

1N-18
7705
P-237

Space Mechanisms Lessons Learned Study

Volume II—Literature Review

Wilbur Shapiro, Frank Murray, and Roy Howarth
Mechanical Technology Incorporated
Latham, New York

Robert Fusaro
Lewis Research Center
Cleveland, Ohio

September 1995



National Aeronautics and
Space Administration

(NASA-TM-107047) SPACE MECHANISMS
LESSONS LEARNED STUDY. VOLUME 2:
LITERATURE REVIEW (NASA. Lewis
Research Center) 537 p

N96-17821

Unclass

G3/18 0098298

LITERATURE REVIEW

A comprehensive literature review was accomplished using a variety of sources including Space Mechanism Symposium proceedings in the United States and Europe, various technical society publications, Pyrotechnic conference publications, Jet Propulsion Laboratory (JPL) Lessons Learned files, Mil Standards and Mil Specs, National Aeronautics and Space Administration (NASA) and Air Force publications, and unpublished contractor reports, memoranda, and presentations. The review has been organized into the three major categories: Deployable Appendages, Rotating Systems, and Oscillating Systems. Subheadings are as presented in the Introduction of Volume I. The reviews conducted by the European Space Tribology Laboratory (ESTL) are included as a separate section, although ESTL material was integrated in the Summary of Lessons Learned.

In conducting the literature review, a specific format was developed which all reviewers adhered to. The format is as follows:

Key Words:	Mechanism, system, problems
Mechanism:	Description
System:	To which mechanism applies
Authors; Experts:	As referred to in paper; all authors listed
Address:	Business address of authors
Telephone Number:	Included if available
Title:	Title of publication
Source:	Where the publication was published
Abstract:	Copied from paper, or else summarized by reviewer
Anomalies:	Description of problems encountered on the ground or in flight
Lessons Learned:	Listing of lessons learned to avoid future anomalies
Description:	Description of mechanism and technical data
Testing:	Results of preflight testing, how accomplished
Experience:	Flight experience, if available

Deployable Appendages

Solar Arrays

Key Words:

Cosmic Background Explorer, Viscous Damper, Pin Pullers, Solar Array

Mechanisms:

Solar Array

Systems:

Cosmic Background Explorer

Authors; Experts:

R. Farley

Address:

NASA-Goddard Space Flight Center
Mail Code 731
Greenbelt, Maryland 20771

Telephone:

Title:

Spacecraft Deployable Appendages

Source:

Goddard Space Flight Center (1992)
Engineering Directorate

Abstract:

This report discusses experience with various spacecraft and provides general guidelines for deployment mechanisms.

PRECEDING PAGE BLANK NOT FILMED

Anomalies:

- One damper required replacement because of an air bubble (reasons not stated).
- Pin puller shaft fractured and rebounded into unfired position. Excessive hole drilling in this puller caused failure.
- Array experienced inconsistent behavior of a microswitch.

Lessons Learned:

- Viscous damper fluid; McGhan-Nusil CY7300 silicone fluid preferred because of stable viscosity and low outgas characteristics.
- Pin pullers used in lieu of bolt cutters to improve reliability.
- Pin pullers should be x-ray inspected.
- Microswitch quality assurance may need improvement.

Description:

Solar Array Appendage Description. The cosmic background explorer solar array consisted of three wings, 120° apart, each with three panels. The three inboard hinges had dampers that were heated with 10-W strip heaters controlled by the thermostats such that there would be minimal temperature variations between the three input dampers. This ensured that the major deployment geometry would be symmetrical. Each hinge line was supported by two hinges, each one with an Elgiloy torsional spring for redundancy and spherical bearings to allow misalignments due to thermal distortions or manufacturing tolerances. This prevented jamming as well as providing a redundant torsional path for the hinge. The top hinge was connected to a potentiometer (position telemetry) through a U-shaped beryllium copper coupler, which would allow large misalignments without affecting either the potentiometer or the deployment. The bottom hinge had the damper. These rotary viscous dampers were modified to use McGhan-Nusil CV7300 silicone fluid, which has very stable viscosity characteristics and has low outgas. This was a vast improvement over the typical DC 93500 resin that has been used to a great extent in these dampers. The new fluid was relatively inexpensive and has infinite shelf life as opposed to the old fluid that was opposite on both counts. The DC 93500 was also extremely viscosity sensitive with regard to temperature.

Solar Array Latch/Release Mechanisms. This system used the high reliability of pin pullers rather than bolt cutters, producing virtually no particular contamination upon firing and retained all of the hardware after firing so it would not pollute space with debris that would affect the sensitive instruments on the cosmic background explorer. There were two different types of release mechanisms used on the solar arrays. The strategy was to structurally decouple the solar array panels from the spacecraft and, thus, prevent them from experiencing launch loads that would otherwise pass through the primary structure. This was accomplished by having each solar array wing determinately supported. Each panel was connected at the top and bottom along the centerline with a release mechanism. The upper release mechanism had a conical connecting surface that reacted loads in three translational and two rotational degrees of freedom. The lower mechanism was a V-guide connection which allowed relative motion in the vertical direction. This was the source of

greatest deflection from the structure and therefore the largest potential contributor of second-hand loading into the panels. Whereas the top restraint required a 450-lb preload, the lower restraint had essentially none, since relative vertical motion was a necessity. However, they were tightened until there was approximately a 0.003-in. gap in the V-guides to prevent rattling, yet preserve its vertical motion capability.

Testing:

Hinge line assemblies were tested in a thermal vacuum chamber for independent characterizations; later, air pad deployments on the flight spacecraft or engineering test unit tested the system performance. A few problems were encountered at the launch site during final testing. First, one of the dampers had to be replaced due to an air bubble in it for reasons that are complicated. A replacement damper was on hand and the wing was redeployed on the air pad table. Second, during one of the last deployment tests, a pin puller shaft fractured and rebounded back into the unfired position. That particular pin had two retaining holes drilled into it where there should have been only one, thereby critically weakening the pin. The solar array release mechanism was designed to be redundant in that only one pin puller needed to actuate. However, this failure had the possibility of being a repeated manufacturing problem so all the x-rays of each pin puller on the spacecraft were intensely scrutinized. It was determined that one pin puller was suspicious, so it was removed and replaced with a one that had been x-rayed.

Experience:

The arrays deployed as planned, with the only anomaly being the minor inconsistent behavior of a microswitch.

Key Words:

Tracking and Data Relay Satellite (TDRS), Solar Array, Space Ground Link Antenna, Omni/C Bank Antenna, Single-Access Antenna

Mechanisms:

Bolt Cutters, Motorized Hinges, Torsion Springs, Pin Pullers, Nonexplosive Actuators, Ball Screw Mechanism

Systems:

TDRS

Authors; Experts:

1. P. Luce
2. John Young

Address:

1. NASA-Goddard Space Flight Center
Mail Code 731
Greenbelt, Maryland 20771
2. SAI

Telephone:

Title:

Spacecraft Deployable Appendages

Source:

Goddard Space Flight Center (1992)
Engineering Directorate

PRECEDING PAGE BLANK NOT FILMED
PAGE 6 INTENTIONALLY BLANK

Abstract:

NASA currently has four TDRSs in geosynchronous orbit. Two more spacecraft are being built by TRW to provide the system with additional redundancy. This constellation of satellites has dramatically increased the data rates and accuracy of communication between spacecraft in near-Earth orbit (including the shuttle) and ground stations. The TDRSs weigh nearly 5000 lb each, including 1200 lb of hydrazine propellant used, as needed, for station keeping. They contain the most complex set of deployable appendages ever launched by NASA.

Anomalies:

- **TDRS On-Orbit Deployment Anomalies.** There have been three noncatastrophic on-orbit deployment-related anomalies. In fact, none of the anomalies has interfered with normal spacecraft operations.
- **TDRS-A.** The field of view for one of the single-access antennas was restricted. This was probably due to a pinched or snagged electrical cable that runs across one of the single-access antenna gimbal joints. This restriction, however, was outside the range of normal operations.
- **TDRS-B.** The single-access antenna delayed deployment by nearly 3 hr when one of the compartment attachment lugs came into contact with the compartment kick-off spring mechanism. It freed itself without any action from the ground.
- **TDRS-D.** One of the single-access antenna drive motors stalled because the bias service loop harness became pinched between the boom and compartment. The motor was reversed to relieve the pinch and deployment proceeded normally.

Lessons Learned:

- Reversible motors can help correct deployment problems.
- Cable circuitry should avoid regions where the cable can get caught or snagged.
- Interference between actuation devices and attachment lugs should be avoided.

Description:

Figure 1 shows the spacecraft in the stowed configuration and Figure 2 shows it in the deployed configuration.

Mounted to an inertial upper stage, the TDRS is launched on the shuttle. A spring-loaded ejection system deploys the TDRS/inertial upper stage stack, and the first burn of the inertial upper stage booster takes the TDRS to geosynchronous orbit. The second and final burn circularizes this orbit.

The solar arrays consist of six large panels that form a hexagonal enclosure around the spacecraft body in the stowed configuration. Structurally, there are two separate solar array assemblies. Each assembly consists of a center panel and two outer panels.

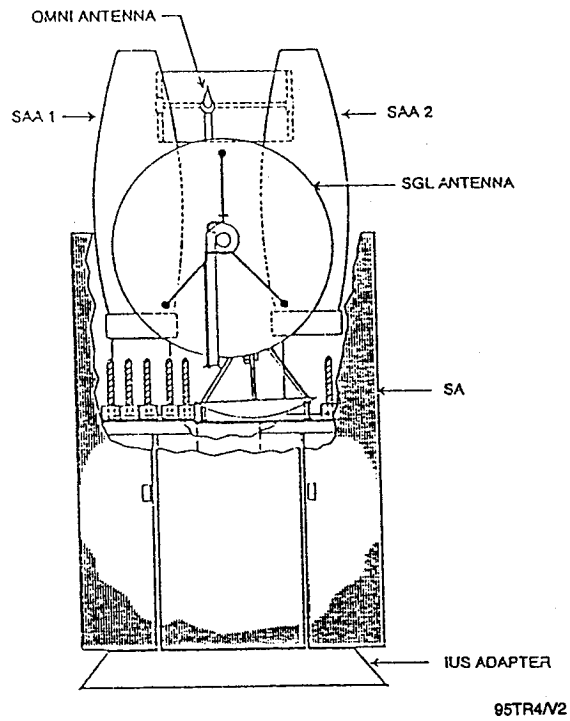


Figure 1. TDRS Stowed Configuration

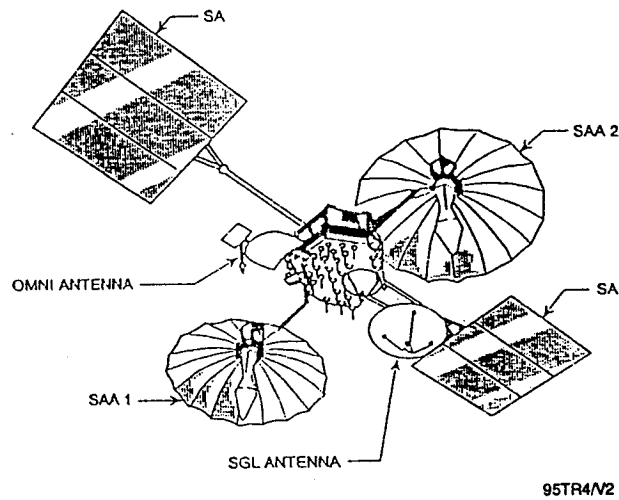


Figure 2. TDRS Deployed Configuration

Testing:

TDRS Appendage Verification Testing. The following functional capabilities were verified by test:

1. Strength and stiffness verified by load deflection testing
2. Margins of safety verified by structural analyses and tests
3. Minimum torque/angle criteria established based on individual and combined resistance torque measurements at worst-case temperature conditions
4. Maximum torque criteria set to ensure that deployment energy remains within safe strength/deformation limits under dynamic latch-up conditions.

Key Words:

Earth Radiation Budget Satellite (ERBS), Electronic Switching Spherical Array, Solar Array, Molybdenum Disulfide (MoS₂) Lubricant

Mechanisms:

Electronic Switching Spherical Array, Solar Array

Systems:

ERBS

Authors/Experts:

R. Mollerick

Address:

NASA-Goddard Space Flight Center
Mail Code 731
Greenbelt, Maryland 20771

Telephone:

Title:

Spacecraft Deployable Appendages

Source:

Goddard Space Flight Center (May 1992)
Engineering Directorate

Abstract:

This article describes the ERBS and two deployable devices; an electronic switching spherical array and two solar array panels. Due to inadequate temperature testing to simulate cold-temperature bearing operation, the solar arrays did not critically deploy. The reason was excessive bearing friction.

Anomalies:

Failure of Solar Array to Deploy. Poor characteristics of MoS₂ lubricant at cold conditions resulted in excessive bearing friction. The problem was resolved by manual manipulation of the bearings into sunlight.

Lessons Learned:

- Insist on the contractor providing sufficient data to verify satisfactory compliance of the test objectives. In this case, makeshift test setup conditions were inadequate to control or achieve temperature extremes.
- Convenience, speed, and cost savings are not always the best criteria for test purposes. Certainly, the high-bay facility turned out to be convenient for the test setup. Quick and inexpensive techniques for temperature control appeared workable. The fact that a suitable chamber was not available in time for the test made all of the above choices desirable. In retrospect, a humidity chamber of the right size including high- and low-temperature control was necessary.
- Insist on testing under realistic thermal conditions. Deployable appendages and associated mechanisms are some of the most difficult subsystems to accurately model and test because of numerous thermally conductive and nonconductive interfaces when using, for example, rolling and point contact surfaces of bearings. Predicting bulk temperatures went well, although temperature gradients for the arrays were neither addressed nor tested. Temperature gradients between sun illuminated and shadowed structures are likely to contribute adversely during deployment.
- MoS₂, while a good dry-film lubricant for space applications, can also be a nemesis for failure. Case in point: each of the deployment drive mechanisms has bearings lubricated with MoS₂. It is known from the literature that MoS₂ has an affinity for moisture. It is not unreasonable to expect that under conditions of cold temperatures (-44°C) and the balling-up phenomenon of MoS₂, moisture molecules could create frozen balls in the path of the rolling elements to impede available driving torque. In fact, this is the major contributor believed to have prevented the solar array from initially deploying while the spacecraft was attached to the orbiter remote manipulator system. Fortunately, with man in the loop we were able to rotate the solar array hinge line into the sun and monitor the deployment drive unit temperature with a box beam thermistor located close to the drive units. Deployment occurred when the temperature climbed through 0°C.
- Spring drives must use a minimum torque ratio of four. The deployment drive systems each had a torque ratio of less than three. However, each drive had redundant torsion springs and analysis indicated ample capacity for successful deployment. In addition, testing indicated only small deployment rate variations between room temperature and hot and cold extremes. In looking at the ERBS solar array deployment, it is conceivable that a combination of cold temperatures, thermal gradients, MoS₂ lubricant, and insufficient torque margins are likely to result in deployment problems.

Description:

The ERBS, launched in October 1984, is an Earth-looking spacecraft with three scientific instruments (ERBS-S, ERBS-NS, and SAGE-II) in a circular orbit of 600-km altitude and 57° inclination. The 2250-kg (4960-lb) shuttle payload was determinately mounted in the cargo bay using three longeron trunnions and one keel trunnion. The spacecraft is illustrated in Figure 1 and is composed of a base, instrument, and keel module.

There were two deployable subsystems on the ERBS spacecraft. These included an electronic switching spherical array antenna and two solar arrays. Both systems use similar deployment drives and release mechanisms. The drive system, illustrated in Figure 2, uses redundant torsion springs and a strike arm that engages a precrushed honeycomb damper and lock system at the end of deployment travel. The release mechanism, illustrated in Figure 3, uses redundant nonexplosive initiators and is designed to release the appendage with either nonexplosive initiator.

The electronic switching spherical array antenna is stowed between the solar arrays, as illustrated in Figure 4, Detail A. The antenna is supported by a boom that pivots through approximately 90° to full deployment and engages a lock.

The solar arrays are stowed on each side of the keel module, as illustrated in Figure 5. Each array is supported by a keel box beam and redundant torsion spring drive systems at each end.

The arrays rotate through 65° and 115°, respectively, at full deployment and engage the respective locks.

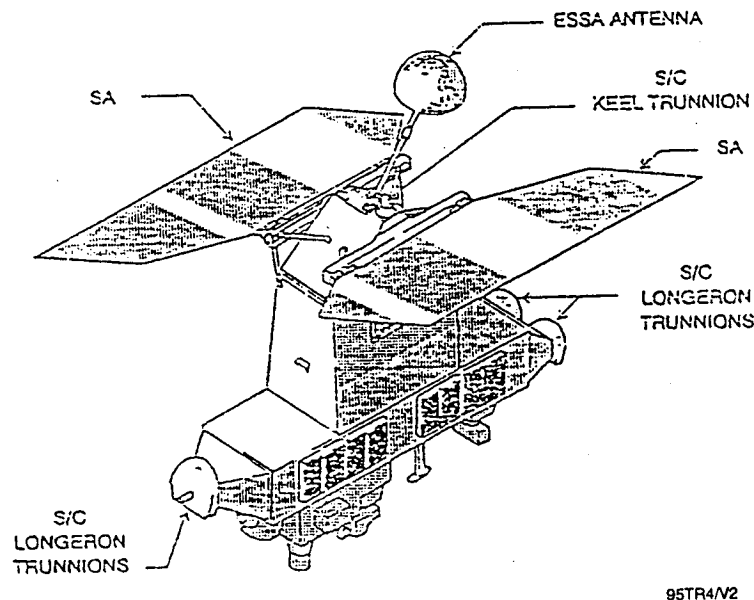
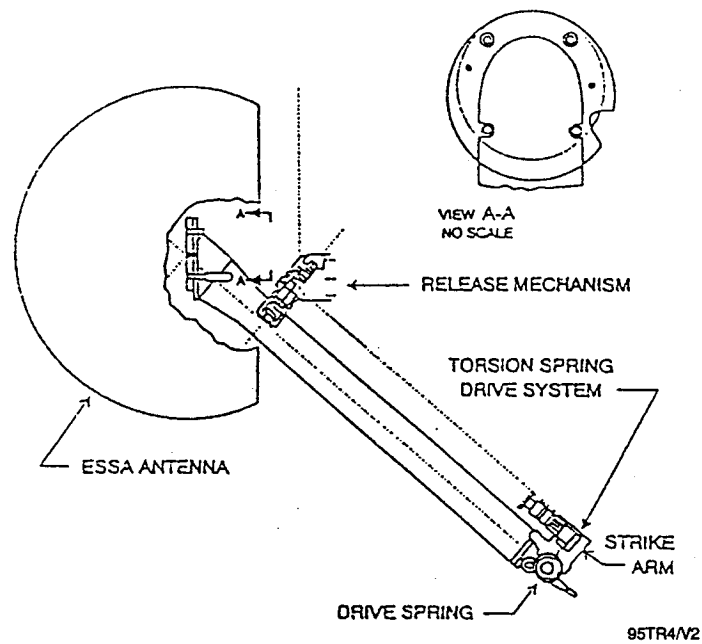


Figure 1. Deployed ERBS Spacecraft Configuration



**Figure 2. ERBS Release Mechanism and Torsion Spring Drive System
(Electronic Switching Spherical Array Antenna)**

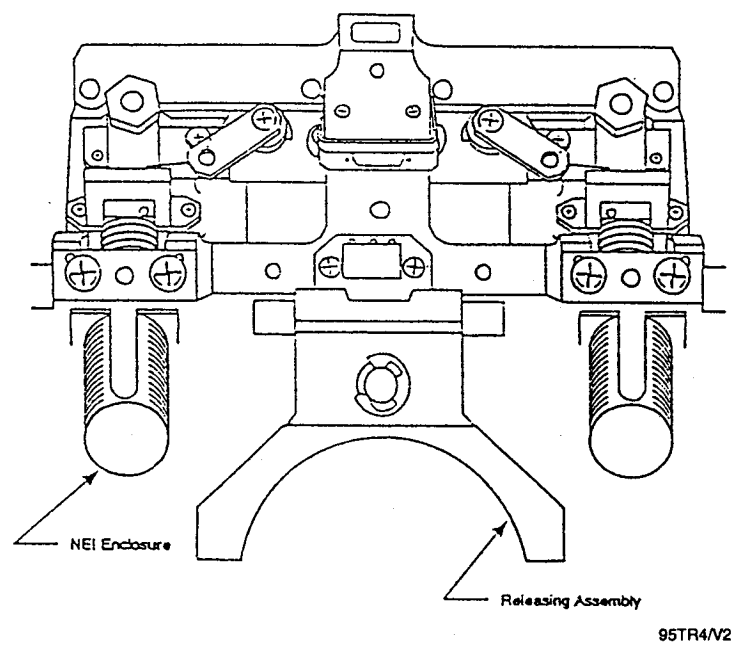


Figure 3. ERBS Release Mechanism

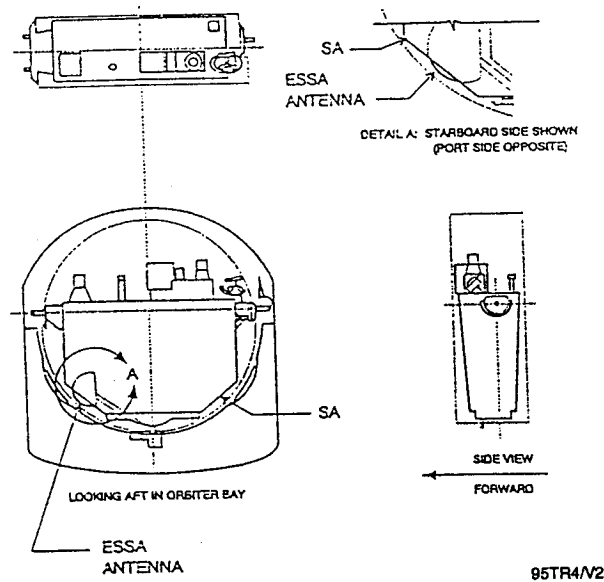


Figure 4. ERBS Launch Configuration

Testing:

ERBS Deployed Appendage Test Objectives and Approach. The test objectives for the deployables were to demonstrate release and deployment under g-negation and to characterize appendage dynamics during hot and cold temperature extremes. Testing of each appendage was configured with flight release and drive mechanisms and with mass simulated arrays and antenna. Rotation of each appendage was around a vertically oriented hinge line to minimize gravity effects. Release and drive mechanisms were instrumented to monitor all motion. Temperature extremes were achieved, although poorly controlled, with heaters for the hot case, and liquid nitrogen vapors for the cold case. The tests were performed by the contractor in a high-bay facility with makeshift wrap-around plastic bags for the mechanisms to help achieve temperature goals. The bags allowed freedom of motion for full appendage deployment.

Deployed Appendage Test Results. Thermal vacuum test results indicated that conditions from room temperature to hot were easily achieved with repeatable data. The steady-state cold case was difficult to achieve because of icing on the components and poor temperature control due to the makeshift test setup. The predicted cold case test temperatures of -49°C and -55°C for the sun and antisun sides of the arrays, respectively, were not achieved under the described conditions. The coldest obtainable test temperature was -33°C . The on-orbit monitored temperature in the center of the array box beam (sun side) was -44°C .

Experience:

Initial deployment of the solar array abated by excessive drive torque, attributable to cold temperatures and MoS_2 lubricant adversely affecting bearing operation. Astronauts rotated the solar array hinge line onto the sun, and higher temperature allowed deployment.

Key Words:

Solar Array, Deployment

Mechanisms:

Solar Array

Systems:

Deployment System

Authors; Experts:

P.L. Vorlicek, J.V. Gore, and C.T. Plescia

Address:

Ford Aerospace and Communications Corporation

Telephone:

Title:

Design and Analysis Considerations for Deployment Mechanisms in a Space Environment

Source:

16th Aerospace Mechanisms Symposium, NASA Conference Publication 2221 (1982).

Abstract:

On the second flight of the INTELSAT V spacecraft, the time required for successful deployment of the north solar array was longer than originally predicted. The south polar array deployed as predicted. A series of experiments was conducted to locate the cause of the difference. Specifically, deployment rate sensitivity to hinge friction and temperature levels was investigated. In conjunction with these experiments, a digital computer simulation of the deployment was created to investigate the effect of parameter changes on deployment. As a result of the experiments and simulation, hinge design was optimized for nominal solar array deployment time for future INTELSAT V satellites. The nominal deployment times of both solar arrays on the third flight of INTELSAT V confirmed the validity of the simulation and design optimization.

PRECEDING PAGE BLANK NOT FILMED

PAGE 16 INTENTIONALLY BLANK

Anomalies:

On the second flight of the INTELSAT V spacecraft, the time required for successful deployment of the north solar array was longer than originally predicted. The south solar array deployed as predicted.

Lessons Learned:

- Adequate theoretical analysis of a mechanism should be undertaken.
- Mechanisms should be tested under conditions that duplicate the range of expected orbital environments in order to identify sensitive conditions.
- During the ground testing of very large complete assemblies, it is very difficult (if not impossible) to adequately duplicate the orbital conditions.
- The difference in deployment time was found to be due to a significant increase in hinge friction at low temperatures.
- The hinge friction problem was overcome by increasing the bearing clearances to allow for greater temperature variations and giving the hinges special lubrication.

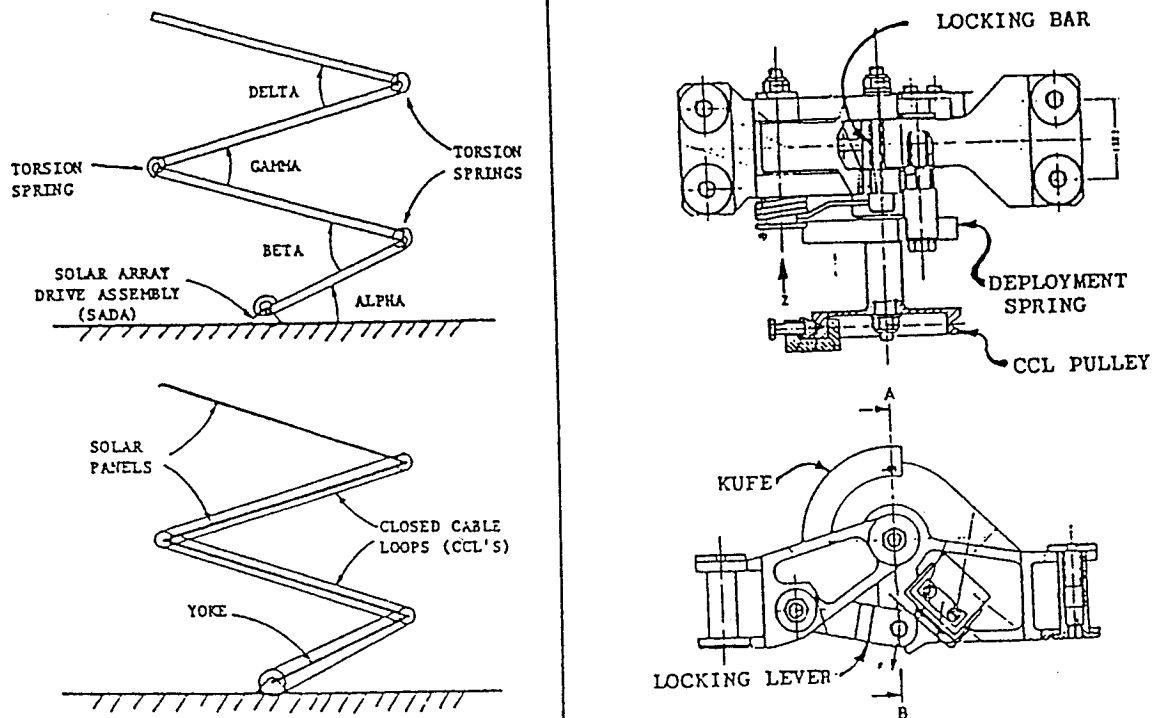
Description:

The solar arrays on INTELSAT V consist of a yoke and three solar panels that deploy in an accordion-type manner as shown in Figure 1. The array has two deployment mechanisms, torsion springs, and closed-cable loops. The torsion springs provide the energy to deploy the array. The closed-cable loops restrain the deployment of transferring torques between the hinges, synchronizing the deployment angles and controlling the deployment rate to a point within the structural capability. Springs on the closed-cable loop cables compensate for changes in cable length due to temperature variation. The springs also allow the hinge lines to be at somewhat different angles during deployment, which adds considerable complexity to the mathematical model of the solar array deployment. On the second flight, the south solar array deployed in 22 sec, while the north solar array took 32 sec. Original predictions were for both solar arrays to deploy in approximately 13.5 sec.

Two sets of ground-based experiments were conducted using an engineering model and flight hinge assemblies in order to determine the cause of the deployment time difference. The deployment tests on the engineering model were divided into two groups:

- Attempts to duplicate the flight data
- Deployment tests with simulated hot and cold closed loops and hinges, duplicating on-orbit conditions.

Attempts to duplicate the flight data were unsuccessful. The orbital configuration of the solar arrays during deployment is edge-on to the sun. This position results in a temperature difference between the sunward and shaded hinges. To evaluate the effects of hot and cold conditions, a test was conducted where the upper hinges were heated to 85°C and the



95TR4/V2

Figure 1. The Deployment Mechanisms and Hinges

lower hinges cooled to -100°C . The deployment time in this configuration was increased from 22 to 24.7 sec. These tests indicated an increasing resistance torque level with decreasing temperature.

Additional tests were conducted to examine the closed-cable loop temperatures on deployment times. Temperature changes affect the length of the cables, which changes the point at which the cables go slack. When the effects of temperature on the closed-cable loops were tested, significant variations in deployment time resulted. Under nominal on-orbit conditions, the south array deployment time was 3 sec faster than the north array during engineering model tests but this still did not account for the differences seen in flight.

The most important findings of the investigation were the measurements of the resisting torques on flight hinge assemblies. These revealed that the resisting torques at low temperatures in vacuum were much larger than values obtained from measurements on development model assemblies and much larger than values obtained in ambient conditions. As a result of these findings, all the hinges were given special lubrication. In addition, the bearing tolerances were increased to allow for greater temperature variations. Tests on the modified hinges showed that the resisting torque was greatly reduced at low temperatures and that it was not as sensitive to temperature variation as the original hinges.

In conjunction with the laboratory experiments, a digital simulation of the solar array deployment was developed. In the simulation, the torques acting on the hinges included:

- The torsion springs at the hinges
- Torques from the closed-cable loops
- Stick-slip Coulomb friction torques (stiction).

Accurate simulation of stiction is important for both designer and analyst to consider, as this was eventually found to account for the differences in the north and south panel deployment times. A simulation of the deployment of the north solar array with the nominally measured friction levels gave a deployment time of approximately 18.5 sec. Additional runs showed that the deployment rate was most sensitive to the friction level on the yoke/solar array drive assembly hinge. Raising the stiction on the yoke/solar array drive assembly hinge 50% and the yoke/inboard panel hinge 50% yielded a deployment similar to that experienced on orbit.

Based on the findings of the simulation runs and the experiments, several changes were made to the hinges. Among the changes were:

- Special application of lubricant to all moving parts in the hinges
- Increased bearing tolerances to allow greater variation in temperature
- Increased polish on locking bars
- Increased torsion spring pretorque level.

Experience:

The modifications described above were included in the third flight of INTELSAT V, which was successfully launched December 15, 1981. Data from the on-board accelerometer showed that the first hinge of the south array locked up at 11.8 sec and the first hinge of the north array began lock up at about 13.8 sec.

Key Words:

Solar Array, Flexible Solar Array, Deployment, Solar Blanket, Solar Array Deployment

Mechanisms:**Systems:****Authors; Experts:**

J. Gibb

Address:

Lockheed Missiles & Space Company, Inc.
Sunnyvale, California

Telephone:**Title:**

MILSTARs Flexible Substrate Solar Array – Lessons Learned

Source:**Abstract:**

MILSTARs flexible substrate solar array is an evolutionary development of the lightweight, flexible substrate design pioneered at Lockheed during the 1970s. Many features of the design are related to the solar array flight experiment flown on STS-41D in 1984. Flexible substrate solar array development has created a substantial technology base for future flexible substrate solar arrays such as the array for space station Freedom. Lessons learned during the development of the flexible substrate solar array can and should be applied to the Freedom array and other future flexible substrate designs.

Anomalies:

- During one of the first development tests, the suspension wire supporting the 10-kg cover broke, causing a chain reaction domino effect to propagate down the blanket. Several panels ended up on the floor of the test facility. After this incident, the cover support wire was increased in size and changed from single-strand music wire to

braided cable to avoid a future mishap. However, the remaining suspension wires continue to plague the test fixture with fatigue-related breakage. They are being converted to heavier gage braided cable as well. The main problem with the music wire cables occurs at their end fittings, which have small radius bends, inducing low-cycle fatigue failure. Revised end termination designs for the braided wire cable have ball end fittings, or relatively large radius cable loops to eliminate these problems.

- Ambient testing of the flexible substrate solar array development unit proved that the basic design was sound. One of the most important test results was the discovery of panel-to-panel sticking, caused by assembly adhesive on the backside of the panels. Because of this, manufacturing and handling procedures were successfully revised to eliminate such problems on flight panels by scrupulous attention to cleanliness during bonding operations.
- Additional testing with the development hardware exposed it to the ascent acoustic environment, the release pyroshock environment, and ascent quasi-static loads. No anomalies occurred during the first two tests, proving that the foam and rubber insulation in the blanket container performed as intended. However, the quasi-static load testing of the blanket container did result in unexpected behavior. In order to properly load the stowed blanket in the preloaded container, the entire assembly was placed on a centrifuge, oriented such that the centrifuge arm was along the resultant load vector for the worst-case peak-load condition. Before maximum load was reached, the blanket panels slipped relative to one another, and the cover also shifted. Experimentation found that the cover required lateral restraint and preload was raised from an initial value of 9.3 to 13.4 kN to avoid slippage. Panel slippage while stowed and preloaded is a concern because it can cause cell cracking. The centrifuge testing also found inadequacies in the preload setting/measurement method.

Lessons Learned:

Many lessons have been learned during the design and testing of the flexible substrate solar array. A summary of these includes:

DO's:

1. Establish written test requirements and a test plan as early as possible.
2. Devote sufficient resources to thoroughly prove 0-g deployment test equipment works, and that it is robustly designed with fail-safe features or high structural margins.
3. Minimize deployed mass at the deployed end of the array or mast (leave the cover at the base).
4. Create a finite-element model of blanket container preload distribution.
5. Perform development acoustic and shock testing as appropriate to establish minimum acceptable blanket preload to survive these environments.
6. Consider pretesting cell assemblies by uniformly preloading prior to incorporation in the blanket. This will eliminate or reduce cell cracking caused by cell assemblies with residual stresses.

7. Insist on high cleanliness standards during panel bonding, especially when the process involves cutting film adhesives, to avoid panel sticking.
8. Use electromechanical measurement of preload when it is critical. Ensure adequate strain reliefs are provided for connection wires.
9. Maximize spreader bar stiffness in the deployment plane, and perform analysis to ensure acceptably low deflection to avoid panel warping or wrinkling.
10. Be aware that molybdenum disulfide (MoS_2) coatings have a coefficient of friction dependent upon humidity. Variations are on an order of magnitude between ambient and vacuum conditions.

DON'Ts:

1. Do not rely on preload and friction to hold a blanket stack in place during ascent; use a positive mechanical load path such as pins, skewers, or interlocking sections. A reduction in applied pressure from 9.7 to 1.2 kPa (a factor of 8) should be possible if this is done.
2. Avoid overly complex electronic test consoles; if a simple power supply with polarity and on/off control suffices, use it.
3. Avoid using notch-sensitive materials, such as threaded fasteners. The original tension rod cam roller bearing screw was 440C CRES and broke at the root of the first thread.
4. Do not apply MoS_2 coatings to both surfaces of a sliding/mating pair, or a higher coefficient of friction will result that if only one surface is coated (this occurred in the tension-rod Belleville washer stack).
5. Do not allow inexperienced engineers to design spacecraft mechanisms without sufficient supervision and design review (many details of the preload/release mechanism have required changes, due to the designer's lack of experience and insufficient review).

Description:

The flexible substrate solar array is a large deployable solar array made up of flexible substrate electrical panels that are fan folded when stored. When deployed, the array is 15.2 m long \times 3 m wide. Each panel is about 0.4 mm thick and, when folded for storage, the blanket stack is 2.5 cm thick. There are 69 active panels with solar cells and 7 spacer panels without cells.

During launch, the stack is compressed between two foam and rubber-lined honeycomb panels. Preload clamp and release action is produced by a multipoint preload/release mechanism. Upon release, the cover panel is rotated up and out of the blanket deployment path by two four-bar hinge mechanisms. Deployment is then effected by a coilable longeron Astromast attached to the blanket by a spreader bar (upper tension bar). The mast pulls the panels out of the stowed stack as it extends. Orderly unfolding and alignment is assisted by three guidelines controlled by tensioning mechanisms. Near the end of the mast travel, the blanket is automatically tensioned by two mechanisms acting on a second spreader bar (lower tension bar).

Retention and Release Mechanisms

Key Words:

Pin Puller, Pyrotechnics, Coatings, O-Rings

Mechanisms:

Pin Puller

Systems:

Deployment Systems (Antenna)

Authors; Experts:

1. L.J. Bement
2. M.L. Schimmel

Address:

1. NASA-Langley Research Center
Hampton, Virginia
2. Schimmel Company
St. Louis, Missouri

Telephone:

Title:

Integration of Pyrotechnics into Aerospace Systems

Source:

27th Aerospace Mechanisms Symposium, NASA-Ames Research Center, California
(May 12-16, 1993).

Abstract:

The application of pyrotechnics to aerospace systems has been resisted because normal engineering methods cannot be used in design and evaluation. Commonly used approaches for energy sources, such as electrical, hydraulic, and pneumatic, do not apply to explosive and pyrotechnic devices. This paper introduces the unique characteristics of pyrotechnic devices, describes how functional evaluations can be conducted, and demonstrates an engineering approach for pyrotechnic integration. Logic is presented that allows evaluation of two basic types of pyrotechnic systems to demonstrate functional margin.

PRECEDING PAGE BLANK NOT FILMED

Anomalies:

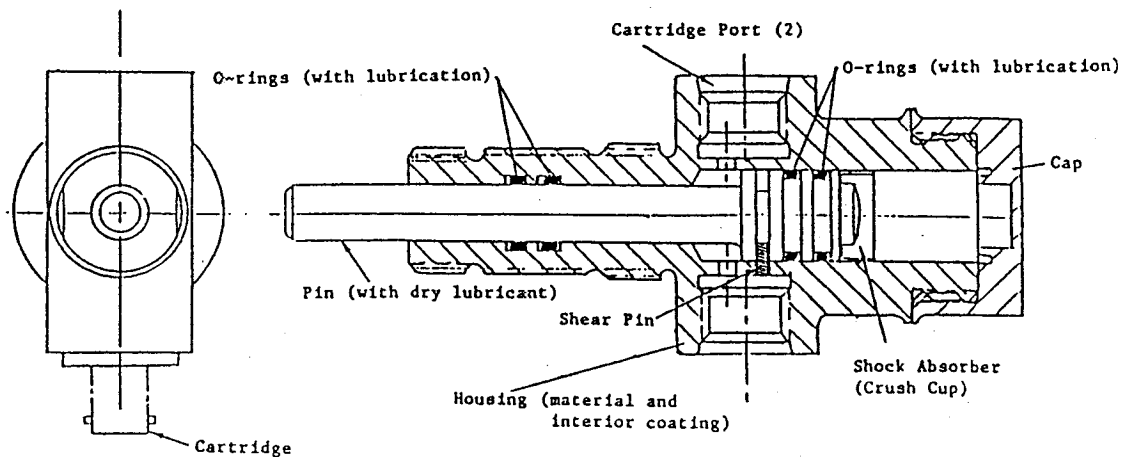
- Blowby across O-ring seals – some of the molybdenum disulfide (MoS_2) coating on the pin deposited on the O-ring, preventing a seal.
- A soft, electrodeposited nickel/Teflon coating on the piston bore wiped off on the O-rings, preventing a seal.

Lessons Learned:

- A principal cause of pyrotechnic device failures is inadequate functional margin. In the case of the pin puller, the initial design could not accommodate lot-to-lot variations in cartridges, combined with improper coatings on the piston and bore.
- Variables of a pyrotechnic system must be evaluated and functional margins established. Tests should be conducted with flight representative hardware and functional dynamics applied to either: 1) measure and compare the energy delivery capability of the explosive or pyrotechnic power source to the energy required by the mechanical function, or 2) quantify and compare key functional performance parameters.
- Soft coatings on pistons and bores can wipe off on O-ring seals reducing sealing effectiveness and degrading pin puller operation. For pistons, electrodeposited nickel/Teflon coating is recommended. Hard anodized aluminum uncoated housings are recommended.

Description:

The Viking pin puller releases an antenna on the mission's Mars Lander. Its design and system variables are shown in Figure 1. Firing either cartridge first fails the shear pin and drives the piston from left to right to withdraw the pin. The pin puller was inconsistent and failed.



95TR4/V2

Figure 1. Viking Pin Puller

Key Words:

Pin Pullers, Pyrotechnics

Mechanisms:

Pin Pullers, Pyrotechnics

Systems:

Deployment Systems (Antenna)

Authors; Experts:

L.J. Bement and M.L. Schimmel

Address:

NASA-Langley Research Center
Hampton, Virginia

Telephone:

Title:

Determination of Pyrotechnic Functional Margin

Source:

Presented at the 21st Annual SAFE Symposium, Las Vegas, Nevada
(November 11-13, 1991).

Abstract:

The purpose of the effort described in this paper was to improve the understanding of how pyrotechnical devices work by demonstrating a method of measuring the performance margin of a pyrotechnically actuated pin puller for use on NASA's halogen occultation experiment instrument, which is on an orbital spacecraft.

Anomalies:

- **Magellan Failures.** Early in the program a functional failure occurred. The pin had strokes approximately half the required distance. The force required to push the pin to the end of its stroke was approximately 50 lb. An inspection revealed that the NSI port had not been chemical-chromate coated, as required by drawing. Additional firings of deliberately uncoated units, and properly coated units showed that coated units produced consistently higher peak pressures, so the failure was considered resolved.

Within three more firings, a second failure occurred. In this failure, the pin stroked less than 0.02 in. The dissection revealed that the web in the port into which the NSI was fired was deformed and had gripped and locked the piston into place. This pin puller design was then abandoned in favor of another previously qualified design. There was no failure resolution.

- **Halogen Occultation Experiment Failure.** An x-ray examination revealed that the pin puller bores on all the Viking units had been drilled off center by as much as 0.009 in., thus, causing the webs to vary by that amount. On removing the caps from the bodies of three pin pullers that had been fired with a single NSI, two units had not fully stroked to contact the end cap, and the third had just contacted without appreciably deforming the energy-absorbing cup to achieve the locking function. The fourth unit had been fired in a nonstandard mode with two simultaneously initiated NSIs. The energy-absorbing cup in this unit was completely flattened. The cylinder bores indicated no appreciable web deflection in the NSI port bottom and only minor scuffing on the walls. There were no obvious indications of blowby around the O-ring seals.

Lessons Learned:

- In summary, the aluminum-bodied test series revealed that a considerable increase in energy required to stroke could be expected with less lubrication on O-ring interfaces. The chemical chromate and molybdenum disulfide coatings reduced the sealing reliability of O-ring interfaces. The aluminum body had a sensitivity to deformation. The steel-bodied test series revealed considerable output variation among VSI and NSI lots and that the combustion efficiency of all lots could be significantly enhanced by using an epoxy nozzle and an external BKN03 booster charge. Also, the steel body exhibited none of the sensitivities to sealing or metal deformation. Finally, the use of a steel body met the requirement that the NSI energy output (127 in.-lb for lot XPF) was at least three times the energy required to stroke (25 in.-lb).
- For the Viking pin puller design, there was an inadequate demonstration of functional margin. That is, not enough information had been obtained on the influence of functional variables and how much energy was consumed by these variables in accomplishing the function. The Magellan failures occurred when production variables reduced the pin puller's performance below its functional threshold: 1) sliding friction increased, 2) O-ring seals were poor, 3) the combustion efficiency of the NSI was reduced, and 4) the aluminum housing deformed.
- Functional margin should be determined, comparing energy deliverable by a cartridge to the energy required for the device to function. The energy deliverable by the cartridge should be measured by firings in the actual device. Energy required should be determined by drop tests on the actual device.

- A further conclusion is that the changes made to the pin puller design, specifically using steel instead of aluminum and using a more durable dry coating on the pin, significantly improved functional performance.

Description:

The Viking application was to release an antenna on the surface of Mars, and the halogen occultation experiment application was to release a gimbal interface in Earth orbit. Both pin pullers had the same basic design: a 0.25-in. diameter pin was withdrawn just over 0.5 in. by firing either of two cartridges. The cartridge output vented through a 0.100-in. diameter opening out of the port to pressurize the pin side of the piston. The shear pin failed at approximately 80-lb static force. Redundant O-rings were used on both the pin and the piston and lubricated with medium-consistency silicone grease. A deep-drawn, 0.15-in. long, 0.010-in. wall thickness, 302 stainless steel energy-absorbing cup (see Figure 1) crushed on impact into the cap to remove the excess energy from the pin-piston and prevent rebound.

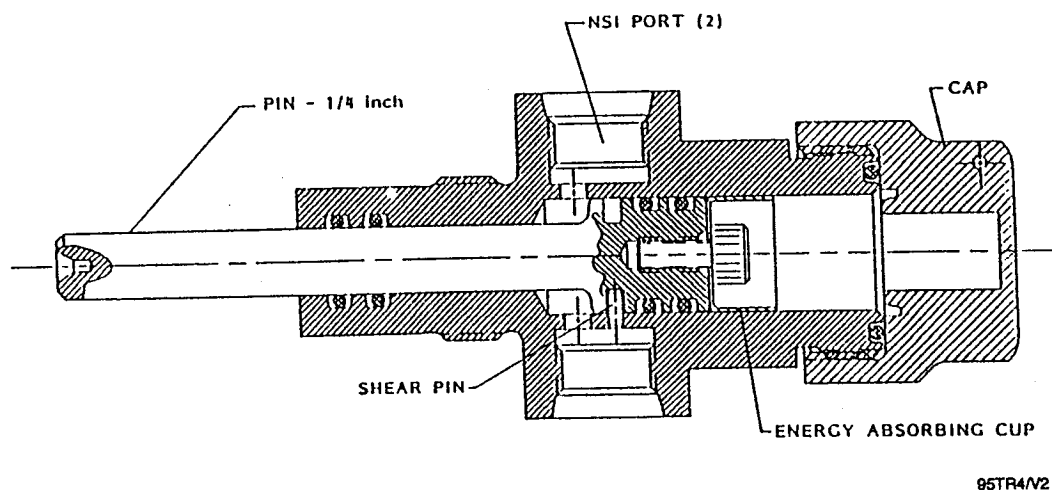


Figure 1. Cross Section of Steel-Bodied Halogen Occultation Experiment Pin Puller

Key Words:

Pyrotechnics, Explosives

Mechanisms:

Pin Puller, Pyrotechnics, Bolt Cutter

Systems:

Deployment Systems

Authors; Experts:

L.J. Bement

Address:

NASA-Langley Research Center
Hampton, Virginia

Telephone:

Title:

Pyrotechnic System Failures: Causes and Failures

Source:

NASA TM100633 (June 1988).

Abstract:

This paper describes a survey compiled for a 23-yr period which includes 84 serious component or system failures (12 occurred in flight with fully developed and qualified hardware). Analyses are presented as to when and where these failures occurred, their technical source or cause, followed by the reasons why and how these kinds of failures continue to occur. The results of these efforts frequently indicated a fundamental lack of understanding of the functional mechanisms of pyrotechnic devices and systems, followed by not recognizing pyrotechnics as an engineering technology, insufficient manpower with hands-on experience which has led to a heavy dependence on manufacturers and too few in-house test facilities.

PRECEDING PAGE BLANK NOT FILMED

Anomalies:

Date	Project	Failure	Source of Failure	Resolution
1976	RSRA	Firing pin assemblies corroded and locked in qualification	Bad design	Redesigned, requalified
1973	Classified	Pin puller failed during system test (cartridge closure blocking port)	Lack of understanding	Redesigned, requalified
1979	Classified	Pin puller body ruptured during system test (inadequate containment margin and variation in metal grain orientation)	Lack of understanding	Redesigned, requalified
1987	Magellan	Pin puller failed to stroke against flight-side load (NSI output restricted, causing reduced output and housing deformation against working piston)	Bad design, misapplication of hardware	Replaced, requalified
1986	Magellan Orbiter	Pin puller failed to function in LAT (NSI produced insufficient pressure caused by coatings of pressurized volume)	Misapplication of hardware, lack of understanding	Changed manufacturer and design
1986	ASAT	Bolt cutter failed LAT (improper compression margin test requirement)	Incorrect specification	Correct specification

95TR4/V2

Lessons Learned:

The 1987 failure of two Magellan pin pullers has far greater potential impact than is initially apparent. This pin puller was the same unit fully qualified for the Viking Lander spacecraft for the 1976 landing on the surface of Mars. After this experience and with its pedigree, two units from a duplicate lot of pin pullers failed to function in a failure mode not recognized in the original design, development, and qualification. First, the extremely dynamic pressure impulse output as designed of the NSI, when fired into a small eccentrically vented cavity, was severely attenuated reducing the energy available to stroke the piston. Furthermore, the bottom of the cavity was deformed by the pressure into a groove in the piston, which had to stroke to pull the pin. This device may have always been marginal when operated by a single-cartridge input.

For the source of failures, the shocking statistic is that 35 of 84 (42%) of the failures were caused by a lack of understanding; i.e., the personnel working the problem at the time did not have the technology needed to understand and correct the failure. Unfortunately, 24 were mistakes, caused by poor designs and misapplication of hardware, which means that personnel did not apply the known technology. The next 22 failures have to be categorized as carelessness through manufacturer's poor procedures and quality control.

Since pyrotechnics are single-shot devices, past approaches for demonstrating reliability have relied heavily on developing a statistical verification without a clear understanding of functional mechanisms and the relative importance of system parameters. That is, once a successful performance was achieved, emphasis was placed on accomplishing large numbers of consecutive successes. (More than 2000 units are needed to establish a 99.99% reliability at a 95% confidence level.) However, the current approach often is to run full-scale systems tests on as few as six assemblies or less with no statistical guarantee of reliability, and without an adequate understanding of how the mechanisms function, which can be a prescription for disaster.

Key Words:

Joint, Release Mechanisms, Pyroactuators

Mechanisms:

Release Mechanism

Systems:

Authors; Experts:

1. L.J. Bement
2. M.L. Schimmel

Address:

1. NASA-Langley Research Center
Hampton, Virginia
2. Schimmel Co.
St. Louis, Missouri

Telephone:

Title:

Investigation of Super*Zip Separation Joint

Source:

NASA TM 4031 (1988).

Abstract:

Following functional failures of two of five Lockheed Super*Zip spacecraft separation joints in a development test series to quantify thermal effects, an investigation program was initiated on this and related systems to assist in preventing recurrence of failure. The Super*Zip joint, applied in a ring configuration, utilizes an explosively expanded tube to fracture surrounding prenotched aluminum plates to achieve planar separation. A unique test method was developed and more than 300 individual test firings were conducted to provide an understanding of the severance mechanisms, the functional performance effects of system variables, and the most likely cause of system failure. An approach for defining functional margin was developed, and specific recommendations were made for improving existing and future systems.

PRECEDING PAGE BLANK NOT FILMED

Anomalies:

- The patented Lockheed Super*Zip spacecraft separation joint was planned for use on the space shuttle to release the Centaur vehicle (120 in. diameter) and the inertial upper stage (91 in.) at the same separation plane as the Centaur and the Galileo spacecraft.
- Following functional failures of two out of a group of five Lockheed Super*Zip spacecraft separation joints in a shuttle/Centaur thermal development test series to quantify thermal effects, an evaluation program was initiated on this and the related inertial upper stage and Galileo systems to assist in preventing a recurrence of failure.

Lessons Learned:

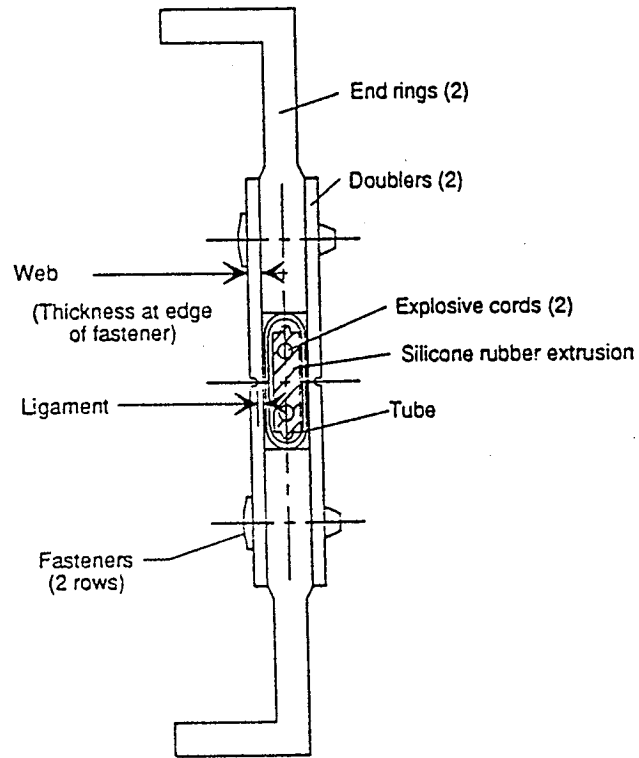
The severance mechanisms of the Super*Zip separation joint are complex. The ligament area is initially impacted by the explosive pressure wave, which induces a structural weakening. An extremely rapid bending stress/strain condition is then induced in the ligament, which ultimately fails in tension at a much smaller energy level than can be achieved with mechanical impact. The most surprising result of this investigation was that thin (0.025-in.) ligaments were more difficult to sever than thicker (0.042-in.) ligaments. This phenomenon can be attributed to the differences in the dynamic stress/strain conditions induced in the two different thickness ligaments; in simpler terms, thin sheets can more easily be rapidly bent around small radii without fracturing than can thick sheets. Tube ruptures are induced by the explosive pressure wave driving the flattened tube radius closest to the explosive source in the dual-cord configuration into the ring structure. The tube is thinned on the peak of the radius by the initial impact and is then flattened across the entire radius against the end ring structure. As the flattened portion of the tube expands, the radius area is dynamically forced into tension, inverting the shape from convex to concave and inducing failures at the thinned sections. The single-cord configuration indicated no trend toward tube rupture with increased explosive load.

Description:

Figure 1 shows the components used in the Super*Zip. The Super*Zip separates into two parts as shown. Separation is accomplished when either explosive cord is fired. The explosive pressure wave expands the tube (which contains all explosive products) against the doublers and fractures are induced in the ligaments progressing around the cylinder.

Testing:

A series of five thermal development tests were conducted: one at approximately -40°F, three at -80°F, and one at -120°F. The failures occurred at -80°F and -120°F. The joints were cooled in a closed chamber free from moisture or frost buildup. The thickness of doublers in all five tests (39 doublers per test) are summarized in Table 1. Functional failures (i.e., no severance) began occurring at a thickness of 0.086 in. and, as thickness increased, more failures occurred even though all ligaments were closely controlled to ± 0.002 in.



95TR4/V2

Figure 1. Component Identification of Separation Joint

Key Words:

Gimbals, Pyro Actuators, Solar Array Driver, Deployable Appendages, Antennas

Mechanisms:

Gimbals, Pin Pullers, Pyro Actuators

Systems:

Solar Array Driver, Antennas, Deployable Appendages

Authors; Experts:

K. Hinkle

Address:

NASA-Goddard Space Flight Center
Engineering Directorate
Greenbelt, Maryland 20771

Telephone:

Title:

Spacecraft Deployable Appendages

Source:

Spacecraft Deployable Appendages

Abstract:

This publication discusses specific spacecraft features and anomalies, under NASA-Goddard cognizance. General guidelines for deployable mechanisms are also discussed.

Anomalies:

- Using bearings for small rocking motion applications has its problems. Even with a porous retainer, there is no fresh supply of oil to replenish the contacting surfaces with small oscillatory motions. Torque can skyrocket as either the oil breaks down or the bearing starves. In a test conducted at Hughes, Bray 815Z had half the initial torque of Apiezon C (with an extreme pressure additive) in a 4° gimbal bearing test. But after 7×10^4 cycles, the Bray 815Z turned to "brown sugar" and the bearing torque quickly increased by a factor of 10.
- During one of the solar array deployment tests in 1989, a pin puller in a release mechanism was actuated, the pin was retracted inside its housing to release the solar array but then rebounded back out of the housing. The normal function of a pin puller is to retract and stay flush inside the pin puller housing. The malfunction of this pin puller did not stop the deployment of the solar array because of the mechanical redundancy of the release mechanism. The rebound of the pin outside the housing forced us to investigate our pin puller design. The result of this investigation showed that an extra shear pin hole was accidentally drilled 120° away from the original shear pin hole on the pin puller.
- Some gas molecules will leak out of the actuator assembly during the actuation and some over a period of time after the actuation because most pyrotechnic actuators have only a single Viton O-ring. If the spacecraft requires an extremely high level of cleanliness, then a hybrid sealing system must be designed for the actuator assembly. A hybrid sealing system design consists of a Viton O-ring and silicon O-ring that are located side by side in the leakage path.

Lessons Learned:

Hinges

The torque generated by the hinge assembly should be greater than the torque required to deploy the appendage in a 1-g and a 0-g environment by a minimum factor of 4.

Bearings

1. The peak contact stress should be kept below 580,000 psi for stainless steel bearings (440C steel).
2. The bearing should withstand launch loads that are estimated by multiplying the estimated weight of the rotating portion by the estimated gravity load value and by an amplification (Q) factor. Q factors have been measured as high as 25, but at the beginning of a design we usually estimate around 10. A Q factor of at least 5 should be used.
3. A 200-hr run-in test of the bearings should be done at operating speeds.

Lubrication

In order to prevent destructive chemistry, the surfaces in contact need to be passivated in some manner. Ceramic hard coatings like TiN or TiC will eliminate catalytic reaction. Conventional nitride hard coatings are also effective. In the case of ball bearings, replacing the stainless steel 440C balls with ceramic Si₃N₄ balls eliminates the breakdown. Also, to prevent oil starvation, it is always good practice to use a porous ball retainer that functions like a reservoir of oil and dilutes any breakdown products.

From past design experience in pyroactuators, we learned that the material impact strength is usually a more critical variable than the ability of the pin puller to withstand the high inertia load of a deployable system, especially if the device is required to operate in a cold environment. Material impact strength drastically drops when the temperature drops. It is recommended that when the inertia load of the deployable system is low, a more ductile material be selected over a brittle material for the actuator housing and piston. It is also recommended that for the pin puller lot acceptance test, at least one test should be to subject the pin puller to zero inertia load in the shear direction and, in a cold operating temperature, actuate the pin puller with 125% explosive power.

In addition, almost every deployment device related to spacecraft on-orbit configuration change is a mission catastrophic single-point failure if it does not function properly. The following are some ground rules from lessons learned for designing such devices:

1. All deployed appendage programs must have engineering test units.
2. All flight units and engineering test units must be testable to determine deployment margins.
3. Analyses must be verified by judicious hardware testing programs.
4. There must be adequate life testing early in the program.
5. There must be redundant backup systems in all critical areas.
6. Worst-case analyses and failure modes effects and critical analyses must be performed and verified by actual hardware testing. Conditions that must be considered include worst-case friction, misalignment, and excessive preload.
7. All devices should be designed as simple as possible to do an adequate job.
8. Consider the effects of mounting system redundancy and structure-induced input forces not only on the devices but also on the internal components of the devices.
9. Look for all possible hostile environmental effects and design to minimize their impact. Pay particular attention to vacuum, thermal control, and 0-g effects that are not always intuitive to the designer.
10. Select devices that are directly testable and reusable to be qualified by analysis rather than single-use devices that are statistically qualified to a pass/fail criterion.
11. Use the largest possible margin of operation in all devices consistent with consideration of undesirable effects on the surrounding hardware. These undesirable effects include large forces developed by end-of-travel latch-up and shock from pyrotechnic device firing.
12. Make installations such that the devices can be verified for proper installation. Knowledge of preloads, position of parts, status of switches, or other electrical interfaces should be known or testable.

Key Words:

Binary Latch Mechanisms, ISTP/Geotail Comprehensive Plasma Instrument, ISTP Polar Spacecraft

Mechanisms:

Binary Latches

Systems:

ISTP/Geotail Comprehensive Plasma Instrument, ISTP Polar Spacecraft

Authors; Experts:

Daryl Maus and Scott Tibbitts

Address:

Starsys Research Corp.
5757 Central Avenue, Suite E
Boulder, Colorado 80503

Telephone:

Title:

Resettable Binary Latch Mechanisms for use with Paraffin Linear Motors

Source:

NASA Conference Publication 3113, 25th Aerospace Mechanisms Conference (1988).

Abstract:

A new resettable binary latch mechanism has been developed utilizing a paraffin actuator as the motor. This linear actuator alternately latches between extended and retracted positions, maintaining either position with zero power consumption. The design evolution and kinematics of the latch mechanism are presented, as well as development problems and lessons that were learned.

Anomalies:

- The polyamide rail failed during initial testing. The rail end points, around which the toggle pivots fractured from unexpected high inertial loads. The toggle impacted the rail ends as it moved into the latched position and again when it rotated. Both motions and the associated impact led to a rapid brittle failure breaking the ends off the rail. More tightly controlling the toggle movement might have eliminated this failure, but it was clear that a more durable material was required for this part to ensure reliability under all conditions.
- Because limiting weight was important and because the rail experienced light loading from the toggle sliding along it, 6Al-4V titanium was initially substituted. Galling occurred within 100 cycles although contact surface loading was less than 25 psi against the stainless steel toggle. The galling produced progressively higher drag and could not be mitigated by smoother surface finishes. The titanium was therefore deemed unsuitable.
- Thermal testing revealed interference between the output shaft and its bushing at low temperatures. The bushing, fabricated from polyimide, shrank onto the output shaft at 60°C and created friction. Enlarging the bushing bore corrected the problem.

Lessons Learned:

- CDA 624 aluminum silicone bronze, CDA 655 silicon bronze, and CDA 630 aluminum nickel bronze were employed for the rails. After initial wear-in (approximately 50 cycles) the toggle was burnished from contact with the rail and neither part demonstrated significant wear during subsequent testing to 20,000 cycles. CDA 630 bronze was selected because of its resistance to corrosion and slightly better wear characteristics.
- Thermal binding must be considered, not only for high-temperature operation, but for low-temperature operation as well.
- Iteratively designing a complex mechanism using computer-aided design (CAD) and using pasteboard mock-ups can be a more efficient process than detailed mathematical analysis of component geometries:
 1. Components can be visualized throughout their range of motion
 2. Interferences can be identified and eliminated
 3. Kinematics and component shapes can be easily optimized by simultaneously seeing the effect of changes in all positions.

Description:

This final design is shown on Figure 1 and has the following characteristics:

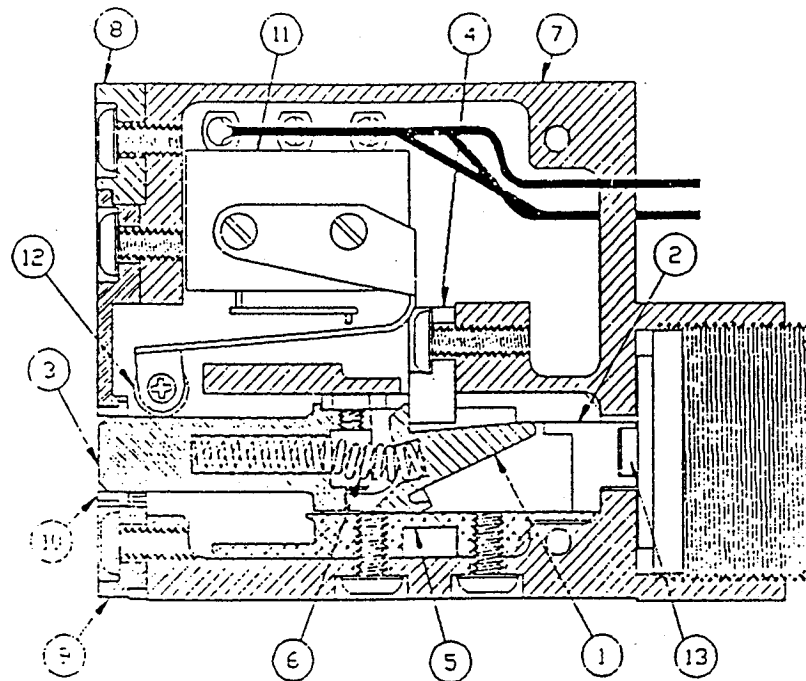
1. To patch and unlatch the mechanism, the logic element, called the toggle, moves between a series of stable positions.
2. The toggle moves through the series of positions by pivoting about different features of the toggle. These movements are created by a separate low-force spring (the toggle spring) rather than by the throughput loads.
3. The toggle does not carry loads during actuator extension or retraction. It locks up the load-carrying components when in the latched position. No motion, and, consequently, no significant wear, can occur when the toggle is loaded.
4. The shapes of the toggle and latch components are optimized to minimize overtravel. Overtravel ideally can be limited to only what is required to accommodate tolerance stack-up.
5. None of the output loads is translated to sliding surfaces during extension or retraction, eliminating significant wear points in the mechanism.

Size/Mass. Final dimensions of the single-switch version of the mechanism are $2.3 \times 4.2 \times 3.2$ cm ($0.90 \times 1.65 \times 1.25$ in.) and mass is 86 gm. Dimensions of the two-switch version are $2.5 \times 4.3 \times 4.5$ cm ($1.0 \times 1.7 \times 1.75$ in.) and mass is 100 gm.

Output Loads. During extension and retraction, output loads are carried axially from the actuator shaft to the mechanism output shaft. None of the output load is translated to normal forces on wearing or moving surfaces. Static load testing at 100 kg (220 lbf) and qualification testing at 80 kg (175 lbf) dynamic load for 15 cycles produced no wear or damage to latch components. This testing established a margin of greater than three above the nominal rated operating load of 23 kg (50 lbf).

Overtravel/Stroke. As currently configured, 0.08 cm (0.030 in.) of overtravel is required to operate the latch. An additional 0.08 cm (0.030 in.) is required to operate the limit switches. A remaining 0.152 cm (0.060 in.) of overtravel is used to ease part tolerance requirements, assembly tolerance, and to accommodate a large variation in environmental temperature. Total overtravel is 0.32 cm (0.125 in.). Overtravel was reduced to 0.19 cm (0.075 in.) by utilizing a custom switch blade and by tightly controlling tolerances.

The use of an SRC IH 5055 actuator with 1.5 cm (0.575 in.) of available stroke provided 1.1 cm (0.45 in.) of stroke between the retracted and extended latched positions, even with the more generous 0.32 cm (0.125 in.) of overtravel.



95TR4/V2

1. **Toggle.** The logic element of the mechanism. Moves inside the slide to latch the mechanism (303 stainless steel).
2. **Slide.** Carries the throughput load from the output shaft around the toggle to the actuator shaft (Envex 1115).
3. **Output Shaft.** Carries the load to the slide and to the toggle in the latched position. Houses the toggle spring (303 stainless steel).
4. **Reset Plate.** Resets toggle to its initial position (Envex 1115).
5. **Rail.** End of the rail captures the toggle forcing it to pivot into the latched position. The toggle slides on the rail (630 bronze).
6. **Toggle Spring.** Applies an axial off-center load to the toggle that forces the toggle to pivot through various overcenter positions (18-8 stainless).
7. **Housing.** Houses components and mounts to spacecraft. Actuator mounts to housing (6061-T6 aluminum).
8. **Cover.** Encloses components after assembly and restrains bushing (6061-T6 aluminum).
9. **End Cap.** Captures bushing and supports output shaft. Allows visual access to components (6061-T6 aluminum).
10. **Bushing.** Guides the output shaft (Envex 1115).
11. **Limit Switch.** Signals actuator extension (Honeywell 9HM1).
12. **Switch Blade and Roller Assembly.** Interfaces with slide to actuate the limit switch (Microswitch JS-151).
13. **Actuator Output Shaft.** Output of paraffin motor (Nitronic 60).

Figure 1. Final Design

Testing:

As initially configured, all sliding surfaces in the mechanism were metal on molydisulfide-impregnated polyamide (Vespel and Envex are trade names for Mil-Spec versions of this material). This required the slide, rail, and bushing to be made of polyamide. Fabricating these parts required developing machining expertise because of the brittleness of the material and its tendency to chip and split when in shear. Carbide tools, backing up edges, high tool speeds, and high feed rates were necessary for fabricating the complex shapes required.

Repeated latch operation at 80 kg (150 lbf), greater than three times normal load, was performed. The mechanism functioned smoothly with no deformation or excessive component wear, confirming satisfactory strength margins for the latch and load-carrying components.

Standard mounting of the Honeywell Microswitch 9HM1 switch and its associated roller blade uses only the clamping friction created by torquing the switch mounting screws to 1728 gm-cm (1.5 in.-lb) to secure the blade in position. Because one of the mechanisms designed required stacking two 9HM1 switches on top of each other, there was a concern that the blades and, therefore, the switch actuation point might shift from vibration. The mounting security was improved by assembling the switches with urethane between all the parts, effectively bonding the assembly.

The mechanism was subjected to vibration testing at 20-, 30-, and 50-g rms. There was no change in mechanism function and the latch stayed in position during vibration. The Honeywell 9HM1 limit switch point of operation shifted by 0.025 cm (0.010 in.) after 20-g vibration. This shift was due to changes in the internal components of the switch and was expected. Mechanism tolerance was sufficient to accommodate this shift and no further shifts were noted at the 30-g and 50-g vibration levels.

Experience:

Initial material selections failed because of shock-loading-induced fracture of brittle polyamide molydisulfide-impregnated parts and galling of titanium parts. Redesigned mechanism using 303 stainless steel and CDA 630 aluminum nickel bronze was successfully tested for 20,000 cycles.

Key Words:

Latches, Latching Mechanisms, Modular Assembly, Coupling

Mechanisms:

Latching Mechanisms

Systems:

Latching System

Authors; Experts:

William McCown and Neal Bennett

Address:

Rexnord Aerospace Mechanisms
Torrance, California

Telephone:

Title:

Structural Latches for Modular Assembly of Spacecraft and Space Mechanisms

Source:

22nd Aerospace Mechanisms Symposium (1988).

Abstract:

Assembling spacecraft systems from modular sections has changed the role of structural latching systems. Docking methods involve controlled berthing techniques using end effector and robotic arm systems. Latches are now required to operate reliably for many connect/disconnect cycles and multiyear lifespans. This paper discusses procedures for selecting latching systems, and outlines a judgement criteria system that can be used to select the best designs. As an example, the authors use the latch selection for the NASA flat-plate interface prototype. This is an integrated modular connector designed to transfer thermal energy, electrical power, and signal data between two structures with very flat mating surfaces.

PRECEDING PAGE BLANK NOT FILMED

Anomalies:

The use of a slip clutch to set preload gave large differences when operating in air or vacuum.

Lessons Learned:

- Coefficients of friction can be quite different in air and vacuum.
- Load control is a particular problem with hook systems where the load is usually preset by rigging. Load changes due to thermal or dynamic fluctuations cannot be compensated.
- The selection methodology described in the paper is an excellent guideline to designers.
- For roller screw latches, thread engagement is improved by providing lead-ins.
- Rolling element latch interfaces reduce particle generation. The addition of Teflon wiper seals control loose particles in the roller screw latch and receptacle nut.
- A run-in and cleanup procedure reduces particle generation from initial actuations.
- The only reliable method to control the roller screw latch preload was to limit motor power.

Description:

Assembling spacecraft systems from modular sections has changed the role of structural latching systems. Docking methods involve controlled berthing techniques using end effector and robotic arm systems. Latches are now required to operate reliably for many connect/disconnect cycles and multiyear lifespans. This paper discusses procedures for selecting latching systems, and outlines a judgement criteria system that can be used to select the best designs. Most spacecraft latch systems in use today are based on actuated hooks or threaded fasteners. Both systems rely on the interlocking of piece parts to retain an object, but differ in their axis and type of movement. The primary advantages of hook systems are rapid actuation and high misalignment tolerance. The major disadvantage is that length and preload are relatively fixed. Threaded fastener systems are variable in preload and length, but require finer alignment and are slower in actuation. Berthing technology has reduced the necessity for rapid actuation because closing velocities are low and alignment is more controllable. Fastening systems with reach and alignment flexibility are being developed for connector and standard interface systems where close prelatch orientation is available.

Load control is a particular problem with hook systems where the load is usually preset by rigging. Load changes due to thermal or dynamic fluctuations cannot be compensated. Fasteners usually control load through their drive systems by either power control, active feedback through a sensor system, positional sensing, or mechanical control such as a clutch system.

Latch selection can consist of seven phases:

1. Definition of functional latch requirements
2. Proposal of candidate techniques
3. Establishment of weighted judgement criteria
4. Selection of final candidates per weighted criteria
5. Formalization of functional latch requirements
6. Optimization of final candidates to functional requirements
7. Selection of final latch system per weighted criteria.

The authors use, as an example, the latch selection for the NASA flat-plate interface prototype. This is an integrated modular connector designed to transfer thermal energy, electrical power, and signal data between two structures with very flat mating surfaces. High preload generation, reliability, life, and low contamination are mandatory. Candidate latching concepts included a powered pawl latch, a roller screw structural latch, a powered claw latch, and a powered nut/bolt latch system. Functional requirements for the latch are shown in Table 1.

Table 1. Functional Requirements for the Flat-Plate Interface Prototype Latch

Structural preload	≥3,600 kg (8,000 lb)
Ultimate load	≥6,800 kg (15,000 lb)
Take-Up load	≥225 kg (500 lb)
Preload adjustable Up to	4,550 kg (10,000 lb)
Actuation time	<100 sec
Lateral, longitudinal misalignment	≤3 mm (0.125 in.)
Angular misalignment	≤2°
Mass	<20 kg (40 lb)
Life	>1,000 cycles over 10 yr
Power	TBD at 28 V dc
Negligible particulate and gaseous contamination	
Simple operation, extra vehicular activity compatible	
Full retractability into interface, damage-resistant design	
Full accommodation to the TRW load distribution and flat-plate system	

95TR4/V2

The latches were evaluated against weighted judgement criteria as shown in Table 2.

From a design standpoint, the roller screw latch was chosen as the best candidate. Figures 1 through 5 show the assembly and details of the drive. The latch is powered by a brushless dc motor acting through a worm drive system that is torque limited by a slip clutch. The drive system advances the screw and tightens it to a predetermined load. Then, the motor direction is reversed to retract the roller screw back into its housing.

Possible modes of failure were considered. These included:

- Thread engagement (possibility of misalignment)
- Roller screw latch preload control
- Slip clutch operation
- Contamination control.

Table 2. Weighted Judgement Criteria

Item	Criteria	Weight Factor (1-10)	Fixed Acme		Powered Nut/Bolt		Roller Screw		Powered Pawl	
			Value	Score	Value	Score	Value	Score	Value	Score
1	Cost	8	4	32	5	40	3	24	5	40
2	Simplicity	5	4	20	4	20	3	15	4	20
3	Function	9	7	63	6	54	9	81	8	72
4	Mass	4	5	20	6	24	3	12	5	20
5	Power	4	5	20	5	20	7	28	6	24
6	Load	9	7	63	8	72	9	81	8	72
7	Envelope	7	4	28	7	49	5	35	5	35
8	Reliability/life	9	5	45	4	36	9	81	8	72
9	Service/maintenance	5	5	25	4	20	7	35	8	40
10	Environment compatible	9	5	45	4	36	8	72	7	63
11	Safety	5	4	20	5	25	6	30	5	25
12	Design flexibility	4	4	16	6	24	8	32	7	28
13	Design maturity	2	5	10	6	12	4	8	8	16
14	Operation simplicity	7	7	49	8	56	9	63	7	49
15	Electronics complexity	5	5	25	6	30	6	30	5	25
16	Schedule	6	5	30	5	30	5	30	6	36
17	Miscellaneous factors	7	7	49	7	49	7	49	4	28
18	Control	7	5	35	5	35	7	49	6	42
Totals		—	—	595	—	632	—	755	—	707

95TR4/V2

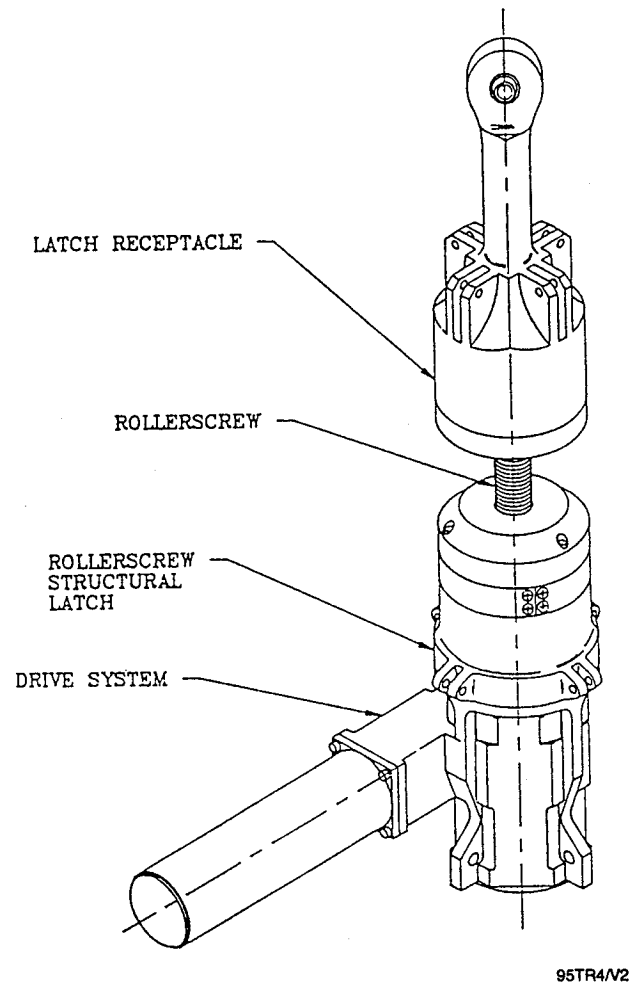


Figure 1. Roller Screw Structural Latch System

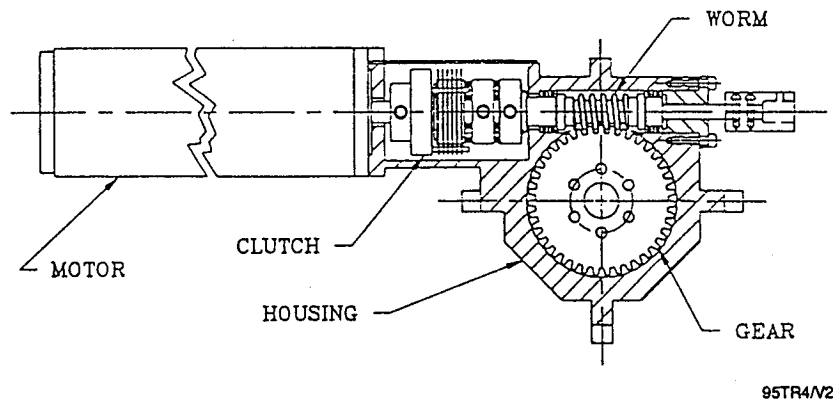


Figure 2. Roller Screw Drive System

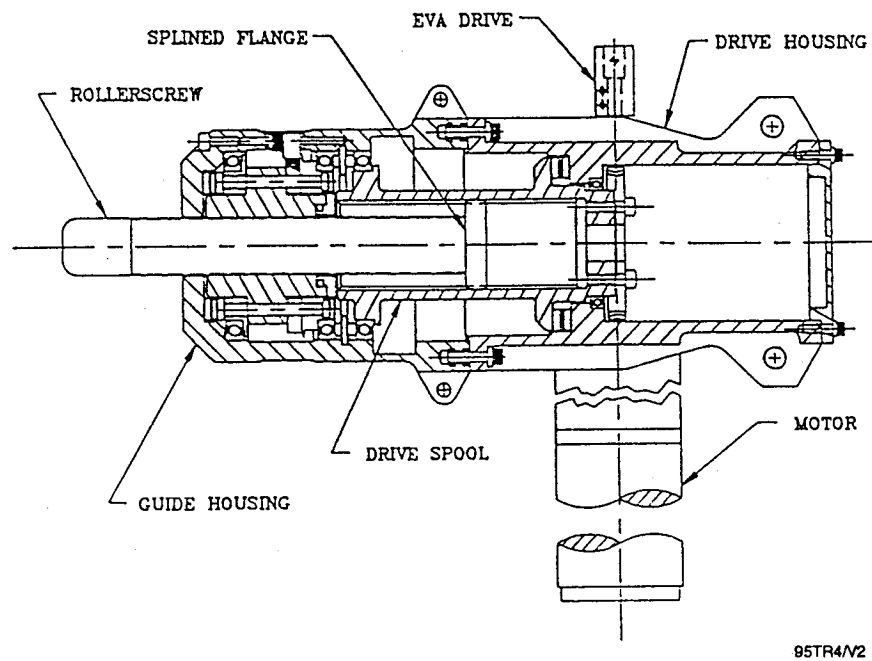
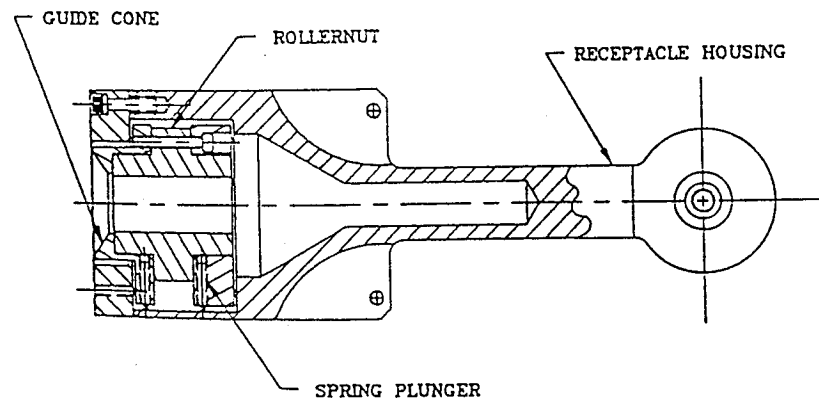
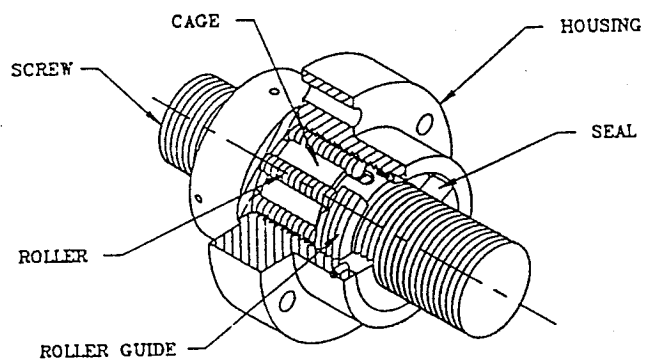


Figure 3. Roller Screw Latch Assembly



95TR4/V2

Figure 4. Receptacle Assembly



95TR4/V2

Figure 5. Recirculating Roller Screw Nut

The following steps were taken to resolve these problems:

- Thread engagement was improved by providing lead-ins.
- The gear stiffness was found to be marginal and was improved by a number of changes such as increased shaft size, revised housing design, and mounting with preloaded bearing sets.
- The gear and worm will both be lubricated with WS₂ and Braycote 601 grease.
- Preload control was supposed to be a single-stage actuation where the drive system would be powered to a stall, but variables in the drive system would have varied preload levels beyond acceptable limits. It will now be done by a two-stage actuation with motor power set by current limiting devices.
- The slip clutch was intended to control the roller screw latch preload, but the wide difference in friction between air and vacuum operation precluded this approach. The function of the clutch was downgraded to an overload protection role.
- A number of techniques were used to minimize contamination. Rolling element latch interfaces were selected, in part, to reduce particle generation. In addition, Teflon wiper seals were added to control any loose particles in the roller screw latch and receptacle nut. A run-in and clean-up procedure reduces particle generation from initial actuations.

Key Words:

Pin Puller, Pyrotechnics, Solar Array

Mechanisms:

Pin Puller, Solar Array

Systems:

Deployment Systems

Authors; Experts:

M. Phan

Address:

NASA-Goddard Space Flight Center
Mail Code 731
Greenbelt, Maryland 20771

Telephone:**Title:**

Spacecraft Deployable Appendages

Source:

Goddard Space Flight Center (1992)
Engineering Directorate

Abstract:

This report is a compendium of satellite experience and mechanism design practices compiled by the engineering staff at NASA-Goddard.

Anomalies:

During one of the solar array deployment tests in 1989, a pin puller in a release mechanism was actuated; the pin was retracted inside its housing to release the solar array, but then rebounded back out of the housing. The normal function of a pin puller is to retract and stay flush inside the pin puller housing. The malfunction of this pin puller did not stop the deployment of the solar array because of mechanical redundancy of the release mechanism. Subsequent investigation showed that an extra shear pin hole was accidentally drilled 120° away from the original shear pin hole.

Lessons Learned:

- Material impact strength is usually a more critical variable than inertia load capability, for pyrotechnic devices, especially when the temperature drops. When the inertia load of a deployable system is low, a ductile material should be selected as opposed to a brittle material for the actuator housing and piston.
- For a pin puller lot acceptance test, at least one puller should be exposed to 125% explosive power in a cold environment.
- If the spacecraft requires a high level of cleanliness, then multiple pyrotechnic seals must be used to prevent gas leakage. A hybrid sealing system consists of a Viton O-ring and silicon O-ring in tandem.

Key Words:

Cover, Ejection

Mechanisms:

Ejection Mechanism

Systems:

Ejection System

Authors; Experts:

P.W. Schaper

Address:

Jet Propulsion Laboratory/California Institute of Technology
4800 Oak Grove Drive
Pasadena, California 91109-8099

Telephone:

(818) 354-2140

Title:

Galileo Near-Infrared Mapping Spectrometer Cooler Cover Ejection Anomaly

Source:

JPL Lessons Learned Reports Nos. 736, 737, 738, and 739.

Abstract:

At launch, the near-infrared mapping spectrometer of the Galileo spacecraft had two covers in place to protect the instrument from contamination. Two and a half months after launch, initial attempts to eject the covers were unsuccessful. It was subsequently determined that this was due to differential expansion caused by the shield heater being energized. The shield heater was turned off, the covers allowed to cool, and then they were successfully ejected.

Anomalies:

Two and a half months after launch, initial attempts to eject the covers from the near-infrared mapping spectrometer of the Galileo spacecraft were unsuccessful.

Lessons Learned:

- Untested flight sequences frequently result in unexpected events. All primary and backup spacecraft flight configurations should be tested or analyzed before launch, including the most probable failure mode configurations.
- Incomplete reviews of mission operations flight rules can cause problems. Subsystem constraints that impose system constraints should be evaluated at system design reviews for their system impacts and their possible elimination.
- The flight rules generation cycle should be initiated early in the mission operations design, and emphasis should be placed on their review, including additions or revisions thereto, by all essential personnel such as design and cognizant engineers.
- Reviews of critical spacecraft operations should be initiated early in the design cycle and should include design specialists. For long duration missions, re-review before initiation of critical operations is highly desirable.

Description:

At launch, the near-infrared mapping spectrometer of the Galileo spacecraft had two covers in place to protect the instrument from contamination. Two and a half months after launch, when contamination was deemed to be negligible, an attempt to eject the covers was unsuccessful. The cooler cover failed to eject, as determined by not receiving expected temperature changes. Analysis of the data revealed that the temperature of the cooler shield was 38°C, due to the shield heater being energized. This resulted in a temperature differential between the cover and the shield that caused a mechanical distortion sufficient to prevent the cover from ejecting. All ejection tests before launch were conducted with the shield heater unenergized, which was the original in-flight plan. Because of a concern for contamination caused by spacecraft outgassing, a flight rule was modified prior to launch requiring the shield heater to be energized ejection. The flight rule was in error by not requiring the shield heater to be off some time prior to cover ejection. The shield heater was commanded off and 22 min later the cooler cover ejected properly, as shown by the instrument temperature telemetry. Had the cooler cover not ejected, the near infrared mapping spectrometer experiment would have been considered a failure.

Key Words:

Pip Pins

Mechanisms:

Connectors

Systems:

Various

Authors; Experts:

Lane P. Skyles

Address:

Lockheed Engineering & Sciences Company
Houston, Texas

Telephone:

Title:

Pip Pin Reliability and Design

Source:

Proceedings of the 28th Aerospace Mechanism Symposium, NASA Conference Publication 3260.

Abstract:

Pip pins are used in many engineering applications. Of particular interest to the aerospace industry is their use in various mechanism designs. Many payloads that fly aboard our nation's space shuttle have at least one actuated mechanism. Often these mechanisms incorporate pip pins in their design in order to fasten interfacing parts of joints. Pip pins are most often used when an astronaut will have direct interface with the mechanism. This interfacing can be done during space shuttle mission extra vehicular activities. The main reason for incorporating pip pins is convenience and their ability to provide quick release of interfacing parts. However, there are some issues that must be taken into account when

using them in a design. These issues include documented failures and quality control problems when using substandard pip pins. A history of pip pins as they relate to the aerospace industry as well as general reliable design features are discussed.

Anomalies:

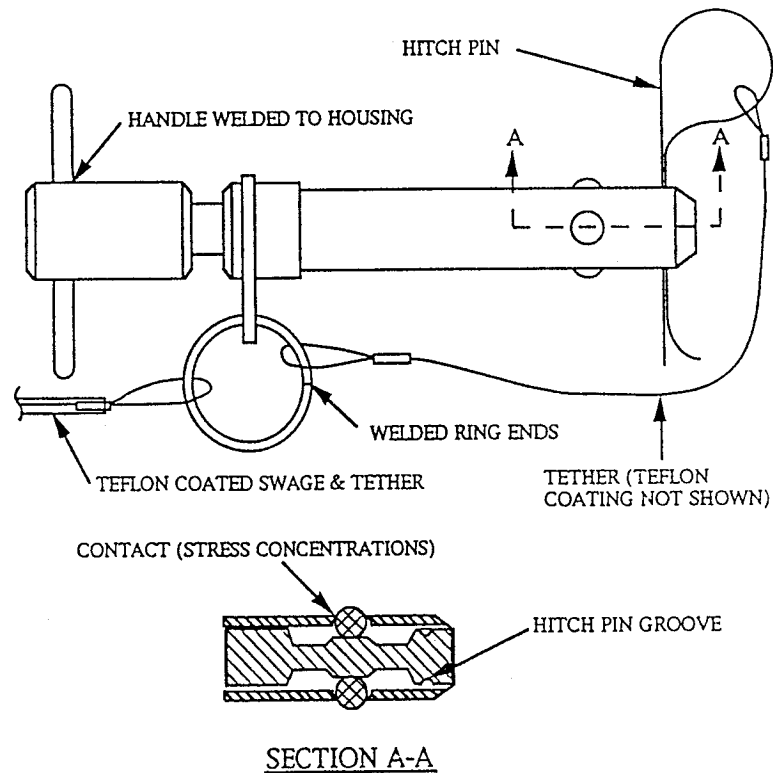
- Locking balls can vibrate out of their sockets.
- Swaged tethers could create a tear hazard to an astronaut's pressure suit.
- Dowel pins for handle attachments could loosen from vibration or thermal effects.
- Liquid lubricants or grease could freeze and cause seizure of the pins.

Lessons Learned:

- Install four balls rather than two to provide sufficient redundancy if one of the balls falls out of its socket.
- Weld handles to the pin and avoid dowel pin loosening from vibration and thermal effects.
- Provide double-acting pins that allow release capability when the handle is either pushed or pulled because they facilitate operation.
- A Teflon sleeve should cover the tether swag fitting and cable termination, providing a smooth surface and preventing the possibility of astronauts contacting frayed or broken cable strands.
- Tether rings should be solid or have welded ends. Split rings can allow disconnect and are also a tear hazard.
- Dry film lubricants should be used to lubricate all internal parts of the pip pin.
- Hitch pins are recommended where the pip pin only has to be removed and not reinstalled.
- Further development of ball retention is required. The present method is by staking which is subject to error. Inspections have shown that incomplete staking would allow the balls to fall out. Also, the staked material is relatively thin and stress concentrations can be created at the tip of the staked material. Vibrations can cause fracture and subsequent failure by ball loss.

Description:

Figure 1 shows a schematic of a pip pin with the improvements noted under Lessons Learned.



95TR4/V2

Figure 1. T-Handle, Double-Acting Pip Pin

Testing:

During 1994, NASA began environmental testing of the extra vehicular activity development flight experiments payload. During vibration testing, several locking balls in the pip pins vibrated out of their sockets. In addition, the lubricant inside of the pins froze and seized the pins during cold-temperature vacuum testing. The design improvements discussed under Lessons Learned and depicted on Figure 1 were prompted by the extra vehicular activity development flight experiment test results.

Key Words:

Paraffin Actuator, Pin Puller

Mechanisms:

Linear Actuator, Pin Puller

Systems:

Linear Motion Systems

Authors; Experts:

Scott Tibbitts

Address:

Maus Technologies
Boulder, Colorado

Telephone:**Title:**

High-Output Paraffin Actuators: Utilization in Aerospace Mechanisms

Source:

22nd Aerospace Mechanisms Symposium (1988).

Abstract:

This paper describes the development of a high-output paraffin linear actuator for use on spacecraft. These types of actuators work on the principle that when paraffin melts, its volume expands approximately 15%, and this expansion can be used to do useful work, for example, push out a cylinder. Actuators of this type are being used in many commercial applications and have been employed on spacecraft such as the Voyager. The goal of this present development was to produce an actuator with characteristics that were specifically designed for space.

Anomalies:

It is not clear if the actuator rod slides through the stationary actuator plug. If it does, then the composition and finish of the actuator plug and the hardness and surface finish of the rod will be very important in determining life.

Lessons Learned:

- The high-output paraffin actuator provides an alternative device to the mechanism designer requiring significant mechanical work from a small, compact, reliable component. The work can be generated from heat provided by internal electrical resistance elements or from environmental temperature changes.
- In the internally heated configuration, the advantages over conventional electrically powered actuators can be significant: low weight, resetability, full verification before flight, high force, long stroke, gentle stroke, and flexibility in materials of construction.

Description:

The high-output paraffin aerospace actuator design requirements are:

- All external components qualifiable to outgassing requirements
- Qualifiable to vibration and acoustic requirements
- Internally heated to provide faster response times, efficient heating, and allowing flexibility in case material selection (thermal conductivity) not a requirement
- Operating range: -70 to +65°C
- Redundant, space qualifiable heating element
- Flexible design allowing custom fabrication for specific requirements:
 - Fabrication from a wide variety of materials including titanium or stainless steel
 - Fabrication from nongamma emitting or nonmagnetic materials
 - Fabricated with a wide range of custom paraffin formulations.

The result of the development program was the internally heated high-output paraffin actuator. Characteristics of the actuator are:

- Useful stroke: maximum nominal stroke is 10 cm
- Output force: maximum nominal output force is 4000 N (900 lb)
- Actuation temperature (temperature at which motion begins): can be varied from -20 to +120°C by selection of paraffin type
- Actuation temperature range (temperature rise necessary for full extension after start of motion): can be varied from 5 to 60°C by selection of paraffin
- Response time (power on to full stroke): 15 sec to 20 min; dependent on power input, amount of thermal isolation, and initial actuator temperature
- Stroke time (extension begins to full stroke): 5 sec to 4 min; dependent on power input

- Efficiency (mechanical power out/electrical power in): approximately 5% once the actuation temperature has been reached
- Actuator size: proportional to stroke times force
- Actuator weight: proportional to stroke times force
- Cycle life: >10,000 cycles at rated stroke distance and force.

A sketch of a typical internally heated high-output actuator is shown in Figure 1.

The actuator is sealed by a redundant O-ring type seal. The squeeze boot is fabricated with an integral O-ring which seals between the actuator body and the actuator plug. This is backed up with a standard Viton O-ring/backup ring seal. This arrangement provides sealing for internal pressures in excess of 48,000 kPa (7,000 psi). Both the O-ring and the urethane boot meet or exceed outgassing requirements according to ASTM E-595-77 (<1% total weight loss, <0.1% recondensable weight loss at 125°C, 10^{-6} torr).

The actuator body is typically fabricated from either 303 stainless steel or titanium. However, it can be fabricated from any material that will provide the necessary strength to withstand the internal hydrostatic pressure. It is preferable to fabricate the case from relatively low thermal conductivity materials such as stainless steel or titanium to reduce heat loss. These materials also have low electrical conductivity, which minimizes Thompson effect currents in the case of magnetically sensitive applications.

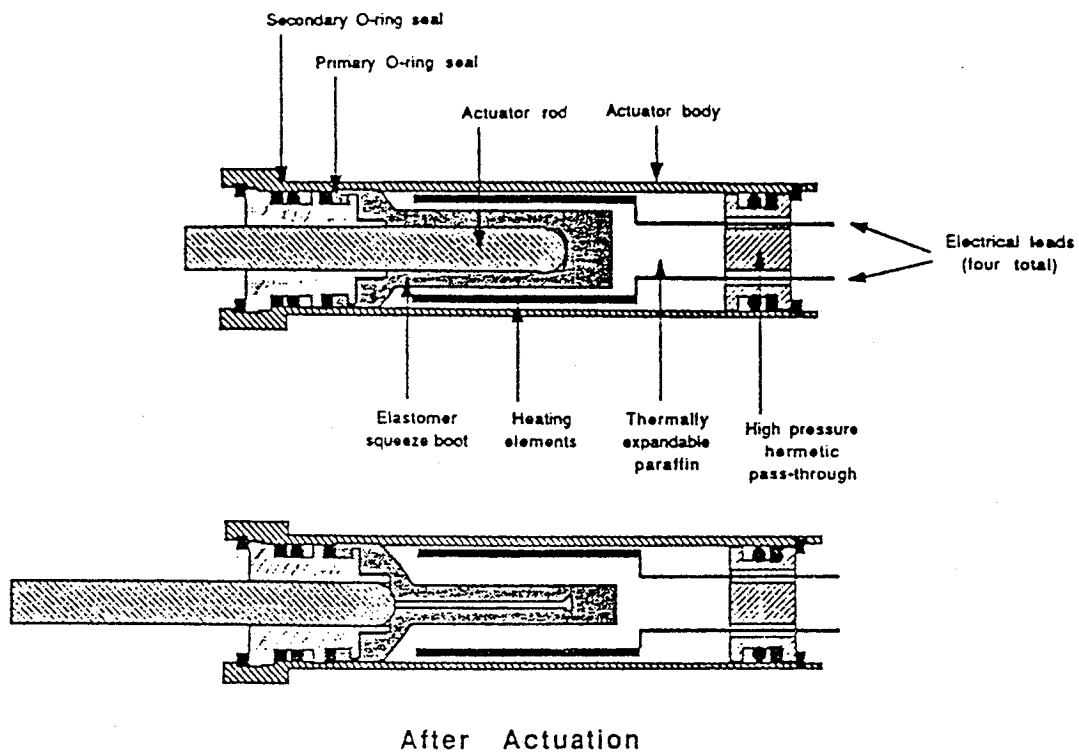
The actuator is filled with a mixture of copper particles and purified paraffin. The copper is an optional component that increases heat transfer rates in the wax, providing even melting in the actuator. The paraffin is a single or multicomponent formulation depending on the application.

The key component in the actuator is the elastomer squeeze boot/seal. A castable two-part polyurethane was chosen as the elastomer for the following reasons:

- Thermoset polyurethanes provide superior outgassing performance (correct stoichiometry produces a single molecule component)
- Superior toughness/flexibility
- Tooling is easily modified for different actuator configurations.

Alternatively, compression-molded Viton B is used for higher service temperatures.

The first aerospace mechanism to utilize high-output paraffin actuators will be a gimbal caging device being designed by Aeroflex Labs for a satellite that was launched in 1988.



95TR4/V2

Figure 1. Cross Section of Internally Heated High-Output Paraffin Actuator

Bearings, Lubrication, and Tribology Considerations

Key Words:

Lubrication

Mechanisms:

Surfaces of Relative Motion

Systems:

General Spacecraft

Authors; Experts:

E. Divine

Address:

NASA-Goddard Space Flight Center
Greenbelt, Maryland 20771

Telephone:

Title:

Deployed Appendage Design Philosophy

Source:

Goddard Space Flight Center (1992)
Engineering Directorate

Abstract:

This report discusses general lubrication practices.

Anomalies:

- Seizures of relative motion surfaces caused by excessive friction.
- Vibration-induced fretting and adhesion due to excessive clearance in caging devices.
- Unlubricated surfaces exceeding bearing yield strength of substrate on hard-coated materials.
- Seizures caused by dissimilar materials with high mutual solid solubility.

Lessons Learned:

- Maximum utilization of rolling surfaces as opposed to sliding motion should be employed.
- Lubrication or separation of all moving surfaces either by suitable aerospace grease or dry lubricant coating should be used. No exceptions are allowed, even for lightly loaded friction-compatible surfaces.
- On hard mating surfaces where hard coatings are used (such as Type III anodizing on aluminum), loads must be kept below the bearing yield strength of the substrate material (e.g., 60 ksi for 6061-T6 aluminum).
- Smooth and polished surfaces are preferred.
- Dissimilar material mating surfaces should have low mutual solid solubility, or at least one of the two should have a heavy dissimilar coating (e.g., nitride, carbide, or oxide).
- Caging devices should be designed to positively preclude relative motion between clamped surfaces when subjected to shipment or launch vibration.
- Wet lubrication is generally preferred because friction is low and predictable. The grease with the most heritage is the Bray 600 series, which is synthetic fluorinated and oil thickened with micron-size Teflon powder. The grease has extremely low outgassing (TML <0.1% and CVCM <0.05% for the standard 125°C 24-hr test) and concerns relative to contamination are negligible for virtually all spacecraft applications. The wet lube usable temperature range is -80 to 200°C.
- For extreme low temperatures and cryogenic applications, solid lubricants are preferred. Epoxy and polyamide-bonded films can be successfully employed with proper application and burnishing to remove excess material.

Key Words:

Solar Array Drives, Deployment Mechanisms, Hinges, Lubrication, Bearings

Mechanisms:

Solar Array Drive Mechanisms

Systems:

Deployment Systems

Authors; Experts:

L. Fehrenbacher

Address:

Technology Assessment and Transfer, Inc.
Annapolis, Maryland

Telephone:**Title:**

Deployment Mechanisms Technology

Source:

Contract No. F33615-89-C-5609, Task No. 24 (1992).

Abstract:

Future United States Air Force and Strategic Defense Initiative Organization (SDIO) space system deployment requirements present substantial tribological challenges. Whereas most deployments on existing systems have been relatively simple (i.e., 1-D, sequential), many of the contemplated designs involve multiaxis synchronous deployment, large solar arrays or antennas and instrument platforms, and complex directly deployable antennas. Many deployable solar arrays, antennas, and instruments will also be required to quickly retract and stow for maneuverability and survivability. Finally, several deployable systems must reliably deploy, function, and retract on demand after long periods of inactivity. This report discusses various problems with deployable systems as related to tribological considerations. Also presented is a discussion of future technologies needed to meet performance requirements.

Anomalies:

- Table 1 summarizes the technology shortfalls currently affecting Air Force and SDIO mission requirements for deployable components, together with suggested tribomaterials (or design) solutions to overcome these shortfalls.
- Based upon a detailed study of the performance records of almost 400 satellites between 1958 and 1983, it was established that about 10% of the successfully launched satellites had some type of deployment anomaly, the majority of which were mechanical.
- Examining three of the reported anomalies will be instructive. The first of these occurred on Apollo 15, on which the spectrometer boom failed to retract completely 5 of the 12 times that it was commanded to do so. The second anomaly was the failure of the latch mechanism on the INTELSAT V maritime communication system antenna. The third anomaly was the failure of the solar array to deploy on the Earth radiation budget satellite (ERBS). When these failures were analyzed, all were attributed to thermal problem or thermal gradient problems that reduced clearances or caused lubricants to fail.

A similarly instructive anomaly occurred in the 1970s during the development of the European solar science satellite HELIOS. This satellite used a despin drive assembly to point a parabolic antenna continuously toward the sun during its entire high elliptical orbit. The despin drive assembly was designed for operation between -50 and +60°C, with a maximum drag torque of 5 oz-in. A qualification model appeared to satisfy the

Table 1. Tribomaterials for Deployment Mechanisms

Mechanisms	Mission Requirement	Technology Shortfall	Tribomaterials/ Mechanisms Solution
Solar Array Drive	<ul style="list-style-type: none"> • Reversible fast, stow, and deploy (10-sec retraction) • 360° continuous rotation (0.3 to 15°/sec) • 10- to 15-yr life, high torque with very small ripple 	<ul style="list-style-type: none"> • Reduced torque and torque noise • Lightweight (reduced size) bearings/gears • Long-life lubrication (thermal gradients, decontamination) 	<ul style="list-style-type: none"> • Solid lubricant (wear-resistant) films • Traction drives with controlled friction solid-lubricant coatings
Antennas and Sensor Platforms	<ul style="list-style-type: none"> • Synchronous and sequential deployment • Pointing accuracy while retracting • Consistent friction over 10- to 15-yr life 	<ul style="list-style-type: none"> • Lubricant life and survivability (thermal gradients, decontamination, laser irradiation) • Low friction, friction noise, and jitter • Reliability under quick transition from stowed to deployed 	<ul style="list-style-type: none"> • Synthetic hydrocarbons (low vapor pressure and additives) • Solid-lubricant films (low friction and wear) • New polymeric retainers for ball bearings
Release Mechanisms	<ul style="list-style-type: none"> • Launch load protection • Operational performance 	<ul style="list-style-type: none"> • Shape memory alloy fatigue/reliability 	<ul style="list-style-type: none"> • Solid-lubricated mechanical release mechanisms

95TR4/V2

torque requirement, but during acceptance testing of the flight model, a torque of 20 oz-in. was observed at -50°C. After three months of testing, this problem was solved through extensive redesign of the bearing mounts, shaft, end plate, and rings. While the end result was a successful despin drive assembly that flew for more than a decade, the reason for the original bearing torque anomaly was never established.

- A very recent problem observed with the Hubble space telescope further underscores the importance of tribological mechanisms for deployable subsystems. The booms used to deploy the solar arrays (illustrated in Figure 1) have been observed to bend in response to an 82°F variation in temperature that occurs within a period of 57 sec. This rate of boom motion is much more rapid than predicted by the dynamic models used to design the system. The result is a jitter that prevents the telescope from providing the precision pointing that was necessary to its mission. It has not yet been established whether this jitter is caused by the spring-loaded drum that deploys the solar panels or by the spreader bars that support the panels between the boom sections.

Lessons Learned:

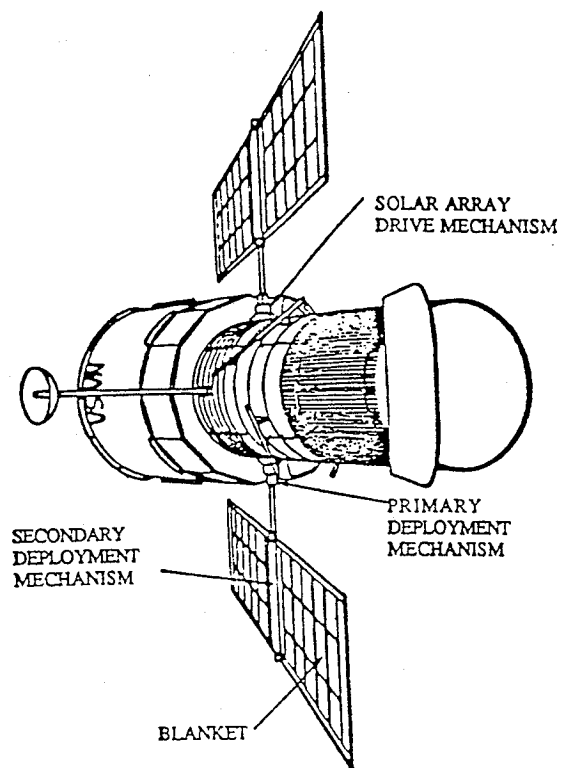
- It was demonstrated on a test of a spacecraft oscillating scanner that a polyalpholefin (PAO) oil provided excellent lubrication, consistent torque with negligible torque noise, and good wear to 22,000 hr with the test still running. The other oils, chloroarylalkylsiloxane (CAS) and perfluoropolyalkylether (PFPE), both exhibited reduction in torque (loss of preload) and increase in torque noise, as well as extensive wear, after a few thousand hours.
- The best options for solid-lubricant films for space applications appear at present to be ion-plated lead and ion-sputter deposition of, and/or ion-assisted deposited, molybdenum disulfide (MoS_2). These lamellar films have demonstrated very low friction operation in sliding and/or high low-load rolling bearings and latch and release mechanisms. They are under development for a variety of ball bearing applications. For example, in a recent study of solid lubricants for satellite gears, lead films were found to provide good lubrication after a breaking-in period that produced a 100 Angstrom elastic film. Best results were obtained for a film thickness of 1 micron. Solid films of MoS_2 and TiN in the same application resulted in unacceptably short gear lives, demonstrating that tribomaterials must be tailored to the system design. MoS_2 has, in fact, been shown to be an excellent lubricant for many space applications, although its reaction with atomic oxygen requires further study. Recent sputtered-deposited films have shown a 10 to 100% increase in film life over previous MoS_2 -coated bearings.
- Both titanium and titanium nitride have been demonstrated to be effective wear coatings under appropriate conditions. Titanium carbide has been applied to gyroscope ball bearings, and has increased operational lifetime by an order of magnitude in this application when used with an uncoated steel raceway and superrefined mineral oil. Titanium nitride has to date been used only on tool steels, but the Aerospace Corporation is currently testing both gimbal and spin bearings with titanium-carbide and titanium-nitride-coated balls.

- The development of new polymeric bearing retainer materials is a critical need to achieve required bearing lifetime. The phenolic materials that are commonly used have been demonstrated to absorb oil in a time-dependent and nonreproducible manner. These retainer materials are unacceptable for the missions under consideration unless an active lubricant supply system is used.

Description:

Hinge: Solar Array. The hinge on the Hubble solar array primary deployment mechanism was designed to a particular exacting specification (Figure 1). The deploy and stow rates were less than 1°/sec, with full deploy or stow in less than 20 min, and with a 5-yr capability of inactive deployment in space followed by correct response to restow commands. The final deployment mechanism used titanium-carbide-coated tungsten carbide balls with lead-bronze cages in place of the usual phenolic cages. The most difficult problem that had to be designed around was the thermal mismatch between the steel bearing race and the aluminum assemblies into which they were placed. The aluminum alloy gears within the primary deployment mechanism were coated by the E-metal electrolytic process, and required no additional lubrication.

Hinge: Antenna. The limited-angle hinge mechanism used for two antennas and an aperture door of the Hubble space telescope has several interesting features. This mechanism was designed to survive five shuttle launches, four returns to Earth, and eight in-orbit docking operations with appendages stowed and locked to close the aperture door within 1 min. It is a rotary drive mechanism using a dc stepper motor with a 200:1 harmonic drive speed reducer. Actuation is achieved through a torsion rod and two torsion tubes. Damping during the movement of the mechanism and at its stops is provided by a polymeric composite lubricant, Delrin AF.



95TR4/V2

Figure 1. Hubble Solar Array Deployment and Drive Mechanism

Key Words:

Lubricants, Slip Rings, Gimbals, Solid Lubrication

Mechanisms:

Slip Rings, Gimbals

Systems:

Solar Array Drives

Authors; Experts:

M.D. Hilton and P.D. Fleischauer

Address:

The Aerospace Corporation
M2/271, P.O. Box 92957
Los Angeles, California 90009-2957

Telephone:

Title:

Application of Solid-Lubricant Films in Spacecraft

Source:

Surface and Coatings Technology, 54/55 pp. 435-441 (1992).

Abstract:

Solid-lubricant films are used in a variety of mechanisms on various spacecraft and launch vehicles. Relative to liquid lubricants, solid lubricants generally have lower vapor pressures, better boundary lubrication properties and relative insensitivity to radiation effects, and operate in wider temperature ranges. This paper reviews the use of solid (dry) lubricants, particularly solid-lubricant thin films, in such space systems. Future opportunities for insertion of solid lubricants as replacements for liquids or greases are identified.

PAGE 76 INTENTIONALLY BLANK

PRECEDING PAGE BLANK NOT FORMED

Anomalies:

Excessive torque in deployment mechanisms.

Lessons Learned:

- Lead coating has had good success as a solid lubricant, in vacuum applications.
- Optimum performance of lead and other metals is achieved at approximately 1 micron thickness.
- Deposition of soft metals (Pb, Au, Ag, In) by ion plating provides excellent adhesion. These films have been particularly effective in spacecraft bearings found in solar array drive mechanism in European satellites and on the Hubble space telescope.
- A particular disadvantage of lead is that it oxidizes rapidly and must be stored in vacuum-dry environments.
- Gold and silver are used in situations requiring electrical conductivity.
- Sputter-deposited molybdenum disulfide (MoS_2) has a lower coefficient of friction than ion-plated Pb (0.01 versus 0.1), which means that MoS_2 -coated components should develop less torque. Figure 1 displays torque characteristics for different application techniques of MoS_2 . Spacecraft usage of MoS_2 is indicated on Table 1.

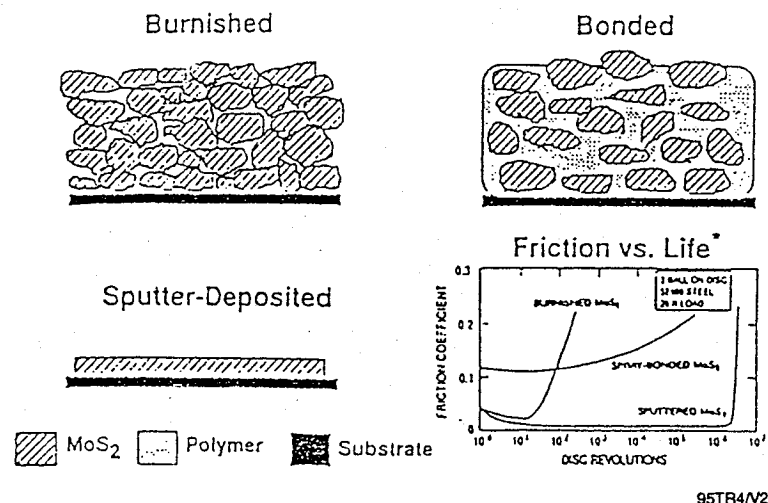


Figure 1. Different Types of MoS_2 Plus Friction Graph

Table 1. Uses of MoS₂ in Active Spacecraft

Device	Function	Comments	Film Type
Inertial properties measurement device	Provides attitude control	Requires constant, low friction, multiple passes	Bonded
Launch clamp for primary sensor	Relieves launch load from bearings	Single-point failure for primary mission	Bonded
Slip rings for microwave sensor	Transmits power signal across rotating contact	Excessive noise degrades sensor performance	Composite
Solar array drive mechanism bearings	Supports solar array drive despin mechanical assembly	Provides sun tracking for power	Bonded
Slip rings for solar array drive mechanisms	Power and signal transfer	Noise sensitive for star tracker	Composite
Slip rings for solar array drive mechanisms	Signal transfer	Noise sensitivity	Composite
Main weather sensor bearings	Scan for weather map	Torque bump sensitivity	Sputtered
Aft support bearings for orbiter interface	Provides pivot for launch from orbiter	Multiple environments, re-use	Bonded
Gimbal bearings, antibacklash springs, jackscrews	Provides pivot and control for antennas	Sensitive pointing	Sputtered, bonded
Solar array drive mechanism bearings	Supports solar array drive despin mechanical assembly	Low-temperature operation	Sputtered, bonded
Gimbal springs, jackscrews, ball and sockets, gears	Controls motion, cradle release	Sensitive pointing	Sputtered, bonded
Bushings, springs, gears, clamps, etc.	Suspension, separation	Single-point failures and wear points	Bonded, burnished
Alignment-release pins	Supports high-gain antenna when folded	High friction prevents deployment, mission failure	Bonded

95TR4/V2

Description:

Release or deployment mechanisms require a lubricant to provide low friction (torque) for a low number of cycles. (Even though a release mechanism generally operates only once in flight, the mechanisms and its lubricant have to undergo multiple cycling, e.g., 10 to 100 operations, during preflight ground tests.) The lubricant cannot be a source of vapor phase contamination once the spacecraft is in orbit because release mechanisms are usually exposed. Lack of thermal control may require the lubricant to function in a wide temperature range. On externally exposed mechanisms, the lubricant must withstand exposure to radiation, electrons, protons, and O-atoms; the nature and quantity of this flux is dependent upon the orbit. All of these requirements favor the use of solid lubricants, and indeed, release and deployment mechanisms are the largest application for solid lubricants in space systems.

Key Words:

Solid-Lubricant Coatings, Sputtered Coatings, Multilayer Films, Composite Coatings

Mechanisms:

No Specific Applications

Systems:

Rolling and Sliding Contacts

Authors; Experts:

1. Michael R. Hilton, Reinhold Bauer, and Stephen V. Didziulis
2. Michael T. Dugger and John M. Keem
3. James Scholhamer

Address:

1. Mechanics and Materials Technology Center
The Aerospace Corporation
El Segundo, California 90245
2. Sandia National Laboratories
Division 1832
Albuquerque, New Mexico 87185-5800
3. Ovonic Synthetic Materials Corporation
Troy, Michigan 48084

Telephone:

Title:

Structural and Tribological Studies of MoS₂ Solid-Lubricant Films Having Tailored Metal-Multilayer Nanostructures

Source:

Surface and Coatings Technology, Vol. 53, pp 13-23 (1992).

PRECEDING PAGE BLANK NOT FILLED

Abstract:

Molybdenum disulfide (MoS_2) solid-lubricant films were prepared by radio frequency (RF) magnetron sputtering on 440C steel, 52100 steel, and silicon substrates. This study concentrated on films that were multilayer coatings of MoS_2 with either nickel or Au-20% Pd metal interlayers. Multilayer thicknesses ranged from 0.2 to 1.0 nm while the multilayer periodic spacing ranged from 3 to 10 nm. Scanning electron microscopy and x-ray diffraction revealed that the multilayer films had dense microstructures that, in some cases, exhibited significant orientation of their basal planes parallel to the substrate. Film endurance was assessed in sliding contact using thrust washer tests and in rolling contact using thrust bearing tests. Some film microstructures exhibited excellent endurance. Brale indentation indicated that the metal layers can improve film fracture toughness. Friction in air and ultra-high vacuum (UHV) was investigated using a UHV-compatible test apparatus. Friction coefficients between 0.05 and 0.08 were measured in UHV.

Lessons Learned:

- Multilayered films exhibited excellent endurance in sliding wear and thrust bearing tests.
- Friction coefficients in UHV ranged between 0.05 and 0.08.
- With metal multilayer films, the optimum structural spacing is on the order of 10 nm.
- MoS_2 should have basal plane orientation between the metal layers.
- Minimum metal layer thickness is best.
- A thin surface overlay of pure MoS_2 seems to facilitate transfer to an uncoated surface.

Description:

Sputter-deposited MoS_2 films often have a porous columnar-plate morphology because of the anisotropic crystal structure of the MoS_2 which causes different reactivities on different facets of the solid. The edge plane surfaces grow faster than the basal surface and these evolve into columnar plates which shadow and inhibit the growth of the basal islands. Wear of these films is often more rapid than it should be. This results in loose wear debris, which causes fluctuations in friction as well as shorter film life.

Chemical modification or passivation of the substrate can suppress the initial edge island formation, but it reappears within 10 to 30 nm of the substrate. By depositing multilayer coatings of MoS_2 separated by sputtered layers of metal, a laminar composite film could be formed without the formation of edge islands or columnar growth. This paper describes an investigation of Ni/ MoS_2 and Au-20% Pd/ MoS_2 multilayer films to see if these would produce better coatings.

Most of the films were applied by RF magnetron sputtering the films on hardened and polished 440C blocks, on 440C or 52100 thrust bearing raceways (INA W1-1/2), and on both silicon (100) wafers and Kapton films. A carousel inside the sputtering chamber was used to rotate the specimens. The deposition pressure was 0.266 Pa of argon, and the sample temperature did not exceed 100°C. The total thickness of the films was about 1 micron.

The authors divided the samples into three groups: I, II, and III. Group I used 52100 steel bearing raceways, and Groups II and III were 440C blocks and Kapton films. Groups II and III also had a 50-Nm overcoat of pure MoS_2 to aid the initial film transfer to the uncoated counterface. All coatings were confirmed by XRD and other techniques. (Note: in designating film composition and structure, the authors used a code where the first number was the metal thickness and the second number was the periodic spacing of the metal interlayers, e.g., 0.3 Nm-Ni/4.8 Nm; 0.3 Nm is the thickness, and 4.8 Nm is the multilayer periodicity and the metal is nickel.) Figure 1 is a schematic diagram of the way the multilayers were structured.

For comparison, two types of straight MoS_2 films (no metal layers) were used as characterization references. Both were RF sputtered. One film, designated as RF-AT, was sputtered at an argon pressure of 2.66 Pa and an ambient temperature of 70°C. It had a columnar plate structure. The other film, designated as a pure MoS_2 RFM film, was sputtered at an argon pressure of 0.226 Pa, and an ambient temperature of less than 100°C. It had a dense morphology with equiaxed features, similar to the other test films applied at this argon pressure. As shown in Figure 2, the pure RFM film had better endurance than the average RT-AT films. The multilayered films with nickel showed considerable scatter. It was hypothesized that the bare steel counterface was not developing an adequate transfer film, so a 50-Nm overlayer of pure MoS_2 was applied to all Group II films to facilitate film transfer. However, since the Group II samples were used in rolling thrust bearing tests, no certain conclusions could be drawn.

Figure 3a presents the endurance data from the 52100 thrust bearing tests. Pure RFM films deposited on the 52100 steel without a nickel interlay failed very quickly, probably because of poor adhesion. Only tests of the 0.3 Nm-Ni/5 Nm showed any promise. The authors reported that only ball cage wear and uniform film removal were observed during the rest of the tests. More promising results are shown in Figure 3b. The 0.7 Nm-Ni/10 Nm films (with 50 Nm pure MoS_2 overlays) had endurance lives consistently better than the RF-AT films. However, they did not appear to be as good as the RFM films. The 0.9 Nm-Au/10 Nm films in Group III were much more promising.

Brale indentations (150-kg load) caused delamination of the pure films with the dense morphologies. Increasing the metal content inhibited delamination and better results were obtained with a 5-Nm spacing than with 10-Nm spacing.

Friction coefficients for the pure RFM film and the 0.9 Nm-Au/10 Nm film (Figure 3b) were similar. At 1000 cycles, the friction was 0.05 to 0.08 in both air and vacuum. In general, lower friction was obtained with MoS_2 in vacuum than in air, which is believed to be due to moisture.

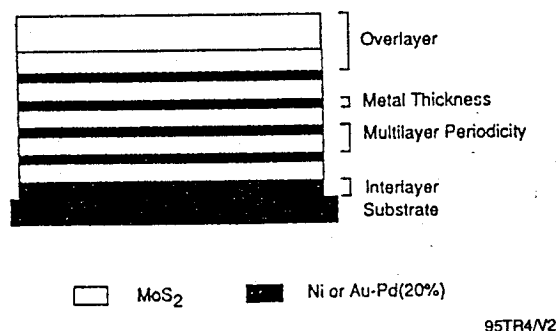
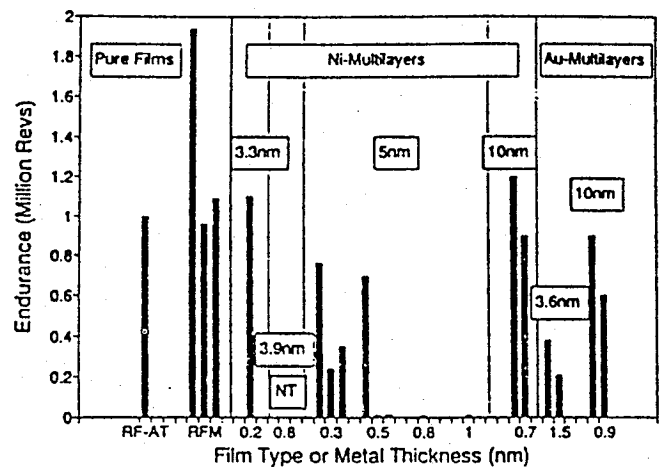
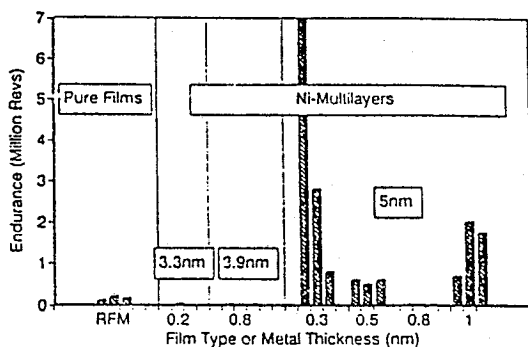


Figure 1. Multilayer Lubricant Film Architecture



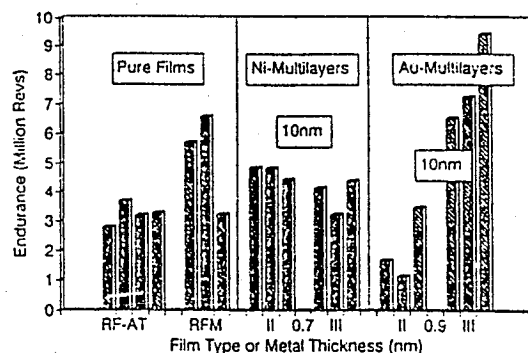
95TR4/V2

Figure 2. Endurance Data for the Various Films in Thrust Washer Sliding Tests from Groups I and II



95TR4/V2

a) 52100 Steel (Group I)



95TR4/V2

b) 440C Steel (Groups II and III)

Figure 3. Endurance Data from Thrust Bearing Rolling Tests of MoS₂

Key Words:

Ball Bearing, Thin Section, Lubricants, Torque, Conductance

Mechanisms:

Ball Bearings

Systems:

Rotating System

Authors; Experts:

Robert A. Rowntree

Address:

European Space Tribology Laboratory
UKAEA
Risley, Warrington, England

Telephone:**Title:**

The Properties of Thin-Section, Four-Point-Contact Ball Bearings in Space

Source:

19th Aerospace Mechanisms Symposium (1985).

Abstract:

Thin-section, four-point-contact ball bearings are increasingly employed in spacecraft mechanisms because of the potential advantages they offer. However, little was previously known of their torque, thermal conductance, and stiffness properties at conditions anticipated for their use in space. The paper describes an investigation of these properties.

Lessons Learned:

- Internal preload, housing design, and external axial clamping force on the bearing rings all have a strong influence upon torque, conductance and stiffness.
- The thermal conductance of a dry or marginally lubricated bearing depends upon the thermal strain and varies linearly with radial temperature difference between the rings. Additionally, conductance is a function of type and quantity of lubricant.
- The Coulomb torque exhibits an almost square-law relation with thermal strain.

Description:

Thin-section, four-point-contact, rolling element bearings have been shown to offer a near-ideal solution for some of the novel demands of spacecraft mechanisms. This type of bearing can take radial loads and thrust loads in both directions so that they are effectively equivalent to two conventional bearings. Since one bearing does the work of two, the prime advantages of low weight, small cross section, and high stiffness can be used to simplify designs. A series of tests were carried out to investigate the mechanical and thermal properties of representative four-point-contact bearings. Details of the bearings are given in Table 1.

Stiffness measurements were made in a specially designed rig. In the rig, the bearing was located against a machined shoulder on both the inner and outer housings and each race was held in place axially by a clamp ring. The axial clamping force on the bearing could be varied by the torque imparted to the 24 × M3 clamping bolts on each clamp ring. For a clamp ring bolt torque of 0.8 Nm, the angular compliance of the bearings are given in Table 2. The axial compliance of the bearings for a clamping bolt torque of 0.8 Nm are given in Table 3. The marked influence of axial clamping force on the axial compliance of Bearing A is summarized in Table 4.

Table 1. Four-Point Contact Bearing Details

Kaydon Bearing No.	KA070XP2
External diameter	190.5 mm
Internal diameter	177.8 mm
Width	6.35 mm
Bearing internal fit (nominal)	0 to 12.7-micron clearance (Bearing A)
Bearing internal fit (nominal)	0 to 12.7-micron preload (Bearing K)
Bearing internal fit (nominal)	12.7- to 25.4- μ m preload (Bearing M)
Number of balls	87
Cage	Snap over crown in brass; nylon or spring separators
Contact angle	30°
Bearing steel	AISI 52100
Precision	Class 6 (equivalent to ABEC 7 in run-out tolerances)

95TR4/V2

Table 2. Bearing Angular Compliance

Bearing	Angular Compliance (rad/Nm)	
	Experimental	Manufacturers Estimate
A	1.62×10^{-6}	2×10^{-6}
K	1.27×10^{-6}	
M	0.85×10^{-6}	

95TR4/V2

Table 3. Bearing Axial Compliance

Bearing	Axial Compliance (m/N)	
	Experimental	Manufacturers Estimate
A	7.25×10^{-9}	8×10^{-9}
K	5.81×10^{-9}	
M	4.04×10^{-9}	

95TR4/V2

Table 4. Influence of Axial Clamping Force on the Axial Compliance of Bearing A

Clamp Ring Bolt Torque (Nm)	Axial Compliance (m/N)
0.2	3.0×10^{-8}
0.8	7.25×10^{-9}
1.86	1.56×10^{-9}

95TR4/V2

The torque and thermal conductance measurements were carried out in a vacuum chamber. The bearing was mounted between the inner housing and heat flux meter. As before, the inner and outer races were clamped axially by two clamp rings. Four radial groups of copper/constantan thermocouples were located at 90° intervals around the heat flux meter. Two measured the inner and outer race temperatures and the other two measured the temperature difference across the heat flux meter. Radiant heat loss from the bearing and heat flux meter was prevented by multiple superinsulation shields. The bearing was rotated using an externally controlled motor via a ferrofluidic feedthrough. Bearing torque was sensed by a strain-gage transducer.

Three space-approved lubricants were used in the torque and conductance tests: two oils and one grease, which are described in Table 5.

In general, conductance values were measured with the bearing stationary and the torque was measured at a rotational speed of 1 rpm, which was slow enough to make any speed-dependent torque effects negligible. Pressure in the vacuum chamber was maintained at 10^{-3} torr to ensure no convective heat transfer between bearing and environment.

The effects of thermal gradient, internal preload, and axial clamping force on the conductance and torque were investigated as well as the different lubricants.

Table 5. Lubricants Used in Torque and Conductance Tests

Lubricant	Manufacturer	Description	Viscosity at 20°C (cS)	Thermal Conductivity (W/m°C)
Fomblin Z25	Montedison	Fluorinated oil	240	0.0840
BP110	British Petroleum	Mineral oil refined to give low vapor pressure	350	0.0153
Braycote 3L-38RP grease	Brayco Oil Company	Based on Z25 with polymer-thickening agent PTFE	—	0.0840

95TR4/V2

Key Words:

Tribology, Lubrication, Solar Array Drive, Despin Mechanisms, Bearings

Mechanisms:

Reaction Wheels, Bearings

Systems:

Deployment Systems, Rotating Systems

Authors; Experts:

R.A. Rowntree and M.J. Todd

Address:

National Center of Tribology
Northern Research Laboratories
UKAE, Risley, Warrington, UK

Telephone:**Title:**

A Review of European Trends in Space Tribology and its Application to Spacecraft Mechanism Design (1991).

Source:**Abstract:**

The development of space tribology and its application in the design of spacecraft moving mechanical assemblies in Europe has followed a different course from that in the United States. This is probably because of the distinct preponderance of three-axis stabilized space vehicles (used for communications and for Earth observation over Europe) together with the preference for solid lubricants in such devices as solar array drives and some types of scanner and despin mechanisms.

The paper reviews the current status and discernible future trends in European space tribology. Examples of current moving mechanical assembly types are given where evolved lubricants and lubrication techniques have been applied.

Lessons Learned:

- The relative merits of solid and liquid space lubricants are indicated in Table 1.
- Avoid the use of wet lubricants where optical devices or sliding electrical contacts are employed.
- Perfluoropolyalkylether (PFPE) fluids have produced high torque noise and excessive ball bearing wear. Table 2 summarizes the factors which have been found to promote or inhibit PFPE degradation.

The precise mechanism of degradation is still not established. In Europe, the evidence points to chemical reaction between nascent wear particles and the exposed oxygen in the Z-type molecule. The product is described as a metal polymer (or "brown sugar") which is autophobic and thus repels the oil from the ball/raceway contact region.

- Ion-plated lead films are extensively used in Europe. In solar array drives alone, more than two million operational hours in orbit have been accumulated.

An important property of the lead film is its high load-carrying ability. Under Hertzian contact, the as-deposited film flows plastically until a thin film (of thickness 10 Nm or less) remains and then elastically deforms with the substrate. In this condition, the film can survive contact loads approaching the static load capacity of a rolling element bearing.

- Thin films of gold have also been investigated as a bearing lubricant, but the higher yield strength and ductile adhesional property result in work-hardened debris and, thus, high torque noise. Silver and indium have been investigated too, but actual usage in space is not reported.
- Sputtered application of molybdenum disulfide (MoS_2) is the preferred and perhaps necessary method. Sputtered films of MoS_2 are currently applied to numerous space components such as screw threads, ball bearings, sleeves, and bushes.

An investigation at European Space Tribology Laboratory (ESTL) of MoS_2 films deposited by so-called magnetron RF sputtering in which the rate of evaporation of the MoS_2 target is greatly increased by magnetic field intensification of the plasma, led to significant gains in triboproperties under vacuum. Not only is the friction coefficient remarkably low under pure sliding motion (values of 0.005 to 0.04 are typical) but the wear resistance of the film is greatly improved. Figure 1 shows a comparison of the friction/time behavior for the three types of film under identical pin/disk experimental conditions.

Table 1. Relative Merits of Solid and Liquid Space Lubricants

Dry Lubricants	Wet Lubricants
Negligible vapor pressure	Finite vapor pressure
Wide operating temperature	Viscosity, creep, and vapor pressure all temperature dependent
Negligible surface migration (debris can float free)	Seals required
Valid accelerated testing	Invalid accelerated testing
Short life in laboratory air	Insensitive to air or vacuum
Debris causes frictional noise	Low frictional noise
Friction speed independent	Friction speed dependent
Life determined by lubricant wear	Life determined by lubricant degradation
Poor thermal characteristics	High thermal conductance
Electrically conductive	Electrically insulating

95TR4/V2

Table 1. Relative Merits of Solid and Liquid Space Lubricants

Promote Degradation	Retard Degradation
Starved conditions	Fully flooded conditions
Low specific film thickness	High specific film thickness
Linear structure (Z)	Branched structure (Y)
Aluminum/titanium substrates	Hydrocarbon contamination
52100 bearing steel	440C steel and ceramic coatings
Temperature 200°C	Low ambient temperatures
Sliding Surfaces (seals, etc.)	Rolling surfaces
Vacuum environment	Atmospheric conditions

95TR4/V2

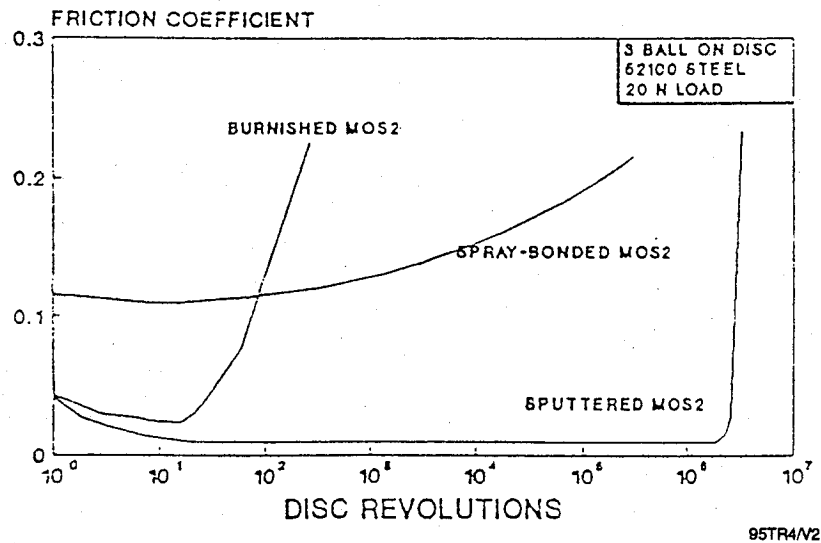


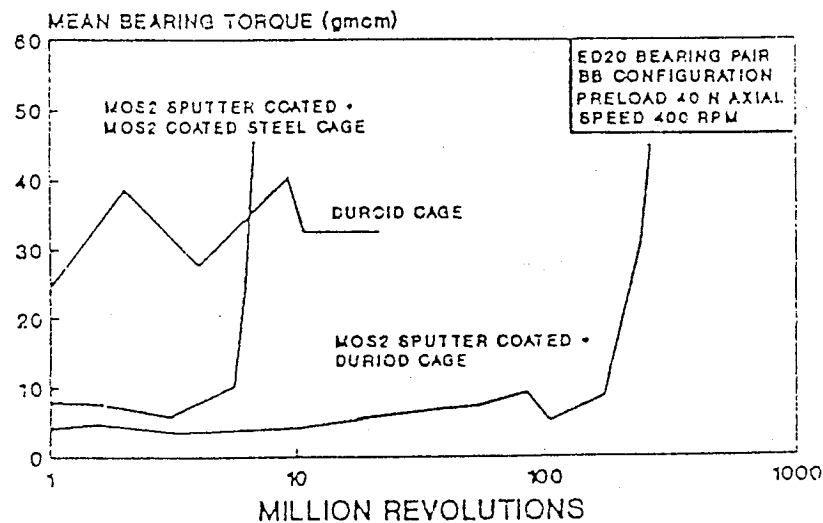
Figure 1. Friction Coefficients of MoS_2 Deposited by Various Techniques

- Ion-beam application of MoS_2 also appears to be promising although it has not been used in space mechanisms. A feature of this method is an increase in the density of the film and it is possible that this compaction may help in extending film lifetime.
- MoS_2 works well with ceramics such as titanium carbide and hot-pressed silicon nitride.
- Polymer use in European space applications is identified in Table 3. An extensive study in the United Kingdom over 10 years ago restricted to air usage, showed that a PTFE/glass fiber/ MoS_2 combination was preeminent in terms of friction torque and endurance, provided that the maximum Hertzian contact stress was kept below 1200 MPa at room temperature.
- Cosputtering of MoS_2 and PTFE onto plain steel gave a ten-fold increase in wear life over pure MoS_2 alone, whereas the same codeposition onto sulphur-enriched interlayers or substrates of Ni, Co, and particularly Rh yielded vast improvements of up to 10,000-fold. The sulphur enrichment was effected by glow discharge treatment in an H_2S /argon atmosphere prior to sputtering. The corrosion properties in moist air were also improved by this chemical activation method. Figure 2 shows a significant gain by combining a PTFE-composite cage (Duroid) with MoS_2 . The combination performs much better than with either lubricant alone.

Table 3. Polymers Used in European Space Applications

Trade Name	Description	Uses
Duroid 6813	PTFE/GF/MoS ₂	Cages and gears
Delrin/Hostaform	Polyacetal	Cages, brushes, and brakes
Tufnol	Reinforced phenolic	Cages and gears
Vespel SP3	MoS ₂ /polyamide	Cages and gears
Glacier DU	PTFE/PB bronze on steel backing	Bushings
Fibreslip	Woven GF/PTFE plus resin	Spherical joints
Rulon	PTFE/GF	Cages
Glacier DP-1	PTFE/bronze	Rotating nuts and bushes

95TR4/V2



95TR4/V2

Figure 2. Mean Torque of Ball Bearings Operating Dry In Vacuum

Description:

Reaction Wheel. A current design of reaction wheel for the Olympus communications spacecraft, made by British Aerospace (BAe), is shown in Figure 3. Rotational speed can be anywhere in the range of ± 3500 rpm depending upon the torque demand for attitude control. The target lifetime of the wheel in space was 7 yr and the bearing torque had to be low and speed insensitive with minimal torque noise.

In connection with this momentum wheel, experimental work on oil quantity and its effect on torque and torque noise pointed to the need for an optimum amount of oil—more oil would raise viscous torque too much at high speeds, and less oil would produce cage instability and vibration peaks. In order to retain the initial inventory of oil, molecular sealing and creep barriers were installed and a heatable porous nylon reservoir was placed between the bearings with the aim of maintaining oil quantity at the optimum throughout the life.

Using these modifications, a real-time life test was performed by BAe with regular cycling of the wheel speed between the limits of $+3500$ and -3500 rpm. The performance of the wheel over a 7-yr period (currently extended to 10 yr) has been excellent and it was found unnecessary to use the heater to replenish the oil.

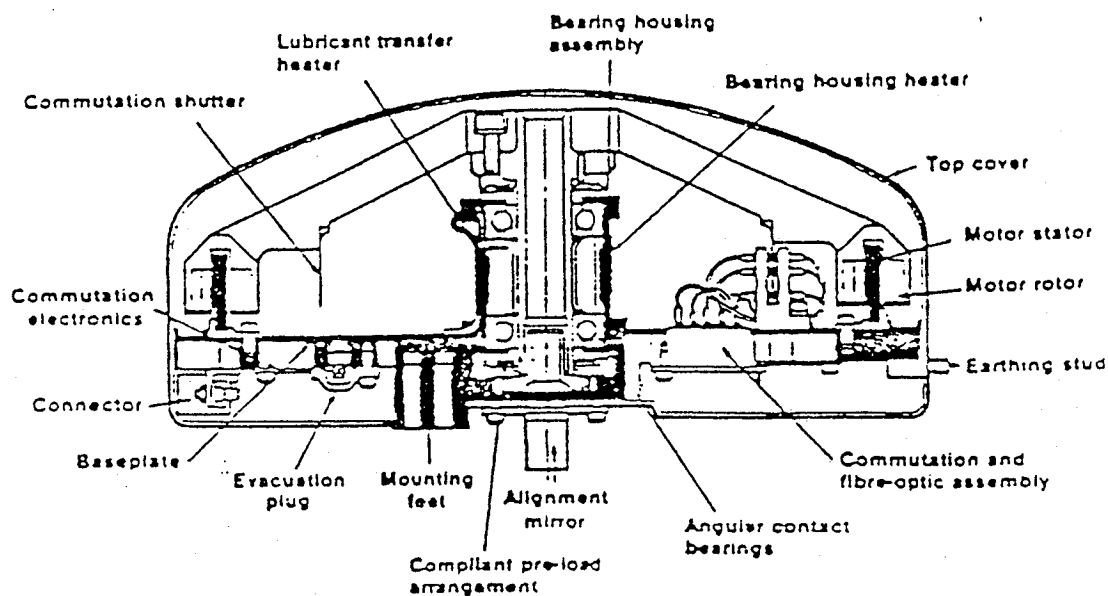
Antenna Pointing Mechanism. The Olympus spacecraft uses the pointing principle involving the relative rotation of two wedges (or swash plates), whose combined angle is the cone half-angle of the pointing vector (Figure 4). Support of the rotating wedges is provided by the thin-section gothic arch (four-point contact) bearings as shown in Figure 4.

The lubricant chosen for this pointing mechanism was the PFPE grease Braycote 601, which, as mentioned above, has been widely used in United States space vehicles. The internal components of the antenna pointing mechanism are vented to space; it has been found that the very low vapor pressure of this grease presented no problem of effusion loss.

Despin Mechanism. The high-gain antenna despin drive mechanism used in GIOTTO spacecraft, designed and built by SEP, France, was an interesting application of solid lubrication to meet the severe environmental conditions that are too severe for a fluid lubricant. The main constraint was the wide temperature range for operation (-40 to 60°C), which would have meant a large change in torque for any fluid lubricant. The choice of ion-plated lead was a result of some preliminary experimental work at ESTL, which showed the lead torque spectrum to be more favorable than that from a PTFE-composite caged bearing. A prelaunch accelerated life test on ion-plated bearings monitored the torque noise over a total of 10^8 revolutions (compared with the Halley mission life of 5 million revolutions). Performance of the despin mechanism during the Halley mission was completely successful.

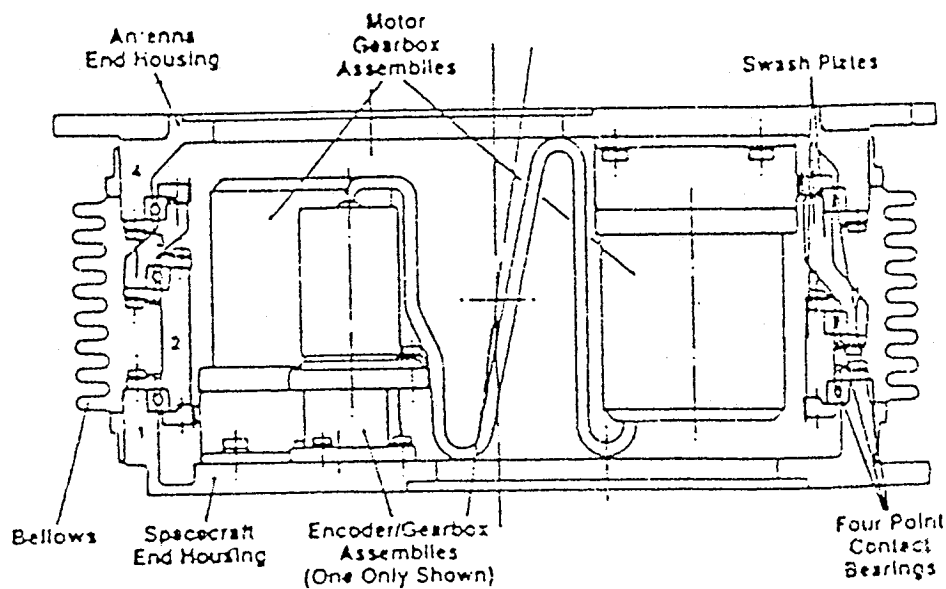
Solar Array Drives. One of the desirable features of solar array drives is that sun orientation of solar arrays on three-axis spacecraft requires a rotating joint between the array and the platform. Electrical energy and signals from and to the array must also be fed across this joint.

A current European design of solar array drive mechanism is shown in Figure 5 for application to Olympus satellite. In this design a pair of back-to-back flexibly preloaded ball bearings is used to support the shaft carrying the solar array. As in the reaction wheel described above, a dual-compliance disk spring preloads the bearings and avoids the need for a separate launch locking of the bearings. The bearing lubricant is ion-plated lead.



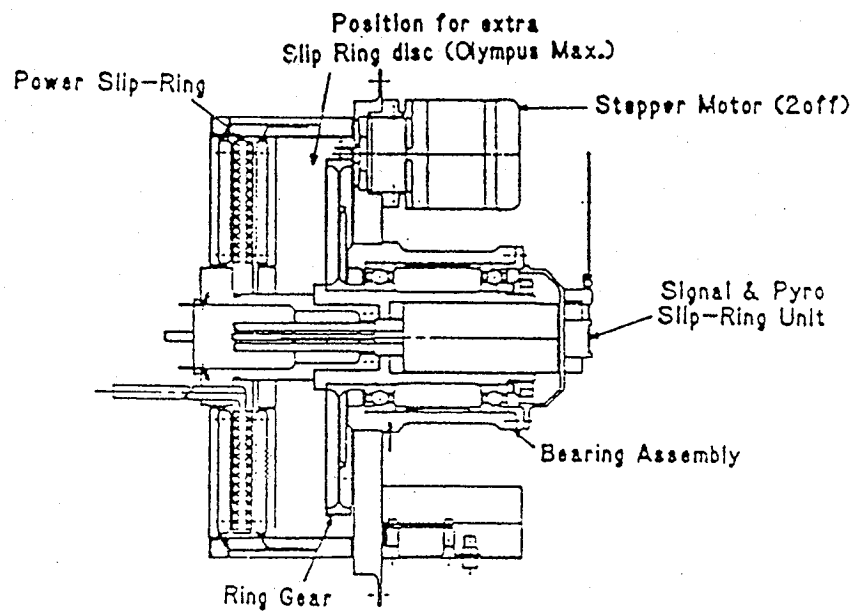
95TR4/V2

Figure 3. BAe Design of Olympus Reaction Wheel (10 Nms)



95TR4/V2

Figure 4. Olympus Swash Plate Antenna Pointing Mechanism (BAe)



95TR4/V2

Figure 5. Olympus Solar Array Drive Mechanism (BAe)

Testing:

- A real-time life test was performed by BAe on the Olympus reaction wheel with regular cycling of the wheel speed between the limits of +3500 and -3500 rpm. The performance of the wheel over a 7-yr period (currently extended to 10 yr) has been excellent and it was found unnecessary to use the heater to replenish the oil.
- A prelaunch accelerated test on ion-plated lead bearings for the despin drive monitored torque noise over a total of 10^8 revolutions (compared with the Halley mission life of 5 million revolutions). Performance during the Halley mission was completely successful.

Experience:

Ion-plated lead film has been featured in numerous spacecraft: OTS, ECS, MARECS, EXOSAT, NIMBUS, Olympus, INMARSAT 2, GIOTTO, SPOT, Eureca, Skynet, and the space telescope. In solar array drives alone, more than 2 million operational hours in orbit have been accumulated to date using this film.

Antennas and Masts

Key Words:

Deployment Mechanism, Hinge, Lubrication

Mechanisms:

Deployment Mechanism

Systems:

Deployment System

Authors; Experts:

Herbert T. Greenfield

Address:

Lockheed Missiles & Space Company, Inc.
Sunnyvale, California

Telephone:

Title:

Appendage Deployment Mechanism for the Hubble Space Telescope Program

Source:

19th Aerospace Mechanisms Symposium (1985).

Abstract:

The paper presents the key requirements, a design overview, development testing (qualification levels), and two problems and their solutions resolved during the mechanism development testing phase. The mechanism described has demonstrated its capability to deploy/restow two large Hubble space telescope deployable appendages in a varying but controlled manner.

PRECEDING PAGE BLANK NOT FILMED

Anomalies:

- The initial predicted aperture door mechanism temperatures could be well below -125°F. This proved to be a problem for the grease plating of Braycote 3L-38RP on the angular contact bearings. The solidification temperature of this lubricant is approximately 120°F. The resulting stiffness of the lubricant caused unacceptably high bearing torques even though the mechanism would operate to as low as -160°F.
- During subsystem testing of the high-gain antenna configuration, the tests were plagued by a problem that was finally diagnosed as lost motion, which resulted in variable performance at the stow position.

Lessons Learned:

- Braycote 3L-38RP grease works well in angular contact bearings (in a vacuum) if the temperature is kept above the grease solidification temperature. The range of motion of the hinges is approximately 90°. For the aperture door mechanism, this motion takes place over 1 min, and for the high-gain antenna hinge the time is 7 min.
- In a mechanism, it is important to eliminate all backlash to avoid lost motion.

Description:

As part of the NASA Hubble space telescope, three appendages are deployed/stowed by an electromechanical hinge mechanism. One use is for the deployment/stowing of two high-gain antennas used to transmit data to the ground station. The second use is to open and close the large aperture door located at the end of the telescope aperture, which must close to preclude the sun from shining on the telescope primary mirror.

The deployment mechanism, a limited-angle hinge device, was designed to meet the following specific requirements:

- The deployment mechanism must be capable of surviving five shuttle launches, four returns to Earth, and eight in-orbit docking operations with appendages stowed and locked
- The deployment mechanism must be redundant so that no single component failure will jeopardize recovery of the spacecraft or result in hazards to personnel
- The deployable appendages must be capable of manual operation and jettison by an extra vehicular activity crewmember to ensure deployment, restowage, and safe return of the space telescope spacecraft to Earth
- The aperture door deployment mechanism must be capable of closing within 1 min after a command from the sun sensor, precluding irreversible damage to the telescope optics if the spacecraft points the aperture towards the sun
- The deployment mechanism must operate in an Earth-orbiting pressure environment and at heater-controlled temperatures from -80 to +110°F
- The hinge mechanism deployed stiffness must meet a first-mode natural frequency of less than 1.0 Hz.

The deployment mechanism consists of an active hinge (actuator-powered dc rotary drive) and a passive hinge.

The large-diameter, angular-contact, output support bearings and the self-aligning spherical bearings are identical in the active and passive hinge assemblies. The active hinge assembly is driven by a permanent magnet dc stepper motor driving through a 200:1 harmonic drive speed reducer. The bidirectional rotary actuator drives a torsion rod via a splined shaft which is keyed to the domed end cover. The torsion rod permits the actuator, with its inherent powered detent torque, to move larger inertias than if direct coupled. This is the point where the aperture door or high-gain antenna is attached. The spring-loaded friction plugs made from Delrin AF rub constantly against the end cover to provide damping during movement of the mechanism. Just prior to the fully deployed position, the adjustable intermediate stops located in the domed cover contact the intermediate torsion tube and the torsion tube. These are both compliant members with different spring rates that reduce the end-of-travel dynamic loads and contribute to the overall deployed mechanism stiffness. The intermediate torsion tube also has Coulomb damping in the form of annular Delrin AF friction segments. A manual wrenching point to rotate the active hinge is provided at the end of the torsion rod opposite the rotary drive actuator. The total travel angle for the high-gain antenna is 92.7°, and for the aperture door it is 105.3°.

Bray Oil Co. wet lubricants, Brayco Micronic 815Z oil, as well as their Braycote 3L-38RP (Braycote 601) grease, are used to lubricate vital components in the mechanism. The angular contact bearings are lubricated with a solvent-thinned solution of the Braycote 3L-38RP grease (grease plating) then vacuum-baked leaving a thin, evenly distributed film of the lubricant. In the passive hinge, the stub shaft is permitted to slide in the inner race of the spherical bearing. A groove is cut in the shaft to provide a reservoir for the Braycote 3L-38RP grease.

Testing:

In-house testing was conducted in three phases.

Phase I: Mechanism Characterization. Key testing in this phase involved nonpowered motion study of the principal mechanism elements at vacuum and cold temperatures. The friction damping elements proved to be within 5 to 10% of the desired damping range.

The spacecraft's thermal control system was based on biasing temperatures toward the colder regimes to reduce thermal gradients. Because of this, initial predicted aperture door mechanism temperatures could be well below -125°F. This proved to be a problem for the grease-plated angular contact bearings. The solidification temperature of the 3L-38RP grease is approximately -120°F. This resulted in unacceptably high bearing torques even though the mechanism would operate to as low as -160°F. Because the Braycote lubricant has low outgassing characteristics and because of a desire to avoid a lengthy lubrication development program, heaters were installed to ensure that the mechanism temperature would not go below -80°F. The high-gain antenna mechanism is not fitted with heaters since the predicted cold operation is -53°F or above.

Thermal testing of the spherical bearing was needed since it was the redundant rotational feature to the angular contact bearings and no cold test data were available from the supplier. The cold test results were acceptable and the bearing torque contribution was factored into the overall mechanism torque margin.

Phase II: Hinge Mechanism Operation. This series of tests involved mechanism operation over the full range of travel at hot and cold temperatures and with the test specimen connected to inertia simulators representing both the high-gain antenna and aperture door. The mechanism rotational axis was mounted vertically and the additional weight was supported by a 0-g line pivoting in line with the mechanism rotational centerline.

This test phase permitted verification of the analytical model as well as providing a test bed for a two-axis, static-proof test and a deploy-direction, dynamic-proof test. These tests at ambient temperature were preceded and followed by functional operation and no anomalies were identified.

The deployed and preloaded natural-mode frequency of the mechanism was verified during this test phase to be 0.875 Hz, below the 1.0-Hz maximum.

The deployed or open position of the mechanism was also verified during this test phase and was shown to be repeatable within 0.033° , well within the aperture door position accuracy needed of $\pm 0.25^\circ$.

The final phase of this test series centered on a three-axis vibration test using the mechanism configured for the high-gain antenna. No unacceptable motions were detected and the mechanism suffered no damage.

Phase III: Subsystem Testing. This test phase addressed, in particular, the high-gain antenna configuration and its deployment and restow. The first portion of the test sequence was plagued by a problem that was finally diagnosed as lost motion, which resulted in variable performance at the stow position. As the mechanism drives into the stow position, it must be positioned correctly for the latches to capture and secure the high-gain antenna. This involves tripping four telemetry switches that indicate to the ground station when the latches may be closed (a separate operation). Although always within latch capture range, the inconsistent performance needed correcting.

Play in the keyway tying the torsion rod to the domed aluminum cover was determined to be the cause. Once corrected by a small shim in the keyway, consistent and reliable results were demonstrated. A redesign, however, was initiated to effect a long-term solution to compression yielding of the aluminum portion of the cover interface brought on by numerous manual deployments and stowings. The solution selected was to provide a conical or tapered fit-up of the stainless steel torsion rod to the aluminum domed housing. The tight friction fit in conjunction with the keyway assured a no-lash joint.

Key Words:

Gamma Ray Observatory, Solar Arrays, High-Gain Antenna, Thermal Blanket,
Bolt Interference

Mechanisms:

Solar Arrays, High-Gain Antenna

Systems:

Gamma Ray Observatory

Authors; Experts:

K. Hinkle

Address:

NASA-Goddard Space Flight Center
Mail Code 731
Greenbelt, Maryland 20771

Telephone:

Title:

Spacecraft Deployable Appendages

Source:

Goddard Space Flight Center
Engineering Directorate

Abstract:

The Gamma Ray Observatory (GRO) had two solar array wings weighing approximately 500 lb each and one high-gain antenna boom assembly weighing approximately 525 lb. The high-gain antenna did not deploy when it was initially commanded. An astronaut extra vehicular activity from the shuttle was required to physically shake the antenna to initiate the deployment sequence.

C-2

Anomalies:

Prior to observatory release from the orbiter remote manipulator system, the high-gain antenna did not deploy when it was initially commanded. An astronaut extra vehicular activity was required to physically shake the antenna to initiate the deployment sequence. Subsequent investigations corroborated with on-orbit photographs taken by the astronaut crew indicated that a portion of the antenna release mechanism (close to the antenna dish) was caught by a piece of thermal insulation blanket. This occurred because of large relative motion between the antenna and its support structure which allowed an exposed bolt to be caught by the neighboring thermal blankets. There were three areas identified which are believed to have caused the problem:

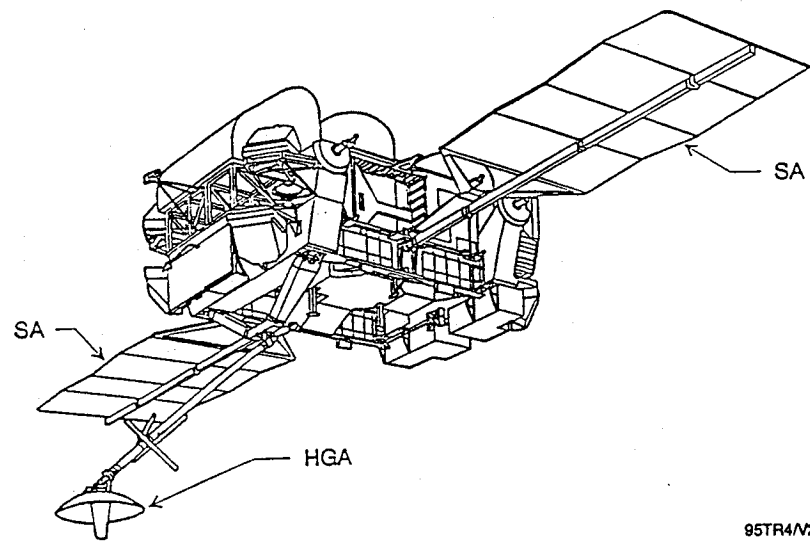
1. Several bolts adjacent to the thermal blankets were installed with the longer nut end of the bolts protruding in close proximity to the blankets. Although this was needed to circumvent a design flaw with the antenna support mechanism, interference with thermal blankets was not envisioned.
2. Structural vibration testing of the assembled high-gain antenna did not include thermal blankets. For practical reasons, these tests also did not include a simulation of the spacecraft relative stiffness between the high-gain antenna support points. It was this low stiffness that allowed large relative motions between the dish end of the antenna and the spacecraft. The only observatory level test with thermal blankets installed was an acoustic test. Acoustic tests generally do not produce large spacecraft loads or motion which would have been needed to uncover the problem prior to launch.
3. The technician and quality assurance personnel who performed the final stowing and inspection of the high-gain antenna, respectively, did not foresee the potential problem of large relative displacements that would have caused the bolts to catch the thermal blankets and prevent the antenna from deploying.

Lessons Learned:

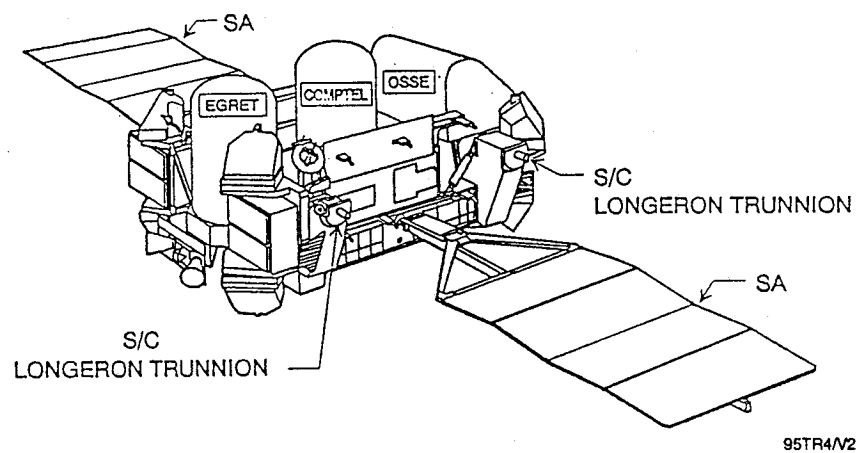
- Deployment tests should be accomplished with final configuration including thermal blankets. Spacecraft attachments should be simulated accurately.
- Interference that might be caused by thermal blankets should be evaluated.

Description:

The GRO was launched on April 4, 1991, aboard the space shuttle Atlantis from the Kennedy Space Center in Florida. The observatory had two solar array wings weighing approximately 500 lb each, and one high-gain antenna boom assembly weighing approximately 525 lb. The array wings and their stowing latches were identical in construction and the -Y system (wing 1) could be mechanically interchanged with the +Y system (wing 2). The two wings were electrically unique in terms of their motor drive direction, microswitch designations, and coarse sun sensor designations. The deployed GRO is shown in Figure 1.



Top View



Bottom View

Figure 1. GRO Deployed Configuration

The high-gain antenna boom and both solar array wings were planned to be deployed while the GRO was being deployed from the orbiter and still attached to the orbiter remote manipulator system. The design of each appendage incorporated redundant mechanisms that allowed for astronaut backup assistance in case of mechanism jam or malfunction.

All unlatch and deployment operations were performed with stepper motors that were electrically redundant. The deployment and unlatch actuators were attached to drive linkage mechanisms, which offered varying degrees of torque amplification during operation. The actuators were built by Honeywell to TRW specifications and provide variable stepping rates from 7.8 to 250 pulses/sec.

GRO High-Gain Antenna Appendage. The high-gain antenna boom supported the antenna reflector dish and the biaxial drive for pointing the antenna. It also supported the magnetic torquers for dumping momentum associated with the attitude control system. The boom was retained in the stowed position by four latches, two near the magnetic torquer bars and two at the antenna reflector. A single-motor-drive latch actuator operated all four latches. The deployment actuator, at the base hinge of the boom that interfaces with the spacecraft keel structure, deployed the boom to the proper position to achieve the required on-orbit field of view.

GRO High-Gain Antenna Support/Release System. The support/release system consisted of four latches housed inside support fittings whose upper ends attached directly to the platform structure. The latches were opened by a single-motor drive actuator that was supported at the outside edge of the platform to provide access for manual operation.

The latches engaged pins in the slide mechanism mounted to the boom. The slide mechanisms allowed axial motion of the boom relative to the supports due to deflections during launch and changes in temperature of the boom. Each aft slide mechanism consisted of a T-shaped bolt mounted to a fitting on the boom and the slider that supported the latch pin. The cylindrical head on the bolts slides in a hole in the slider. The forward sliders are similar except each has two bolts. These bolts are mounted to the horseshoe shaped antenna frame.

The boom loads are reacted by the latches and support fittings. Each of the forward and aft supports carry the loads through shimmed fittings which mate with the slides. Loads along the boom are reacted at the keel hinge.

High-Gain Antenna Boom Structure. The main boom element consists of 6.0-in. diameter by 0.125-in. wall aluminum tube, with the rotating hinge on the keel end and a flanged fitting on the outboard end.

High-Gain Antenna Hinge/Deployment Mechanism. The hinge mechanism consisted of a stationary hinge half and a rotating hinge half joined with two 0.750-in. diameter hinge pins. Toggle links are used to drive the rotating hinge half and preload it against adjustable stops on the stationary hinge half in the deployed position. The driving link is powered by a motor-driven actuator attached to one side of the stationary hinge.

Normal deployment of the high-gain antenna boom was accomplished by the actuator driving the toggle linkage until stop pads (an integral part of the linkage) engage, preventing further rotation. This stop provides +0.06/-0.02 in. overcenter travel of the linkage so that the high compressive preload prevents the hinge from unlocking. Extra vehicular activity deployment was accomplished by backing out a captive pin to disengage the actuator and then using a wrench on the hex end of the drive shaft to drive the toggle links overcenter and preload the hinge in the deployed position.

Testing:

The overall test program for deployables was quite extensive. Tests performed on both the solar array and high-gain antenna boom hinges and single latches were used to understand the effects of thermal environments and evaluate the resistive torque effects of cable bundle wraps. Later tests subjected flight-like deployment hardware of one full solar array wing and the high-gain antenna boom assembly (including latches) to deployment, vibration, and static load tests. The flight hardware was then subjected to a range of tests including acoustics, thermal vacuum, and deployments.

Key Words:

Deployment Mechanism, High-Gain Antenna, Pin Friction, Ball Screw

Mechanisms:

High-Gain Antenna

Systems:

Galileo Spacecraft

Authors, Experts:

Michael R. Johnson

Address:

California Institute of Technology
Jet Propulsion Laboratory
Pasadena, California

Telephone:

Title:

The Galileo High-Gain Antenna Anomaly

Source:

Proceedings of 28th Aerospace Mechanisms Symposium, NASA Conference Publication 3260.

Abstract:

On April 11, 1991, the Galileo spacecraft executed a sequence that would open the spacecraft's high-gain antenna. The antenna's launch restraint had been released just after launch, but the antenna was left undeployed to protect it from the heat of the sun. During the deployment sequence, the antenna, which opens like an umbrella, never reached the fully deployed position. The analyses and tests that followed allowed a conclusion determination of the likely failure mechanism and pointed to some strategies to use for recovery of the high-gain antenna.

PRECEDING PAGE BLANK NOT FILMED

Anomalies:

The high-gain antenna on the spacecraft failed to deploy.

Lessons Learned:

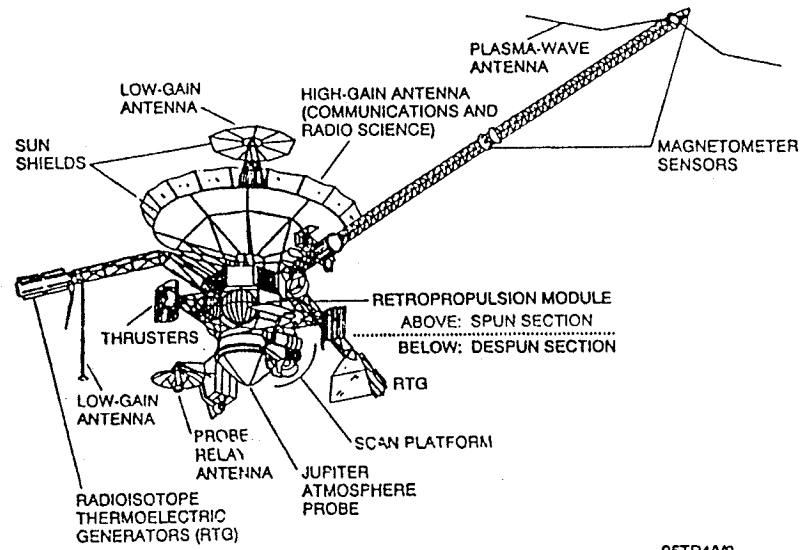
- The failure was caused by galling and excessive friction in the midpoint restraint pins and V-groove socket of the struts that required mechanical drive torques in excess of motor capacity to free the pins and permit deployment.
- Contact stress of any mating surfaces should not be great enough to cause plastic deformation and/or destroy applied coatings.
- Friction in vacuum can substantially exceed friction in atmosphere especially when coatings are destroyed and galling occurs.
- Moments applied to ball screws severely degrade their capacity.
- The use of a dry lubricant, specifically molybdenum disulfide (MoS_2), on a mechanism that is going to be operated in an atmosphere should be carefully evaluated. The wear rate of the MoS_2 in air is so much higher than in a vacuum that any coatings could be worn out by in-air testing and shipping lubrication and not provide the desired lubrication when needed.
- Replacing dry lubricated surfaces just prior to launch so that virgin lubricant surfaces are available is recommended if feasible.
- Shipping vibrations and ground testing can destroy coatings and dry lubricants.
- Vacuum deployment tests, on the ground, should include simulated vibrations prior to deployment.

Description:

The Galileo spacecraft (Figure 1) is a spin-stabilized spacecraft and has three Earth-to-spacecraft communications antennas for commanding and returning spacecraft telemetry.

The high-gain antenna is the one that failed to deploy. To protect the antenna from the sun, it was left in the undeployed position until the sun-to-spacecraft distance was large enough to avoid thermal danger.

Figure 2 shows the Galileo high-gain antenna in the stowed position; Figure 3 shows the antenna in the deployed position. The high-gain antenna is deployed and stowed by a mechanism located in the base of the antenna called the mechanical drive system. This system consists of a dual-drive actuator, a 0.5-in. (12.7-mm) diameter, eight-threads-per-inch (0.125-in., 3.175-mm pitch) ball screw/ball nut assembly; a carrier assembly; 18 pushrods; and 18 ribs (Figure 4). The ribs have a gold-plated wire mesh connected to them that stretches and forms the reflector surface when the antenna is fully deployed. Figure 5 shows the mechanical drive system in the fully deployed position. The lower end of the ball screw is supported by a bearing housing containing a radial roller bearing and two roller thrust bearings. As the ball screw is turned by the dual-drive actuator, the



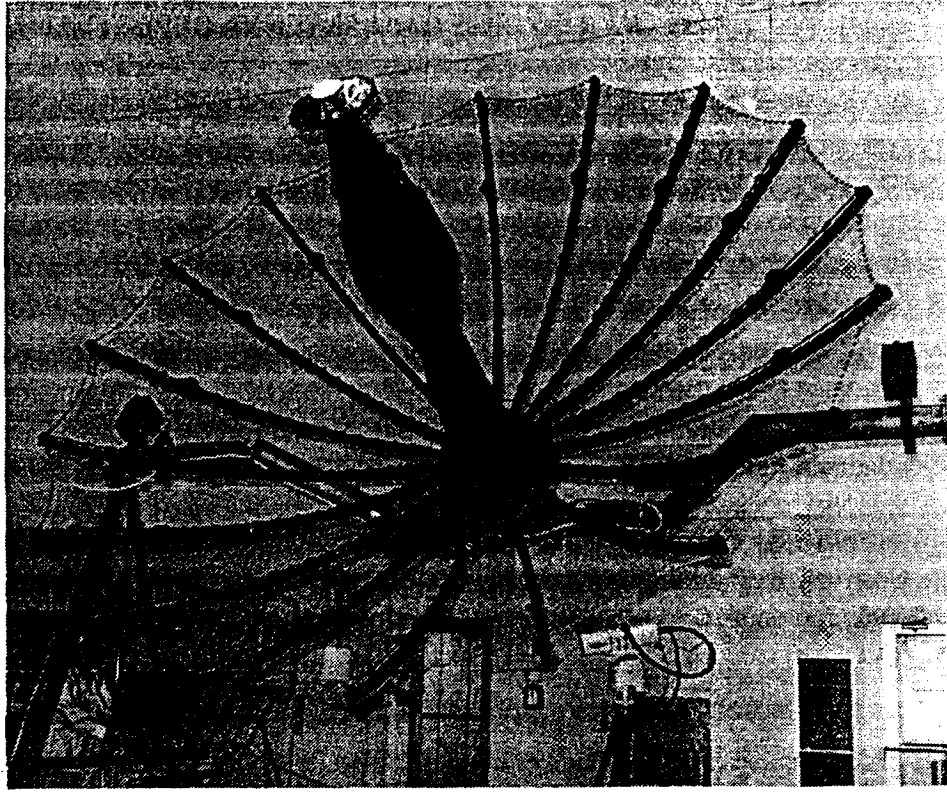
95TR4/V2

Figure 1. Galileo Spacecraft Configuration



95TR4/V2

Figure 2. High-Gain Antenna in the Stowed Position



95TR4/V2

Figure 3. High-Gain Antenna in the Deployed Position

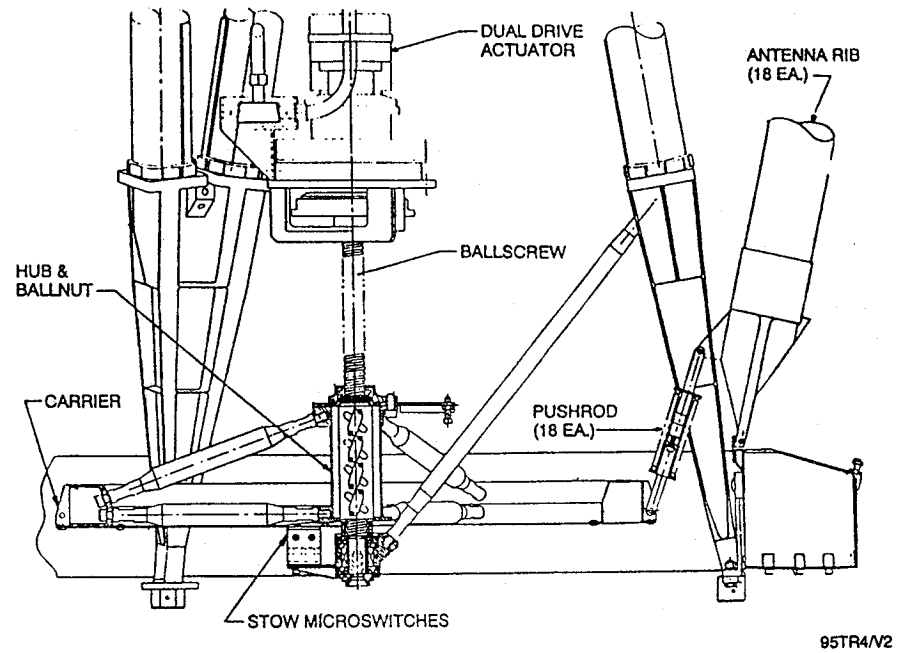


Figure 4. Galileo High-Gain Antenna Mechanical Drive System (Stowed)

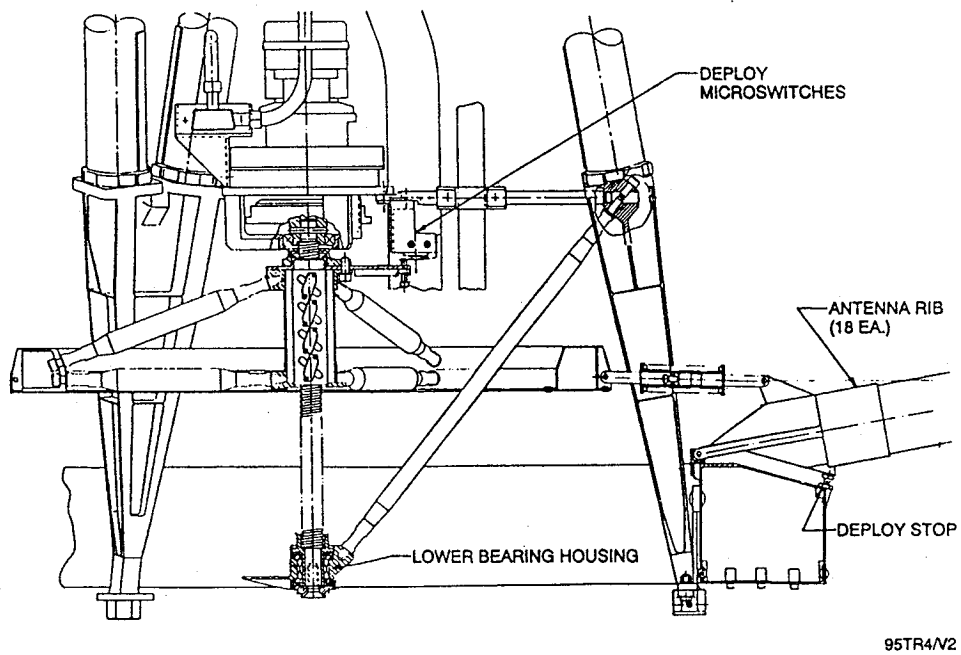


Figure 5. Galileo High-Gain Antenna Mechanical Drive System (Deployed)

carrier, which is prevented from rotating by the pushrods, moves toward the dual-drive actuator. This motion results in the pushrods forcing the ribs to rotate about their pivot point and open out like an umbrella. The motion of the ribs pulls the wire mesh out and stretches it tight, creating the reflector surface. The ribs open out until each rib fitting contacts a mechanical stop, preventing any further deployment of the rib. The continued motion of the carrier compresses a spring on each of the pushrods, preloading the ribs against their stops, and continues until the pushrods pass over center. This maintains a constant preload on the ribs in the deployed direction after the dual-drive actuator is shut off at the fully deployed position.

Figure 6 depicts a rib assembly sectioned to show the pertinent components. The ribs are restrained during launch at the restraint fitting by a spoke assembly that is held in place by the central release mechanism (Figure 7). This mechanism is opened by a spring when the retaining shaft, held in place by a nonexplosive initiator, is released. After launch, the central release mechanism is actuated, releasing all 18 spokes and allowing the mechanical drive system to deploy the antenna. For launch, the spoke assemblies are each preloaded to 378 N (85 lb) and this preload is reacted by two pin-socket combinations called the midpoint restraint (inset, Figure 8). Both pins are titanium 6A1-4V with spherical ends that engage the sockets. The pin receptacle design is shown in Figure 9. One receptacle is a cone and the other a V-groove, which both have included angles of 90° and are made from Inconel 718. The reason for the different receptacle designs was to avoid multiple load paths in case the pins did not have the exact same separation as the receptacles. The two receptacles balance the tension from the spoke preload, the cone locates the rib in the plane of the receptacles, and the V-groove reacts any rotation about the cone receptacle. The tip restraint of the ribs is a pin (shown in Figure 6) in a tuning-fork-like receptacle. This design prevents rotations of the ribs about their midpoint restraints and allows the ribs to move out freely during deployment. A combination of analysis and testing indicated that the primary cause of failure was excessive friction at the pin and socket interface.

Several pin and socket pairs were removed from the spare high-gain antenna for evaluation and testing. The spare high-gain antenna had been through a significant amount of vibration testing that caused relative motion between the pins and sockets. The sockets were made of Inconel 718 with a surface finish of 0.2 microns rms (8 microinch rms). The pins were made from titanium 6A1-4V and were finished with the Tiodize Type II and the Tiolube 460 processes. These processes consist of putting an anodized coating on the titanium and following this with an MoS₂ coating for dry lubrication.

A V-groove socket and its mating pin are shown in Figure 10. The surface of the pin is plastically deformed to a flat spot, as shown by the arrow. Although x-ray diffraction scans of the surface show the presence of MoS₂ on the contact area, scans of some other pins from other ribs showed no presence of MoS₂ on their contact patches. This indicates that the deformation of the surface destroyed the Tiolube and Tiodize coatings. The contact stresses actually exceeded the capability of the pin coatings by about five times. A higher magnification of the upper spot on the V-groove receptacle in Figure 10 is shown in Figure 11. The surface has been deformed and worn away. Scans of the contact surface on the receptacle show a large amount of Ti 6A1-4V, indicating a transfer of base material from the titanium pin.

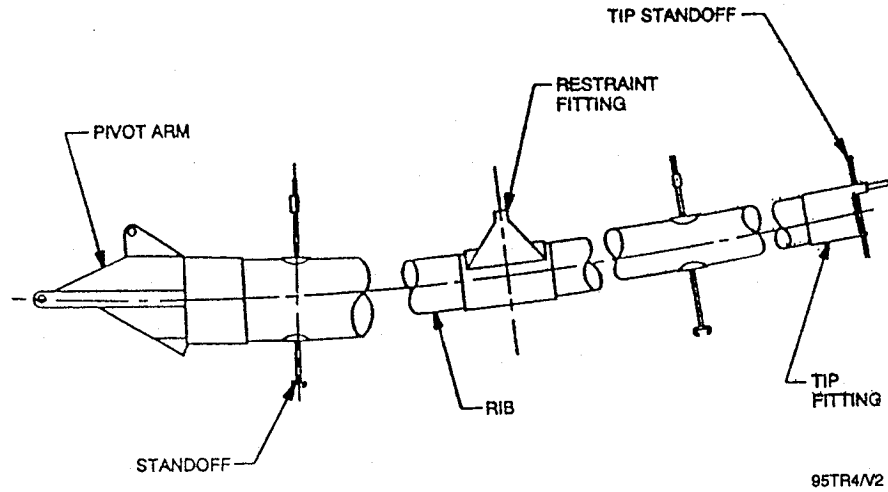


Figure 6. Rib Assembly

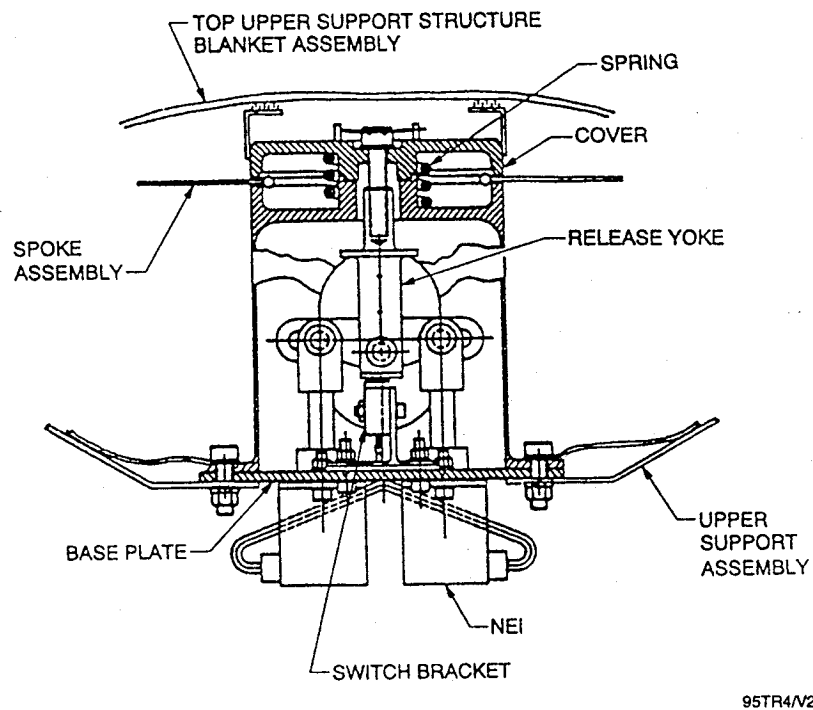


Figure 7. Central Release Mechanism

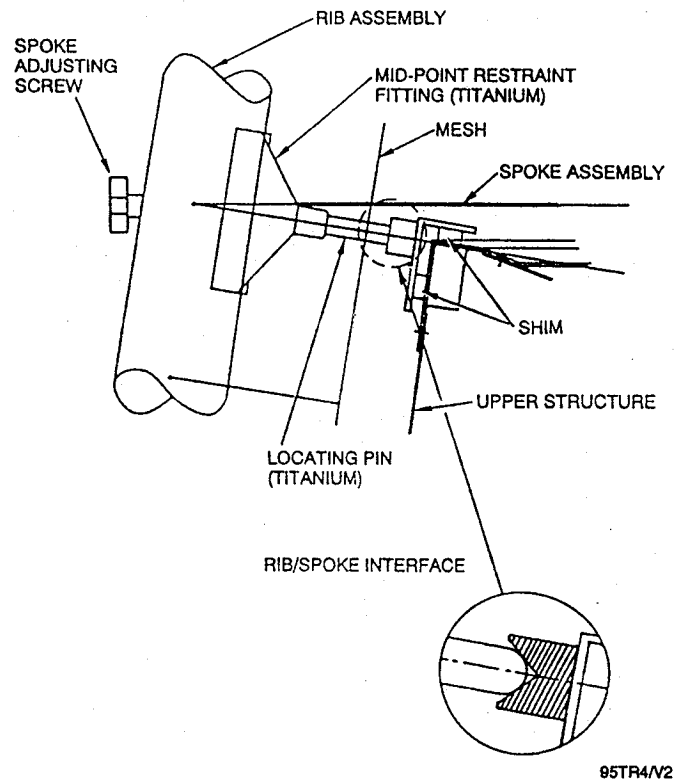


Figure 8. Rib/Spoke Interface

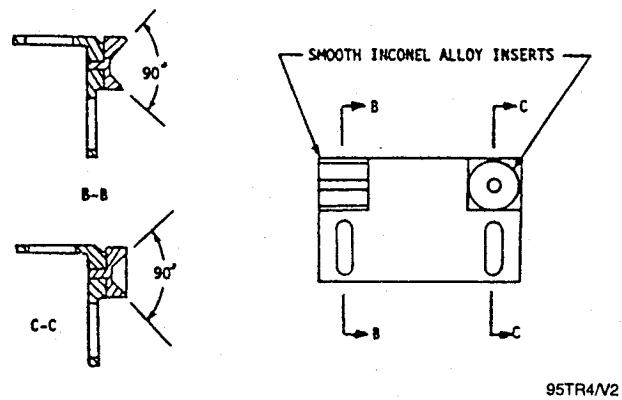


Figure 9. Receptacle Design

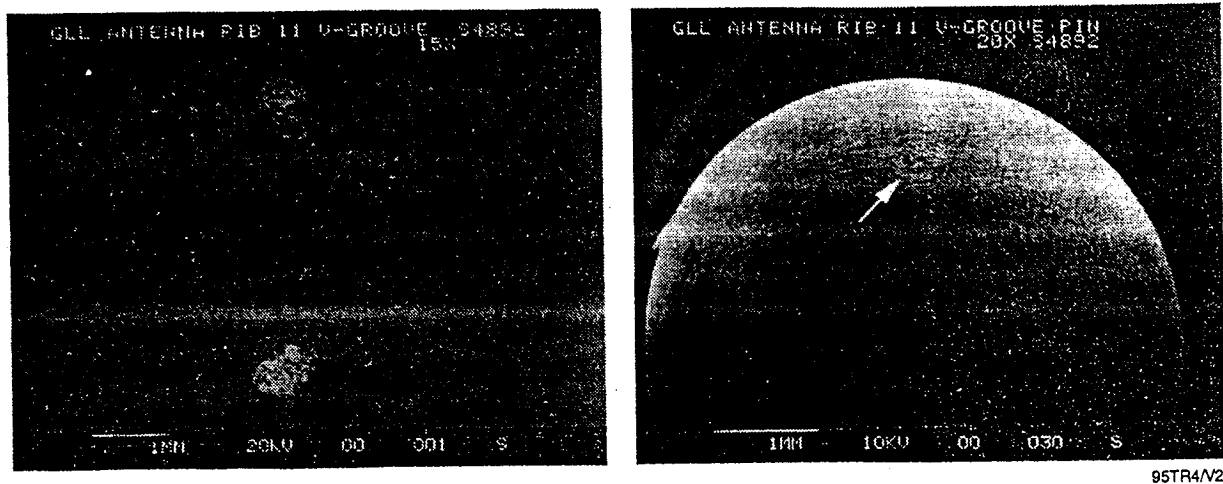


Figure 10. V-Groove Socket and Pin

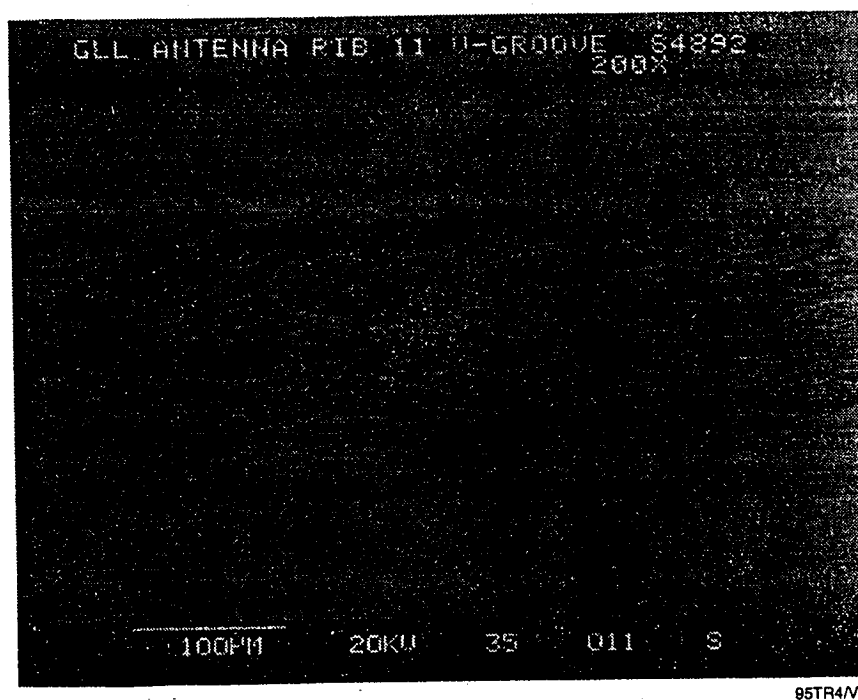


Figure 11. Magnification of Upper Spot on V-Groove Socket in Figure 10

ORIGINAL PAGE IS
OF POOR QUALITY

A series of tests was performed at NASA-Lewis Research Center on the friction properties of dry lubrication and base titanium against Inconel 718. The results of these tests showed that if the two surfaces are displaced relative to each other under load and in air then displaced relative to each other under load in a vacuum, the sliding friction between the surfaces increases nearly ten times. When a dry lubricated and anodized pin was operated in an atmosphere, the dry lubricated surface was quickly destroyed and, as a result, exposed the base titanium. The testing also showed that with an atmosphere present to continue to react with the bare titanium as it was worn by sliding contact, the friction coefficient never exceeded 0.35. However, once a pin's dry lubrication was damaged by operation in air and then operated in a vacuum, the surfaces started to gall and produce coefficients of friction in excess of 1.0.

The failure mechanism required a special set of circumstances in a specific order to cause the deployment anomaly. The events necessary to produce the failure of the Galileo high-gain antenna are summarized in the required order of sequence below:

1. Generate a high enough contact stress to plastically deform the titanium pins and break the ceramic coating that was used to bond the dry lubricant.
2. Produce relative motion between the pins and sockets in an atmosphere to remove the damaged coating and dry lubricant from the contact areas and to produce a rough surface on the mating parts.
3. Produce relative motion between the pins and sockets in a vacuum to remove the oxidized and contaminated titanium from the surface of the pins and then gall both parts so the friction is very high.
4. Produce an asymmetric deployment of the ribs so that the ball screw has a large moment applied to it and cannot produce the force necessary at the midpoint restraint to eject the ribs.

Key Words:

Dynamic Explorer Deployable Devices, Plasma Wave Instrumentation

Mechanisms:

Plasma Wave Instrument

Systems:

Dynamic Explorer Satellite

Authors/Experts:

J. Metzger

Address:

NASA-Goddard Space Flight Center
Mail Code 731
Greenbelt, Maryland 20771

Telephone:**Title:**

Spacecraft Deployable Appendages

Source:

Goddard Space Flight Center (1991)
Engineering Directorate

Abstract:

The dynamics explorer payload was a 1981 Delta vehicle launch and consisted of two spacecrafts: the dynamics explorer A (DE-A) and the dynamics explorer B (DE-B) joined by an 1809-A separation adapter. The 1929-lb payload included a total of 375 lb distributed among 15 instruments, many of which had deployable features. Of particular interest is the DE-A spacecraft, which was spin stabilized and carried the plasma wave instrument. The deployables for this instrument were four radial long-wire antennas; two spin-axis spin antennas; and a group consisting of a search coil, short electric antenna, and a 1-meter² loop

antenna. This group was mounted to a single plate and deployed to a radial distance of 6 meters by means of an Astromast boom. Due to its physical size, the loop antenna was folded and secured along the side of the spacecraft body to fit within the launch vehicle shroud. Consequently, successful deployment of the loop was required before extension of the Astromast could commence. A similar boom carrying a magnetometer was located on the opposite side of the spacecraft and provided a counterbalancing effect. These deployments were mission critical and appropriate analysis and testing were conducted to demonstrate design adequacy and reliability.

Anomalies:

An end-of-travel shutoff switch failed to activate during Astromast deployment. The Astromast was returned to the manufacturer for investigation of a switch problem.

Lessons Learned:

- Comprehensive testing is required to assure proper operation of deployable device.
- Microswitch failure is serious; redundancy may be necessary.

Description:

The design of these deployed appendages was conducted primarily with hand calculations, with some computer-aided design simulations for verification. In order to accommodate the plasma wave instrument, the stowed position of the loop was compared to the deployed position and the intersection of the two planes represented the hinge axis for initial deployment of the loop (see Figure 1). Due to a nonintegral number of turns to deploy the Astromast, which rotates as it deploys, combined with a nonperpendicular alignment of the loop with

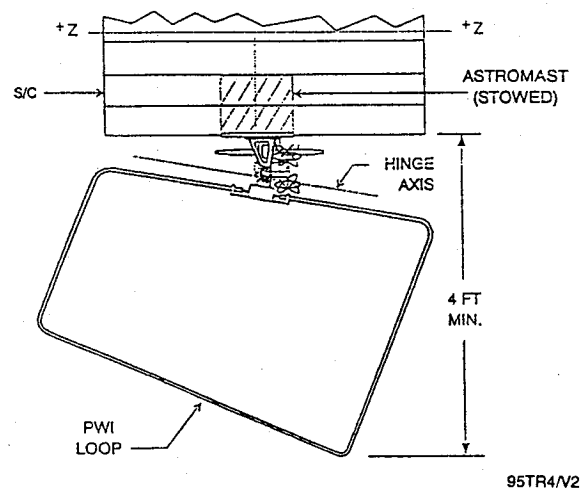


Figure 1. Plasma Wave Instrument Loop

the boom axis, the hinge axis was placed at a skew angle. A coil-type deployment spring was included for the loop to ensure a wide range of spacecraft spin rates. This spring was sized using energy principles to also account for loop strain at lockup, flexing of electrical cables and friction where only a dry film lubricant was used. Lockup was achieved by bending a leaf spring which contained a cutout to capture a detent on the moving part of the hinge and also helped to reduce the shock loads. With deployment ranging between 0 and 30 rev/min, the worst-case stresses were calculated and showed a margin of safety of 1.5 against yielding for the loop. The stowed position of the loop is shown on Figure 2, and the Astromast deployment configuration is shown on Figure 3.

Testing:

For hardware qualification, a series of tests was conducted using a relatively high fidelity mechanical test model, which included most protoflight structure and mechanisms.

The structural dynamics test sequence consisted of a model survey, several sine vibration runs, an acoustics test, pyroshock/separation, and qualification tests for all the mechanisms. Thermal-vacuum testing was also conducted. The plasma wave instrument loop was designed to be handled and installed in a 1-g environment but the effect of gravity would distort the loop in the deployed configuration with the spacecraft spin axis in the normal upright position. Since the flight deployment would take place with a spinning spacecraft and a radial acceleration field that would be equivalent to slightly less than 1 g, it was decided to tilt the mechanical test module on its side and test the loop downward with an approximately 1-g radial force field. This provided 20% margin over the maximum design spin rate for deployment of 30 rev/min and eliminated the need for any special g-negation equipment. The testing was successfully completed with no significant problems reported and no design changes were needed.

The deployment was initiated by firing one of two pyrotechnic dimple motors and the motion was recorded on high-speed film. The test setup is shown in Figure 2.

Plasma Wave Instrument Antenna Deployment Test Results. Prior to installation, the weight of the plasma wave instrument loop and preamp assembly was measured at 895 gm (1.97 lb). The loop antenna was released and deployed in 543 msec with microswitch closure occurring approximately 30 msec prior to lockup. The predicted deployment time was 423 msec and the difference can be attributed to hinge friction, air drag on the loop, and stiffness of the electrical cabling.

Dynamics Explorer Astromast. Two diametrically opposed Astromasts were deployed nearly simultaneously on the DE-A spacecraft. The deployment began at a spacecraft spin rate of approximately 25 rev/min. It took place in several steps, with a spin-up maneuver occurring at some intermediate position. Each Astromast achieved its full length of 20 ft at a spacecraft spin rate of 10 rev/min. The centrifugal acceleration experienced by the tip mass, tending to extend the Astromast, ranged between 0.5 g and 0.8 g, depending upon the spin rate and length of mast deployed. Final tip position and alignment were required to be within $\pm 0.2^\circ$ of nominal. The Astromast was caged for launch and pyrotechnically released for deployment. Since the coiled elements of the mast contained more than enough energy to effect deployment, a motor-driven lanyard was used to restrain and control the deployment and even retract it if desired.

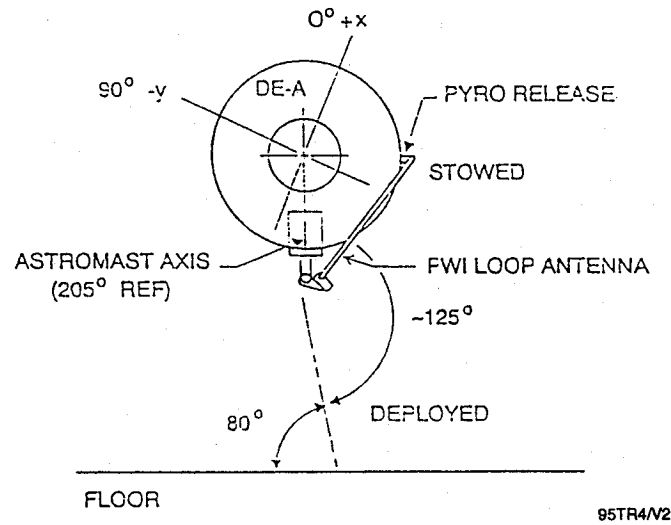


Figure 2. Plasma Wave Instrument Loop Deployment Test Configuration

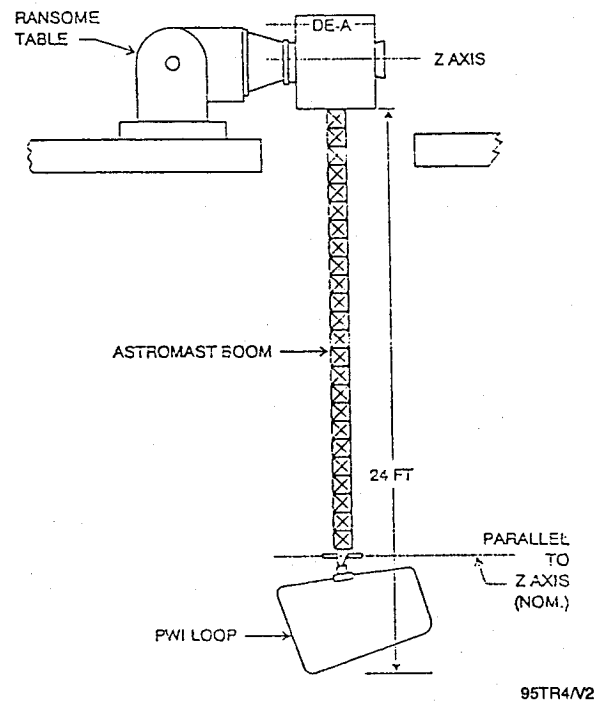


Figure 3. Astromast Deployment Configuration

Dynamics Explorer Astromast Deployment Test Description. With the spacecraft in the horizontal position, the Astromast was deployed straight down with the force of gravity representing the centrifugal force from spinning spacecraft and tending to aid the deployment.

The objective of this test was to complete qualification of the plasma wave instrument loop and stub boom hardware by demonstrating compatibility with the Astromast and its unique deployment dynamics. Specific areas of interest included clearance between the plasma wave instrument short electric antenna and the spacecraft during initial Astromast motion. The entire deployment was photographed at normal speed from two camera angles. The test setup is shown in Figure 3.

Dynamics Explorer Astromast Deployment Test Results. Observation of the plasma wave instrument group (attached to the end of the Astromast) during each step of the deployment revealed no incompatible problems. It was noted, however, that the final tip orientation was rotated approximately 1° counterclockwise from its normal position. Although this was a crude measurement, it did warrant further investigation for the flight units to ensure proper final instrument alignment. It was also noted that the deployed length potentiometer displayed voltage changes opposite to those expected from the given schematic and also warranted further investigation. One significant anomaly was encountered during this test when the end-of-travel shutoff switch failed to actuate. The mast was observed to reach full extension but drive power did not terminate automatically. Power was controlled manually for an additional 12 sec in an unsuccessful attempt to produce switch actuation. A continuity check verified that the dual switch had remained closed. In order to avoid the loss of the lanyard, no further extensions were attempted. Retraction of the mast was accomplished without incident. Following this test, the Astromast was removed from the spacecraft and returned to the manufacturer for investigation of the switch problem.

Experience:

Following launch of the spacecraft, both loop and Astromast were successfully deployed according to plan and no anomalies were reported. The key philosophy in this effort was to keep things as simple as possible and to draw upon design experience gained from previous programs.

Dynamics Explorer Plasma Wave Instrument Loop Antenna. Once the DE-A spacecraft was placed in orbit, the various instrument deployments took place. Among these was the plasma wave instrument loop antenna release that occurred nominally at a spin rate of 25 rev/min. The antenna was preloaded to enhance the initial motion and pyrotechnically released. The motion terminated against a hard stop and end of travel was indicated by the actuation of a microswitch. A latch prevented backlash. The nominal radial acceleration during deployment ranged from 0.5 g to 0.9 g, due to spin rate. The stub boom and loop antenna are shown in Figure 1 as they appeared prior to Astromast extension.

Plasma Wave Instrument Antenna Deployment Test Description. A Ransome table was used to place the spacecraft in the horizontal position with the stub boom oriented straight down so that the loop antenna would experience 1-g acceleration during its free-fall deployment. Although deployment was expected to take place at a spin rate of 25 rev/min, it was designed for at least 30 rev/min. Justification for such a free-fall deployment lies in the fact that the energy absorbed by the loop in this test was calculated to be 1.2 times the energy during a deployment at 30 rev/min. This represents a 20% overtest for design qualification. In addition, a stress analysis on the loop design showed a margin of safety of 51% for the 1-g deployment.

Actuators, Transport Mechanisms, Switches

Key Words:

Brake Materials, Friction Materials

Mechanisms:

Systems:

Author; Experts:

H.M. Hawthorne

Address:

Tribology and Mechanics Laboratory
NRCC
Vancouver, Canada

Telephone:

Title:

Tribomaterial Factors in Space Mechanism Brake Performance

Source:

Abstract:

Dehydration of brake materials and accumulation of wear debris trapped between the opposing surfaces can cause a marked reduction in the friction of brake materials. Problems have been encountered with the friction elements of the shuttle remote manipulator system. These elements are pairs of annular pads of an asbestos/phenolic composition. When slip-tested under load, the pads show a greatly diminished friction in vacuum, which is fully recovered on return to atmosphere. It has been established that a reduced friction torque is normal when this composite material has reached an equilibrium in vacuum. Experimental studies have been made to find materials that will give stable, high friction values, even after long exposure to high vacuum.

PRECEDING PAGE BLANK NOT FILMED

Anomalies:

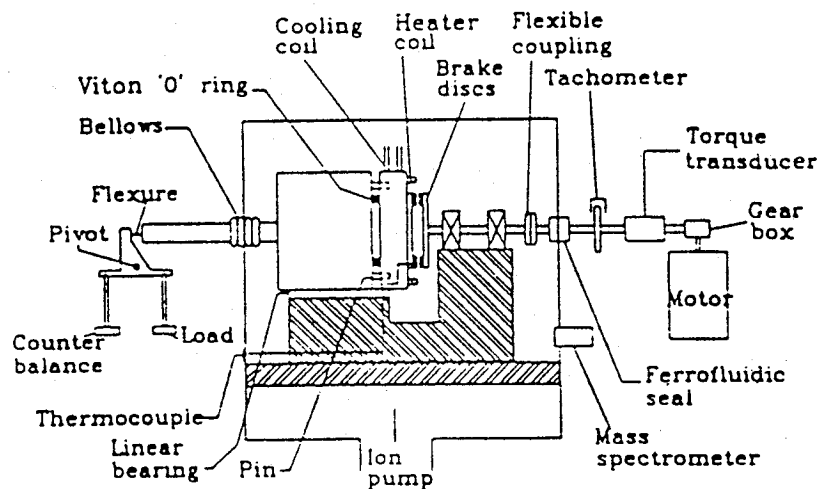
- The asbestos/phenolic considered as a candidate brake material produced unacceptably low friction in vacuum, although it was acceptable in air.
- Polymers will not provide sufficient friction for use as a brake material in vacuum.

Lessons Learned:

- Dehydration of brake materials and accumulation of wear debris, trapped between opposing surfaces can cause a marked reduction in the friction of brake materials.
- Some ceramics or cermets can provide stable and moderately high friction as brake materials. This group includes Cr_2O_3 and $\text{Al}_2\text{O}_3/\text{SiC}$.
- To ensure in-vacuo stable friction, run-in of opposed surfaces is recommended.

Description:

Figure 1 is a schematic of the test rig that was used. It was designed to provide an oil-free vacuum, below 1.3×10^{-4} Pa (10^{-6} torr). The friction and wear behavior of materials was determined from tests that involve continuous unidirectional, or reciprocating (60 sec clockwise, 10 sec off; 60 sec counterclockwise) sliding of one specimen versus another at 100 rpm with loads up to 70 N (bearing stress 0.14 MPa).



95TR4/V2

Figure 1. High-Vacuum Tribometer

Figure 2 shows the results of tests with the asbestos/phenolic. The initial drop in friction corresponds to a reduction in water vapor. Although the first step must be dehydration, the low-slip torque develops as a result of microstructural changes at the sliding interface. Wear debris is generated at the rubbing surface and is trapped in the contact area. It is the structure and properties of this debris that determines the frictional behavior. Figure 3 shows the friction trends for a number of polymers. The author believes that the low friction of these materials is the result of localized wear debris features being formed on worn surfaces. Measurements show that these topographical features are raised above the surface. During sliding, they confine the load to a small contact area. Although the shear strength of the debris will have some effect, the low-torque output is mainly due to this restricted contact area.

Ceramics showed widely different trends when they were evaluated in vacuum. After run-in, the friction behaved in a variety of ways, as shown in Figure 4. Low friction was obtained when the interface developed a few isolated contacts as islands of raised wear debris. In contrast, surfaces that developed a matte appearance gave moderate to high friction. The appearance of the surfaces was a good explanation as to why or how this relates to friction. It was concluded that:

1. The low friction anomaly of the asbestos/phenolic is an inevitable consequence of its use in vacuum.
2. The friction in vacuum is determined by the residual moisture level and then by the structure and properties of the dry interfacial debris layer.
3. All polymers studied gave low friction through the development of minimal contact wear debris patches.
4. Ceramics can give a variety of frictional outputs, depending on the interfacial wear debris characteristics. Limited contact gives low friction, more extensive (matte) contact gives higher friction.
5. Some ceramics can be tailored by run-in to form finely distributed wear debris and to provide stable, high friction.
6. Some of the compositions that meet the No. 5 criteria may be useful for brakes in space.

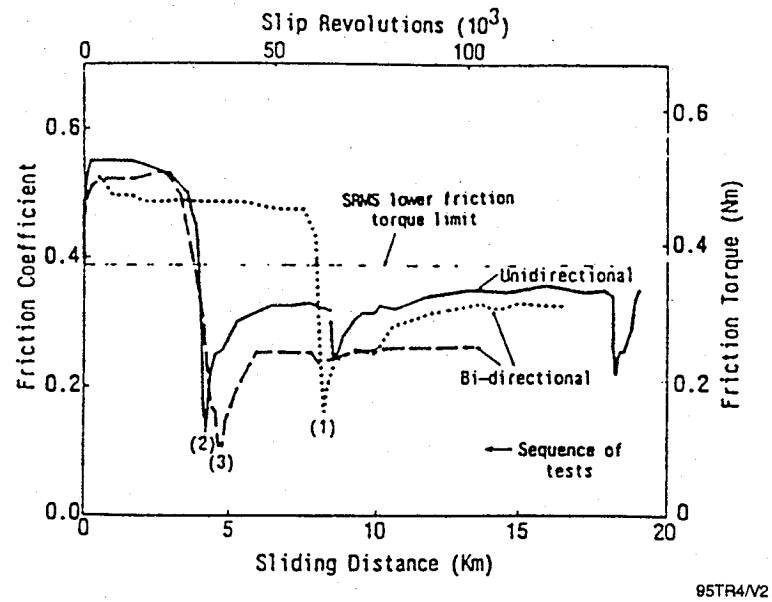


Figure 2. Friction Trends from Slipping of SRMS Brake Material in Vacuum

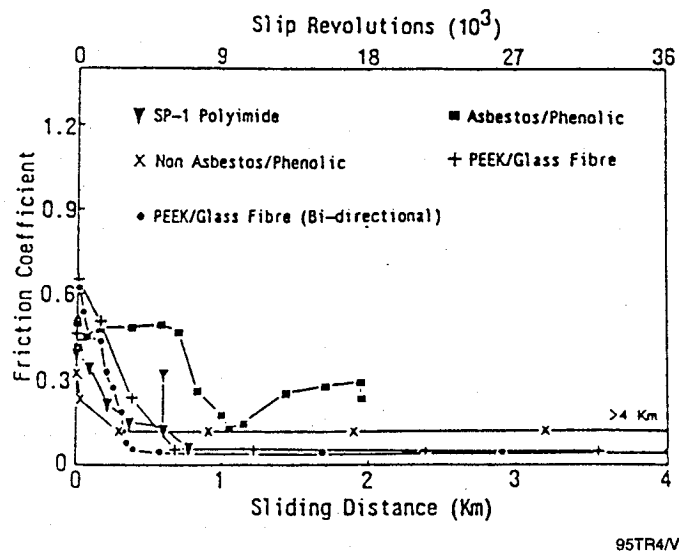


Figure 3. Friction Trends from Sliding of Various Polymeric Compositions in Vacuum

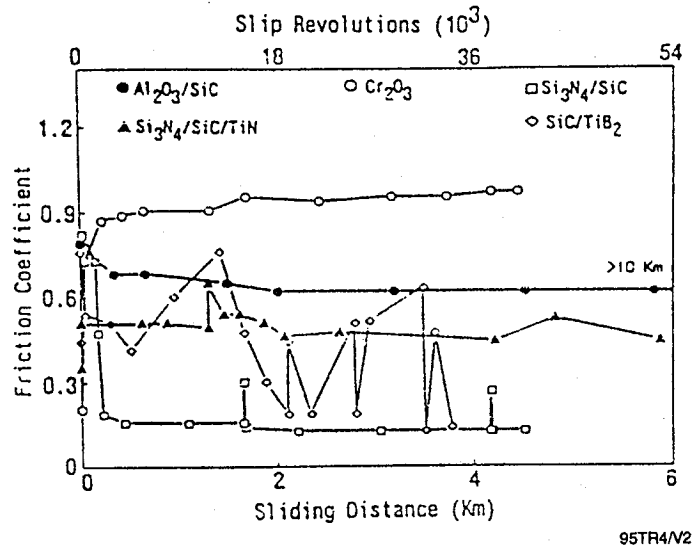


Figure 4. Friction Trends from Sliding of Various Polymeric Compositions in Vacuum

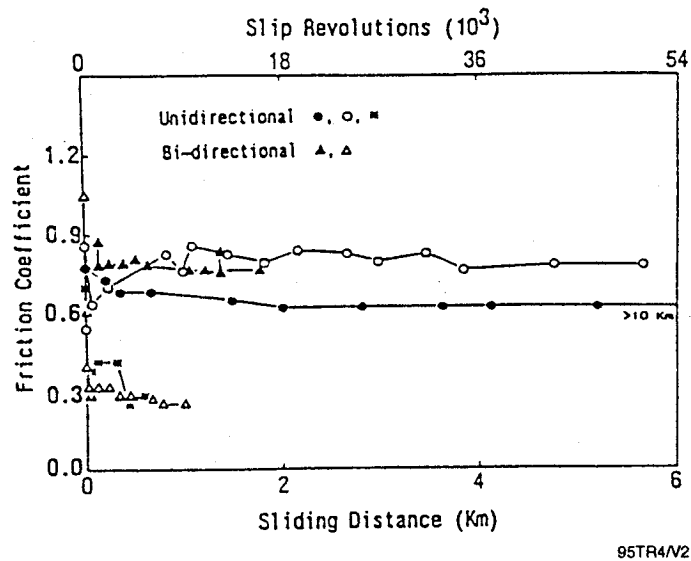


Figure 5. Different In-Vacuo Friction Trends from Separate Tests of the Same Pair of $\text{Al}_2\text{O}_3/\text{SiC}$ Specimens

Table 1. Wear of Polymeric and Ceramic-Based Materials in High Vacuum Conforming Contact Sliding Tests

Material	Specific Wear Rate* ($\times 10^{-5}$ mm ³ /Nm)
Polyimide (SP 1)	29.
Asbestos/phenolic	1.5 (high μ)
Asbestos/phenolic	1.0 (mixed μ)
Nonasbestos/phenolic	1.1 (mixed μ)
PEEK/glass fiber	0.7
Al ₂ O ₃ /TiO ₂	43
Si ₃ N ₄ /SiC	15. (high μ)
WC/Co	13
Al ₂ O ₃ /SiC	11. (high μ)
Al ₂ O ₃	7.5
Si ₃ N ₄ /SiC/TiN	6.5
SiC/TiB ₂	4.5
Cr ₃ C ₂ /NiCr	0.8
MoS ₂ /Nb/Mo/Cu	0.6
Cr ₂ O ₃	0.6
Si ₃ N ₄ /SiC	0.5 (low μ)
Cr ₂ O ₃ versus 440C steel	0.4
Al ₂ O ₃ versus 440C steel	0.2

95TR4/V2

*Mean value of two sliding specimen disks.

Key Words:

Deployment Actuator, High-Gain Antenna, Actuator, Springs, Fluid Dampers

Mechanisms:

Systems:

Author; Experts:

S.R. Jones

Address:

Honeywell Satellite Systems Operation
Glendale, Arizona

Telephone:

Title:

Topex High-Gain Antenna System Deployment Actuator Mechanism

Source:

Abstract:

A deployment actuator mechanism has been developed to drive a two-axis gimbal assembly and a high-gain antenna on the Topex satellite. The design and test phases are discussed in this paper.

Anomalies:

- Post-vibration inspection showed that the dry lubricant film in the journal bearing was flaking, causing an increase in torque. The problem was determined to be excessive lubricant film thickness. Applying the lubricant to one bearing surface, rather than both, and burnishing the film to reduce thickness resolved the problem.

- During thermal-vacuum deployment testing, noise appeared on one channel of the redundant potentiometer. A failure analysis investigation revealed contamination on the windings. A review of the materials and processes used in the manufacture of the part showed that the contamination is not an inherent problem and is probably an isolated incident. Five qualification parts are being tested for signs of contamination. In addition, the spare flight part is being screened to establish flight worthiness.
- The most serious problem is related to thermal-vacuum operation of the viscous fluid rotary damper and is characterized by a region of undamped travel immediately after deployment has been initiated, followed by normal operation throughout the remainder of the travel. The phenomenon is random in nature and has occurred at hot and cold temperatures. The maximum undamped travel was 15°, resulting in unacceptably high impact loads in the damper input shaft as damper operation returned to normal. Because a potentiometer was not installed to provide positional telemetry during engineering model thermal-vacuum testing, the problem did not become apparent until acceptance testing of the flight unit.

It was suggested that an air pocket or void might be the cause of this problem, or that the method used for compensating changes in the fluid volume overtemperature was responsible. In spite of procedural changes, the anomaly still existed and the decision was made to replace this unit with a customer-furnished damper.

Lessons Learned:

- Although the viscous rotary damper has been used successfully in other satellite applications, there are some unknowns that must be resolved before it can be used with high confidence.
- Excessive lubricant can cause increased torque. Lubricant should be applied sparingly and burnished in to reduced film thickness.

Description:

Figure 1 shows the deployed high-gain antenna system on the Topex satellite. The major components are a two-axis gimbal assembly, a high-gain antenna, a cradle assembly, and a deployment actuator mechanism with a 1.4-meter long, 0.15-meter diameter thin-wall aluminum mast. A layout of the stowed high-gain antenna system is shown in Figure 2.

The high-gain antenna system will be launched in a stowed configuration and deployed once the satellite is in orbit. During launch, the two-axis gimbal assembly and the high-gain antenna are supported by the cradle assembly using three pyrotechnically actuated separation bolts. Once in orbit, the bolts are fired, and the deployment actuator mechanism drives the two-axis gimbal assembly and the high-gain antenna to a fixed 90° position with respect to the spacecraft. As the deployment nears completion, a pair of lockpins engage to secure and align the system.

This is a one-time deployment with manual retraction capability for ground testing. Redundant motors, bearings, lock assemblies and lock and position telemetries are required. Full deployment must be complete in 1800 sec. The mechanism must also be thermally isolated from the spacecraft.

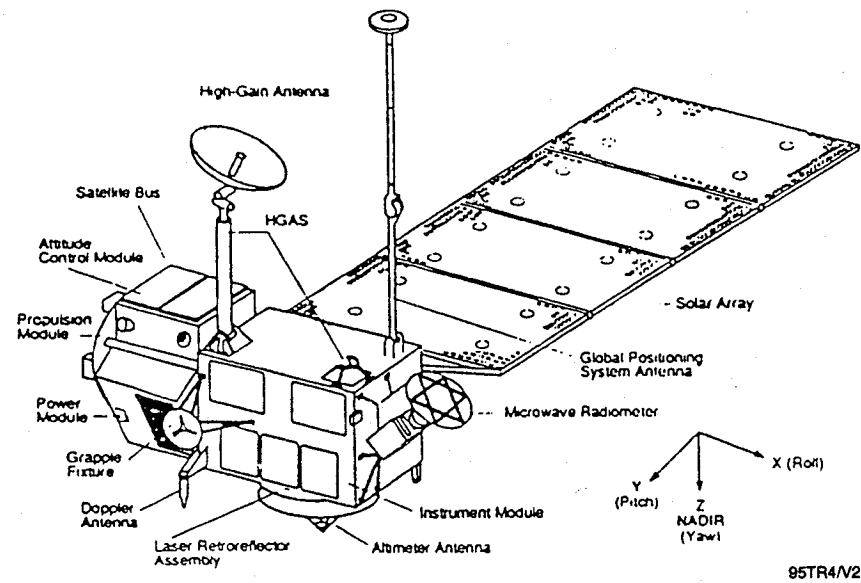


Figure 1. Topex Spacecraft High-Gain Antenna System

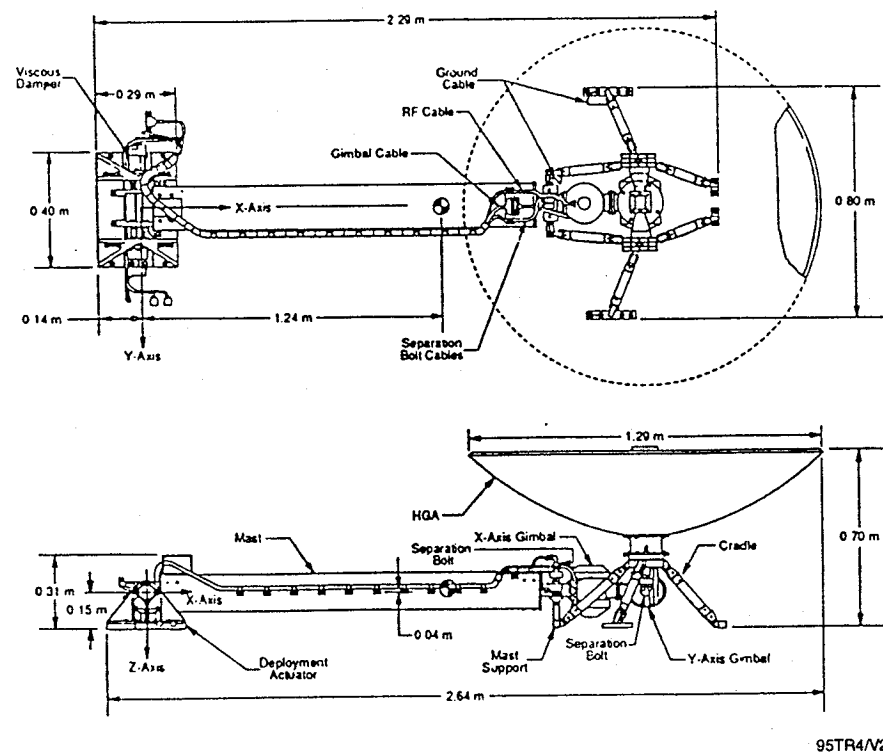


Figure 2. Topex High-Gain Antenna System Layout

Mechanical Design. The deployment actuator mechanism is a passive device, driven by a pair of multileaf negator springs. A viscous fluid rotary damper limits the rate of actuation. A pair of spring-driven, wedge-shaped lock pins align and secure the system as the deployment is finished. A redundant bearing design is used that features a lined spherical bearing and a dry lubricated journal bearing. Either can act as the rotating surface. A two-channel ganged potentiometer provides positional telemetry during deployment and a pair of microswitches indicate the locked position. Figure 3 shows the layout of the actuator and Figure 4 details the negator spring. A pair of 3.6-Nm six-leaf springs were used, each capable of deploying the system.

Table 1 presents the requirements and capabilities of the system; Table 2 shows the thermal vacuum deployment test results.

The selected viscous fluid rotary damper is a small, light, limited-rotation device that produces approximately 452-Nm damping at room temperature. Similar devices have flight history on commercial satellites as well as the Goddard cosmic background explorer satellite. Damping is produced through viscous shear of 30,000-centistoke McGahn Nusil CV7300 silicon fluid between a rotating vane shaft and a stationary housing. A bypass valve provides adjustability of pressure side of the vane shaft to the low-pressure side. The damper uses a reservoir with a flexible diaphragm to compensate for fluid volume changes with temperature. The reservoir interfaces with the damping chamber through a set of check ball valves that isolate the high-pressure side of the vane shaft from the reservoir during damper operation. A cross section is shown in Figure 5.

The bearing design must be capable of carrying launch and thermal-induced loads and must provide for a single, limited-rotation, low-speed deployment once in orbit. A spherical bearing with a Teflon-impregnated Nomex liner, in conjunction with a dry lubricated journal bearing at the shaft-to-inner-race interface, proved adequate. A layout is presented in Figure 6. The spherical bearings are manufactured to MIL-B-81820 and feature a low no-load breakaway torque, tight radial clearance, and a high static load-carrying capability. The dry lubricant meets the requirements of MIL-L-81329 and consists of molybdenum disulfide (MoS_2) and graphite in a sodium-silicate bonding agent.

The lock assembly must align and lock the deployment actuator mechanism in the deployed position. The lock assembly consists of a pair of wedge-shaped, spring-loaded pins, which preload adjustment screws against a hard stop, as shown in Figure 7. The adjustment screws allow for precise alignment of the deployed system, and the preload provided by the wedge-shaped pins results in zero backlash. A tool allows the pins to be retracted for restowing during test.

The thermal isolation requirement was met by installing NEMA FR4 epoxy laminate thermal isolating pads on each side of titanium mounting bolts at the spacecraft interface. The damper utilizes a heated cover and is thermally isolated from the surrounding structure to ensure that it is maintained above its minimum operating temperature. Additional thermal control measures consist of gold plating and thermal blankets.

Positional telemetry is provided during deployment by a redundant, single-shaft, wire-wound potentiometer that interfaces with the deployment actuator mechanism shaft. A pair of microswitches indicate when the system is fully deployed and lock pins are engaged.

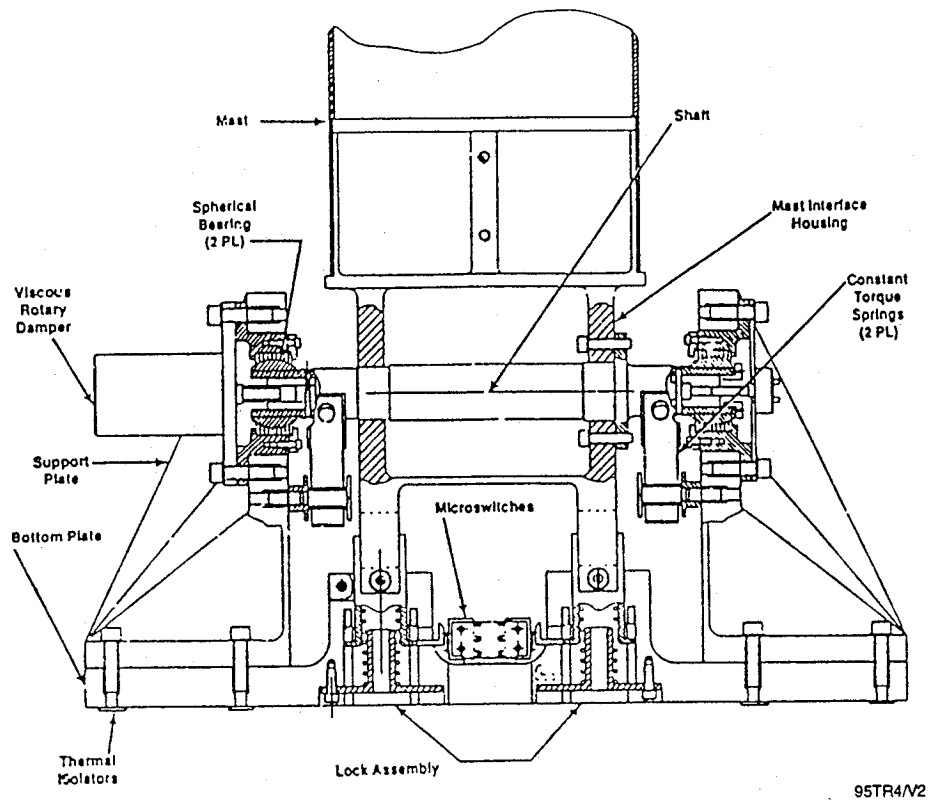


Figure 3. Deployment Actuator Layout

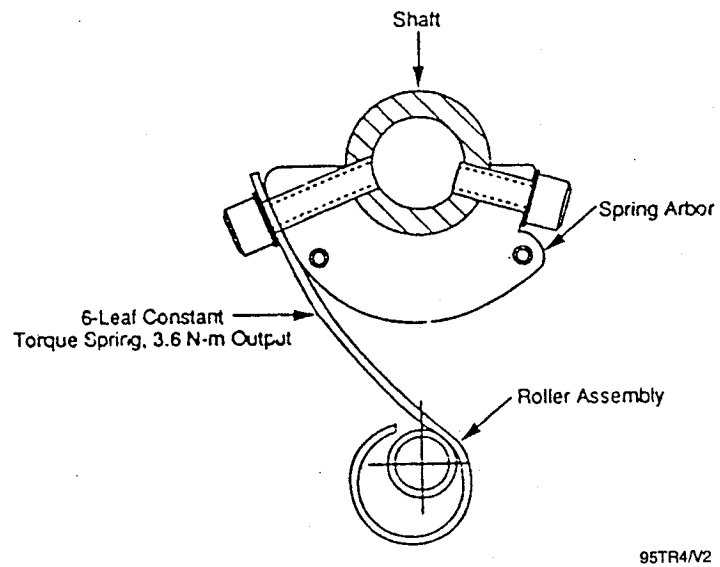


Figure 4. Constant Torque Spring Detail in the Deployed Position

Table 1. Requirements and Capabilities

Parameter	Requirement	Capability
Mass (kg)	<18.1	12.6
Footprint (m x m)	0.40 x 0.29	0.40 x 0.29
Operating Temperature (°C) Maximum Minimum	38.0 11.5	58.0 -8.5
Nonoperating Temperature (°C) Maximum Minimum	63.0 -7.5	83.0 -27.5
Deployment Time (sec) 58°C -8.5°C	>45 <1800	45 300
Spring Torque (Nm)	6.8	7.0
Drag Torque (Nm)	<1.7	0.9
Torque Margin	>4.0	7.8
Damping Rate (Nm/rad/sec) 58°C -8.5°C	>147 <4859	169 at 75°C 1356 at -20°C
Alignment (degree) Initial Repeatability	0.05 0.05	0.05 0.02
Deployed Stiffness (Hz)	>5.0	7.2

95TR4/V2

Table 2. Thermal-Vacuum Deployment Test Results

Test	Temperature (°C)	Deployment Time (sec)	Average Damping (Nm/rad/sec)	Undamped Travel (degree)
1	29.8	87	376	1.9
2	-8.8	220	943	2.2
3	-7.5	218	956	4.2
4	59.0	45	210	6.4
5	-6.8	214	917	1.9
6	-8.4	238	1022	1.8
7	58.3	48	1965	3.9
8	22.4	108	4166	2.1
9	58.5	46	1997	10.1

95TR4/V2

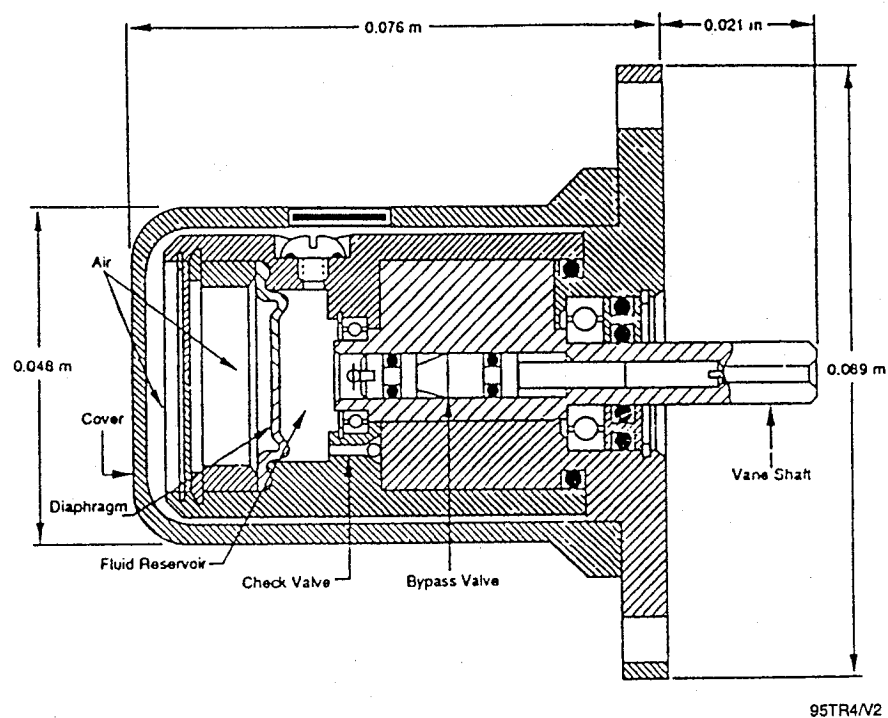


Figure 5. Rotary Damper Cross Section

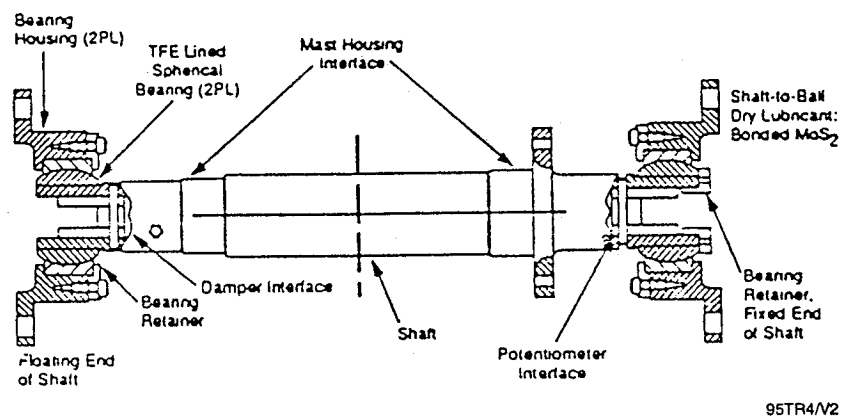
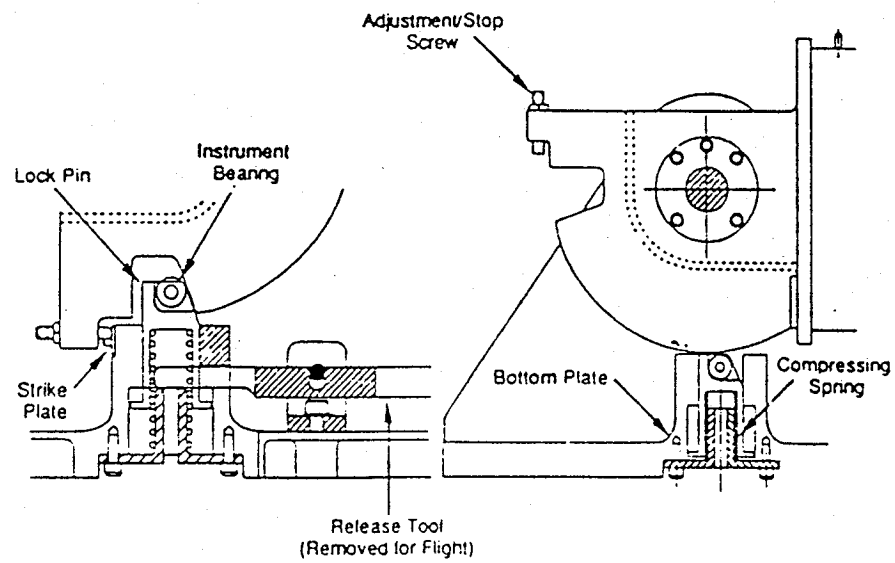


Figure 6. Bearing Detail



95TR4/V2

Figure 7. Lock Assembly Detail

Key Words:

Upper Atmospheric Research Satellite (UARS), Solar Array Retention, Deployment, and Jettison Assembly

Mechanisms:

Solar Arrays, High-Gain Antenna, Zenith Energetic Particle System (ZEPS) Boom

Systems:

UARS

Author; Experts:

W. Leary

Address:

NASA-Goddard Space Flight Center
Mail Code SAI
Greenbelt, Maryland 20771

Telephone:

Title:

Spacecraft Deployable Appendages

Source:

Goddard Space Flight Center (1990)
Engineering Directorate

Abstract:

The UARS is described and an anomaly discussed with a plunger-activated, hermetically sealed switch. The problem was due to gravity effects during ground testing. The problem was resolved by reorienting the switch and covering the plunger.

Anomalies:

- The switches used on all mechanisms were Honeywell 10HM30-5RELPGM miniature hermetically sealed units. The auto-stow function operated the two gimbal motors to their respective ready-to-latch position, where actuation of the switches caused power shutoff to the motor. One set of switches was actuated by a rotary cam with its travel being at 90° to the switch axis, the other by a linear plunger which moved parallel to the switch axis. A problem occurred with the design when attempting to adjust it on the ground under 1-g conditions. In the orientation at the time, gravity effects caused the plunger to deflect away from the switch preventing motor cutoff at the desired position. The switch was limited in its overtravel capability, so adjustments to make it work properly on the ground would cause destruction of the switch on orbit (in 0-g conditions).
- The design solution was to redesign the switch activation device and make it similar to the cam operated switches. Instead of a rotary cam, however, the actuation was done by using the linear motion of a rod which was stepped with two diameters (Figure 1). This arrangement was not critical to linear motion. Overtravel was limited by the two diameters. This allowed for both ground testing and on-orbit operation.

Lessons Learned:

- Mechanisms must be designed for both ground test and space operation.
- Plunger designs of switches could pose problems on ground test due to gravity. Cam actuation may be preferable.

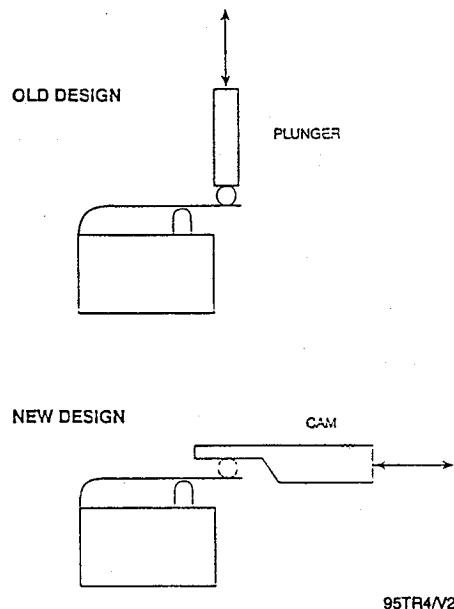


Figure 1. UARS Switch Actuation Redesign Solution

Description:

The deployed UARS is shown on Figure 2. The UARS contained three deployable appendages.

1. Solar Array Retention, Deployment, and Jettison Assembly. The solar array retention, deployment, and jettison assembly contained redundant springs in the solar array panel and strut hinges for deployment, redundant stepper motors to regulate the rate of deployment, and redundant initiators in the separation nuts for jettison release.

The six panels of the solar array were stowed by four retention bolts. Solar array deployment was initiated by firing the separation nuts. Deployment was completed by motor drive.

2. Solar Stellar Position Platform Instrument and High-Gain Antenna Gimbal Retention Subsystems. The solar stellar position platform and the high-gain antenna used identical two-axis gimbal mechanisms. The solar stellar position platform was restrained at two points between the gimbal interface and the front face of the solar stellar position platform and at two points between the platform structure and the gimbal support structure. Gimbal lockout for the high-gain antenna was provided at three points between the antenna extension boom structure and the gimbal support adapter. Each retention point consisted of a cup/sphere assembly held together by an overcenter in-line linkage operated by dc motors. The drive motors were operated in series for redundancy and incorporated a specific detent torque to retain the proper linkage position during all mission phases.
3. UARS Deployable ZEPS Boom. The ZEPS boom was a truss assembly consisting of three 13-ft long glass/epoxy longerons, triangular battens, and diagonal stiffeners between battens. The boom was stored in the instrument canister by coiling the longerons into interlacing helices. The ZEPS instrument mounting plate was attached to the end of the longerons and was latched to the canister until deployment. Boom extension was initiated by activating the latch and the deployment mechanism motor. Deployment was effected by the stored energy in the longerons and regulation was provided by redundant dc motors that metered out a lanyard connected to the instrument mounting plate. The boom could be restowed by reversing the direction of the motor. The retention system of the ZEPS boom prevented boom deployment until a safe separation distance had been reached by the orbiter.

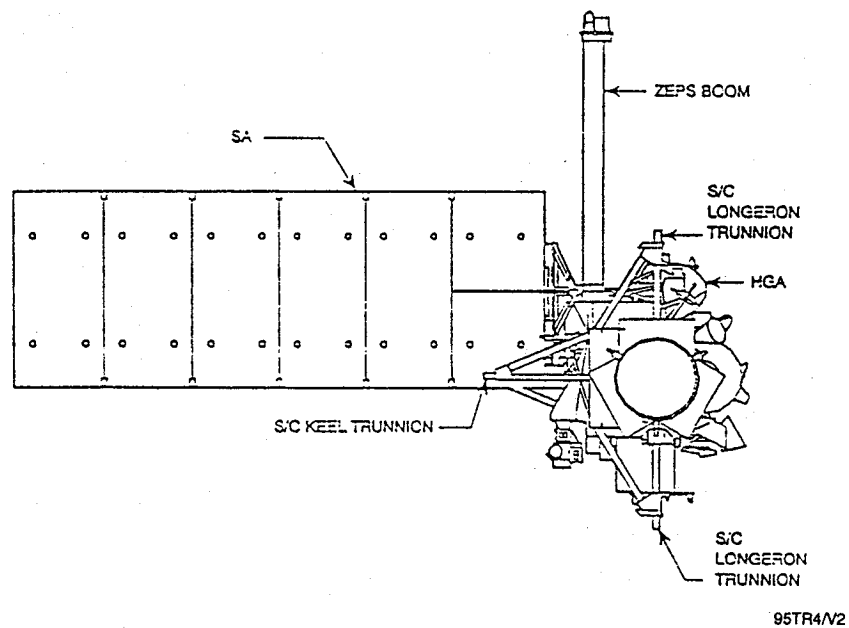


Figure 2. UARS Solar Array Retention, Deployment, and Jettison Assembly

Key Words:

Antenna, Deployment Mechanism

Mechanisms:

Pin Pullers, Pins

Systems:

Deployment Systems (Antennas)

Authors; Experts:

D.F. Lewis and T. O'Donnel

Address:

Jet Propulsion Labs
Pasadena, California

Telephone:**Title:**

Materials Analysis in Support of the Galileo High-Gain Antenna Deployment Anomaly

Source:

JPL Report No. JPL D-9814 (1989).

Abstract:

On April 11, 1991, a command to unfurl the Galileo spacecraft high-gain antenna resulted in a stalled motor about 50 sec into deployment. The motor had stalled considerably short of a full antenna deployment. Evaluation of this situation over many weeks after the deployment anomaly revealed: 1) maximum antenna rib deployment was approximately 34°, 2) antenna ribs were asymmetrically deployed, and 3) flight data and modeling appeared to support a condition where 3 or 4 ribs were undeployed (i.e., stuck in the stow position). The prevalent theory of cause has been that the undeployed ribs' locating pins were still locked or stuck in their receptacles due to a misalignment taper plus a high-friction condition.

This report is a summary of only the major materials analysis performed during 1991 and 1992 in support of the primary hypothesis for the Galileo high-gain antenna deployment anomaly.

Anomalies:

- The attention of most of our work was the midrib locating pin to receptacle interface area of the antenna. Each graphite/epoxy antenna rib (18 total ribs) has two titanium 6A1-4V pins that were Tiodized and coated with a molybdenum disulfide (MoS_2)-based dry lubricant Tiolube 460. These pins would seat into two mating receptacles that were fabricated from Inconel 718. The receptacles were attached to the upper structure of the antenna tower at the midpoint restraint location.
- On examining three S/N 001 antenna pin/V-groove receptacle interfaces, it was apparent that the restraining forces and or the material response to the restraining forces varied from rib to rib. It is apparent that there was some degree of pin misalignment, especially at Rib 15, with lesser amounts for Ribs 6 and 9. It was estimated that for a pin misalignment of 9° , the difference in the sizes of the two contact areas between the V-groove receptacle and its mating pin would be approximately 34%.

Lessons Learned:

From our tests, we believe that the transportation environment resulted in what might be considered a classic fretting condition. Since the fretting condition of small oscillatory translational movement coupled with high-frequency cycling was not duplicated in our friction testing, there is some concern that a coefficient of friction higher than 1.4 could have resulted. Simulated transportation environment exposure followed by vacuum friction testing is proposed as the next step if more accurate determination of the resulting coefficient of friction is required.

Description:

Figure 1 shows the high-gain antenna in deployed position.

Key Words:

Actuator, Optical System, Reflector, Large Reflector, Astronomical Optical System

Mechanisms:

Systems:

Authors; Experts:

K.R. Lorell, J.N. Aubrun, D.F. Zacharie, and E.O. Perez

Address:

Lockheed Palo Alto Research Laboratory
3251 Hanover Street
Palo Alto, California 94304

Telephone:

Title:

Development of a Precision, Wide-Dynamic-Range Actuator for Use in Active Optical Systems

Source:

23rd Aerospace Mechanisms Symposium, NASA Conference Publication 3032, NTIS 89-23892, pp. 139-156 (1989).

Abstract:

This paper describes the design, operation, and performance of a wide-dynamic-range, optical-quality actuator. The actuator uses a closed-loop control system to maintain accurate positioning. It has an rms noise performance of 20 Nm. An offloading mechanism allows the actuator coil to dissipate less than 3 mW under quiescent conditions. The total available mechanical range is 2 mm. Operation of an experimental segmented optical system that uses 18 of these actuators is described to show how the actuator is integrated into an actual system.

PRECEDING PAGE BLANK NOT FILMED

Lessons Learned:

- The use of a motor-driven screw or gear mechanism was rejected because of mechanical inaccuracies. Piezoelectric devices require high voltages. The best choice appears to be a voice-coil type of actuator that can have high bandwidth capabilities and is both simple and reliable.
- The force unloading system that Lockheed has proposed in this paper may be useful in other satellite applications where it is necessary to maintain a continuous power input. Eliminating the need for bearings and lubricants by the use of flex pivots also has merit.

Description:

In astronomical optical systems, large reflectors improve sensitivity and resolution of the instrument. There are three ways to make these reflectors: 1) use a spin-casting technique to make optical blanks, 2) make a thin monolithic meniscus mirror and attach several hundred actuators to the back surface, and 3) use segmented mirrors with actuators that can align the mirror segments. This third approach is described. It requires actuators with very low noise level and the ability to generate substantial forces over a wide mechanical range. It must also have a bandwidth to accommodate the spectra of the observances. In addition, because of thermal and power considerations, energy dissipation must be minimized.

The greatest drawback of a voice-core actuator is that it needs a constant supply of power to maintain a given force level. This problem of maintaining position in the face of a constant load, without having a continuous power input, is resolved by using a force offloading system. This separately controlled automatic system uses a special control loop with a very long time constant that has a small separate actuator to move a spring attached to the main linkage mechanism of the actuator. When steady-state conditions are reached, the spring supplies a force to the output shaft that almost exactly balances the constant load seen by the main actuator. Schematic diagrams of the operation of the actuator and closed-loop control system are presented in Figures 1 through 3.

Table 1 summarizes the approaches taken by the Lockheed design to overcome the limitations of conventional designs. Table 2 compares the performance of the Lockheed actuator design with other actuators that have been used or proposed. Table 3 lists the performance characteristics of the Lockheed actuator.

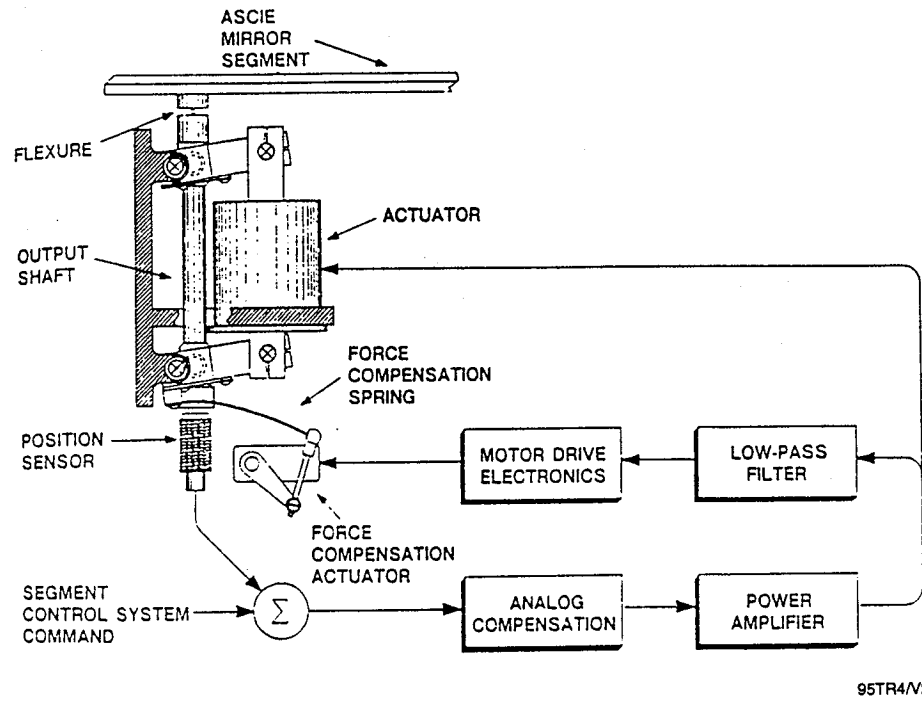


Figure 1. Lockheed Actuator and Closed-Loop Control System

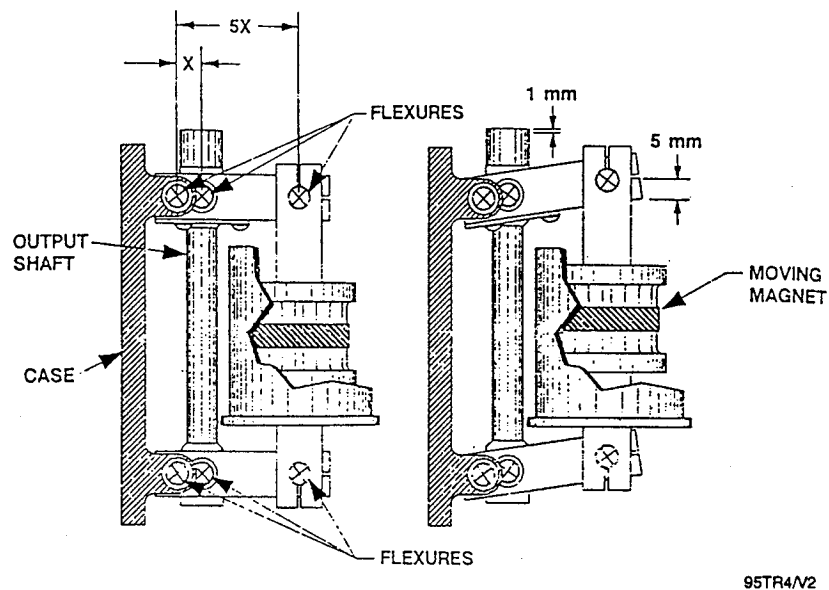


Figure 2. Four-Bar Linkage with 5:1 Reduction Ratio

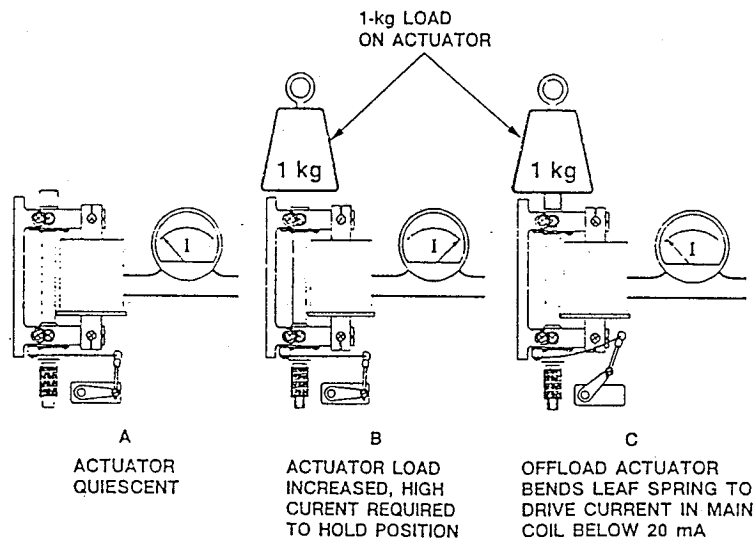


Figure 3. Operation of Force Off-Loading System

Table 1. Lockheed Solution to Limitations of Conventional Designs

Problem	Solution
Dynamic range	Use of electromagnetic actuator in an analog closed loop using special low-noise sensor electronics
Bandwidth	Use of electromagnetic actuator and moderate equivalent gear ratio
Stiction/friction	No bearings or lubricants; exclusively flex pivots
High power consumption	Four-bar linkage (lever) and force unload system
Inability to cancel static forces	Force unload system

95TR4/V2

Table 2. Comparison of Actuator Characteristics

Actuator Type	Dynamic Range	Accuracy	Resolution	Smoothness	Bandwidth	Idle Power	Reliability
Stepper or dc motor-driven gear/screw	Large	Medium	Medium	Poor	Low	Lowm	Poor-Med.
Hydromechanical (Keck telescope)	Medium	Good	Good	Good	Low	Low	Medium
Piezoelectric (open loop)	Small	Poor	Good	Good	High	Low	Medium
Piezoelectric (with feedback)	Small	Good	Good	Good	High	Low	Medium
Inch worm	Large	Good	Medium	Medium	Low	Low	Medium
Voice coil (open-loop)	Medium	Poor	Good	Good	Medium	High	Good
Lockheed design	Large	Good	Good	Good	Medium	Low	Good
Ideal actuator	Large	Good	Good	Good	High	Low	Good

95TR4/V2

Table 3. Performance Characteristics of the Lockheed Actuator

Dynamic range	100,000:1
Total mechanical range	± 1 mm
Noise-equivalent position	20 Nm (rms, measured using a 100-Hz filter)
Friction/stiction	None
Typical static power required	10 mW
Maximum available bandwidth	140 Hz
Maximum available force	± 45 N
Weight	700 g
Operational features	<ul style="list-style-type: none"> • Soft start-up and shutdown • Automatic force unloading • All-analog electronics

95TR4/V2

Key Words:

Robotics, Robots, Manipulators, Rotary Joints

Mechanisms:

Systems:

Author; Experts:

Klaus Priesett

Address:

Dornier GmbH
Friedrichshafen, Germany

Telephone:

Title:

Experiences in the Development of Rotary Joints for Robotic Manipulators in Space Applications

Source:

Abstract:

This paper describes European work on rotary joints and robotic manipulators for space. Two general applications have been targeted:

1. Internal robots for experiments inside laboratory modules
2. External robots for exchange of orbital replacement units, support of extra vehicular activity, and inspection tasks.

Anomalies:

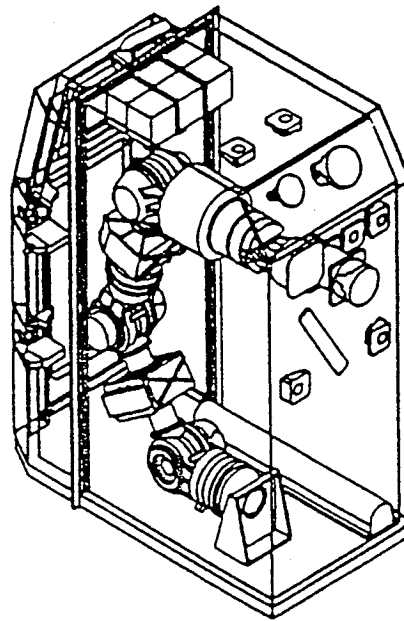
Phenolic/asbestos brake materials present torque anomalies under thermal vacuum conditions.

Lessons Learned:

- Only ceramic-based brake materials could provide consistent friction characteristics in vacuum.
- The brake friction of cobalt-bonded tungsten carbide (WC/Co) is excellent but abrasive wear occurs under load since hard WC particles are embedded in a soft cobalt matrix. The wear rate is too low to affect the brake, but carbide wear debris must be trapped so that it does not affect the rest of the system.
- Molybdenum disulfide (MoS_2) in a dry environment was the superior lubricant (over Braycote 601) for the harmonic drive. However, the atmosphere must be dry.
- Robotic joints must be rugged, but with accurate positioning.
- Robotic joints require high torque capability, low backlash, high stiffness, and low friction.
- A brushless torque motor was selected. A reluctant motor was rejected on the basis of nonlinear torque/current behavior. A brushless, toothless torque motor was also rejected because of lower motor constant for a given mass and size.
- Optical sensors provide best performance but resolvers are more robust and reliable. Additional trade-offs are necessary.
- Harmonic drive provides the lowest mass and dimensions for the required performance. A cycloid drive was less sensitive than the harmonic drive to temperature effects and showed no wear except for a light burnishing.

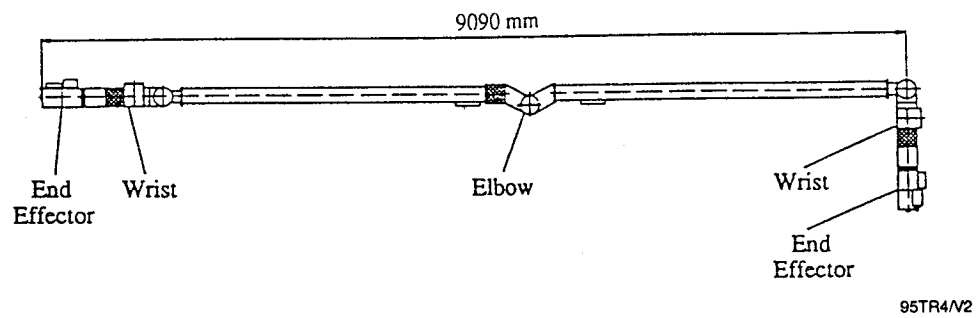
Description:

A robotics technology experiment is in progress. Part 1 is the internal robot, a small six-joint manipulator arm located inside a spacelab rack, as shown in Figure 1. Part 2, the external robot is the Hermes robot arm. This is a relocatable seven-joint arm with a useful range of 9.09 m. As shown in Figure 2, the Hermes robot arm has two identical end effectors, wrist assemblies, limbs, and a single-elbow assembly in the middle of the arm. Each wrist has three rotary joints, roll, yaw, and pitch. During operation, the wrist that is



95TR4/V2

Figure 1. Rotex Arm Inside Spacelab Rack



95TR4/V2

Figure 2. Hermes Robot Arm Configuration

located at the base will act as the shoulder, with the yaw joint kept in the fixed position. This paper is mainly concerned with the design of the Hermes robot arm joint assemblies. The joint design drivers must be rugged, but with accurate positioning. They need high-torque capability, low backlash, stiffness, and low friction. Table 1 lists the requirements and Figure 3 is a schematic of the joint. The following components/features make up the joint design:

- Brushless dc torque motor
- Optical sensor on motor shaft for commutation and speed measurement
- Electromagnetic friction brake with manual lifting device
- Backdriveable gear – a harmonic drive with a planetary gear prestage
- Optical, absolute encoder (17-bit resolution) for joint angle measurement
- Thin section ball bearings
- Titanium structure to reduce mass
- End switches and end stops at limits of range.

The pancake-type dc motor is driving a hollow shaft supported on two preloaded angular contact ball bearings. On the same shaft, there are the (metal) code disk of the motor sensor and the brake disk. The motor sensor provides feedback signals for motor commutation and speed control. The motor shaft is coupled to the input element of the gear (the pinion of the planetary gear stage). This planetary gear is integrated into the main gear (a harmonic drive). The flex spline of the harmonic drive is connected to the joint housing and the dynamic spline is the output element and is fixed to the joint output flange. The total gear ratio is 260.6.

The housed optical absolute encoder is mounted inside the motor section and coupled to the joint output flange by a long shaft running through the gear. The external mounting interfaces of the joint are at the side, perpendicular to the axis of rotation, leading to a yoke-type construction of the rotary output element. Two preloaded angular contact bearings support this rotating output member. The angular rotation range of the joint is $+120^\circ$ with respect to the upright position.

Figure 4 shows how the Hermes robot arm joint design has evolved through experience:

- Motor and sensor have been combined on common sleeves
- Eliminated manual brake lifting
- Provided astronaut override
- Considering change of harmonic drive
- Resolver for joint angle readout
- Make both output bearing pairs the same size
- To reduce the structural mass, consider changing from titanium to beryllium
- Redundancy is needed for the motor windings, the brake and resolver, as well as the readout station of the motor sensor and the switches at the ends of travel
- The redundant motor must fit in the same space; therefore, the gear ratio must be increased to about 400 to get the same torque.

Table 1. Joint Performance Requirements

Parameter	Hermes Robot Arm	Rotex
Angular Range (°) Wrist pitch/yaw Wrist roll Elbow pitch	± 120 ± 185 $+30/+180$	± 125 pitch ± 185 roll —
Angular Speed (rad/sec) Maximum Minimum	0.05 4.5 E-05	0.15 —
Output Torque, T (N) At minimum speed At maximum speed	≥ 450 ≥ 50	≥ 15 —
Torque Ripple T > 25 Nm T \leq 25 Nm	$\leq 2\%$ (TBR) ≤ 0.5 Nm (TBR)	— —
Backdrive Threshold Torque (Nm)	≤ 40	≤ 10
Brake Torque Referred to Output Level (Nm)	500 to 650	—
Rotational Stiffness (Nm/rad) T \leq 13.5 Nm T > 13.5 Nm	≥ 1.1 E+05 (TBC) ≥ 1.3 E+05 (TBC)	≥ 0.5 E04 —
Joint Position Measurement (arcsec) Resolution Accuracy	9.9 (17 bit) ≤ 27	9.9 (17 bit) ≤ 24
Motor Speed Measurement (%) Resolution Accuracy	0.5 ≤ 1	— —
Power Consumption (W)	≤ 30	≤ 3
Mass (kg) Wrist (3 joints + electronics) Elbow (1 joint + electronics)	≤ 45 (TBR) ≤ 19 (TBR)	4.4 (1 pitch joint) 4.0 (2 roll joint)
Lifetime	10 yr, periodic operations (20-hr total)	1 spacelab mission
Temperature range (°C)	-40 to +80	+6 to +65

95TR4/V2

TBC = to be confirmed; TBR = to be reviewed.

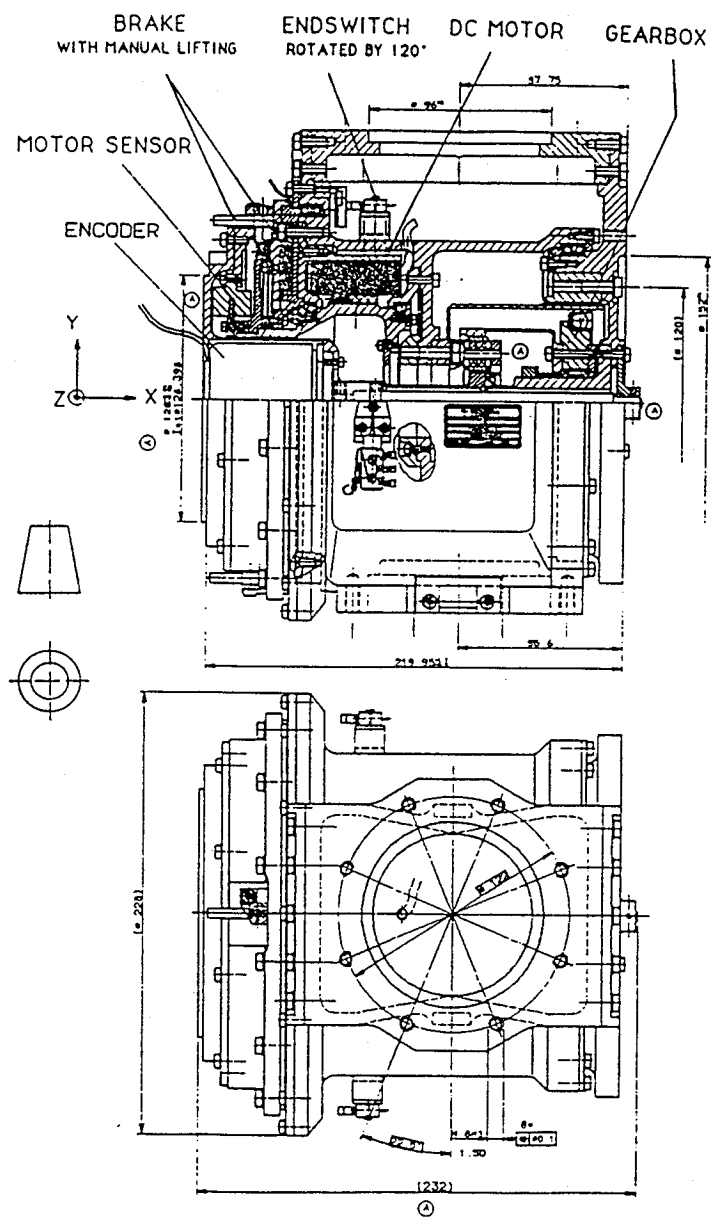


Figure 3. SMS Joint Design

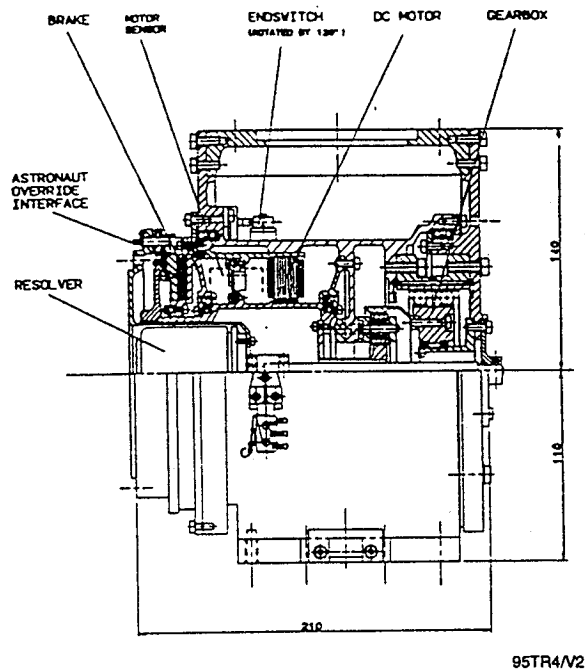


Figure 4. Hermes Robot Arm Joint Design

Table 2 lists possible component trade-offs and tentative replacements. The motor appears to be well in hand. Although optical sensors have desirable characteristics, their reliability is being questioned. More studies are needed.

Lubrication and tribological material selection are major problems in the Hermes robot arm joint development. The author listed some of the lubricant choices in Table 3. His tentative choices for the Hermes robot arm joints include:

- Ball bearings
 - Perfluorinated oil (e.g., Fomblin Z25 or Bray 815Z), TiC coating of balls
 - Sputtered MoS_2
 - Ion-plated lead
- Gearbox
 - Grease (e.g., Braycote 601), possibly gold-coated harmonic drive teeth
 - MoS_2 (sputtered or spray bonded).

A common lubricant for both the ball bearings and the gears is anticipated, with the gears being the determining factor.

Table 2. Summary of Trade-Offs

Alternative Solutions	Main Arguments for Selection of Baseline
Motor <ul style="list-style-type: none"> • Brushless torque motor • Brushless, toothless torque motor • Reluctant motor 	<ul style="list-style-type: none"> • Reluctant motor has nonlinear torque/current behavior • Baseline provides higher motor constant than toothless motor for given mass and size
Sensors <ul style="list-style-type: none"> • Resolver • Optical encoder • Inductosyn 	<ul style="list-style-type: none"> • Optical devices provide best performance • Resolver is more robust and reliable • Trade-off will continue to arrive at a common technology for both sensors
Lubrication Method (Treated Separately)	
Main Gear System <ul style="list-style-type: none"> • Cycloid drive • Harmonic drive • Planetary gear 	<ul style="list-style-type: none"> • Provides lowest mass and dimensions for the required performance • Is available with space-compatible materials
Brake Pad Material (Treated Separately)	

95TR4/V2

Table 3. Relative Merits of Dry and Liquid Lubricants

Dry Lubricants	Liquid Lubricants
Negligible vapor pressure	Finite vapor pressure
Wide operating temperature range	Viscosity, creep, and vapor pressure are temperature dependent
Negligible surface migration (debris can float free)	Creep barriers and seals required
Valid accelerated testing	Invalid accelerated testing
Short life in laboratory air	Insensitive to air or vacuum
Debris cause frictional noise	Low frictional noise
Friction speed independent	Friction speed dependent
Life determined by lubricant wear	Life determined by lubricant degradation
Poor thermal characteristics	Good thermal conductance
Electrically conductive	Electrically insulating

95TR4/V2

Gear tests have been run with a harmonic drive gearset. One test was lubricated with Braycote 601 grease, the other with sputtered MoS₂ on the circular spline, and spray-bonded MoS₂ on the flex spline and on the wave generator. It was concluded that MoS₂ can provide the best overall efficiency, but these were relatively short-term tests. The author pointed out that MoS₂ should only be used in a dry environment. It was stated that humidity would drastically reduce the wear life. A cycloid drive was also run with the same lubricants. It was less sensitive than the harmonic drive to temperature effects and showed no wear except for a light burnishing.

Although these were short-term tests of a unit that is supposed to survive for 10 yr in space, as stated in Table 1, it is important to note that the actual operating life is about 20 hr (2 hr each year).

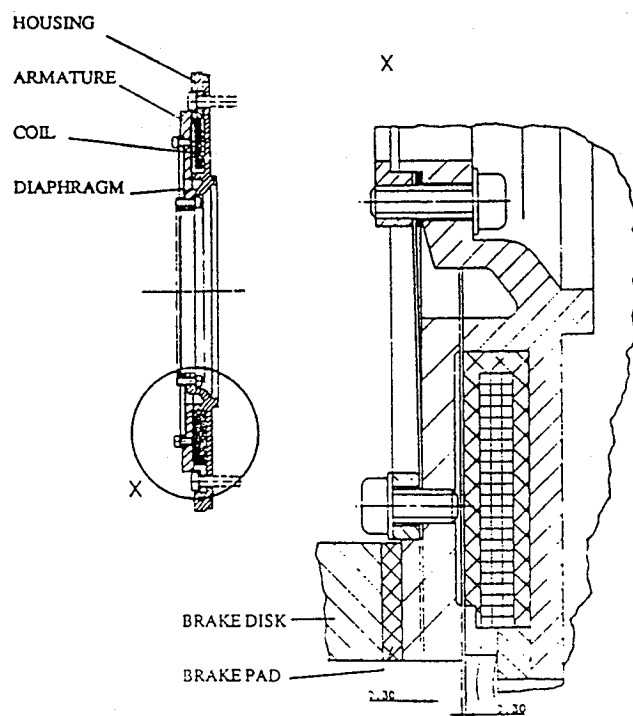
The brake material presented another problem, mainly because the torque variations must be held to less than 10%. This brake is a failsafe, electromechanically actuated friction device. It consists of a rotor (or disk) fixed to the motor shaft, carrying the friction layer and a stator assembly, comprising housing, coil, diaphragm, and the armature with the other friction layer (Figure 5). The brake is "on" when the diaphragm is pressing the armature against the disk with a defined preload.

Obtaining good constancy in friction by selecting the right materials is difficult. Standard brake materials such as phenolic/asbestos present a torque anomaly under certain thermal vacuum conditions. For the Hermes robot arm, a number of different materials were investigated by a comprehensive literature search. It was concluded that only ceramic-based materials could provide constancy in friction. Three materials were selected for test using a representative brake configuration: Al₂O₃/ZrO₂, Al₂O₃/TiO₂, and WC/Co.

Tests were conducted in both ambient and thermal vacuum conditions. The results were as follows:

- Friction decreases when going from vacuum to air
- Temperature has very little effect
- The friction of cobalt-bonded tungsten carbide (WC/Co) is excellent, but abrasive wear occurs under load since hard WC particles are embedded in a soft cobalt matrix.

The wear rate is too low to affect the brake, but carbide wear debris must be trapped so that it does not affect the rest of the system. Two other anomalies were experienced with the motor sensor and the absolute optical joint position encoder. The former could be resolved by including signal preconditioning electronics directly at the sensor and the latter could be corrected by an appropriate adjustment step.



95TR4/V2

Figure 5. SMS Brake Design

Key Words:

Springs, Deployable Appendages

Mechanisms:

Solar Arrays, Antennas, Robotic Arms

Systems:

General Spacecraft

Authors; Experts:

R. Sharma, A. Tyler, and R. Farley

Address:

NASA-Goddard Space Flight Center
Greenbelt, Maryland 20771

Telephone:

Title:

Spacecraft Deployable Appendages
Deployed Appendage Design Philosophy

Source:

Goddard Space Flight Center (1992)
Engineering Directorate

Abstract:

This report discusses experience with various spacecraft and provides general guidelines for deployment mechanisms.

Lessons Learned:

- Redundant push-off springs should be incorporated for initial release of all spacecraft deployable appendages.

Description:

- Rate-controlled, constant force, spring-driven hinges are used for deployable appendage actuation.

Key Words:

Infrared Absolute Spectrophotometer (FIRAS), Mirror Transport Mechanism,
Cosmic Background Radiation

Mechanisms:

Mirror Transport Mechanism

Systems:

FIRAS

Authors/Experts:

Kenneth W. Stark and Meredith Wilson

Address:

NASA-Goddard Space Flight Center
Greenbelt, Maryland 20771

Telephone:

Title:

A Mirror Transport Mechanism for Use at Cryogenic Temperatures

Source:

21st Aerospace Mechanisms Symposium (1992).

Abstract:

This report describes the mirror transport mechanism, which supports a pair of dihedral mirrors and moves them in a very smooth and uniform scanning motion normal to a beamsplitter. Each scan is followed by a quick flyback and repeat.

Included in the report will be material selection, design, and testing of all major components of the mirror transport mechanism in order to meet the stringent performance requirements under cryogenic conditions and survive the launch environment of the shuttle. Areas to be discussed in detail will be those in which failures or performance anomalies occurred and

their solutions. Typically, this will include (but not to be limited to) flex pivot failures during vibration testing, excessive dihedral platform sag under 1-g operation, electronic and fiber-optic characteristics, and tolerancing considerations.

As of this writing, development of the mechanism has reached the final phase of thermal and vibration qualification. Environmental testing of the complete FIRAS experiment is just beginning.

Anomalies:

- Loads were developed during vibration testing that caused a rocking motion of the dihedral platform resulting in pivoting motion about the latch cone axis. This placed excessive loads on the pivot flexures causing them to fail.
- There were two major problems that developed during the vibration testing that necessitated significant redesign in the latch mechanism. Loads were developed during testing which caused a rocking motion in the dihedral platform resulting in pivoting motion about the latch cone axis. This placed excessive loads on the pivot flexures causing them to fail.

To reduce this motion, a third-point latch was developed (Figure 8) that limited motion to ± 0.0051 cm (± 0.002 in.). This was arrived at by a compromise of how tight a clearance could be maintained without possible binding and the allowable stress buildup in the flexures at that excursion. The third-point latch consists of a slot in the latch motor housing and a tang attached to the rear of the dihedral platform connecting link. The spacing is adjusted so that when the tang is moved into the slot during the latch mode there is a clearance gap on each side of the tang of 0.0051 cm (0.002 in.). This arrangement was retested and worked.

- Later in our test program there was a condition in which the mirror transport mechanism was vibrated but because of a misadjustment in the relationship of the latch motor to latch spring, the cones were not seated properly in their respective sockets. This allowed excessive motion at the sockets even though the third-point latch was engaged. In effect, the platform could rotate about the third-point latch. This caused failure in several pivots. At this point it was decided that the pivots themselves should be protected from excessive loads in case of another overload condition. After an extensive investigation, it was decided to enclose each pivot in a sleeve that would limit radial movement to an acceptable level. This level was selected at a maximum of 0.0076 cm (0.003 in.) after an analysis showed a stress level of 248 MPa (36,000 psi) was reached with 0.0076 cm (0.003 in.) deflection and that buckling occurred at approximately 303 MPa (44,000 psi).
- Testing in a fixture showed that buckling occurred slightly above 0.0076 cm (0.003 in.), which probably put the stress close to 303 MPa. The sleeves were designed to have tightly machined tolerances to minimize the sleeve-to-sleeve dimensional variations. Taking into account the tolerances on the pivots, sleeves, and the center shift at 4° (rotation of flex pivot in latch position) of each pivot, a maximum radial clearance of 0.008 cm (0.0032 in.) and a minimum radial clearance of 0.0011 cm (0.00045 in.) is possible. The upper pivot section is bonded to the sleeve. Each sleeve and corresponding pivot have recessed grooves machined into the mating surface to allow for epoxy retention. Subsequent room temperature vibration testing showed no failed pivots.

- The initial motor design used niobium titanium wire that became superconducting below approximately 9.5 K. The mirror transport mechanism was tested and operated at 4.5° with a motor of this type. However, some anomalies were noted: an apparent increase in spring constant and a large hysteresis effect. Because of these poorly understood factors, it was decided to redesign the motor using normal copper wire if power dissipation could be made low enough.
- Since copper has finite resistance, it was important to reduce the required current as much as possible by maximizing motor force constant. Redesign included the following:
 - Samarium cobalt magnets were replaced with neodymium-iron, a newly developed material having about 50% higher gauss-oersted product
 - The flux return path was at or near saturation; the cross sectional area was increased about 50%
 - Overall diameter was increased to allow for 30% more turns.

Lessons Learned:

- To limit the load on the pivots, they were enclosed in sleeves that limited radial movement to acceptable levels.

Description:

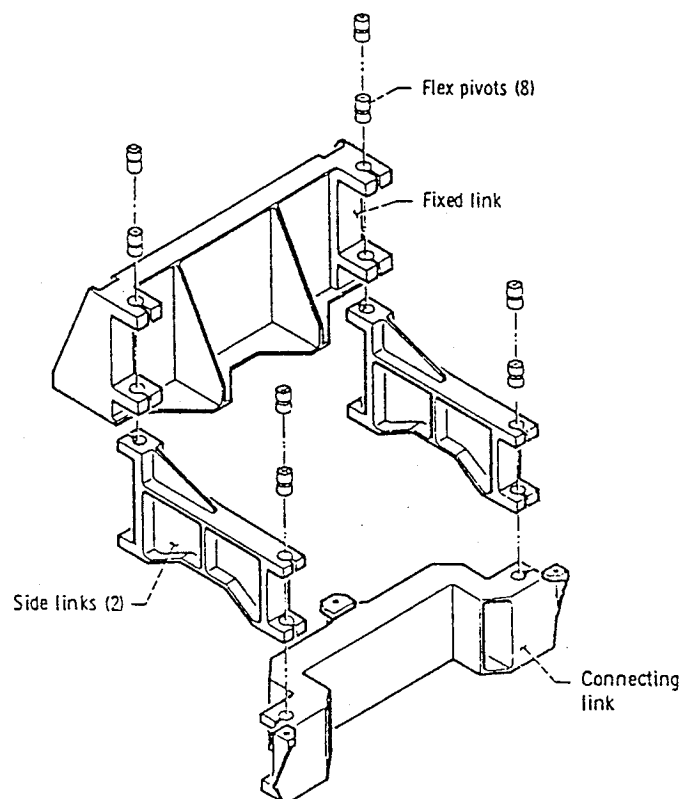
The mirror transport mechanism is an integral part of the FIRAS instrument. The FIRAS measures the spectrum of the 3 K cosmic background radiation, the interstellar dust emission, and any unknown sources in the wavelengths ranging from 100 micron to 1 cm.

The FIRAS is a cryogenically cooled (LHe), rapid-scan interferometer spectrophotometer. A pair of dihedral mirrors is moved with respect to a beamsplitter, producing the optical path differences that generate an interferogram. Incoming radiation, which is channeled into the interferometer by a skyhorn, is balanced against an internal reference source.

An external calibrator is also provided that, when commanded, will swing into place in front of the skyhorn, at which time the temperature of the internal reference source is adjusted to nearly null the signal. Proper operation requires that the entire instrument be maintained at a temperature below 2 K. Thus, it is enclosed in a large dewar filled with superfluid helium at 1.8 K. Spacecraft orbit is such that complete coverage of the universe requires about six months. For double coverage, a lifetime of at least a year in orbit is desired. Since any power dissipated in the dewar increases boil-off of the cryogen, strict limits are placed on the allowable dissipation. The FIRAS power budget is 5 mW. Lifetime in orbit is reduced by about 3 days/mW.

The dihedral mirrors are mounted on the mirror transport mechanism platform and the mirror transport mechanism is designed as a basic four-bar linkage connected by a set of eight flexural pivots (see Figure 1). These flex pivots are essentially frictionless and provide only a small linear restoring force. Angular rotation is low enough that expected lifetime at normal temperature is infinite. However, the entire mechanism must operate at 1.8 K for more than a year and there is no such previous experience. Flex pivots were fabricated with a special material and life tested for more than 20 million cycles at LHe temperature and with greater than normal rotation. The mirror transport mechanism is

driven by a unique linear motor whose only moving part is completely passive (no contact, no flexing wires). Scan operation is controlled by an optical encoder, which consists essentially of a pair of gratings having 50 lines/mm. Thus, a pulse is generated at intervals of exactly 20 μm . By counting these pulses, the scan motion reverses at the proper position. These encoder pulses are also used to command the analog-to-digital (A/D) converters to sample the detector outputs. Since each pulse is generated at a precise position of the mirrors, data from successive scans can be added for greater reliability and noise reduction. Actually data sampling must be at a higher rate than the basic encoder resolution so these pulses are accurately subdivided by a phase-lock loop. In normal optical encoder applications of this type, the light sources and detectors for the encoder are located outside the dewar and optical fibers transmit the signals. Launch environment requires rugged caging and locking to prevent damage. The dihedrals are quite large (about 8 in. high) and heavy (about 1.5 lb each) and must withstand launch vibrations. Protection is provided by moving the platform beyond its normal stroke and by locking into a pair of cones and sockets. A latch motor rotates a roller shaft deflecting a leaf spring that forces the cones into the sockets. As further protection, each flex pivot is fitted with a sleeve that limits deflection in the lateral direction.



95TR4/V2

Figure 1. Mirror Transport Mechanism Exploded View

Testing:

Thermally, the mirror transport mechanism must survive launch conditions at LHe temperatures, and once in orbit it must operate at this temperature. Although we were able to performance test the mirror transport mechanism at LHe temperatures, vibration testing could not be done at LN₂ temperatures due to the test dewars that were available. The sequence for vibration testing was to perform a room temperature vibration and if everything was successful then an LN₂ vibration would follow. The reasons for two separate tests was that the room temperature test was out in the open allowing clear visual observation during tests, but the LN₂ tests had the mirror transport mechanism mounted inside a dewar where no visibility was possible.

Vibrational testing consisted of: 1) a sine burst test at approximately 20 cps to simulate the steady-state component of the vibration, and 2) a random test. These tests were performed separately and in each of three mutually perpendicular directions. The vibration test specification levels used are shown in Table 1.

Table 1. Vibration Test Levels

Parameter	X	Y	Z
Random (GRMS)	6.75	3.8	3.3
Sine Burst (G's)	10.0	10.0/83	10.0

95TR4/V2

Key Words:

Movable Stop, Four-Bar Linkage, Telescope

Mechanisms:

Four-Bar Linkage

Systems:

Rotary Flap Drive

Authors; Experts:

R.E. Tweedt and R.N. Poulsen

Address:

Hughes Aircraft Company

Telephone:

Title:

A Movable Stop Mechanism for the Space Infrared Experiment (SIRE) Program Telescope

Source:

16th Aerospace Mechanisms Symposium, NASA Conference Publication 2221 (1992).

Abstract:

The movable stop mechanism is to activate flaps that change the size and shape of the SIRE telescope aperture stop on command. Operating at the cryogenic temperatures of the optic system, it consists primarily of a rotary solenoid that drives dual four-bar linkages in synchronism that in turn rotate the butterfly flaps into position. The paper discusses the design, performance characteristics, and testing of this mechanism. Specific problems that occurred during test and the solutions that were adopted are also described.

PRECEDING PAGE BLANK NOT FILMED

PAGE 170 INTENTIONALLY BLANK

Anomalies:

- During the initial 5000-cycle test of the engineering model, unexplained stoppages occurred. Although two subsequent 6000-cycle tests of this model were successfully completed, it was decided that a 20,000-cycle life test of both the engineering model and the flight unit should be conducted in order to establish confidence that this unit would be able to meet its 5,000-cycle life requirement.
- After the 20,000-cycle test on the engineering model had been successfully completed, the unit was brought up to room temperature when it was found that the mechanism was jammed in the open position. This was found to be due to galling or scuffing of the surfaces of a fixed-stop and mating-stop surface on the actuating arm.
- During testing of the flight unit, stoppages occurred in the open and partially open positions at operating temperature and pressure. However, at room temperature, the unit operated normally. The reason was found to be that the clearances between the shafts and the holes were slightly smaller than those in the engineering model.

Lessons Learned:

- Testing an engineering model is useful in debugging the initial design and test procedures for any mechanism that must meet stringent requirements for low friction, close tolerances, and precise balancing of the spring output torque against solenoid output torque. However, each subsequent mechanism assembly must be subjected to a level of testing that will demonstrate that assembly parameters relating to friction, tolerances, and spring/solenoid output torque balance have been satisfied.
- The ion-plated lead lubrication has proved to be satisfactory for a lightly loaded, low-speed, intermittent, journal bearing type of application at cryogenic temperature and in a vacuum.
- The tungsten carbide coating was effective in preventing galling and cold welding of the contacting surfaces on the fixed stop and the mating surface of the actuator arm when subjected to impact on contact.
- The importance of exactly replicating the fits, geometry, and assembly parameters of the engineering models in the subsequent production of flight units has been very positively demonstrated.

Description:

The primary objective of the SIRE Program was to develop an infrared sensor system that could make a variety of star and space target measurements from space in several different spectral wavelength regions. During the course of this program, a requirement was added for a dual-aperture stop configuration. The principal design requirements for the movable stop mechanism were:

- Operating temperature: 15 to 25 K
- Power dissipation: ≤ 200 mW to close aperture stop and keep it closed

- Power dissipation in open position: ≤ 10 mW
- Hold in closed position for at least 5 min
- Fail-safe in open position
- Life: 5000 cycles (minimum)
- Switches to indicate end-point positions
- Time to actuate: ≤ 1 sec
- Noncontamination of cryogenic optics in vacuum
- Compatible with current telescope hardware.

The final design of the movable stop mechanism is shown in Figure 1. The aperture stop and its actuating arm support bracket are made of beryllium. The arm, connecting links, link pins, and flap shafts are made of A-286 steel. The stop flaps are made of 6061 aluminum. The diameters of the journal-type bearing areas of the flap shafts and of the actuating arm shafts are sized to provide 0.015/0.025 mm (0.0006/0.0010 in.) of clearance in the respective mating pivot holes. The link pins are sized to provide 0.010/0.020 mm (0.0004/0.0008 in.) of diametral clearance in the respective mating pivot holes.

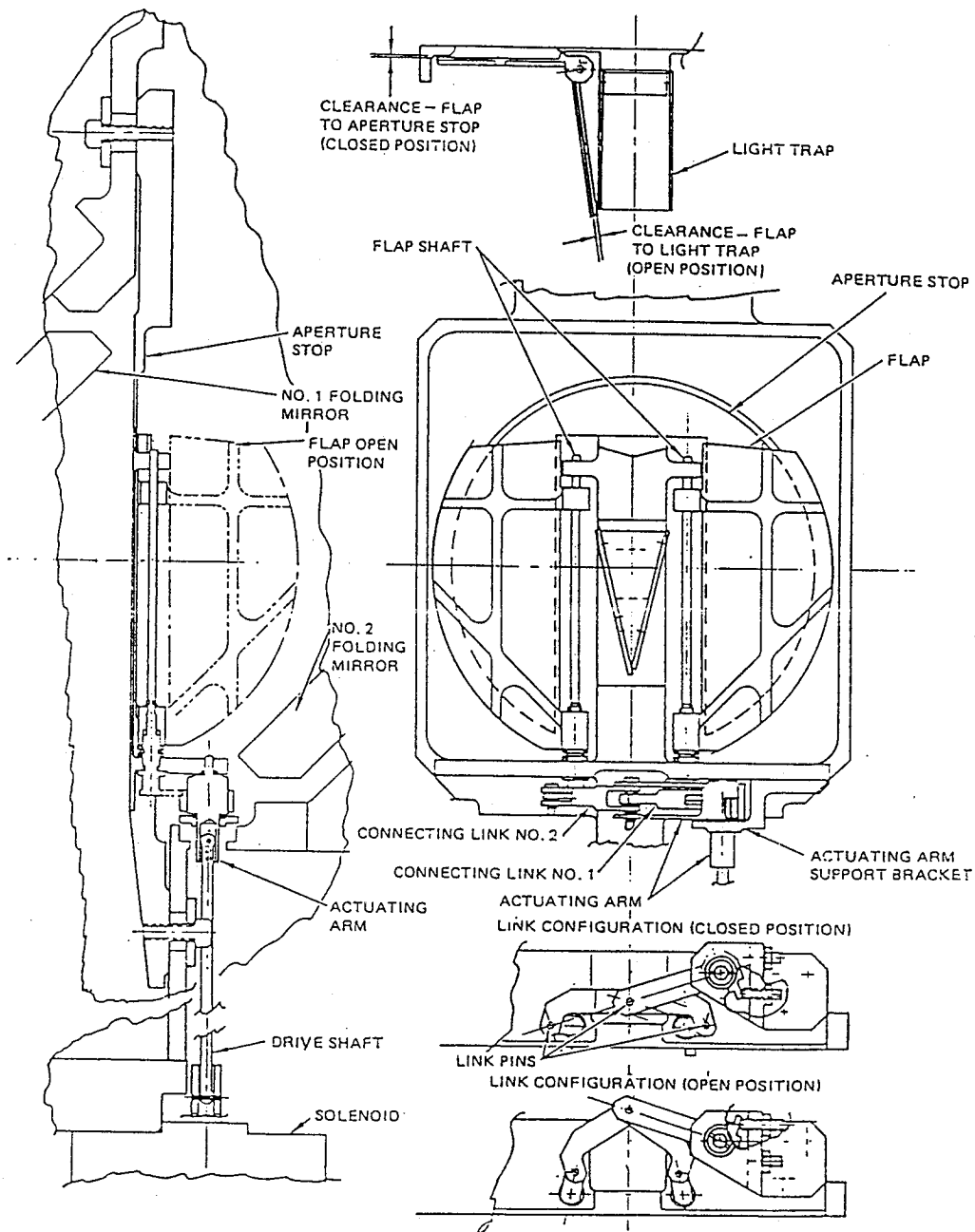
It was necessary to make several different length configurations of the actuating arm and the No. 2 connecting link in length increments of 0.025 mm in order to be able to select parts at assembly to ensure symmetrical flap clearances in both the open and closed positions. Adjustable stop screws are used to set the open and closed positions of the flaps.

The drive shaft connecting the solenoid output shaft to the actuating arm is made of A-286 steel and is designed to float axially in order to accommodate differential expansion. The drive shaft also accommodates slight positional mislocations between the solenoid and the actuating arm.

Although the movable stop mechanism is to operate in a 0-g environment, 1-g loading of the contacting link and actuating arm surfaces can occur during ground tests because of the vertical orientation of the unit. To prevent the creation of excessive friction loads during test and during ground operation, Teflon washers are installed.

The solenoid ball bearings and all shafts, link pins, stop-flap shims, and pivot holes are coated with 99% pure commercial lead lubricant, ion plated to a thickness of 2000/3000 Å. This lubricant was chosen because of its ability to meet the requirements imposed by operation in space at cryogenic temperature, low friction, and minimum contaminant generation.

The solenoid rotor is mounted on ball bearings in a titanium housing. The radial air gap between the rotor and pole pieces is 0.23/0.30 mm (0.009/0.012 in.). Magnetic detent stops on the pole pieces reduce the air gap to zero at the closed position and thereby allow a reduction in the holding current needed. Redundant torsional springs made of beryllium-copper alloy are installed with an adjustable anchor post at the fixed end to permit the spring output torque to be accurately set. Reed switches indicate position, and in the closed position, the switch causes the 0.170-A current to be reduced to a holding current of 0.050/0.060 A. Reed switches housed in glass-filled polycarbonate resin were designed and built for this cryogenic application. A samarium-cobalt magnet attached to the rotor actuates these switches.



95TR4/V2

Figure 1. Movable Stop Mechanism

Testing:

The original test plan called for a 5000-cycle life test of an engineering model in a test dewar at a pressure of less than 10^{-4} torr and at a temperature less than 25 K. The test equipment provided automatic cycling to close the moveable stop, maintained this position for 3 sec, and released the stop to the open position for 1.5 sec. The use of a manual override made it possible to keep the stop in the closed position for extended periods. At regular intervals during the test, the minimum actuating and minimum holding currents as well as the closing and opening times were measured in order to monitor changes in the performance characteristics of the movable stop mechanism.

During the initial 5000-cycle test of the engineering model, unexplained stoppages occurred. Although two subsequent 6000-cycle tests of this model were successfully completed, it was decided that a 20,000-cycle life test of both the engineering model and the flight unit should be conducted in order to establish confidence that this unit would be able to meet its 5000-cycle life requirement.

Before the extended life test, the engineering model was refurbished by relubricating all parts of the linkage with ion-plated lead. The 20,000-cycle life test of the engineering model was completed without failure. However, when the movable stop mechanism was brought up to room temperature at the end of the test, it was jammed in the open position and the solenoid torque was insufficient to operate the linkage. During inspection, a slight pressure applied to one of the flaps released the unit and it then operated normally at room temperature. The same phenomenon occurred after an additional 6000-cycle test. Further inspection revealed that the area of contact between the actuating arm and the stop screws was galled and the contact conditions were such that it generated a locking force when exposed to differential expansion. The jamming was eliminated by modifying the angle of contact between the stop screw and the actuating arm and applying a 0.050/0.076-mm (0.002/0.003-in.) coat of plasma-sprayed tungsten carbide to the contact surface on the arm.

During initial tests of the flight version of the movable stop mechanism, stoppage occurred in the closed position after less than 500 cycles. This was caused by galling and cold welding of the solenoid rotor and one of the magnetic detent stops. In a subsequent test of the engineering model, the same type of stoppage occurred after 47,000 cycles. The marked difference in the test results was due to differences in the electrical discharge machine tooling and different manufacturing setups used in fabricating the two models. The stoppage was eliminated by reworking the detent stops to eliminate sharp corners and to bring the rotor into simultaneous contact with both detent stops. In addition, a plasma-sprayed layer of tungsten carbide was applied to the rotor. The coating increased the minimum holding current from 0.013 to 0.027 A.

During continued testing of the flight unit, stoppages occurred in the open and partially open positions at operating temperature and pressure. Careful comparison of the engineering model and flight units revealed a slight difference in the diametral clearances between the shafts and holes. Because of rework on the engineering model, these clearances were 0.0025/0.0050 mm (0.0001/0.0002 in.) greater than the drawing tolerance that the flight unit met. The drawings were changed and the flight unit shaft diameters were reworked to provide the 0.015/0.025-mm (0.0006/0.0010-in.) clearances that characterized the engineering model.

A problem related to the maintenance of end play on the flap shafts was also encountered. In the engineering model, the flap was keyed to the shaft by means of a coiled spring pin. Apparently, the friction between the pin and the flap slot maintained the axial position of the

flap on its shaft and thereby ensured that the amount of end play set during assembly was maintained. During the design review, the use of the coiled spring pin was criticized; the attachment of the flap shaft was therefore redesigned (a flattened shaft, a flat-sided hole, and a retaining ring were substituted). The flap can now move on the shaft in a way that tends to eliminate the end play established at assembly. The attachment of the flight unit flap shaft was redesigned to incorporate an additional retaining ring and thereby ensure the maintenance of the proper shaft end play.

With these changes in the shaft-to-hole diametral clearances and in the flap-to-flap shaft attachment, the movable stop mechanism flight unit successfully completed the 20,000-cycle life test.

General and Miscellaneous

Key Words:

Moving Mechanisms, Solar Array Drives, Momentum Wheels, Lubricants

Mechanisms:

Pin Pullers, Bearings, Rotating Wheels, Gears

Systems:

Deployment Systems, Scanning Systems, Rotating Systems

Authors; Experts:

Anonymous

Address:

USAF Space Division, SD/ALM
P.O. Box 92960
Los Angeles, California 90009-2960

Telephone:**Title:**

Assemblies, Moving Mechanical, for Space and Launch Vehicles, General Specification For

Source:

United States Air Force Mil Standard MIL-A-83577B (1 February 1988).

Abstract:

This specification sets forth the general requirements for the design, manufacture, quality control, and testing of moving mechanical assemblies to be used on space and launch vehicles. Before the application of MIL-A-83577B to Air Force spacecraft programs, a number of anomalies had occurred with spacecraft deployables. In addition, a number of more recent failures have occurred on spacecraft that were not designed and tested to the moving mechanical assembly specification. Most of these problems could have been avoided had the design and test requirements of the moving mechanical assembly specification been observed. These failures could have been avoided through proper design and testing. Properly designed and perceptive tests would have ferreted out things like interference between the deployable and adjacent thermal blankets or thermal distortion-related problems. Also, it is interesting to note that many of the failures could have been uncovered only by testing at the vehicle level (i.e., after the deployable was fitted to the spacecraft).

Anomalies:

Program	Problem	Cause
Program 461 (1964)	Solar array failed to deploy fully	Mishandling during storage
STP 67-2 (OV2-5) (1968)	Solar array booms failed to deploy fully	Field modification problem
777 (1970)	Omni-antenna latch broke during spin-up	Attitude control instability
Program A (1971)	Antenna failed to deploy fully	Wire harness binding
Program B (1971)	Solar array deployed late	Silicon rubber sticking
STP 71-5 (1972)	Boom not deployed	Dynamic clearance problem
Skylab (1973)	Solar array failed to deploy	Interference with cabling or thermal blankets
Transit (1975)	Solar array failed to fully deploy; cable hung up	Anomalous flat trajectory caused high heating rates
Viking (1975)	Sampling arm failed to deploy	Debris in gear train
STP 74-1 (SOLRAD) (1976)	Solar panel failed to deploy	Release mechanism binding
DMSP-F-1 (1976)	Solar array failed to deploy fully	Excessive wire harness stiffness
DMSP-F-2 (1977)	Solar array delayed release	Friction welding
Voyager 2 (1972)	<ul style="list-style-type: none"> Science boom failed to fully deploy Scan platform gearbox seized Magnetometer boom misalignment 	<ul style="list-style-type: none"> Microswitch failed Lubricant failure Unknown
SEASAT (1978)	Spacecraft power failed	Slip ring debris between power/ground rings
VUE (1988)	Telescope failed to rotate about azimuth	Inadequate torque margin on azimuth caging arm
Galileo (1989)	High-gain antenna failed to deploy	Excessive friction in ball and socket joint
Galileo (1989)	Instrument cover jettisoned late	Thermal binding
Magellan (1989)	Solar array failed to latch at end of travel	Microswitch misadjusted
MACSAT (1990)	Gravity-gradient boom failed to deploy	Inadequate force margin
CRRES (1990)	Magnetometer boom failed to fully orient	Interference between thermal blanket velcro and wiring
Ulysses (1990)	Spin stabilized spacecraft wobbles	Antenna boom thermal distortion caused spacecraft center of gravity offset
Hubble Space Telescope (1990)	Solar array deployment booms oscillate as telescope goes from shade to sun	Thermal gradient across boom diameter
ANIK E2 (1991)	C-band antenna did not fully deploy	Thermal blanket interference
Unknown	Sampling arm failed to deploy	Screw backed out and wedged against housing
Upper Atmosphere Research Satellite (1992)	Solar array failed to track sun	Clutch failure

95TR4/V2

Lessons Learned:

Deployables

Deployables shall, where practicable, be designed so that they are self supporting when placed in any orientation relative to gravity, while in either the stowed or deployed configuration. Deployables shall be designed with sufficient motive force to permit full operation during ground testing without depending upon the assistance of gravity to demonstrate deployment.

Retention and Release Devices. Positive retention provisions shall be provided for deployables in the stowed and in the deployed position. The effects of deflections such as those induced by centrifugal forces or differential thermal growth of any deployable with respect to its space vehicle attachments shall be considered in the design of the attachments. Devices that may be subject to binding due to misalignment, adverse tolerances, or contamination shall not be used. Slip joints shall be avoided, where practicable.

Pin Pullers. Where pin pullers are used, such as cartridge-actuated or nonexplosive pin pullers, they shall be designed to be in double shear. The design, installation, and checkout procedures for pin pullers shall ensure that loads due to misalignment of the pin are within design limits. A minimum retraction force margin of safety of 100% at worst-case environmental conditions and under worst-case tolerances shall be maintained for all nonexplosive pin pullers.

Bearings. For deployables, hinges, and linkages, self-aligning bearings shall be used (where practicable) to preclude binding due to misalignments. Bearings shall not be used for ground current return paths or to carry electrical current. All ferrous material bearings shall employ (where practicable) a corrosion-resistant steel that is in accordance with QQ-S-763. Rolling element bearings shall, where practicable, be of 440C stainless steel; however, 52100 or M50 steels may be employed providing they are suitably protected from corrosion.

Dry Film Lubrication. Application of dry film lubricants to the surfaces of bearings, V-band clamps, coil springs, leaf springs, clock springs, constant force springs, gears, or other items shall be by an appropriate process. Bonding, peening, sputtering, vacuum deposition, ion plating, or any other process that provides a predictable, uniform, and repeatable lubricant film may be appropriate. Composite materials containing dry film lubricant in their composition may be used in appropriate applications. Where appropriate, dry film lubricants should be burnished to provide a uniform film that reduces the coefficient of friction from the as-applied condition and minimizes the generation of lubricant powder. Corrosion-resistant materials shall be used in bearings employing dry film lubricants. Consideration shall be given to protection of molybdenum disulfide dry film lubricants from adverse affects due to exposure to atmospheric humidity. Testing in a humid environment shall, where practicable, either be avoided or minimized.

Hard Coatings. Hard coatings such as titanium carbide, titanium nitride, and chromium may be used to extend life, reduce wear, prevent welding, reduce friction, and to prevent corrosion either with or without a liquid or dry film lubricant.

Rotating Wheels

Ball Bearings. Bearings used in critical applications such as reaction wheels, control moment gyros, gimbals, despin mechanisms, and pointing devices shall meet ABEC 7, 7P, or 7T tolerance or better in accordance with the AFBMA Standards.

Lubrication Requirements. Bearings operating in the boundary lubrication regime (i.e., contact of asperities) shall be avoided, where practicable. If bearings must be operated in the boundary lubrication regime, a boundary lubricant with good antiwear characteristics shall be used. Perfluorinated polyether and silicone lubricants should be avoided in this regime except where light loads and limited travel are expected. Where bearing lubricant reservoirs are used, the reservoir shall be attached (where practicable) to an area of relatively high temperature to enhance molecular and surface flow into the bearing. Barrier films or shielding or both may be used to separate the bearing from the reservoirs to minimize surface migration such as that caused by loss of lubricant due to wicking action of the reservoir. Incorporation of the above techniques dictates that the lubricant transfer mechanism be primarily by molecular flow. The preferred approach to lubrication of bearings involves placing the reservoirs in intimate contact with the bearing races and adding a larger amount of lubricant than would be ordinarily required to provide acceptable lubricant films. The above method of lubrication is preferred providing that any increase in churning torques can be tolerated.

Bearing lubrication tests and supporting analyses shall be used to show that the chosen lubricant transport mechanisms such as surface migration, vaporization, and wick action provide effective lubricant films over the expected operating temperatures, thermal gradients, and internal environments. If providing adequate life of bearings depends on their operating in an elastohydrodynamic lubrication regime and not in the boundary lubrication regime, and it cannot be clearly shown by analysis that the bearing operating range is well within the regime, then a test method, such as contact resistance measurements, shall be used to establish that an elastohydrodynamic film is being generated. In general, the lubrication system variables that should be substantiated by component development tests include (as appropriate) the amount of lubricant, retainer design, reservoir design, and the reservoir proximity to the areas requiring lubrication. When liquid lubrication is used, the design shall ensure that migration of the lubricant through the seals is not excessive or detrimental to the space vehicle.

Gears. All gears used in moving mechanical assemblies shall be in accordance with the standards of the American Gear Manufacturers Association (AGMA). Hunting-tooth gear ratios shall be used (where the application is appropriate) to distribute wear. For better protection of the gear teeth, the through hardness or surface hardness or both may be increased, and the surface finish of the teeth improved through grinding, honing, lapping, and prerun-in. The through hardness may be increased by material or heat treatment changes. The surface hardness may be increased by nitriding, carburizing, induction hardening, or anodizing. Undercutting of spur gear pinions should be avoided.

Key Words:

Deployable Appendages

Mechanisms:

Solar Arrays, Antennas, Robotic Arms

Systems:

General Spacecraft

Authors; Experts:

R. Farley and E. Devine

Address:

NASA-Goddard Space Flight Center
Greenbelt, Maryland 20771

Telephone:

Title:

Spacecraft Deployable Appendages
Deployed Appendage Design Philosophy

Source:

Goddard Space Flight Center (1991)
Engineering Directorate

Abstract:

This report discusses experience with various spacecraft and provides general guidelines for deployment mechanisms.

Anomalies:

- Nonredundancy of the motion-producing elements
- Snagging
- Stiction
- Torque ratio and torque margin insufficient
- Binding of panel hinges
- Excessive impact loads from deployment
- Poor selection of solid lubricants. Molydisulfide solid lubricants absorb water that can freeze and jam hinges and V-cone guides
- Improper cone angle for cone supports
- Excessive bending stiffness of wire harness at low temperatures
- Insufficient instrumentation

Lessons Learned:

- Torque Ratio: $T_r = \text{available torque} / \text{resisting torque} > 4$
Torque Margin: $T_m = (\text{available torque} - \text{resisting torque}) / \text{resisting torque} > 3$
 $T_m: T_r - 1$
- Panel hinges should have spherical bearings with axial clearance to avoid binding.
- Dampers are necessary to reduce kinetic energy at impact.
- Tioxode V provides an acceptable hard slippery coating. Avoid molydisulfide solid lubricants.
- Cone support angle $< 30^\circ$ to avoid locking.
- Joint actuators must have sufficient margin to overcome low-temperature wire harness torque. Capability should be tested at temperature with wire harness.
- Sensors should be applied to deployment devices to determine:
 - Initial motion
 - Intermediate position
 - Latch lock indication.
- For articulation motors, sensors should be applied for:
 - Output shaft position
 - Null reference indication
 - Speed
 - Current.

Key Words:

Coalignment, Kinematic Support, Mechanical Isolation

Mechanisms:

Experiment Support Plate

Systems:

Coalignment System

Authors; Experts:

Robert E. Federline

Address:

NASA-Goddard Space Flight Center
Greenbelt, Maryland 20771

Telephone:**Title:**

Coalignment of Spacecraft Experiments

Source:

15th Aerospace Mechanisms Symposium, NASA Conference Publication 2181 (1981).

Abstract:

On February 14, 1980, the solar maximum mission satellite was launched into orbit with experiments to monitor solar activity. To obtain common object observations, experiments must be coaligned within 90 arc-sec of the spacecraft pointing vector. Hardware was designed to minimize structural and thermal distortions of the experiment support plate. Coalignment was provided through control of a unique interface, which combined flexible blades to limit load transfer and spherical seats for alignment reference.

The paper describes the hardware used to achieve coalignment and identifies the techniques used to achieve coalignment of experiment on solar maximum mission.

Anomalies:

A detailed structural analysis of the support plate and mounted experiment was carried out using NASTRAN. This was used to predict optical vector alignments, which were compared with measured data. Cross checking the two sets of data identified questionable values that were then subjected to detailed investigation. This resulted in the discovery and correction of several inconsistencies in both the measurement technique and the analysis.

Lessons Learned:

- Using kinematic principles and good design practices it is possible to produce a stable support platform that is isolated mechanically and thermally from its supporting structure and from experiments mounted on it.
- Through the use of reference surfaces, gages, and optical measuring techniques it is possible to coalign experiments to a high degree of accuracy.

Description:

The specific requirement was to provide a stable platform for in-orbit solar observation where the experiment boresights would be coaligned to the solar pointing vector within 90 arc-sec. The solar pointing vector is defined as the boresight of the fine-pointing sun sensor. Because its location could be adjusted in orbit by software modifications, the specification translated to coalignment of experiment boresights within 180 arc-sec of each other.

The approach selected was to provide a single plate where experiments could be mounted on both sides. The plate is isolated from thermal and mechanical distortions originating in its support structure and in the experiments; this provides the stable platform. To align the experiments, an alignment template is used that accurately defines the experiment interface. With optical reference surfaces for three-axis determination, the alignment template provides the common link between the experiment boresight through the interface to the spacecraft hardware. With a unique template for each experiment, individual experiment boresights are aligned to a common optical vector.

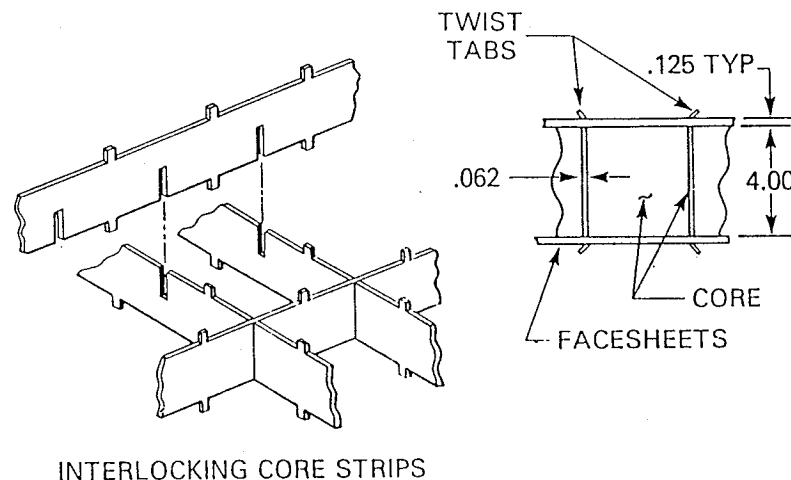
Isolation of the support plate from its support structure is effected mechanically by true kinematic support. The plate is supported at only three points; one at each side and one in the center. A spherical bearing with a breakaway torque of less than 0.9 Nm is installed at each support point. Additional bearings are installed at the base of the center strut and in a trapeze joint at one side of the plate. Thermal isolation of the support plate is achieved by wrapping the plate and support structure in 20 layers of aluminized mylar super-insulation. The support structure is made from welded titanium plates and the center strut is made from graphite-reinforced epoxy. The use of titanium and graphite epoxy provides thermal resistance and conductively insulates the plate from the support structure.

The second step was to isolate the support plate from the experiments. Thermal isolation was achieved with thermal blankets and titanium in the experiment mounts. The experiment interface can be precisely aligned with the plate while a flex-blade type of mount minimizes load transfer. Forces resulting from hardware shifts during launch and thermally induced dimensional changes are first localized by the flex mounts and then converted to bending within the mount itself.

The construction of the support plate is shown in Figure 1. After assembly, the plate is dip-brazed then heat treated, fog-quenched, and aged. Holes 3.8 cm in diameter were centered through the face sheets in each of the core cells. Magnesium corner reinforcement brackets were installed internal to each cell where experiment mounts were to be installed and where loads require stiffening doublers. Experiment mounts fit through the holes in the face sheet and into the cell, as shown in Figure 2. With the aid of a backing plate, the experiment mounts are rigidly bolted to the front and back face sheets. Internal to the mount is a titanium stud machined in the form of a flex blade. Experiments are constrained to use three mounts. The weak axis of two blades is radially oriented to the stiff blade. The configuration is a right triangle with the stiff blade at the apex. Spherical bearings and seats on the top of each mount define a unique interface for each experiment.

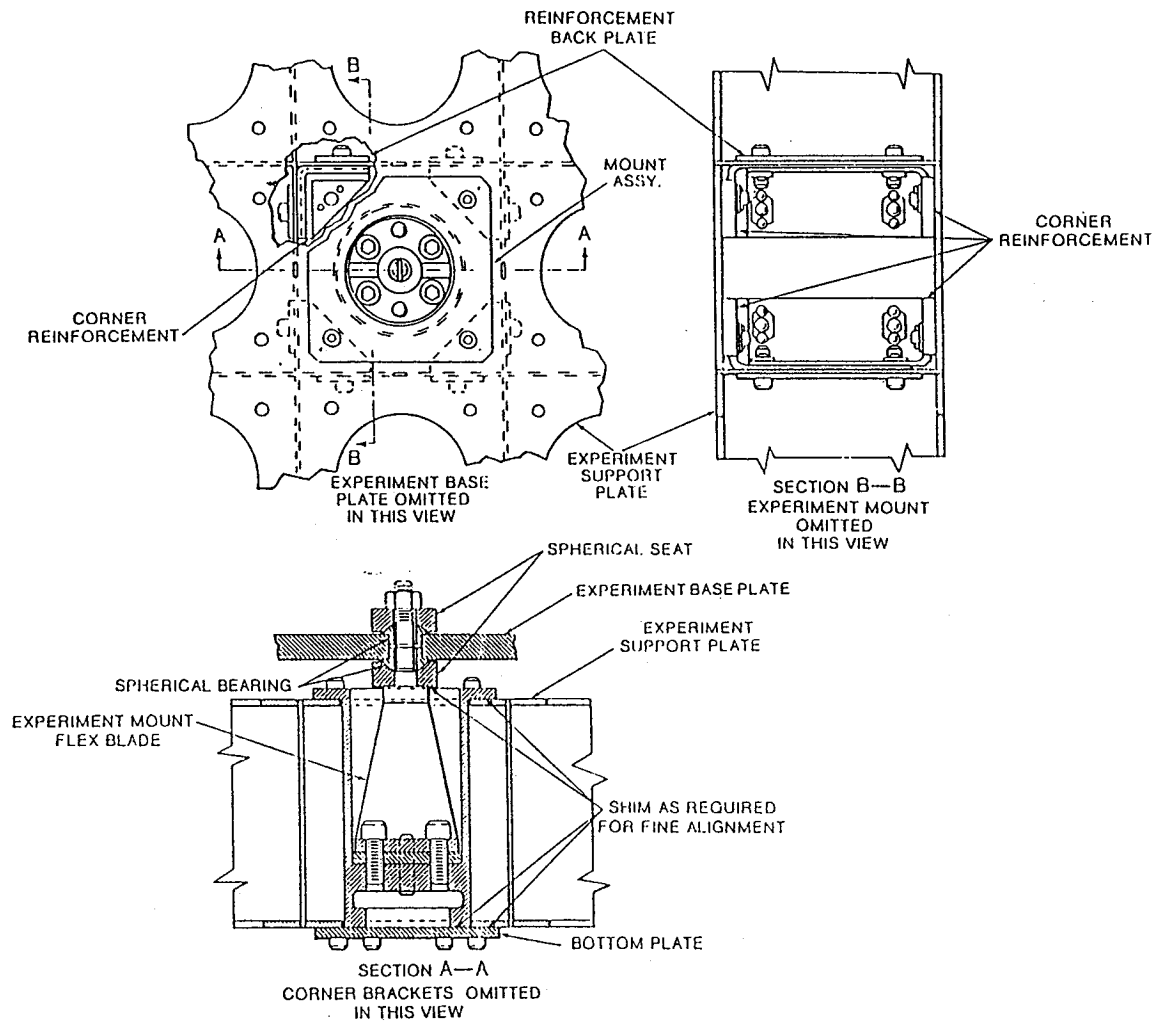
The alignment templates are accurately machined from a tooling plate and contain an integral interface to accommodate a master alignment gage. Optical measurements are made between an optical cube installed on the template and the master gage. The alignment template is attached to the experiment base structure and the mounting holes are simultaneously machined into both pieces in an in-line machine operation. When separated from the template, assembly of the experiment onto its base structure continues with the following restrictions:

- The completed instrument must be aligned to the hole pattern in the base structure.
- An alignment reference must be installed on a stable portion of the experiment structure. The reference must be aligned with the boresight within the tolerance of the measurement facility to see it. For the facility used on the solar maximum mission, this value was 5°.
- The three-axis bias values between the experiment boresight and the experiment reference cube, and between the experiment reference cube and the alignment template cube must be measured.



95TR4/V2

Figure 1. Experiment Plate Construction



95TR4/V2

Figure 2. Experiment Mounts

Bearing halves are installed in the holes in the alignment template and these define a single unique interface. The alignment template and the bias values are used to locate the experiment mounts in the support plate. Shims are installed between the experiment mount housing and the support plate to coplanarize mount sets and ensure a good fit to the support plate. The mounts are then adjusted to optically align the template reference to the main pointing vector. The mounts are then dowel-pinned to the support plate. From now on, only fine alignment adjustments can be made. In two of the axes, this is achieved by placing ground shims between the bearing seat and the top of the flex blade in the mount. Adjustment of the third axis is accomplished by exchanging the nominal concentric bearing seats with seats of a known offset.

When all the experiments are mounted on the support plate, a final optical measurement is made. This becomes the baseline from which alignment shifts are monitored throughout the observatory integration and test program.

Testing:

A detailed analysis using NASTRAN was carried out in parallel with the collection of measured data to predict optical vector alignments. This provided a check on the measured data by identifying questionable values for detailed investigation. Conversely, the measured data were used to validate and revise the math model. This cross-check of alignment data accounted for the discovery and correction of several inconsistencies in both the measurement technique and the analysis. It also produced a high level of confidence in the accuracy of the math models used for structural analysis.

Experience:

Results in orbit indicate that the coalignment goal was achieved. One month after launch, quick-look data were extracted for the critical instruments and this showed that they lay within a 90-arc-sec error circle.

Key Words:

Cryovalve, Liquid Helium Valve, Cryogenic Mechanisms

Mechanisms:

Cryogenic Mechanisms

Systems:

Linear Motion

Authors; Experts:

K.R. Lorell, J.N. Aubrun, D.F. Zacharie, and D.J. Frank

Address:

Lockheed Palo Alto Research Laboratory
Palo Alto, California

Telephone:

Title:

Development of a Motorized Cryovalve for the Control of Superfluid Liquid Helium

Source:

22nd Aerospace Mechanisms Symposium (1988).

Abstract:

Recent advances in the technology of infrared detectors have made possible a wide range of scientific measurements and investigations. The infrared astronomy satellite, The cosmic background explorer, the Space Infrared Telescope Facility (SIRTF), and the Infrared Space Observatory (ISO) are all examples of this new generation of instruments. One of the requirements for the use of sensitive infrared detectors is that the entire instrument be cooled to temperatures approaching absolute zero. The cryogenic cooling system for these instruments is commonly designed as a large dewar containing liquid helium which completely surrounds the apparatus. Thus, there is a need for a remote-controlled, motorized cryovalve that is simple, reliable, and compact and can operate over extended

PRECEDING PAGE BLANK NOT FILMED

periods of time in cryovac conditions. This paper describes the design, development, and test of a motorized cryovalve with applications to a variety of cryogenic systems currently under development at Lockheed.

Anomalies:

In one test of the cryovalve, the 1000-N seating force damaged the copper valve stem. A modification was made to the lift rod and the spring housing to improve the alignment and this resolved the problem.

Lessons Learned:

- At low speed and for a limited number of cycles, electric motors and gearboxes may run without lubrication.
- In general, the mechanical problems that are encountered with cryomechanisms are the result of: 1) mismatches in the coefficients of thermal expansion, and 2) the friction and wear properties of moving parts.
- Motors should be of the brushless or stepper design because brushes are unreliable in vacuum. They must have adequate power to overcome friction even with unlubricated surfaces. Motor leads to the outside are also thermal paths along which heat can travel.
- There are two sources of heat which can be of concern: 1) thermal energy generated by the equipment inside the shell, and 2) thermal energy leakage from the outside traveling along the wires.
- Reliability. Since the mechanisms are usually located inside the shell where they are inaccessible, it is critical that they function with a high degree of reliability.

Description:

The use of sensitive infrared detectors for scientific investigations, such as telescopes, has made it necessary to be able to cool the entire instrument to temperatures approaching absolute zero. The cryogenic cooling system for these instruments is commonly designed as a large dewar containing liquid helium that completely surrounds the apparatus. There is a need for a remote-controlled, motorized cryovalve that is simple, reliable, and compact and can operate over extended periods of time in cryovac conditions. This paper describes the design, development, and test of such a valve.

The valve must be virtually leak proof and the mechanisms that open and close the valve must operate reliably at temperatures just above absolute zero. It is estimated that a force of 1000 N will be required to close a 1/4-in. valve. This will require a motor acting through a gear reduction set to shut off the valve and maintain closure. To function properly, the stem and seat must be able to open and close over the entire operating temperature range from ambient to 1.5 K.

The valve design that was selected is similar to the valve used in automobiles. Figure 1 shows how the valve is actuated. A stack of Belleville washers is used to provide the spring force for closure. Valve opening is accomplished by using a lever and pivot arrangement. This concept has the advantage that the seat force is constant, predictable, and repeatable.

To develop enough force with a small motor to open the valve, a spindle-and-tape arrangement was used as shown in Figure 2. The spindle-and-tape arrangement has several advantages. It is a simple and direct way of converting rotary motion into linear motion. It requires no pivots or gears and attaches directly to the lift arms. Because the tape pulls on the spindle from both sides, there is zero net side force on the gearbox output shaft. This is particularly important because the gearbox must run without lubrication and the friction losses in the gearbox are a noticeable part of the motor torque requirement.

The other aspect of the spindle-and-tape drive is the means of balancing the forces on each of the lift arms. If the tape were attached directly to each of the arms, even a slight decentering of the spindle with respect to the arms would cause the arms to have very different engagement forces at the lift pin. Figure 3 shows a continuous steel-tape drive. Instead of being directly attached to the arm, the metal tape is made as a continuous loop and, thus, the tension force of each arm is balanced.

The motor and gearbox drive is shown schematically in Figure 4. Since the speed was so low and the total number of cycles was limited, both the motor and gearbox were run with no lubricant. No problems were encountered.

The valve was a commercially available sealed-stem unit manufactured by Nupro. Figure 5 shows the cryovalve assembly.

Test experience indicated that in one trial the 1000-N seating force may have been detrimental to the copper valve stem. A modification was made to the lift rod and the spring housing to improve the alignment and this resolved the problem.

A full-scale test of the motorized cryovalve was apparently successful, although no details were given.

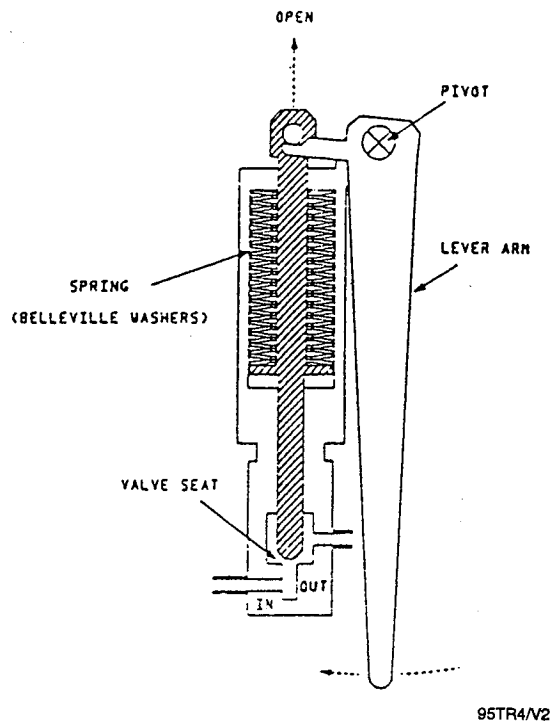


Figure 1. Valve Actuation Showing Spring and Lever Mechanism

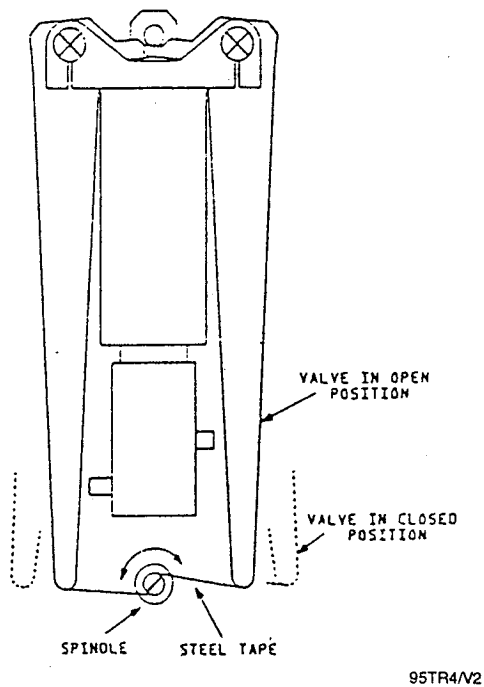
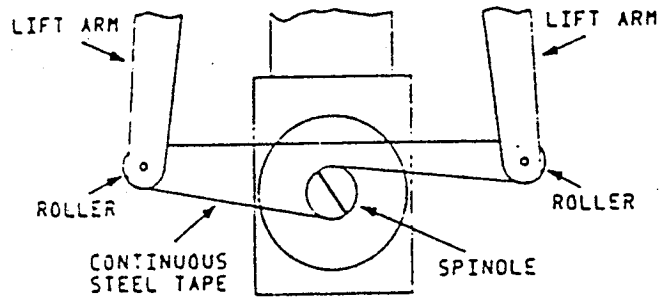
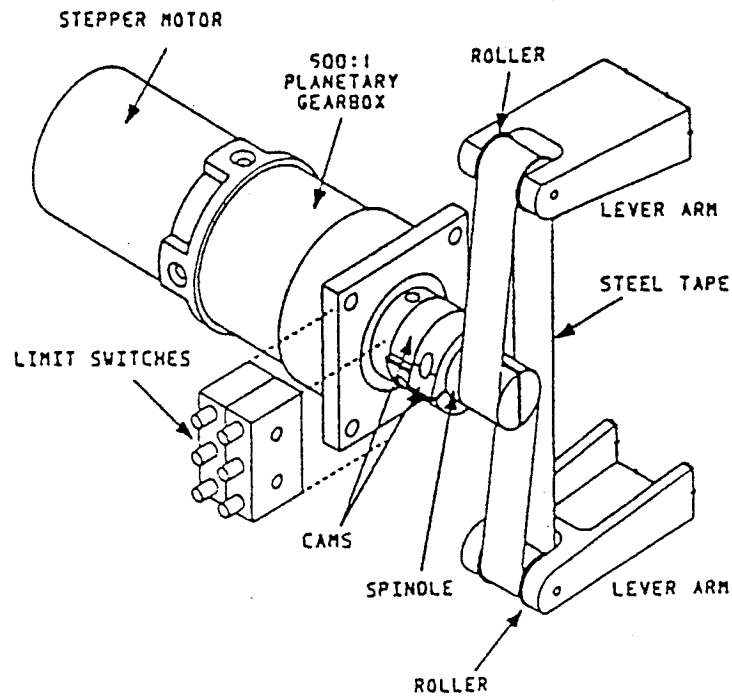


Figure 2. Spindle and Steel-Tape Drive for Lift-Arm Actuation



95TR4/V2

Figure 3. Continuous Steel-Tape Drive



95TR4/V2

Figure 4. Motor and Gearbox Drive Mechanism Detail

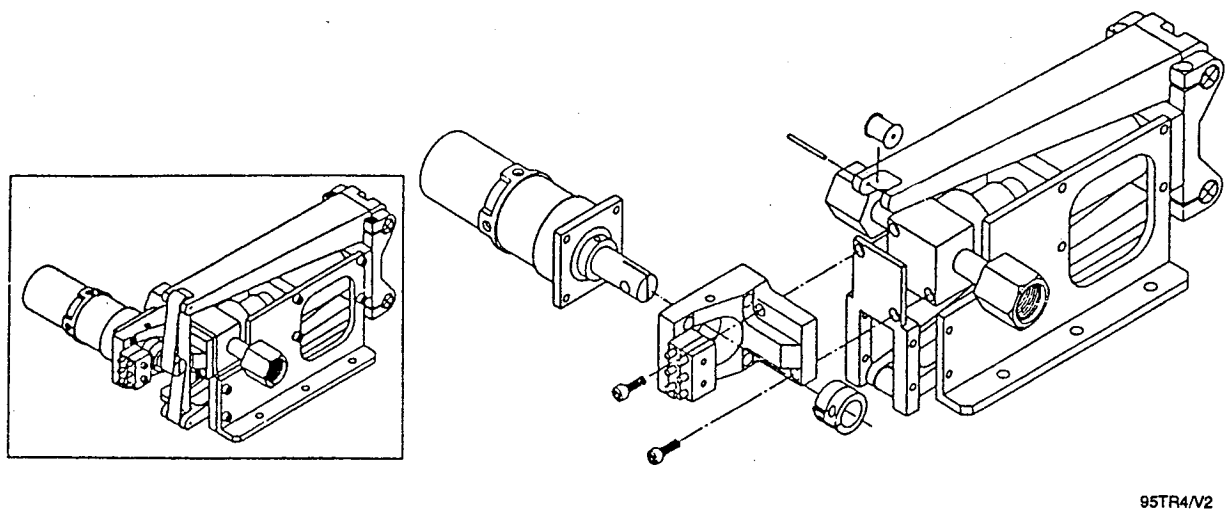


Figure 5. Cryo Valve Assembly

Key Words:

Thermal-Vacuum Testing, Solar Arrays, Despin Mechanisms, Slip Rings,
Pointing Mechanisms, Momentum Wheels

Mechanisms:

Solar Array Drive, Despin Mechanisms, Motor Drive Systems, Slip Ring Assemblies,
Antenna Pointing Mechanisms, Gimballed Momentum Wheels

Systems:

Rotating Systems, Deployable Systems

Authors; Experts:

K. Parker

Address:

European Space Tribology Laboratory
Risley, Warrington, United Kingdom

Telephone:

Title:

The Importance of Thermal-Vacuum Testing in Achieving High Reliability of Spacecraft
Mechanisms

Source:

18th Aerospace Mechanisms Symposium (1984).

Abstract:

The paper describes the work performed at the European Space Tribology Laboratory (ESTL) on thermal vacuum testing of complex mechanisms for the European Space Agency and several European customers. The objective of these tests is to assess the mechanism reliability by monitoring performance in an environment that closely resembles that which will occur during flight. To be both valid and cost effective, these tests must be performed in a detailed, formally controlled manner.

A review of the major test observations at ESTL over a 10-yr period is given, during which time some totally unexpected failure modes have been detected. Full confidence now exists in many mechanisms and component designs, and much valuable data were obtained that are available to mechanism designers for improving reliability.

Lessons Learned:

- Thermal-vacuum testing has proved to be essential in providing a detailed assessment of the reliability of complex mechanisms by subjecting them to realistic simulations of the anticipated flight conditions, where lifetimes in excess of 10 yr are now expected.
- Thermal vacuum test have been proved to be cost effective in avoiding delays and disturbances to a number of European projects, as several previously unknown failure modes have been detected. There is now complete confidence in many designs following independent, fully documented performance assessment.
- Much valuable data were obtained on many mechanisms and components about their operational parameters, power dissipation, and wear processes. There is frequent evidence of how important it is to implement comprehensive inspection and product assurance systems at all stages of mechanism development and construction, to avoid the human factors of accidents, errors, and poor judgement.

Description:

Even with elaborate thermal control systems and detailed analysis, it is not always possible to accurately predict the temperature distribution in a mechanism. When several components may be operating to different control sequences, resulting in variable power dissipation, thermal gradients can occur over very small areas of a device. The performance of individual components may have been assessed before assembly but it is still possible that unpredictable behavior and possibly failure of a component will occur in systems subjected to extreme temperatures and temperature gradients. Complete confidence in a particular design is only achieved when every possible failure mode has been identified and either designed out of the system or accepted with adequate demonstration of reliability.

At ESTL, certified clean room conditions have proved to be essential in the success of thermal-vacuum testing, particularly with regard to the handling and inspection of mechanisms. ESTL has several different types of ultra-high vacuum test chambers. Emphasis is always placed on maintaining very clean test systems and for this reason the only types of pumps used on the vacuum chambers are high-reliability turbomolecular, titanium-sputter ion, and cryogenic pumps. The environment is often determined by the amount of vapor outgassing from the mechanism under investigation. It is usually considered that a valid tribological test can be performed below 10^{-7} mbar. Each system is fully instrumented with mass spectrometry facilities for residual gas analysis. This is very important as undesirable gas species such as oxygen and other active gases must be identified and, where possible, excluded. Usually, it is necessary to ensure that the partial pressure of oxygen, for example, is well below 10^{-9} mbar. A thermal interface enclosure is built around the mechanism in such a way that there are two independently controlled boundary interface temperatures. These two temperatures are determined by radiation to and from thermal shrouds whose temperatures are controlled in the range -90° to $+120^{\circ}\text{C}$ by high-reliability fluid circulation systems and electrical heating units. Space-approved materials of certified

purity are used throughout the construction of the thermal test environment. Instrumentation systems are available to monitor to very fine limits such test parameters as thermal distribution, speed, torque, angular motion stability, and slip ring noise. Selected parameters of the thermal control system, the pumping units, and the mechanism under test are linked to high-reliability, redundant protection systems so that any deviation from prescribed limits can be sensed and the appropriate corrective action can be taken. This is vital to ensure that there is never any risk of the test itself causing the possibility of additional failure modes.

The majority of solar array drive mechanisms tested at ESTL have been intended for communications satellites in geostationary orbit where the mechanism is subjected to thermal gradients. Typical test temperatures are shown in Table 1. Additional tests may be necessary to simulate the extreme conditions experienced in an eclipse, typically a drop of 60°C in the shaft temperature in 72 min followed by an increase of 60°C in 30 min.

Many European solar array drive mechanisms use bearings of the highest available precision that have been lubricated by a thin film of lead deposited by an ESTL ion-plating process.

The solar-generated power, typically 2 kW, is transmitted by slip rings that are often fabricated from silver or copper with a gold plating. A common brush material is a composite of silver/copper/molybdenum disulfide (MoS_2) in volume ratio 82.5/2.5/15, respectively. Assessment of the electrical noise across the interface is necessary as this could result in unacceptable power loss and radiation interference.

In 1975, ESTL commenced a 7-yr real-life test on a solar array drive mechanism, to fully quantify the time-dependent parameters and to obtain data that would enable them to assess the validity of accelerated life testing on systems using solid lubrication. Many thermal changes were made in this test, including 420 eclipse simulations. The test was very successful; only minor changes occurred in the measured parameters. Of significant interest was that the test chamber pressure took several years to stabilize at about 1×10^{-8} mbar because of continuous outgassing from the mechanism surfaces and cable looms. It is important to note that this outgassing can be a primary cause of failure due to degradation of materials. The rotational stability and motor power requirements were remarkably consistent, showing that the friction in the slip rings and brushes had remained substantially constant. The slip rings were tested with various current levels ranging from 100 mA to 7 A. Most gave variable amounts of electrical noise, within specification, but two circuits passing 500 mA produced intermittent noise pulses that were equivalent to a resistance change of 2 ohm. The characteristics of these transients were such that they could only have been caused by the presence of variable amounts of brush wear debris, and an inevitable conclusion is that some suspicion must fall on the use of MoS_2 as brush lubricant.

Table 1. Typical Test Temperatures (°C)

Parameter	Shaft Interface	Housing Interface
Hot soak	+90	+55
Cold soak	-50	-25
Positive differential	+50	0
Negative differential	-35	+15

95TR4/V2

A second 7-yr real-life test on a different type of mechanism had to be abandoned after 4 yr because of excessive deviation from the position control stability criterion. Subsequent examination revealed that time-dependent degradation of the efficiency of an optical encoder had occurred. This failure was completely unexpected.

In 1975, ESTL started a unique real-life test on a despin mechanism in which the bearings were lubricated by BP2110 grease with BP110 oil impregnated in the cages and in Nylasint reservoirs. At 60 rpm, the conditions were bordering on boundary lubrication. One area of uncertainty was the effectiveness of oil-creep barriers and oil seals. If oil migration did occur it was essential to investigate the effect on the slip rings. Modest thermal conditions were imposed on the device, with the shaft temperature at either -5° or $+45^{\circ}\text{C}$.

Again, because of continuous outgassing, the test chamber pressure took several years to stabilize at about 1×10^{-8} mbar. Although there was no significant overall deterioration in the performance of the slip rings, there were large but temporary increases in the interface resistance following a change of thermal conditions. This may have been due to the presence of oil or differential axial expansions causing the brushes to run on a slightly different track, several days of running-in being necessary before the resistance returned to normal. There was a gradual increase in motor current probably due to a continuous reduction in the field strength of the permanent magnets in the motor. This aging process was known to occur at about 7% per year for the magnetic materials available in 1973 when the mechanism was designed. At the end of the test, the bearings were in very good condition with adequate reserves of clean oil. Although there was a significant amount of wear debris in the slip ring unit this did not effect their operational efficiency.

Many different types of motor drive systems have been evaluated. Of particular interest are torque stability, power dissipation, bearing performance, brush stability, stability of potting compounds, generation of wear particle contamination, and magnetic circuit stability.

Slip ring assemblies are present in several types of mechanisms. Much valuable data have been obtained on reliability in terms of contact resistance variation, power loss, stability of materials, friction, wear, and distribution of wear particles. Some problems have been identified in units that have been widely used and assumed to be of high reliability under all conceivable operating conditions. These test observations have resulted in ESTL embarking on a review of current slip ring technology, particularly with regard to the reliability of MoS_2 as brush lubricant. The presence of silver sulfide can have a significant effect on surface properties.

Tests on a large double-gimbal momentum wheel showed that oil lubrication was preferable to lead lubrication in the gimbal bearings. This could only be found by doing a thermal-vacuum accelerated life test.

Many measurements have been made on a large number of critical items such as stepper motors, actuator motors, spring assemblies, flexure pivots, lead screws, lead-lubricated bearings, plastic gears, and electromagnetic position sensors. The mechanisms were typical examples of the dilemma often experienced by a mechanism designer, who must guarantee that the complete mechanisms will conform to the required specification but must use components that, although of the highest quality available, are not guaranteed by the various suppliers to fulfill the required specification.

Rotating Systems

Momentum Wheels

Key Words:

Moving Mechanisms, Solar Array Drives, Momentum Wheels, Solar Array Drives, Lubricants

Mechanisms:

Pin Pullers, Bearings, Rotating Wheels, Gears

Systems:

Deployment Systems, Scanning Systems, Rotating Systems

Authors; Experts:

Anonymous

Address:

United States Air Force Space Division (SD/ALM)
P.O. Box 92960
Los Angeles, California 90009-2960

Telephone:**Title:**

Assemblies, Moving Mechanical, for Space and Launch Vehicles, General Specification For

Source:

United States Air Force MIL Standard MIL-A-83577B (1 February 1988).

Abstract:

This specification sets forth the general requirements for the design, manufacture, quality control, and testing of moving mechanical assemblies to be used on space and launch vehicles.

Before the application of MIL-A-83577B to Air Force spacecraft programs, a number of anomalies had occurred with spacecraft deployables. In addition, a number of more recent failures have occurred on spacecraft which were not designed and tested to the moving mechanical assembly specification. Most of these problems could have been avoided had the design and test requirements of the moving mechanical assembly specification been observed. These failures could have been avoided through proper design and testing. Properly designed and perceptive tests would have ferreted out things like interference between the deployable and adjacent thermal blankets or thermal distortion-related problems. Also, it is interesting to note that many of the failures could have been uncovered only by testing at the vehicle level (i.e., after the deployable was fitted to the spacecraft).

Anomalies:

Program	Problem	Cause
Program 461 (1964)	Solar array failed to deploy fully	Mishandling during storage
STP 67-2 (OV2-5) (1968)	Solar array booms failed to deploy fully	Field modification problem
777 (1970)	Omni-antenna latch broke during spin-up	Attitude control instability
Program A (1971)	Antenna failed to deploy fully	Wire harness binding
Program B (1971)	Solar array deployed late	Silicon rubber sticking
STP 71-5 (1972)	Boom not deployed	Dynamic clearance problem
SKYLAB (1973)	Solar array failed to deploy	Interference with cabling or thermal blankets
Transit (1975)	Solar array failed to fully deploy; cable hung up	Anomalous flat trajectory caused high heating rates
Viking (1975)	Sampling arm failed to deploy	Debris in gear train
STP 74-1 (SOLRAD) (1976)	Solar panel failed to deploy	Release mechanism binding
DMSP-F-1 (1976)	Solar array failed to deploy fully	Excessive wire harness stiffness
DMSP-F-2 (1977)	Solar array delayed release	Friction welding
Voyager 2 (1972)	<ul style="list-style-type: none"> Science boom failed to fully deploy Scan platform gearbox seized Magnetometer boom misalignment 	<ul style="list-style-type: none"> Microswitch failed Lubricant failure Unknown
SEASAT (1978)	Spacecraft power failed	Slip ring debris between power/ground rings
VUE (1988)	Telescope failed to rotate about Azimuth	Inadequate torque margin on azimuth caging arm
Galileo (1989)	High-gain antenna failed to deploy	Excessive friction in ball and socket joint
Galileo (1989)	Instrument cover jettisoned late	Thermal binding
Magellan (1989)	Solar array failed to latch at end of travel	Microswitch misadjusted
MACSAT (1990)	Gravity-gradient boom failed to deploy	Inadequate force margin
CRRES (1990)	Magnetometer boom failed to fully orient	Interference between thermal blanket velcro and wiring
Ulysses (1990)	Spin stabilized spacecraft wobbles	Antenna boom thermal distortion caused spacecraft center of gravity offset
Hubble Space Telescope (1990)	Solar array deployment booms oscillate as telescope goes from shade to sun	Thermal gradient across boom diameter
ANIK E2 (1991)	C-band antenna did not fully deploy	Thermal blanket interference
Unknown	Sampling arm failed to deploy	Screw backed out and wedged against housing
Upper Atmosphere Research Satellite (1992)	Solar array failed to track sun	Clutch failure

95TR4/V2

Lessons Learned:

Deployables

Deployables shall, where practicable, be designed so that they are self supporting when placed in any orientation relative to gravity, while in either the stowed or deployed configuration. Deployables shall be designed with sufficient motive force to permit full operation during ground testing without depending upon the assistance of gravity to demonstrate deployment.

Retention and Release Devices. Positive retention provisions shall be provided for deployables in the stowed and in the deployed position. The effects of deflections such as those induced by centrifugal forces or differential thermal growth of any deployable with respect to its space vehicle attachments shall be considered in the design of the attachments. Devices that may be subject to binding due to misalignment, adverse tolerances, or contamination shall not be used. Slip joints shall be avoided, where practicable.

Pin Pullers. Where pin pullers are used, such as cartridge-actuated or nonexplosive pin pullers, they shall be designed to be in double shear. The design, installation, and checkout procedures for pin pullers shall ensure that loads due to misalignment of the pin are within design limits. A minimum retraction force margin of safety of 100% at worst-case environmental conditions and under worst-case tolerances shall be maintained for all nonexplosive pin pullers.

Bearings. For deployables, hinges, and linkages, self-aligning bearings shall be used (where practicable) to preclude binding due to misalignments. Bearings shall not be used for ground current return paths or to carry electrical current. All ferrous material bearings shall employ (where practicable) a corrosion-resistant steel that is in accordance with QQ-S-763. Rolling element bearings shall, where practicable, be of 440C stainless steel. However, 52100 or M50 steels may be employed providing they are suitably protected from corrosion.

Dry Film Lubrication. Application of dry film lubricants to the surfaces of bearings, V-band clamps, coil springs, leaf springs, clock springs, constant force springs, gears, or other items shall be by an appropriate process. Bonding, peening, sputtering, vacuum deposition, ion plating, or any other process that provides a predictable, uniform, and repeatable lubricant film may be appropriate. Composite materials containing dry film lubricant in their composition may be used in appropriate applications. Where appropriate, dry film lubricants should be burnished to provide a uniform film that reduces the coefficient of friction from the as-applied condition and minimizes the generation of lubricant powder. Corrosion-resistant materials shall be used in bearings employing dry film lubricants. Consideration shall be given to protection of molybdenum disulfide dry film lubricants from adverse affects due to exposure to atmospheric humidity. Testing in a humid environment shall, where practicable, either be avoided or minimized.

Hard Coatings. Hard coatings such as titanium carbide, titanium nitride, and chromium may be used to extend life, reduce wear, prevent welding, reduce friction, and to prevent corrosion either with or without a liquid or dry film lubricant.

Rotating Wheels

Ball Bearings. Bearings used in critical applications such as reaction wheels, control moment gyros, gimbals, despin mechanisms, and pointing devices shall meet ABEC 7, 7P, or 7T tolerance or better in accordance with the AFBMA Standards.

C-3.

Lubrication Requirements. Bearings operating in the boundary lubrication regime (i.e., contact of asperities) shall be avoided, where practicable. If bearings must be operated in the boundary lubrication regime, a boundary lubricant with good antiwear characteristics shall be used. Perfluorinated polyether and silicone lubricants should be avoided in this regime except where light loads and limited travel are expected. Where bearing lubricant reservoirs are used, the reservoir shall be attached (where practicable) to an area of relatively high temperature to enhance molecular and surface flow into the bearing. Barrier films or shielding or both may be used to separate the bearing from the reservoirs to minimize surface migration such as that caused by loss of lubricant due to wicking action of the reservoir. Incorporation of the above techniques dictates that the lubricant transfer mechanism be primarily by molecular flow. The preferred approach to lubrication of bearings involves placing the reservoirs in intimate contact with the bearing races and adding a larger amount of lubricant than would be ordinarily required to provide acceptable lubricant films. The above method of lubrication is preferred providing that any increase in churning torques can be tolerated.

Bearing lubrication tests and supporting analyses shall be used to show that the chosen lubricant transport mechanisms such as surface migration, vaporization, and wick action provide effective lubricant films over the expected operating temperatures, thermal gradients, and internal environments. If providing adequate life of bearings depends on their operating in an elastohydrodynamic lubrication regime and not in the boundary lubrication regime, and it cannot be clearly shown by analysis that the bearing operating range is well within the regime, then a test method, such as contact resistance measurements, shall be used to establish that an elastohydrodynamic film is being generated. In general, the lubrication system variables that should be substantiated by component development tests include (as appropriate) amount of lubricant, retainer design, reservoir design, and the reservoir proximity to the areas requiring lubrication. When liquid lubrication is used, the design shall ensure that migration of the lubricant through the seals is not excessive or detrimental to the space vehicle.

Gears. All gears used in moving mechanical assemblies shall be in accordance with the standards of the American Gear Manufacturers Association (AGMA). Hunting-tooth gear ratios shall be used (where the application is appropriate) to distribute wear. For better protection of the gear teeth, the through hardness or surface hardness or both may be increased, and the surface finish of the teeth improved through grinding, honing, lapping, and prerun-in. The through hardness may be increased by material or heat treatment changes. The surface hardness may be increased by nitriding, carburizing, induction hardening, or anodizing. Undercutting of spur gear pinions should be avoided.

Key Words:

Momentum Wheel Bearings, INTELSAT VII, Long-Duration Missions

Mechanisms:

Ball Bearing Momentum and Reaction Wheels

Systems:

INTELSAT VII, SYMPHONIE, IRAS, ECS, INTELSAT VI, TV-SAT, EUTELSAT 2,
and DFS-KOPERNIKUS

Authors; Experts:

W. Auer

Address:

TELDIX GmbH
Heidelberg, Germany

Telephone:

Title:

Test Results and Flight Experience of Ball Bearing Momentum and Reaction Wheels

Source:

NASA Conference Publication 3062
24th Aerospace Mechanism Symposium

Abstract:

The required satellite mission durations and levels of reliability have been considerably increased. In the beginning of the 1970s, 3- to 5-yr missions were planned (the standard is now 10 yr with an expansion to 15 yr and more for such programs as INTELSAT VII). Based on a 20-yr test and flight experience with basically the same design, ball bearing momentum and reaction wheels with the required 15-yr mission capability can be provided.

Lessons Learned:

- Ball bearing lubrication remains the principal life-limiting problem on momentum and reaction wheels.
- Means for lubricant replenishment can improve life characteristics. The wheel described in this paper incorporated a lubrication reservoir actuated by centrifugal force to relubricate the bearings. The base oil is stored as a grease in a ring-type chamber, which is centrifuged out through orifices. The rate is limited by the thickener of the grease that forms a microporous filter in the vicinity of the orifices. Overlubrication, as measured by torque increase, does not appear to be a problem for this system.
- Oil lubrication is favored over grease because of superior torque characteristics and means for replenishment.
- The minimum amount of initial lubricant required is 2 mg.
- Extended life appears promising. The test results and flight operations are promising but not conclusive. Two ground test wheels (3000 and 3800 rpm) had run for 16 yr after full qualification. These wheels had been subjected to temperature cycling and showed minimal changes in torque. The longest operation time in space was the OTS wheel, which had run 11.5 yr at the time this paper was presented.

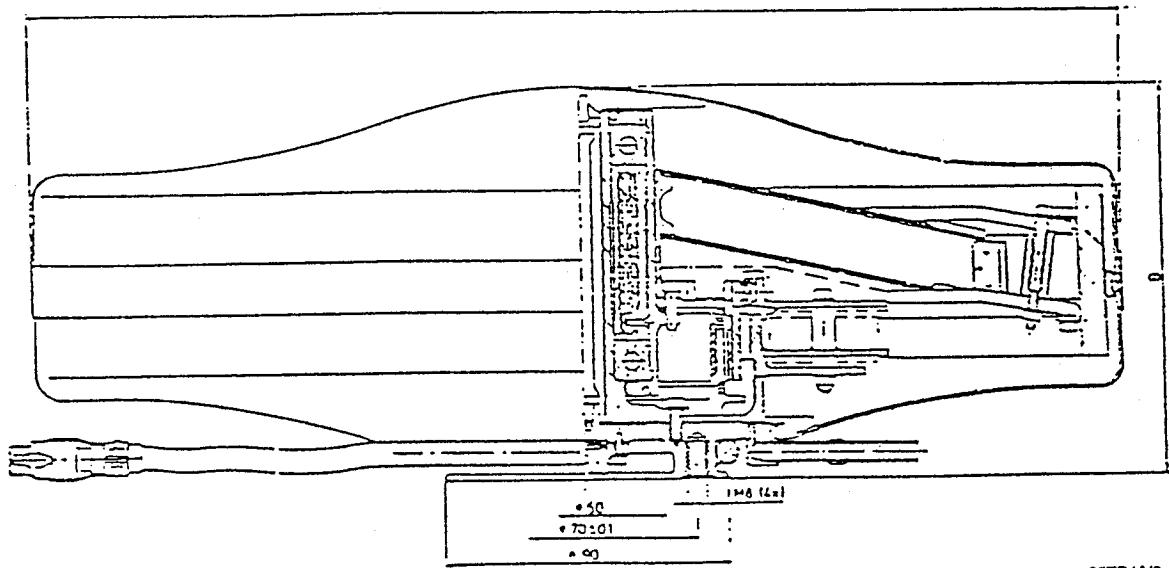
Description:

Many engineers are taking the approach that modular design of components, such as momentum wheels, is the most reliable way to build and upgrade these components as needed. The modular design that was selected uses one type and size of ball bearing for three wheel diameters ranging from 22 to 35 cm. The largest (35 cm dia), which is most often used, has the following main parameters:

- Wheel diameter: 35 cm
- Height: 12 cm
- Angular momentum: 12 to 80 Nms
- Mass: 5 to 8.4 kg

A sketch of the wheel is shown in Figure 1. It has five subassemblies:

1. Housing. Two parts spun from sheet metal. The upper half is soldered to the lower half. The lower half contains the base plate, which is fixed by electron beam welding. The curvature of the housing, plus the center stud bolt, is responsible for the ability of the housing to withstand air pressure during and after evacuation.
2. Flywheel. For a favorable inertia-mass ratio, the flywheel rim is linked to the hub by stiff, double-T-shaped, sheet metal spokes. To avoid resonance problems, the flywheel mass is damped by two damper rings in frictional contact with the spokes.



95TR4/V2

Figure 1. Momentum Wheel

3. Ball Bearings. Two 20-mm bore ball bearings (assumed to be angular contact bearings), are preloaded to each other by spacer sleeves and nuts. It was stated that the materials and design were chosen to maintain an almost constant preload regardless of temperature level or temperature gradients, but no specifics were given. The retainer material was not specified, but it sounds like a conventional cotton or linen fabric-laminated phenolic. Both SRG-60 and KG-80 mineral oils were evaluated as lubricants, but neither the results nor the final selection were reported. It was stated that the initial amount of oil in the bearing is sufficient to maintain an elastohydrodynamic film for years of service.
4. Motor. The motor is a brushless and ironless dc motor. Depending on the torque required, either one of the two cylindrical surfaces of the U-shaped rotor are covered with samarium cobalt permanent magnets.
5. Motor Stator. The motor stator with commutation electronics has stator coils inserted into the holes of the cylindrical support of the armature. The stator is mounted between the above-mentioned rotor surface. Thus, the permanent magnet flux is cutting the wires of the windings. To avoid eddy currents, stranded wire is used in most applications. The commutation sensors, together with a shutter ring, control the currents in the coils of the motor via electronics.

Testing:

Lubrication and Bearing Tests. Bearing life prediction, using a modified AFBMA formula, indicated that at 6000 rpm, the life of the bearings should be about 18 yr. Oil lubrication was selected over grease because grease often shows wide torque changes, especially when the temperature is varying. Oil is also easier to resupply.

Bearing tests, using torque, speed, and electrical contact resistance measurements to demonstrate elastohydrodynamic lubrication, showed that 2 mg of oil was adequate for full elastohydrodynamic lubrication, while 1 mg of oil showed signs of oil starvation. The use of 2 mg of oil also showed that the friction torque of the bearing changed only about 10% over the temperature range from -10 to +55°C.

The initial charge of lubricant into the bearings was enough to provide an elastohydrodynamic film for years of operation. To supply additional oil, a lubricant reservoir (activated by centrifugal force) was located between the outer rings of the bearings. After a period of time, this reservoir was designed to start bleeding oil back into the outer rings of the bearing. The approach seems feasible, but rather complex. To demonstrate that overlubrication would not be a problem, some tests were run with excess oil supplied to the bearings. Higher currents and an increase in torque noise were noted, but steady-state conditions were restored with running time.

Evaluation and Life Testing. A test on a wheel that had been qualified, then stored for 5 yr, demonstrated that no deterioration had occurred. Extensive life testing has been done. Ground tests have completed more than 16 yr of operation after they had been fully qualified. Tests at varying temperatures have been consistently successful after 10 yr of operation.

Flight Experience. At the time this paper was written, 40 satellites were using this design. As of November 1989, the OTS wheel has the longest service time (11.5 yr in orbit). No ball bearing failures have occurred. Tables 1 and 2 show some test and flight results.

Table 1. Test and Flight Results of OTS-B

Speed (rpm)	Acceptance Test (November 1976)			Flight (18 October 1989)
	at 22°C (mA)	at -5° (mA)	at 45°C (mA)	4000 rpm at 31°C (mA)
3600	220	284	186	Minimum: 206
4000	230	292	192	Maximum: 292
4400	234	294	198	Average: 248

95TR4/V2

Table 2. Test and Flight Results of INTELSAT V

Launch	Acceptance Test (A)	Pre-Launch (A)	Post-Launch (A)	July 1985 (A)	May 1988 (A)
F1 December 1980	0.17	0.21	0.19	0.19	0.19
F2 May 1981	0.23	0.22	0.20	0.19	0.19
F3 December 1981	0.20	0.23	0.20	0.19	0.20
F4 March 1982	0.21	0.20	0.20	0.21	0.20
F5 September 1982	0.20	0.21	0.20	0.19	0.19
F6 May 1983	0.19	0.18	0.17	0.19	0.18
F7 October 1983	0.21	0.25	0.20	0.21	0.21
F8 March 1984	0.20	0.18	0.17	0.20	0.20
F10 April 1985	0.17	0.21	0.20	0.20	0.17
F11 July 1985	0.17	0.20	0.20	0.20	0.17

95TR4/V2

Note: temperatures were 20 to 35°C; speeds in the nominal range.

Key Words:

Reaction Wheels, Momentum Wheels, Bearings

Mechanisms:

Momentum Wheels

Systems:

Rotating System

Authors; Experts:

B. Bialke

Address:

ITHACO, Inc.
735 W. Clinton Street
Ithaca, New York 14851-6437

Telephone:

(607) 272-7640

Title:

A Combined Earth Scanner and Momentum Wheel for Altitude Determination and Control of Small Spacecraft

Source:

Abstract:

In order to satisfy the stringent cost and power requirements of small satellites, an advanced SCANWHEEL® has been designed, built, and qualified by ITHACO, Inc. The T-SCANWHEEL is a modular momentum/reaction wheel with an integral conical Earth scanner. The momentum wheel provides momentum bias and control torques about the pitch axis of a spacecraft. An angled scan mirror coupled to the rotating shaft of the momentum wheel provides a conical scan of the field-of-view of an infrared sensor to provide pitch-and-roll attitude information. By using the same motor and bearings for the momentum wheel and Earth scanner, the overall power consumption is reduced and the system reliability is enhanced. The evolution of the T-SCANWHEEL is presented, including design ground rules, trade-off analyses, and performance results.

PRECEDING PAGE BLANK NOT FILMED

Lessons Learned:

- Bearing lubricant condensation on a rotating scan mirror cannot interfere with the infrared radiation reflection of the mirror. Pennzane X2000 was the preferred lubricant over Bray 815Z because it has a much higher transmission in the region of the horizon sensor infrared bandpass.
- With the exception of its lower viscosity index, the Pennzane X2000 was superior to the Bray 815Z.

Description:

A summary of the relevant design specifications is presented in Table 1. For the sake of modularity, the design of the momentum wheel subassembly required that it be able to be used as an independent momentum wheel or reaction wheel. The size was established as that required for a small satellite on the order of XSAT. The 6-V bus was chosen because that is the bus voltage on XSAT. The typical bus voltage for spacecraft is 28 V, but smaller spacecraft have fewer solar cells to string together, so the available bus voltage may be lower. One design goal was to make it usable with either a 28- or a 6-V bus. The final design met all of the minimum requirements, and met every goal with the exception of steady-state power consumption. The goal of <0.5 W at 1000 rpm was impossible to attain within program constraints.

Structural support of the flywheel is provided by a pair of spoked flexures separated by a cylindrical ring. This can be seen in the cutaway portion of Figure 1. The spokes allow visual and mechanical access to the flywheel when it is completely assembled into the housing. This eliminates a blind assembly that would occur if the enclosure and support structure were combined into a single part. With open flexures on both sides of the housing, inspection can be performed prior to close-up to detect the presence of contamination and to verify correct direction of rotation polarity.

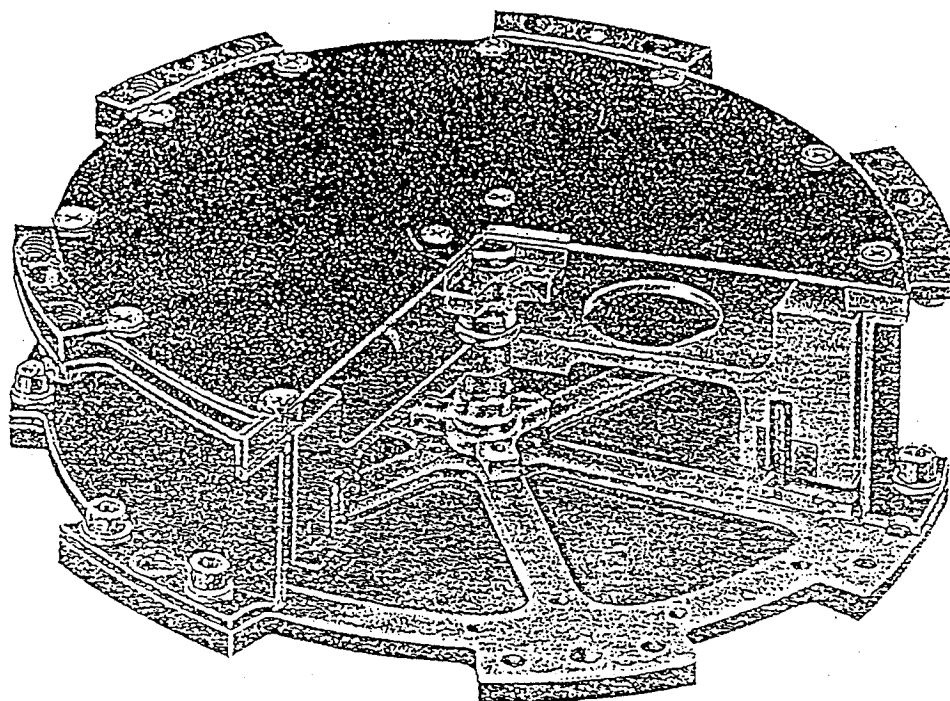
Test Experience:

The development effort succeeded in producing a low-cost, low-power consumption SCANWHEEL as an elegant solution for small satellite attitude determination and control with a minimum amount of hardware. Simplistic and reliable techniques were employed to result in a rugged, yet efficient, design. The versatile T-SCANWHEEL has since been commissioned for several small satellite programs, including the Air Force space test experiment platform mission series, and the NASA total ozone mapping spectrometer spacecraft. These spacecraft typically use a pair of T-SCANWHEELs and an independent reaction wheel in their reconfigurable attitude control systems. In addition, an independent momentum wheel has been built for BREMSAT. This gas-canister-launched satellite is being built for the University of Bremen in Germany to perform microgravity experiments.

Table 1. SCANWHEEL Baseline Design Specifications

Parameter	Minimum Requirement	Goal
Momentum Wheel Subassembly		
Nominal operating speed, rpm	1000	±5000
Operating life, yr	1	3 to 5
Storage life, yr	5	5
Torque capability, N-m (oz-in.)	>0.02 (2.8)	Increasable
Torque ripple, N-m	N/A	<0.002
Angular momentum at 1000 rpm, N-m-s (ft-lb-sec)	0.67 (0.5)	Increasable
Power consumption at 1000 rpm, W	<1.0	<0.5
Weight, kg (lbm)	<2.5 (5.5)	—
Temperature range, °C	0 to 50	-34 to 71
Bus voltage, V	6	6, 15, or 28
Scanwheel Assembly		
Scan cone half angle, °	45 ±1	45 to 85
Scan beam width, °	1.5 (0 ±0.75)	—
Blanking, °	90 Allowed	—
Optical passband, μ	14 to 16	14.3 to 15.6
Optical efficiency, %	65 minimum	—
Sun rejection	No Damage	—
Aperture	Restricted by XSAT structural opening	φ1.25 in. minimum
Position sensor	1/rev index pulse	—
Accuracy, °	±0.5	±0.1

95TR4/V2



95TR4/V2

**Figure 1. The Modularity of the Momentum Wheel Subassembly of the New Design
Allows it to be Used as an Independent Momentum Wheel or Reaction Wheel**

Key Words:

Momentum Wheel Spin Bearings, Rolling Element Bearing Dynamics

Mechanisms:

Spin Bearings for Momentum Wheels

Systems:

Generic Technology

Authors; Experts:

1. Edward A. Boesiger
2. Mark H. Warner

Address:

1. Lockheed Missiles & Space Company, Inc.
Sunnyvale, California
2. Honeywell Corporation
Satellite Systems Operations
Glendale, Arizona

Telephone:**Title:**

Spin Bearings Retainer Design Optimization (1991).

Source:

NASA Conference Publication 3113, 25th Aerospace Mechanisms Symposium.

Abstract:

The dynamic behavior of spin bearings for momentum wheels (control moment gyroscope, reaction wheel assembly) is critical to satellite stability and life. Repeated bearing retainer instabilities hasten lubricant deterioration and can lead to premature bearing failure and/or unacceptable vibration. These instabilities are typically distinguished by increases in torque, temperature, audible noise, and vibration induced into the bearing cartridge.

Ball retainer design can be optimized to minimize these occurrences. A retainer was designed using a previously successful smaller retainer as an example. Analytical methods were then employed to predict its behavior and optimize its configuration.

Anomalies:

Retainer instability and failure in a control moment gyroscope bearing.

Lessons Learned:

- There is a critical friction level associated with each retainer design beyond which the retainer is unstable.
- Ball pocket friction is more critical to stability than retainer land friction for the bearing investigated.
- The nature of the bearing dynamics problem makes retainer optimization a very difficult task for the following reasons:
 - The parameters are coupled
 - The high accuracy of input data required
 - The specific operating conditions are important.
- It is difficult to discern the effects of small changes on the indicators of stability from the bearing dynamics program.
- The steepest descent optimization method appears to be the most promising, but is hard to implement accurately for bearing dynamics.

Description:

Minimal design details are given in the article. Efforts included a parametric analysis of the effects of the following five primary characteristics of the retainer on stability:

1. Retainer pocket-ball diametral clearance (values from 0.05 to 0.5 mm)
2. Retainer race diametral clearance (values from 0.05 to 0.5 mm)
3. Number of balls
4. Force bias
5. Moment bias.

The optimization study was carried out while operating under the nominal operating conditions, which included gravity, a small radial load, a shaft speed of 6000 rpm, and retainer race and ball-retainer friction coefficients of 0.12.

Testing:

Two bearing test fixtures were used to observe stability. An existing fixture, universal bearing test system (UBTS) was considered a retainer screening tool. The bearing stability tester (BeST) tests an end-item duplex bearing pair and was developed in parallel to complement the testing on the UBTS. Since the UBTS tests were done with one of the bearings from the duplex pair, the BeST more closely simulates the actual bearing system configuration.

UBTS Fixture. The UBTS is a fixture that was developed to perform ball bearing dynamics research. The fixture was designed primarily as a single-bearing screening device, but it can also be configured to accept a preloaded pair. The spindle is suspended on an air bearing, and the axial preload on the bearing can be varied by adjusting the gas pressure. Radial- and axial-induced vibration forces are measured using two piezoelectric load cells. In addition, two linear variable differential transformer deflectionometers measure bearing drag torque. The amplitude variation of the induced vibration radial component at the retainer frequency, as well as audible noise and an increase in drag torque, give indications of retainer instability.

BeST Fixture. The BeST fixture was developed to simulate the end-item configuration while being able to measure the forces, motor current, accelerations, bearing temperatures, speed, and retainer motions. The bearings were rotated by a dc servo motor through a flexible coupling. The fixture was also designed to be compatible with mounting onto a shaker table.

A servo motor controlled the rotating speed of the bearing pair. The drive motor current is an indirect measure of the torque required to turn the bearings. A three-axis accelerometer was mounted on the side of the housing to measure radial and axial accelerations. Thermocouples measure the outer race temperature at two places on each bearing. An infrared pyrometer measured the temperature of the inner race. Two three-axis piezoelectric load cells were intended to measure the forces and torques in the bearing. However, the poor quasi-static performance and high thermal sensitivity of the cells on the BeST fixtures made it difficult to obtain useful steady-state information.

Key Words:

Momentum Wheels, Lubrication, Bearings

Mechanisms:

Momentum Wheels, Reaction Wheels, Control Moment Gyroscope Bearings

Systems:

Rotating Systems

Authors; Experts:

L.L. Fehrenbacher

Address:

Technology Assessment and Transfer
Annapolis, Maryland

Telephone:

Title:

Tribomaterials Technology for Momentum Transfer Devices

Source:

Final Report, Contract No. F33615-89-C-5609, Task 3L (April 1991).

Abstract:

This report summarizes the requirements for momentum wheels, reaction wheels, and control moment gyroscopes for the Strategic Defense Initiative Organization (SDIO) systems such as brilliant pebbles. It also outlines the technology limitation of existing momentum exchange devices.

PRECEDING PAGE BLANK NOT FILMED

Anomalies:

A recent Aerospace Corporation review of past problems with space mechanisms has revealed that the number one recurrent tribomaterials problem is momentum wheel bearings. As reflected in Table 1, these problems manifest themselves in pointing errors (degraded pointing capability) that are traceable to increased bearing torque and vibration in the momentum wheels. These bearing degradation characteristics are symptomatic of bearing cage instability. Close inspection of telemetered data by aerospace bearing specialists and tribologists suggests that the cage instability is induced by lubricant depletion between the ball race and ball retainer contact regions.

Lessons Learned:

- Bearing lubricant depletion between the ball race and retainer causes cage instability and subsequent pointing errors, increased bearing torque, and wheel vibration.
- The past practice of using steel bearings lubricated with mineral-oil-based greases or super-refined mineral oils with porous phenolic cages is unacceptable. Recent tests by aerospace tribologists have shown that the phenolic cages continue to absorb oil from the bearing ball contact regions during operation instead of supplying oil, thereby hastening the onset of cage instability.
- An active oiling system can be incorporated to periodically lubricate bearings and avoid erratic torque behavior. The trade-off is added complexity.

Table 1. History of Momentum/Reaction Wheel and Control Moment Gyroscope Experience

Program	Wheel Type	Problem	Comments
DSP	Large momentum wheel constant speed	Torque/temperature anomalies pointing errors; 6- to 8-yr life (some shorter)	Previously life limited by thermal control sensor warm-up
NAV/GPS	Reaction wheels; four per satellite	Torque/temperature runaway pointing errors	Symptoms consistent with lube loss and starvation
CDP	Medium control moment gyroscopes; > one per satellite	Torque anomalies degrade pointing capability	Redundancy adequate for 4- to 6-yr mission life
CDP	Large control moment gyroscopes; > one per satellite	Runaway torque, cage fracture, lube break down	Life test failures at <1/2 life lube starvation, cage instability using active oiler
DMSP	Medium momentum wheel	Torque noise, vibration	Other systems fail first
DSCS III	Momentum wheels	Torque noise, vibration	Redundancy

95TR4/V2

Description:

British Aerospace produces a 2-Nms and a 10-Nms reaction wheel. For the last two and a half years, they have had a 70-Nms wheel under development. The two production wheels use spokes for structural stiffness and Nylasint (polyamide: nylon) oil reservoirs that can be heated to release oil on demand. Twenty microliters of oil are initially placed on the bearing ball race surfaces which are fabricated from ED-20 (52100 alloy steel). The oils are the standard superrefined KG-80 and SRG 60 mineral oils used by most United States companies. In the larger 10-Nms production wheel, British Aerospace has gone to an outer race riding bearing design for structural strength and uneven ball spacing to solve the cage instability problem. In contrast to the 2-Nms wheel, the brushless dc motor was also placed in the outer rim of the 10-Nms wheel to achieve additional momentum.

Key Words:

Bearings, Lubrication, Instability

Mechanisms:

Momentum Wheels, Reaction Wheels

Systems:

Rotating Systems

Authors; Experts:

S. Lowenthal, E. Boesinger, and A. Donley

Address:

Lockheed Missile & Space Company, Inc.
Sunnyvale, California

Telephone:

Title:

Observation of Cage Instability

Source:

International Rolling Element Symposium 91, Sponsored by C.S. Draper Lab and DOD Instrument Bearing Working Group (April 8-11, 1991).

Abstract:

Tests were conducted to investigate the characteristics of ball bearing cage instability and the means to predict it. Precision-305 size angular-contact bearings with standard and biased retainers were tested. Accelerometers mounted on the bearing housing showed that the cage instability frequency was invariant with respect to bearing speed, external vibration, or lubricant viscosity. Measured bearing cage motions showed basic agreement with both a Lockheed Missile & Space Company, Inc. real-time bearing dynamics simulation, and also with the commercial code ADORE.

PRECEDING PAGE BLANK NOT FILMED

Anomalies:

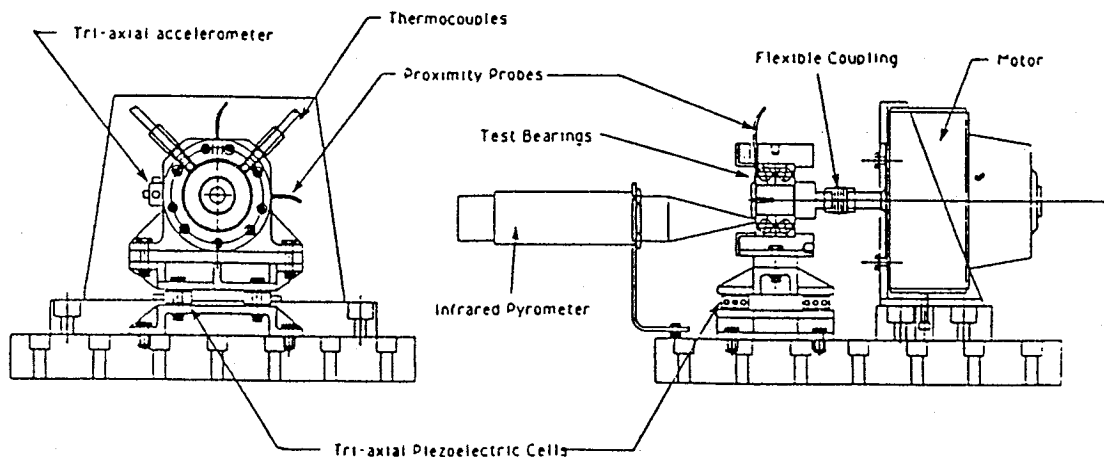
Cage instability in rolling-element bearings.

Lessons Learned:

- The characteristic instability frequency is an inherent geometric mass property of the cage/bearing system and is essentially invariant to external vibration, bearing speed, or lubrication condition.
- The biased cage has a different instability pattern and frequency than the commercial unbiased cage. Both the cage motion pattern and the instability frequencies are reasonably predictable.
- Each cage-bearing design has a critical friction coefficient for instability. The ball cage interface is much more critical than the cage land. This was also predictable by the simulations.
- Increased lubricant viscosity enhances the changes and severity of instability. Room temperature grease triggered instability, while room temperature oil and warm grease did not.
- Simulation computer codes can predict cage instabilities for steady-speed conditions. They cannot predict stability onset as speed is ramped up.

Testing:

Tests were conducted with a hard preloaded, duplex bearing pair in the test rig shown schematically in Figure 1. The test bearings were driven by a low noise, brushless dc motor through a flexible bellows coupling. The drive motor current was used as a measure of bearing torque. Radial and axial accelerations were measured by a three-axis accelerometer mounted on the housing along the shaft centerline.



95TR4/V2

Figure 1. Bearing Tester

Key Words:

Magnetic Bearing, Momentum Wheel, Gimbal

Mechanisms:

Momentum Wheel

Systems:

Rotating System

Authors; Experts:

1. K. Yabu-uchi, M. Inoue, and S. Akishita
2. C. Murakami and O. Okamoto

Address:

1. Mitsubishi Electric Corporation, Amagasaki, Japan
2. National Aerospace Laboratory, Tokyo, Japan

Telephone:

Title:

A Compact Magnetic Bearing for Gimballed Momentum Wheel

Source:

17th Aerospace Mechanisms Symposium (1983).

Abstract:

A three-axis controlled magnetic bearing and its application to a momentum wheel are described. The four divided stators provide a momentum wheel with high reliability, low weight, large angular momentum storage capacity, and gimbal control.

Lessons Learned:

- The magnetic bearing had suitable characteristics for attitude control of biased momentum spacecraft.
- The magnetically suspended gimballed momentum wheel was small, had large angular momentum storage capacity, and high reliability.

Description:

Momentum wheels are widely used for attitude control of satellites. For precise active control, the momentum wheel is often mounted on a gimbal mechanism. The momentum wheel is supported on two pairs of bearings whose axes are usually parallel to the roll or yaw axes of the spacecraft. Two gimbal torquers provide the roll/yaw attitude control. The mechanically suspended gimballed momentum wheel has the disadvantages of large size and mass and disturbance torques from the gimbal bearings.

A magnetically suspended momentum wheel is an attractive alternative. The magnetically suspended rotor has no contact with the stators, which eliminates the problems associated with friction and lubrication in a vacuum environment providing long life and high accuracy. In addition, the rotor axis can tilt (gimbal) within the clearance between the rotor and the stator. Although the gimbal angles might be small (1° at most), such vernier attitude error correction is sufficient if it is used with some other course attitude control devices such as thrusters or magnetic torquers. Rotor gimbaling without any contact means that it does not require heavy gimbal frames and there are no frictional disturbances.

A magnetic bearing has to stabilize five degrees of freedom of the rotor: one axial, two gimbal, and two radial motions. Five active control mechanisms would make the system complex and reduce reliability. In the bearing, there are only three active controls: one axial and two gimbal. The two radial motions of the rotor are passively stabilized by samarium cobalt permanent magnets.

The stator is made up of four identical segments each of which has active axial control and passive radial control. Each segment has an associated sensor that monitors the axial position of the rotor relative to the segment. The control system varies the magnetic flux in each segment to maintain the axial position of the rotor and eliminate tilt of the rotor. The outputs from all four sensors are used for axial control. For tilt control, the system uses the outputs from pairs of opposed sensors to control the tilt about two orthogonal axes.

A spoked wheel design was adopted to provide a high inertia/mass ratio. Five pairs of spokes connected the wheel ring and the hub. The wheel ring, spokes, and hub were machined from one super duralumin block to eliminate problems associated with mechanical connections between different parts. In order to withstand the large axial acceleration during launch and the gimbal reaction torques, the spokes were made in the form of thin blades. The pairs of spokes were also merged into one near the hub to increase the resonant frequency.

The wheel drive was a brushless dc motor with stator coils composed of thin copper films insulated and formed by fiber-reinforced plastics. Three coils were laminated around a cylinder for each of the three phases. The nine coils had a total thickness of 1.8 mm. The thin stator coil and small permanent magnets, which yielded sufficient magnetic field to generate drive torques, made the motor very compact. The motor phase angle was identified by three commutation sensors which also played the role of tachometer with an output of 24 pulses/rev.

Testing:

The performance of the momentum wheel was as follows:

- Maximum angular momentum: 70 Nms
- Maximum speed: 10,000 rpm
- Maximum gimbal angle: 0.5°
- Maximum motor drive torque: 0.02 Nm
- Maximum gimbal reaction torque: 5.0 Nm
- Weight (without electronics): 5.5 kg
- Bearing power consumption (zero gimbal position): 8 W
- Motor power consumption (maximum torque): 50 W
- Bearing supply voltage: ± 18 V
- Motor supply voltage: 15 V

Reaction Wheels

Key Words:

Momentum Wheels, Reaction Wheels, Control Moment Gyroscope, Lubricants, Bearings

Mechanisms:

Momentum Wheels

Systems:

Rotating Systems

Authors; Experts:

Anonymous
(B. McConnell viewgraph handout; internal presentation material)

Address:

Telephone:

Title:

Momentum/Reaction Wheel Experience

Source:

Phillips Laboratory (B. McConnell)

Abstract:

The presentation tabulates anomaly experience and suggests lubrication mechanisms.

PRECEDING PAGE BLANK NOT FILMED

Anomalies:

Program	Wheel Type	Problem	Cause	Action
Navstar/GPS (January 1991)	Reaction wheel; four per satellite	On-orbit and test failures; high torque	Lubricant depletion	New lubricant qualification
GPS IIR (1991-Present)	Reaction wheel	High-speed cage instability	Force, mass resonance	Force, mass biased cages
DMSP (1992)	Reaction wheel	Bearings/lube could not be delivered	Lubricant degradation	Extensive bearing run-in and screening
DMSP (1993)	Reaction wheel	Torque instability	Unknown	Under study
DSP (1980s)	Large momentum wheel	Torque/temperature anomalies	Lubricant starvation	Passive oil delivery system
DSP (October 1992)	Large momentum wheel	Torque/temperature anomalies	Lubricant starvation	Modify passive oiler
DCSS III	Reaction wheel vibration	Torque noise	Unknown	Redundant wheels
MILSTAR (1991)	Rate gyroscopes	Drive rate/torque instability	Lubricant starvation	Improved lubrication, cage processing
CDP (1988-Present)	Large control moment gyroscopes; > one per satellite	Excessive torque	Lubricant loss, cage instability	Active oiler system, new oil
NASA-GOES (1993)	Momentum wheel; ~5500 rpm	Related wheels; torque noise on orbit	Suspect lubricant loss, instability	Revised cage process- ing; lubricant supply system under study

95TR4/V2

Lessons Learned:

- Passive oilers that are programmed to release lubricant at a predetermined rate do not apply lubricant as needed. Overlubrication or underlubrication can occur. Data from digital signal processor (DSP) indicates that after about three years of operation, the spacecraft again manifests instabilities associated with lubricant depletion.
- Need exists for an active oiler commandable from the ground.

Key Words:

Reaction Wheels, Motors, Sensors, Bearings

Mechanisms:

Sensors, Bearings

Systems:

Rotating Systems

Authors; Experts:

B. Bialke

Address:

ITHACO, Inc.
735 W. Clinton Street
Ithaca, New York 14851-6437

Telephone:

(607) 272-7640
(800) 847-2080

Title:

On-Orbit Problems with Scanning Earth Sensor Bearing Lubrication: A Testimonial for Realistic Life Testing of Long-Life Space Flight Mechanisms

Source:

17th Annual AAS Guidance and Control Conference, Keystone, Colorado (February 2-6, 1994).

Abstract:

A scanning Earth sensor was developed in the early 1980s using a flight-proven stepper motor design. The sensor was successfully flown on LANDSAT 4 and LANDSAT 5, with a single unit failing after 34 months of operation. Subsequent process controls placed on the bearing lubrication and screening processes were intended to enhance the bearing lifetime.

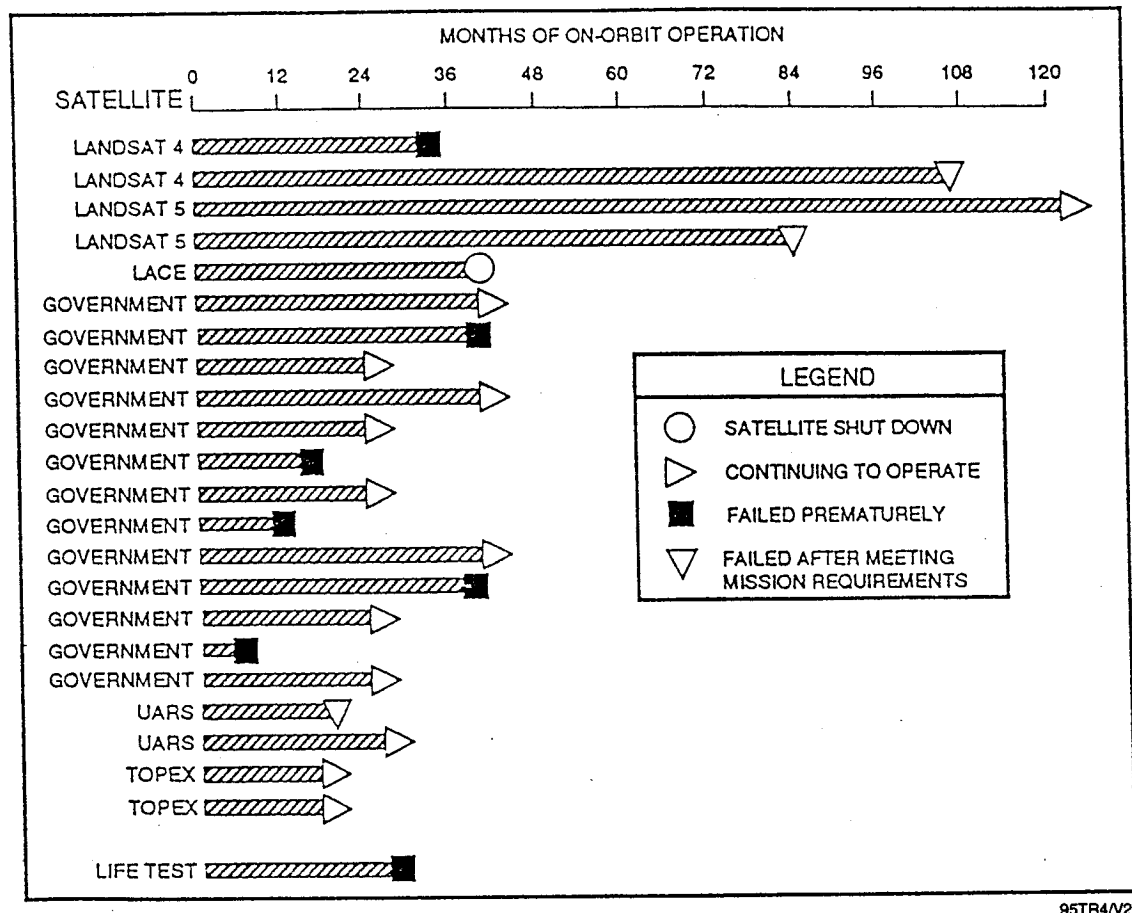
The design was then flown on many missions, including NASA's upper atmosphere research satellite (UARS) and Topex satellites. Several of the programs experienced on-orbit problems believed to be caused by lubricant failure. One of the UARS sensors failed shortly after the 18-month mission requirement was met.

Some of these problems may have been avoided if more extensive and realistic life testing had been performed. A single life test was performed, which was inadvertently accelerated. This discounted its validity and resulted in dismissal of its negative results.

This paper provides a history of the referenced lubrication problem and an analysis of the design change that has been implemented to correct it, including a summary of the status of the life testing that is currently underway using a new, more suitable lubricant.

Anomalies:

- The first flight of the conical Earth sensor design was on LANDSAT 4. One of the sensors on that 36-month mission failed after 34 months of operation. The failure was characterized by erratic data from the sensor and subsequent heating of the sensor motor. During the investigation of this failure, it was noted that the sensor output went quiet when the sensor was not pointed toward the Earth. This effect, plus temperature data, confirmed that the failure indeed involved the motor/bearing system, and was not related to the electronics or the detector. The heating is also a primary indicator of motor failure, since the motor draws significantly more current when it is unable to maintain synchronous speed.
- Several other programs experienced a problem with conical Earth sensor performance, which was eventually isolated to the motor, and most likely due to lubricant failure. One particular application experienced problems as soon as six months into the mission. Many missions have not seen any anomalous motor behavior, and the low-power atmospheric compensation experiment satellite successfully completed a 3-yr mission with no problems.
- The UARS spacecraft was launched in September 1991 on an 18-month mission. After 19 months of operation, one of the two Earth sensors failed. Telemetry data showed a loss of synchronous speed of the motor and heating of the motor. Attempts to recover the motor by implementing the high-torque mode were successful, but only for a few hours. Because of the presence of a redundant sensor and the fact that the conical Earth sensor is not the primary attitude sensor, the extended mission has not been affected by loss of the sensor motor.
- The Topex spacecraft was launched on August 10, 1992, with two conical Earth sensors. With the exception of minor anomalies in Earth sensor data attributed to charged particle radiation (definitely unrelated to the motor), there have been no problems.
- A summary of the spacecraft with ITHACO conical Earth sensors and their on-orbit performance is presented in Figure 1.



95TR4/V2

Figure 1. Conical Earth Sensor On-Orbit Performance Summary

Lessons Learned:

- Four lubricants were compared in a lubricant trade-off analysis: Pennzane X222 from Pennzoil; Apeizon C, distributed by Biddle Instruments; Coray 100 from Exxon; and Nye 188B from Nye Oil Co. The candidate lubricants were compared against the baseline Bray 815Z in a variety of categories. The most significant of these are listed in the trade-off summary presented in Table 1. The parameter with the most significant negative aspect is highlighted for each of the rejected lubricants.
- The candidate lubricants were selected from among available space flight-qualified lubricants with the same nominal viscosity as the Bray 815Z. A higher viscosity lubricant would not be tolerable without a complete redesign of the motor for increased torque, and a lower viscosity lubricant would be undesirable for increasing wear.
- The primary flaw in the Bray 815Z is its instability while operating in the boundary region. Typically, extreme pressure additives are used to improve this performance, but the Bray 815Z is unable to dissolve any additives and is thus vulnerable to chemical decomposition catalyzed by metal-to-metal wear. The four alternate lubricants examined in the trade-off analysis have proven to be stable during boundary region operation when used with extreme pressure additives such as tricresyl phosphate (TCP) or lead naphthenate (PbNp).
- The lesson learned from our analysis is that overly conservative life testing of oil-lubricated space flight mechanisms can lead to fatal conclusions as easily as under-testing. For oil-lubricated mechanisms, there is no substitute for a real-time life test with multiple test units. Extrapolations of accelerated life test data have never proven to be effective due to the varied time dependence of a large number of parameters. Although it is possible to accelerate a test, the derivation of an appropriate acceleration factor has proven to be unreliable. Thus, if only a single life test can be afforded, the test environment and operating conditions must be as realistic as possible. Overly conservative tests should only be performed to supplement real-time life testing.

Table 1. Candidate Lubricant Trade-Off Summary

Parameter	Bray 815Z	Pennzane X2000	Apeizon C	Coray 100	Nye 188B
Viscosity	Good	Good	Good	Good	Good
Stability	Poor	Good	Good	Good	Good
Vapor pressure	Excellent	Excellent	Fair	Poor	Excellent
Viscosity index	Excellent	Good	Poor	Poor	Good
Infrared clarity	Poor	Excellent	—	—	Poor
Heritage	Poor	Limited	Good	Good	Limited

95TR4/V2

- We believe the lubrication problem in the conical Earth sensor has been corrected by changing to a chemically stable synthetic hydrocarbon fluid. A flight-proven extreme-pressure additive has been included in the lubricant formulation to minimize wear and enhance the lifetime of the sensor. Life testing of two flight units is currently progressing with no signs of degradation.
- The lifetime of oil-lubricated bearings is very temperature dependent. Higher temperatures reduce the expected lifetime in two ways. A high temperature results in higher evaporation rates and more surface migration for the bearing lubricant, which depletes the available supply more quickly than lower temperatures. In addition, higher temperature lowers the viscosity of the lubricant which reduces the elastohydrodynamic film thickness, resulting in more wear.

Description:

The conical Earth sensor is a scanning horizon sensor designed to determine pitch-and-roll spacecraft attitude based on measurements of the location of the edge of the infrared Earth. The instrument consists of a sensor head and an electronics assembly. The sensor head contains a set of infrared optics, a bolometric infrared sensor, a motor, a ball bearing suspension system, and a small preamplifier. The sensor head is sealed with O-rings and backfilled with one half atmosphere of dry nitrogen. The layout of the sensor head is shown in Figure 2.

Light enters the front of the sensor head through an optical band-pass filter on the front window. The desired infrared energy passing through the window is deflected 45° by a prism and then focused onto the detector. A motor rotates the prism which causes the sensor head line of sight to sweep a 45° half apex angle scan cone in space. The sensor head preamplifier magnifies the detector signal and sends it to an external electronics assembly. This signal, along with rotor position information, is used to generate pulse width and phase (roll and pitch) information for use by the spacecraft for attitude determination. The motor rotor/prism is suspended on two angular contact ball bearings, preloaded by a spring. A hollow shaft motor is required to afford space for the optics and the infrared sensor. This requires the use of relatively large diameter bearings.

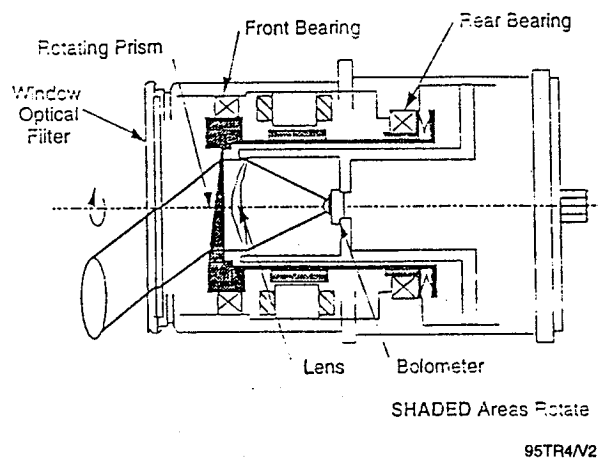


Figure 2. Sensor Head Layout

The predecessor to the motor used for the conical Earth sensor was a 3° stepper motor for a steerable horizon crossing indicator. Since the suspension system used in that design was vented to space, a low-vapor-pressure oil was required to minimize lubricant depletion due to evaporation. The Bray 815Z oil, which was selected, was chosen due to its extremely low vapor pressure and its unparalleled viscosity index for optimum performance over temperature. Bray 815Z is a synthetic fluorocarbon, PFPE oil. When the motor was redesigned for the enclosed scanning earth horizon sensor, the same lubricant was specified, since it was still state-of-the-art for space flight applications at the time.

The operation of the conical Earth sensor requires synchronous rotation of the prism at 120 rpm. The motor is driven quasi-open-loop by a fixed-frequency, regulated-voltage power supply. Some thermal compensation is incorporated to increase motor voltage when low temperatures are sensed by a thermistor located in the sensor head. If bearing drag torque increases beyond the torque provided by the motor at the voltage applied to the motor, the motor goes asynchronous, and the conical Earth sensor will not function properly.

Testing:

The life test was performed in a small thermal chamber temperature cycled to 50°C for 6 hr each day. During the remaining time, the temperature was not actively controlled. Heat rejection from the motor was accomplished only by convection and radiation. When the thermal chamber was operating at 50°C, the fan in the chamber induced forced convection, but when the chamber was turned off, natural convection was the only effective form of heat rejection from the motor. The result was that the motor bearings were continually between 52 and 62°C for the entire duration of the test.

Key Words:

Reaction Wheels, Motors, Lubricants, Bearings, Momentum Wheels

Mechanisms:

Momentum Wheels, Reaction Wheels

Systems:

Rotating System

Authors; Experts:

B. Bialke

Address:

ITHACO, Inc.
735 W. Clinton Street
Ithaca, New York 14851-6437

Telephone:

(607) 272-7640
(800) 847-2080
(607) 272-0804 (Fax)

Title:

A New Family of Low-Cost Momentum Reaction Wheels

Source:

American Astronautical Society Paper No. AAS 92-025 (1992).

Abstract:

This paper discusses the trade-off analysis and design features of an ITHACO momentum wheel development. Significant trade-offs were involved with bearings, lubrication, drive motor, and tachometer. Performance specification and information is also presented. The selection of Pennzane X2000 lubricant is the most significant result of the paper.

Anomalies:

The Bray 815Z lubricant, which has the positive qualities of low-vapor-pressure and high-viscosity index, is not a suitable lubricant for the momentum wheel application. Bray 815Z is a synthetic fluoro-carbon that is unable to dissolve antiwear additives. It performs well when operating speeds are sufficient to form an elastohydrodynamic film that separates the balls from the races, but it has poor performance in the boundary lubrication regime. Thus, the Bray lubricant is not acceptable for a reaction wheel that must go through zero speed.

Lessons Learned:

- An acceptable lubricant available from Pennzoil is Pennzane X2000 with 5% lead naphthanate (PbNp) as air antiwear additive. It has a very low vapor pressure, good viscosity index, and good boundary lubrication qualities. Lubricant properties for both the Bray 815Z and Pennzane X2000 are shown on Table 1.
- An ironless armature motor is ideal for the reaction wheel drive being both power and weight efficient.
- A Hall generator was selected for the tachometer. It has good accuracy, low complexity, low power consumption, and zero speed measurement.

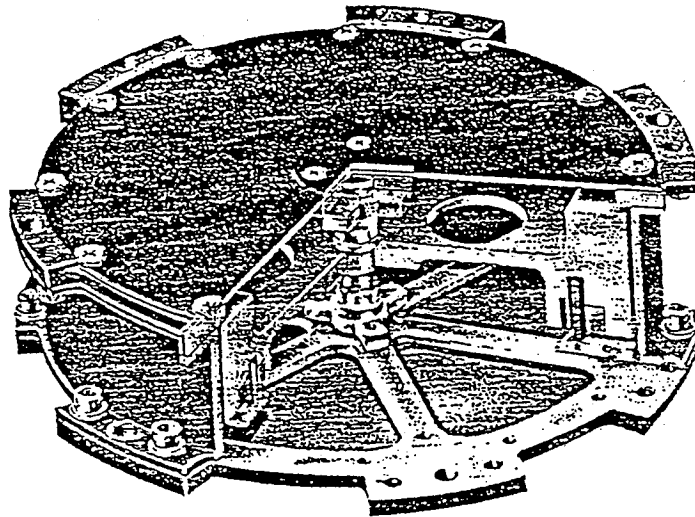
Description:

The ITHACO T-wheel configuration is shown on Figures 1 and 2. It consists of an aluminum flywheel suspended on angular-contact ball bearings and driven by an ironless armature brushless dc motor. Hall sensors are integrated directly into the motor stator to provide commutation information as well as a high-resolution tachometer signal. The aluminum housing consists of a cylindrical enclosure with supporting flexures to suspend the rotor. The housing is vented to space to eliminate viscous drag torque from the flywheel due to windage.

Table 1. Lubricant Property Comparison

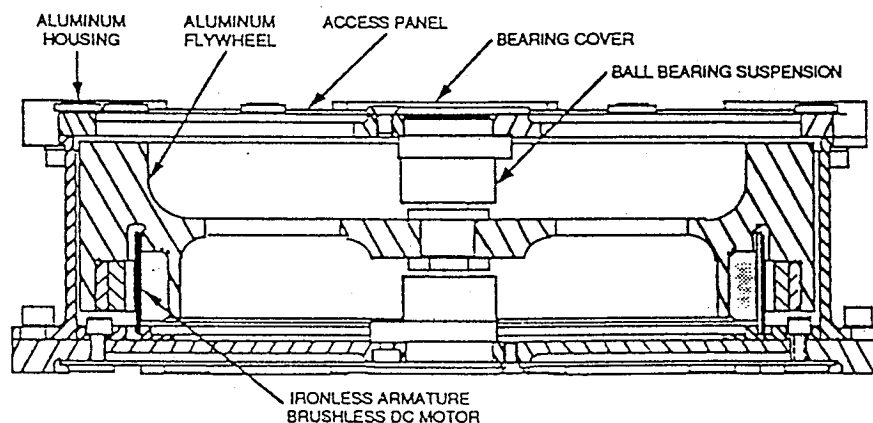
Lubricant Type	Bray 815Z Synthetic Fluorocarbon	Pennzane X2000 Synthetic Hydrocarbon
Viscosity (cSt)		
100°C ASTM D445	45	14.7
40°C ASTM D445	148	112.0
0°C ASTM D2602	—	1,182
-20°C ASTM D2602	1,125	7,092
-40°C	11,500	78,608
Viscosity Index ASTM D2270	350	135
Flash Point ASTM D92 (°C)	299	315
Fire Point ASTM D97 (°C)	330	326
Pour Point ASTM D97 (°C)	-112	-57
Molecular Weight (gm/mole)	7,000	910
Density ASTM D1298 (gm/ml)	1.866	0.846
TML (%)	0.8	0.160
VCM (%)	0.05	0.056
Vapor Pressure 125°C (torr)	2×10^{-7}	4×10^{-7}
Vapor Pressure 20°C (torr)	9×10^{-12}	1×10^{-12}

95TR4/V2



95TR4/V2

Figure 1. The Symmetrical Outline Chosen for the T-Wheel Allows a Variety of Mounting Options (identical assemblies can be bolted together for increased momentum capacity or redundancy)



95TR4/V2

Figure 2. The T-Wheel Mechanical Layout Consists of a Precision-Balanced Aluminum Flywheel Suspended on Ball Bearings and Driven by an Ironless Armature Brushless dc Motor

Structural support of the flywheel is provided by a pair of spoked flexures separated by a cylindrical ring. The spokes allow visual and mechanical access to the flywheel when it is completely assembled into the housing. This eliminates a blind assembly that would occur if the enclosure and support structure were combined to form a single part. With open flexures on both sides of the housing, inspection can be performed prior to close-up for presence of contamination and to verify correct direction of rotation polarity.

Aluminum was selected as the primary structural material due to its relative low cost, low weight, and high thermal conductivity. A variety of aluminum alloys are categorized as highly resistant to stress corrosion cracking, as shown in Table 1 of MSFC-SPEC-522A. Beryllium, magnesium, titanium, and composites are frequently used in spaceflight hardware to minimize structural weight, but in the interest of maintaining low cost and simplicity, these materials were not used in the design.

A pair of preloaded ball bearings support the rotating assembly. Preloading is desirable for a precision device such as the momentum wheel in order to remove radial and axial play for more precise shaft positioning. By maintaining ball race contact, noise is reduced by preventing ball skidding, and load sharing is improved between bearings. The only disadvantage with preloading is that increased wear and higher drag torque results when compared to a bearing with zero load. However, the precision and stability required for a momentum wheel dictate that a preloaded scheme be incorporated. The simplest method of preloading is with a spring. This turns out to be the preferred method for the momentum wheel due to its simplicity and the fact that it easily accommodates differential thermal expansion between the shaft and housing. Spring preloading also accommodates minor misalignment better than alternate methods. A stainless steel wavy washer spring was selected to preload the bearing pair. The final bearing suspension layout is shown in Figure 3.

The final bearing selection was based on capacity. A high-capacity R4 bearing was selected from the Barden Corporation. This bearing is a hybrid of a conventional R4 bearing which has a high load rating. Thin section bearing tolerances, larger balls, and a low conformity ratio were designed into the bearing to lower the contact stresses and increase the capacity. The capacity of the Barden bearing allows it to be used with nearly any current launch vehicle random vibration spectrum.

A stainless steel bearing mount was chosen due to its close coefficient of thermal expansion match with the bearing material. The sleeve within the mount in which the outer race of the bearing is installed is coated with titanium nitride to prevent the fretting corrosion, which would be inevitable at the bearing and mount interface due to the microscopic movements of the race during operation. The suspension scheme selected requires one bearing pair to be fixed, and one bearing to float axially during relative changes in the shaft and housing dimensions due to thermal expansion and pressure differentials on the housing. The titanium nitride coating ensures that this floating action of the second bearing is preserved.

A cross section of an ironless armature brushless dc motor is shown in Figure 4. It consists of a thin armature that supports the windings with a set of magnets and backiron on one side and a flux return path on the other side. The result is a motor that exhibits no cogging or eddy current drag, since there is no relative movement between the magnets and the iron flux return ring. Because of this, the iron components need not be laminated, which reduces the cost of these parts. The efficiency of an ironless armature motor is optimized by utilizing the largest possible diameter, since this results in a high number of poles and a large torque radius. By using a high number of poles, the resolution of the tachometer pulses generated from the commutation signal is also increased, and the torque ripple frequency is pushed beyond the range where torque disturbances are likely to be a concern on the spacecraft. Hence, the ironless armature motor is ideal for the reaction wheel drive by being both power and weight efficient.

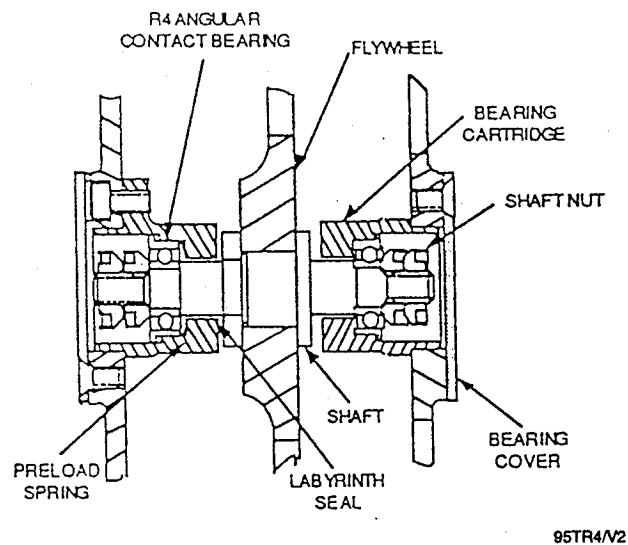


Figure 3. The Suspension System Accommodates Differential Expansion Between the Shaft and Housing by Using a Compliant Spring Preload

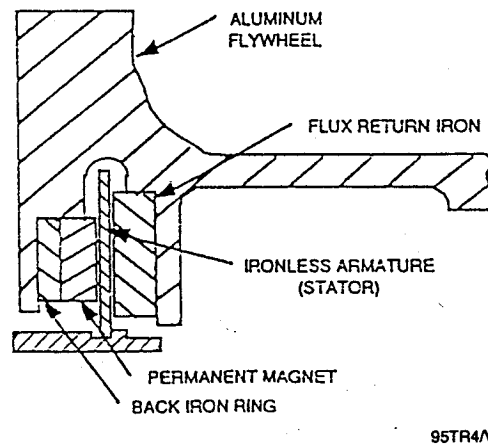


Figure 4. The Ironless Armature Brushless dc Motor is an Optimum Drive for Momentum Wheels Due to its Unique Combination of High Efficiency and High Inertia/Weight

Hall effect generators are commonly employed for commutation of brushless dc motors. The Hall regenerators can be stimulated directly from the permanent magnets in the motor so a separate gear or code wheel is not required. The phasing of the Hall sensor signals when stimulated by the actual motor magnets is exactly correct for commutation, eliminating any alignment procedure required to clock a separate gear to the motor. The circuitry to bias the Hall sensors is very simple, requiring only a constant current source. The sinusoidal output of the Hall sensors when excited by the motor magnets can be easily processed into commutation and tachometer signals.

The Hall generators were selected for the tachometer for the fact that their simplicity eliminated the need for many additional parts. They can be integrated directly into the armature assembly to minimize the packaging requirements for the commutation and tachometer components.

The performance specifications for the standard sizes of the T-wheel series momentum/reaction wheels are presented in Table 2 and Figures 5 through 7. Higher angular momentum capacities and higher torque versions can be made available as nonstandard designs. The currently manufactured Type A and Type B T-wheels are shown in Figure 8.

Table 2. T-Wheel Performance Specifications

Parameter	Type A	Type B	Type E*
Speed range (rpm)	0 to ± 5100	0 to ± 6000	0 to ± 6000
Angular momentum capacity (Nms)	4	19.5	68
Reaction torque (Nm)	20.0	40.0	140.0
Weight (kg)			
Wheel	2.55	5.1	11.3
Driver	0.91	0.91	Included
Outline (mm)			
Diameter	204	254	398
Height	63.5	90.0	16.5
Tachometer (pulses/revolution)	54	72	144
Static imbalance (gm-cm)	1.5	1.5	1.5
Dynamic imbalance (gm-cm ²)	40	40	40
Minimum operating Life (yr)	3	3	8

95TR4/V2

*Projected

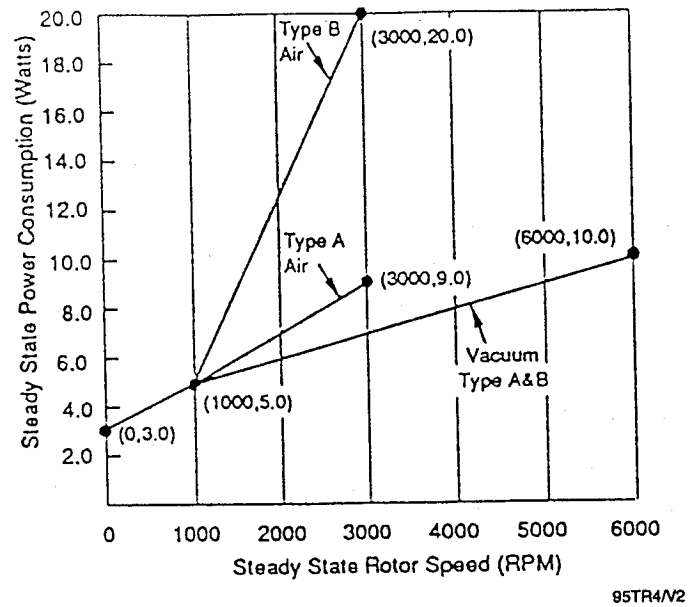


Figure 5. Steady-State Power versus Speed for the Type A and Type B T-Wheels is Similar Due to the Use of the Same Suspension System

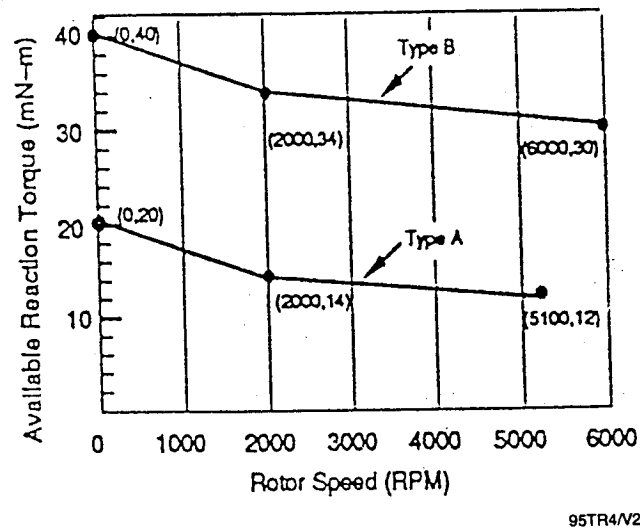
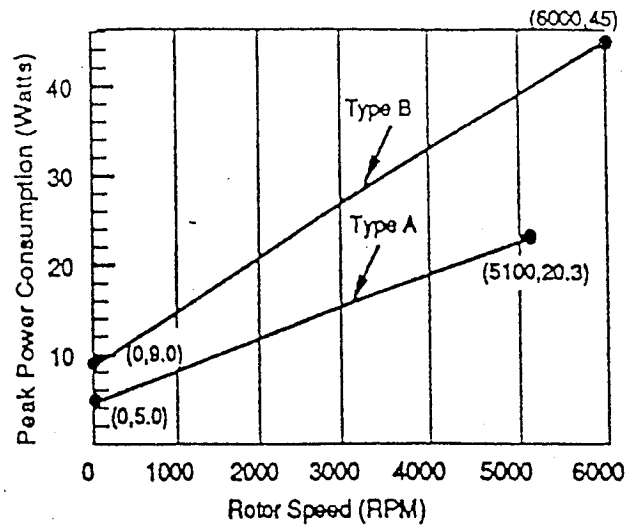
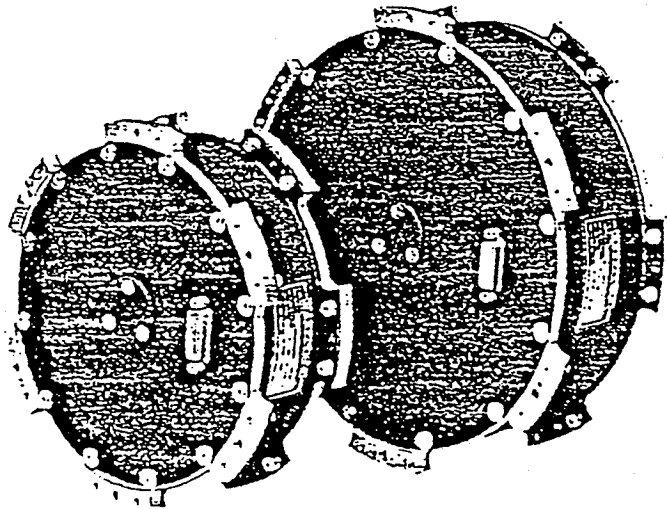


Figure 6. Available Reaction Torque



95TR4/V2

Figure 7. Peak Power Consumption



95TR4/V2

Figure 8. The Type A and Type B T-Wheels Share the Same Basic Mechanical Configuration

Experience:

The first flight T-wheel was delivered in September 1991 to the University of Bremen in Germany for BREMSAT, a small microgravity experiment to be launched from a getaway special canister on a space shuttle mission. Deliveries have also been completed for T-wheels and T-SCANWHEELs for the Air Force space test experiment platform mission, with follow-on contracts for this series of small satellites in process. NASA's total ozone mapping spectrometer will fly one T-wheel and two T-SCANWHEELs for attitude control.

The type B T-wheel is being built for an attitude control system for the Wake Shield Facility, which is a free-flying commercial spacecraft delivered to orbit by the space shuttle and retrieved on a single mission. The hardware to be delivered on this program includes a 6.5-Nms T-SCANWHEEL operating at 2000 rpm and a supplementary 19.5-Nms T-wheel operating at 6000 rpm.

Key Words:

Passive Isolation, Noise

Mechanisms:

Passive Mounts

Systems:

Rotating System

Authors; Experts:

Martin D. Hasna

Address:

Lockheed Missiles & Space Company, Inc.
Sunnyvale, California

Telephone:

Title:

Passive Isolation/Damping System for the Hubble Space Telescope Reaction Wheels

Source:

21st Aerospace Mechanisms Symposium (1987).

Abstract:

The need to reduce structural-borne vibration and resultant optical jitter induced by the reaction wheels has prompted a feasibility investigation and eventual development of a passive isolation system. Alternative design concepts considered were required to meet a host of stringent specifications and pass rigid tests to be successfully verified and integrated into the already-built flight vehicle. The final design employs multiple arrays of fluid-damped springs that attenuate over a wide spectrum, while confining newly introduced resonances to benign regions of the vehicle dynamic response. The paper presents the basis, evolution, and performance of the isolation system.

Anomalies:

Stability of highly accurate pointing devices can be destroyed by reaction wheel assembly-induced vibrations.

Lessons Learned:

- A passive isolation system was successfully developed, built, verified, and integrated into the existing Hubble space telescope vehicle.
- The development program attained a significant improvement in a critical pointing stability parameter/reaction wheel assembly jitter with a cost-effective solution.
- The isolator design met or exceeded the numerous requirements/constraints imposed by the Hubble space telescope application

Description:

The Hubble space telescope has the most stringent pointing requirements imposed on any spacecraft to date. During data acquisition, the stability of the pointing control system shall not exceed 0.007 arc-sec rms. To achieve this, structural-borne noise (particularly that from continuous operating systems) must be kept to an absolute minimum. The Hubble space telescope has four reaction wheel assemblies that are the constantly operating and has torque-producing components critical to the pointing control system. Their constant operation produces minute structural-borne sinusoidal vibrations that must be controlled with very tight criteria. Key design goals for minimizing reaction wheel assembly mechanical vibration output noise are: 1) extremely precise dynamic balancing of the rotor-bearing assembly, and 2) state-of-the-art mechanical bearing manufacture, quality control, and selection process. Reaction wheel assemblies are grouped in pairs. The spin axes are skewed $\pm 20^\circ$ from the plane normal to the Hubble space telescope optical axis and the pairs are 90° apart. Underlying mounting structures are at the heart of the Hubble space telescope primary load-bearing structure and are, hence, very stiff.

When powered and rotating, each reaction wheel assembly emits mechanical vibrations parallel to its spin axis and in directions radially outward in its equatorial rotational plane. The generation of these force and moment disturbances are caused by combinations of: 1) motor ripple/cogging, 2) electronic and resolver imbalance, and 3) rotor-bearing mechanical unbalance/geometry error. These vibrations emanate at the rotor rotational frequency and at other set harmonic ratios of rotational speed (e.g., 2.0, 2.8, 4.0, 5.2). These harmonic ratios are caused by minute bearing alignment and surface irregularities, specifically rotor imbalances, bearing raceway and ball geometric imperfections, and ball retainer interaction. The precise ratios all have their basis in consistent physical parameters of the bearing rotor assembly and have been empirically verified. Any isolation or attenuation scheme must be capable of addressing the entire range of harmonics as well as the primary unbalance harmonic. Early reaction wheel assembly-induced jitter analysis indicated that key harmonics that create the most deleterious optical system jitter were midratios (primarily 2.8 and 5.2) producing vibratory motion along the reaction wheel assembly spin axis. Therefore, these were the characteristics targeted for reduction.

A list of preliminary requirements was created to serve as a starting point for surveying existing damping devices and assessing basic feasibility/viability. This led to a development program. Some major concerns were: 1) dynamic performance at such low through-put load levels, 2) obtaining target ratios of lateral-to-axial stiffness, 3) control of large excursions under launch conditions without harming the reaction wheel assembly, and 4) placement of new isolator resonances.

After thorough screening, a Sperry concept was chosen for further development. Induced-vibration tests were conducted using a reaction wheel assembly, which showed that the device functioned as a second-order spring-damper system. The central element is basically a viscous fluid-damped coil-spring suspension system. Each reaction wheel assembly is suspended on three units. Damping is provided by a low-volatility silicone-based fluid (Dow Corning 200 series), confined by metal bellows to internal cavities. The design effectively fixes the internal fluid volume as far as dynamic motion is concerned.

The four sets of flight-qualified isolators were installed with their complement of reaction wheel assemblies on the assembled Hubble space telescope vehicle that was suspended vertically by cables from an array of three airbags. This nearly complete vehicle was instrumented with sensitive accelerometers and perturbed with shakers and onboard equipment to simulate actual orbital operations and predicted situations. A review of the pointing control system stability analyses showed that with the isolator system, it was acceptably stable.

Control Moment Gyroscopes

Key Words:

Gyroscope, Control Moment Gyroscope, Double-Gimbal Gyroscope

Mechanisms:

Control Moment Gyroscope, Gimbal

Systems:

Rotating Systems

Authors; Experts:

1. Lewis Cook, Paul Golley, and Henning Krome
2. Joseph Blondin, Charles Gurisi, and John Klovek

Address:

1. NASA-Marshall Space Flight Center
Huntsville, Alabama 35812
2. Allied-Signal Aerospace Company
Guidance Systems Division
Teterboro, New Jersey 07608

Telephone:**Title:**

Fabrication and Test of a 4750-Nms Double-Gimbal Control Moment Gyroscope

Source:

23rd Aerospace Mechanisms Symposium (1989).

PRECEDING PAGE FLANK NOT FILMED

Abstract:

In recognizing the need to develop future technologies in support of the space station, NASA's Advanced Development Program (ADP) placed as its goal the design and fabrication of a prototype 4750-Nms (3500-ft-lb-sec) control moment gyroscope. The control moment gyroscope uses the principle of momentum exchange to impart control torques to counteract vehicle disturbances. This paper examines the selection of the double-gimbal over the single-gimbal control moment gyroscope and describes the major subassemblies of the selected device. Particular attention is given to how the man-rated mission requirement influenced the choice of materials, fabrication, and design details employed.

Physical characteristics and the result of functional testing are presented to demonstrate the level of system performance obtained. Comparisons are made of the measured system responses against the predictions made by computer simulation.

Anomalies:

- Torque noise is the undesirable component of torque produced by the actuator when a constant rate is commanded. A typical measured rms value was 0.1 Nm. Major contributors to this error were identified as the dc offset in the drive voltages and the transmission gearing.
- A small amount of cross coupling between the inner and outer gimbal servo loops caused variations in frequency response as a function of the inner gimbal angle. These variations appear to be acceptable for current applications but future improvements are planned.

Lessons Learned:

- A single gimbal can provide greater torque capability for the same angular momentum than a double gimbal. However, a double gimbal has less complex control laws and greater flexibility to support a large variation in vehicle inertia. Ultimately, this proved to be the main reason for selection for the space station.
- Custom 455 stainless steel was identified as the optimum rotor material since it could provide the necessary angular momentum (4750 Nms at 6600 rpm) and provide a safety factor of 4 for the yield stress at 105% of nominal wheel speed.
- A two-stage, parallel-path spur gear with installed wind-up of one gear with respect to the other provides a preload that eliminates backlash.

Description:

In support of the space station, NASA's ADP set as its goal the design and fabrication of a prototype 4750-Nms (3500-ft-lb-sec) control moment gyroscope. It uses the principle of momentum exchange to counteract vehicle disturbances by imparting control torques. The first part of this paper was concerned with the reasons for selecting the double-gimbal control moment gyroscope over the single-gimbal control. The advantages of the double gimbal include:

- Much simpler control laws
- No impact of unit failure on control laws
- No impact of failure on spherical momentum envelope shape
- Growth capability by adding individual double-gimbal control moment gyroscopes without impacting control laws
- Simpler vehicle mounting geometry.

Single-gimbal control moment gyroscopes can provide greater torque capability for the same angular momentum. However, the space station has no rapid maneuvering requirements necessitating greater torque capabilities. The flexibility of the double-gimbal control moment gyroscope to support a large variation in vehicle inertia, especially during station build-up, ultimately proved to be the main consideration for the selection. Figures 1 and 2 show the layout of the system, while Figure 3 shows the inner gimbal assembly.

A detailed survey of available materials was then made to select a suitable material for the rotor. The rotor was designed to be 63 cm (25 in.) in diameter with an angular momentum of 4750 Nms at a speed of 6600 rpm. The maximum rotor speed was to be less than 9000 rpm. A safety factor of 4 for the yield stress at 105% of nominal wheel speed (6390 rpm) was also used as criterion. The plan emphasized reliability and a 10-yr operating life. Custom 455 stainless steel was identified as the optimum rotor material.

A bearing configuration was chosen that would make it feasible to replace the bearings on orbit if any deterioration was detected. Preloaded angular contact bearings made of 52100 vacuum-melted chrome steel were selected. The bearings would have cotton-fabric-base phenolic retainers impregnated with KG-80 petroleum oil. Fresh oil would be supplied by a once-through system with the lubricant being discarded after it passed through the bearing. If bearing replacement was necessary, the gyroscope would be placed into a space station "shirt sleeve" work area.

For the required torque of 272 Nm (200 ft-lb), a torque motor and geared transmission are used. The motor is a brushless dc type capable of developing 12 Nm (9 ft-lb) of torque. The gear train is shown in Figure 4 and consists of a two-stage, parallel-path spur gear arrangement. Wind-up of one gear train with respect to the other provides a preload that eliminates backlash. A gear ratio of 27.76:1 supplies the required torque. This configuration has been used before and was very successful. These components are housed in the torquer module assembly, along with a multispeed resolver used for rate feedback. Figure 5 shows a cross section of the assembly. The arrangement is identical for both the inner and outer gimbal pivots.

The paper gives reasonably detailed descriptions of the gyro design and the gimbal and rotor drive electronics.

The test results demonstrated that this prototype would meet all requirements. Future plans are to improve signal characteristics.

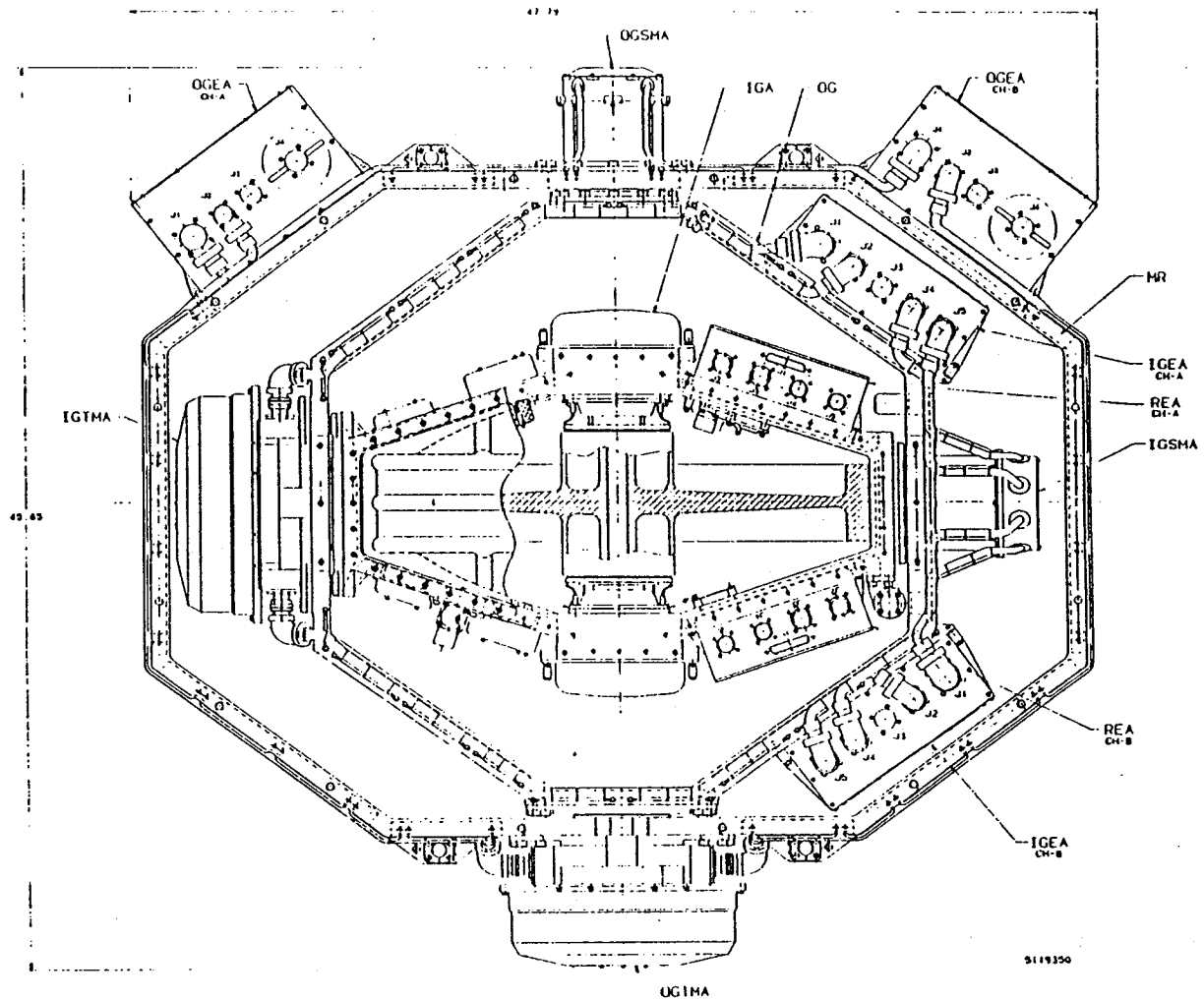


Figure 1. Prototype Double-Gimbal Control Moment Gyroscope System Layout

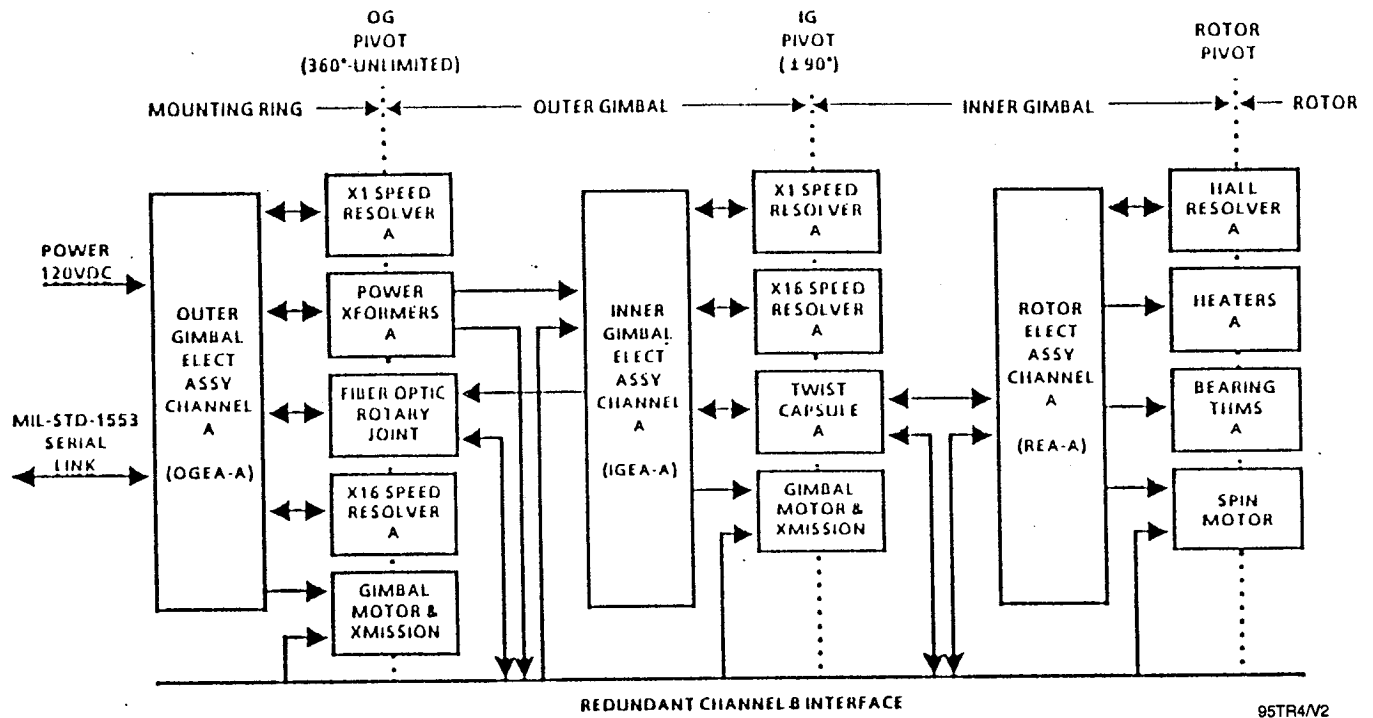
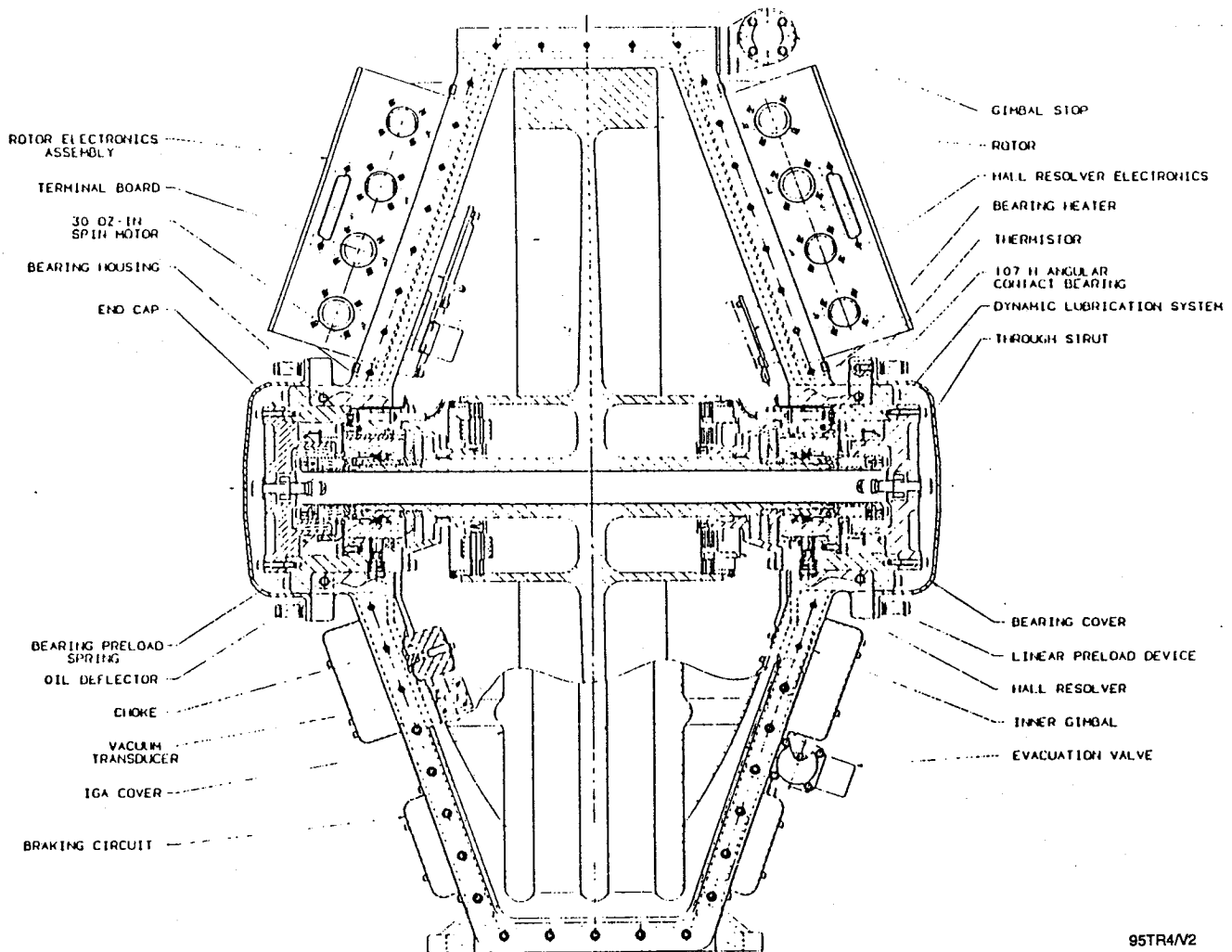


Figure 2. System Block Diagram



95TR4/V2

Figure 3. Inner Gimbal Assembly

ORIGINAL PAGE IS
OF POOR QUALITY

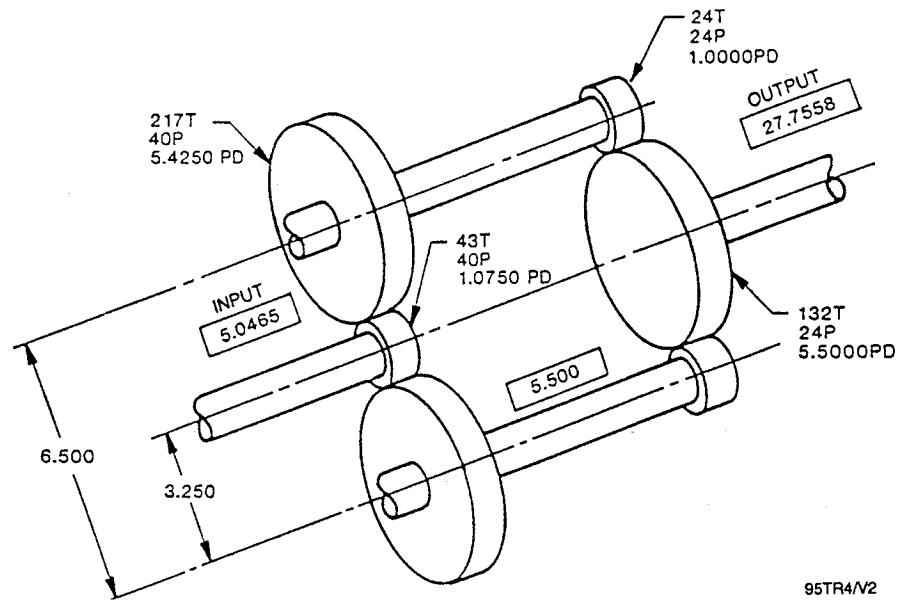


Figure 4. Parallel-Path Gear Train Transmission

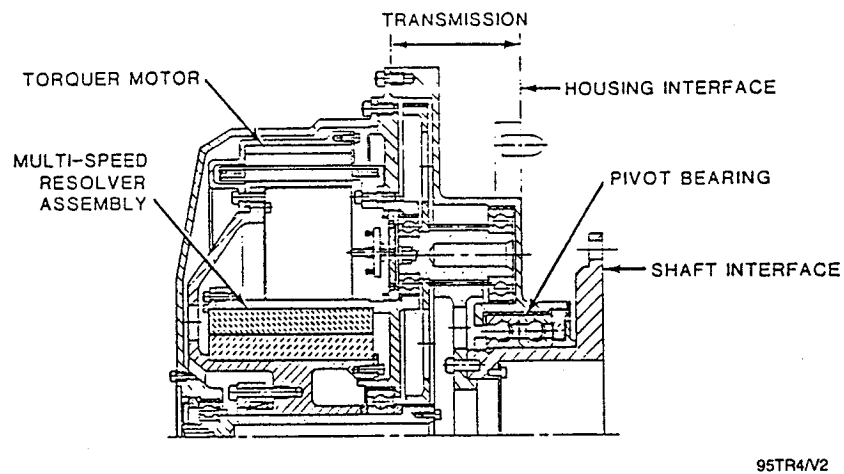


Figure 5. Torquer Module Assembly Cross Section

Testing:

The prototype model has been evaluated on a specially designed force and moment table. Further work is planned to reduce cross coupling between the inner and outer servo loops even though they are within specification for the space station. Life testing is also being planned.

Experience:

Past experience gained from the Skylab mission provides confidence that this type of gyroscope with a double-gimbal control moment can satisfy the goals of this work.

Gears

Key Words:

Worm Gearing, Spacecraft Power Transmission

Mechanisms:

Worm Gears

Systems:

Deployable Systems, Naval Research Laboratory (NRL)/Sundstrand Worm Gear Ball Screw Actuator, Shuttle Payload Capture Mechanism, Deployable Mast Worm Gear Drive, Roller Screw Latch Mechanism

Authors; Experts:

1. William Purdy
2. William McCown

Address:

1. Naval Research Laboratory
Washington, D.C.
2. Rexnord Aerospace Mechanisms
2530 Skypark Drive
Torrance, California 90505

Telephone:**Title:**

Practical Experiences with Worm Gearing for Spacecraft Power Transmission Applications

Source:

NASA Conference Publication 3032, 23rd Aerospace Mechanisms Conference.

Abstract:

Experiences of several organizations using worm gearing for spacecraft power transmission are discussed. Practical aspects and subtleties of using worm gearing in a space environment are also covered. An overview of advanced considerations for design and operation is included. Knowledge gained from these applications is analyzed and guidelines for usage are discussed.

Anomalies:

- Excess torque under cold vacuum conditions.
- Lubricant starvation.
- A dry film lubricant can cause massive gear tooth wear.

Lessons Learned:

- Careful run-in is essential to good operation. Break-in gradually with light loads and abundant lubrication.
- Low-temperature operation can be problematical because of lubricant starvation. Soft extreme pressure greases that contain molybdenum disulfide (MoS_2) are effective in resolving this problem (e.g., Braycote 608).
- Techniques for replenishing the lubricant as it is wiped off the tooth surfaces are beneficial. On the Rexnord mechanism, a wiper system was installed to force grease back onto the gear teeth.
- Unacceptable lubricant starvation can be caused by allowing the gears to reach a stall condition.
- Torque reserve is important.
- A list of general guidelines is useful for the initial design. These guidelines apply to most worm gear systems and are taken from worm gear specific texts (see Table 1).

Table 1. General Guidelines for Worm Gear Systems

Guideline	Reason
Make the hob as nearly identical to the worm as possible. Use larger center distance for hobbing.	Optimize contact prior to break-in.
Make face width a maximum of 50% of worm diameter.	Avoid high-contact load on outer edges of gear teeth.
Avoid low-pressure angles on low-tooth-count gears.	Avoid undercutting.
Total tooth count (worm + gear) should be a minimum of 40.	Avoid geometric interference.
Avoid low speeds and stall.	Low speed promotes severe boundary lubrication.
Grease lubrication may require special techniques to maintain performance.	Oil film benefits from replenishment such as in oil bath.
Use fine surface finishes.	Improves lubrication and wear.
Set the gearset up so that initial contact pattern is on the leaving side of the gear.	Provide oil reservoir on the entering side. Pattern will grow to cover entire width over life.
Break in gradually with light loads and abundant lubrication.	Break-in greatly increases life.

95TR4/V2

Description:

NRL/Sundstrand Worm Gearing Ball Screw Actuator. Two similar worm gear systems were used to drive a ball screw actuator built by Sundstrand Corporation in conjunction with the NRL for a spacecraft application. The first gearset (referred to as the primary system) had an 86:2 ratio and consisted of a 20.2-mm (0.797-in.) diameter steel worm and beryllium copper gear. There were two of these type worm gear systems in the actuator called the primary and back-up drivers. The second type of system, called the emergency system, was on a redundant drive for the first two systems. This gearset consisted of a two-start worm of the same design as the primary system and a 58-tooth gear cut into a steel bull nut, called the emergency drive. The actuator was required to drive under a constant load for 15 min, generate a sufficient stall load, then reverse its cycle. The emergency system had to drive against constant load for 30 min.

NASA-Goddard Cone Drive System Design. At the Goddard Space Flight Center, a 50:1 cone drive (double enveloping) worm gear system was used to drive an overcenter latch for a shuttle payload capture mechanism. The worm gear drives for approximately 10 sec against a torque that increases to a peak at 5°-before-center position. The worm is driven by a motor with a peak torque at stall of 27.5 Nm (250 in.-lb) and has a requirement to produce a minimum 339-Nm (3000-in.-lb) peak output at the gear. The system must operate from -70 to +70°C in a vacuum environment.

The reduction ratio was changed from 50:2 to 50:1 after galling. Poor efficiency was observed in cold-vacuum testing of a development motor/worm gear system. The development system was lubricated with Braycote 601, which was changed to a mixture of 50% Bray 815Z oil for the final system. The 802 extreme pressure grease is different from the Braycote 601 in that it contains a molybdenum disulfide (MoS_2)-based compound, and it is based on a different oil than the Braycote 601, which is based on Bray 815Z oil. The system was designed to operate properly with a worm gear efficiency of 40%.

Astro Aerospace Worm Gear System Design. Astro Aerospace has successfully used two worm gear systems as drivers and governors in deployable masts. The worm gear systems are used as a drive to retract the mast and as a brake/governor when the mast deploys under its own spring energy. This paper discusses the system's characteristics only when used as a drive. Two systems used in this capacity are being examined. One system, detailed in Table 1, was a 30:1 ratio gearset with a 25.4-mm (1.000-in.) worm and 63.5-mm (2.500-in.) gear. The other system will not be discussed in detail. However, lubrication failed completely allowing massive gear tooth wear when a dry film lubricant was the sole lubricant. Following a switch to grease lubrication, the system was successful.

The first system mentioned had to produce an output torque of 4.8 Nm (42 in.-lb) for several minutes after briefly producing a torque of 25 Nm (225 in.-lb). The system had to operate in vacuum at temperatures from -85 to 70°C.

One of the most important aspects of this design is the grease lubrication and its application. A thin coat of Braycote 601 grease is used as the only lubricant for the worm gearset. The grease is applied before run-in and then cleaned off, first using Freon and then toluene to remove Freon residue after the run-in is finished. A thin film of grease is then applied in the final assembly.

Rexnord Aerospace Mechanism Worm-Gear-Driven Latch System Design. A worm gear system is used in a roller screw latch, which is used to clamp a connector system together. The gearset features a 40:1 ratio consisting of a 15.9-mm (0.625-in.) diameter

steel worm and an aluminum-bronze gear of 63.5 mm (2.500 in.) diameter. This system undergoes minimal loads for latch extension and engagement, then is driven under power to stall as the screw and nut tighten.

This system operates in vacuum at ambient temperatures with a peak torque output of 12 Nm (107 in.-lb) and a maximum available input torque of 2.0 Nm (18 in.-lb). Output load variance using governed motor power was limited to 10% in a life-cycle test of 20 full actuations. Sliding velocities run from as great as 1.52 m/sec (60 in./sec) down to stall, going from high to low extremes in as little as 3 sec. Design details are listed in Table 1. Braycote 601 grease is applied to lubricate this system. Tungsten disulfide dry film is applied and is worn away during break-in.

Testing and Experience:

NRL/Sundstrand Systems. The two systems operated as designed in ambient air, ambient vacuum, and hot vacuum testing. All systems demonstrated an unexpected failure mode during cold vacuum qualification testing. The actuator would start a cycle working normally, but would gradually slow down during the cycle indicating increasing torque demand on the drive motor. The emergency and one of the primary systems would actually slow down to the point of stall under a constant load. After much investigative testing it was shown that the efficiency of the worm gearing was dropping over time. The worm gear system efficiency has to drop to approximately 12% for the primary drive to stall in these conditions and to 19% for the emergency system to stall. This is a very low efficiency as compared to the 40% efficiency the systems demonstrated in ambient tests and at the start of each cold vacuum cycle. Design calculations predicted efficiency to be between 47 and 62%.

This decay was severe in cold vacuum conditions, minimal in ambient vacuum conditions, and nonexistent in hot vacuum and ambient conditions. The severity of the decay varied for each system and for each drive direction of each system. The cause was shown to be lubrication depletion in the worm gearing. The decay, and therefore the lubrication problem, was not permanent. Whenever the actuator was retested in cold vacuum, it exhibited the same behavior of starting well and then decaying. This decay problem was eliminated by switching from Braycote 601 to Braycote 608 grease for the worm gear lubrication. This fix was demonstrated only on the emergency system, although it is expected to succeed on the primary systems also.

The decay phenomenon was attributed to a gradual wiping away of the grease, with the poor efficiency demonstrating a weakness in the boundary lubrication regime. The MoS₂-bonded dry film lubricant applied to the gear teeth wore off the driving surfaces during run-in, and provided no lubrication during operation. The manner in which the Braycote 608 grease solved the problem is not fully understood because it has two major differences from the Braycote 601 grease. The Braycote 608 grease has MoS₂ added, which could be improving the boundary lubrication. The Braycote 608 grease also has much higher oil content, which could help the healing process of lubricant after it has been wiped away. It has not been determined whether the problem was solved by either one or both of these changes.

An interesting discovery was the healing ability of the worm gear system lubrication. The primary systems would show normal efficiency when restarted after they had been turned off for a 20-min period after decaying to stall.

Astro Aerospace Worm Gear Testing. This system performed successfully with no difficulties encountered. A critical factor in the success of this design is the ample torque margin of the drive motor at nominal loads. At nominal loads, the motors had greater output. It is important that the system succeeded at extremely cold temperatures as low as -85°C .

NASA-Goddard Cone Drive System. The final system operated as designed between -50 and $+70^{\circ}\text{C}$ in thermal vacuum testing. Below -50°C , however, the worm gear efficiency was significantly lower, dropping as low as 21% at -70°C . Gear efficiencies in test were from 40 to 50% at ambient and hot vacuum conditions. With the system's ample torque margin, it barely passed its -70°C vacuum operation requirement. At the time of this writing, the system has not yet been disassembled and examined for galling or other degradation.

Tests on the development system showed generally poor efficiency during operation below -10°C . The efficiency was anywhere from 5 to 50% lower than efficiencies measured at higher temperatures. The original system failed during these cold vacuum tests, having wiped bronze from the gear onto the worm. Data on torque versus speed at high and low temperatures showed that at low-speed, high-torque conditions, the efficiency was significantly lower and more inconsistent in the cold case. Data taken at low torque, higher speed conditions showed equal performance in hot or cold conditions.

Some important worm gear performance characteristics were demonstrated by this system. At extreme low-temperature conditions, the worm gear efficiency dropped from normal efficiencies of 40 to 50%, to 21%. The system was highly successful at temperatures above -50°C . As a result of development testing, the performance of the system was significantly improved by the switch to a wetter grease that contained MoS_2 .

Rexnord System. The drive system demonstrated a load degradation after 10 full-load cycles, decreasing steadily to 60% level at 20 cycles. Gear lubrication was found to be at fault, as relubrication brought back initial loads. A wiper system was installed to force grease back onto the gear teeth eliminating the load decay and providing successful operation.

Stall conditions under peak loading aggravated the tendency of the worm to wipe grease from the gear teeth. A healing effect was evident, but produced output loads of only 80%, at best, from previous well-lubricated runs.

Motors

Key Words:

dc Brush Motor, Gearhead, Solar Array

Mechanisms:

Brush Motor Gearhead

Systems:

Deployment Systems, Rotating Systems

Authors; Experts:

Barnie W. Henson

Address:

European Space Agency
Noordwijk, Holland

Telephone:

Title:

Dual-Wound dc Brush Motor Gearhead

Source:

NASA Conference Publication 2423, Revised, 20th Aerospace Mechanism Symposium (1988).

Abstract:

This paper describes the design, design requirements, development tests and problems, qualification and life tests, and the findings of the strip examination of a dual-wound dc brush motor gearhead. At the time of this writing, it is the only space-qualified, dual-wound dc brush motor gearhead in Europe.

PRECEDING PAGE BLANK NOT FILMED

Anomalies:

Bearing Failures. The first 160:1 gearhead tested was coupled to a Size 11 motor. The unit was subject to thermal vacuum testing and a life test. After 39 hr of operation, a gearhead failure was observed. Investigation revealed that a bearing on the third layshaft had collapsed, although the rest of the gearhead was in good condition. This was an unexpected failure mode and, from a brief examination, it was considered to be a random failure.

The second 160:1 gearhead was coupled to a dual-wound Size 18 motor. The unit was subject to sine and random vibration at qualification levels. Subsequent derivation of Q factors due to fixture design and mounting resonances indicated that the unit was subject to random levels of the order of 100 g (rms). To improve this situation for future vibration tests, a new fixture was designed. The unit was then subjected to thermal vacuum testing and life testing. A total of 82-hr running time had been accomplished when the unit failed. Investigation revealed that the identical bearing on the third layshaft had collapsed. The gearhead was generally in good condition, but the appearance of the grease had deteriorated and some evidence of debris existed. This failure eliminated the random bearing failure theory previously supposed.

Shaft Failure. The gearhead that had accomplished 200 hr of operation was still running smoothly and it was decided to continue the test to obtain more confidence. At 240 hr, a catastrophic failure occurred. The third layshaft fractured at a change in the cross section from a gear face to the bearing spigot. This formed an almost square corner, less than 0.125-mm (0.005-in.) radius to facilitate seating of the bearing.

A thorough metallurgical examination revealed that during final machining, the Tuffride layer had been ground away on the bearing spigot. Thus, at a critical change of section with a sharp radius attracting a stress concentration factor of about 4, the material properties also changed.

The running time equated to approximately three million revolutions of the shaft (i.e., some six million stress reversals). Analysis of the load/fatigue curve indicated that the expected life had been reached. While the running time was some five times more than required for the intended application, it was considered essential to initiate design and process changes to improve the product in view of the wide variations associated with fatigue failures. The changes required were quite straightforward:

1. Increase the blend radius from 0.125 mm (0.005 in.) to 0.250 mm (0.101 in.) and, thus, reduce the stress concentration factor from 4 to 1.5.
2. Finish grinding the bearing spigot prior to applying the Tuffride process because the growth in size due to the Tuffride process is insignificant.

These changes were consequently incorporated in the qualification and life test model for formal testing.

- Post-test examination revealed brush debris that had been blown around by the gaseous purge applied during air operation.
- During the initial phase of the ambient life test, the winding 1 current trace became noisy and the shaft speed reduced. It was concluded that the temporary anomalous performance was caused by a brush fragment.

Lessons Learned:

- Drawing dimensions should not allow bearing axial preload under worst-case tolerance conditions.
- Examine bearing loads carefully and apply a double bearing, if necessary.
- Apply the Tufftride process to gears and shaft. The process reduces wear debris and avoids bearing contamination. The Tufftride process should be applied *after* the bearing spigot is finished ground. The growth of the Tufftride process is insignificant; if it is applied prior to grinding, it could be removed by wear.
- Examine the design for stress concentrations carefully and be sure there is adequate safety margin.
- Motor winding redundancy is recommended in the event of winding or connection failure. A clever scheme is described below.
- The brush material is Boeing Compound 046-45 because of good wear resistance in vacuum. It consists primarily of molybdenum disulfide (MoS_2), which requires purging for operation in normal atmosphere.
- Brush debris caused problems and reinforces the view that brushless motors should be applied, if possible.

Description:

Motor. The motor is a two-pole permanent-magnet device in a frame Size 18. A fundamental feature of the unit is the dual-wound armature with a commutator at each end. This arrangement provides electrical redundancy using a common armature, shaft, housing, and magnet system. The configuration is shown in Figure 1.

The principal electrical system is duplicated to provide redundancy in the event of winding or connection failure. The two windings are radially separated and electrically isolated in the armature stack by wrapping the respective windings in Melinex slot liners. The winding layout is shown in Figure 2. The inner winding (redundant) is connected to the front commutator and the outer winding (prime) is connected to the rear commutator.

The armature wire size has been carefully chosen to give the same torque from each winding and the same number of turns per winding to ensure that the no-load speed is equal. The resulting performance per winding is higher than a normal Size 11 motor and the stall torque is approximately double.

Two ceramic magnets are bonded to the stainless steel housing. They are made of barium ferrite and was chosen because it has a good resistance to demagnetization. This permits the rotor to be removed and replaced without affecting the performance. Although the magnetic characteristics of the material exhibit a knee in the BH curve, it is not possible to demagnetize the motor under normal operations or by reversing the motor while running at ambient temperature.

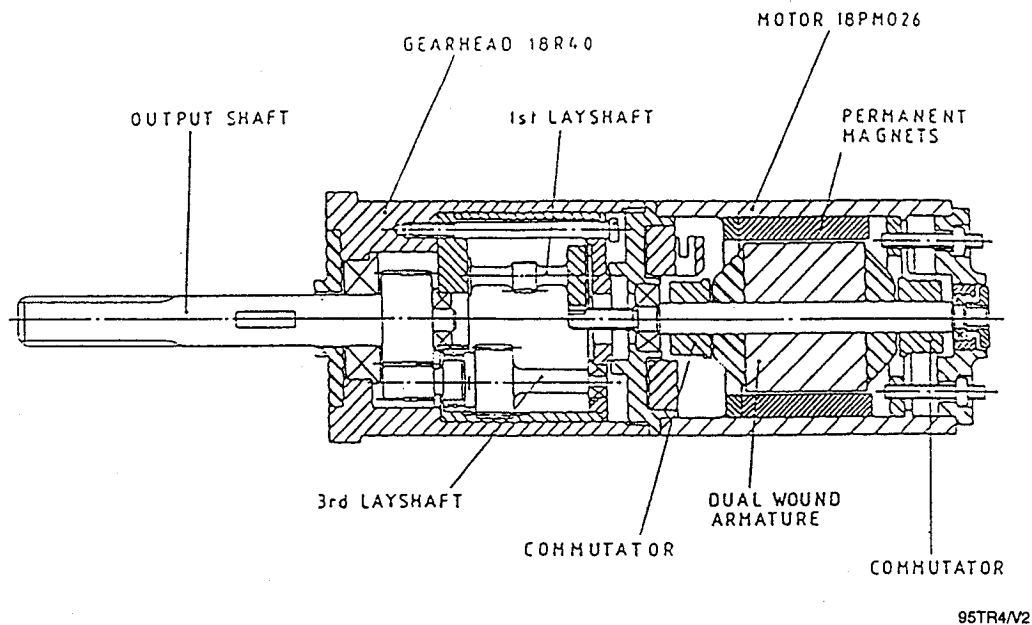


Figure 1. Dual-Wound Motor Gearhead (Section View)
(Note: Second Layout Omitted for Clarity)

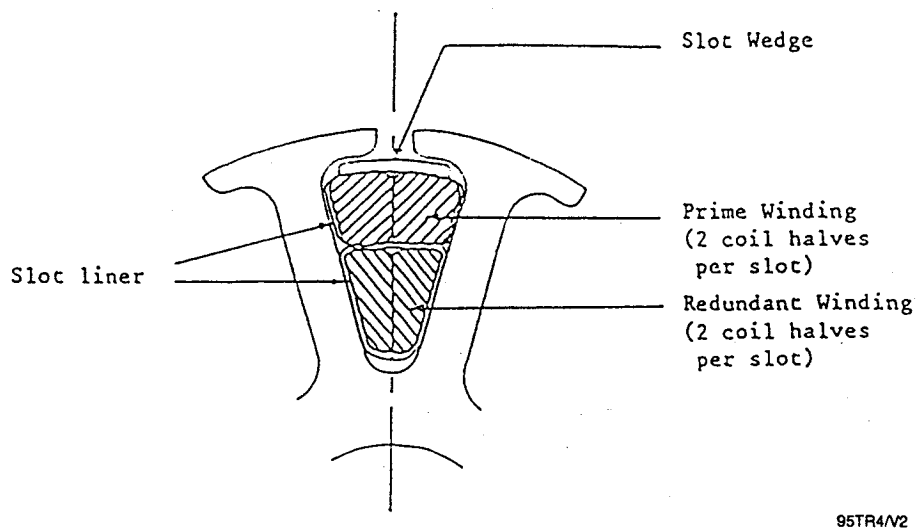


Figure 2. Winding Layout

The commutators are made of copper and are comprised of eleven segments set in a molding. A pair of spring-loaded brushes are located in a holder adjacent to each commutator. The wires from the front brush assembly pass through a tube located in the gap between the magnets and exit through the rear end cap where terminal posts are provided for external connections.

The brush material is Boeing Compound 046-45. The material is supplied in a compact form and comprises mainly MoS_2 . It has a low rate of wear in vacuum but has the disadvantage that it requires purging when used in air. Because it has a high MoS_2 content, the commutator film has a relatively high and variable resistance that influences the performance characteristics at low voltages and loads. In normal operation, these effects disappear. For this reason the motor run-in tests are made at 18 V and a torque of 100 g-cm. The motor shaft is supported on Bartemp dry lubricated bearings. Lubrication is achieved by transfer from a sacrificial cage made of a PTFE/ MoS_2 /glass fiber composite.

Gearhead. The gearhead is manufactured entirely from stainless steel. It has a conventional spur gear and layshaft configuration and has a ratio of 160:1. There are five layshafts and each one is mounted on miniature ball bearings. This arrangement results in a high overall efficiency (~90%) and permits the unit to be backdriven. A cross section of the gearhead is shown in Figure 1. The bearings used are mainly the caged type with shields, but in two cases different bearings had to be used to accommodate the loads and envelope constraints. All bearings are lubricated with Braycote 601 grease.

All the gears and layshafts are hardened by a diffusion process known as Tufftriding. This is a proprietary type of nitriding process and is used to improve the wear characteristics. It also improves the fatigue life.

Motor Gearhead Assembly and Mounting Arrangements. The motor-gearhead interface comprises a spigot location with a screw fixation and the motor shaft pinion meshes directly with the first layshaft gear in the gearhead. Locking of the interface is achieved by four small spots of adhesive.

Choice of Lubricant. Braycote 601 grease was chosen because its low pour point ensured consistent performance even at -45°C .

Choice of Brush Material. Brush material is Boeing Compound 046-45 because of good wear resistance.

Testing:

Performance of the unit with one winding powered at 28 V is show:

- No-load speed: 38 to 43 rpm
- No-load current: 50 to 100 mA
- Speed at 1.5 Nm: 30 to 34 rpm
- Current at 1.5 Nm: 300 to 420 mA.

The performance with both windings powered is very similar, but the speed at rated torque is slightly higher and, of course, the total current is shared between the two windings. The torque required to backdrive the unit is less than 0.7 Nm (100 oz-in.).

The purpose of the two windings is to provide redundancy rather than to increase the torque capability. The gearhead is designed for the rated torque of 1.5 Nm and has a safety factor of two based on static loads. The motor gearhead should not be operated above the rated torque.

Vibration Tests. The qualification level vibration test comprises:

- Sinusoidal
 - 5 to 20 Hz: 20-mm peak to peak
 - 20 to 100 Hz: 16.3 g
 - Duration: 1 sweep/axis at 2 octaves/min
- Random
 - Level: 19.5 g (rms)
 - Duration: 3 min/axis

During these tests, the actual level on the motor was also monitored. It was noted that a substantial degree of cross-coupling occurred even with the new fixture. Q factors up to 3 resulted in levels up to 60 g (rms) on the motor. Post-vibration function tests confirmed that the unit was still in good working order.

Thermal Vacuum. The thermal vacuum and life tests were performed at the European Space Tribology Laboratory (ESTL), Risley, United Kingdom. The motor gearhead was subject to function tests at a torque of 1.27 Nm (180 oz-in.) at ambient temperature with a nitrogen purge and in vacuum over a temperature range of +80 to -45°C. The unit was also subject to temperature survival tests at +95 and -60°C. Performance was nominal throughout the tests and all motor configurations were demonstrated.

Life Tests. The planned life test comprised of operations on each winding at a torque of 1.27 Nm (180 oz-in.) at ambient and in vacuum over a temperature range of +50 to -30°C. During the initial phase of the ambient life test, the winding 1 current trace became noisy and the shaft speed reduced. After some brief checks of no-load speed, start voltage, and breakaway torque measurements, the performance reverted to nominal. It was concluded that the temporary anomalous performance was caused by a brush fragment. The motor gearhead continued to function well for the planned duration of 100 hr, 50% of which were in vacuum.

Extended Life Test. Due to the satisfactory performance obtained, the life test was extended until a total running time of over 250 hr had been accomplished; 50% of this testing was in vacuum and the motor gearhead was still giving a nominal performance.

Examination After Test. Brushes were in good condition but had worn slightly unevenly; at least 50% of their length remained. Some brush debris was evident in various places having been blown around by the gaseous purge applied during air operation. Insulation resistance had reduced to values of 10 K Ω and 80 K Ω . It is believed this was due to tracking across debris paths possibly formed by centrifugal deposition of MoS₂.

Experience:

The gearhead has been applied to the Hubble telescope. Actual space experience was not cited.

Key Words:

Stepper Motor, Hybrid Stepper Motor, Stepper Motor Instability

Mechanisms:

Positioning Mechanisms

Systems:

Rotating Systems

Authors; Experts:

Russell Kackley and Sean McCully

Address:

Lockheed Missiles & Space Company, Inc.
Sunnyvale, California

Telephone:**Title:**

Stepper Motor Instabilities in an Aerospace Application

Source:

26th Aerospace Mechanisms Symposium (1992).

Abstract:

Stepper motors are frequently used in positioning mechanisms because they have several advantages over ordinary dc motors. However, there is frequently no feedback loop and the motor may exhibit instabilities under some conditions. A stepper motor in an aerospace positioning mechanism was investigated.

During testing, the motor exhibited unstable behavior, such as backrunning and forward running. The instability was dependent on voltage pulse characteristics, temperature, positioning angle, step rate, and interaction between the two motors in the system. Both testing and analysis results verified the instability. A special-purpose FORTRAN code was

written to simulate the system. This code was combined with another simpler code to show the performance of the system in the phase plane so that instability boundaries could be displayed along with the motor performance. The analysis was performed to verify that the modifications would produce stable performance before implementation in the hardware. Subsequent testing verified the analytical stability predictions.

Anomalies:

During thermal vacuum testing of a multiple boom assembly, serious instabilities occurred arising from the stepper drive motors.

Lessons Learned:

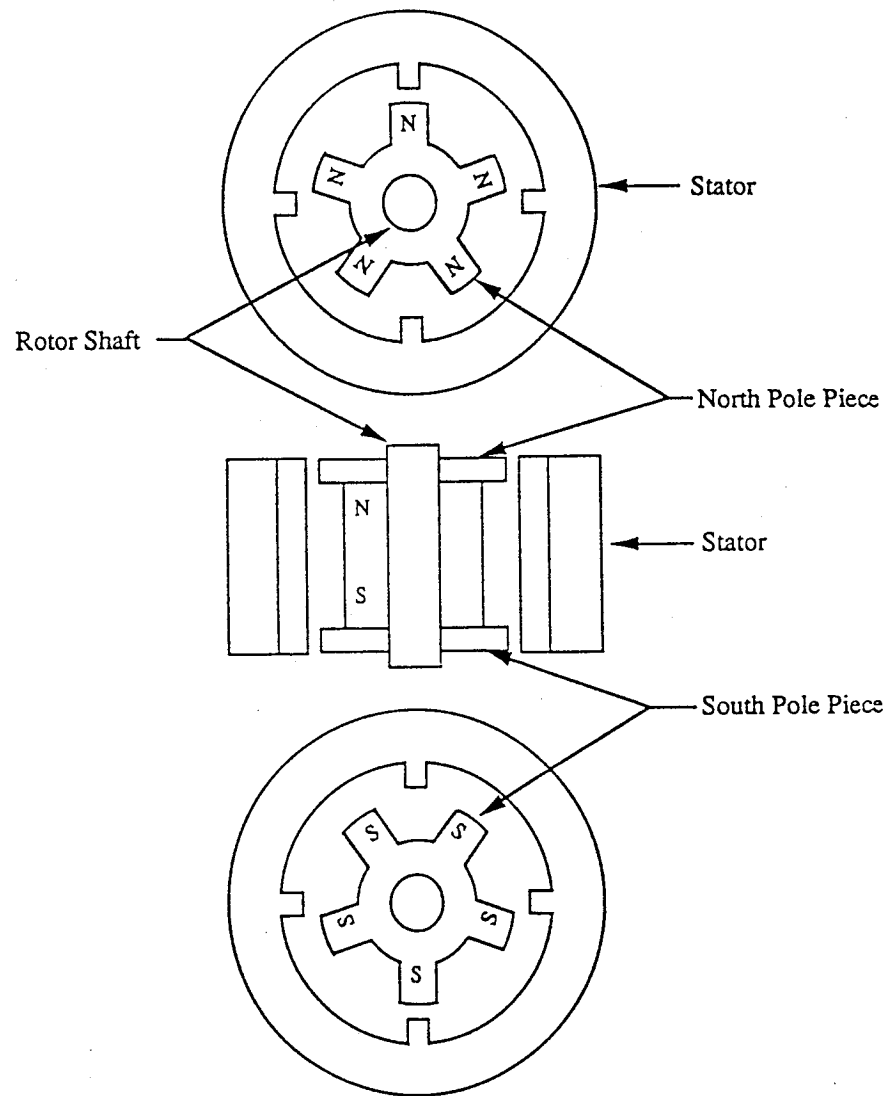
- Stepper motors can exhibit instabilities, which should be addressed early in the development process.
- Stepper motor stability is very dependent on friction and damping and it is important to ensure that adequate friction and damping are present over the range of operating conditions.
- Superimposing rotordynamic behavior and separatrices on the phase plane technique is a valuable tool for analyzing stepper motor stability.
- Simulation analysis is valuable to determine problems and solutions prior to building and testing expensive hardware.

Description:

Stepper motors are frequently used in positioning mechanisms because they have certain advantages that include no brushes to wear out and simple mechanical and electrical construction. However, each step applies a torque pulse that can cause structural modes to be excited. In addition, the motors may have problems dissipating heat into the vacuum of space. To minimize heat buildup, many motors are operated with a shaped, rather than square, voltage pulse. This can also aggravate stability.

There are three basic types of stepper motors: permanent magnet, variable reluctance, and hybrid (which combines features of both). The motor of concern here is a hybrid. It is made up of three components: an axially magnetized rotor and two pole pieces (one at each end of the rotor). Each pole piece is a toothed disk. The basic arrangement is shown in Figure 1. The pole pieces are staggered by one-half tooth pitch.

The stator is wound with wire to provide electromagnetic poles that interact with the rotors' permanent magnet poles. Stepper motors can have two, three, or more stator phases. This motor is two phase. It has four electromagnetic poles on each phase for a total of eight stator poles. In addition, the rotor has 50 poles for a total of 200 possible stable rotor positions. This results in a step angle of 1.8° .



95TR4/V2

Figure 1. Motor with Five-Tooth Rotor

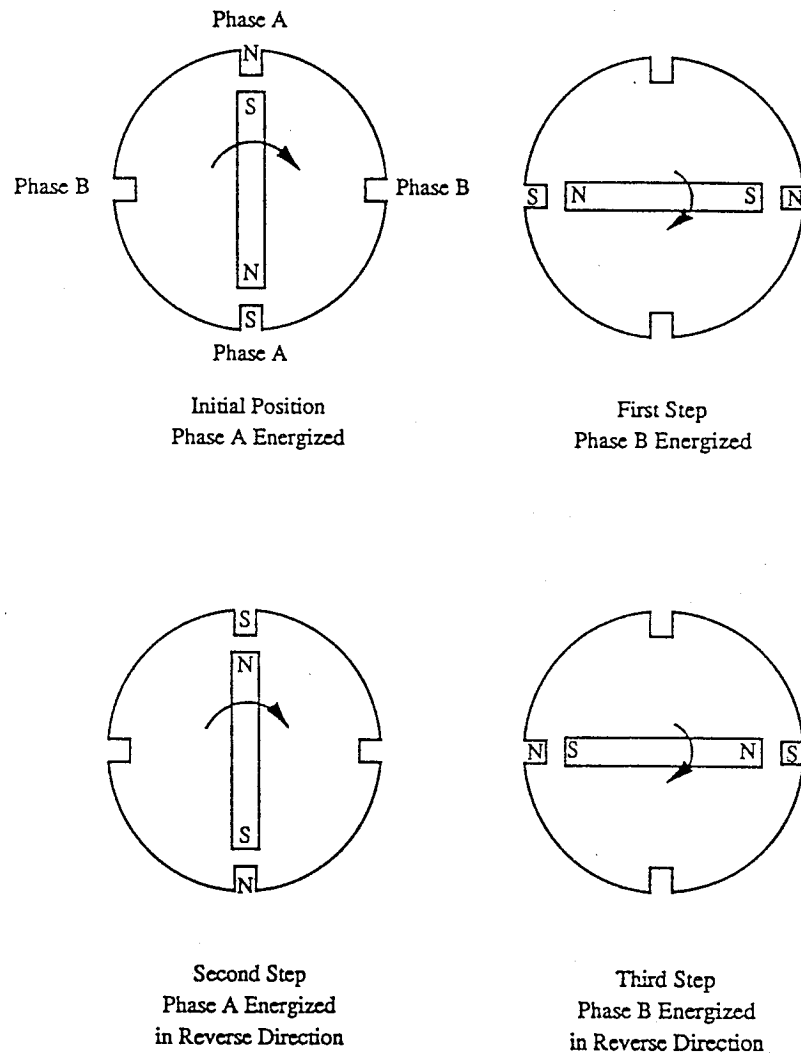
Figure 2 shows the operation of a 90° two-phase stepper motor in which each stator phase is sequentially energized. The motor can run forward or backward by reversing the phase excitation sequence. When the rotor runs synchronously with the phase excitation, the motor is said to be maintaining step integrity. The operation of the 1.8° two-phase motor involves 200 steps for each rotor revolution.

The desired behavior of a stepper motor is shown in Figure 3. If there is insufficient damping or friction, or if the motor is stepped at a frequency close to its natural frequency, the motor can backrun at three times the command rate, as shown in Figure 4. With low damping or friction, the rotor can also overshoot the commanded positioned move to the next stable equilibrium position, which is four steps ahead of the commanded position. This is called forward running and is shown in Figure 5.

In this application, a multiple boom assembly (Figure 6) uses stepper motors to position the booms. Both forward and backrunning were exhibited by the motor during a thermal vacuum test. The test temperature range was 10 to 170°F. The first failure occurred on the elbow. The outboard boom was gaining, or losing, steps at random. However, the motor was stable at 10°F because the viscous damping in the system was high to eliminate any oscillations.

Several solutions were offered, but cost and time ruled against them. The problem was finally resolved by making three modifications to the system. First, the duration of maximum voltage was shortened to reduce the energy delivered to the motor. Second, the driving circuitry was modified to introduce additional electromagnetic damping. Third, the minimum temperature was raised to 35°F to be sure that adequate torque capability was provided at low temperature with the reduced energy input and the additional damping.

The rest of the paper discusses analyses that were used to validate these solutions. Two analyses were undertaken to investigate the stability. The first analysis modeled one rotor and boom with Pro-Metlab and Simulab, two commercial servo-control simulation codes. The second analysis modeled the two-boom, two-motor system with a special-purpose FORTRAN code called STEPPER. The analysis technique was found to be very useful in verifying this stability. Based on the results of the analyses, the hardware was modified and run through the test program, successfully passing all the qualification tests.



95TR4/V2

Figure 2. 90° Stepper Motor

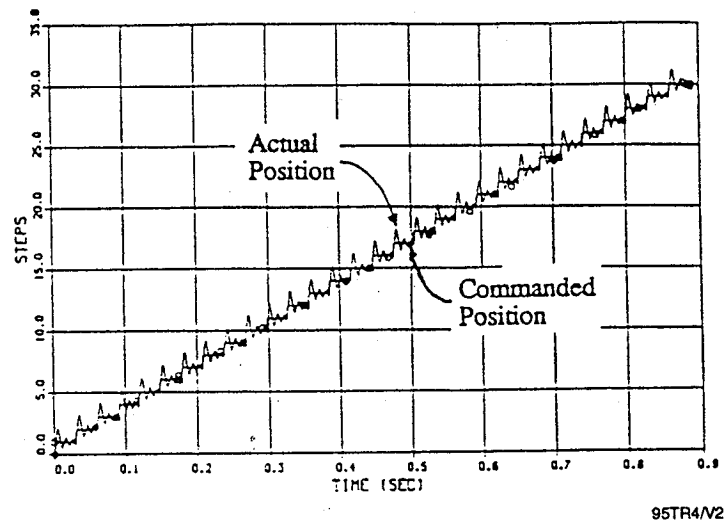


Figure 3. Rotor Position versus Time; Rotor Following Command

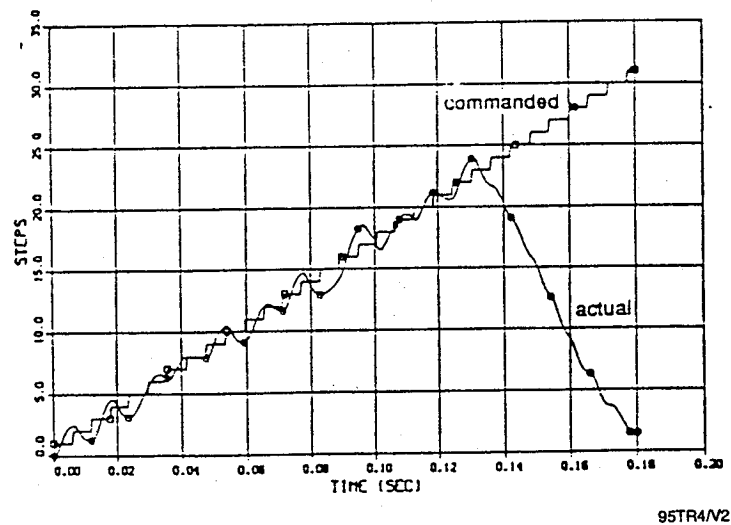
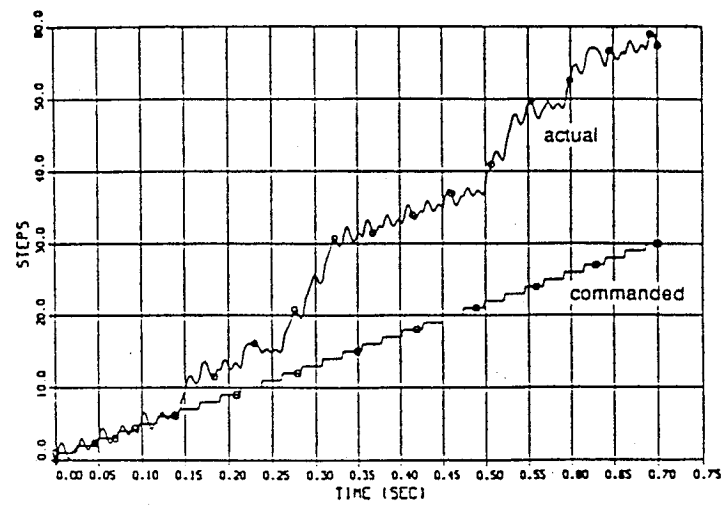
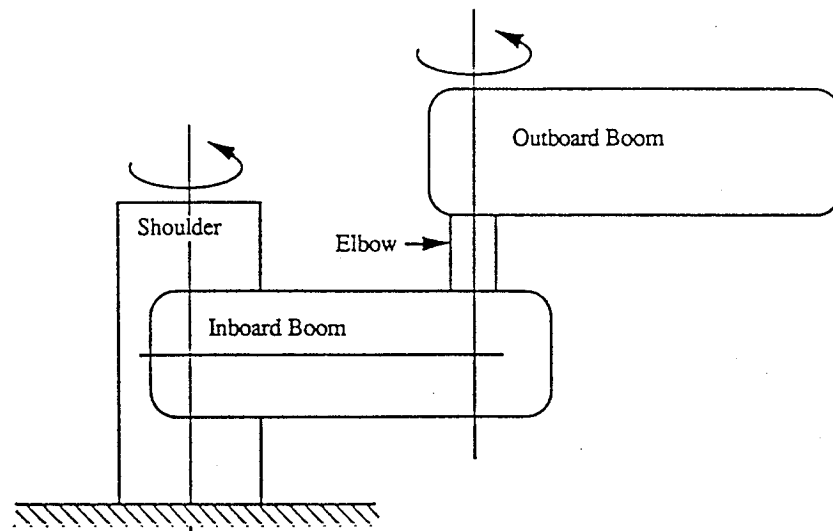


Figure 4. Rotor Position versus Time; Rotor Running Opposite of Command Direction (Backrunning)



95TR4/V2

Figure 5. Rotor Position versus Time; Rotor Running Ahead of Command (Forward Running)



95TR4/V2

Figure 6. Multiple Boom Assembly

Key Words:

Drive Motors, Deployable Appendages, Stepper Motors, dc Torque Motors

Mechanisms:

Drive Motors for Deployable Appendages

Systems:

Solar Arrays, Antennas, Robotic Arms

Authors; Experts:

R. Sharma, A. Tyler, R. Farley, and E. Devine

Address:

NASA-Goddard Space Flight Center
Greenbelt, Maryland 20771

Telephone:**Title:**

Spacecraft Deployable Appendages
(Internal Document)

Source:

Goddard Space Flight Center (1991)
Engineering Directorate

Abstract:

Various aspects of stepper motors used to actuate deployable appendages are discussed. Comparisons are made with dc torque motors. Brush motors are considered unacceptable because of excessive wear and consequent debris contamination.

PRECEDING PAGE BLANK NOT FILMED

Anomalies:

- Motor failures of brush motors were experienced on MAPS/MDRA and ISTP/GGS.
- Carbon brushes of brush-type motors wear excessively in vacuum
 - Wear debris contaminates the bearings, increasing drag and reducing life
 - Accumulated debris shorts the commutator, increasing current and resulting in motor failure.
- Stepper motors can have positioning errors due to:
 - The encoder
 - The drive electronics
 - The attitude control electronicsor
 - A power supply interruption
 - A single-event upset in the electronics
 - A mechanical failure of the unit.

Lessons Learned:

- Brush-type motors should not be used for space applications.
- Brushless dc, permanent magnet dc, and brushless stepper motors should be selected.
- The torque margin (TM) for any motor ≥ 3 .
 - $TM = (T_a - T_r) / T_r$
 - T_a = available torque
 - T_r = maximum resistance torque.
- The design torque margins should be verified during flight testing.

Description:

Brushless dc, permanent magnet dc, and brushless stepper motors should be used for space flight applications. Stepper motors are essentially brushless dc motors with special construction and properties that are capable of converting digital signals into fixed increments of shaft rotation. This is achieved by magnetic alignment of teeth on the stationary and rotating parts of the motor. This makes stepper motors useful and reasonably accurate devices for positioning a load without the need for direct feedback systems.

The only error induced by the motor is its final positioning accuracy, which is usually within 5% of the last step taken, depending on the Coulomb friction in the system. The error is noncumulative and, with a reduction drive, the final position of the output shaft is within extremely small tolerances. Because the motor is an incremental device, it can be easily integrated into a microprocessor-based control system.

The load (inertia, friction, damping) can effect many motor parameters, such as motor resonance, instability, overshoot, ringout time, and pull-in rate. Stepper motors are characterized as lightly damped spring-mass systems where the motor has several torsional frequencies that can reduce the available torque or go unstable if driven at a resonant frequency. There are three general types of stepper motors: variable reluctance, permanent magnet, and hybrid.

The advantages of a stepper motor over a dc torque motor is that the control of a stepper is very simple compared to the dc torque type. Open-loop control of a stepper motor is simple to implement and the motor also has the advantage of an internal magnet detent to hold the last position without dissipating power. This detent gives the system high torsional stiffness with a reduction drive, whereas the direct-drive dc torque motor must be held in position by the control system at all times and has low torsional stiffness.

Simpler, smaller, lower-cost electronics utilizing open-loop and microprocessor control are the key advantages of stepper motors. Even though the motions are small, they are still impulsive in nature creating a set of frequencies that need to be avoided to minimize spacecraft jitters and motor resonance. Those are the key disadvantages.

A dc torque motor is commutated (coordinated phase switching) for maximum torque/minimum ripple, where the motor torque is only dependent on the current in the windings (or rotor speed and applied voltage). The stepper motor is uncommutated and the torque then depends not only on the current in the windings, but also on the position of the shaft with respect to those fixed windings. The motor torque can then be saw toothed during multistep operation and the exact wave form will depend on the load (friction, inertia, viscous effects), step rate, and intrinsic motor characteristics. This makes a closed-loop control system based on assumptions regarding motor/speed characteristics very difficult to implement.

Experience:

See brush motor failures under anomalies.

Key Words:

Rotary Actuators, Deployment Mechanisms, Harmonic Drive, dc Motors, Stepper Motors

Mechanisms:

Solar Arrays, Booms, Antennas

Systems:

Satellites

Authors, Experts:

R. Sharma, A. Tyler, and R. Farley

Address:

NASA-Goddard Space Flight Center
Mail Code 716
Greenbelt, Maryland 20771

Telephone:

Title:

Spacecraft Deployable Appendages

Source:

Goddard Space Flight Center
Engineering Directorate

Abstract:

This report is a compendium of satellite experience and mechanism design practices compiled by the engineering staff at NASA-Goddard Space Flight Center.

PRECEDING PAGE BLANK NOT FILMED

Anomalies:

Hard-stop collision can cause the motor rotor to continue to turn, which elastically winds up the harmonic drive. The spring energy of the harmonic drive can catapult the motor backward three steps as it unloads. The motor then picks up the pulse signals as if it were starting from standstill and drives into the hard stop repeating the same series of events over and over.

Lessons Learned:

- Hard stops must be avoided by proper application of end-of-travel limit switches.
- Motor drives for rotary actuators should be a dc torque motor or stepper motor. The dc motor should be of the brushless permanent-magnet type with position and velocity sensors.
- The output shaft should be supported by a pair of back-to-back duplex bearings (for high-moment resistance), preloaded for a desired stiffness and life span.

Description:

There are three main constituents of a rotary actuator: motor, reduction gearing, and output shaft support. The motor can be a dc torque motor or stepper motor. A magnetic detent can be provided for position hold. The straight dc torque motor should be of the brushless permanent-magnet type with position and velocity sensors.

The preferred reduction gearing is the harmonic drive that has three principal components: a fixed circular spine, a flex spine that engages the circular spine when deformed, and an elliptical wave generator that deforms the flex spine.

The last major component is the output shaft support. Typically, a pair of back-to-back duplex bearings (for high moment resistance), preloaded for a desired stiffness and life span are employed. Other optional components are added for specific applications such as limit switches, travel hard stops, incremental and absolute position encoders, tachometers, and slip rings or cable wraps.

As an example, the design of the tropical rainfall measuring mission solar array drive actuator will use a three-phase permanent-magnet type stepper motor with a step size of 15° through a harmonic drive reduction of 200:1. This will result in an output step size of 0.0075° . This baseline actuator has a starting rate of 300 steps/sec when an inertia of 350 slug-ft^2 is rigidly attached, which is approximately six times greater than the tropical rainfall measuring mission array inertia. Thus, no steps are lost in the initial transient acceleration. In fact, when there is no-load inertia attached, the starting rate is about 1000 steps/sec. This excellent performance is explained by a very small step size at the output shaft and the compliance of the harmonic drive. The rotor can get ahead of the load an equivalent of three to four steps during initial acceleration due to the fact that the harmonic drive is elastically winding up at a displacement equal to three to four steps. This windup will unload when the output load reaches a constant speed.

Typically, a Type 5 Schaeffer Magnetics rotary actuator will have internal losses due to harmonic drive generator friction of 5 in.-oz (input end) and a torque efficiency of 75%. The flex spine has a torsional stiffness of 100,000 in.-lb/rad and the transverse stiffness provided by the duplex bearing has been measured at 500,000 in.-lb/rad. The motor rotor/wave generator inertia is 2500 gm-cm². The duplex bearing pair is preloaded to 100 lb resulting in a drag torque of 1.0 in.-lb at the output end. The peak motor torque produced by energizing the coils is on the order of 80 in.-oz and the detent torque can be as high as 33% of the motor torque (27 in.-oz).

Bearings and Lubrication

Key Words:

Chopper, Ball Bearings, Lubricants

Mechanisms:

Optical Chopper System

Systems:

Rotating System

Authors; Experts:

Terry Allen

Address:

Honeywell Inc.
Satellite Systems Operation
Glendale, Arizona

Telephone:**Title:**

Optical Chopper Assembly for the Mars Observer

Source:

27th Aerospace Mechanisms Symposium (1993).

Abstract:

The paper describes the Honeywell-developed optical chopper assembly, a component of the Mars observer spacecraft pressure modulator infrared radiometer science experiment that will map the martian atmosphere during 1993 to 1995. The optical chopper assembly is unique because of its constant accurate rotational speed, low electrical power consumption, and long-life requirements.

Anomalies:

The power loss in the angular contact ball bearings in the assembled flight unit was higher than that measured in bench tests.

PRECEDING PAGE BLANK NOT FILLED

Lessons Learned:

- The power loss in ball bearings is very sensitive to the amount of lubricant in the bearings.

Description:

The specification required that the total steady-state power consumption of the optical chopper assembly not exceed 1 W while operating at a nominal shaft speed of 67 Hz in a 10 to 45°C temperature range. A cross section of the optical chopper assembly is shown in Figure 1. The optical chopper assembly is directly coupled to an ac hysteresis synchronous, two-phase, six-pole motor excited by a 28-V, 200-Hz supply. The motor was based on an existing, proven design to minimize cost and schedule.

To meet the schedule, off-the-shelf Size R-3H angular-contact bearings were selected to support the motor rotor. The bearings were disassembled and the radii of the races were measured. The data were then reviewed to select races to match the diameters of separately procured titanium-carbide-plated 440C balls. The retainer was designed by Honeywell to have conical pockets and is machined from sintered nylon or Nylasint. The Nylasint material, which can hold up to 25% of its weight in oil, acts as a lubricant reservoir. The lubricant used was Coray 55. By selecting acceptable preload and lubricant quantity, the bearing drag torque was minimized during bench tests to meet the steady-state power requirements. Applied to the race surfaces of each bearing, was 2 mg of Coray 55 oil; approximately 20 mg was absorbed by each cage. Another sacrificial lubricant reservoir is mounted within the optical chopper assembly housing. This reservoir stores 1.05 g of Coray 55 and maintains a constant lubricant vapor partial pressure within the housing. This constant pressure extends lubricant life by replacing molecules that escape through the labyrinth seal.

After assembly, the optical chopper assembly was shipped to the Jet Propulsion Laboratory (JPL) for integration and system testing. These tests showed that the bearing power loss was greater than the 1 W specified. However, the motor efficiency was higher than predicted and the system was acceptable. The higher power loss in the bearings could be due to excess lubricant or misalignment. The bearing power loss is very sensitive to the amount of lubricant present and, from observations during the tests, it appears that this was the probable cause for the anomaly.

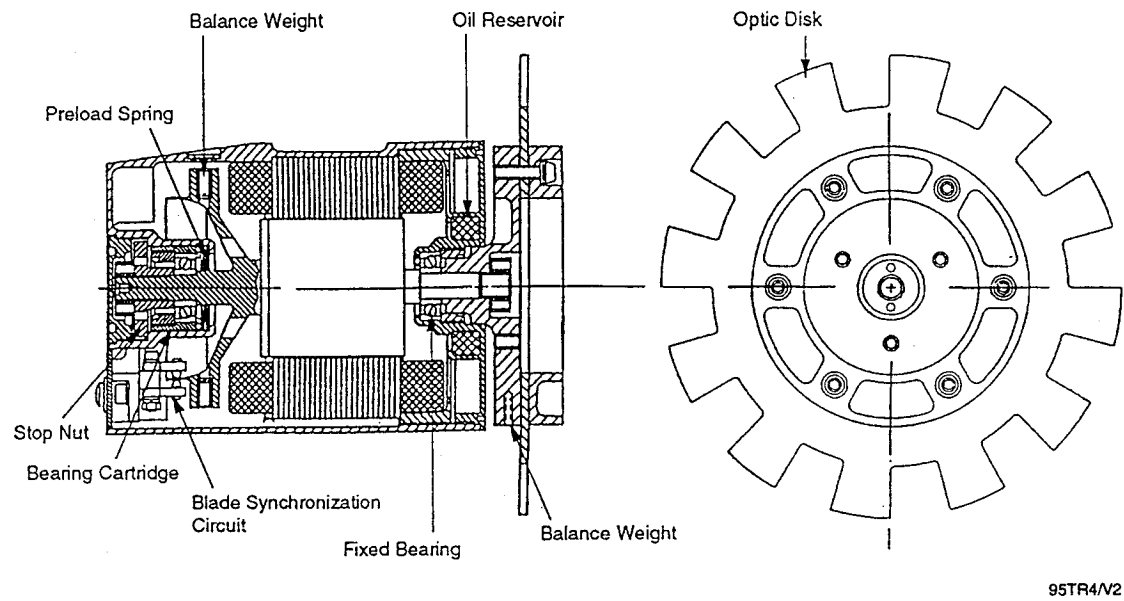


Figure 1. Optical Chopper Assembly Cross Section

Key Words:

Bearings, Lubrication, Momentum Wheels

Mechanisms:

Momentum Wheels, Control Moment Gyroscopes, Reaction Wheels

Systems:

Rotating Systems

Authors; Experts:

Anonymous

Address:

Allied Signal Aerospace Company
Bendix Guidance Systems Division

Telephone:

Title:

Attitude Control System Hardware - Momentum Exchange Devices

Source:

Viewgraph Handout (1992).

Abstract:

The Bendix Guidance Systems Division (BGSD) of Allied Signal Aerospace Company is a major supplier of momentum and reaction wheels and control moment gyroscopes. This presentation comprehensively describes BGSD technology and experience in these areas.

PRECEDING FILMS PLAIN NOT FILMS

Lessons Learned:

Reaction Wheel/Momentum Wheel Spin Bearings and Lubrication

- Low-speed operation (<3000 rpm)
 - Contact bearings (shielded): R4A, R6, R8, R10
 - Charged with fixed amount of oil
 - Metal retainers
 - Lubrication (Winsor lube L245X (MIL-L-6085A) plus 5% tricresyl phosphate (TCP), SRG40 superrefined mineral oil).
- High-speed operation (>3000 rpm)
 - Angular contact bearings: 104H, 106H, 107H, 305H
 - Proprietary design phenolic retainers
 - Active continuous lubrication system
 - Lubrication (KG-80 (MIL-L-83176A) superrefined mineral oil).

Lubrication System Choice

- For low-speed operation (<3000 rpm), a fixed-lubricant oil quantity in a shielded bearing is adequate for a 10-yr life.
- For high-speed bearings (>3000 rpm), a make-up mechanism must be provided to overcome the oil loss due to centrifugal force.
- The active flow-through lubrication system was chosen as a means of enhancing the bearing life by continuously supplying additional new oil to the spinning ball bearing at a controlled rate.
- Grease lubrication is not recommended
 - Higher running torque
 - Torque variations
 - Lubricant supply uncertain
 - High viscosity can lead to retainer instability.

Description:

Some typical Bendix momentum wheels are shown in Figure 1. The wheels are machined from a single piece of stainless steel (300) and the housing is made from magnesium and designed to meet stress corrosion criteria. Control moment gyroscopes are shown in Figure 2.

Experience:

The list of the control moment gyroscopes designed and built by Allied Signal Bendix is given in Table 1. Additional experiences are shown on Tables 2, 3, and 4.

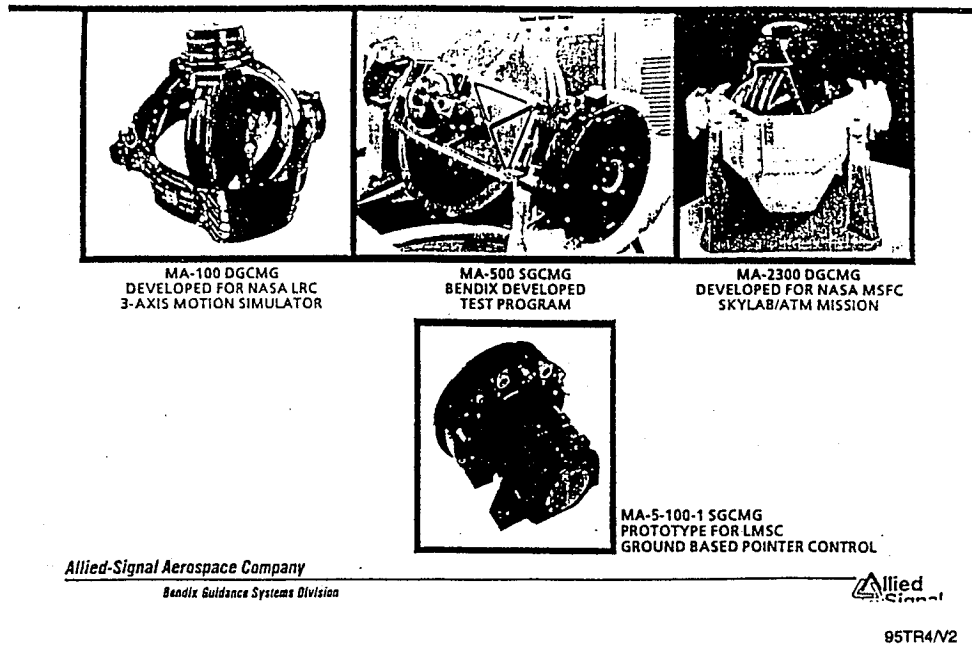


Figure 1. BGSD Reaction/Momentum Wheels

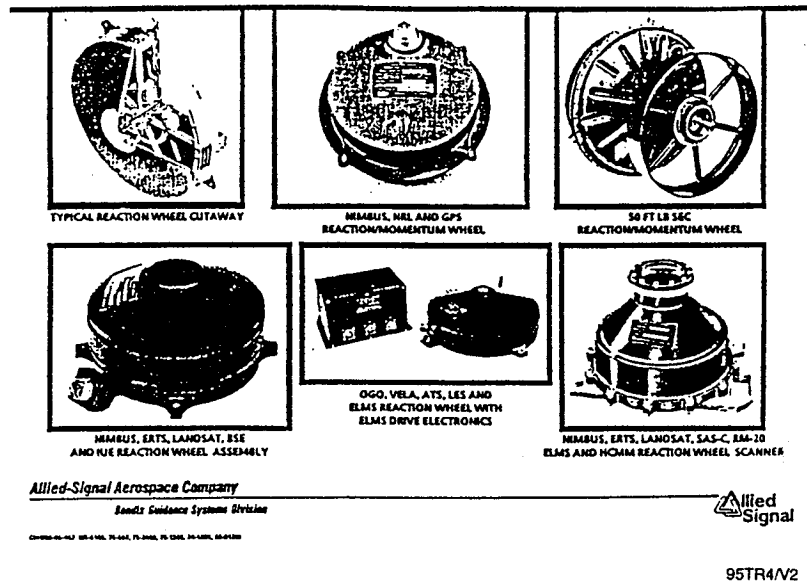


Figure 2. Control Moment Gyroscopes

Table 1. BGSD Control Moment Gyroscope Designs

PROGRAM	MOMENTUM	YEAR	TYPE	ELECTRONICS	DC MOTORS	LUBE SYSTEM	GEARS	SLIP RINGS	FUT GND
LANGLEY	1000 H	1963	DGCMG	X			X	X	G
SKYLAB	2300 H	1967	DGCMG	X		X	X		F
AIRFORCE	500 H	1972	SGCMG	X	X	X	X		G
ADVANCED	2300 H	1973	DGCMG	X	X	X	X	X	G
XPT	5 H	1975	SGCMG	X				X	G
INSAT	50 H	1978	MW	X	X	X			F
DSP	1200 H	1978	MW			X			F
H. TORQUE	1700 H	1981	SGCMG	X	X	X	X	X	G
ARABSAT	50 H	1982	MW	X	X	X			F
DSP-1	1800 H	1983	MW			X			F
ASTRO C	50 H	1984	MW	X	X	X			F
COBE	15 H	1984	MW	X	X				F
TEST BED	2300 H	1985	DGCMG	X		X	X	X	G
ADP-DG/CMG	3500 H	1985	DGCMG	X	X	X	X	X	G
SSCMG	3500 H	1988	DGSMG	X	X	X	X	X	F

Allied-Signal Aerospace Company

APM/A81

Bendix Guidance Systems Division



95TR4/V2

Table 2. Chronological History of BGSD Reaction/Momentum Wheel Programs

	<u>QTY BUILT</u>	<u>TIME FRAME</u>
NIMBUS/NRL/NTS/LMSC	62	1960-PRESENT
ADVENT/NIMBUS/ERTS (PITCH WHEEL)	55	1960-1972
OGO	53	1960-1968
OA0	51	1961-1971
NASA III-REL/VELA/LES/ATS/ELMS/SEASAT/ERBS	35	1963-PRESENT
NIMBUS/LANDSAT/HCMM (SCANNER)	21	1964-1978
TD OGO/LANDSAT-C/SEASAT/ETS-III/INSAT/ARABSAT	20	1966-1985
SAGS/RM-20/APL/ELMS/HCMM/SAESAT/JAPAN/ERBS (SCANNER)	18	1966-1984
NIMBUS/LANDSAT/BSE/UE/BS-II	33	1967-1985
GPS/MARTIN	209	1974-PRESENT
INSAT/ARABSAT/MW-50/ASTRO-C	13	1978-1985
DSP-1200/DSP-1800	10	1978-PRESENT
SSM/I	7	1979-PRESENT
EXOS-C/ERBS (SCANNER)	3	1980-1984
COBE	3	1984-PRESENT

Allied-Signal Aerospace Company

Bendix Guidance Systems Division

APW/AB1
CUCM 66-345

95TR4/V2

Table 3. Recent BGSD Momentum Exchange Programs

PROGRAM	WHEEL TYPE	H (lps)	SPIN MOTOR	MOTOR TORQUE (oz-in)	WHEEL SPEED (rpm)	WHEEL WEIGHT (lbs)	WHEEL SIZE (dia x high)	DESIGN STATUS
SSCMG (IGA)	DGCMG ^{1,3}	3500	BDC	37	6600	280	26" x 19"	E/M, FLIGHT
HTCMG (IGA)	SGCMG ^{2,3}	1700	BDC	37	6000	195	25" x 25"	E/M
DSP-B14/B18	RW	1800	AC(2PH)	18	9000	170	26" x 18.5"	Flight
DSP-5R6R	RW	1200	AC(2PH)	18	6000	170	26" x 18.5"	Flight
INSAT	MW ³	50	IBDC	14	6600	23	12.1" x 6.1"	Flight
ARABSAT	MW ³	37	IBDC	14	6600	20	12.1" x 6.1"	Flight
COBE	RW ³	15	IBDC	45	2200	20	12.1" x 5"	Flight
SSM/I	MW ³	3	AC(2PH)	5	1800	11	7.8" x 3.8"	Flight
INSAT/ARAB	RW ³	2	IBDC	5	3000	8	7.8" x 4.3"	Flight
ETS III	RW	1.4	AC(2PH)	5	1450	9	7.8" x 3.8"	Flight
GPS I/II, SMEX	RW	0.8/1.2	AC(2PH)	4	3000	5/6	6" x 3"	Flight
BS-II	RW	0.3	AC(2PH)	5	2100	5	6.5" x 3.5"	Flight

- NOTE 1. - CMG Output torque is 200 foot pounds
 2. - CMG Output torque is 3400 foot pounds
 3. - Provided with drive electronics

THE ABOVE IS A SAMPLE OF THE VARIETY OF WHEELS WHICH HAVE BEEN BUILT BY BENDIX GSD. OVER 600 WHEELS HAVE BEEN BUILT. OVER 250 HAVE BEEN FLOWN WITH MORE THAN 7 MILLION HOURS IN SPACE.

Allied-Signal Aerospace Company

A/PWAB1

Bendix Guidance Systems Division



95TR4/V2

Table 4. Control Moment Gyroscopes

LANGLEY	- 1,000 FT-LB-SEC 12,000 RPM
SKYLAB	- 2,300 FT-LB-SEC 9,000 RPM
MA-500	- 500 FT-LB-SEC 8,000 RPM
ATM - IMPROVEMENT	- 3,000 FT-LB-SEC 12,000 RPM
MA-6,000	- 6,000 FT-LB-SEC 8,000 RPM
XPT 5-100	- 5 FT-LB-SEC 8,000 RPM
HTCMG	- 1,700 FT-LB-SEC 6,000 RPM
SSCMG	- 3,500 FT-LB-SEC 6,600 RPM

Allied-Signal Aerospace Company

VPMIAD1

Bendix Guidance Systems Division

95TR4/V2

Key Words:

Perfluoroether

Mechanisms:

Ball Bearings

Systems:

Rotating System

Authors; Experts:

Bryan H. Baxter and Barry P. Hall

Address:

British Aerospace
Stevenage, England

Telephone:

Title:

The Use of Perfluoroether Lubricants in Unprotected Space Environments

Source:

19th Aerospace Mechanisms Symposium (1985).

Abstract:

The paper describes a series of ball bearing tests carried out in a simulated space environment to determine the durability of perfluoroether lubricants. The results of the examination of the test bearings for each stage are described and experimental techniques designed to overcome lubricant degradation are outlined.

PRECEDING PAGE BLANK NOT FILMED
[PAGE 296] INTENTIONALLY BLANK

Anomalies:

The perfluoroether group of lubricants, which is manufactured by a variety of companies around the world, has physical properties suggesting that they would be ideal for space applications. The available range of products in this class of fluids is very large and is complicated by the fact that several different manufacturing routes are used, resulting in different families of products with different properties.

Lessons Learned:

- Operating ball bearings lubricated with Z25 oil in a vacuum results in an interaction between the lubricant and the races. This results in race wear and oil degradation.
- When ball bearings lubricated with YVAC 40/11 are operated in a vacuum, there is no oil degradation and no wear. However, the higher viscosity of the YVAC 40/11 leads to undesirable high running torque.
- At this stage, it appears that modification of the bearing surfaces with inert coatings, resulting in decoupling of the lubricant from the active bearing surfaces, offers the best course to ensure maximum lubricant life.

Description:

The bearings used in the tests were 42-mm OD angular-contact bearings with 10 balls. The balls and races were 440C and the bearings had a one-piece fabric-reinforced phenolic retainer.

Four bearings were used in the first test. They ran as preloaded pairs within the vacuum chambers (10^{-6} torr), one at 200 rpm and the other at 1400 rpm, for a total for each pair of 10^8 revolutions. The bearings were supplied with Z25 lubricant. During the test, the running torque of both bearing pairs fell steadily, reaching a minimum after 10^6 revolutions. If the tests were stopped for 15 min, the torque on restarting was found to be equal to that at the start of the test; this fell rapidly to the minimum level within a short time. Bearing noise increased with this fall in running torque and bearing surface temperatures also increased slightly as the minimum torque level was reached.

On completion of the test, it was found that all the bearings were contaminated with brown/black deposits along each ball track and in the pockets of the retainers. Preliminary analysis of the contaminant showed that it was rich in Fe and Cr, both contained in a significant level of organic material. A spectroscopic examination showed that the contaminant was free of carbon hydrogen absorption and had a strong carbon fluorine absorption. This indicated that the contaminant was derived directly from the perfluoroether lubricant and was not a foreign product, such as phenolic polymer constituents of the retainer or residues of cleaning agents remaining in the bearings. Microscopic examination of the ball tracks on the races showed a well-defined wear track with surface pitting. The surface within the wear track carried a very thin, highly adherent film that could not be removed by repeated washing in solvent.

This initial test suggested that under the test conditions, the Z25 test lubricant was liable to form a surface reaction product that would wear away sacrificially, building up in the bearing as described.

A second bearing test was carried out. This was identical to the first test except that the bearings were obtained from a different source. The results were quite different. The torque level remained constant throughout the test and after the test there was not even a trace of contaminant in the bearings. Also, the ball tracks were smooth and free of pitting. However, the oil film in the raceways was seen to be cloudy. Closer examination revealed that the cloudiness was due to the presence of two immiscible fluids in the bearings; one in the form of a dispersion of droplets and fluid in the second. Using pyrolysis gas chromatography mass spectrometry it was shown that there was hydrocarbon oil present. The reason for the difference in bearing performance between the first and second test runs was then obvious. The presence of the hydrocarbon oil would have successfully decoupled the Z25 from the surface and, thus, prevented any disruption of the PFPE lubricant.

This result did little to resolve the problem of the apparent sensitivity of the Z25 lubricant to active metal surfaces. In fact, it could have been seen as supporting the theory since decoupling by the accidental use of a second lubricant had completely prevented a recurrence of the degradation.

Two techniques were investigated to overcome the apparent difficulties associated with the use of the Z-series oil. The first technique was to decouple the lubricant from the wearing metal surface by the application of nonmetallic layers to the bearing surfaces. The system adopted was to use tungsten-carbide balls that had been coated with titanium carbide and races that had been coated with zirconium nitride. A total bearing test of 10^8 cycles was completed without any change in running torque and, on completion of the test, no evidence of oil degradation could be found. The titanium-carbide coating on the balls had not been destroyed but the zirconium-nitride coating on the races had worn and a low level of solid debris had been generated as a result.

The second part of the hypothesis concerning the sensitivity of the Z-type of oil to decomposition in ball bearings was that the particular linear structure of the polymer could contribute to the effect. Other types of perfluoroether lubricant are available. One of which is a member of the Y-series; YVAC 40/11 is also recommended for instrument bearings. This carries certain penalties such as higher viscosity, higher vapor pressure, and higher pour point. However, a fourth bearing test was carried out using the YVAC 40/11 lubricant. After the test the oil was unchanged, there was no wear of the races.

Key Words:

Momentum Wheels, Despin Mechanisms, Despin Mechanical Assembly, Lubrication, Slip Rings

Mechanisms:

Antenna Pointing Mechanisms, Despin Mechanical Assemblies, Momentum Wheels

Systems:

Authors; Experts:

R.J. Benzing and J.R. Strang

Address:

Air Force Materials Laboratory
Wright-Patterson Air Force Base, Ohio 65433

Telephone:

Title:

Failure Mode Analysis of Lubricated Satellite Components

Source:

Air Force Report AFML-TR-73-88 (May 1974).

Abstract:

A failure mode study performed to examine lubrication malfunctions or failures in 10 different spacecraft identified 12 possible failure modes. These were: lubricant degradation, lubricant dewetting, slip ring and brush wear, improper lubricant transfer, inadequate lubricant quantity, lubricant volatility effects, lubricant incompatibility, torque variations, cage and bearing instability, cage wear, lubricant creep, and film thickness. This report also includes a discussion of a four-phase effort required to develop accelerated tests for predicting lubricant life performance in space systems. A program is recommended for the development of accelerated tests for selecting long-life lubricants for space systems.

PRECEDING PAGE BLANK NOT FILMED

Anomalies:

System A. This satellite system's despin mechanical assembly employs a brush-type torque motor, power and signal slip rings, and a pulse generator encoder for spin axis pointing control. The despin mechanical assembly employs a 150-millimeter bore bearing that is spring preloaded to 40-lb axial. The bearing rotates at a nominal 55 rpm and has an operating temperature range requirement of 0 to 100°F.

Dewetting of bearing surfaces by the lubricant has been experienced in ground vacuum bearing and despin mechanical assembly tests. The contractor attributes this dewetting to contamination of the bearing surfaces by unreacted phenols from the cotton-phenolic separator.

In thermal vacuum tests of both a qualification and a flight despin mechanical assembly, torque transients were experienced either at low temperatures (<10°F) or with rapidly changing temperatures. The cause for each occurrence has been attributed by the contractor to some combination of the following four probabilities: decreased bearing contact angle, increased bearing preload, bearing race distortion, and increased lubricant viscosity at lower temperatures.

A gradual decrease in despin mechanical assembly friction torque has been experienced in space over a period of about one year. The contractor attributes this anomalous performance mainly to oil film reduction in the despin bearing due to an increase in lubricant evaporation rate during the long period of over 80°F bearing temperature condition during a summer season in space.

Periodic antenna pointing anomalies have been experienced in orbit due to bearing torque fluctuations of up to 0.04 or 0.05 ft-lb caused by spacecraft nutation of approximately 1°. The spacecraft's nutational instability apparently is caused by the clearance of the bearing in the outer race being designed to permit axial movement due to differential thermal expansion.

System B. This system's antenna drive mechanism consists of a despin bearing/lubrication system, a dc brushless torque motor, and a magnetic pick-off to indicate antenna position and rate. Since the antenna weighs only about 0.5 lb, there are no significant dynamically imposed loads in space.

The antenna drive support bearings are small (approximately 1.3 in. bore) angular-contact bearings (modified from radial bearings because of size considerations) that are spring preloaded to 5-lb axial. The bearings are outer race floating and rotate at a nominal 90 rpm. The operating temperature range requirement is -10 to +130°F.

The bearings are lubricated with Vac Kote and contain Nylasint retainers having a minimum porosity of 5%.

A gradual decrease in bearing torque in space has been experienced over a period of several years in two of the satellite vehicles. One suggested explanation is that the oil film is gradually being lost with a consequent loss in viscous drag.

A one-time, one-day incident of abnormal performance occurred in one spacecraft (Satellite B-3) about 1 yr from launch. The contractor postulated that a piece of contaminant, either metallic or nonmetallic, may have been dislodged from the housing or from the bearing cage and entered the ball-race contact area causing additional friction until it was either dissipated by the grinding action of the balls or cast off from the bearing race. The contaminant might have been introduced externally during manufacture.

In the despin mechanical assembly life test unit, an audible click developed after about 11 months of operation. The click occurred at a frequency of once per revolution due to the combined effect of a radial magnetic force between the motor rotor and stator and a slip-fit interface between the despin bearing outer race and the housing sleeve bore. Apparently, at one angular position of the motor rotor with respect to the stator, the magnetic force was strong enough to pull the bearing off center thus allowing the outer race to strike the housing sleeve. To correct the problem, all despin mechanical assembly units were modified in the following manner:

- The bearing outer race fit was changed from a diametral clearance of 0.0010/0.0017 to 0.0000/0.0004 in. It was felt that the tighter fit would reduce the magnitude of the unbalanced forces of the motor by more perfectly centering the rotor, and thereby would eliminate impacting of the outer race in the housing.
- The type 416 stainless steel sleeves in the housing were changed from a hardness of approximately Rockwell C20 to Rockwell C 35-42 to decrease the possibility of fretting.
- Grease was removed altogether from the drive systems since it was felt that the grease might provide a means of transfer of wear products (if any would develop) from the outside to the inside of the bearing.

System C. System C's despin mechanical assembly has a dc brushless torque motor, power and signal slip rings, and magnetic pulse generators. This assembly performs the task of despinning a payload equipment platform with respect to a rotating coordinate set.

The despin mechanical assembly employs back-to-back angular contact bearings spring preloaded to 60-lb axial. The bearings rotate at a nominal 60 rpm and have an operating temperature range requirement of 20 to 140°F.

Lubricant (Vac Kote) dewetting of bearing surfaces has been experienced in ground vacuum bearing life tests. In general, the contractor believes that the phenomenon of lubricant dewetting is related to surface contaminants.

System D. This satellite system's despin mechanical assembly uses a synchronous stepper motor for driving the antenna, a rotary RF coupling for signal transfer, and a magnetic shaft encoder for antenna positioning reference. Five of eight satellite vehicles have achieved orbit.

The despin mechanical assembly bearings rotate at a nominal 90 rpm, contain phenolic cages, and are lubricated with Vac Kote. Nylasint blocks impregnated with Vac Kote are located near the bearings to provide additional lubricant during long-term operation. The despin mechanical assembly contains a beryllium shaft, 52100 steel bearings, beryllium bearing inserts, and an aluminum housing.

Thermal lock-up and excessive torque variations have been experienced in space by Satellite D-2. The malfunction mechanism appeared to be that thermal displacements of the duplex bearing races induced frictional bearing torques sufficient to cause system stall when the bearing outer races were operating at lower temperatures than the bearing inner races.

Having apparently identified the failure as a thermally-induced mechanical problem, the despin mechanical assembly motor housing heaters were added as a fix to later flight units. These were used to overcome stalling when it occurred and to prevent it when an impending stall became evident.

Fretting was observed between the bearing ball and race surfaces during one thermal vacuum test. The bearings ran well for several months before the torque gradually increased and the despin mechanical assembly motor stalled. Classical iron-oxide debris was observed upon disassembly and visual inspection. The contractor and his outside bearing consultants attributed this failure to overloading of the duplex bearing due to the undersized bore of the outer race seat.

System E. This advanced, high-capacity communications satellite system employs both wide-beam Earth-coverage (17°) antennas and narrow-beam spot-coverage (4.5°) dish antennas. The spot-beam antennas are steerable and may be pointed at specific areas of the world. The despin mechanical assembly rotates at a nominal 60 rpm on two flexurally mounted angular-contact Vac Kote-lubricated bearings mounted in a titanium alloy housing.

Antenna pointing errors due to excessive bearing torque fluctuations have occurred in space in two satellite vehicles. The problem is caused by a retainer instability due to the combined effect of lubricant viscosity and cage ball pocket design that leads to wobble of retainer. Recommended means to reduce the wobble amplitude of the retainer were to raise temperature to reduce lubricant viscosity and/or to change the cone angle of the retainer ball pocket. Also, it was found that reducing the separator mass would improve the retainer stability.

System F. This system's despin mechanical assembly employs a brushless torque motor that drives the antenna support ball bearings, a slip ring assembly that provides the electrical interface (both signal and power) between the despin and spinning portion of the spacecraft, and a master index pulse generator for antenna positioning purposes. The despin bearings rotate at a nominal 60 rpm and are axially preloaded to 150 lb. The bearings are lubricated with a proprietary lubricant. Nylasint reservoirs are located near the bearings for the purpose of lubricant replenishment. The normal despin mechanical assembly operating temperature range in orbit is 40 to 85°F.

The major problem with this system has been a lubricant dewetting condition of bearing surfaces after ground vacuum tests. This may be due to:

- The retainer material (an inadequate cure giving rise to free or unreacted phenols or incompatible chemicals used in processing, e.g., possibly the hexamethylene tetramine catalyst); shredding of the retainer material; and/or starch in the cotton fabric
- Improperly controlled cleaning and handling processes
- Incompatible surface energies.

As a result of various laboratory tests, materials and processes were changed, which resulted in bearings that were fully wet at room ambient conditions. The bearing material was changed from 440C (CEVM) stainless steel to 52100 (CEVM) steel and the bearing retainers were ordered from another vendor according to a revised processing specification that included a Soxhlet extraction of the retainer blanks.

The lubricating procedure was also changed. The 52100 bearings were lubricated with the contractor's proprietary lubricant with the metal parts being kept separate from the retainer and aged in the lubricant. Specifically, the clean balls and races were vacuum baked for 24 hr and then soaked in lubricant for 6 days.

System G. This satellite system spins during the day, is stationary at night, and has an antenna pointing accuracy requirement of 0.1° . The despin mechanical assembly operates on a 90-min duty cycle (60 min on and 30 min off). Slip rings effect power and signal transfer between the spacecraft and the antenna system. The antenna support bearings are driven at 30 rpm by a dc brush motor and are lubricated with thick Vac Kote films (20,000 to 60,000 angstroms).

The anomalous torque decline of satellite G-2 was due to a magnetic imbalance problem dealing with coupling of the spacecraft with the Earth's magnetic field. All subsequent satellite vehicles were properly balanced.

Lubricant dewetting has been observed on highly polished 440C balls after ground bearing tests in vacuum. In general, the experience of System G's contractor has been that the harder they tried to clean the 440C bearings, the more likely lubricant dewetting became. Their explanation for this phenomenon is that the lubricant may be autophobic (i.e., polar additives in the lubricant become strongly attached to clean metal surfaces), thereby forming a jacket that the oil will not wet.

Two torque motors exhibited excessive wear of brushes during laboratory testing in 220 to 300 hr of operation. It was concluded by the contractor that this type of problem could be eliminated in future motor processing by procuring all brushes as separate detail parts and by conducting hardness and oil absorption tests on brushes before use.

System H. This satellite system, which has a design lifetime of one year, utilizes a momentum wheel assembly or flywheel as part of a three-axis stabilization system that stabilizes the spacecraft to a pointing accuracy of better than 1° in all three axes (pitch, yaw, and roll). The assembly contains a pair of bearing drive motors for purposes of redundancy, one located on each side of the wheel bearing. Power is supplied to only one motor at a time, although operation of both motors simultaneously is possible. These motors originally were Inland Type 4437A dc brush motors containing 50/50 (by weight) silver/graphite brushes; however, because of brush wear problems, the system contractor has subsequently switched to brushless drive motors having a stall torque of 130 in.-oz.

The major problem of this satellite system has been one of motor brush wear. The excessive brush wear was attributed to marginal lubrication and inefficient distribution of DOA oil within the momentum wheel assembly.

System I. System I satellites employ two major rotating components: a momentum wheel assembly for spacecraft stabilization and an instrument package. These components are built by separate contractors. The major problem experienced by this satellite system has been one of motor brush wear.

Satellite I-1 experienced excessive momentum wheel assembly motor brush wear with the dioctyl adipate-based oil and failed after about 80 days in orbit. Due to this failure, the momentum wheel assembly contractor switched to Vac Kote thin-film lubricant (about 5000 angstroms average static film thickness for the bearing) for the wheel bearing and the motor brushes of Satellites I-2 and I-3. Also, the contractor at this time changed from a bronze- to an oil-impregnated porous phenolic ball separator.

System J. System J employs reaction wheels for three-axis stabilization. Although this system does not employ a despin mechanical assembly, the performance problems that have been experienced are relatable to lightly loaded, slow-speed satellite systems.

C-4.

Satellite J-1 failed after 24 days in orbit due to failure of the solar array drive mechanism. Specifically, the drive mechanism operated satisfactorily for 21 days, built up friction for a few days, and finally stalled completely. The solar array drive bearings rotated at approximately 1 rpm and were lubricated with G300 grease (F-50 silicone oil with a lithium soap thickener). It was determined in vacuum by an infrared spectrometer that excessive temperatures in the drive's motor bearings were the cause of failure.

A reaction wheel bearing failed in Satellite J-4 after 22 months in orbit. This failure was believed to be due to thermal degradation of the MIL-L-6085A diester lubricant (based on ground test experience; see below). The system contractor believed that boundary lubrication conditions existed in the satellite which, together with heating, caused the lubricant to degrade.

Lessons Learned:

- Advanced elastohydrodynamic computer simulation techniques can provide benefit in design of space lubrication systems.
- Failure modes of despin mechanical assembly operation include the following:
 - Insufficient bearing lubricant film thickness
 - Lubricant incompatibility with system materials
 - Inadequate lubricant quantity
 - Improper lubricant transfer
 - Lubricant creep
 - Lubricant dewetting
 - Lubricant degradation
 - Bearing and cage instability
 - Torque variations due to lubricant properties
 - Slip ring and brush wear
 - Lubricant volatility
 - Cage wear.
- The authors recommended developing accelerated test methods for predicting lubricant performance and reliability.

Key Words:

Porous Reservoirs, Phenolic Retainers, Wick Lubrication, Vacuum-Impregnated Retainers, Plastic Retainers

Mechanisms:

Systems:

Author; Experts:

P.A. Bertrand

Address:

Aerospace Corporation
2350 East El Segundo Boulevard
P.O. Box 92957
Los Angeles, California 90009

Telephone:

Title:

Oil Adsorption into Cotton-Phenolic Material

Source:

Journal of Materials Research, Vol. 8, No. 7, pp. 1749-1757 (July 1993).

Abstract:

This paper is concerned with the absorption of oil into laminated cotton fabric ball bearing retainers and the ability of the retainer to function as a supply reservoir to feed oil back to the balls and races during bearing operation.

Lessons Learned:

- Phenolic retainers must be carefully and thoroughly dried to remove any absorbed moisture before they are impregnated with oil. Otherwise, the retainer will not saturate and can absorb and remove oil from the bearing it is intended to lubricate. Thus, the retainer becomes a liability rather than an asset.
- Changing the weave of the cloth will not have much effect on the amount of oil stored in the retainer.
- Oils of different viscosities will absorb at different rates. This can be calculated from the model described in the paper.

Description:

Laminated phenolic materials were developed in the late 1920s and their properties quickly made them attractive candidates for various bearing applications. Their use as ball bearing retainers was probably initiated by the low density and toughness of these composites as well as their ability to absorb lubricant. As long as there is some kind of lubricant present (even water), they are compatible with metals. However, once they run dry, frictional heating causes the low conductivity phenolic to char and wear at a rapid rate.

The author of this paper demonstrated that the oil was impregnated into the retainer by a two-step process. The first step was due to the capillary action of the voids associated with the fibers within the cotton threads. This was followed by a slow diffusion of the oil into the bulk of the phenolic resin. Figure 1a shows the unnormalized weight increase versus time; Figure 1b shows the unnormalized weight gain versus the square root of the time. The oil is Coray 100, a naphthenic-based petroleum oil produced by Exxon. Its properties are shown in Table 1 along with the properties of the other lubricants that were evaluated in this work.

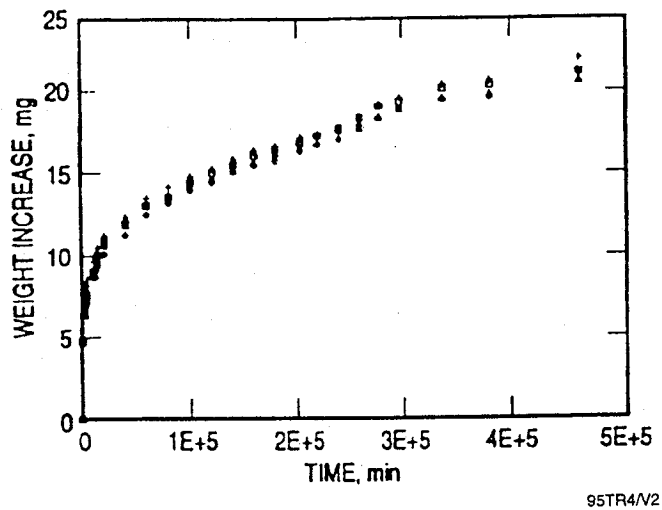
The amount of oil stored in Step 1, first capillary fill, can be calculated from the intercept of the region 3 line, as shown in Figure 1b. (Note that the author's model is for two-step absorption. Regions 1 and 2 are the first step and region 3 is the second.) The results of the tests, as plotted in Figures 2a and 2b, show that the amount of oil absorbed with the phenolic composite is dependent on the volume of the sample, not the surface area.

A particular point was made that moisture would absorb preferentially into the cotton-phenolic and act as a barrier to oil penetration. Thorough drying the material before oil impregnation is an important step.

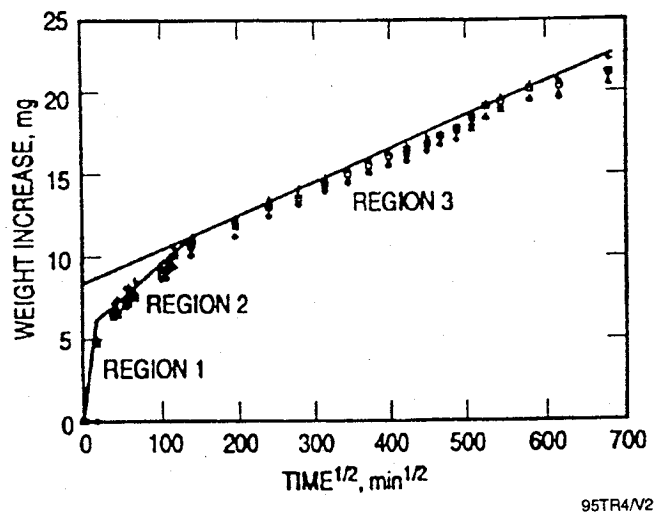
Based on the results of these tests, the author has proposed a two-step mechanism for the oil absorption process. Initially, oil is absorbed into unconnected capillaries in the threads of the cotton cloth. The rate is determined by the fluid properties and the number of capillaries per unit area. It is also affected by the source of the phenolic, which may vary considerably depending on the supplier. The long-term, Step 2 process is modeled as diffusion of the oil from the capillaries and voids associated with the cotton threads into the phenolic resin. The author reports that the saturation amount of oil into the phenolic resin is about 2 to 3% v/v. The diffusion coefficient calculated from this model is 3×10^{-12} cm²/sec.

Results from this work have direct implications for the use of cotton-phenolic retainers in oil-lubricated ball bearings. First, retainers must be dried before immersion in oil or else very little oil will be absorbed. Second, oils of different viscosities will absorb at different rates, which can be calculated from the model. Soaking a retainer in oil for a few hours probably results in an incomplete fill. Such a retainer may then continue to absorb oil from its bearing during storage. Saturation of the material with oil occurs only after about two years of storage in a room temperature oil bath. If this diffusion takes place in a stored, lubricated bearing, it may affect the availability of oil during later bearing use. For a lightly lubricated bearing where a thin oil film is in contact with the retainer, creep of the oil and absorption into the retainer over long storage times could constitute a serious oil depletion mechanism.

This reviewer has no quarrel with the author's analysis as far as it goes, but it seems to present a good picture of the uptake of lubricant by capillary effects and a vague picture of how and why the oil is supplied from the retainer back to the bearing.

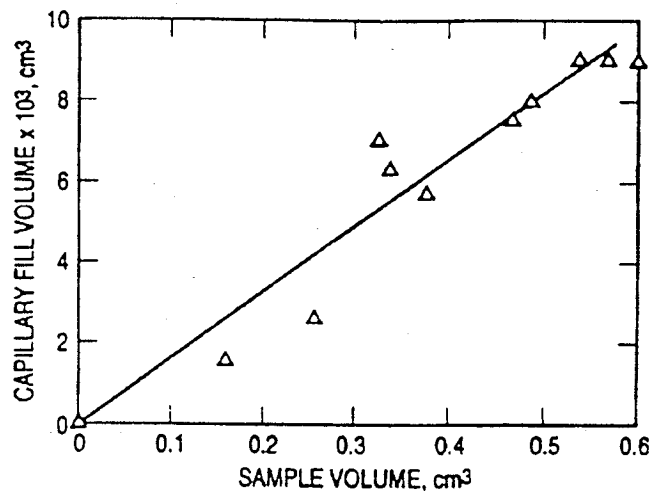


a) Unnormalized Weight Increase versus Time



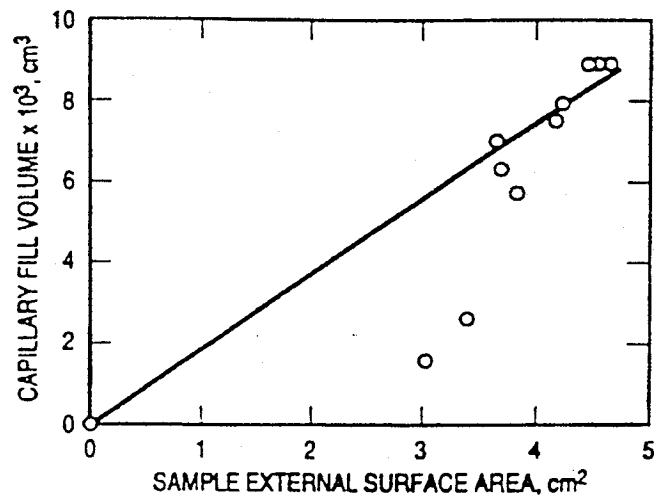
b) Unnormalized Weight Increase versus Square Root of Time

Figure 1. Coray 100 Absorption into Westinghouse 97 Cotton-Phenolic



95TR4/V2

a) As a Function of Sample Volume



95TR4/V2

b) As a Function of Sample External Surface Area

Figure 2. Final Volume of Liquid Absorbed in the First Step for Westinghouse 97 Material

Table 1. Selected Fluid Properties (25°C)

Lubricant	η (Poise)	ρ (g/cm ³)
Coray 100	3.67	0.9176
Nye 176H	10.2	0.85
Krytox 143AB	3.78	1.89
Pennzane SHF X2000	2.21	0.85
Heptane	0.00386	0.684

95TR4/V2

Key Words:

Momentum Wheel Spin Bearings, Rolling Element Bearing Dynamics

Mechanisms:

Spin Bearings for Momentum Wheels

Systems:

Generic Technology

Authors; Experts:

1. Edward A. Boesiger
2. Mark H. Warner

Address:

1. Lockheed Missiles and Space Company
Sunnyvale, California
2. Honeywell Corporation
Satellite Systems Operations
Glendale, Arizona

Telephone:**Title:**

Spin Bearings Retainer Design Optimization

Source:

NASA Conference Publication 3113, 25th Aerospace Mechanisms Symposium.

Abstract:

The dynamic behavior of spin bearings for momentum wheels (control moment gyroscope, reaction wheel assembly) is critical to satellite stability and life. Repeated bearing retainer instabilities hasten lubricant deterioration and can lead to premature bearing failure and/or unacceptable vibration. These instabilities are typically distinguished by increases in torque, temperature, audible noise, and vibration induced into the bearing cartridge.

Ball retainer design can be optimized to minimize these occurrences. A retainer was designed using a previously successful smaller retainer as an example. Analytical methods were then employed to predict its behavior and optimize its configuration.

Anomalies:

Retainer instability and failure in a control moment gyroscope bearing.

Lessons Learned:

- Retainer instability is a major cause of bearing failure.
- There is a critical friction level associated with each retainer design beyond which the retainer is unstable.
- Ball pocket friction is more critical to stability than retainer land friction for the bearing investigated.
- The nature of the bearing dynamics problem makes retainer optimization a very difficult task for the following reasons:
 - Parameters are coupled
 - High accuracy of input data required
 - Specific operating conditions are important.
- It is difficult to discern the effects of small changes on the indicators of stability from the bearing dynamics program.
- The steepest descent optimization method appears to be the most promising, but is hard to implement accurately for bearing dynamics.
- Optimization of the retainer design was accomplished by computer simulations coupled with experimentation.
- Computer predictions were a useful tool and qualitatively compared to experiment.

Description:

Minimal design details are given in the article. Efforts included a parametric analysis of the effects of the following five primary characteristics of the retainer on stability:

1. Retainer pocket ball diametral clearance (values from 0.05 to 0.5 mm)
2. Retainer race diametral clearance (values from 0.05 to 0.5 mm)
3. Number of balls
4. Force bias
5. Moment bias.

The optimization study was carried out while operating under the nominal operating conditions, including gravity, small radial load, shaft speed of 5000 rpm, and retainer race and ball retainer friction coefficients of 0.12.

Testing:

Two bearing test fixtures were used to observe stability. An existing fixture, the universal bearing test system (UBTS), was considered a retainer screening tool. The bearing stability tester (BeST) tests an end-item duplex bearing pair and was developed in parallel to complement the testing on the UBTS. Since the UBTS tests were done with one of the bearings from the duplex pair, the BeST more closely simulates the actual bearing system configuration.

UBTS Fixture. The UBTS is a fixture that was developed to perform ball bearing dynamics research. The fixture was designed primarily as a single-bearing screening device, but it can also be configured to accept a preloaded pair. The spindle is suspended on an air bearing, and the axial preload on the bearing can be varied by adjusting gas pressure. Radial- and axial-induced vibration forces are measured using two piezoelectric load cells. In addition, two linear variable differential transformer deflectionometers measure bearing drag torque. The amplitude variation of the induced-vibration radial component at the retainer frequency, as well as audible noise and an increase in drag torque, give indications of retainer instability.

BeST Fixture. The BeST fixture was developed to simulate the end-item configuration while being able to measure the forces, motor current, accelerations, bearing temperatures, speed, and retainer motions. The bearings were rotated by a dc servo motor through a flexible coupling. The fixture was also designed to be compatible with mounting onto a shaker table.

A servo motor controlled the rotating speed of the bearing pair. The drive motor current is an indirect measure of the torque required to turn the bearings. A three-axis accelerometer was mounted on the side of the housing to measure radial and axial accelerations. Thermocouples measure the outer race temperature at two places on each bearing. An infrared pyrometer measured the temperature of the inner race. Two three-axis piezoelectric load cells were intended to measure the forces and torques in the bearing. However, the poor quasi-static performance and high thermal sensitivity of the cells on the BeST fixture made it difficult to obtain useful steady-state information.

Key Words:

Lubrication, Momentum Wheels, Testing

Mechanisms:

Momentum Wheels, Control Moment Gyroscope, Reaction Wheels, Slip Rings

Systems:

Rotating Systems

Authors; Experts:

Paul Fleischauer and Michael Hilton

Address:

Aerospace Corporation
2350 East El Segundo Boulevard
P.O. Box 92957
Los Angeles, California 90009

Telephone:

Title:

New Developments in the Lubrication of Spacecraft Mechanisms

Source:

Viewgraph Presentation, Aerospace Corporation (1992).

Abstract:

This presentation reviews lubrication problems in moving mechanical assemblies, testing methodologies, and directions for research. A few case studies of lubrication problems are also included. Solutions include synthetic lubricants and hard, antiwear coatings for contacting pairs.

PRECEDING PAGE BLANK NOT FILMED

Anomalies:

- Recurrent problem with bearings in reaction/momentum wheels, control moment gyroscopes, and gyroscopes.
- Problems with actuators, gears, and gimbals operating in boundary lubrication regime.
- Consistent difficulties with low-noise operation of slip rings
 - Noise not understood
 - Materials development missing
 - Primary application in solar array drives.

Lessons Learned:

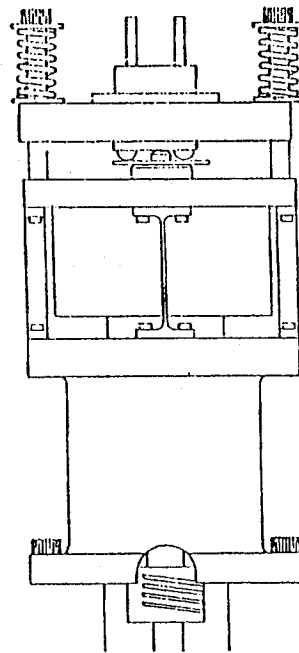
- Most mechanical problems are lubrication problems.
- Subsystems with the most problems include momentum wheels, gimbal and other boundary-lubricated devices, sliding electrical contacts, and gyroscopes.
- Two primary types of lubrication problems:
 - Supply or loss of lubricant
 - Chemical reaction (oxidation, polymerization) of lubricant.
- Lubricants
 - Synthetic oils can increase life by a factor of 10
 - Sputter-deposited solid-lubricant thin films provide low friction and noise and long life.
- Wear-resistant materials
 - Hard coatings and ceramic parts are used for low-torque noise.
- Lubricant additives
 - Provide protection of contacting surfaces to reduce wear and minimize torque.
- Subsystems with the most problems include momentum wheels, gimbal and other boundary-lubricated devices, sliding electrical contacts, and gyroscopes.

Testing:

Aerospace Corporation has test equipment for qualifying lubricants for space applications. The eccentric bearing lubricant screening tester has capability to apply load and speed to balls under vacuum conditions and determine life of lubricants. A schematic of the tester is shown on Figure 1; test results are shown on Figures 2 and 3.

Test Conditions:

- 60 μ L oil
- 50 lbs load (~4 lbs/ball)
- speed 1800 rpm
- base pressure 1×10^{-8} Torr
- torque, temperature, # of revolutions monitored
- run to failure, 3x initial torque
- post test lube and disk analysis



Mechanics and Materials Technology Center
The Aerospace Corporation



95TR4/V2

Figure 1. Eccentric Bearing Lubrication Screening Tester

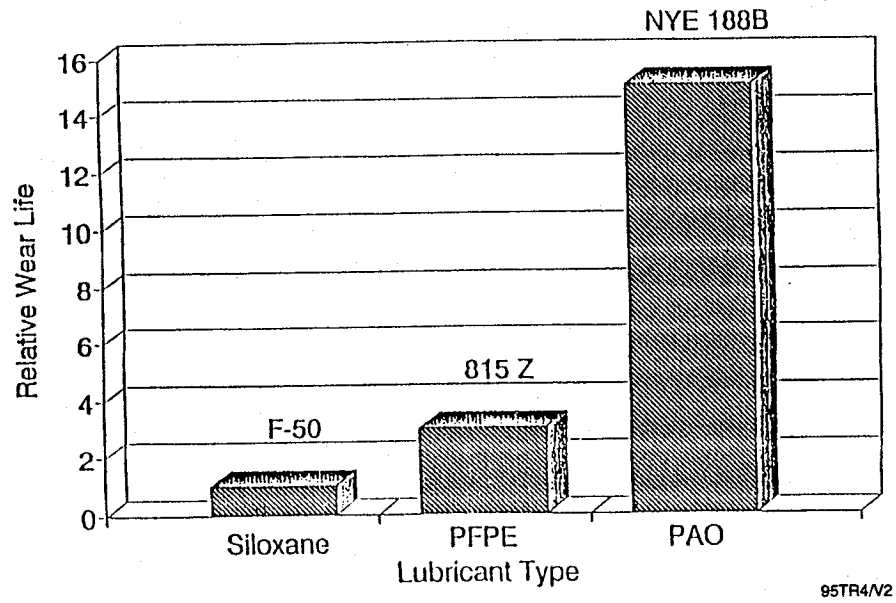


Figure 2. Lubricant Screening Test Results

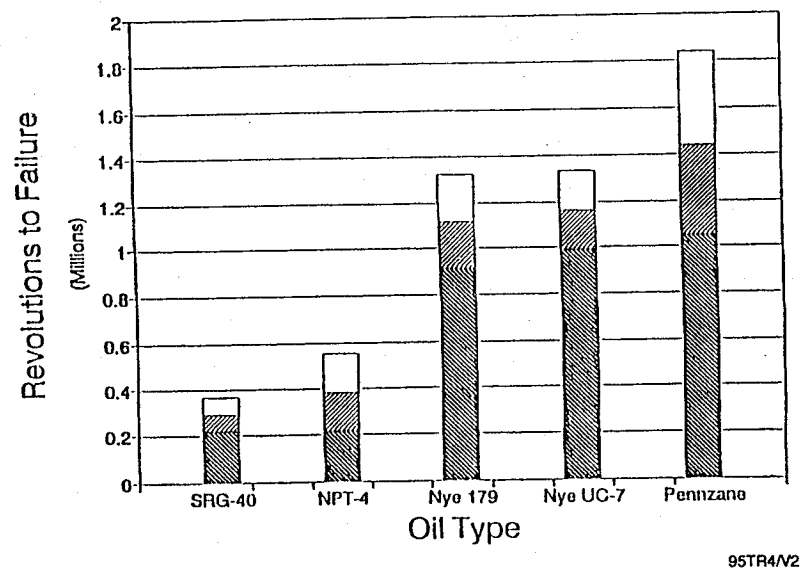


Figure 3. Eccentric Bearing Lubricant Screening

Experience:

Program	Wheel Type	Problem	Cause	Action
Navstar/GPS	Reaction wheel; four per satellite	On-orbit and test failures; high torque	Lubricant depletion	New lubrication qualification
GPS IIR	Reaction wheel	High-speed cage instability	Force, mass resonance	Force, mass; biased cages
DMSP	Reaction wheel	Bearings/lubricant could not be delivered	Lubricant degradation	Extensive bearing run-in and screening
DSP	Large momentum wheel	Torque/temperature anomalies	Lubricant starvation	Passive oil delivery system
DSCS III	Reaction wheel	Torque noise, vibration	Unknown	Redundant wheels
MILSTAR	Rate gyroscopes	Drift rate/torque instability	Lubricant starvation	Improved lubrication, cage processing
CDP	Large control moment gyroscopes; > one per satellite	Excessive torque	Lubricant loss, cage instability	Active oiler system, new oil

95TR4/V2

Key Words:

Lubricants, Bearings, Reaction Wheels, Slip Rings

Mechanisms:

Reaction Wheels, Slip Rings, Gimbals

Systems:

Rotating Systems, Scanning Systems

Authors; Experts:

P.D. Fleischauer

Address:

Aerospace Corporation
Mechanics and Material Technology Center
El Segundo, California 90245

Telephone:

Title:

Performance of Fluid and Solid Lubricants in Spacecraft Applications (1993).

Source:

Not specified.

Abstract:

Results of a series of lubricant screening and performance tests are described that provide criteria for the selection of proper lubrication for precision spacecraft mechanisms, such as reaction wheels, gyroscopes, solar array drives, and gimbals. An eccentric thrust bearing apparatus was used for rapid screening and relative ranking of lubricants; results are compared to life-test data for a series of oils. Synthetic hydrocarbon oils and greases are recommended for the first three types of mechanisms, while newly developed, high-density-oriented molybdenum disulfide (MoS_2) films are recommended for gimbals.

PRECEDING PAGES BEARING IDENTICAL

Lessons Learned:

- Polyalphaolifins (PAO) and multiple-alkylated cyclic compounds (Pennzane) are excellent candidates for use in spin bearings of reaction/momentum wheels, solar array drives, and rate gyroscopes. The PAO lubricant did well in both hard vacuum and in an atmosphere of 380-torr helium gas.
- The formulation of Pennzane with tricresyl phosphate (TCP) in solution outperformed the other systems tested although considerable wear was noted.
- Pennzane plus naphthalene had less torque life than with TCP additive, but there was no evidence of wear. The increased torque failure was caused by the accumulation of excessive protective additive film containing metallic lead and carbonaceous material. The conclusion is that varying the amount of naphthenate could lead to superior friction and wear performance. Future tests are planned.
- A run-in period is recommended for lubricated ball bearings to transfer lubricant from the ball pockets of the sacrificial retainer to the balls and then to the raceways. Approximately 1.3×10^6 cycles of run-in were accomplished.
- For oscillating gimbal applications, sputter-coated MoS_2 films were recommended. Benign ball retainers (those that do not form transfer films) were tested with good results.

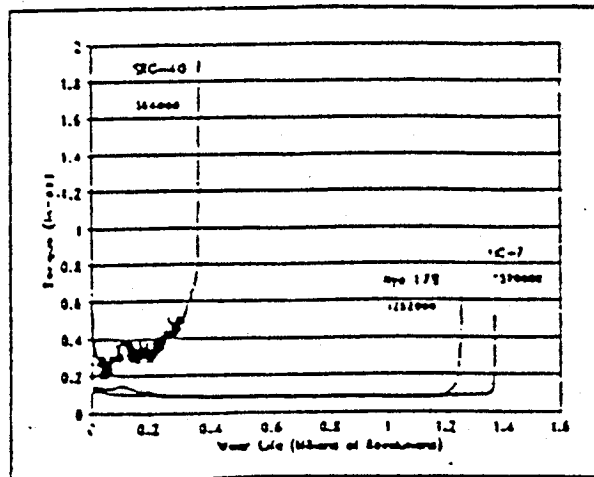
Testing:

For reaction wheel assembly lubricant assessment, the performances of two synthetic hydrocarbon oils (polyolester: Nye UC-7 and PAO: Nye 179) were compared to that of a superrefined mineral oil, SRG 40. In addition, the behavior of another synthetic, Pennzane SHF 2000, together with two different boundary additives was investigated. Finally, for the scanner bearings three different synthetics (siloxane: GE Versilube F50, perfluoropolyalkylether: Braycote 815Z, and PAO: Nye 188B) were compared.

Typical torque traces for eccentric bearing screening tests of reaction wheel assembly lubricants in vacuum are shown in Figure 1. Lubricant failure was defined as the time when the reaction torque of the system exceeded three times the average running torque. Clearly, the synthetic oils outperformed the mineral oil under these conditions.

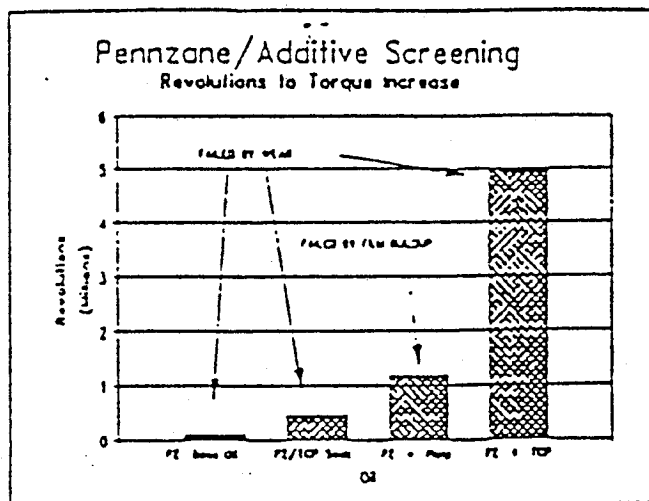
Under these conditions, the PAO (179) lasted in excess of 150 million revolutions, while the polyolester (UC 7) failed at just over 20 million cycles. Screening test results of Pennzane SHF 2000 (PZ) are shown in Figure 2. Data are presented for the pure base oil (base oil on metal parts precoated with TCP, but with no additive in the oil); the base oil plus lean naphthenate (PbNp, 5% w/w) in solution; and for the base oil plus 1% TCP in the solution, but not precoated parts. For these test conditions and on the basis of revolutions to torque increase, the formulation with TCP in the solution clearly outperformed the other systems.

The performances of three different synthetic oils (siloxane, perfluoropolyalkylether (PFPE), and PAO) in both screening tests and life tests are compared in Figure 3. The life test operated in an oscillatory mode with an arc of $\pm 60^\circ$ and a frequency of ~ 6 Hz, while the screening test ran under the customary conditions of continuous, though eccentric, motion. In this case, both the screening and life tests show that the formulated PAO (TCP) is a much superior boundary lubricant than either of the other two oils.



95TR4/V2

Figure 1. Typical Torque Traces for Eccentric Bearing and Screening Tests of Reaction Wheel Assembly Lubricants



95TR4/V2

Figure 2. Screening Test Results of Pennzane SHF 2000

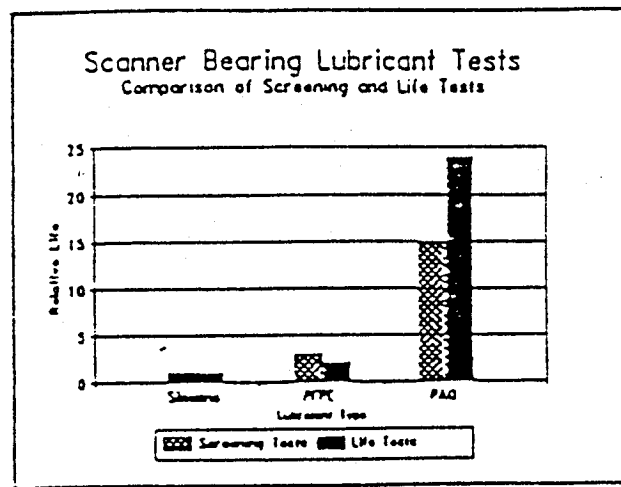


Figure 3. Siloxane, PFPE, and PAO Synthetic Oil Screening Test Comparison

Key Words:

Lubrication, Bearings, Anomalies, Momentum Wheels, Control Moment Gyroscopes, Gimbal Mechanisms, Slip Rings, Motors

Mechanisms:

Momentum Wheels, Control Moment Gyroscopes, Motors, Slip Rings, Gimbal Bearings

Systems

Rotating Systems

Authors; Experts:

1. P.D. Fleischauer and M.R. Hilton
2. R.A. Rowntree and M.J. Todd

Address:

1. Aerospace Corporation
2350 East El Segundo Boulevard
P.O. Box 92957
Los Angeles, California 90009
2. National Tribology Center
United Kingdom (ESTC)

Telephone:**Title:**

Assessment of State-of-the-Art and Tribology of Advanced Spacecraft Mechanisms

Source:

Air Force and SDI Publication.

Abstract:

A survey of existing technologies for precision moving mechanical assemblies used in spacecraft applications was conducted. The purpose was to identify areas where future requirements for lifetimes in excess of 10 yr with anticipated speeds, loads, and temperatures might not be attained. Some specific mechanisms, such as momentum/reaction wheels, high-speed turbines, pointing and tracking mechanisms, despin mechanisms, and gimbal mechanisms, were identified as areas for potential application of existing but unused technologies. Two major problem areas identified involve boundary regime lubrication and lubricant supply (active or passive) for long life. Areas where substantial, near-term improvements appear practical include the use of hybrid bearings, new synthetic fluid lubricants, new bearing retainer materials, and properly designed solid film lubricants.

Anomalies:

Problems experienced on a variety of AFSD programs are summarized in Table 1. Some problems are due to inappropriate design and the failure to involve the tribologist in the design and testing phases of the programs.

Control Moment Gyroscope Bearings. Analysis of lubricants from laboratory tests on control moment gyroscope bearings show depletion of oil from grease samples taken from control moment gyroscope spin bearing cage surfaces and no depletion from samples of bulk grease. Analysis of metal parts show little evidence of wear although some metal is found in degraded lubricant. Analytical simulations and measurements of bearing motions suggest cage instability may be involved in retainer wear and ultimate bearing torque increases.

Gimbal Mechanisms. Typically for gimbal mechanisms, ball bearings are forced to oscillate over very small arcs (dither) and then turn to a new position and continue to dither.

The gimbal system combines the severity of boundary lubrication with fretting motion of contacting surfaces. Gimbals are critical elements of most pointing mechanisms; antennas, sensors (telescopes), and weapons platforms; and of control moment gyroscopes. Usually, performance levels are met when systems are first tested, but with time, lubricant degradation, bearing wear, or both degrade performance levels so that mission requirements no longer can be satisfied.

Slip Ring Assemblies. Slip ring assemblies were constructed of gold- or silver-plated rings and wire wipers lubricated with the same fluid lubricants used in the bearings of the despin mechanical assemblies. However, extreme care is required to prevent excessive oxidation of the molybdenum disulfide (MoS_2) lubricant and simultaneous tarnish formation that results in unacceptable electrical noise and even measurable torque increases. Many such problems with electrical noise can be traced to the fabrication and assembly practices during construction of the slip ring mechanisms, but even after incorporation into satellites it is still necessary to protect the brushes from atmospheric exposure.

Table 1. Tribology Anomalies in Spacecraft

System	Conditions	Problem	Impact
Momentum wheel spin bearing	3600-rpm, grease-packed bearings, room temperature to 100°F	Torque/temperature anomalies	Single-point mission failure, possible indication of failure
Sensor support bearing	Preloaded ball bearings oscillatory motion	Failure in test	>\$500K testing
Sensor launch clamp	Located inside craft thermal blanked	Seizure on launch pad	Single-point failure prohibited launch or mission failure
Harmonic drive ATP control	Very low speed, temperature <150°F, fluorocarbon lubricant, boundary condition	Excessive wear, lube failure in test	Failure will degrade mission or possible mission failure; changed lubricant
Slip rings, brush contacts	MoS ₂ /Ag/C brushes on Ag rings; numerous recurrences	Excessive electrical noise due to moisture and corrosion	Inability to point communications antennas; reduced mission objective
Potentiometer for ATP control	Low temperature, light-load fluid lubricant	Electrical noise lube thickening open circuit	Loss of pointing reduced mission ~\$500K testing
Control moment gyroscope	Oil injection on bearing land	Bearing failure lube design wrong	Premature mission failure
Control moment gyroscope	Very high torque for slewing	Bearing failure	Loss of mission, >\$1M test and anneal
Momentum wheel	Grease, etc.	Torque/temperature anomalies	Possible mission failure
Propellant pump gearbox	High speed	Contractor switching lubricants	Possible launch failure with new lube
Slip rings, brush contacts	MoS ₂ /Ag/C brushes on Ag rings	Excessive noise due to oxidation of MoS ₂	Rework brushes and rings; delivery delay
Gear mechanism	High loads, fluorocarbon grease, boundary conditions	Lube degradation	System failure
Synchronous motor assembly	Mineral oil grease-packed bearings	Motor failure due to increased bearing drag	Failure would degrade mission
Momentum wheel spin bearings	High speed, mineral oil grease	Possible lubricant degradation in testing	Single-point mission failure
Inertial guidance synchronous motor bearing	High speed, mineral oil grease	Possible chemical reaction between grease & iron surface during storage	Guidance failure
Harmonic drive	Low-temperature operation; fluorocarbon grease	Low-temperature viscosity of grease causes excessive torque	Failure will degrade mission
Momentum wheel, active lubrication system	High-speed, long-life requirement	Inability to deliver adequate lubricant quantity	System will not meet lifetime requirement
SADM	Large launch loads on MoS ₂ -lubricated bearings	Test of static loads	Possible single-point failure; passed test
Gimbal bearings on telescope	Low-temperature, dry (MoS ₂) lubricant	Tested in air friction increase	Modified specification to do inert gas test; passed
Spin bearing	Large diameter, thin cross section bearing	Humidity-induced dimensional instability of cotton-phenolic retainer	Possible target acquisition failure, changed to metal ball separator
Gas bearing, gyroscope	Alumina surfaces; stearate lubricant	Erratic friction on start-up; uneven lube during test	Reliability problem for flight units; major rework if failure
Foil bearings for turbo-machinery	High-strength alloy, CF _x -polyamide lubricant; temperature extremes	High friction start-up after standing	Potential system failure; inability to start turbine

95TR4/V2

Lessons Learned:

- Accuracy, mobility, and lifetime requirements of future mechanical systems require tribological interaction early in the design phase.
- Gimbals and electrical contacts have consistently been the source of anomalies and failures. Gimbal bearings that operate in an oscillatory (dithering) mode and rarely make a full revolution are troublesome.
- Problems in rotating assemblies are often caused by ineffective lubricant supply, which is caused by inadequate initial amount, loss via transport processes, normal consumption without resupply, and chemical degradation.
- Perfluorinated lubricants cannot dissolve antiwear additives, and thus are not suitable for boundary-lubricated applications.
- Polyalphaolefin (PAO) lubricants significantly outlast a silicone oil for oscillatory motion. It is expected that these synthetic oils can be applied to high-speed applications to provide added protection against retainer instability and wear.
- Ultra-low friction-durable films of MoS_2 are deposited by various ion-sputter deposition processes. They can be used for some sliding applications, very low-load bearings, or for latching and release mechanisms. There is very encouraging evidence that ion-assisted, sputter-deposited MoS_2 films can provide ultra-low friction operation even in air applications.
- Titanium-carbide-coated bearing balls have been used in gyroscope bearings with uncoated steel raceways and superrefined mineral oil to produce operational lifetimes a factor of ten or more longer than for uncoated balls. The commercial process for coating bearing parts with TiC is available in the United States but has only been used for instrument bearings of the type used in gyroscopes. Titanium nitride coatings are used for tool steels to provide much longer service lives and considerable research and development is underway to use TiN for bearings and gears. Tests are currently under way to test the performance of both gimbal and spin bearings with TiC- and TiN-coated balls.

Testing:

In typical tests for slip ring bearings, the systems bearings tested were of the order of 90- to 150-mm bore, ABEC 7 or better precision, operated at speeds of 30 to 60 rpm, and lubricated with an oil comparable to Vac Kote 36233. The contact stresses on the bearings were low, so that even though they operated in the mixed (elastohydrodynamic boundary) lubrication regime, the antiwear additives in the oil prevented any significant bearing wear over 6 to 10 yr of operation.

Key Words:

Contact Angle, Angular Contact Bearing, X-Ray Kinematography

Mechanisms:

Despin Mechanical Assembly

Systems:

Rotating System

Authors; Experts:

1. Peter H. Fowler
2. Frank Manders

Address:

1. TRW Space and Technology Group
Redondo Beach, California 90278
2. Ball Aerospace Systems Division
Boulder, Colorado 80306

Telephone:

Title:

Estimation of Bearing Contact Angle In-Situ by X-Ray Kinematography

Source:

16th Aerospace Mechanical Symposium, NASA Conference Publication 2221 (1982).

Abstract:

The DSCS II satellite has a stationary section and a spinning section. The two sections are joined by the despin mechanical assembly consisting of drive motors, slip rings, and a pair of ball bearings on which the spinning section revolves, all enclosed in a load-bearing case. The need arose to measure the bearing contact angles in assembled units that had completed acceptance tests. The usual bench methods of estimating contact angle are not applicable to a bearing assembled in an opaque case. In any case, the contact angle (as assembled) includes the effects of preload and assembly tolerance. The paper describes a technique that can be used in this type of situation and uses an x-ray system to provide an image of the balls in-situ.

Lessons Learned:

- X-rays can be used to provide images of balls in a bearing that are not directly visible.
- Using the X-ray technique, it is possible to measure the contact angle in assembled bearings.

Description:

The x-ray system is shown schematically in Figure 1. In this case, the test article was the despin mechanical assembly. With this system, a very clear picture of the balls was generated. From this it was possible to relate the rotation of the ball train to the rotating part of the despin mechanical assembly, which provided the basis for estimating the bearing contact angles.

The contact angle can be estimated by counting the number of balls passing a given point as a function of the number of turns of the shaft.

- If, β = contact angle
 E = bearing pitch diameter
 d = ball diameter
 n = total number of balls in bearing
 θ_i = shaft rotation (degrees)
 N = number of balls observed passing a fixed point

$$\beta = \cos^{-1} \left[\frac{E}{d} \left(1 - \frac{720N}{n\theta_i} \right) \right]$$

Using this technique and estimating the bearing individual errors, the test accuracy can easily be determined. For the purpose of illustration, take one of the bearings. The basic bearing parameters are:

- $d = 0.5$ in.
 $E = 5.14$ in.
 $\beta = 15^\circ$
 $n = 23$.

Add to these the following variations and uncertainties:

- Ball diameter variation (known) = 0.00001 in.
 Pitch diameter variation (estimated) = ± 0.001 in.
 Ball train uncertainty (estimated) = $\pm 0.2^\circ$
 Shaft angle uncertainty (estimated) = $\pm 0.25^\circ$.

The contact angle accuracy improves with increased ball count. With the values above, counting 300 balls the contact angle will be accurate to approximately $\pm 0.2^\circ$. Increasing the ball count to 700, the contact angle will be accurate to approximately $\pm 0.1^\circ$.

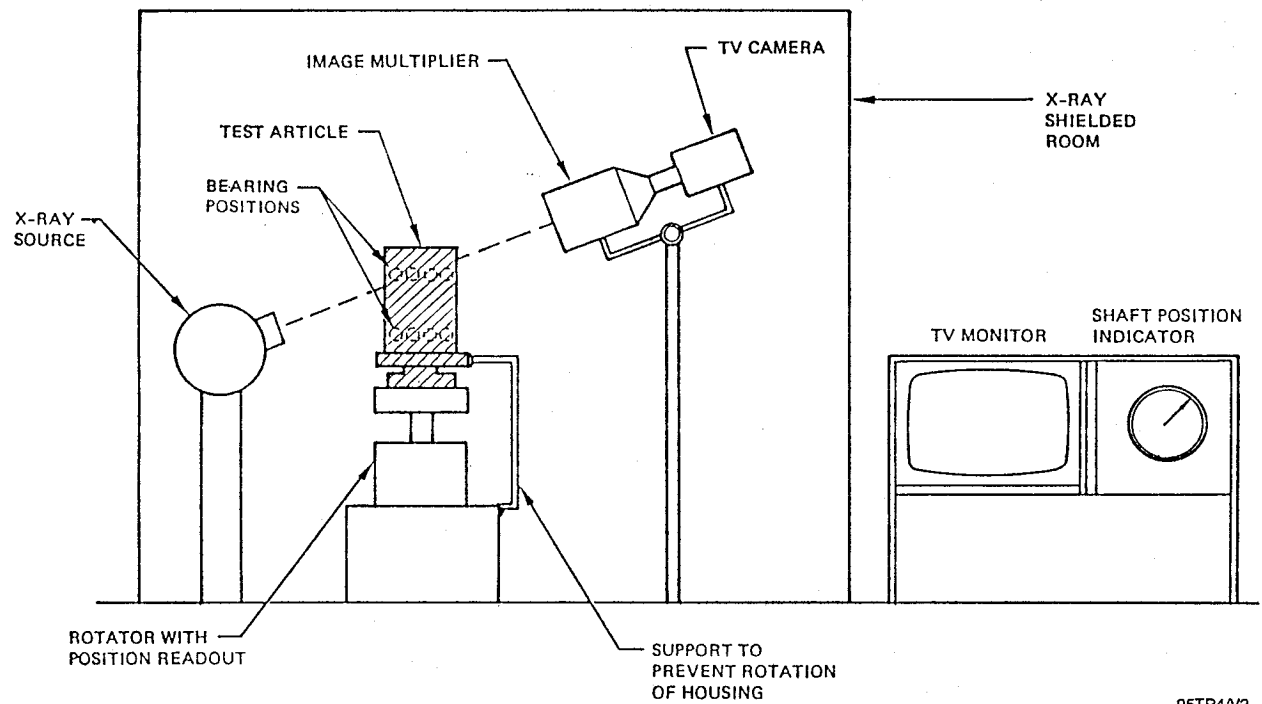


Figure 1. Measurement System

Key Words:

Lubricants, Ball Bearings, Cleaning

Mechanisms:

Slip Ring Bearings

Systems:

Rotating System

Authors; Experts:

J. Langmaier

Address:

Jet Propulsion Laboratory
Pasadena, California

Telephone:

(818) 354-2031

Title:

Galileo Spin Bearing Lubricant Problem

Source:

JPL Lessons Learned No. 775.

Anomalies:

After approximately 3 months of life testing, the lubricant in the Galileo slip ring bearing (KG80 oil) had a thick, black, gooey appearance and the bearing friction torque was higher than expected.

PRECEDING PAGE BLANK NOT FILMED

Lessons Learned:

- Even careful cleaning of spaceflight components can leave residues that may eventually react with adjacent materials. Cleaning processes must be followed by an outgassing vacuum-bake treatment. This is particularly important for porous materials that may have absorbed various fluids, including the cleaning medium itself.

Description:

The Galileo flight control slip ring test fixture bearings had once been lubricated with a synthetic lubricant. This was eventually replaced with KG80 oil to simulate actual spin bearing assembly operating conditions in space. After approximately 3 months of life testing under vacuum at 3 rpm, the bearing lubricant had a thick, black, gooey (??) appearance and the bearing friction torque was higher than expected. It was discovered that, even with careful cleaning prior to the test, some of the original synthetic lubricant had remained in the porous, phenolic retainer. Under vacuum, this residual lubricant migrated to the surface, and reacted with the KG80 to form the black material. A new bearing with a nonporous steel retainer was installed.

Key Words:

Antenna Despin Drive, Bearings

Mechanisms:

Antenna Despin Drive

Systems:

Solar Science Satellite, HELIOS

Authors; Experts:

Damon D. Phinney

Address:

960 6th Street
Boulder, Colorado 80302

Telephone:

(303) 442-7824

Title:

Anatomy of a Bearing Torque Problem

Source:

NASA Conference Publication 2470, 21st Aerospace Mechanisms Symposium.

Abstract:

Torque anomalies were encountered on the despin drive assembly of the HELIOS solar science satellite. The shaft of the inside-out despin drive assembly was fixed to the spacecraft, supporting the antenna feed at its outboard end, while the antenna was attached to the housing (see Figure 1). The specified despin drive assembly temperature range was -50 to 60°C and the minimum lifetime was to be 18 months.

Anomalies:

High bearing torque was encountered on two flight models.

Lessons Learned:

- The relative position of two parts can lead to either compensating or aggravating effects due to dimensional errors and thermal distortion. Bearing draw is affected by assembly accuracy and thermal distortions. Improving the perpendicularity of the lower bearing inner race seat from 0.8 to 0.3 arc-min dropped bearing drag at -50°C about 40%.
- Distortions can significantly add to bearing torque. In this case, a favorable indexed rotation of the end plate reduced torque significantly. The end plate and aluminum housing were distorted.
- Anisotropic material properties designed for use over a wide temperature range can lead to problems due to thermal distortion.

Description:

- An isometric view of the despin drive assembly is shown on Figure 1. Further details are shown on Figure 2.
- A three-piece shaft assembly consists of a 7.8-in. long 7075-T652 aluminum tube with 6A1-4V titanium stubshafts at each end. Bearing journals were on the stubshafts, whose function was to isolate the bearings from the high expansion rate of the aluminum tube.
- Two angular-contact ball bearings were spaced 6.4 in. apart with outer race thrust shoulders facing each other. All bearing rings were slight interference fits except for the outer race of the right-hand bearing. This was slip fitted and acted on by a set of coil springs with a force of 5 lb. The springs were in a carrier machined to length at assembly to produce an end play of 0.0055/0.0065 in. Because of the mix of aluminum and titanium pieces in the shaft and housing, the end play would be reduced by 4 mil at -50°C.
- The 440C bearings were lubricated with a thin film of molybdenum disulfide (MoS_2) approximately 1/4 micron thick, and had inner-land-rigging Rulon-A separators with full cylindrical pockets. The normal ball complement was reduced from 42 to 38 to provide additional separator material between pockets and increased dimensional stability.

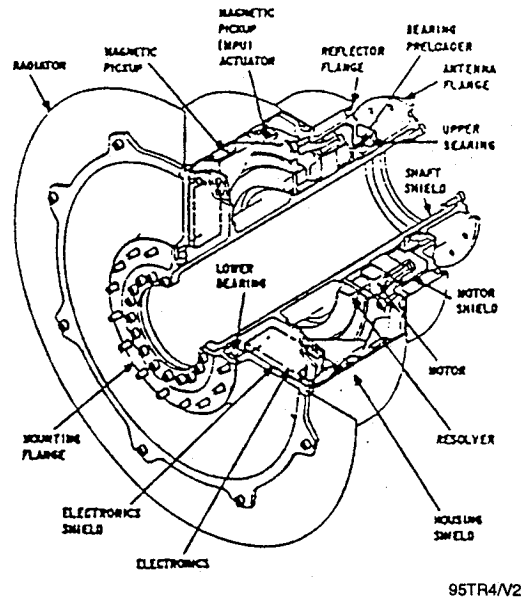


Figure 1. EMS-331 Despin Drive Assembly

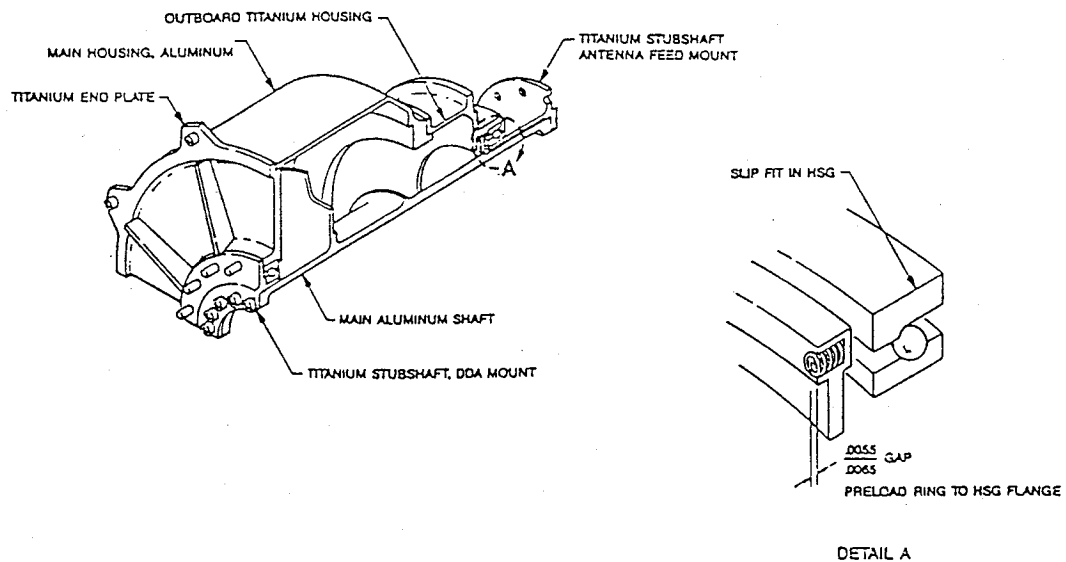


Figure 2. Bearing Installations

Testing:

Early experience indicated a flight unit problem. Despin drive assembly requirements included operation between -50 and 60°C (-60 and 75°C for qualification) with a maximum drag torque of 5 oz-in. In addition to the bearings, the only significant drag source was motor hysteresis (1.3 oz-in.).

To confirm bearing lubrication, a thermal vacuum life test on six bearing pairs had been run at 60 rpm for 18 months. Temperatures were -35°C, 10°C, and 60°C. Torques varied from 0.5 to 1.5 oz-in. with brief excursions to 2.5 oz-in. on two sets at 22°C.

An 18-month thermal vacuum life test had also been conducted on an engineering model despin drive assembly at 60 rpm and temperatures of -40°C, 22°C, and 50°C. After some fixturing problems were corrected, drag torque varied between 2 and 4 oz-in. There were two brief excursions as high as 8 oz-in. at 22°C and 120 rpm while we were catching up after some downtime.

The qualification unit had shown drag torques of 6.4 and 4.5 oz-in. at -60 and 75°C. The 6.4-oz-in. reading, although above the 5-oz-in. limit, was rationalized away on the basis of a probable adverse temperature gradient (housing warmer than shaft) unlikely to occur during flight. An excessive gradient would have completely eliminated end play and caused an increase in bearing load.

With this favorable experience preceding acceptance tests of the two flight despin drive assemblies, we were rudely surprised when drag torque climbed to 20 oz-in. on the first unit while it was being taken down to -50°C.

By process of elimination, two significant findings were discovered:

1. Torque was sensitive to the indexed position of the end plate.
2. Parallelism between the lower shaft flange face and the bearing thrust shoulder was off by 0.0007 in. Improving parallelism between the bearing thrust shoulder and shaft flange, and slightly opening the inner bearing ring fit made a significant reduction in -50°C torque.

Experience:

HELIOS-B was operational for four years until a TWT failure occurred. HELIOS-A was still going in December 1984, 10 yr after launch. We were told that its drive had been turned off for 29 days during 1982 to conserve battery power because solar cell degradation had occurred. Apparently the despin drive assembly, whose travails are discussed here, ran nearly continuously at 60 rpm for 10 yr. It may still be running as this is written in December 1986, 12 yr from launch.

Key Words:

Lubrication, Momentum Wheels, Reaction Wheels

Mechanisms:

Ball Bearings, Momentum Wheels, Reaction Wheels

Systems:

General Satellites

Authors; Experts:

1. Herbert Singer and Erik Gelette
2. Dr. Edward Kingsbury

Address:

1. The Charles Stark Draper Laboratory
Cambridge, Massachusetts
2. The Bearing Consultants
1063 Turnpike Street
Stoughton, Massachusetts 02072

Telephone:

1. Phone: (508) 660-1391/Fax: (508) 660-0146

Title:

Design of a High-Speed Reliable Ball Bearing

Source:

28th Aerospace Mechanism Symposium, NASA Conference Publication 3260.

Abstract:

A high-speed, reliable ball bearing has been designed for at least 15 yr of operation in space effectors, momentum wheel assemblies, and reaction wheel assemblies. Advance bearing concepts have been used in this design, such as no ball retainer, which eliminates all retainer-related problems; an external lubricating system that will supply the lubricant at a specified flow rate; and a cartridge assembly that will allow the instrument user to purchase a ready-to-use bearing assembly with lubricator. Currently, two assemblies are on life test at 12,000 rpm and have accumulated over 20,000 hr, each with consistent low-torque losses. The paper will describe each of the salient features.

Anomalies

The paper does not cite anomalies, but possibilities include:

- Thermal lockup
- Lubricant contamination that can clog feed mechanism
- Ball-to-ball impact.

Lessons Learned:

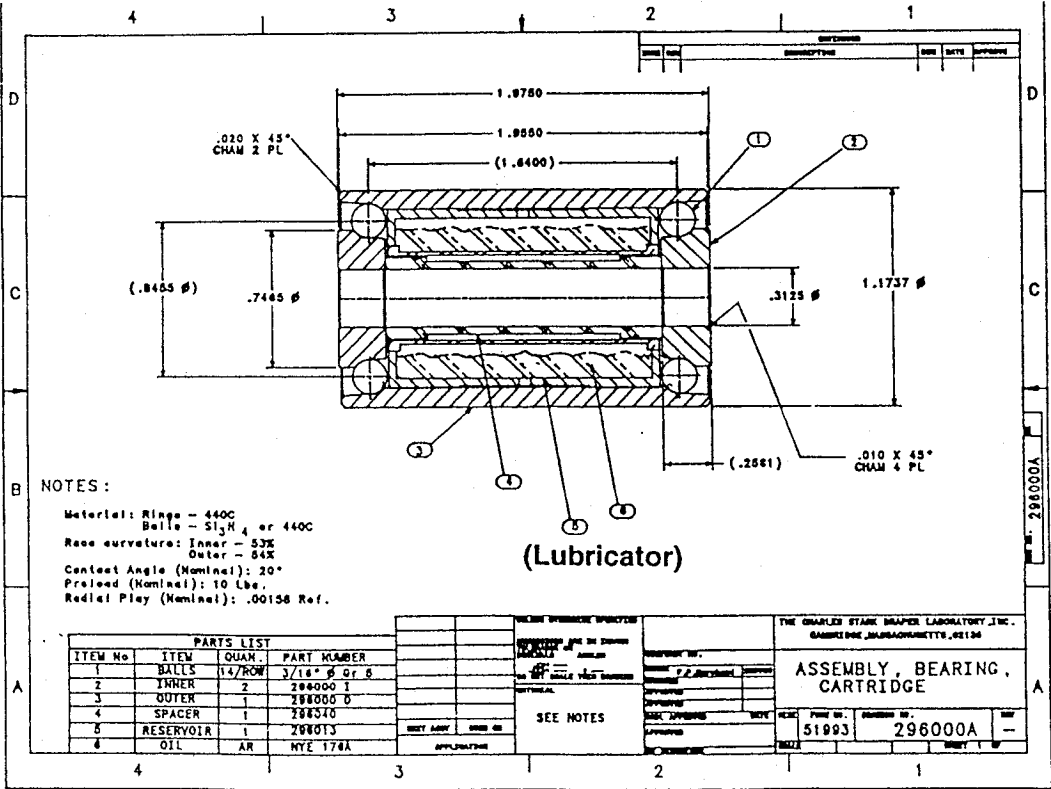
- Screening tests provide an accurate and expeditious approach to determining bearing cartridge performance.
- Lubricant replenishment is a major problem with spacecraft bearings. The design presented in this paper provides a clever scheme for a continuous and controlled supply of lubricant without incurring excessive torque.
- Retainerless instrument bearings avoid cage instability and are advantageous if ball impact is not a problem.

Description:

Salient Features

Retainerless Design. The ball retainer has been eliminated to ensure no retainer-related problems, such as retainer instability (squeal). Dr. Kingsbury has shown that contrary to current theory, there is a lubricant film between the balls to ensure no ball damage during operation.

External Lubricator. An external lubricator, named an oozing-flow lubricator, has been designed to give a specified flow rate of lubricant to the ball contacts. The oozing-flow lubricator is shown schematically in Figure 1. The lubricant is driven through the interface by the centrifugal pressure head caused by the rotation of the lubricator. Thus, at storage conditions, no oil is lost from the lubricator.



95TR4/V2

Figure 1. Oozing-Flow Lubricator

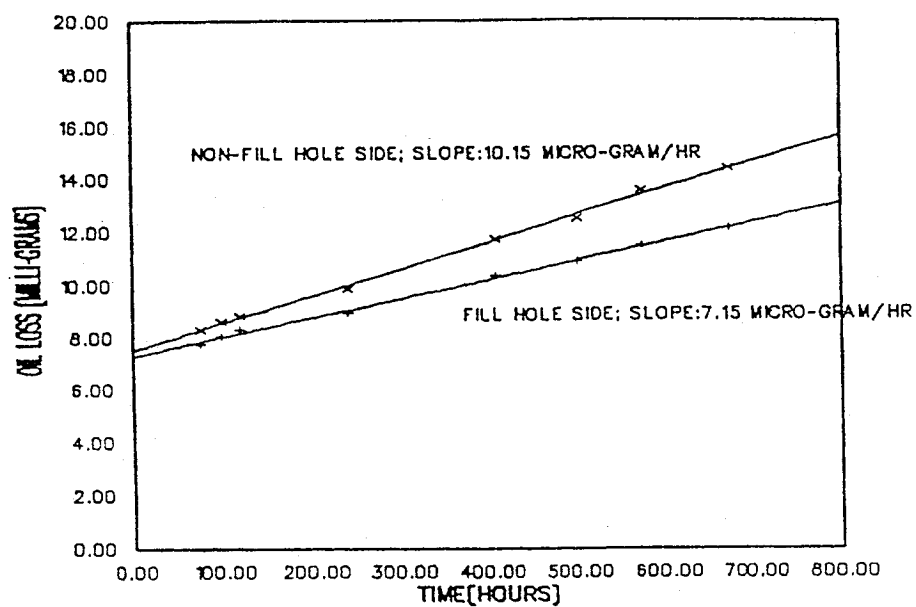
The flow rate of the oil is controlled by the properties of the interface; for high interfacial pressures, the flow is only proportional to the cube of the flow channels' dimension. These channels can be controlled either through surface finish controls or other means. The flow is also controlled by the oil viscosity. As the oil is lost from the lubricator, the head and the flow rate change exponentially with running time.

Cartridge Bearing Design. A cartridge bearing design was selected for this bearing assembly (see Figure 1). Based on the expected loads and environment, the bearing was designed to have a pitch diameter of Size 100 bearing. There are 14 0.1876-in. diameter balls in each bearing row. The reservoir and the ID of the outer races comprise the oozing-flow lubricator. Nye 176A oil, a polyalphaolefin (PAO) with a kinematic viscosity of 437 cs at 100°F, is the lubricant of choice. This cartridge design with the lubricator and shaft is configured so that a competent bearing manufacturer can produce and screen the assembly. This will relieve the instrument manufacturer from handling the ball bearing.

Optimum Flow Rate Determination. Parched elastohydrodynamic theory was used to determine the optimum flow rate for the bearing size (basic Size 100 design), preload (10 lb), and speed (12,000 rpm). A flow of at least 0.2 micrograms/hr is needed to maintain a parched elastohydrodynamic film.

Testing:

Figure 2 shows oil losses versus time. Two bearing assemblies (one with a wheel and one as a cartridge only) are running at 12,000 rpm for over 20,000 hr. Torque and oil flow rates are periodically measured. The change of oil flow rate with time follows the prediction (see Figure 3). The torque losses at 12,000 rpm are around 0.4 in.-oz and are consistent with time for both bearings (see Figure 4).



95TR4/V2

Figure 2. Oil Flow versus Time

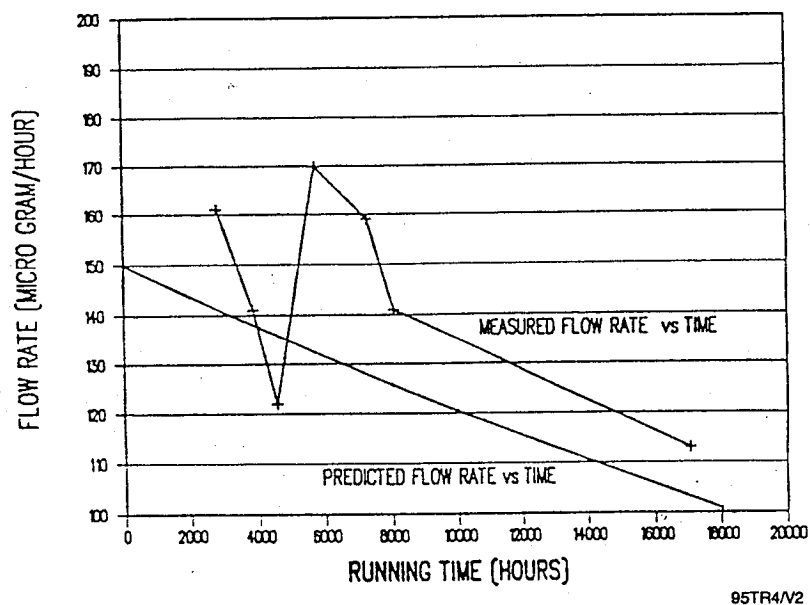


Figure 3a. Flow Rates for S/N 005

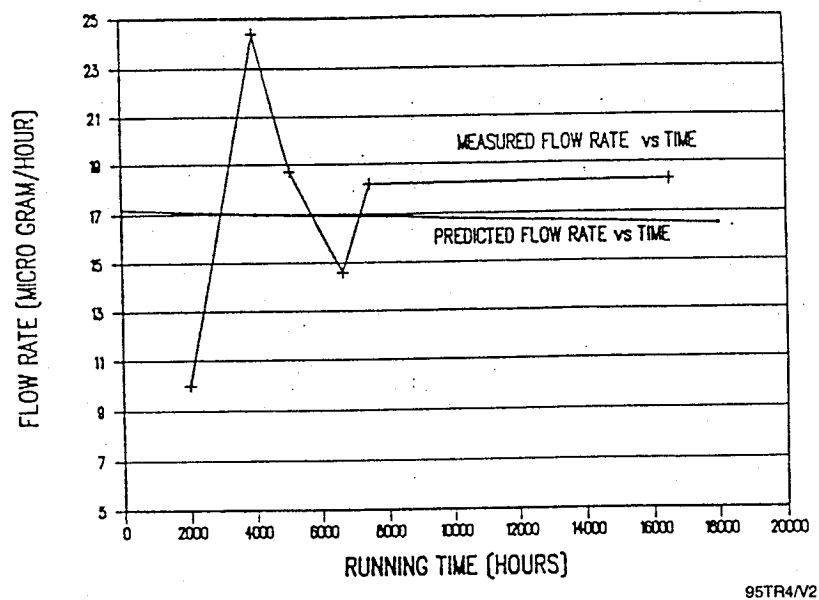
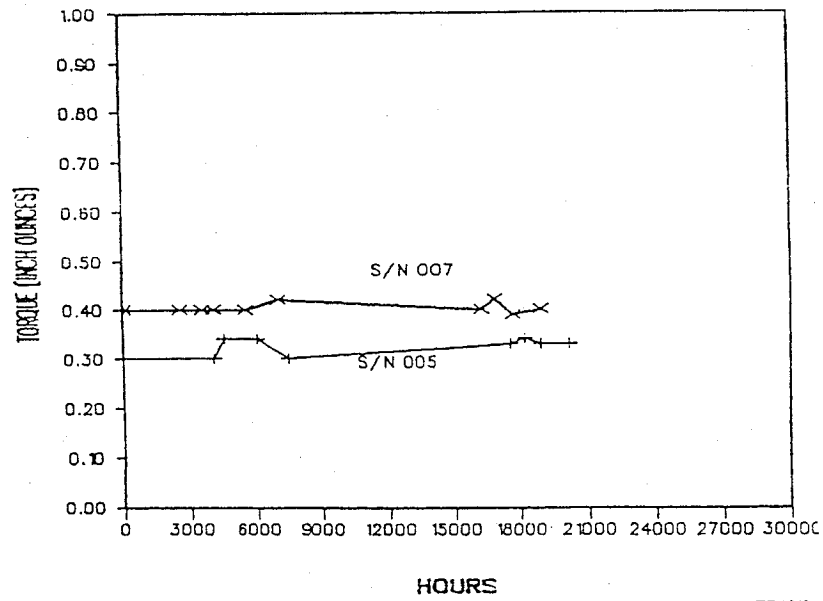


Figure 3b. Flow Rates for S/N 007



95TR4/V2

Figure 4. Cartridge Bearing Life Test

Key Words:

Ball Bearings, Relubrication

Mechanisms:

Control Moment Gyroscope, Reaction Wheel, Momentum Wheel

Systems:

Rotating Systems

Authors; Experts:

Dennis W. Smith and Fred L. Hooper

Address:

Honeywell Corporation
Satellite Systems Operations
Glendale, Arizona

Telephone:

Title:

Positive Lubrication System

Source:

24th Aerospace Mechanisms Symposium (1990).

Abstract:

The goal of this work was to increase the effective life of grease-lubricated bearings in space by designing an auxiliary lubrication system that could deliver fresh oil to the bearings on demand. The useful life of control momentum gyroscope, reaction wheels, and momentum wheels is strongly dependent on the availability of lubricant for the support bearings. Current lubrication systems are passive and consist of grease-filled bearings or controlled-leak oil systems. Greases have been found to be effective for lifetimes of up to 3 yr for most control moment gyroscopes, up to 8 yr for small control moment gyroscopes, and 11 yr in momentum wheels. The controlled-leak (or once-through) systems look

PRECEDING PAGE BLANK NOT FILMED

promising in the laboratory but there is very little experience in space. To provide longer life, an active oil system is offered that would back up the grease-lubricated bearings and would also supply oil based on bearing requirements.

Anomalies:

- The lives of control moment gyroscopes, reaction wheels, and momentum wheels are essentially determined by the lives of the supporting ball bearings. The bearings are usually grease lubricated and fail due to loss of oil from the grease. The current lives can be as short as 3 yr and may be mission limiting.
- In a weightless environment, there are questions about how a drop of oil will behave. Even at a distance of 0.04 in., the drop may not transfer smoothly. It may touch and then be slung off the moving surfaces to create a number of finer droplets that will float around the bearing housing.

Lessons Learned:

- Grease-lubricated bearings can be automatically supplied with additional oil as required to compensate for oil loss from the grease.
- Any lubrication scheme should be evaluated in a weightless environment.
- Resupplying oil to a grease-lubricated bearing after the grease has lost some oil is a very feasible approach to the goal of extending bearing life. Eventually, some kind of a system like the one proposed in this paper will have to be used in space.
- Centralized lubrication systems are widely used in industry. With a few modifications for the space environment and an evaluation of weightless performance, a reliable, long-life system could be had.

Description:

One grease that is being used for these applications is Andok C. This is a channeling, nonbleeding-type grease with a naphthenic oil and a sodium soap-base thickener. The authors are proposing to use Coray 100 as the lubricating oil that would resupply the grease when it was needed. Coray 100 is an Exxon product, which is an uninhibited, naphthenic-base machine and engine oil with a viscosity of about 110 cs at 40°C. The authors are also trying to develop a sensor to detect when the grease lubricant needs additional oil. Current telemetry can detect spin motor current, which is proportional to the drag torque, and an increase in bearing temperature, which is also indicative of the increase in drag torque. These measurements provide an indication of the need to supply fresh oil to the system.

Much of the rest of the paper is concerned with bench tests that were done to fine tune the design of the positive lubrication system. The system is essentially a pressurized reservoir with a solenoid valve that will supply oil at 100 psi through 0.016-in. inside diameter CRES tubing and feed this oil into the bearing at a point within 0.004 in. of the ball surfaces. Originally, it was planned that one reservoir would supply a pair of bearings (inboard and

outboard), but only one bearing received adequate oil so it was necessary to have a separate reservoir for each bearing. The oil volume requirement for each reservoir was based on supplying 20 to 30 mg of oil per month for 3 yr, plus about 200 mg for the initial system fill. This volume of 3 ml (2.8 gm) is more than a factor of two greater than the estimates of oil needed. Figure 1 is a schematic of the pressurized reservoir/solenoid valve. Figure 2 is the 28-V dc type 316 CRES solenoid valve, and Figure 3 shows a typical flight installation. Figure 4 shows the details of the bearing geometry with the oil holes.

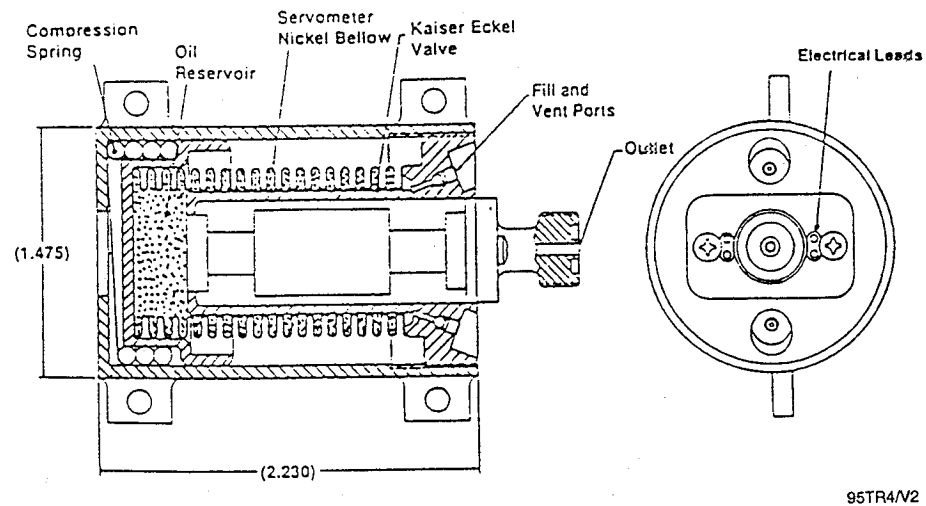


Figure 1. Pressurized Reservoir/Valve

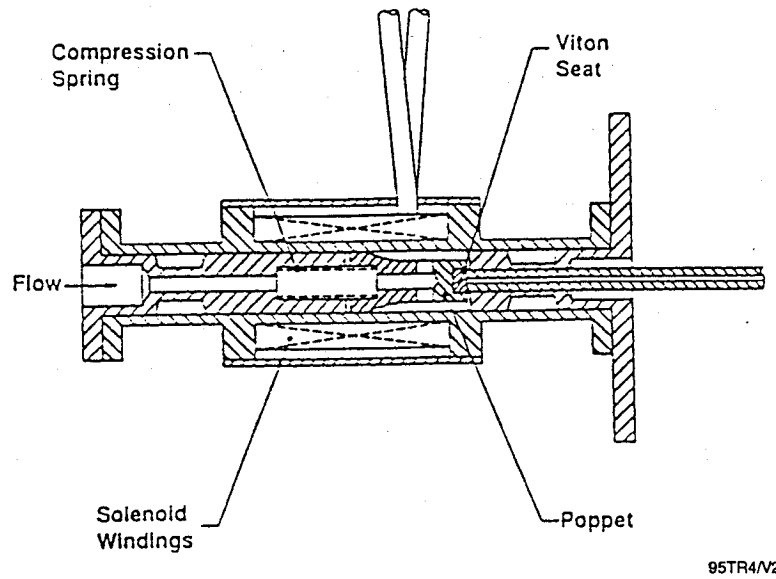


Figure 2. Kaiser-Eckel Solenoid Valve

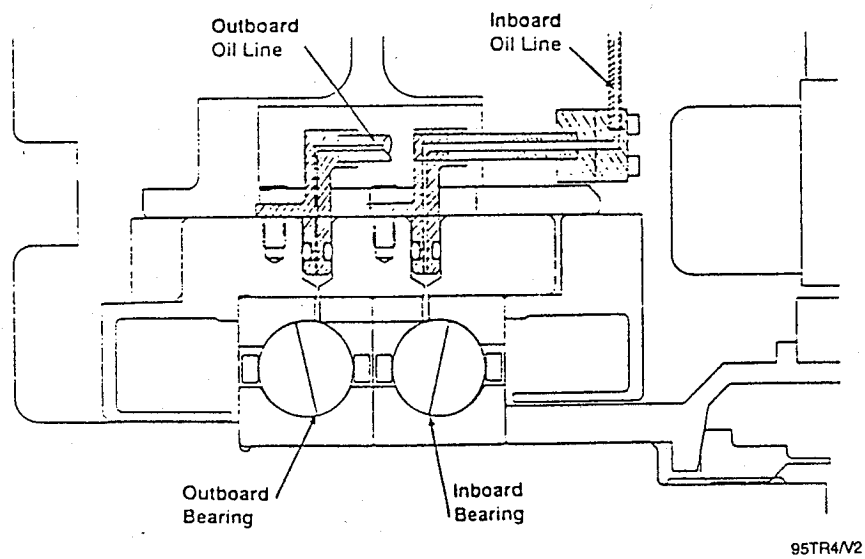


Figure 3. Typical Flight Installation

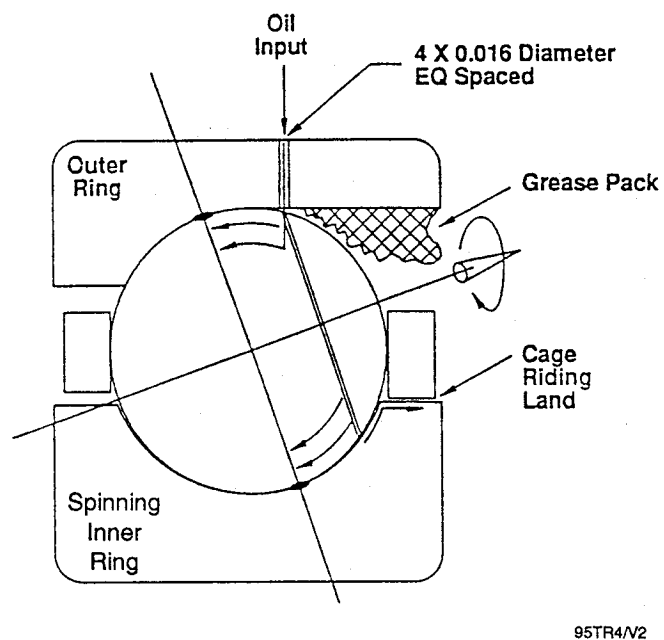


Figure 4. Nominal Bearing Geometry with Oil Holes (Option 5)

Key Words:

Despin, Angular Contact Bearings, Dry Lubricants

Mechanisms:

Despin Mechanism

Systems:

Rotating System

Authors; Experts:

M.J. Todd and K. Parker

Address:

European Space Tribology Laboratory
Risley Nuclear Power Development Laboratory
UKAEA, Risley, Cheshire, England

Telephone:

Title:

GIOTTO's Antenna Despin Mechanism: Its Lubrication and Thermal Vacuum Performance

Source:

21st Aerospace Mechanisms Symposium (1987).

Abstract:

During GIOTTO's mission to comet Halley, its high-gain antenna was the only means of up/down communications. The spacecraft spin stabilization required that the high-gain antenna be despun at the same rotational rate of nominally 15 rpm. The despin mechanism runs on angular contact ball bearings and for the expected thermal environment dry lubrication was preferred for the bearings. Since there was no existing data on the torque noise spectrum of candidate solid lubricants, torque noise tests were run with two solid lubricants: ion-plated lead film with a lead-bronze retainer and a PTFE composite retainer only. The lead lubrication showed the better spectrum up to the mission lifetime point so it was selected for continued test over some 20 times the Halley mission life, with periodic torque spectrum monitoring. The spectrum remained well within the pointing error budget over the 100 million revolutions covered.

Anomalies:

Stepper motor harmonics excited a torsional resonance of the antenna.

Lessons Learned:

- Bearings lubricated with ion-plated lead were capable of meeting the mission life and had a noise spectrum that was rather insignificant compared with the tolerable noise.
- Tests of the complete energized despin mechanism showed that the stepper motor harmonics excited a strong undamped torsional resonance of the antenna at certain motor speeds.
- The tests identified a safe operating regime for the GIOTTO despin mechanism and contributed to the eventual mission success.

Description:

The rotating shaft of the despin mechanism is supported by two flexibly preloaded angular contact bearings. The Earth-pointing accuracy required of the antenna (maximum constant error $\pm 0.1^\circ$ /maximum jitter $\pm 0.05^\circ$) together with the anticipated range of working temperature, from -20 to $+40^\circ\text{C}$, imposed limits on the tolerable torque noise, part of which would be generated by the bearings.

The criteria for the despin mechanism lubrication were:

- Long-term stability in space vacuum
- Low torque noise over the mission life
- Insensitivity of mean torque to temperature change
- Validity of accelerated testing
- Simplicity in design (preferably no lubricant reservoirs or molecular seals).

The third and fifth criteria effectively ruled out wet lubricants; thus, a solid lubricant was favored.

The long experience in Europe with ion-plated lead film made it a strong contender for this duty. Another solid lubricant (a transferred PTFE film from a composite retainer) was also included in the testing.

For the initial tests, bearings of the same type used in the despin mechanism were lubricated either by ion-plated lead with a cast lead-bronze cage or by a PTFE composite cage (PTFE/glass fiber/molybdenum disulfide (MoS_2)). The tests were carried out in a vacuum chamber. After a short 10,000-rev test in air to simulate likely ground testing, the chamber was evacuated to $<10^{-6}$ torr and the main test was begun. To fit the tests into a reasonable timescale, they were carried out at 100 rpm with regular reductions to a nominal despin speed of 16 rpm for the recording of torque spectra. Since with these solid film lubricants, temperature was known to have little effect on bearing torque, the tests were carried out at a nominal ambient temperature of 20°C . Comparisons of the power spectral density of the two types of bearings at a similar number of revolutions showed that the spectra for the PTFE-lubricated bearings had more and larger peaks than the lead lubricated bearings. This was probably due to thick, uneven transfer of the PTFE to the

balls and races. The PTFE bearings also had prominent peaks in the sensitive bandwidth of 1 to 3 Hz. On these grounds, the test on the PTFE-caged bearings was discontinued. The Halley mission lifetime was 6×10^6 rev, but the test on the lead-lubricated bearings was continued to 1×10^8 rev. The highest rms torque measured during the test was 0.009 Nm, which was small compared with the design limit of 0.12 Nm.

The bearing tests were followed by an accelerated thermal vacuum life test on a model of the despin mechanism. The mechanism was driven mainly at 200 rpm except for periods of torque measurement and analysis which were at 15 rpm. Tests were carried out under the following thermal conditions:

- Shaft = 20°C, housing = 20°C
- Shaft = 20°C, housing = -25°C
- Shaft = -25°C, housing = -5°C.

Torque spectra were taken in all these temperature states every 5×10^5 rev until a total of 6×10^6 rev had been completed. The different thermal conditions did not have any significant effect on the torque spectra.

Following the driven despin mechanism tests described above, it was decided to measure directly (in vacuum) the torque that would be experienced by the spacecraft in driving the antenna. A dummy antenna with the same polar moment of inertia as the actual antenna was attached to the despin mechanism with the mechanism mounted on a piezo-electric torque transducer in the vacuum chamber. Torque measurements over a range of speeds showed up a number of resonances that could cause excessive antenna jitter. From the data, it was possible to select a spin speed at which there would be no significant jitter.

Key Words:

Lubricants, Testing

Mechanisms:

Hinges, Gears, Bearings

Systems:

Rotating Systems, Scanning Systems

Authors; Experts:

C.E. Vest

Address:

Applied Physics Laboratory
Pennsylvania

Telephone:

Title:

Lubrication of Spacecraft Mechanisms

Source:

John Hopkins Applied Physics Laboratory (APL) Technical Digest, Vol. 14, No. 1, pp. 68-75 (1993).

Abstract:

The instruments were designed by APL using ball bearings, gears, pins, hinges, and other types of moving components lubricated with materials such as thin gold plate, hand-burnished molybdenum disulfide (MoS_2) or graphite, plastic cages/retainers, inorganic/organic-bonded solid films, or oil and grease. For each instrument, the lubricants were selected for a specific reason; for example, electrical conductance across the bearing was needed; a short (30 sec) or long (20 yr) lifetime was required; a motor with a large torque margin was used, where wear was not a consideration; or continuous exposure to the space environment was involved.

PRECEDING PAGE BLANK NOT FILMED

[PAGE 358 INTENTIONALLY BLANK]

Lessons Learned:

- To produce a boundary-lubricating film using a liquid lubricant, a run-in must be performed.
- For high-load boundary-lubricated contacts, a bonded solid film lubricant such as MoS_2 is recommended.
- For slow-speed ball bearing rotation, a Teflon or MoS_2 -filled grease or a transfer film lubricating polymeric cage is recommended.
- Sliding motion applications are mostly boundary lubricated. A high load-carrying grease with an extreme pressure gradient additive must be used. The grease produces a high load-carrying solid film such as Teflon, MoS_2 , graphite, or tricresyl phosphate (TCP) between the rubbing surfaces

Slip Rings and Roll Rings

Key Words:

Solar Array Drive, Slip Rings, Dry Lubrication

Mechanisms:

Solar Array Drives

Systems:

Rotating Systems

Authors; Experts:

G. Atlas and G. Thomin

Address:

Société Européenne de Propulsion (SEP)
Vernon, France
Centre National d'Etudes Spatiales (CNES)
Toulouse, France

Telephone:**Title:**

Experience of CNES and SEP on Space Mechanisms Rotating at Low Speed

Source:

21st Aerospace Mechanisms Symposium (1987).

Abstract:

The paper describes some developments in the field of space mechanisms carried out by SEP and CNES. The experience described centers on the development of the following major mechanism programs:

- MEGS (Mechanisme d'Entraînement du Générateur Solaire). This is a solar array drive mechanism developed and flown under a CNES-led program and is now flying on the Earth observation SPOT-1 satellite.

- MOGS (Mechanisme d'Orientation de Générateur Solaire). This is a solar array drive designed by SEP under CNES contract and currently being developed for application in the EUTELSAT II program.

The paper highlights the key design features and the performance of the mechanisms.

Anomalies:

Anomalous values of contact resistance was found in both the pyrotechnic and the power/signal slip ring assemblies.

Lessons Learned:

- Contamination of slip rings can occur if they are exposed to the atmosphere for any length of time.

Description:

MEGS. The SPOT mission was to provide precise images of the Earth with a resolution of 10 meters. This was a very severe requirement for the control stability of the satellite and the stability and uniformity of motion of the MEGS. The speed stability was required to remain within 10% of the nominal speed of 1 rev/100 min (no stepping allowed). Particularly important was the avoidance of frequencies between 0.15 and 0.2 Hz that might have excited the solar arrays.

Careful attention was given to the drive motor to ensure that it ran at a constant speed. Because of nonuniformities in the motor coils, there is usually a small ripple on the speed. By varying the currents in the coils, it was possible to eliminate this ripple.

The bearings selected were 25° angular-contact bearings, SNFA SEA 55, with a lead-bronze retainer and lead-coated raceways. Preload was provided by a diaphragm, which was radially stiff but axially compliant. For launch, the bearings were off loaded to prevent brinelling.

The slip ring material was chosen after a series of tests by CNES with materials from Le Carbone Lorraine. The material chosen was Ag/C/molybdenum disulfide (MoS_2) (12% MoS_2). One year after delivery of the MEGS during integration testing, anomalous values of contact resistance were found in both the pyrotechnic and the power/signal slip ring assemblies. The problem was particularly severe for the pyrotechnic slip rings where a typical value found was a 1000-ohm resistance compared with the expected 1 ohm. It was determined that the high resistance was due to surface contamination, possibly Ag_2O or Ag_2S . The slip rings were cleaned just prior to launch in 1986 and subsequently operated well within their specifications in orbit.

MOGS. Following the successful development of the MEGS, CNES decided to fund the design of a solar drive specifically for GEO applications. The main requirements were:

- Low mass mechanism: <5 kg
- Load capabilities:
 - 800 N along rotation axis
 - 1500 N perpendicular to axis
 - 200 Nm perpendicular to axis
- Power capability: 6 kW at 50 V
- Accuracy: $\pm 0.2^\circ$
- Life: 10 yr

The bearings used in the design were SNFA SEA 55 angular-contact bearings with lead-bronze retainers and lead-coated raceways, the same as used in the MEGS.

To reduce the overall dimensions and mass, the slip ring assembly is located between the bearings. The power slip rings utilize four cylindrical modules, each with six rings capable of carrying up to 8 A. The same slip ring and brush materials as for the MEGS are used for the power circuits but, for the 20 signal circuits, Nye ORO brushes sliding against gold rings are used.

The drive is an off-shaft stepper motor driven by a shaped pulse to improve the dynamic characteristics. The high pointing accuracy is achieved by using a 200-step/rev Moore Reed stepper motor driving a 15:1 gear giving a shaft step of 0.12° . The gear system has a steel pinion and a Nuflon-N treated steel gear. This combination was selected after load representative vacuum testing.

The effect of temperature differentials on the MOGS performance is minimized by the use of a diaphragm-loaded bearing, linking the motor to the MOGS drive shaft by a flexible connection, and using a special constant-gap device that maintains the gear pinion play at a constant value.

Key Words:

Roll Rings, Space Station, Solar Alpha Rotary Joint, Beta Gimbal, Thermal Radiator Rotary Joint

Mechanisms:

Roll Rings

Systems:

Solar Arrays, Space Station

Authors; Experts:

J. Batista, J. Vise, and K. Young

Address:

Honeywell, Inc.
Satellite Systems Operation
Phoenix, Arizona

Telephone:

Title:

Roll Ring Assemblies for the Space Station

Source:

28th Aerospace Mechanism Symposium, NASA Conference Publication 3260.

Abstract:

Space station Freedom requires the transmission of high power and signals through three different rotational interfaces. Roll ring technology was baselined by NASA for rotary joints to transfer up to 65.5 kW of power for 30 yr at greater than 99% efficiency. Signal transfer requirements included MIL-STD-1553 data transmission and a 4.5-MHz RS250A base-band color video. A unique design for each rotary joint was developed and tested to accomplish power and signal transfer. An overview of roll ring technology is presented, followed by design requirements, hardware configuration, and test results.

PRECEDING PAGE BLANK NOT FILMED

PAGE 364 INTENTIONALLY BLANK

Anomalies:

- Roll rings can produce excessive noise if not geometrically correct and of proper materials.
- The utility transfer assembly had a 9.0-Nm drag torque after initial assembly, which increased to approximately 27.1 Nm during functional testing after X-axis vibration. This was considered a failure because the drag torque requirement was <13.6 Nm. The unit was inspected and analyzed to determine the cause of the failure. The high drag torque was caused by two design problems:
 - The outer contact ring track geometry was spoiled by a twist in the ring caused by the radial clamping pressure of the heat transfer spring between the ring and the housing. This resulted in flexure interference and then higher drag torque.
 - The idler guide tracks had windows manufactured in them to reduce weight and to aid in assembling the power circuits. It was found that an idler got lodged in the window causing a flexure to break and created high drag torques, which created the 27.1-Nm drag torque.

Lessons Learned:

- Roll rings are effective rotary joint electrical transfer devices and avoid the deficiencies of slip rings and flex capsules. Flex capsules are limited with respect to rotation and fatigue life. Slip rings wear due to sliding electrical contacts, generate debris, and require lubrication.
- Roll rings have had considerable development for both high- and low-power applications. They are reliable, low noise drag torque devices and should receive primary consideration for rotary joint electrical transfer applications.
- To accomplish noise reduction, plating processes, plating purity, and cleaning processes must be carefully controlled.
- High purity plating and elimination of metallic oxides from surfaces by stringent reduction of low-nobility metals in gold plating enhances noise reduction.
- Progress in noise reduction is evident by the data provided in Table 1.
- Software that models geometric tolerances and maximizes rolling efficiency is very helpful in roll ring design.

Table 1. Roll Ring Noise Resistance

Unit	Background Noise (mΩ)	Peak Noise (mΩ) ⁽³⁾	Current
Utility Transfer Assembly Signal ⁽¹⁾	<10 (13x)	15 to 30 (4x) 15 to 50 (5x) 15 to 89 (1x) 15 to 143 (3x) 15 to 243 (1 x) 20 to 300 (2 x)	0.1 mA
PDТА Signal ⁽¹⁾	6 to 10	13 to 32 (1x) 18 to 66 (1x) 13 to 18 (1x) 18 to 347 (1x)	0.1 mA
BGRRS Signal ⁽¹⁾	2 to 4	5 to 9 (2x)	0.1 mA
BGRRS Low Power ⁽²⁾	2	4 to 6 (2x)	2 A

1. Signal roll rings have two flexures in parallel per crossing.
2. Low-power roll rings have three flexures in parallel per crossing.
3. Peak noise levels seen by the number of circuits in parentheses, e.g., 4x.

95TR4/V2

Description:

Roll rings are a new technology developed to perform the same function as a slip ring/brush assembly, but by means of rolling instead of sliding electrical contact. Consequently, there is no measurable wear, lubrication is not required, and long fatigue life can be met. Two types of roll rings have been developed: one type for signal and low power, another for high-power applications.

The space station Freedom design featured three rotary joints. The solar alpha rotary joint provides continuous rotation of the solar arrays to account for orbital rates, and transfers 65.5 kW of power as well as signals. The beta gimbal rotates the solar arrays to track the seasonal changes of the sun angle and transfers 45 kW of solar array power, low power, and signal. The thermal radiator rotary joint keeps the radiators pointed at deep space and transfers low power and signal. Each rotary joint incorporates a unique roll ring design.

The roll ring electrical signal/power rotary transfer device evolved from ball bearing and electrical transfer technologies and has been under development since mid-1970. The device consists of two or more concentric conductive rings and at least one rolling, flexible, conductive element (Figure 2). The conductive element (or flexure) is fitted to and captured in the annulus space between the concentric rings. When the rings are suitably attached to two structures that are aligned with a common axis, the conductive flexure provides a precise, mechanically stable, electrical coupling between the two structures.

The theoretical torque of the roll ring is zero. Actual torque levels are very small and exist because the flexure and the ring grooves cannot be fabricated perfectly. The bulk of roll ring life testing has been conducted in a vacuum environment. This imposes the most severe conditions from a life and wear standpoint because water vapor is present in a laboratory environment and acts as a lubricant. The ring tracks and flexures are plated with a gold/cobalt alloy, which acts as a dry lubricant during vacuum operation and ensures the integrity of the electrical contact surfaces. The gold plating is backed by a nickel plating to enhance the wear life, reduce porosity in the gold plating, and act as a migration barrier to the copper in the base metal.

Signal and low-power applications utilize a multiple-crossing module design made up of inner and outer housings, as shown in Figure 3. The inner and outer housings consist of inner and outer contact rings, each encased in a dielectric epoxy material. Depending upon the application, each crossing utilizes one or more flexures. Multiple flexure designs employ parallel tracks in each contact ring. A typical signal module design utilizes a pair of flexures in parallel tracks and can transfer up to 10 A at 120 V dc. Isolation of 45 to 70 dB can be provided between crossings. Surge currents to 100 A, shock loads to 300 g, and frequencies from dc to 200 MHz have been tested. Assembly of roll ring modules is straightforward, requiring only installation of flexures between inner and outer housings.

Power crossings utilize a multiple-flexure design for high-power transfer. Each power crossing consists of an equal number of flexures and idlers, an inner and outer contact ring, and two idler guide tracks. A typical power crossing is depicted in Figure 4. Power is transferred from one contact ring, through multiple flexures, to a second contact ring. Idlers separate each flexure and are captured by idler guide tracks, which are in turn attached to the inner contact ring. Idlers allow contact velocities of each interfacing component to be matched, minimizing sliding and associated drag torque and wear. Operational drag torque less than 1.1×10^{-2} Nm (0.1 in.-lb) per crossing is a measure of near-zero interface sliding.

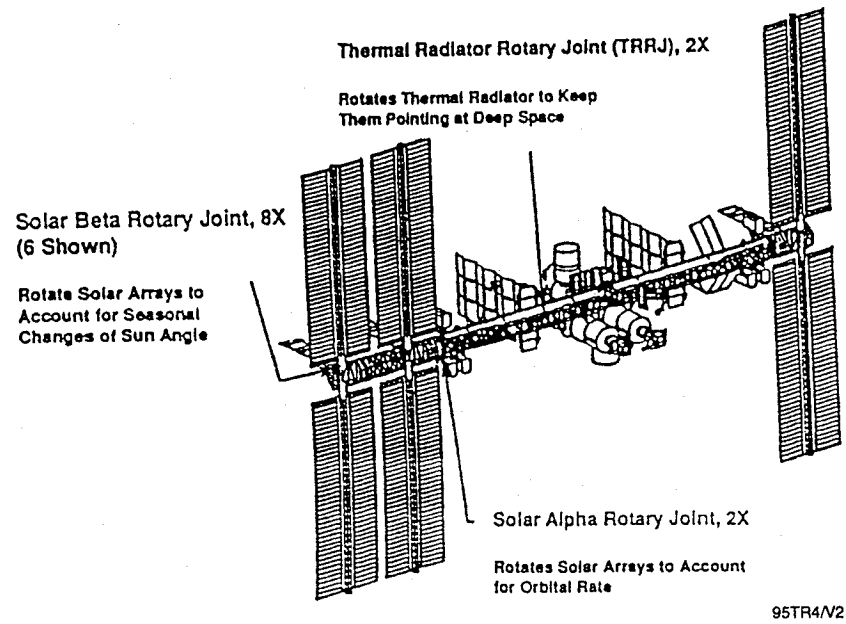


Figure 1. Roll Ring Locations on Space Station Freedom

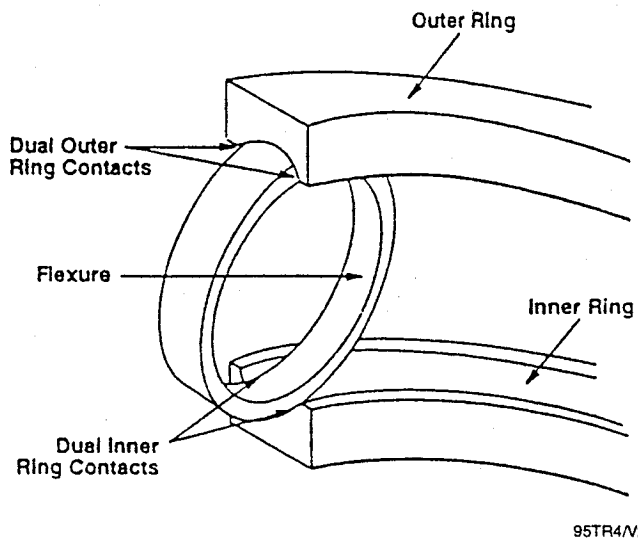
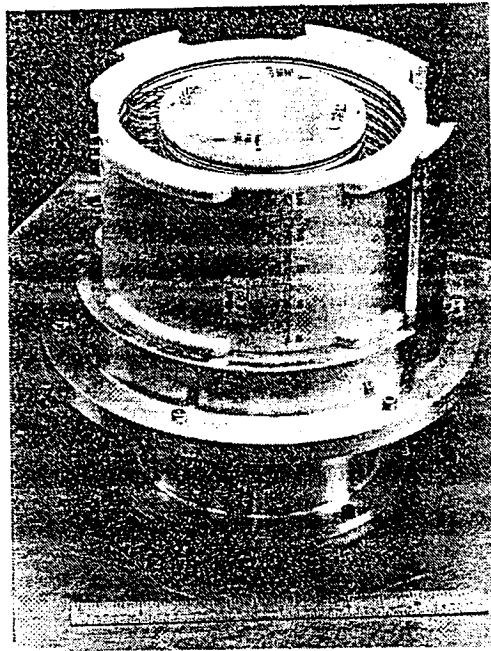
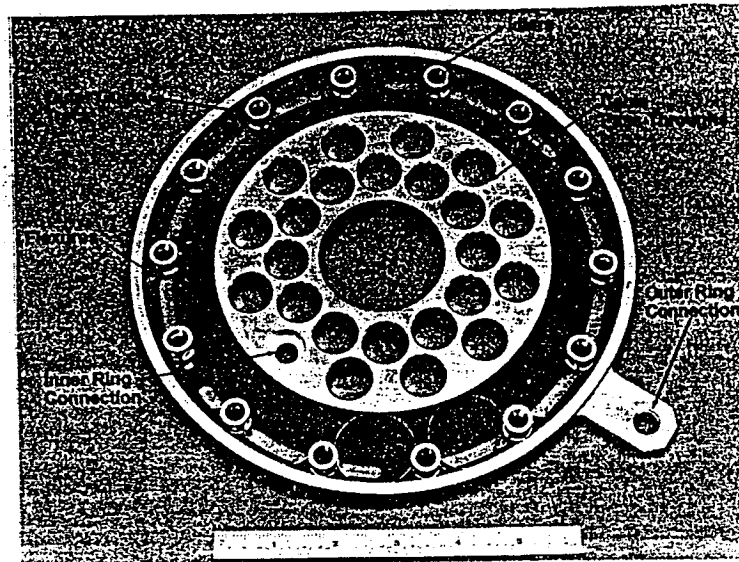


Figure 2. Signal Roll Ring



95TR4/V2

Figure 3. Signal Roll Ring Subassembly



95TR4/V2

Figure 4. High-Power Roll Ring Crossing

Testing:

Wear and flexure fatigue testing has been conducted to over 3.2×10^7 revolutions of the inner ring in a vacuum environment and 1.6×10^8 revolutions in air. The resultant wear debris of the latter unit was of extremely low volume and consisted of gold dust adjacent to the running tracks. In summary, the roll ring design exhibits low and consistent torque, has near-zero wear debris, and has no time-related effects; thus, it is an excellent choice where long-life requirements are to be met.

The space station roll rings were subjected to noise resistance, word error rate, high-frequency video, resistance tests, current in-rush, and drag torque with excellent results.

Key Words:

Slip Rings, Brushes

Mechanisms:

Slip Ring Assemblies

Systems:

Rotating System

Authors; Experts:

Donald N. Matteo

Address:

General Electric Company
Space Systems Operations
Valley Forge, Pennsylvania

Telephone:

Title:

Improving Slip Ring Performance

Source:

18th Aerospace Mechanisms Symposium (1984).

Abstract:

The use of dry film lubricated, silver bearing slip ring/brush combinations is not new to space applications. This type of slip ring assembly has enjoyed considerable on-orbit success; however, recent experiences have indicated the need to improve the dynamic noise performance of the slip rings. The paper describes the original slip ring design for the DSCS III spacecraft, the handling and testing of the slip ring assembly before launch, the on-orbit performance indicating the need for the improvement in dynamic noise, the subsequently incorporated design improvements, and the results of testing to verify noise performance improvement.

PRECEDING PAGE BLANK NOT FILMED

PAGE 372 INTENTIONALLY BL

Anomalies:

Dry film lubricated, silver bearing slip ring/brush combinations have enjoyed considerable on-orbit success but, recent experiences have indicated the need to improve the dynamic noise performance of the slip rings.

Lessons Learned:

- To initiate noise, some form of dielectric contamination must exist at the slip ring/brush interface.
- A reduction in brush spring force to significantly less than the design minimum force must occur to render the slip ring assembly susceptible to the contamination.
- The fewer the number of brush/ring sets in contact with each signal circuit, the more statistically susceptible the circuit is to contamination-induced resistance variations.
- Critical sensor signals should be carried by two parallel slip rings, thus placing four brushes in parallel.
- Synchronization of sensor sampling times and drive pulses must be maintained at all times.
- Slip ring assemblies of this type must be purged with clean, dry nitrogen at all times (except when precluded by other tests) up to as close to launch time as possible.
- Margin above nominal brush force (approximately 80%) should be provided to account for in-process or in-service degradation.
- The individual brushes of a brush pair should be electrically separated to enable in-process measurement of individual brush/ring contact resistances during testing.
- Whenever possible, critical signals should be amplified before passing across the slip rings.

Description:

The slip ring assembly in question is part of the solar array drive and power transfer assembly for the DSCS III spacecraft. The paper concentrates on the slip rings that carry control signals only.

The slip rings are hard silver plated, over copper, which is plated over the epoxy rotor. Epoxy barriers between the rings prevent shorting. The brushes are stackpole SM-476 (a silver, MoS₂, and graphite composition) that are soldered to Glidcop AL20 brush arms. There are two brushes per signal ring that are electrically and mechanically interconnected by the brush arms. Brush force is maintained at 23 gm nominal. Many of the signals passing through the slip rings are used in the attitude control systems of the spacecraft. Recognizing the sensitivity of the spacecraft performance to slip-ring-induced noise, several precautions were taken before the first DSCS flight to control any noise to a tolerable level.

These precautions were:

- A specification of 800-m Ω maximum (at the system level) was established for any variations in signal ring resistance during all ground testing.
- Analog signals are converted into digital words (counts) for use in the attitude control algorithms. It was determined that proper yaw control would result if noise-induced effects represented less than one count. It was calculated that the sensitivity of the system to slip ring noise was 0.5 to 0.6 counts/ohm.
- During all periods when the slip rings were rotated or vibrated during ground testing (other than thermal vacuum testing), the slip ring assembly was purged with filtered, dry, gaseous nitrogen. This prevented the buildup of a partially insulating film of MoS₂ forming in a moist atmosphere.
- End-to-end systems tests were run stimulating the sensor eyes and monitoring the output of the difference amplifiers, verifying that the output was within tolerance limits.
- The system was designed to sample Sun sensor signals at the time when the contact resistance of the brushes/rings was expected to be most stable, that is when the slip rings/solar array drive shaft were at rest between bursts of motor pulses.

Shortly after DSCS III orbit injection, the solar array drive was commanded to track the Sun, and an oscillation in yaw was detected. The redundant roll Sun sensor loop was selected for control and the oscillations were eliminated. The most likely cause of the oscillations was resistance variation noise introduced by contact resistance changes at the slip ring/brush interface.

A number of possible factors that might have led to the noise were investigated but it was finally determined that variations in brush forces were the most likely reason. Increasing the brush force greater than the nominal 23 gm did not reduce the noise, but any significant reduction in brush force increased the noise. Furthermore, it was established that processes used in fabricating the Glidcop AL20 springs could have resulted in a wide variation of brush force.

For subsequent DSCS spacecraft, the following changes are being implemented:

- All critical signals are now brought across the rotating joint on two parallel slip rings using four parallel brushes. This paralleling drastically reduces slip ring noise.
- The nitrogen purge has been extended so that it now covers the total vehicle life (with the exception of a few hours). This eliminates the possibility of contamination caused by oxidation.
- The brush contact force has been increased from 23 gm per brush nominal to 41 gm per brush nominal.

The brush pairs that were mechanically and electrically interconnected have been electrically separated to enable testing of individual brushes for noise during acceptance testing at the vendor.

The brush spring material has been changed from 0.010-in. Glidcop AL20 to 0.012-in. beryllium copper and the brush attachment has been changed from silver solder to soft solder. Buffer amplifiers have been relocated so that now, amplified signals are transmitted across the slip rings making the system much less sensitive to noise.

Key Words:

Slip Rings, Orbiting Solar Observatory (OSO), Despin Drives, Global Positioning System

Mechanisms:

Slip Rings

Systems:

OSO, Despin Drives, Global Positioning System

Authors; Experts:

Damon D. Phinney

Address:

Ball Aerospace Systems Division
960 6th Street
Boulder, Colorado 80302

Telephone:

(303) 442-7824

Title:

Slip Ring Experience in Long-Duration Space Applications

Source:

NASA Conference Publication 2423, Revised 20th Aerospace Mechanism Symposium.

Abstract:

In 1978, SEASAT suffered a disastrous power system failure after three months of successful operation. The probable cause was a short somewhere inside a slip ring assembly.

This paper reviews Ball Aerospace Systems Division (BASD) experience with slip rings in space, presenting design and application experience for several different types.

PRECEDING PAGE BLANK NOT FILMED

Anomalies:

- A power failure happened on SEASAT in 1978. The probable cause was a short in the slip ring assembly.
- A high-resistance short between two rings occurred during the 18-month life test of the slip rings for OSO-6. A minute crack in one of the 0.010-in. thick epoxy barriers between rings was discovered, into which debris had infiltrated. Cracks are not tolerable and must be weeded out by microscopic inspection.
- For self-lubricating contact-type slip rings, BASD has experienced high electrical noise levels during or immediately following operation in air. The Ag/MoS₂/C brush on silver is outstanding in vacuum, but it is not good in air.

Lessons Learned:

- Provide adequate and proper lubrication of the rings and brushes when self-lubricating contacts are not employed. A liquid lubricant is necessary if significant rotation is involved. BASD's most widely used lubricant consists of a highly refined mineral oil with extreme pressure additive. Recently, a synthetic oil with improved characteristics has come into use. With the mineral oil, reservoirs are placed along the brush access slots in the housing. The vapor pressure of the new oil is so low that the surface films are sufficient for multiyear missions and reservoirs are not required.
- Measure brush forces and correct if required. Brush force must be set carefully. BASD rings have used 3 to 5 gm of force and lubricants that produce a friction coefficient of 0.3 to 0.5.
- Brush wear particles remain under the brush pad and provide an additional lubricating medium which prevents further wear.
- The precaution of side-side brushes is unnecessary because of the 5-yr demonstrated life with single-groove rings.
- For self-lubricating brushes:
 - Coat the brush springs with thin films of polyurethane.
 - To minimize vibration problems on brush assemblies of this type, brush pads should be a minimum height of <0.090 in.
 - The Ag/MoS₂/C brush on silver is outstanding in vacuum, but it is not good in air. To eliminate electrical noise, slip rings with this brush material should only be operated in dry nitrogen or vacuum.
 - Remove all humidity before starting.
 - Power brushes are operated at current densities in the 100- to 150-A/in.² range for space applications and contact pressures of 6 psi. Signal brushes commonly have pad face areas in the 7×10^{-3} in.² range (0.060 × 0.12 in.) or less and brush force is set at approximately 20 gm.
 - Friction coefficients are in the 0.25 to 0.50 range.

- Conduct hard vacuum run-in tests followed by disassembly, run-in wear debris removal, reassembly, and checkout.
- Evaluate slip ring performance during drive acceptance tests, which should always include thermal vacuum operation.
- Maintain coordination with suppliers. They have developed significant experience and knowledge. Sources include: Electro-Miniatures Corp., Moonachie, New Jersey; KDI Electro-Tec, Blacksburg, Virginia; and Litton Industries, Inc., Poly-Scientific Division, Blacksburg, Virginia. Prepare definitive specifications; conduct detailed review of suppliers design, materials selection, and processes; and inspect critical manufacturing and test operations at the supplier's facility.

Description:

First OSO Slip Rings. The slip ring design is available from Electro-Miniatures Corp., Moonachie, New Jersey. Figure 1 shows three views of the 22-ring Electro-Miniatures assembly used on OSO-6. Slip rings are coil-silver disks clamped against opposite sides of a laminated phenolic washer by short tubular phenolic spacers. Brushes are silver graphite buttons on the ends of beryllium copper leaf springs (two per ring). The buttons are 0.090 in. diameter, 0.060 in. long, with hemispherical ends. The hard vacuum rating was 3 A per ring. Brush springs are stacked between rectangular phenolic spacers. The two large cylindrical objects are porous sintered nylon blocks impregnated with lubricating oil. No bearings were used in the slip ring itself, the rotor was mounted on the end of the despin drive shaft, and the brush rigging was fastened to the drive housing inside a sheet metal cover.

Wire-Brushed Slip Ring, Double-Grooved Type (manufacturer KDI Electro-Tec, Blacksburg, Virginia). A variation of the slip ring just described is shown on Figure 2. It uses rings with two V-grooves. Brush wires are bent into a tight hairpin and the ends lie side by side in the two grooves (instead of straddling the ring). This design was used in the slip rings for DSCS-II despin drives developed in the early 1970s.

Two variations of the DSCS-II slip rings were built, one with 90 rings and another with 100. Each of these had 58 signal rings on a 0.5-in. diameter section of the rotor, with the balance being power rings rated at 2 A each on a 1 in. diameter. Signal brushes used 0.012-in. diameter wires flattened at the ends, while power brushes were 0.015 in. in diameter. Axial ring pitches were 0.0066 and 0.078 in. for signal and power, respectively, and included 0.015-in. wide debris barriers. The 100-ring unit was 9.38 in. long by 2.62 in. in diameter and weighed less than 3 lb.

Experience:

Between 1962 and 1969, six OSOs were flown accumulating a total of more than 18 yr of operating time before shutdown. With the despin drive turned off during orbit night, about 200 million drive revolutions or 3 billion slip ring revolutions were accumulated with no known slip ring problems. One of these units with its tiny brushes operated at 30 rpm for more than five years (60 min on, 30 min off) in OSO-5. One contributing factor was the effectiveness of the lubricating oil (used to replace the effectiveness of water vapor in air for terrestrial applications) and the wear mechanism that this oil helped to promote. A small amount of brush wear, generated during early operation, remained under the brush pad and provided additional lubrication, effectively eliminating further wear.

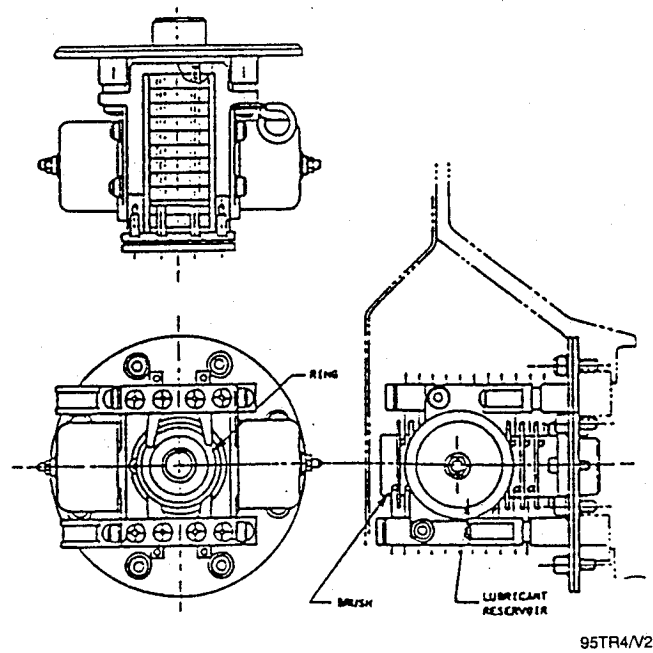


Figure 1. OSO-6 Slip Ring Assembly

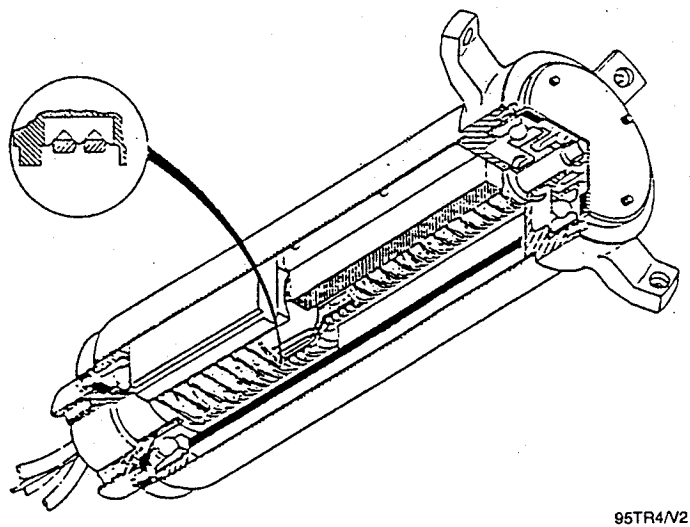


Figure 2. Wire-Brush Slip Ring with Double V-Groove Rings and Side-by-Side Brushes

Wire-Brushed Slip Ring, Single-Groove Type. The units are made by Litton Industries, Inc., Poly-Scientific Division, Blacksburg, Virginia. Figure 3 shows a slip ring widely used for low power and signal applications. It has hard gold wire brushes and soft gold rings with a hard gold flash. Rings are V-grooved so that the brushes are laterally stabilized, while the bottom of the groove provides a lodgement for wear debris away from the brush track. In the more common configuration, the brush wire is formed into a U-shape with both ends in the ring groove.

The advantage of this design is high ring density. BASD has used them with 25 rings/in. in 40- and 66-ring assemblies. Many more rings can be provided, and even closer ring spacing is used, especially with very tiny slip rings. With 15-mil brush wires, a ring and brush set would be conservatively rated for 2 A in vacuum.

The rotor consists of rings embedded in epoxy cast over a metal shaft rather than being assembled by stacking individual components. Rings are plated into grooves that are machined in the plastic, machined to final shape, and then flashed with hard gold. For space applications, a ceramic filler is usually added to the epoxy to bring its expansion coefficient down into the range of the shaft that holds the brushes for every other ring (Figure 3). The housing is slotted to let the brushes onto the rings and provide access to the brush ends for brush force checking and adjustment.

A new OSO slip ring with 40 rings replaced a 22-ring assembly in the same space on OSO-6. The units were made by Poly Scientific and two assemblies underwent life tests. The assemblies were 2.15 in. diameter by 2.5 in. long.

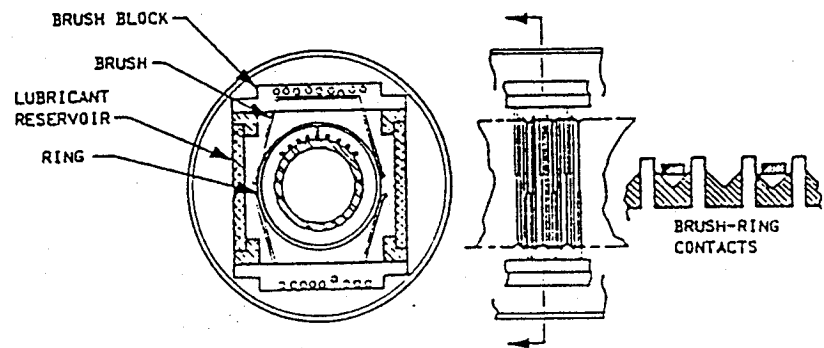
Two BASD spacecraft flew with these slip rings. OSO-7 operated continuously at 30 rpm for 2.8 yr and then reentered. P78-1 operated continuously for 6.4 yr at 30 rpm until it was intentionally shut down. There were no slip ring problems on these two spacecraft.

Ten units have been flown in space and six are still in operation. Launched in pairs, these six units had been going 8.1, 7.1, 6.1 years as of January 1986.

Slip Ring with Self-Lubricating Contacts. For self-lubricating materials, composite brushes of silver, molybdenum disulfide (MoS_2), and graphite (85%, 12%, and 3%, respectively) running on coin silver (90/10 silver/copper) were found to be most satisfactory.

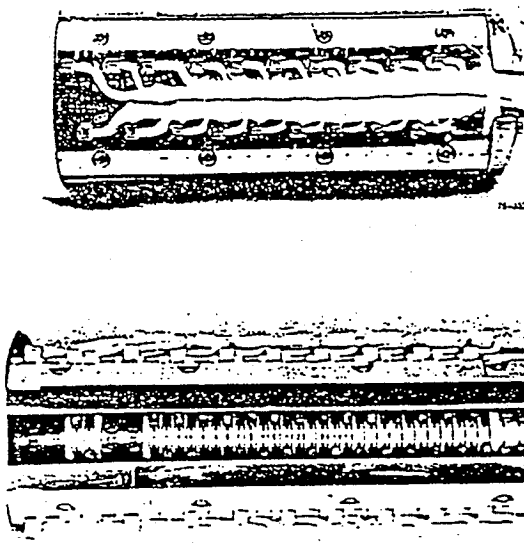
Figure 4 shows the slip ring assembly for the global positioning system spacecraft made by Rockwell International, which had two solar arrays each driven by a separate single-ended drive. Since axial space was restricted, the slip ring assembly was installed inside the shaft with the brush assembly bolted into the shaft. The slip ring rotor cantilevered from a nonrotating plate at the inboard end of the housing. No separate slip ring bearings were used. These assemblies contained 35 rings including four power rings (10-A each), 30 single rings, and 1 electrical bonding ring. Figure 4 shows this assembly from the back of one brush block and from one side looking through a brush inspection slot. The assembly is 4.75 in. long by 1.75 in. diameter. In the global positioning system, slip ring brush assemblies consisted of small rectangular blocks of the $\text{Ag/MoS}_2/\text{C}$ brush material on the ends of U-shaped beryllium copper finger springs. Power rings used four brushes, each operated at a nominal 147 A/in.². Braided copper shunts in parallel with the springs helped carry current from the brush pads to the leads. Signal rings used two brushes each that were individually fastened to a molded plastic brush support structure.

As of January 1, 1986, nine global positioning system satellites with 18 array drives have been launched. Array motion varies from a few degrees to 360° per orbit (two orbits per Earth day) and occurs in steps of approximately 0.1°. Total drive operating time on January 1, 1986, was 89.5 yr with 7.8 yr on the oldest pair. No slip ring problems have occurred.



95TR4/V2

Figure 3. Wire Brush Slip Ring Details



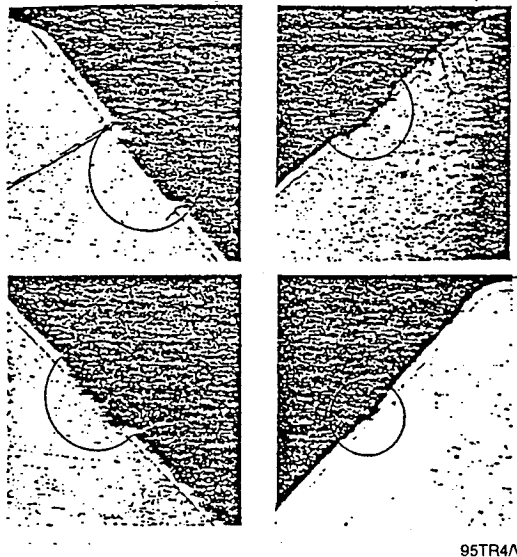
95TR4/V2

Figure 4. Global Positioning System Block 1 Slip Ring Assembly

High-Power Slip Rings. Large spacecraft require high-power slip rings. BASD has completed life tests on four 48-A and two 24-A 125-V dc rings (15-kW total power capacity). The 48-A rings were 2.38-in. diameter fine silver with a hard silver flash, plated up in 0.25-in. wide grooves in a ceramic-filled epoxy. Raised barriers 0.188 in. high and 0.020 in. wide separated pairs of high-side and return rings. The barriers were grooved 0.090 in. deep and stationary disks mounted on the brush blocks fit down into the grooves, providing isolation between the rings and preventing line of sight between exposed elements and ground. Surface creepage distance between rings of opposite polarity was 0.75 in. (enough for more than 500 V). The remainder of the power section included 12 additional rings with a total capacity of 94 A. A 1-in. diameter section of the shaft contained 43 signal rings. Overall length of the complete assembly was 13.1 in. The high-power section of the slip ring described above could handle 500 V because of the built-in isolation and the negligible wear of its contact materials. At 500 V, the 3.6-in. long high-power section would be delivering and returning 60 kW.

Testing:

When suitably lubricated, the tiny brush wires do not wear. Rings only wear until the hard flash is penetrated then wear effectively ceases. In hard vacuum tests on 40-ring assemblies, BASD demonstrated this in two tests lasting 6 and 18 months. In both units, ring wear scars stopped at the soft gold interface. Ring wear on the 18-month sample, based on measured wear scar cross sections, was actually slightly less than that of the 6-month specimen, possibly because the hard gold was not quite as thick. Figure 5 shows microphotos of four representative ring wear scars from the 18-month life test specimen.



95TR4/V2

Figure 5. Wear Scars on Gold Slip Rings After 18 Months at 30 rpm

A single DCSC-II slip ring made by Electro-Tec was exposed to a 6-yr thermal vacuum life test at 60 rpm by Aerospace Corporation, while TRW tested several others for up to three years.

In early development, a vibration test on sample brushes in contact with a dummy slip ring rotor showed brush resonance at approximately 300 Hz. Brushes moved laterally from the weights of the overhung brush pads. The random input was 0.5 g²/Hz. Brush resonance caused chipped brush pads resulting from brushes bearing against the raised plastic debris barriers between rings. Coating the brush springs with thin films of polyurethane completely eliminated this problem.

Toward the end of the 1960s, BASD participated in a slip ring materials test program with INTELSAT and Poly-Scientific. Several brush and ring combinations in self-lubricating and fluid-lubricated combinations were evaluated at the COMSAT Laboratories of INTELSAT in the multispecimen test sets. Each set was run in a hard vacuum at 100 rpm for more than a year (52.5×10^6 revolutions/yr).

Additional References:

1. *Lubrication of dc Motors, Slip Rings, Bearings, and Gears for Long-Life Space Applications*, B.J. Perrin and R.W. Mayer, NASA Technical Memorandum 33-382, Proceedings of the 3rd Aerospace Mechanism Symposium.
2. *The Testing of Contact Materials for Slip Ring and Brushes for Space Applications*, C.J. Pentlicki, 17th Annual Meeting of the Holm Seminar on Electric Contact Phenomena.
3. *Improving Slip Ring Performance*, Donald N. Matteo, NASA Conference Publication 2311, 18th Mechanisms Symposium.
4. *BASD TN70-02, Reliability Analysis for TRW Despin Mechanical Assembly*, Subcontract BE501-SC.
5. *BASD System Engineering Report 3779-003*, 1 July 1981, M.L. Kahn.

Key Words:

Roll Rings, Slip Rings, Signal Roll Rings, Power Roll Rings, Roll Ring Noise and Contamination

Mechanisms:

Solar Arrays, Antennas, Screening Devices

Systems:

General Satellites

Authors, Experts:

Dennis W. Smith

Address:

Honeywell Corporation
Satellite Systems Division
Phoenix, Arizona

Telephone:**Title:**

Signal and Power Roll Ring Testing Update

Source:

23rd Aerospace Mechanisms Symposium, NASA/MSFC (1989); NASA Conference Publication 3032, NTIS No. N89-23892.

Abstract:

The roll ring was developed as a long-life, low-torque alternative to the slip ring. Roll rings showed significant advantages in two orders of magnitude lower torque, low debris generation, and transfer efficiencies well in excess of 99% (including high-power applications). Roll rings have also shown little sensitivity to storage and operating environments, minimizing handling problems and service requirements. A variation of the slip ring, the signal roll ring, was developed to achieve a low transfer noise factor. Life tests of signal

roll rings have accumulated 15 million revolutions with signal noise levels still below the requirements of other programs. Data on these life tests are presented, along with test results from the most recent signal roll ring design. The latest design operates at speeds of hundreds of rpm, with demonstrated life in the tens of millions of revolutions. Power roll rings were later developed, meeting the needs of large power transfers across a rotating joint (as in the space station application). Power roll rings have been tested by NASA-Lewis to the equivalent of 200 yr of space station operation and have carried currents of 200 A per circuit and 500 V dc. In addition, alternating currents have been applied at frequencies of 20 kHz, with 440 V, and 60-A current. Detailed results of these tests are presented, indicating that roll rings are ideal for low-noise-requirement applications.

Anomalies:

Potential problems include: flexure fatigue, signal noise (the presence of silicones is deleterious), circuit isolation, and corona discharge.

Lessons Learned:

- Flexure fatigue of the roll rings must be considered and the rings designed to accommodate specified life cycling.
- Corona effects can be prevented by avoiding line of sight between conductors of different potential and by using appropriate insulation.
- To reduce noise electroplating, matrices have been developed and plating purity and surface cleaning improved. These matrices consist of a copper flash for adhesion, followed by either sulfamate or electroless nickel as a copper migration barrier and a hard underlayment of one of several types of gold outerplatings. The most recent surface analyses indicated that a principal source of noise is from copper and lead oxides on the surface. One of the potential sources of these oxides is the migration through the plating matrix of active substrate metal. As a result, the thickness of the nickel layer was increased from a minimum of 2.5 microns (100 microinches) to a minimum of 5 microns (200 microinches).

The type of nickel was also changed from sulfamate to electroless to provide a denser barrier. The final gold layer is either a hard gold alloy, used particularly on the flexures and sometimes on the rings as well, or pure soft gold, often used on the rings to provide a relatively compliant track for the harder flexures. The gold-plated layers are typically about 125 microinches thick. If the hard gold alloy is used on both the flexure and ring, very little wear is evident; however, the contact resistance is somewhat increased. This outer gold layer is also a potential source of contaminating oxides, due to impurities in the plating itself. Extreme care is required in the plating process to minimize the potential for contaminants, particularly copper and lead, which are commonly present in plating equipment. Careful monitoring and scavenging of the plating baths are required to minimize contaminants, particularly when other specimens are plated in the same bath.

- A high correlation was found between the presence of silicones in the system and resultant electrical noise. Although the exact form of the nonconductive silicone-containing film was never identified, several sources of silicone contamination were eliminated from the test system. The primary source was silicon grease used to lubricate gearheads in the test fixture drive located in the vacuum chamber with the roll ring. Elimination of these silicone sources resulted in greatly improved electrical performance.
- Once the plating is applied with great care and purity, contamination from outside sources must be avoided. Primary sources of outside contaminants include organic films, silicone and metallic oxides. Outside sources of metallic oxides include migration from nearby components, such as solder used to attach the lead wires. For that matter, the lead wires themselves provide a potential source of copper contamination. The location of solder lugs for the rings in the Holloman signal roll ring design reduces the potential for noise. These lugs were molded into the inner and outer rings. When the curvature of the raceway was subsequently machined into the ring, it also cut into the lug. Therefore, when the raceways were plated, the lugs were part of the substrate. The result is that the soldering operation is separated from critical surfaces by the plastic ring.
- Particularly important in a signal roll ring application is the isolation of adjacent circuits.
- For high-power transfer, a multiple flexure design in which the flexures are separated by rolling idlers, is required

Description:

Roll rings, as replacements for slip rings, have been under development since 1975. Their configuration is essentially one or more circular flexures (rings) captured by their own spring force in the annular space between two concentric conductors or contact rings. These inner and outer contact rings are rigidly mounted to the rotating and fixed sides, respectively, of the rotating axis. The advantages claimed for roll rings include: extremely low drag torque, high-power transfer efficiencies, little wear debris, long life, and low weight (even for high-power usage).

Three basic roll-ring configurations were under development: a single-flexure, 0 to 15-A configuration (Figure 1); a single-flexure, 0 to 3-A, high-speed (200-rpm) configuration (Figure 2); and a 2 to 200-A, high-power configuration (Figure 3).

Testing:

- Life tests have been conducted on a number of assemblies. Table 1 provides data on 8- and 4-circuit assemblies.

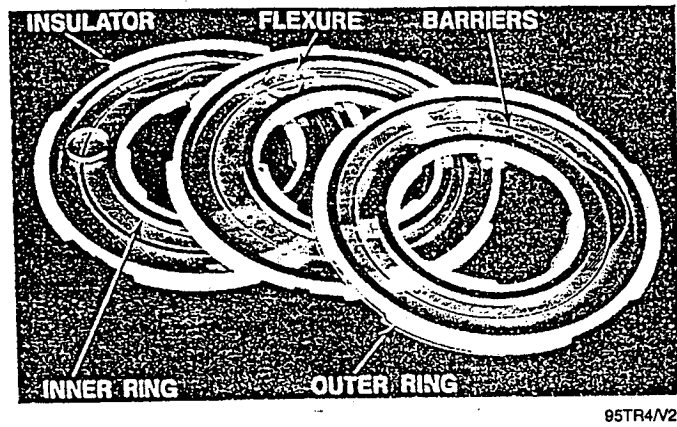


Figure 1. Single Flexure Roll Ring Circuits

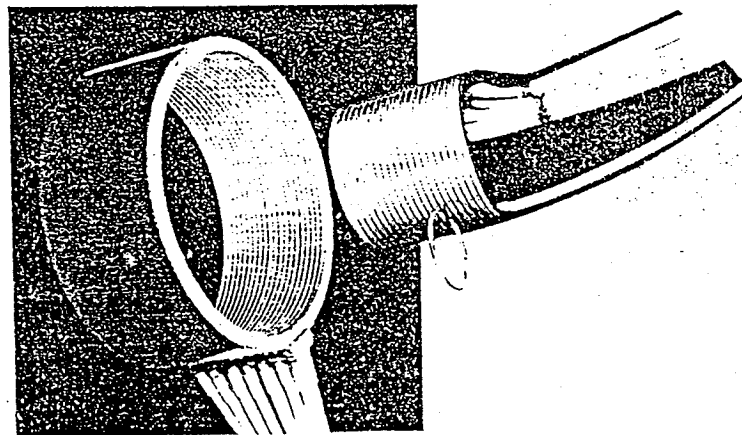


Figure 2. High-Speed Signal Roll Ring

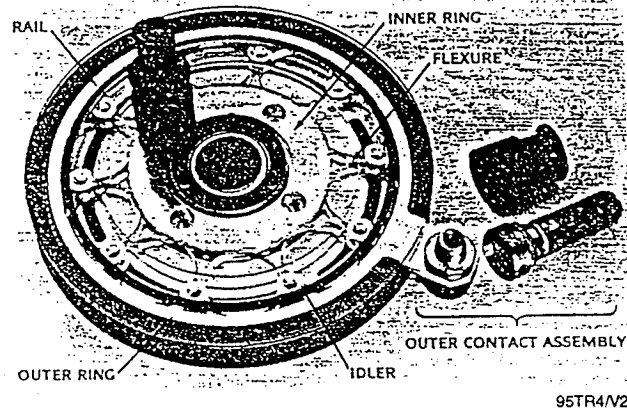


Figure 3. Multiflexure Power Roll Ring

Table 1. Power Transfer Efficiency Data

8-Circuit Roll Ring Assembly		4-Circuit Roll Ring Assembly	
Rolling, SS Years	Efficiency	Rolling, SS Years	Efficiency
20	99,995	20	99,997
40	99,987	40	99,970
60	99,987	60	99,975
—	—	80	99,974
—	—	100	99,966
—	—	114	99,966

Note: Lifetime (rolling station years) and average efficiency (500 V dc, 200 A).

95TR4/V2

Miscellaneous

Key Words:

Space Infrared Telescope Facility (SIRTF), Infrared Spectrograph, Grating Drive Mechanism

Mechanisms:

Filter Wheel, Slit Wheel, Grating Wheel, and Echelle

Systems:

SIRTF

Authors; Experts:

Michael J. Dubitschek

Address:

Ball Corporation
Aerospace Systems Group
Electro-Optics/Cryogenics Division
Boulder, Colorado

Telephone:

Title:

SIRTF/Infrared Spectrograph Cryogenic Grating Drive Mechanism (arc-sec Positioning at 4 K)

Source:

25th Aerospace Mechanisms Symposium (May 1991).

Abstract:

This paper describes the requirements, design, and test results of a grating drive mechanism for the infrared spectrograph science instrument on the proposed superfluid helium-cooled Space Infrared Telescope Facility (SIRTF). The infrared spectrograph grating drive mechanism (tested in fall 1989) satisfied all performance requirements in vacuum at 4 K. Measured mechanism performance included: 1.5-arc-sec rms error positioning resolution, 2.2-arc-sec rms position repeatability error, less than 10-milli-joules/° dissipated power, and $\pm 170^\circ$ angular range of travel. Mechanisms that precisely position optical elements at very low cryogenic temperatures (at or below 4 K) are vital to the operating success of a number of proposed infrared scientific instruments like those in SIRTF.

PRECEDING PAGE IS AWK, NOT FILMED

Lessons Learned:

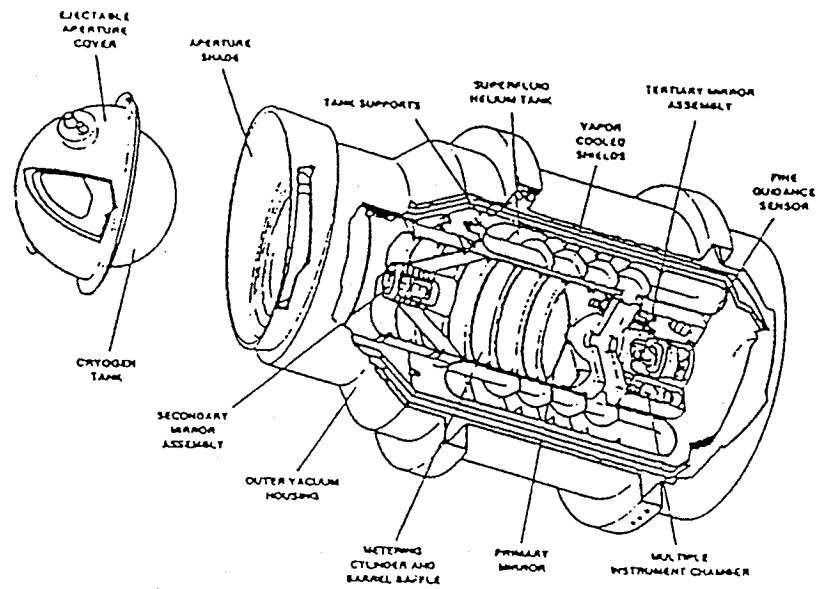
- The amount of preload necessary to maximize mechanism positional performance characteristics in the arc-sec regime involves a trade-off between maximizing system response stiffness in all extraneous degrees of freedom yet minimizing resistive (and most important) nonlinear or discontinuous resistive torques (stiction, Dahl effects, etc.) opposing pure rotation. As the axial preload on a bearing increases, the system response stiffness to undesired motions increases, but so do the unwanted resistive and nonuniform torques (both are functions of preload and lubrication). The approach adopted was to apply 5 lb of preload to the bearings via a diaphragm deflection, which corresponds to approximately a 60,000-psi Hertzian contact stress between the bearing balls and races, and yields an empirical torque minimum for a particular bearing.
- The test data revealed only a slight change in the mechanism stiffness and position resolution performance between temperature limits of 300 to 4 K. The reduction in preload was, in all probability, significant enough to account for the decrease in position resolution by reducing mechanical hardware stiffness and frequency response to the point of introducing nonlinearities that were not as tightly controllable. It is believed that the performance of the mechanism at 4 K could be made to match that measured at 300 K by using a bearing spacer fabricated out of the identical material as the housing (6A1-4V Ti), thus ensuring that the bearing preload remains unchanged over the temperature excursion.
- To avoid undesirable temperature gradients, and barrelling of the bearing, flexible copper thermal strapping was added to both rotating and stationary components.
- To ensure precise accuracy control of bearing preload over temperature range, a flexible diaphragm of similar thermal characteristics was incorporated.

Description:

The infrared spectrograph grating drive mechanism was designed, built, and tested to meet the following requirements in vacuum environment at 4 K: ± 4 -arc-sec positioning resolution for eight separate, equally spaced $\pm 3^\circ$ ranges of grating motion; ± 2 -arc-sec command position repeatability; < 1 mW average power dissipation; $\pm 170^\circ$ rotational travel in a maximum package size of 6 in. dia \times 6 in. length.

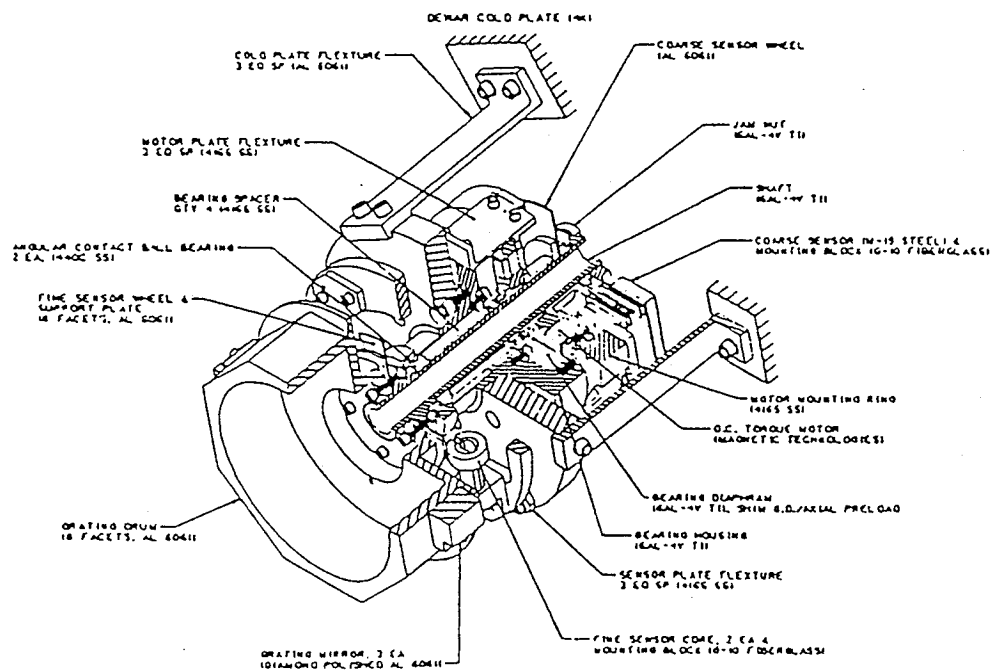
Figure 1 shows the overall design of the SIRTf system and the key elements. Figure 2 shows an isometric cutaway view of the infrared spectrograph grating drive mechanism. The unit is a simple drive mechanism that consists of a hollow rotating shaft that is simply supported by a single pair of angular-contact ball bearings. An 8-faceted grating drum is used to mount test mirrors to the near end of the shaft. The mirrors were later used to verify the angular motion of shaft and drum. The bearings are mounted into the stationary housing and preloaded axially by means of a diaphragm. The physical envelope of the unit is approximately 5 in. dia \times 6 in. length.

The rotating assembly is driven by a brushless dc torque motor. The permanent-magnet rotor is mounted integral to the mechanism shaft, and the stator with armature windings, is mounted into a stationary ring on the housing. The radial and axial spacing of the rotating components is accomplished by individual spacers that fit over the shaft and are shimmed at assembly to coincide with the respective stationary part (stator, housing, etc.) axial locations. The rotating assembly is axially loaded and retained by a jam nut screwed onto threads provided at the far end of the mechanism drive shaft.



95TR4/V2

Figure 1. Cutaway View of SIRTf Telescope Assembly



95TR4/V2

Figure 2. Isometric Cutaway View of the Infrared Spectrograph Grating Drive Mechanism

The mechanism employs two position sensor configurations that indicate the coarse (± 10 arc-min) and fine position (± 1 arc-sec) of the rotating assembly. The coarse sensor is located at the far end of the unit near the torque motor and consists of a rotating, Nautilus shell-shaped cam sensor wheel and a stationary sensor reading head coil. The fine position sensor assembly is located at the near end of the unit, adjacent to the grating drum, and is comprised of a rotating 8-toothed sensor wheel (corresponding to the 8 facets of the grating drum) and two stationary fine sensor reading cores. These sensors will be discussed in more detail later in this paper.

The stationary portion of the mechanism is comprised of the main bearing housing, diaphragm and separate mounting rings for the torque motor stator and fine sensor assemblies. The radial location and axial spacing of the mounting rings and housing are handled with three separate, 3-piece sets of mounting flexures that physically link the stationary components together. The cold-plate flexure set also serves as a tripod base that mounts the entire mechanism assembly to the dewar cold plate.

Bearings and Lubrication. The infrared spectrograph mechanism design approach focused on two main objectives: arc-sec position accuracy at 4 K and $\pm 170^\circ$ of rotational travel. The large range of travel dictated the use of ball bearings to support the mechanism shaft. Operation at cryogenic temperatures necessitated dry lubrication in order to maintain bearing torques at uniform, acceptable levels during operation at 4 K. The ball bearings also required a compliant preload scheme to avoid brinelling during cooldown and required precise control of the preload in order to meet the position accuracy requirements for operation at both 300 and 4 K.

The bearings used for this application were 440C stainless steel, precision (ABEC-7), angular contact ball bearings (bore diameters 0.875 and 0.750 in., respectively), with 440C stainless steel ball separators, manufactured by Miniature Precision Bearing Corp. (MPB). The bearing balls, separators, and races were lubricated with a sputtered, 800 Angstroms-thick coating of molybdenum disulphide (MoS_2). This particular combination of bearing and lubrication was chosen for a number of reasons based on meeting the most severe position/design-driving requirements at 4 K. Angular contact ball bearings in particular were selected so that the internal radial clearance of the bearing could be eliminated with sufficient preload. The thin, hard-sputtered MoS_2 lubrication coating was selected to ensure smooth rotational motion, minimize torque nonuniformities due to lubrication pile-up, and maintain absolute minimum contamination levels at 300 and 4 K.

Bearing function torque is nominally a function of the bearing geometry (pitch diameter), bearing preload, and ball lubricant. To achieve the required positional accuracy in a cryogenic environment, a single pair of reasonably sized ball bearings consistent with the mechanism package was chosen. The larger diameter bearing (0.875-in. bore) was positioned just beneath the grating drum in order to provide the most stable shaft restraint as close to the grating drum and critical mirror surfaces as possible. The other bearing (0.750-in. bore diameter) was mounted into an axially compliant diaphragm. The compliant diaphragm ensures that the preload level is closely maintained at both 300 and 4 K, without overstressing the bearings throughout the temperature transition. Snubbers were designed and would be used to carry the axial loads on the diaphragm for a launch environment.

The thermal contraction of 6A1-4V titanium (6A1-4V Ti) most closely matches that of 440C, while avoiding the extremely brittle properties of the 400-series stainless steels at low temperatures. Therefore, it was chosen for the mechanism shaft, housing, diaphragm, and flexure/motor mounting ring materials. The decision was made to fabricate the bearing spacers and mounting plate flexures out of 416S stainless steel. At the same time, this choice was accounted for by increasing the bearing preload slightly (by approximately 2 lb) at room temperature to offset the anticipated decrease in bearing preload at 4 K, due to the differential thermal contraction between the titanium housing and the 416S stainless steel bearing spacers. Test results show that the bearing preload did decrease somewhat between 300 and 4 K, as predicted, but the diaphragm was compliant while maintaining a preload on the bearings as designed.

There is, however, an unavoidable disadvantage of using either 440C stainless steel or titanium; the lower thermal conductivity of both materials. Low thermal conductivity slows the overall mechanism cooldown, increases temperature gradients, and could possibly limit the mechanism moves or available scientific observation time, due to inefficient removal of local dissipative heat inputs during flight operation. Temperature gradients of more than 100 K between rotating and stationary assemblies were analytically estimated to occur, if uncontrolled during mechanism cooldown. This is due to the small contact area and poor thermal conduction across the interface between the 440C bearing balls and races. There was serious and immediate concern, since temperature gradients of this size were certain to cause brinelling of the outer bearing races. Flexible copper thermal strapping (multiple strands of 44 AWG Litz-wire) was added to both rotating and stationary portions of the mechanism to speed cooldown, efficiently remove dissipative heat inputs, and minimize the undesirable temperature gradients.

Key Words:

Potentiometers, Solar Array Drives

Mechanisms:

Solar Arrays

Systems:

Topex/Poseidon Spacecraft, and Others

Authors; Experts:

Mr. Theodore C. Iskenderian

Address:

Jet Propulsion Laboratory/California Institute of Technology
Guidance and Control Section
4800 Oak Grove Drive
Pasadena, California 91109-8099

Telephone:

(818) 354-2972

Title:

Lessons Learned from Selecting and Testing Spaceflight Potentiometers

Source:

28th Aerospace Mechanism, NASA Conference Publication 3260.

Abstract:

A solar array drive was designed for operation on the Topex/Poseidon spacecraft that was launched in August 1992. The experience gained in selecting, specifying, testing to failure, and redesigning its position sensor produced valuable lessons for future component selection and qualification. Issues of spaceflight heritage, cost/benefit/risk assessment, and component specification are addressed. It was found that costly schedule and budget

PRECEDING PAGE BLANK NOT FILMED

overruns may have been avoided if the capability of the candidate sensors to meet requirements had been more critically examined prior to freezing the design. The use of engineering models and early qualification tests is also recommended.

Anomalies:

- Excessive electrical noise
- Unacceptable wear of beryllium-copper contacts
- Beryllium-copper contact breakage
- When lubricated with Bray 815Z, the lubricant beaded and contained wear debris.

Lessons Learned:

- Wiper contacts of Paliney-7 (a precious metal alloy primarily comprising palladium), silver, gold, copper, and platinum proved effective.
- To assure adequate contact, the contact force was increased to 20 ± 4 cN.
- The above two Lessons Learned indicate that potentiometer contacts must have compatible rubbing characteristics, low friction coefficient, and sufficient preload to assure contact.
- Hub connections should not loosen during vibrations. In this instance, each steel hub was first mechanically fastened to the shaft with two set screw joints (one cone point, one cup point) at 90° to each other, then bonded with a bead of epoxy at the shaft hub interface. The set screws themselves were blocked from backing out by a drop of epoxy.
- The pots should not be contaminated by shipping packages. Individual nylon bags were employed.

Description:

A cross section view of the pot is shown in Figure 1. The resistive and conductive tracks are two annular rings on each element, comolded into the diallyl phthalate (DAP) disk substrate during fabrication. Each pot element is manually trimmed to specified linearity by grinding away small fractions of these comolded resistive tracks by removing material from an annular channel that is cut adjacent to the track for this purpose. A thin electrical wiper contact, whose contact force is controlled to approximately 15 cN, sweeps over each track. As seen in Figure 2, two wipers per element originally made of beryllium copper alloy, are resistance welded to their wiper arm. The wiper arm grips an insulating ring on its respective hub by friction generated through spring force when the arm is sprung open (much like a retaining ring) to install it on the hub.

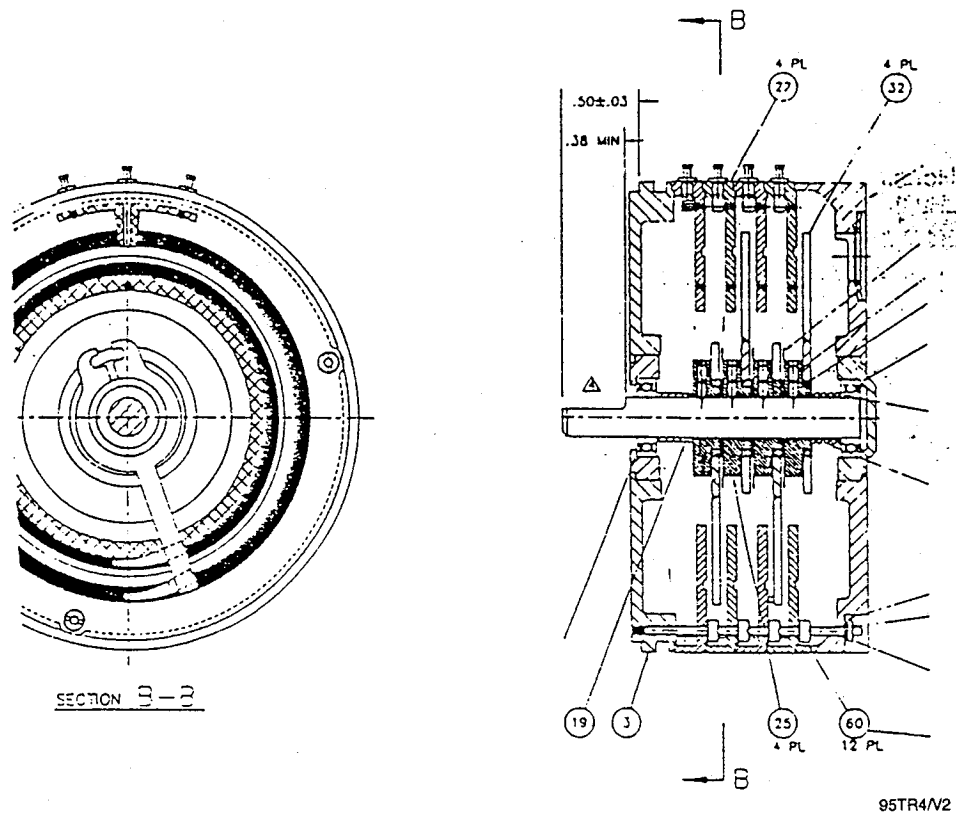


Figure 1. Potentiometer Cross Section

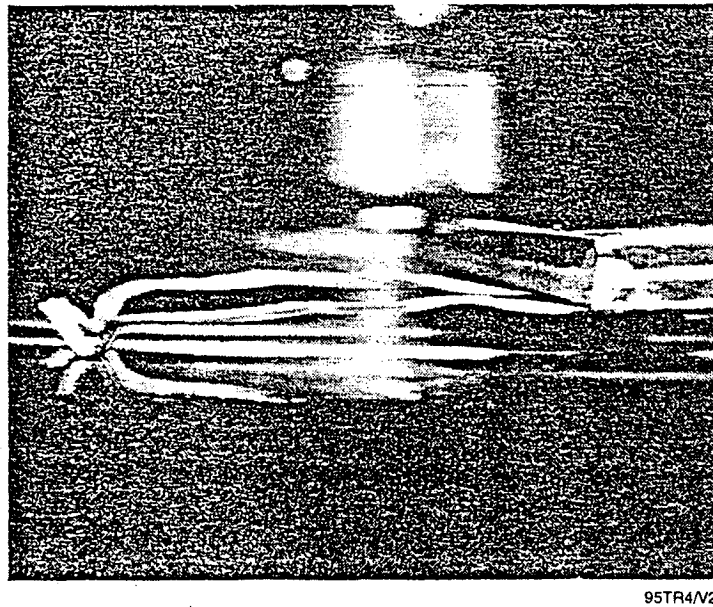


Figure 2. Typical Wiper Contact Pair

Testing:

The purchased pots were exposed to electrical, vacuum, and vibration testing with various progressive improvements. For each of the first three lots of four each, at least one representative unit was completely disassembled and subjected to failure analysis with the hope of finding a solution to pot noise and the other problems. This was a troublesome process because the pot was designed such that epoxy bonds had to be chiseled loose, which generated debris. This debris interfered with the investigator's search for particulate contamination, sometimes yielding ambiguous results.

The failure analysis comprised the following:

- Radiographic x-ray inspection of the units before disassembly
- Scanning electron microscope (SEM) visual and chemical analysis of internal surfaces
- Wiper force measurements
- Macroscopic video records of the pot elements as they were exposed one by one in disassembly.

The first lot displayed a high degree of contamination. It was concluded that the electrical noise was due to loose particles interfering with the electrical contact, and vibration damage to the contact surface.

Pot numbers 005 through 007 were lubricated. Bray 815Z oil was applied to each track during assembly. Severe noise resulted and the oil beaded and mixed with wear debris. Contact lubricant was subsequently abandoned.

The wiper contact force was increased to ± 18 cN, which resulted in crack propagation and fatigue breakage during vibration testing.

New wiper contacts of Paliney-7 were fabricated to a contact force specification of 20 ± 4 cN, and assembled into the final lot, serial numbers 0013 through 0018. This lot passed all screening, qualification, and life testing.

Key Words:

Chopper System, Spectrometer

Mechanisms:

Chopper System

Systems:

Rotating System

Authors; Experts:

1. Arlin J. Krueger
2. August O. Weilbach

Address:

1. NASA-Goddard Space Flight Center
Greenbelt, Maryland 20771
2. Helvart Associates
Fullerton, California

Telephone:**Title:**

Multichannel Chopper System for a Total Ozone Mapping Spectrometer

Source:

15th Aerospace Mechanisms Symposium, NASA Conference Publication 2181 (1981).

Abstract:

The paper describes a multichannel chopper system designed and built to stringent NASA specifications for a total ozone mapping spectrometer. State-of-the-art machining technology, suitable material selection, and a unique way to hold and position the slit plate resulted in the instruments better-than-expected performance. A shutter method used for internal calibration allows compensation for the occurrence of an unlikely wave length shift during testing, launch, or during the orbiting life of the instrument. The total ozone mapping spectrometer was part of a payload on NIMBUS 7 launched October 24, 1978.

Anomalies:

- The required accuracy and alignment of the slit plate and chopper disk could not be achieved when they were rigidly mounted.
- In the presence of thermal gradients and varying environmental conditions, alignment of the slit plate and chopper disk could not be maintained using materials with significant thermal expansion coefficients.
- Conventional milling processes for machining the slit plate and chopper disk resulted in unacceptable distortions of the components. Attempts to overcome the problem using stabilizing and stress-relieving processes were not successful.
- Dry lubrication of the sliding interface between two shafts gave unacceptably high friction.

Lessons Learned:

- Special floating mounts had to be developed for the slit plate and chopper disk to maintain their dimensional accuracy and alignment.
- To maintain dimensional tolerances under varying environmental conditions and in the presence of thermal gradients, the slit plate and chopper disk were made from INVAR 36, a low-expansion metal.
- To achieve the required accuracy and minimize possible distortion from internal machining-induced stresses, electrical discharge machining was used for the final machining of the slit plate and the chopper disk and for machining the apertures in these components.
- For a close sliding fit of two shafts with limited motion, the dry lubricated approach was unsatisfactory and increased the friction between the two parts to an unacceptable level. A very small amount of Krytox oil applied to the inner shaft was the solution.

Description:

The electro-optical design and performance of the total ozone mapping spectrometer required implementation of the sequential display and measurement of each of six selected wave lengths on to a common photomultiplier. Proper processing of the signal output depends, among other factors, on wave length accuracy and repeatability and uniform chopper speed. Accuracy and stability of both the entrance and especially the exit energy is achieved by most accurate and stable slit and chopper apertures and exact registration between both of them.

The total ozone mapping spectrometer housing and all other major supporting and enclosing parts are made of magnesium. The housing is subject to expansion and contraction depending on which temperature level is working. If the expansion/contraction displacements were transmitted to the slit plate or there was an equivalent radial displacement of the chopper disk, it would be impossible to maintain the specified wave length accuracy. This problem was resolved by selecting a low expansion metal, INVAR 36, for both the slit plate and the chopper disk.

Disadvantages of INVAR 36 are high specific weight, difficulties in applying an approved black finish, and its susceptibility to distorting stress buildup under machining operations. To reduce the weight of the chopper disk and to maintain a thin surface around the many apertures, the backside of the disk was reinforced with a web of ribs that provided stiffness and stability to the disk. The need for removal of substantial amounts of material between ribs by conventional milling procedures resulted in immediately unacceptable bending and wobble of the front surface of the disk. Stabilizing procedures and several attempts to relieve stress did not result in sufficient improvement. Consequently, after rough machining, all further material and detail removal was done by electrical discharge machining. Apertures, radial distances, and angular separation were achieved to tolerances less than 0.005 mm (0.0002 in.). Wobble on the front surface was held to better than 0.01 mm (0.0004 in.).

The problems associated with applying a black finish to the slit plate and chopper disk were resolved by plating the part with a controlled thickness of copper and then oxidizing the copper. The temperatures involved in these processes did not create distortion of the parts.

The slit plate is held flat against its mount by six spring-loaded retainers that allow it to move laterally and maintain its axial alignment with the chopper disk.

Figure 1 shows the drive shaft assembly. The chopper disk shaft is supported by a pair of duplexed bearings. The preloaded bearings lubricated by grease plating provide precise, no-play radial control. The chopper disk shaft has an extension that is a slip fit on the motor shaft. To accommodate relative axial motion, the motor shaft and the disk shaft extension are connected by welded metal bellows. There was an obvious need to lubricate the motor shaft/disk shaft interface. Tests with a dry lubrication approach proved to be negative. The MoS₂ particles had a tendency to accumulate in a spotty manner and increase friction between the two parts to an unacceptable level. This problem was solved by applying a very small amount of Krytox oil to the motor shaft.

Vibration tests showed that the motion of the periphery of the chopper disk could be excessive. This problem was easily overcome by Vespel snubber pins on both sides of the disk close to the edge.

Experience:

The total ozone mapping spectrometer instrument was launched into sun-synchronous polar orbit on October 24, 1978, and was activated shortly after. At the time the paper was written (more than two years after the launch), the instrument still continues to function flawlessly in its normal 50% duty cycle of operations.

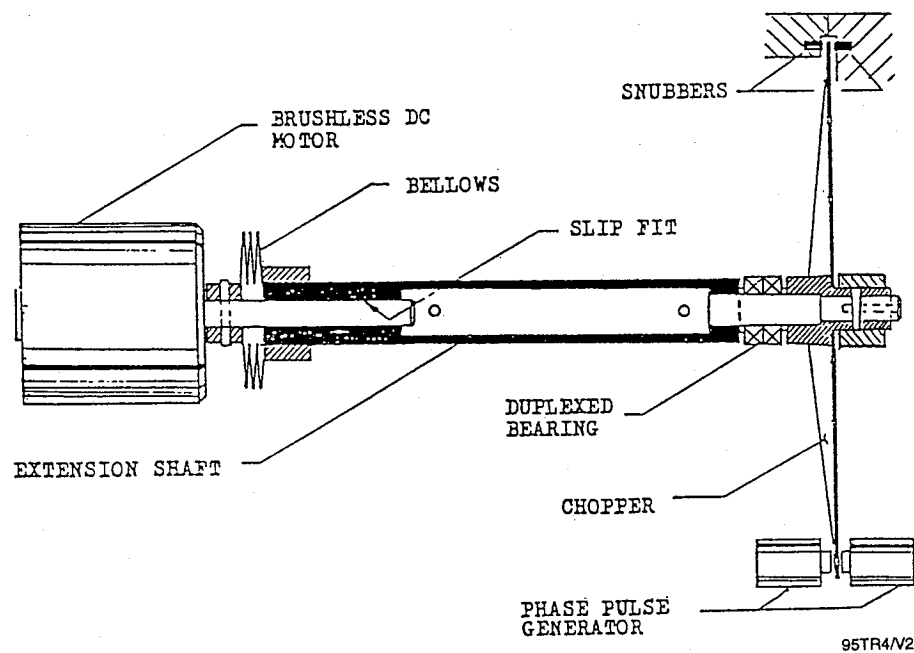


Figure 1. Chopper and Chopper Drive Assembly

Key Words:

Satellite Spin-Up, Payload Spin Assembly, Satellite Launch

Mechanisms:

Systems:

Author; Experts:

1. Wilf Robinson
2. Greg Pech

Address:

1. Honeywell Inc.
Satellite Systems Operation
Glendale, Arizona
2. Martin Marietta
Denver, Colorado

Telephone:

Title:

Payload Spin Assembly for the Commercial Titan Launch Vehicle

Source:

25th Aerospace Mechanisms Conference.

Abstract:

Honeywell Inc., Satellite Systems Operation has completed a contract to design, build, and test a payload spin assembly for installation onto the Martin Marietta Titan III commercial launch vehicle. This assembly provides launch support for satellite payloads up to 5783 kg (6.37 tons) and controls release, spin-up, and final separation of the satellite from the second stage. Once separated, the satellite's Perigee kick motor boosts the satellite into its transfer orbit. The first successful flight occurred December 31, 1989. This paper discusses requirements, design, test, and problems associated with this unique mechanical assembly.

Anomalies:

- dc drive motor assemblies failed insulation testing because of brush wear debris and insulation cracking. The problem was resolved by applying a coating of chemglaze to the windings.
- Separation bolts did not fracture after pyrotechnic ignition; it was resolved by changing mix of powder charge and changing undercutting of bolt.
- The slip ring assembly unit had problems in establishing a no-interrupt requirement, as well as equipment needed for verification. Once those problems had been resolved, the unit performed well.
- The spin bearing drag torque, especially at -23°C , was too high. A torque budget of 41 Nm had been set as a goal, but drag numbers as high as 136 Nm were initially measured. The problem was due to a mismatch in the coefficient of thermal expansions of aluminum housings and steel bearing races. This was resolved by interference fitting the steel races into the aluminum housings and then final grinding the steel raceways in place.
- During qualification tests, a major failure occurred during the third spin-up. The spin electronics assembly failed 3 min after test start. All six MOSFET transistors had failed because of thermal overload. It was found that during rapid switching, the MOSFETs became unstable because the designed scrubber circuit could not control the speed of these S-level components. The engineering model components were of lesser quality and therefore slower. The circuit was changed and more inductance was added in the transistor source lead. This resolved the problem.
- Analysis of high-speed V-band separation films showed that the energy absorbers were not being activated and were, in fact, going overcenter and impacting the structure. The links to these absorbers were shortened and a mechanical stop included; lightweight honeycomb was also used. All these measures cured this impact problem, which arose through lack of understanding the fine details of V-band dynamics.
- The payload spin assembly failed to attain full 70 rpm during testing in the thermal cycle environment, the problem being that six of the spin-bearing separators had been displaced from the bearing and wedged together. This displacement occurred because incorrect bearing retainers had been installed, which stemmed from the need to thermal fit the bearing prior to final race grind. Machine access for this grinding had made a reconfiguration of the bearing installation necessary, part of which was redesigned retainers. These were not available at assembly time, so the obsolete configuration was used against the advice of the bearing manufacturer. Schedule pressure is never a reason to ignore sound advice.
- In thermal-vacuum testing, the payload spin assembly again failed to spin-up during the second cold cycle after having shown nominal performance during the first cycle; however, during the first cycle, the payload spin assembly had been clamped together with the spin V-band, which, after the 1-hr soak, had been released. The second cycle configuration was, therefore, entirely different thermally and allowed a major thermal mismatch to occur. The problem should never have occurred because the unit, at that time, was in a nonoperational configuration.

- The electromagnetic interference/electromagnetic compatibility demands on the payload spin assembly were extensive, and testing was a lengthy affair. A total of 80 complete spin-ups were required to cover the entire spectrum and stay within the despin mechanical assembly thermal limits. The test equipment was more of a problem than the unit.

Lessons Learned:

- Motor brush wear debris can present problems. Brushless motors are preferable; otherwise appropriate coatings and lubricants should be applied to reduce debris formation.
- Thermal mismatch of bearing components and housing can cause serious torque and cage problems. The potential problem should be recognized and analyzed prior to build.
- Provide interface with Titan III aft payload adapter and the upper payload Perigee kick motor.
- Provide a system that can support a range of payloads between 1814 kg (4000 lb), $I_z = 868 \text{ kg-m}^2$ (640 slug-ft²), 5783 g (12,750 lb), and $I_z = 5424 \text{ kg-m}^2$ (4000 slug-ft²).
- Accelerate selected payload from 0 rpm to desired speed (between 4 and 70 rpm) in 7 min while applying less than 13.8 kg-m (100 ft-lb) to Titan vehicle.
- Separate the 5783-kg (12,750-lb) payload from a 12,247-kg (27,000-lb) mass at minimum velocity of 0.61 m/s (2 ft/sec) with a tip-off rate not to exceed 0.10 deg/sec.
- Provide structural stiffness of:
 - Axial: $81.35 \times 10^5 \text{ Nm}$ ($5 \times 10^5 \text{ lb/in.}$)
 - Torsional: $9.45 \times 10^8 \text{ Nm/rad}$ ($4 \times 10^8 \text{ in.-lb/rad}$)
 - Moment: $0.11 \times 10^9 \text{ Nm/rad}$ ($1 \times 10^9 \text{ in.-lb/rad}$).
- Payload spin assembly mass to be 195 kg (430 lb) maximum.
- Provide redundant drive motors and electronics with bus current limited to 65 A per channel.
- Environment:
 - Operational temperature of -23 to +60°C (-10 to +140°F)
 - Vacuum level of $>1 \times 10^{-5}$ torr
 - Random vibration at component level
 - Acoustic test at system level
 - An exploded view of the payload spin assembly is shown in Figure 1.

Description:

The principal challenge of the launch vehicle was to spin the payload at rates up to 70 rpm before release. Spin stabilization of satellites destined for geostationary service (altitude 22,000 miles) is required in low earth orbit (altitude 100 miles) before ignition of the satellite's Perigee kick motor to improve orbit insertion accuracy and thus extend the satellite's operational life. This is an adaptation of enhancing rifle accuracy with a spinning bullet.

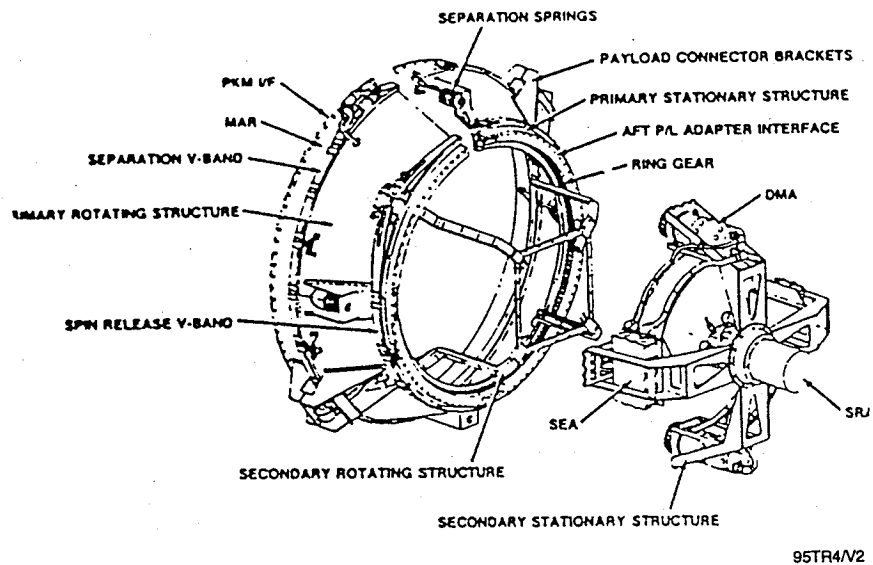
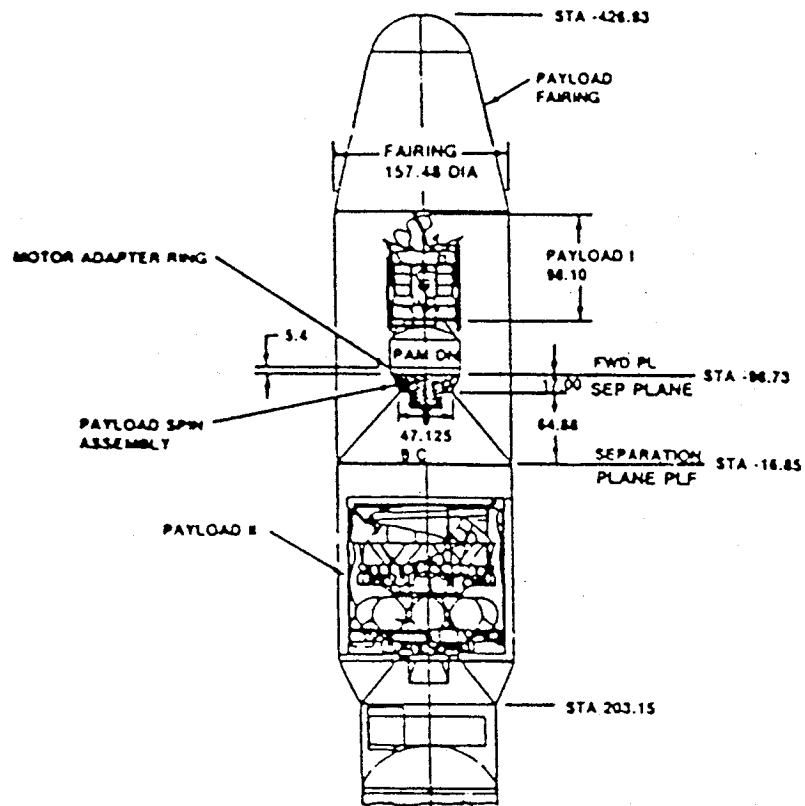


Figure 1. Payload Spin Assembly

The payload spin assembly has been designed and developed to provide structural and electrical interfaces between satellite payload and the Titan III expendable launch vehicle and perform controlled satellite spin-up and release.

The location of the payload spin assembly in its first launch application is shown in Figure 2. This configuration flew and performed flawlessly on the first commercial Titan launch, December 31, 1989, when it spun the SKYNET 4A satellite to 60 rpm. The precise injection of this payload has extended the satellite's operational life well beyond the user's expectations.



95TR4/V2

Figure 2. Commercial Titan JC SAT/Skyenet Mission

Oscillating Systems

Key Words:

Lubricants, Ball Bearings, Shutter, Filter Wheel, Tuning Motor

Mechanisms:

Shutter, Tuning Motor, Filter Wheel

Systems:

Intermittent Rotating Systems

Authors; Experts:

David Akin, Ralph Horber, and Jake Wolfson

Address:

Lockheed Palo Alto Research Laboratory
H. Magnetics Corporation

Telephone:

Title:

Three High-Duty-Cycle, Space-Qualified Mechanisms

Source:

27th Aerospace Mechanisms Symposium (1993).

Abstract:

The Michelson Doppler Imager (MDI) is a scientific instrument aboard the Solar and Heliospheric Observatory (SOHO) spacecraft. In 1995, the spacecraft will be put into a halo orbit about the L1 Lagrangian point (equal sun and Earth gravity). The MDI looks at the sun continuously and takes a picture with a large format CCD (??) camera every 3 sec. The design goal of the mission is 6 yr, during which time 60 million pictures will be taken. The sun, being a high-intensity source, provides a signal with a pixel noise level of 0.2%. Many images are combined to measure the oscillatory motion of the sun so very high performance is required of the mechanisms in order that they do not add noise to the data. This paper describes the design and testing of three mechanisms on the MDI that are required to operate large numbers of times.

0-5. PRECEDING PAGE BLANK NOT FILMED

Anomalies:

The thin-section ball bearings in the tuning motors lubricated with Bray 815Z oil exhibited rapidly increasing friction and did not meet the design life goal.

Lessons Learned:

- For the angular contact ball bearings in the shutter and filter wheel mechanisms, lubrication with Bray 815Z oil met and exceeded the design life goals.
- For the thin-section ball bearing in the tuning motors, lubrication with Bray 815Z oil did not meet the design life goals but lubrication with Braycote 600 grease did.

Description:

The mechanisms described are the shutter, tuning motors, and filter wheels. The shutter precisely controls the exposure time of the CCD camera, and also selects either a magnified or unmagnified beam path. The shutter mechanism is shown in Figure 1. The rotor is supported on a pair of preloaded ball bearings lubricated with Bray 815Z oil.

The Michelson tuning motor assembly, shown in Figure 2, is used to tune the passband of the Michelson interferometers by rotating 1/2-wave retarders. The rotor of each motor is supported by a single, thin-section ball bearing. The bearing is preloaded magnetically.

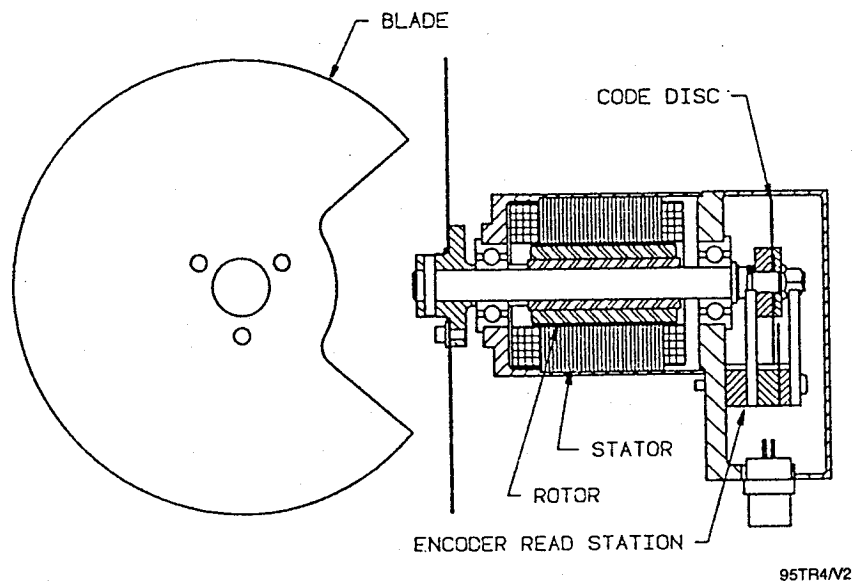
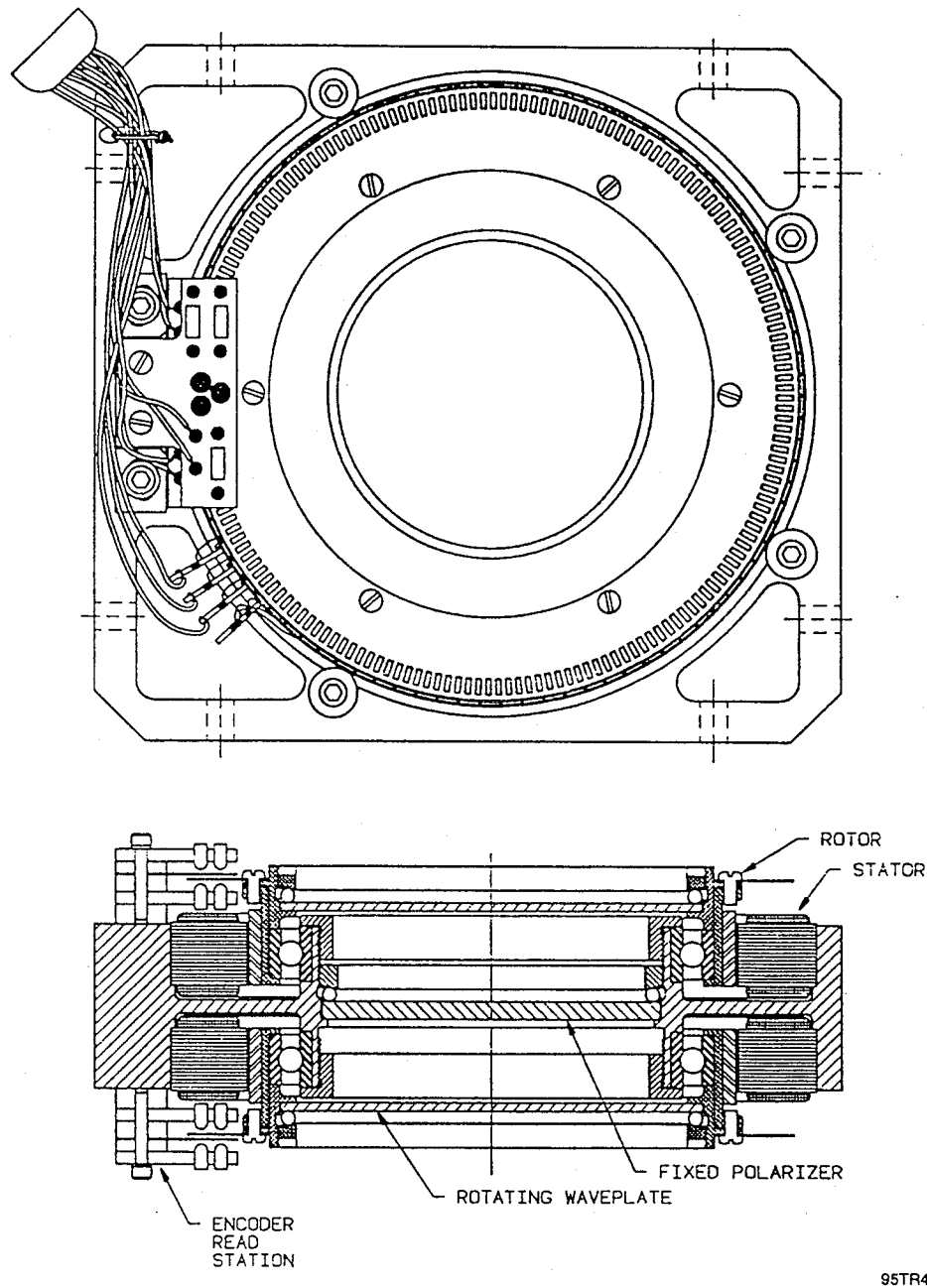


Figure 1. Shutter



95TR4/V2

Figure 2. Michelson Tuning Motor Assembly

The MDI has three filter wheels that are used to place different optical elements into the beam path. The filter wheel assembly is shown in Figure 3. The rotors are supported by pairs of preloaded ball bearings lubricated with Bray 815Z oil. All three mechanisms operate with intermittent small angular motions (less than 360°).

The mechanisms have all undergone extensive life testing in a vacuum chamber. Pressures in the vacuum chamber varied from approximately 10^{-6} to 10^{-7} torr. The shutter and wheel mechanisms were at room temperature and the tuning motors were in a temperature-controlled oven at 35°C . The design goal of the shutter and tuning motor mechanisms is 60 million operations of each, while the design goal for the filter wheels is 2 million operations.

The shutter life test put the equivalent of 67 million exposures on the motor. The friction during the test was essentially constant. Examination of the bearings after the test showed them to be in perfect condition.

The filter wheel test also went to 67 million cycles. It showed a gradual trend of increasing friction and was considered a success because the design life was only 2 million operations. The filter wheel continued to function perfectly throughout the test. Examination of the bearings after this very excessive over test showed them to be in poor condition.

In the first test of the tuning motor, the bearings had Teflon toroid separators and were lubricated with Bray 815Z oil. After 34 million moves, the friction of one of the motors increased at an unsatisfactory rate and the test was stopped. The Teflon separators showed considerable wear.

In the second tuning motor test, the bearings had separators made from SALOX-M, a mixture of Teflon and bronze, and were also lubricated with Bray 815Z. This second test was stopped when one of the motors again exhibited rapidly increasing friction. Examination of the bearings showed a lack of lubrication and a considerable amount of wear debris.

In the third test of the tuning motors, the bearings also had SALOX-M separators but this time it was lubricated with Braycote 600 grease. This test lasted 7 months, put 66 million moves on one motor and 102 million moves on the other, and was stopped after a 6-yr equivalent mission life was reached. Visual examination of the bearings showed them to be in fine condition. Braycote 600 grease-lubricated bearings are being used in the flight tuning motors.

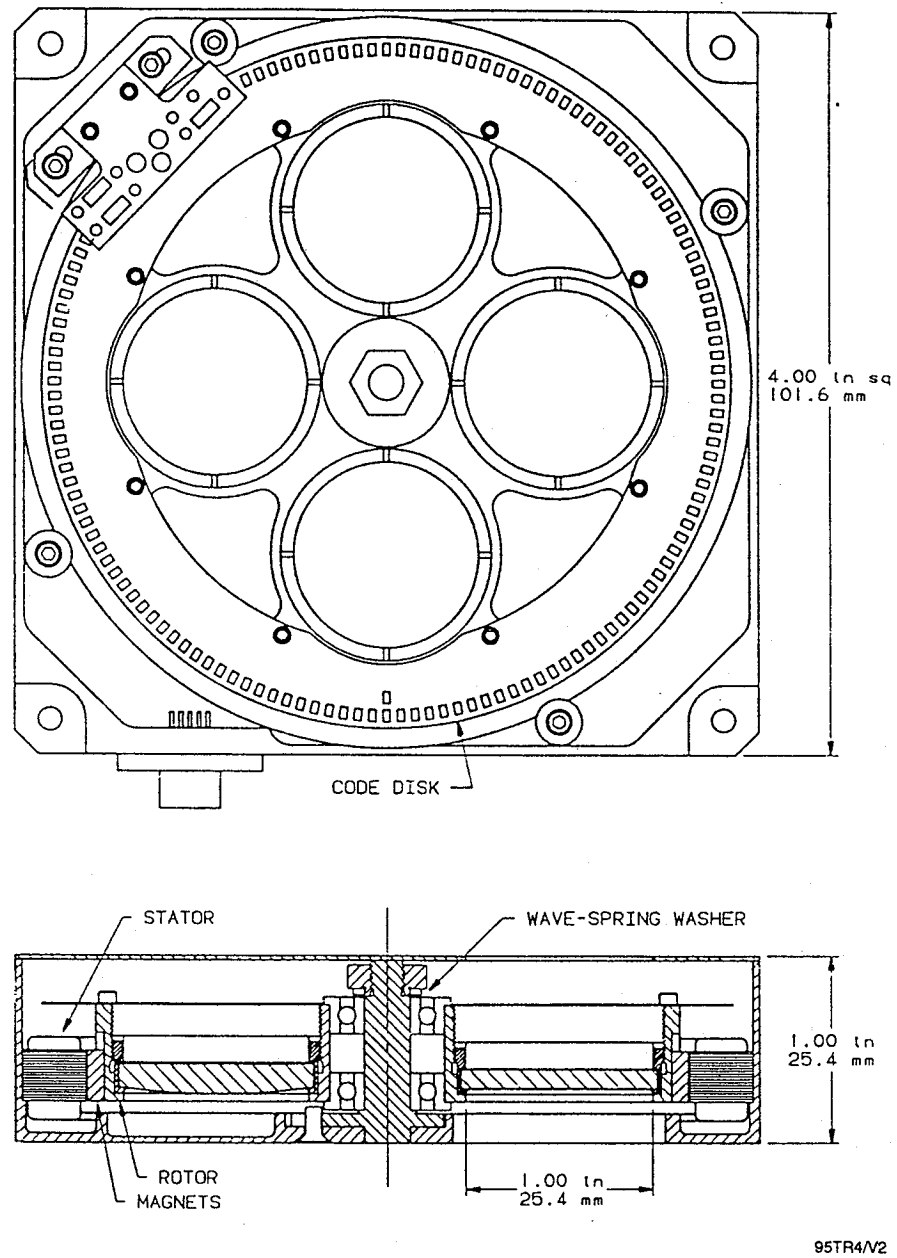


Figure 3. Filter Wheel Assembly

Key Words:

Lubrication

Mechanisms:

Oscillating Mechanisms, Gimbals

Systems:

Author; Experts:

D.J. Carre, P.D. Fleischauer, C.G. Kalogeras, and H.D. Marten

Address:

Aerospace Corporation

Telephone:

Title:

Comparison of Lubricant Performance in an Oscillating Spacecraft Mechanism

Source:

Trans. ASME, Journal of Tribology, Vol. 113, pp. 308-312 (April 1991).

Abstract:

This paper is concerned with a specific application; an oscillating scanner with instrument bearings lubricated by chloroarylalkylsiloxane (CAS). Anomalies in torque values were uncovered during ground tests. To determine if the lubricant was the cause, an experimental program was set up.

PRECEDING PAGE BLANK NOT FILLED

Anomalies:

- CAS oil and perfluoropolyalkylether (PFPE) were seriously degraded under oscillating load and vacuum testing and produced excessive bearing wear and torque noise for <2500 hr of operation.
- One ball in one of the sets of bearings was found to be 0.01 mm oversized and it produced higher torque levels than uniform balls.
- A large piece of metal from the surface of one ball detached and migrated into the cage of the other bearing without getting into the ball track.

Lessons Learned:

- A polyalphaolefin (PAO) lubricant with a tricresyl phosphate (TCP) wear additive did not cause bearing failure and had run 11,000 hr with no indication of a problem. The authors have attributed its success to the TCP antiwear additive. This type of oil should be used for oscillating applications.

Description:

Test Equipment. The test equipment consisted of two ball bearing test cells mounted horizontally on either side of an oscillating drive mechanism, as shown in Figures 1 and 2. The test bearings were R2, ABEC 7 instrument bearings with 7 balls (1.58 mm in diameter) and a cotton-phenolic crown-type retainer. The bearing alloy was not specified (probably 440C). The bearings were used as duplex pairs loaded against each other, so that four pairs of bearings could be tested simultaneously. Three different lubricants were evaluated; some of their characteristics are shown in Table 1.

The drive mechanism consisted of an inertial mass to simulate the optics and sensor array of the actual scanner, a brushless dc motor, and two coiled springs that were installed opposite each other to provide a restoring force for the oscillatory motion. Each bearing test cell consisted of two pairs of R2 bearings that were connected by a shaft to the dc motor. The drive motor was supported on two R4 ball bearings lubricated with the same oil as the closest test bearings. The R2 pair of test bearings farthest from the motor was supported by an SR186 bearing mounted in the housing of the test cell. Torque was measured with four piezoelectric force transducers, which sensed the torque of each pair of test bearings. The tests were run at ambient temperature. However, the temperature of each test cell was monitored so that temperature increases (resulting from higher torque) could be observed. No data were reported in the paper.

Test Conditions. The scanner simulator was oscillated through an arc of +57° at a frequency of about 6 Hz. Each duplex pair of bearings had a preload of 13.4 + 2.2 N. The bearing test facility was mounted in a vacuum test chamber that was evacuated to a vacuum of about $<1.3 \times 10^{-6}$ Pa (-10 torr).

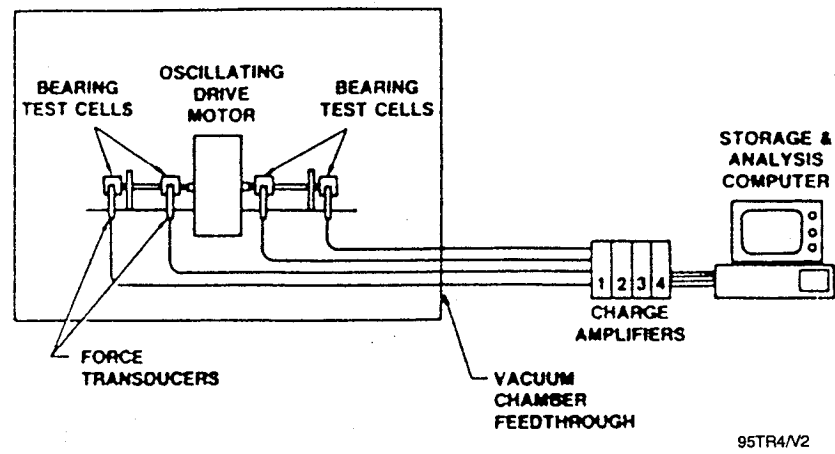


Figure 1. Bearing Test Facility

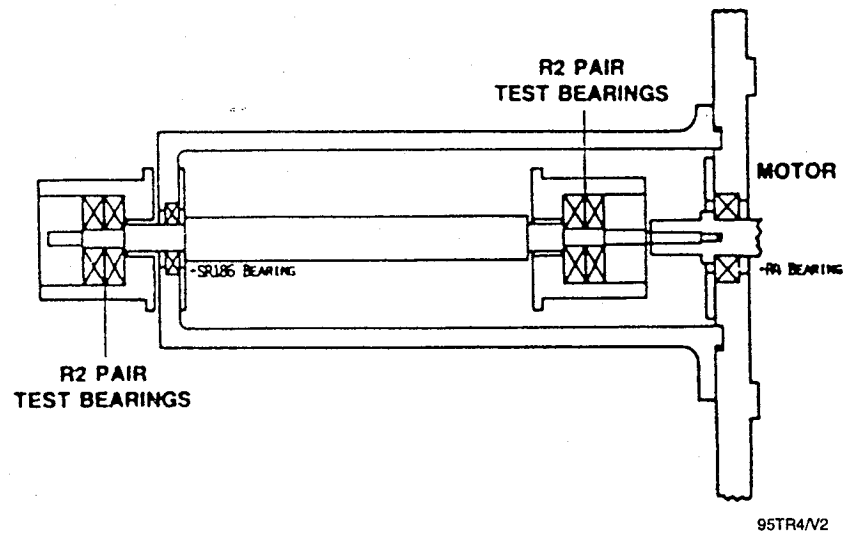


Figure 2. Cross Section of Bearing Test Cell

Table 1. Selected Oil Properties

Property	CAS	PFPE	PAO
Viscosity (cS)			
-40°C	640	2600	—
40°C	52	129	107
100°	16	40	14.5
Viscosity Index	—	350	145
Pour Point (°C)	-73	-73	-55
Specific Gravity	1.045	1.866	—

95TR4/V2

Test Data. In the first tests, CAS and PFPE were evaluated using two bearing pairs. During those tests, malfunctions in the torque transducers on one set of bearings (the ones lubricated with PFPE) resulted in that set being removed temporarily. The other set (with the CAS oil) was run to failure for a life of 1500 hr. The PFPE-lubricated bearings were then returned to the fixture and were also tested to failure (2350 hr).

After reviewing the results with those two lubricants, a new set of four bearing pairs were lubricated with a PAO synthetic hydrocarbon oil containing TCP as an additive, and were put on test. Two pairs were removed for examination after 4300 hr, and a third pair at 6400 hr. None of those bearings had failed. The fourth pair was still running after 11,000 hr.

Results. The wear lives of the bearings with the three lubricants are shown in Table 2. Figure 3 shows the torque traces for one pair of the CAS-lubricated bearings at the beginning and at the end of the 1500-hr test. The torque values decreased, but the trace was noisier. In three of the four bearings, the lubricant was a black solid debris. The fourth bearing showed signs of degradation, but was still lubricated with oil. Similar results were obtained with the PFPE-lubricated sets. The torque trace was noisy and the amplitude had decreased substantially, as shown in Figure 4. This drop in amplitude could be the result of a loss of preload. Inspection of the bearings also showed that in three of the four bearings the lubricant was completely degraded, and the fourth bearing showed signs of lubricant breakdown.

The PAO-lubricated bearing sets gave much better results. Figure 5 shows the torque traces for one of these bearing sets, initially and after 4300 hr of testing. There is essentially no difference in performance. A second set was run for 6400 hr with no apparent problems. Two bearing pairs, one set from the 4300-hr test and the other from a 6400-hr test, were sent to the supplier for inspection. One pair had a preload change from 12.7 to 8.9 N, the other was unchanged at 15.1 N. Slight wear was observed in the ball track.

Two anomalies were found. The first was that one ball in one of the sets was 0.01 mm oversize. This bearing set had given higher initial torque readings, but it was used in these tests because it was the only set that was available. The second anomaly was that a large piece of metal from the surface of one ball had apparently become detached and migrated to the cage of the other bearing, without getting into the ball track.

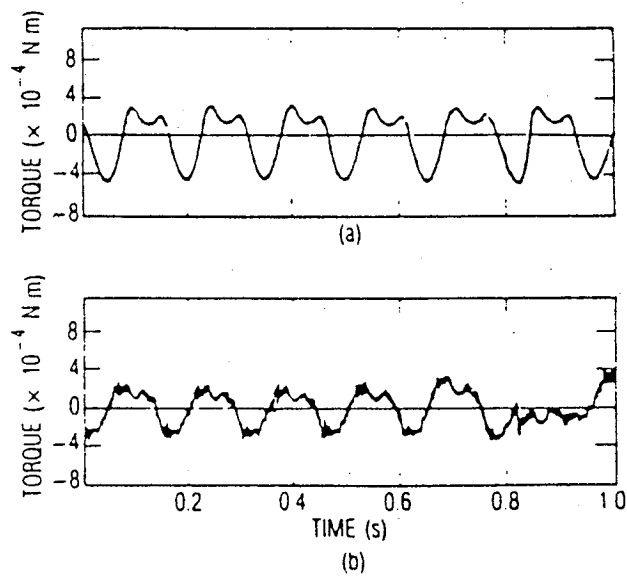
As of January 22, 1990, the third PAO-lubricated bearing set had run for more than 11,000 hr with no indication of a problem. Its success has been attributed, by the authors, to the TCP antiwear additive in the oil.

Table 2. Test Wear Life Data

Oil	Wear Life (hr)
CAS	1500
PFPE	2350
PAO	>11,000*

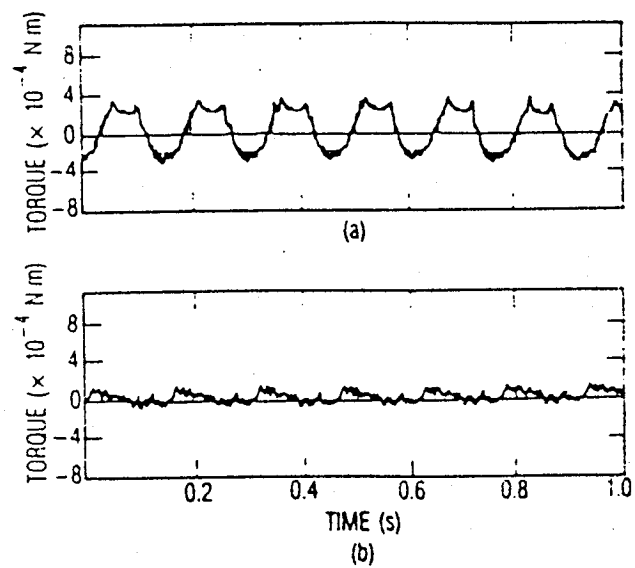
95TR4/V2

*Continuing under test.



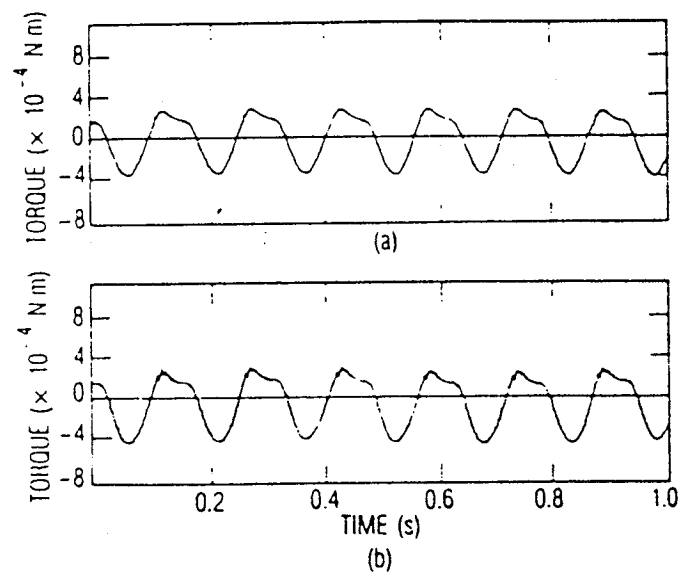
95TR4/V2

Figure 3. High-Resolution Torque Traces for CAS Oil



95TR4/V2

Figure 4. High-Resolution Torque Traces for PFPE Oil



95TR4/V2

Figure 5. High-Resolution Torque Traces for PAO Oil

Key Words:

Molybdenum Disulfide (MoS_2), Dry Lubricants, Bearing Torque, Encoder, Scan Mirror

Mechanisms:

Scan Mirror Mechanism

Systems:

Oscillating System

Authors; Experts:

John J. Bohner and Peter L. Conley

Address:

Hughes Aircraft Company
Space and Communications Group
Los Angeles, California

Telephone:

Title:

On the Torque and Wear Behavior of Selected Thin-Film MoS_2 -Lubricated Gimbal Bearings

Source:

22nd Aerospace Mechanisms Symposium (1988).

Abstract:

During the thermal vacuum test phase of the GOES-7 spacecraft, the primary scan mirror system exhibited unacceptably high drive friction. The observed friction was found to correlate with small misalignments in the mirror structure and unavoidable loads induced by the vehicle spin. This paper describes an intensive effort to understand and document the performance of the scan mirror bearing system under these loads. This effort involved calculation of the bearing loads and expected friction torque, comparison of the computed values to test data, and verification of the lubrication system performance and limitations under external loads. The study culminated in a successful system launch in 1987 and the system has operated as predicted since that time.

Anomalies:

- During the thermal vacuum test phase of the GOES-7 spacecraft, the primary scan mirror system exhibited unacceptably high drive friction.
- Friction becomes too high at ends of travel (oscillating motion). During spacecraft spin tests, torque was also found to be sensitive to spin speed and load.

Lessons Learned:

- The friction torque in dry lubricated bearings can be very sensitive to moments induced by misalignment and other factors.
- Reduce moment loads by using larger race curvatures to reduce alignment sensitivity. Also, shift the frame limit about 5° whenever torque becomes too high so that the balls can roll over the torque bumps at end of travel.

Description:

A schematic of the mirror drive is shown in Figure 1. The mirror is attached at four points to a beryllium support structure. The support is hard mounted to the beryllium shaft of each encoder. The primary encoder is hard mounted to the frame, while the redundant encoder is mounted to the frame through a flexible diaphragm that permits axial motion but maintains radial stiffness. Each encoder contains a pair of thin-section preloaded angular-contact bearings that support the shaft. The balls and races are made from 440C. The bearings are lubricated by a very thin film (3×10^{-8} m) of MoS₂, applied by radio frequency sputtering. The thickness was selected to provide the maximum operational life before the lubricant would pile up and form torque bumps at the ends of travel.

During spacecraft spin testing, the main scan mirror friction torque had to remain below a prescribed maximum throughout the entire mirror scan. During anechoic testing, the drive torque for the spinning vehicle reached a peak of 0.1 Nm. The launch requirement was 0.076 Nm. During the test, it was noted that the drive torque increased significantly as the vehicle spin speed increased.

Tests revealed that the loads on the bearings were much higher than expected. The higher loads were induced by small misalignments in the mirror structure and the vehicle spin. Since changes could not be made to reduce the bearing loads, there was concern that the bearings would not achieve the required life or that the torque might continue to increase with time. Under normal loads, the life of the MoS₂ film was greater than two mechanism lifetimes. Further bearing tests with additional moment loads showed that the life was reduced but it was still between one and two lifetimes. Increases in end-of-frame torque due to debris and race wear were found to be manageable by periodic changes to the frame limits.

During the investigations, it was discovered that the bearings used in earlier vehicles, which had lower torque during spin-up, had been designed with slightly different race curvatures to reduce their alignment sensitivity.

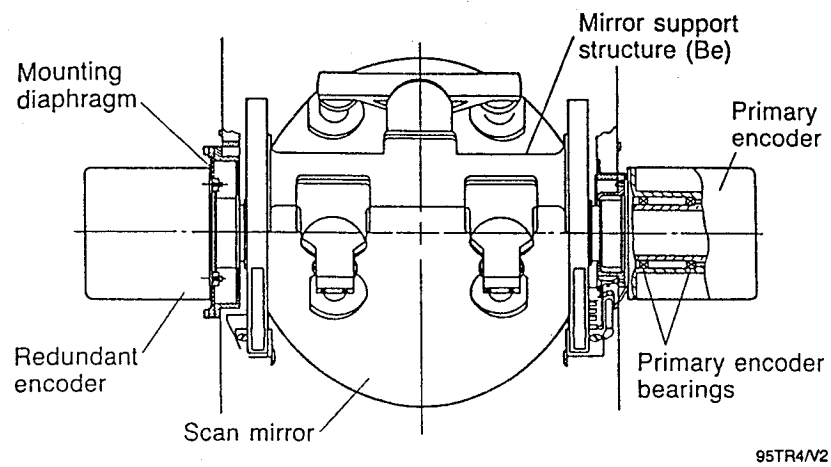


Figure 1. GOES-7 Scan Mirror Drive

Key Words:

Oscillating, Bearings, Solid Lubricants, Cage Lubricants, Liquid Lubricants

Mechanisms:

Gimbals, Oscillating Mechanisms

Systems:

Scanning Devices, Control Moment Gyroscopes

Authors, Experts:

Steven Gill

Address:

European Space Tribology Laboratory
AEA Technology
Risley Warrington, United Kingdom

Telephone:**Title:**

A Comparison of Solid and Liquid Lubricants in Oscillating Spacecraft Ball Bearings

Source:

28th Aerospace Mechanism Symposium, NASA Conference Publication 3260; Viewgraph Presentation at 28th Aerospace Mechanism Symposium.

Abstract:

The European Space Tribology Laboratory (ESTL) has been engaged in a program to compare the performance of oscillating ball bearings when lubricated by a number of space lubricants, both liquid and solid. The results have shown that mean torque levels are increased by up to a factor of five above the normal running torque, and that often torque peaks of even greater magnitudes are present at the ends of travel. It is believed that these effects are caused by a buildup of compacted debris in the contact zone, thus reducing the ball/race conformity ratio.

Anomalies:

- Oscillation = $\pm 0.5^\circ$ (see Tables 1 and 2).
- Self-lubricating cages
 - A rapid torque increase occurs four to five times over the initial 100,000 passes, then the torque stabilizes.
- Dry lubricant films
 - Pb: rapid increase in torque (5x) followed by a gradual rise
 - MoS₂: initial fall then gradual rise (4 to 5x).
- Oil/greases
 - Z25: rapid increase (4x) then stable
 - SHF: X2000 - gradual increase (2x).

Lessons Learned:

- Conformity ratio has a dramatic effect on torque levels (see Figure 1). A buildup of compacted debris in the contact zone, reduces the ball/race conformity ratio and can cause a torque increase of a factor of 5 above normal torque levels.
- Liquid lubricant torque levels are less than cage lubricants or solid lubricants.
- Of the systems tested, the Pennzane SHF 2000 lubricant was the best for all conditions of operation.
- Torque levels dramatically increase when direction changes (see Figure 2).
- Variable angle of oscillations are preferred, particularly for solid lubricants.

Description:

Eight lubricant/cage combinations have been tested as shown in Table 3. The material combinations can be split into three groups: dry-coated bearings (Groups i and ii); dry cage-lubricated bearings (Groups iii through v); wet-lubricated bearings (Groups vi through viii).

For the coated bearings (Groups i and ii), 0.2 to 0.5 μm of lubricant film was applied to each race and, in addition, the MoS₂ coating was also applied to the balls. For the wet-lubricated bearings (Groups vi through viii), the phenolic cages were vacuum impregnated with oil prior to fitting (using Fomblin Z25 in the case of the grease; Group vii).

The test bearings were standard 20-mm bore profile (conformity 1.14) ED20 ball bearings to ABEC 7 specification manufactured from 52100 steel by SNFA. Further details are shown in Table 4.

Table 1. Oscillation = ± 5 Degrees (Anomalies in Bold)

Lubricant	Mean Torque (gm-cm)		Peak Torque (gm-cm)	Comments
	Start	End		
Duroid*	30	550	1200	Very high reversal
Vespel SP3 Cage	170	116	520	Recovered, stable
Salox-M Cage	10	22	60	Stable
Sputtered MoS ₂ /Duroid Cage	12	30	150	Mean stable; peak increasing
Pb + Pb - Bronze Cage	19	220	400	Stabilizing
Fomblin Z25	15	18	25	Stable
Braycote 601	18	17	50	Recovered, stable
Penzane SHF X2000	23	18	25	Stable

95TR4/V2

*130-N preload, test stopped at 6 million passes.

Table 2. Oscillation = ± 20 Degrees (Anomalies in Bold)

Lubricant	Mean Torque (gm-cm)		Comments
	Start	End	
Pb/Pb - Bronze Cage	20	80	Rising at test end
Sputtered MoS ₂ /Duroid Cage	16	84	Rising at test end
Salox-M Cage	145	69	Reducing
Vespel SP3 Cage	60	71	Variable
Duroid Cage*	143	131	Variable
Fomblin Z25	22	18	Stable
Braycote 601	25	19	Stable
Penzane SHF X2000	21	14	Stable

95TR4/V2

*95-N preload.

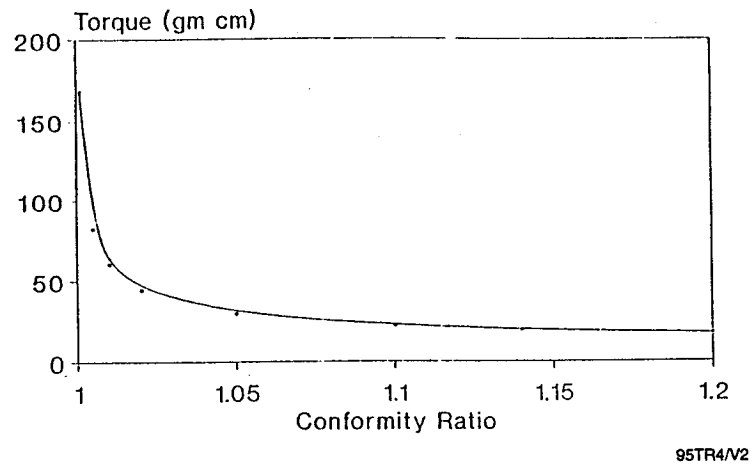


Figure 1. Calculated Torque versus Conformity for a Pair of Test Bearings

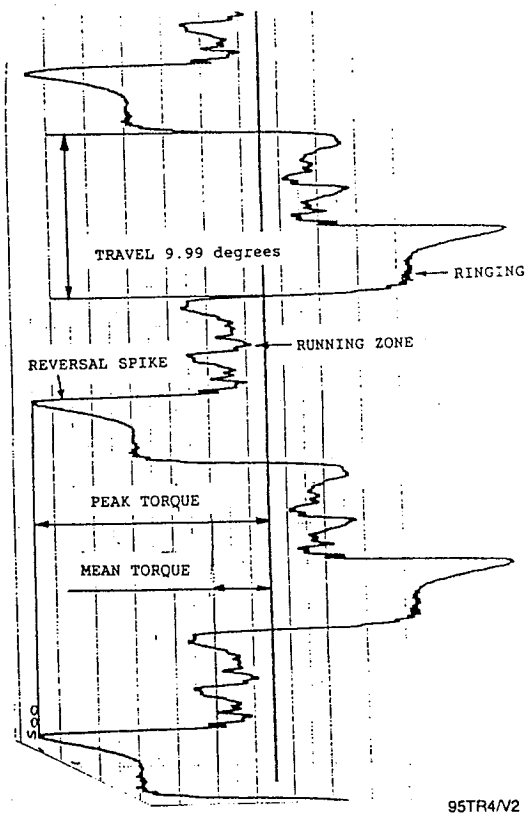


Figure 2. Typical Torque Trace Torque Against Time ($\pm 5^\circ$ Test; Vespel SP3 Cage-Lubricated Bearings)

Table 3. Lubricant/Cage Combinations Tested

Group	Lubricant	Cage Type
i	Sputtered-Coated MoS ₂	Duroid 5813
ii	Ion-Plated Lead	Lead Bronze
iii	Race Uncoated	Duroid 5813
iv	Race Uncoated	Vespel SP3
v	Race Uncoated	Salox-M
vi	Fomblin Z25	Phenolic
vii	Braycote 601	Phenolic
viii	Pennzane SHF X2000	Phenolic

95TR4/V2

Table 4. ED20 Bearing Size Parameters

Outer Diameter (mm)	42
Inner Diameter (mm)	20
Bearing Width (mm)	12
Ball Size (mm)	7.14
Ball Complement	10
Contact Angle (°)	15

95TR4/V2

Testing:

Oscillation Angle $\pm 0.5^\circ$. The coated bearings (Groups i and ii) performed with lower torques than the cage-lubricated bearings (Groups iii through v), although the MoS₂-coated bearings had reached torque levels of 100×10^{-4} Nm by the end of the tested 10^7 oscillatory passes. The cage dry lubricated bearings (Groups iii through v) quickly registered torques of 100 to 130×10^{-4} Nm. For the oil lubricated bearings, the Fomblin Z25 (Group vi) showed a rapid increase to 100×10^{-4} Nm before settling back to 80×10^{-4} Nm, whereas the Pennzane-lubricated bearings (Group viii) only showed a gradual increase from 20 up to 40×10^{-4} Nm over the duration of the test. The Braycote 601 grease-lubricated bearings (Group vii) showed a rapid increase over the first million passes to around 60×10^{-4} Nm and then stayed stable for the rest of the test.

Oscillation Angle $\pm 5^\circ$. The MoS₂-coated bearings (Group i) performed better than the lead (Group ii) in this instance. The lead mean level increased to 150 to 200×10^{-4} Nm over the first 3 million passes, while the MoS₂ mean level remained low at 20×10^{-4} Nm throughout. Both types suffered a reversal peak torque, 300 to 400×10^{-4} Nm, for the lead and 100×10^{-4} Nm for the MoS₂ by the end of the test. Turning to the cage-lubricated bearings (Groups iii through v), the torque of the Duroid-caged bearings rapidly rose to 200×10^{-4} Nm and continued to increase to 600×10^{-4} Nm by 6 million oscillatory passes. At the same time, a reversal peak level of 1200×10^{-4} Nm was attained and so the test was stopped to protect the torque transducer. The torque of the Vespel-caged bearings (Group iv) also rose quickly to a mean level of 200×10^{-4} Nm for the duration of the test. The peak level on reversal reached a maximum value of nearly 600×10^{-4} Nm at 3 million oscillatory passes, but in this case fell back to 300×10^{-4} Nm by the end of the test. The Salox M caged bearings (Group v) performed the best in this category and held a mean torque level of 20×10^{-4} Nm, with a peak of 50 to 60×10^{-4} Nm after an initial short stabilizing period. The wet lubricants (Groups vi through viii) performed in a very similar manner throughout this test, with mean torque levels around 20×10^{-4} Nm and peak torque levels up to 40×10^{-4} Nm.

Oscillation Angle $\pm 20^\circ$. The MoS₂- and lead-coated bearings (Groups i and ii) performed similarly for over half of the test duration, although the lead bearings were noisier on reversal and ran at higher mean torque levels. By the end of the test however, starting at around 7 million oscillatory passes, the mean torque levels for both types had risen to 100×10^{-4} Nm with peak levels on reversal as high as 200×10^{-4} Nm for the lead. The cage dry lubricated bearings (Groups iii through v) showed no major variations after the initial settling period. The Salox M (Group v) caged bearings again performed the best of the trio with mean levels of around 50×10^{-4} Nm compared with 100×10^{-4} Nm for the Vespel (Group iv) and 150×10^{-4} Nm for the Duroid (Group iii). Again, the wet lubricants (Groups vi through viii) performed in a very similar manner throughout this test, with mean torque levels around 15 to 20×10^{-4} Nm and peak torque levels up to 30×10^{-4} Nm for the Braycote grease and Pennzane oil (Groups vii and viii). The Fomblin Z25 (Group vi) recorded higher mean levels, 30×10^{-4} Nm, with peak torque levels up to 60×10^{-4} Nm during the second half of the test.

Post-Test Inspection. Inspection of the post-test bearing condition has revealed very obvious contact zones in most cases, especially in the case of the dry lubricants (Groups i through v). In the case of the coated bearings (Groups i and ii), the motion has worn a groove into the lubricant with a buildup of debris around the edge. In the case of the cage dry lubricated bearings (Groups iii through v), compacted zones of material have been generated on the bearing surface during the motion. These details have been confirmed by a small number of Talyrond measurements, and also by removing the debris in the latter case. The wet-lubricated bearings also show obvious contact zones of sizes similar to those in the dry lubricated bearings, however the height of these features has not been measured at this time. However, it is not believed that any steel bearing surface material wear has occurred in any of these tests.

The paper concludes that it is difficult to explain the torque increases seen in oscillating bearings purely by a change in friction or preload levels or by a reduction in the number of balls in contact. Therefore, ESTL postulates that the change in conformance at the contact due to compacted debris buildup is the cause of the increased torque levels.

Key Words:

Lubricants, Ball Bearings

Mechanisms:

Oscillating Scanner, Harmonic Drive, Reaction Wheel

Systems:

Rotating System, Oscillating System

Authors; Experts:

Chris Kalogeras, Mike Hilton, David Carré, Stephen Didziulis, and Paul Fleischauer

Address:

Mechanics and Materials Technology Center
The Aerospace Corporation
El Segundo, California

Telephone:

Title:

The Use of Screening Tests in Spacecraft Lubricant Evaluation

Source:

27th Aerospace Mechanisms Symposium (1993).

Abstract:

A lubricant screening test fixture has been devised in order to satisfy the need to obtain lubricant performance data in a timely manner. This fixture has been used to perform short-term tests on potential lubricants for several spacecraft applications. The results of these tests have saved time by producing qualitative performance rankings of lubricant selections prior to life testing. To date, this test fixture has been used to test lubricants for three particular applications. The qualitative results from these tests have been verified by life test results and have provided insight into the function of various antiwear additives.

PRECEDING PAGE BLANK NOT FILMED ^{PAGE 434} INTENTIONALLY BLANK

Anomalies:

Bearing failures due to improper lubricant.

Lessons Learned:

- The screening tester has been used to evaluate lubricants for a number of applications. The lubricant rankings from the tests have subsequently been confirmed by the results of life tests on the real components/assemblies.
- For oscillating scanner bearings, three oils were tested:
 - G.E. Versilube F-50, a chloroarylalkylsiloxane (CAS) oil.
 - Bray 815Z, a perfluoropolyalkylether (PFPE) oil.
 - Nye 188B, a synthetic hydrocarbon oil (polyalphaolefin, PAO).

The PAO outperformed the other oils by a wide margin. The primary reason for this was the presence of the antiwear additive, tricresyl phosphate (TCP), in the PAO oil. The other two oils suffered rapid degradation.

- For harmonic drive support bearings, two oils were tested: NPT-4 (a neopentylester spacecraft oil) and Pennzane SHF-2000 (a synthetic hydrocarbon oil). The effects of antiwear additives, TCP, and lead naphthenate (PbNb) were also investigated. Pennzane with TCP gave the longest life. The failure mechanisms with the two additives were different. Bearings tested with oils plus TCP failed due to wear. Bearings tested with oils plus PbNb failed due to formation of a hard, lead-containing carbon film, which resulted in high friction. From this, it appeared that TCP would be effective in light-load applications where low friction was important, while PbNb would be more suitable for high-load applications where friction was of secondary importance.
- For reaction wheel support bearings, three oils were tested: SRG-40 (a highly refined mineral oil), Nye 179 (a synthetic PAO oil), and Nye UC-7 (a synthetic polyolester (POE)) oil. All of the oils were formulated with TCP and tests were carried out in different atmospheres. The tests showed that the TCP did not function as an antiwear additive in UC-7. Nye 179 was considered the best choice for this application. Its performance in vacuum was far better than that of SRG-40, and its performance in helium was the best of all the oils tested.
- The use of oxygen as a component of the fill gas of reaction wheels was determined to be unnecessary and generally harmful to the life of the bearing lubricant.

Description:

The test fixture utilizes low-cost bearing components. The bearings used are INA GT-1 thrust bearings that have a complement of 12 balls. The balls and races are made from 52100 steel. Instead of using the grooved raceways for top and bottom, the flat side of the bottom (rotating race) is polished to a 0.25-micron finish and used instead of the raceway. This change in configuration was done so the bearing could be run with a controlled amount of lateral misalignment. The misalignment introduces skidding, which serves to accelerate the wear process. In addition, the flat surface gives a higher Hertzian stress

and more severe tribological conditions. The flat surface is also much easier to analyze than a grooved raceway. The overall test fixture is shown in Figure 1. In order to simulate the space environment, the test apparatus operates in a vacuum chamber that has a baseline pressure of 1×10^{-8} torr. The chamber can also be sealed off and backfilled with gases, such as helium, for certain reaction wheel bearings.

Case 1: Oscillating Scanner Bearings. The goal was to find a suitable replacement lubricant for a pair of R2 bearings that support the shaft of an oscillating optical scanner. The original lubricant used in this application was G.E. Versilube F-50, a CAS oil. This oil has very low vapor pressure and excellent low-temperature properties, but it does not function well under boundary lubrication conditions. In this application, the oil degraded very quickly and resulted in substantial bearing wear and reduced life.

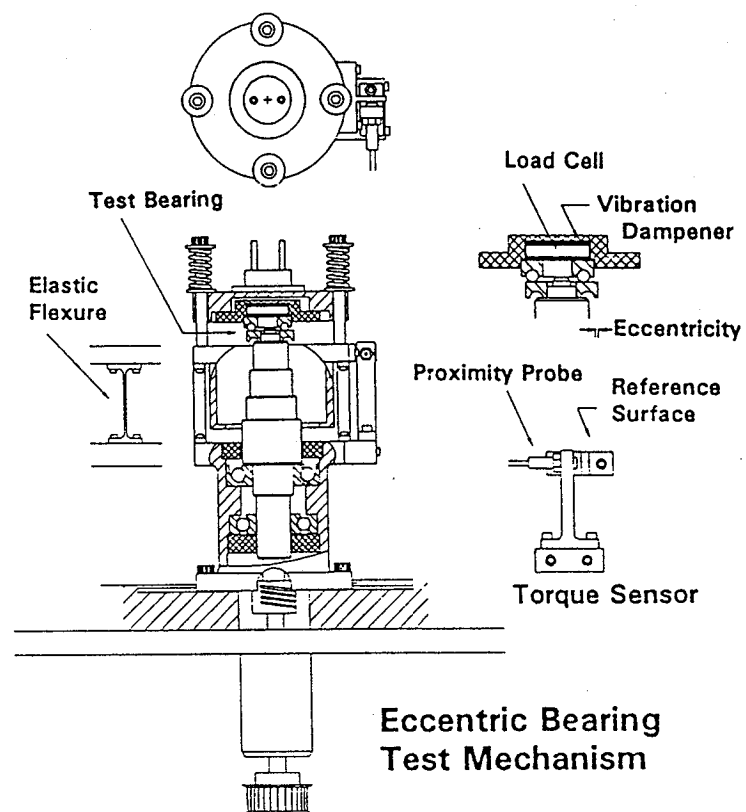
After preliminary investigation, substitute oils were chosen for the test as follows:

- PFPE (Bray 815Z) - is a PFPE oil and was selected for its low vapor pressure and viscosity properties.
- PAO (Nye 188B) - is a synthetic hydrocarbon oil and was chosen for its excellent physical properties and because it could be formulated with the antiwear additive TCP. The inclusion of an antiwear additive was considered to be essential for boundary lubrication operation.
- CAS oil was also tested for comparison.

For these tests, a thrust bearing was utilized that had the same dimensions as the INA GT1 bearing, but incorporated a custom 440C disk and 440C Grade 10 balls. The test specimens were run in a vacuum at a speed of 1750 rpm and the load ranged between 20 and 50 lb (229- to 310-ksi peak contact stress). The drive motor current was measured to get an estimate of the bearing reaction torque and bearing failure was defined to occur when the motor current reached a level 50% higher than the starting current. The PFPE gave a life approximately three times that of the CAS oil, but the PAO oil increased the life approximately fifteen times. The primary reason for this result appears to be the superior boundary protection provided by the antiwear additive TCP in the PAO oil. In addition, both the CAS and PFPE oils decomposed during the test. The CAS oil was the most reactive, forming a hard sand-like grit, which caused significant wear and subsequent failure after only a short period of operation.

After the screening tests, the same three oils were used in life tests of flight-grade bearings under simulated orbit conditions. The relative lives were very similar to those in the screening tests. The PAO oil outperformed the other oils by a wide margin. The CAS and PFPE oils exhibited the same failure mechanism as they had in the screening tests. The PAO-lubricated bearings operated over 3.5 yr and did not display abnormal wear on removal. The bearings still contained an adequate amount of lubricant and there were no signs of degradation.

Case 2: Harmonic Drive Support Bearings. The goal of this study was to obtain comparative performance data between a frequently used neopentylester spacecraft oil (NPT-4); a new synthetic hydrocarbon oil (Pennzane SHF 2000); and a multiple-alkylated cyclopentane (MAC), which has some outstanding physical properties. Additionally, it was desired to gain a better understanding of the role of wear additives in oils and the mechanisms by which they provide protection. The additives of interest were TCP and lead naphthenate (PbNp).



95TR4/V2

Figure 1. Lubricant Screening Test Apparatus

The screening tests were carried out using the INA GT1 bearings and were run in a vacuum (1×10^{-7} torr) at 1800 rpm. For the tests, a 4-lb per ball load (288-ksi peak contact stress) was used. The bearing reaction torque was monitored and failure was defined to occur when the torque exceeded three times the initial run-in torque. The screening test results are summarized in Figure 2. From this, it is clear that the oils formulated with antiwear additives outperformed the base stock oils. Of the combinations tested, Pennzane with TCP gave the longest life. The addition of PbNp to Pennzane also improved the life, but not to the same extent.

Following the screening tests, the surfaces of the test specimens were analyzed with energy-dispersive x-ray and/or Auger electron spectroscopy. This revealed that the bearings lubricated with TCP and PbNp containing oils failed by different mechanisms. The bearings lubricated by Pennzane plus TCP failed by a wear process that involved surface distress and metal removal from the wear track. The bearing appeared to have failed at a point when the additive could no longer provide satisfactory boundary lubrication protection. In the bearing lubricated with Pennzane plus PbNp, there was no wear. Instead, the increased friction appeared to have been caused by the formation of a tough, lead-containing carbon film on the surface of the disk. These apparent differences suggest that the two additives cannot be directly compared. The surface film generated by PbNp would make it suitable for high-stress applications where maximum protection against wear is desired and increased friction is not a factor. On the other hand, TCP would be more suited to light or intermediate loads, where low friction and long life are desired. For the harmonic drive, low friction is not as important as wear protection. Based on this, Pennzane would be the best combination. Life tests on harmonic drive mechanisms with NPT-4 and Pennzane plus PbNp confirmed the results of the screening tests.

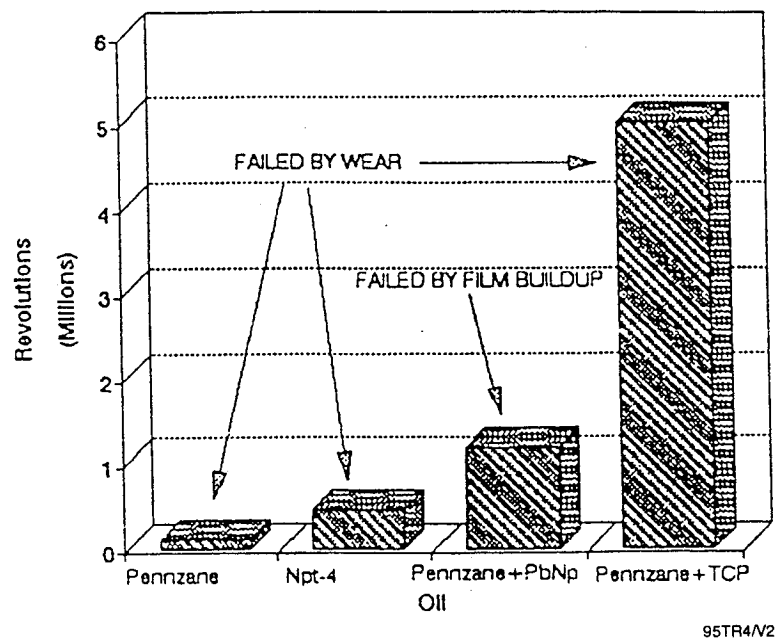


Figure 2. Screening Test Results (Harmonic Drive)

Case 3: Reaction Wheel Support Bearings. The screening apparatus was used to test a well known spacecraft lubricant SRG-40 (a highly refined mineral oil) and two synthetic oils that were considered as replacements for SRG-40. The synthetic oils were Nye 179 (a PAO oil) and Nye UC-7 (a POE oil). All of the oils tested were formulated with TCP. The particular reaction wheel assembly of interest operates in a helium-oxygen mixture ($P_{\text{tot}} = 0.5 \text{ atm}$ with 2% oxygen), so it was decided to perform lubricant screening tests in a number of different environments. These environments consisted of: 1×10^{-7} torr simulating a worst-case scenario of an orbit leak; 1/2 atmosphere of 98% helium, 2% oxygen (the operating environment used on orbit); and 1/2 atmosphere of pure helium. The last environment was chosen to see if the inclusion of oxygen was really necessary for the antiwear additive TCP to function. Our concern was that the inclusion of oxygen in the fill gas may actually be detrimental to the life of the bearing because it could degrade the lubricant. Therefore, several additional tests were run in a 7-torr atmosphere of oxygen. This amount was equivalent to the 2% oxygen added to the helium and it was felt that this condition would accentuate both the reactive effect of oxygen on the lubricant and any potential effects of oxygen on TCP.

In the vacuum tests, the synthetic oils gave lives that were an order of magnitude longer than the SRG-40. The main factor that accounts for this difference seems to be the high vapor pressure of the SRG-40, which led to rapid lubricant loss from the bearings and subsequent failure. The synthetic oils had much lower vapor pressures.

In the oxygen environment, there were no increases in life, and in the case of UC-7, the life was significantly decreased. Visual inspection after the tests revealed extensive lubricant degradation.

In the 1/2-atmosphere environments, the tests ran for a much greater period because the presence of the fill gas reduced lubricant evaporation and allowed the bearings to operate at lower temperature. The tests that were performed in the helium-oxygen mixture confirmed the results from the 7-torr oxygen tests. The test lives in this case were significantly shorter than any of those performed under a helium-only atmosphere. With helium only, UC-7 was the only oil that failed consistently. In contrast, the tests performed with the other oils were either terminated before failure (due to time constraints) or were run for a great length of time in order to fail.

Post-test surface analyses revealed that TCP does not appear to function as an antiwear additive in UC-7. The reactive nature of the ester oil probably interfered with the normal protective mechanism of the TCP. By contrast, all of the samples run with 179 and SRG-40 contained phosphorus in the wear track, indicating that TCP was active in this region and indicating that oxygen was not required for TCP to function.

Profilometer measurements revealed large wear troughs in the wear tracks of the UC-7 test specimens. SRG-40 gave less wear than UC-7; however, 179 gave the lowest wear of all.

The wear lives and the post-test analyses indicated that Nye 179 was the best overall choice for this application. Furthermore, the use of oxygen as a component in the fill gas of reaction wheels was determined to be unnecessary and generally harmful to the life of the bearing lubricant.

Key Words:

Gimbal Bearings, Thin-Section Bearings, Bearing Torque

Mechanisms:

Gimbals

Systems:

Rotating System

Authors; Experts:

Stuart H. Loewenthal

Address:

Lockheed Missiles & Space Company, Inc.
Sunnyvale, California

Telephone:

Title:

Two Gimbal Bearing Case Studies: Some Lessons Learned

Source:

22nd Aerospace Mechanisms Symposium (1988).

Abstract:

The paper addresses two subtle, but not uncommon, torque problems that can be encountered with spacecraft gimbal bearings. The first example illustrates the surprisingly high torque thermal sensitivity of hard-preloaded, thin-section bearings. A thermal bearing performance code was useful in establishing the acceptable operating temperature envelope. Active heater control was then used to manage the bearing torques.

In the second case study, a blocking torque anomaly was encountered with oscillatory gimbal bearings during life-cycle tests. The remedy was opening the race conformity slightly and switching to alternating ball toroid separators. Again, bearing analysis was illustrative in assessing the relative options to combat this problem.

Anomalies:

- In a large gimbal actuator bearing with a beryllium shaft and housing, temperature gradients and, to a lesser extent, bulk temperature could lead to large variations in race interferences. Consequential changes in contact angle would lead to large variations in bearing torque.
- During life-cycle tests of a gimbal bearing, greatly increased torques were experienced in the end-of-travel regions.

Lessons Learned:

- Race conformity and separator type can have a dramatic effect on bearing torque. Opening the race conformity slightly and switching to alternating ball toroid separators reduced the excessive torque problem to an acceptable level.
- Excessive thermal gradients across the races will have significant effect on internal preload and contact stress and can cause torque problems in gimbal bearings. Bulk temperature effects are much less severe. If tight control over preload is necessary, heaters are recommended to maintain proper temperature.
- Blocking is a condition in which high torque occurs at the extremity of a cycle. Table 1 shows the effects of various factors on blocking.
- A thermal bearing performance code was used to establish the acceptable operating temperature envelope. Active heater control was then used to manage the bearing torques.

Table 1. Factors Tending to Increase Blocking

Factor Increased	Effect
Conformity (tighter)	Increases spin; higher spin torque and drag
Contact angle	Increases spin; higher spin torque and drag
One-piece cage	Restricts ball speed spacing; increases cage wind-up
Misalignment	Increases ball speed variation; increases cage wind-up
Preload	Increases traction forces; increases anomalous torque
Friction coefficient	Increases traction forces; increase animals torque
Contact angle variation	Increases ball speed variation
Ball diameter tolerance	Increases ball speed variation
Thrust versus radial bearing	Thrust bearing has all balls loaded; no opportunity for ball spacing to readjust

95TR4/V2

Description:

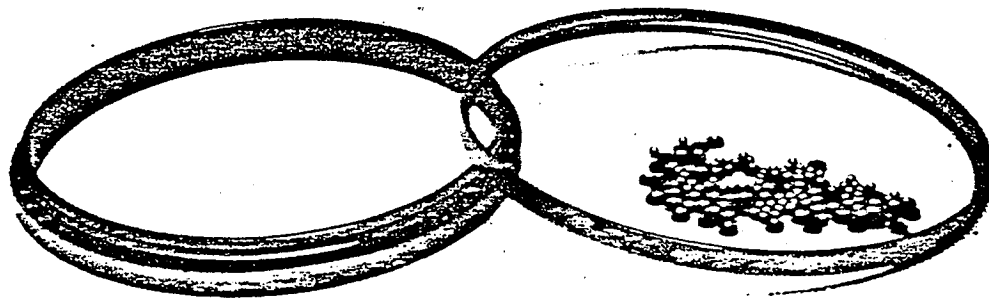
Large Gimbal Actuator. The need to maintain the precise location of a high-precision encoder under ascent loads necessitated a very stiff bearing mount for a large gimbal actuator. Hard-preloaded, thin-section duplex bearings were mounted between a beryllium shaft and housing for maximum stiffness on both the yaw and pitch axes (Figures 1 and 2). Internal preload sensitivity, hence torque sensitivity, of these bearings to temperature gradients was particularly great due to the hard mount. The coefficient of thermal expansion disparity between the steel bearing races and the beryllium mounting structure in combination with the bearings large size also contributed to this sensitivity. The immediate concern was the effects that bulk temperature and radial thermal gradients may have on the bearing preload and drag torque. Loss of significant bearing preload might permit a shift in encoder position, while increased torque might exceed the bearing's allocated torque budget.

The author found it more expedient to construct a special-purpose thermal mechanical bearing code to investigate the problem rather than modify existing general-purpose codes, which could not address the 104 ball bearing at hand. Analyses showed that the effect of radial thermal gradient on the large gimbal actuator internal preload were very significant. A modest, 10°F increase of inner race temperature would raise the internal preload from 250 to 1000 lb. Moreover, with a temperature difference of only 20°F between the outer and inner races, the internal preload could be reduced to zero. The effect of bulk temperature was not as dramatic. The beryllium shaft and housing have a slightly higher coefficient of thermal expansion than the bearing. Consequently, as the temperature increases, the interference between the outer race and the housing decreases and eventually falls to zero. With decreasing temperature, the interference between the inner race and the shaft decreases and may become zero. If the inner race expands faster than the outer race, the internal preload increases and the ball/race contact stresses become unacceptably high. With these limiting conditions, it was possible to identify a thermal window that the bearing had to operate in.

The bearing torque was very sensitive to thermal gradients. A 6°F change in the temperature difference between the inner and outer races doubled the torque. In contrast, a 100°F change in bulk temperature only increased the torque by 10%. To ensure positive torque margins throughout the flight envelope, it was necessary to thermally manage the large gimbal actuator bearing race temperatures via active heater control.

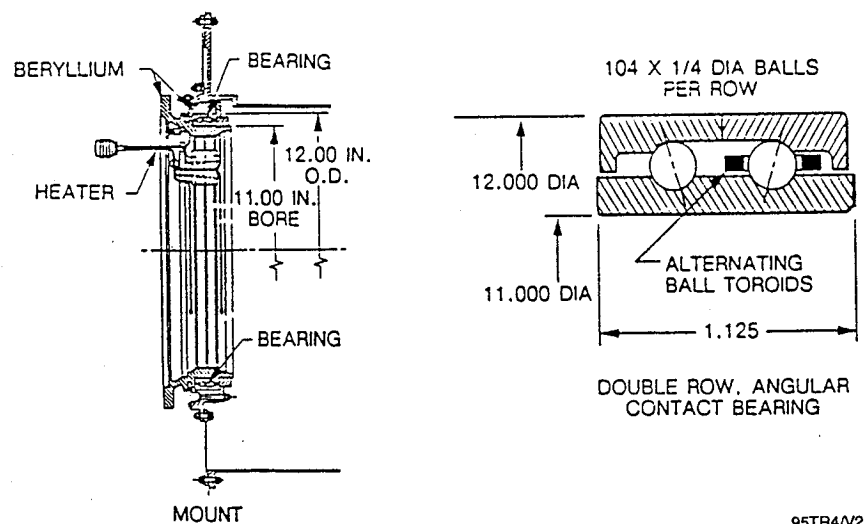
Space Telescope Gimbal Bearings. The Hubble space telescope has two high-gain antennas that are used for ground station communication. The two high-gain antenna drives are cross mounted to provide pitch and yaw positioning over a hemispherical field of view in excess of 180° (Figure 3). The high-gain antenna gimbal is supported by a pair of hard-preloaded A451, duplex angular-contact ball bearings mounted face to face. The bearings have 24 0.125-in. diameter balls and the inner and outer race conformity is 51.8%. The one-piece, inner-land riding, phenolic-laminated cage and balls were lubricated with a Kendal superrefined mineral oil, KG-80.

During life tests under repeated limit-to-limit cycling, the gimbal drag torque increased precipitously from a nominal 2 in.-oz. to as high as 18 in.-oz. This drag torque approached the stall torque of the motor. There were several curious aspects to this problem. The high drag torque always took some time to develop, from a few hours to a few weeks, at the 0.5°/sec cycling rate, and the high torques only occurred at the end-of-travel reversal point. Tapping and/or inverting the gimbal caused the torque to temporarily disappear, but it would eventually return. Finally, torque anomalies were observed with all six of the high-gain antenna gimbals, even though their design was essentially identical to an earlier gimbal that exhibited no such problem.



95TR4/V2

Figure 1. Large Gimbal Actuator Bearing



95TR4/V2

Figure 2. Geometry of Large Gimbal Actuator Bearing and Mounting to Beryllium Structure

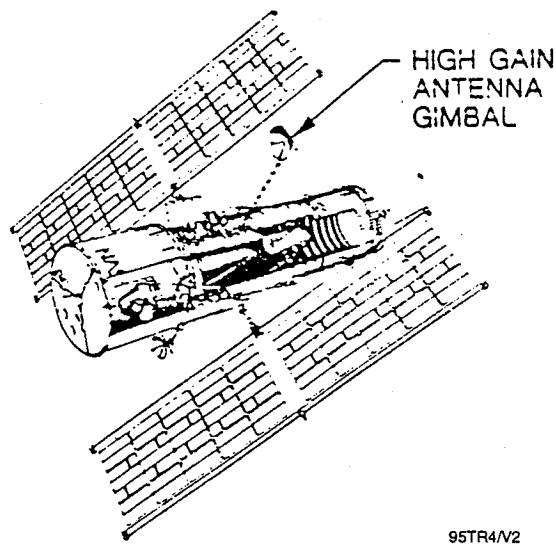
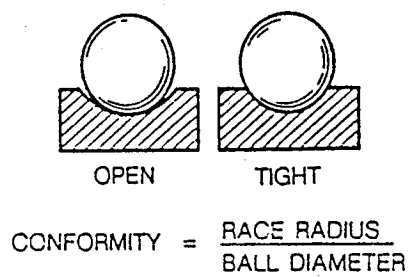


Figure 3. Hubble Space Telescope Two-Axis Gimbal

One hypothesis was that cage wind-up was occurring. This refers to the cage pinching forces that can occur when individual balls are orbiting at different speeds due to small variations in contact angle or ball size. The most common cause of this is bearing misalignment. In an oscillatory bearing such as this, the severity of the cage wind-up could increase with rotation and possibly reach a maximum at the end of travel and then decrease as rotation is reversed. The operating conditions of the high-gain antenna bearings would tend to make cage wind-up effects more pronounced and this suggested that it was a major contributor to the high torques experienced.

Another possible contributory source was blocking, which leads to high torque related to contact spin. With highly conformal bearings, it has been observed that the balls tend to creep outward leading to a situation where the spin axis of the balls is no longer normal to the bearing axis. This phenomenon is less prevalent with lower conformity bearings (see Figure 4). Analysis showed that the bearing conformity could be reduced to 54% while maintaining acceptable contact stresses during launch. This also predicted that the drag torque would be 39% less than the 51.8% bearing. Tests on a bearing with 53% inner race and 54% outer race showed a bigger reduction and, when the one piece cage was replaced with toroids, the reduction was even greater. Further tests with a 51.8% bearing and toroids showed that the toroids essentially eliminated the cage wind-up but with cycling the torque still increased with time up to 60% and this increase was attributed to blocking.



95TR4/V2

Figure 4. Bearing Race Conformity

Key Words:

Duplex Bearings, Bearing Torque

Mechanisms:

Gimbals

Systems:

Rotating/Oscillating System

Authors; Experts:

D.D. Phinney, C.L. Pollard, and J.T. Hinricks

Address:

Ball Aerospace Systems Division
Boulder, Colorado

Telephone:

Title:

Experience With Duplex Bearings in Narrow Angle Oscillating Applications

Source:

22nd Aerospace Mechanisms Symposium (1988).

Abstract:

Duplex ball bearings are matched pairs on which the abutting faces have been accurately ground so that when the rings are clamped together, a controlled amount of interference (preload) exists across the balls. Because the bearings have no internal clearance, they are vulnerable to radial temperature gradients, blocking when oscillating and increased sensitivity to contamination. Duplex bearings were to be used in a gimbal application where motion of the shaft could consist of rotation to a pointing direction, followed by narrow-angle oscillation (less than $\pm 0.3^\circ$) at a 6 cycle/min rate that could last as long as several years in one position. Although bearings with one Ball Aerospace Systems Division (BASD) space lubricant had demonstrated their ability to operate successfully for many years in a narrow-angle dither mode,

a different lubricant (BASD 36234) with improved properties was to be used for the gimbal application. Consequently, it was decided that an accelerated thermal vacuum life test should be conducted. The results of bearing bench tests and tests on gimbal assemblies are presented.

Anomalies:

- High and variable torques were experienced during thermal vacuum bench testing of hard-preloaded duplex bearings.
- High torques and torque spikes were experienced during tests on gimbal assemblies with duplex bearings.

Lessons Learned:

- When properly made and installed, lightly preloaded duplex bearings having phenolic laminate separators and lubricated with thin films of BASD 36234 liquid lubricant can withstand more than 16 million low-angle oscillating cycles without any signs of degradation or without significant torque variation.
- Blocking can occur in oscillating duplex bearings even at extremely narrow angles of motion. Blocking is a condition where some of the bearing balls jam into the ends of the separator pockets as a result of creeping away from their centered positions.
- Races should be slip fits, if possible, to assure proper performance and prevent blocking.
- Soft (spring) preloading is better than hard preloading if bearing torque is critical.
- Bearings must be scrupulously clean.
- Torque spikes are the result of buildup of debris at the ends of the ball travel.
- The debris is primarily aluminum particles with small amounts of titanium debris and dry lubricant from the inner race retaining nut threads.
- Using aluminum tools during assembly can produce aluminum debris that contaminates the bearings. Use titanium tools instead.

Description:

Duplex ball bearings are matched pairs on which the abutting faces have been accurately ground so that when the rings are clamped together, a controlled amount of interference (preload) exists across the balls. Because the bearings have no internal clearance, they are vulnerable to radial temperature gradients, blocking when oscillating, and increased sensitivity to contamination. Duplex bearings were to be used in a gimbal application where motion of the shaft could consist of rotation to a pointing direction, followed by narrow angle oscillation (less than $\pm 0.3^\circ$) at a 6 cycle/min rate that could last as long as several years in one position. Although bearings with one BASD space lubricant had demonstrated their ability to operate successfully for many years in a narrow-angle dither mode, a different lubricant (BASD 36234) with improved properties was to be used for the gimbal application. Consequently, it was decided that an accelerated thermal vacuum life test should be conducted.

Five sets of bearings (two per set) were matched into face-to-face (DF) sets with a very light preload. The characteristics of these inch-series bearings were:

- Ball and race material: 440C
- Separator material: cotton cloth phenolic laminate
- Inside diameter: 58.74 mm (2.3125 in.)
- Outside diameter: 73.025 mm (2.875 in.)
- Number of balls: 48
- Ball diameter: 3.18 mm (0.125 in.)
- Raceway conformities: 0.52 to 0.528 (inner and outer)
- Contact angle: 18-25°
- Raceway surface finish: $<0.05 \mu\text{m}$ (2 $\mu\text{in.}$) AA
- Ball grade: 5
- ABEC tolerance class: 7T (SBB Super Ultra)
- Preload: 13.3-22.2 N (3 to 5 lb).

The five life-test bearing cartridges were mounted on one common vertical shaft and oscillated by a lever and bearing on an eccentric. Strain-gaged beams were used to measure torque. The goal was to simulate 6 yr of orbit operation at 6 cycles/min with a laboratory test of 1 yr or less. The authors rationalized their way to a set of test conditions that called for a bench test at 50°C and a speed of 42 cycles/min. In 8.6 months, this was supposed to simulate 6 yr in space.

During the initial stages of the test, torques on bearing sets 1 and 2 became erratic and increased severalfold. Bearing sets 3, 4, and 5 ran well. After 151 hr, all bearings were disassembled, cleaned, and relubricated. The phenolic separators in sets 1 and 2 were replaced with Teflon toroids to see if the retainers were the cause of their high friction. It was necessary to take out 18 of the 48 balls in each of the two sets to make room for the toroids.

These bearings were supposed to run for 39.5 weeks. However, in the 10th week, the torque values on sets 1 and 2 were still high. They were removed, examined, and cleaned. No changes in the lubricant or buildup of contaminants could be found. New phenolic retainers were installed. The 18 balls taken out of each bearing were replaced. Sets 1 and 2 were put back on test during the 23rd week.

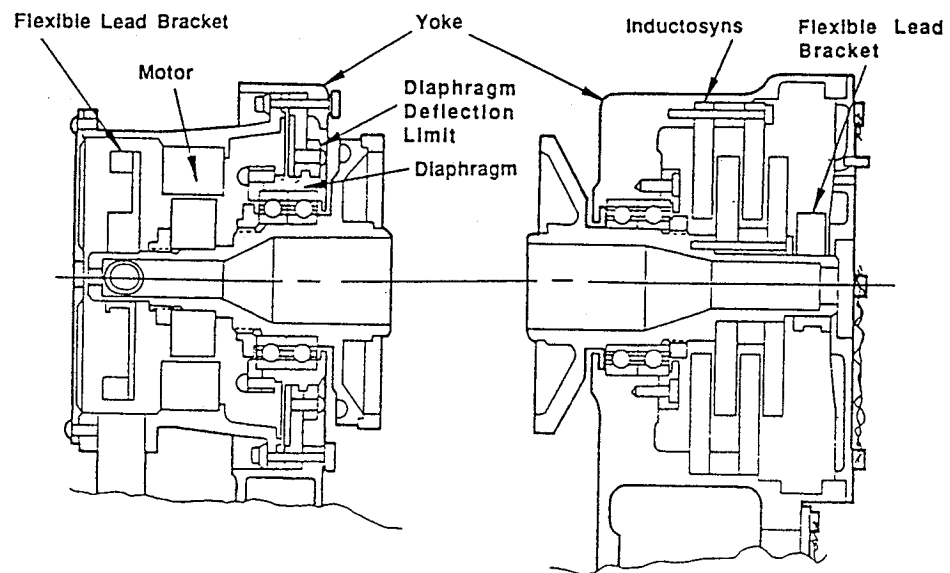
At 151 hr, it was also noted that bearing set 3 showed an odd hysteresis loop when the outer shaft was rotated just enough to relocate the ball contacts away from their initial position. The bearings were inspected and no raceway deterioration was found. However, there were thin films of an unknown material on the surfaces and significant particulate contamination was found when the bearings were rinsed with solvent. The bearings were recleaned, relubricated, and put back on test. No further torque problems were observed.

When the tests were finished, bearing set 1 was examined. The bearings appeared to be well lubricated and no chemical changes were detected in the oil. Some contamination was observed, but it was considered minimal. However, bearing set 1 was found to have a preload of 162 N, instead of 13.3 to 22.2 N, when the outer races were just brought into contact. At that time, it was also discovered that the 18 balls that had been removed from each bearing to make room for the Teflon toroids had been put back in the wrong bearings. This was significant because, one set of balls was 0.0762 mm (0.0003 in.) larger than the other. When the toroids were later replaced by the new phenolic retainers, there was no way of knowing if the oversize balls were grouped together or scattered randomly around the retainer. Any test results obtained with this set of bearings after the 23rd week are open to question.

At this point, the authors had determined that bearing set 1 was too tight and they reworked the bearing fixtures until they could be assembled with less than 9 N of force. This slip-fit bearing assembly was run in air for 57 days with a solid preload. The torque started at 0.007 Nm and increased to 0.024 Nm after 25 days when it stabilized. A softer preload gave a torque of 0.007 Nm, which remained constant for 30 days.

The authors attributed the torque increases that were observed with bearing sets 1, 2, and 5 to blocking. This is a condition where some of the bearing balls jam into the ends of the separator pockets as a result of creeping away from their centered positions.

Subsequently, tests were carried out on six full-scale gimbal assemblies. Figure 1 shows the configuration for the inner axis drive-line components. The inner axis has a 31° rotation range, but its normal mode is narrow angle oscillation in one location. Spring-loaded stops are used at each end of the travel range. In tests, the axis was rotated at constant speed by an external motor. At the end of travel, the axis was driven into the stop, slightly compressing the stop spring to assure complete travel. Of the six gimbal assemblies tested, two had large torque spikes just inside of the stops. Any problems with the mechanical assembly or blocking were eliminated by the authors as the cause of the torque anomalies. It was demonstrated that pile-up of debris just before the ends of the ball paths were the cause of the torque spikes. The torque anomalies were traced to the presence of debris, especially aluminum particles, in the bearings. The sources of the aluminum particles were the aluminum tools used during assembly and aluminum components in the gimbal assemblies.



95TR4/V2

Figure 1. Final Configuration of Inner Axis Drive-Line Components

Key Words:

Gimbals, Bearings

Mechanisms:

Gimbals

Systems:

Deployment Systems

Authors; Experts:

R. Sharma, C. Woods, and R. Farley

Address:

NASA-Goddard Space Flight Center
Mail Code 731
Greenbelt, Maryland 20771

Telephone:

Title:

Spacecraft Deployable Appendages

Source:

Goddard Space Flight Center
Engineering Directorate

Abstract:

This report is a compendium of satellite experience and mechanism design practices compiled by the engineering staff at NASA-Goddard. The information on gimbal bearings is from the source document, Section 3.5.5.5, Bearings/Lubrication, page 55.

PRECEDING PAGE BLANK NOT FILMED

PAGE 452 INTENTIONALLY BLANK

Anomalies:

- Oil replenishment for small oscillatory motions as experienced by gimbal bearings is difficult. Torque magnitudes increase significantly due to oil breakdown or bearing starvation.
- In a test conducted at Hughes, Bray 815Z had half the initial torque of Apiezon C (with an extreme pressure additive) in a 4° gimbal bearing test. However, after 7×10^4 cycles, the Bray lubricant turned to brown sugar and the bearing torque quickly increased by a factor of 10. The Apiezon C continued without torque increase to the end of the test (8×10^6 cycles).

Lessons Learned:

- To prevent destructive chemistry, surfaces in contact must be passivated in some manner.
- Ceramic hard coatings, like TiN or TiC, will eliminate catalytic reaction.
- Replacing stainless steel 440C balls with ceramic SiN_4 balls eliminates lubricant breakdown.
- To prevent oil starvation, it is good practice to use a porous ball retainer that functions like a reservoir of oil and dilutes any breakdown products.

Key Words:

Deployment Mechanisms

Mechanisms:

Hinges, Bearings, Lubrication, Testing

Systems:

Deployment Systems

Authors; Experts:

R. Sharma, C. Woods, and R. Farley

Address:

NASA-Goddard Space Flight Center
Mail Code 731
Greenbelt, Maryland 20771

Telephone:

Title:

Spacecraft Deployable Appendages

Source:

Goddard Space Flight Center
Engineering Directorate

Abstract:

This report is a compendium of satellite experience and mechanism design practices compiled by the engineering staff at NASA-Goddard. Some general mechanism lessons learned are indicated in the back of the source report starting on page 35.

Lessons Learned:

- Hinges
 - The torque generated by the hinge assembly should exceed the resistance torque of the appendage in a 1-g and 0-g environment by a minimum factor of 4.
- Bearings
 - The peak contact stress should be kept below 580,000 psi for 440C stainless steel bearings.
 - The bearing should withstand launch loads that are estimated by multiplying the estimated weight of the rotating portion by the estimated gravity load and by a Q (amplification) factor. Q factors have been measured as high as 25, but at the beginning of a design, a value of 10 is used. The minimum Q factor is 5.
 - A 200-hr run-in test of the bearings should be completed at operating speeds.

Testing:

- All deployed appendage programs must have an engineering test unit.
- All flight units and engineering test units must be testable to determine deployment margins.
- Analyses must be verified by judicious hardware testing programs.
- There must be adequate life testing early in the program.
- There must be redundant backup systems in all critical areas.
- Worst-case analyses and failure modes effects and critical analyses must be performed and verified by actual hardware testing. Worst-case friction, misalignment, and excessive friction must be considered.
- The effects of mounting system redundancy and structure-induced input forces on the device and its internal components must be considered.
- Particular attention should be paid to vacuum, thermal control, and 0-g effects.

***European Space Tribology
Laboratory (ESTL)***

Introduction

The European Space Tribology Laboratory (ESTL) has undertaken a review of open literature to identify European space mechanisms that have failed on satellites or in laboratory qualification tests.

The literature review incorporates relevant text and figures from the source publication. The source text has not been changed, except to correct grammatical errors, which are assumed to have occurred when certain papers were translated into English. For clarity, figure numbers may have been changed since the source text was rearranged to fit MTI's format as well as source text being excerpted.

We have also included a brief additional section, detailing satellite mechanism malfunctions for which the cause does not appear to have been published in open literature.

Deployable Appendages

Solar Arrays

Key Words:

Solar Array Drive Mechanism, Flexible Wire Harness, Anomalous Torque and Hysteresis

Mechanisms:

Flexible Wire Harness

Systems:

Space Telescope

Author; Experts:

Raimund G. Hostenkamp

Address:

Dornier System GmbH,
Friedrichshafen, Germany

Telephone:

Title:

Features of the Solar Array Drive Mechanism for the Space Telescope

Source:

Proceedings of 19th Aerospace Mechanisms Symposium, Moffett Field, California,
pp.315-327 (1985).

Abstract:

The solar array drive mechanism for the space telescope embodies several features not customarily found on solar array drives. Power and signal transfer is achieved by means of a flexible wire harness for which the chosen solution, consisting of 168 standard wires, is described. The torque performance data of the harness over its temperature range are presented. The off-load system, which protects the bearings from the launch loads, is released by a trigger made from Nitinol, the memory alloy. The benefits of memory alloy and the caveats for the design are briefly discussed. The design of the off-load system is described and test experience is reported.

PRECEDING PAGE BLANK NOT FILMED

Anomalies:

Following testing of the qualification model solar array drive mechanism in a dynamic test rig, and to verify pointing accuracy and interactive torque between the space telescope and the wings, it was demonstrated that the torque characteristics of the flexible wire harness had an unexpectedly large impact on the system performance. Both maximum torque and hysteresis of the flight-configured qualification model exceeded the corresponding values of the breadboard model by a factor of 3, even though the flex leads inside were identical. The difference was attributed to the harness located outside the flex lead section. In contrast to the short-circuit looms of the breadboard model, the cables of the qualification model harness outside the mechanism were twisted, shielded, bundled, and fixed as required to form the conventional harness between the solar array panel and the diode box (see Figure 1). These measures had resulted in a deterioration of the torque and hysteresis characteristics to an unexpected extent.

Lessons Learned:

- Based on the experience with the solar array drive mechanism harness, similar flexible wire harnesses have been implemented in further space mechanisms (e.g., the gimbal drives of the instrument pointing system for the spacelab).
- By corrective actions (e.g., deletion of most of the spare lines and provision of slight slack at those tie-down points where the bundles emerge from the housing), it was possible to recover the original harness performance.
- Torque fluctuations can be experienced with wire harnesses due to thermal effects (cold temperature) and to complex wiring paths. Testing is required at simulated environments to resolve torque problems.

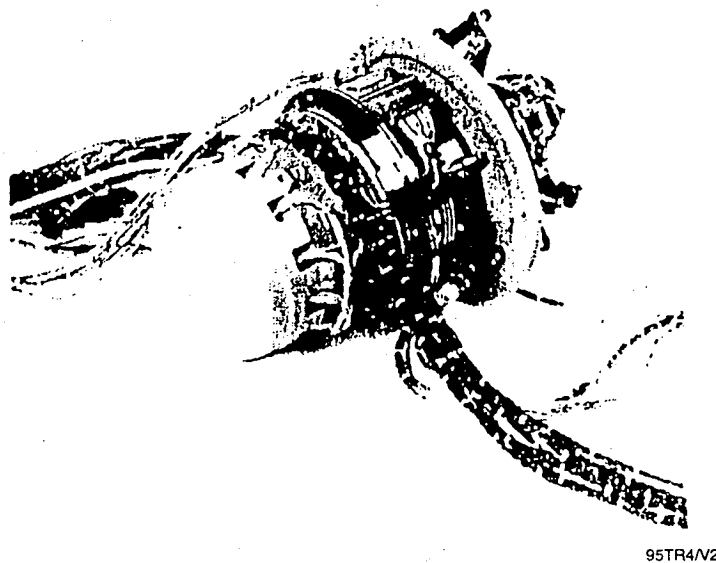


Figure 1. Harness Configuration Qualification Model

Description:

The solar array drive mechanism and its electronics are a subassembly of the solar array. The rotational range of the wings is limited to some 340° because of vehicle pointing constraints, which prevent sunlight from getting into the space telescope aperture. Under these circumstances, a flexible wire harness is an obvious choice for the transfer of a large number of electrical channels.

In the launch configuration, the solar arrays are stowed along the space telescope body and fixed by clamps. Since the loads induced into the solar array drive mechanism through the primary deployment mechanism exceed the load-carrying capability of the bearings, it was necessary to provide an off-load system in order to protect them. Because pyrotechnic devices were banned from use in the solar array drive mechanism, memory alloy elements were chosen to trigger the release of the bearing off-load device.




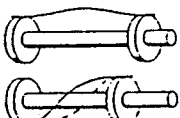
Flexible Wire Harness. Each solar array wing provides 10 solar cell modules, each with a nominal current of 7.5 A. These modules were wired independently from each other, and the wiring had to be redundant. This resulted in a minimum of 40 lines of American Wire Gauge (AWG) 16 for 50% derating. In addition to these solar array power lines, 20 wires with a maximum capacity of 3 A were required for the redundant motors of the primary and secondary deployment mechanisms, the redundant resolvers of the solar array drive itself, and for bonding. Finally, 68 housekeeping data lines were needed with a current capacity of up to 250 mA. Those data lines had to be separated from the power lines by a screen.

Since a high wind-up torque was anticipated from the AWG 16 wires needed for the solar array power, it was necessary to find an alternative that met the redundancy approach, which aimed to avoid single-point failures for vital functions. The chosen approach utilized 80 cables of AWG 22, of which 20 cables are for redundancy purposes. Four options of flexible wire harnesses were studied by breadboarding and analysis. The trade-off is presented in Table 1.

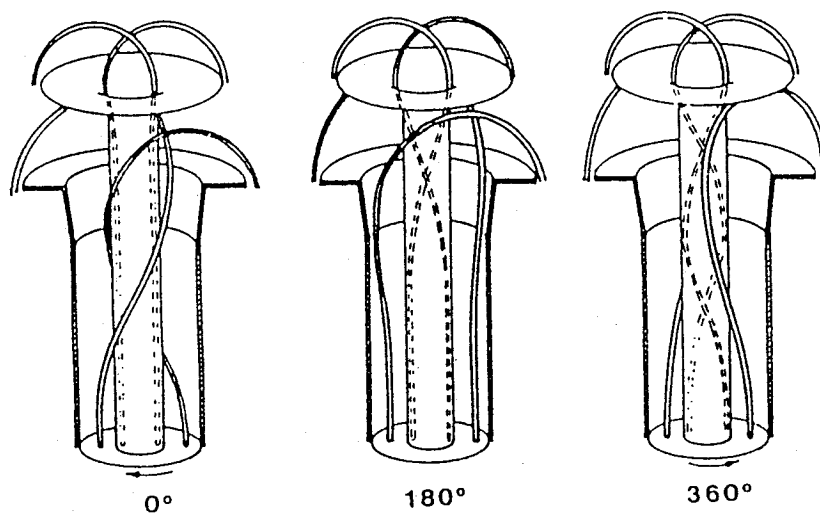
Though torque, torque noise, and hysteresis of the flexible wire harness played an important role in the design of the solar array drive mechanism control system, the printed circuit, which is best in these respects, was not selected. The printed conductors for power transfer would have had to be very wide in order to achieve the necessary cross section. In addition to serious difficulties at the printed circuit/connector interface, this design would have exceeded the given envelope, even with a double-layer arrangement of the printed circuit belts and a reduced derating. In fact, the criterion of compatibility with the given volume rendered the option with the single wires the only feasible solution.

The principle of the chosen solution is shown in Figure 2. The axial degree of freedom required for one cable end of this twisted wire configuration was provided by rotating the cables in a half circle from their shaft location toward their fixation points at the stator. Twisting and shielding of cable pairs within the flexible wire harness was discarded because it impaired cable flexibility. The required shielding between the signal lines and the power lines is achieved by a screening tube. The signal lines (68 off, AWG 24) pass through the screening tube and the power lines (100 off, AWG 22) are arranged in the annulus between the tube and the hollow shaft. The length of the flexible wires amounts to 580 mm. Although the wires are neither fixed nor tied together over that length, both a centrifuge test (giving up to 4.5 g) and vibration tests showed that the wires would suffer no permanent deformation as a result of the launch mechanical environment.

Table 1. Flexible Wire Harness Trade-Off

Flexible Wire Harness Type				
Cable Design	Standard Belts	Standard Belts	PC Special Design	Standard Wires
Qty. of Power Segments	2	1	1	1
Qty. of Signal	2	1	1	1
Cable Arrangement in Segments	Multi-Layer	Multi-Layer	Double Layer	Separate Wires
Connector	Conventional	Conventional	Special Design	Conventional
Shielding Between Power & Signal	Easy	Difficult	Easy	Easy
Rel. Cable Length	1.5	1	0.3 - 0.4	1
Rel. Power Dissipat.	1.5	1	1.8 - 2.4	1
Heat Radiation	Poor	Poor	Poor	Fair
Torque & Torque Characteristic	Low; Constant	Low; Spring	Very Low; Const.	Low; Spring
Torque Noise	High (Multi-Layer)	High (Multi-Layer)	Very Low	Low
Hysteresis	Large	Large	Very Small	Large
Growth Flexibility	Margin by Design	Moderate	Poor	Good
Assembly	Fair	Difficult	Easy	Easy
Compatibil. with Given Volume	No	No	No	Yes

95TR4/V2



95TR4/V2

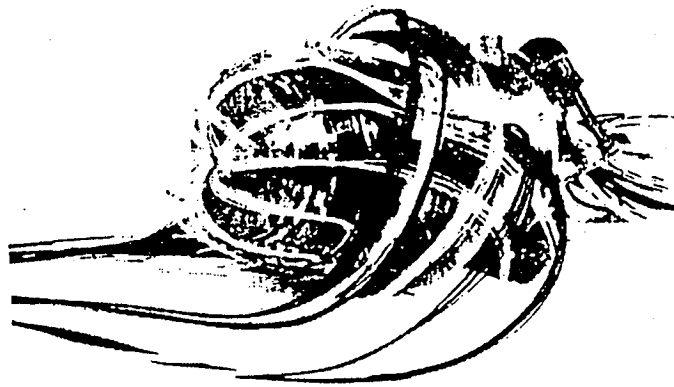
Figure 2. Flexible Wire Harness

The torque at the boundaries of the rotational range is adjusted to about the same level by suitable preorientation of the power and signal leads during assembly. A breadboard model (see Figure 3) was built in order to determine the spring constant, torque noise, and hysteresis characteristics of the harness. The wires were short circuited outside the flex lead compartment. This allowed the routing of current through the leads and the determination of their performance at elevated temperatures. Low-temperature tests down to -25°C were carried out in a large temperature chamber. The results met expectations and, with a margin of 2, were taken into account for the design of the control circuit.

The harness torque and hysteresis characteristics of the flight model mechanisms are summarized in Figures 4, 5, and 6.

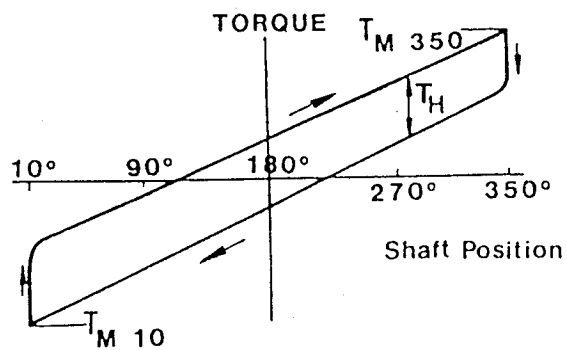
Figure 2 shows the basic shape of the torque/hysteresis loop for the full angular range. Torque rises linearly as the shaft is rotated in one direction. Upon reversal, there is a steep (1°) decay of torque followed by a steady transition (10°) toward the linear wind-back behavior. The area between wind-up and wind-back torque is due to hysteresis as a result of the deletion of spare lines, which were mainly in the signal section, the hysteresis is not constant over the whole angular range. The mechanical properties of the wire insulation are changed by temperature fluctuations of the harness. This affects the whole torque envelope (i.e., the slopes and resulting maximum torques as well as the hysteresis).

Figures 3 and 4 show the maximum torque values at the ends of the angular range and the corresponding hystereses as functions of temperature. The data for a specific temperature give the corners of the torque envelope trapezoid.



95TR4/V2

Figure 3. Flexible Wire Harness Breadboard Model



95TR4/V2

Figure 4. Flexible Wire Harness Torque Envelope as a Function of Shaft Position

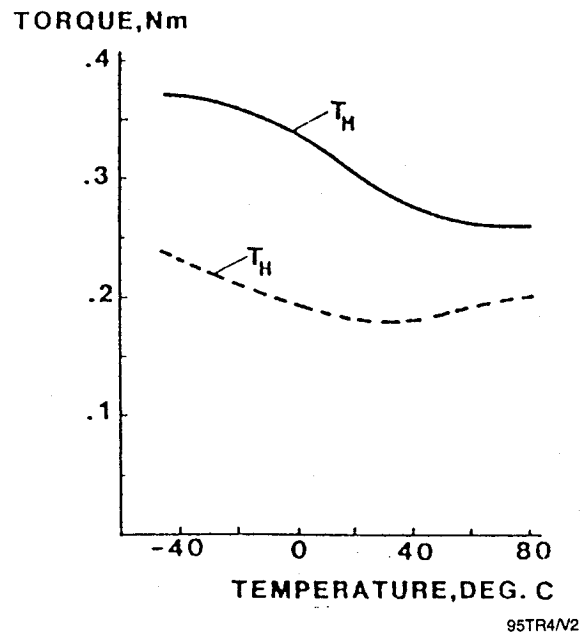


Figure 5. Maximum Torque (T_M) and Hysteresis (T_H) at Position 10°

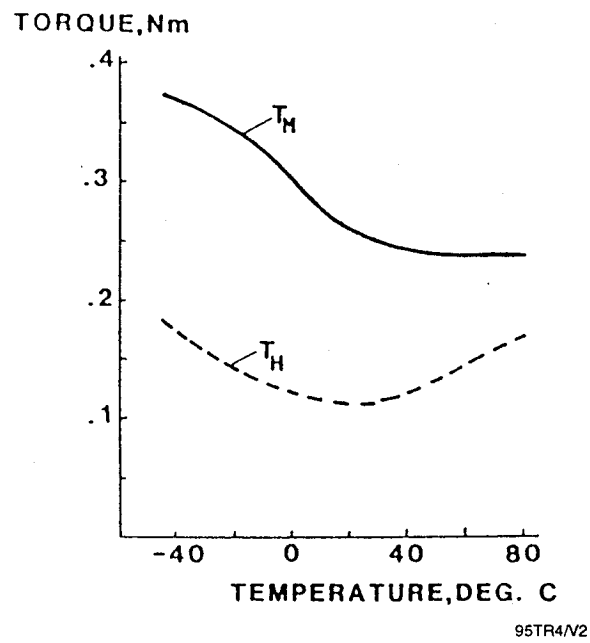


Figure 6. Maximum Torque (T_M) and Hysteresis (T_H) at Position 350°

Retention and Release Mechanisms

Key Words:

Microwelding, Random Vibration, Latch Device, Dynamic Behavior, Expertise, Failure Duplication, Validation

Mechanisms:

Latching Devices, Boom Deployment Mechanisms.

Systems:

HISPARSAT

Author; Experts:

D. Coquelet and G. Gallay

Address:

Bertin & Cie
France

Telephone:

BP. No. 3-78370 PLAISIR Cedex

Title:

Microwelding Due to Random Vibration

Source:

Proceedings of the Fifth European Space Mechanisms and Tribology Symposium (ESTEC), Noordwijk, The Netherlands, 28-30 October 1992, ESA, SP-334 (April 1993).

Abstract:

In the development phase of the HISPARSAT program, Bertin is dealing with the nonactuation of the latching devices of the DBS antenna and the boom deployment mechanisms. In order to suppress any backlash and functional play and to guarantee the pointing performance of the antenna, latch actuation should normally have occurred at the end of the deployment test performed after the mechanical environment test.

PRECEDING PAGE BLANK NOT FILMED

It should be noted that the deployment mechanism design was inherited from ARABSAT (partially) and TELECOM2 (mainly) experiences, and had sustained a full satisfactory development plan during the above-mentioned programs.

The aim of this paper is to show the logic of the examination of the problem of microwelding of contact areas due to random vibration, which is at the source of the jamming of the latching device, and to propose a solution to the problem.

Anomalies:

Jamming of latch device following vibration testing.

Lessons Learned:

- An extensive investigation in the latch subsystem hardware operation failure has been performed, and has allowed us to guarantee the good functioning of the system. This was made possible due to the logic presented in this paper.
- The main conclusions are:
 - The expertise activity (inspection, analysis) was of prime importance in order to understand the different effects that jointly contributed to an unacceptable performance of the mechanism, and then to have a good confidence in the proposed modifications.
 - The test campaign was totally successful mainly due to test conditions that had duplicated the maximum foreseen environmental disturbances and boundary conditions.
 - The on-site statements and the visual inspection that took place during test campaign lead to the following comments: 1) the blocking of the latch s/s was probably initiated by microwelding or surface bonding, evidenced by metal transfer; 2) the system recovers its nominal performance once the system is manually activated by shearing of the microwelding spots; and 3) the failure occurs only during dynamic vibration once a threshold level is passed over, giving sufficient energy to initiate the surface bonding.

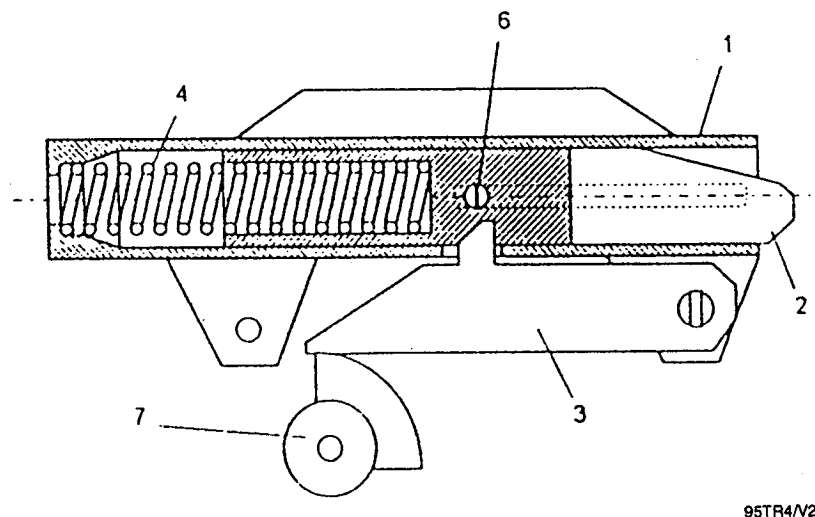
Future activities will focus on the design modification weight with regards to the threshold level, and we will propose a Research and Development (R&D) plan based on the tribologic aspect of high-load contact surfaces.

- Microwelding of high-load contact areas can occur from induced random vibrations.

Description:

The system involved in this paper is the locking device of appendage deployment mechanism shown in Figure 1. The device is made up of a tubular latch body (1), and a finger known as the latch pin (2) that slides inside the latch body. The latch pin is activated by means of a latch spring (4). Guiding capability of the translation movement is provided by means of two screw heads (6) sliding along two symmetrical slots machined in the latch body. A notch is made in the latch pin to allow the finger to be kept in place during the stowed and deployment phases by means of the pawl key, which is a small bit that fits into the notch before release. The pawl (3) itself is set in position by means of a cam (7).

After completion of deployment, the appendage must be locked in position by the latches and adjustable stops. The locking sequence is: near completion of deployment ($\sim 1^\circ$), the cam is designed to set free the pawl. This causes the pawl to carry out a rotational movement around its articulation axis. The result of this is to release the pawl key from the latch pin notch. After ejection of the latch pin, the appendage must be locked in position by the latches and adjustable stops to ensure no any backlash and to retrieve all the kinematics functional plays. Although, the design for antenna and booms locking devices are quite different, only the latch pin is similar, both having to face the same operation problem.



95TR4/V2

Figure 1. Latch Device Subassembly

Testing:

The on-site observation after latch disfunctioning had shown that the appendage was fully deployed. The pawl was set free from the cam, but no latch pin ejection occurred. The pawl was then unjammed by an extra measured load application at pawl key level. This latch pin ejection allowed the satisfactory locking of the appendage. After this action, every deployment test led to successful locking of the device.

Once the latch subsystem was meticulously dismantled, a visual as well as an x-ray inspection were performed. This showed mainly wear, degradation, material transfer and uncohesion of the material at the degradation level of contact surfaces between the finger and the key of the pawl.

After discounting the cause as being incorrect manufacturing and/or assembly, housing deformation induced by mounting condition, deployment geometry, or misunderstanding of mechanism use recommendations and procedures, the contact between the latch pin and the pawl key was identified as a critical point. This led us to consider this area as the source of the malfunction.

Those investigations led us to think that possibly microwelding occurred at pawl/latch contact level. The welded area was then sheared by extra and manual load action. The probability of this scenario being correct is reinforced by the fact that in every subsequent deployment test, there was successful locking of the device without evolution on the pawl motorization margin of safety.

Analysis. Looking at the history of the different failures, it was clear that the functional failure arose from the dynamic behavior of the system being responsible for the degradation of:

- The two contact areas located on the pawl
- The two corresponding contact areas, one on the latch finger notch, the second on the cam.

In order to understand the involved phenomena, the whole latch subsystem is considered together with its interfaces, and the consequences of the necessary functional plays are analyzed when vibration is applied.

Threshold Detection. The aim of this test is to reproduce the blocking of the latch subsystem during random vibration. The blocking is foreseen to happen when the injected level has passed over a threshold level to be determined. The test sequence is:

- Ten actuations are performed before a vibration campaign; a visual inspection is then performed.
- The random vibration starts at 0.5 g rms (1-min duration) and the level is increased by a 0.5-g rms step.
- After each random vibration step, the strut is actuated for latch operation control.

The first blocking occurred with an input level of 7.5 g rms. The figure shows the step-by-step mass acceleration results (g^2/Hz) along the X-axis.

The random test succeeded in reproducing the latch failure that occurred during DBS (R+M) acoustic test. The latch pin is retracted with the dedicated tool to avoid surface contact damage due to pawl actuation and then a visual inspection is performed. The next test phase must confirm the threshold effect with or without aging/dispersion effects on the threshold.

Threshold Aging/Dispersion Effects. The aim of this test is to evaluate the aging or dispersion on the threshold value. The test loop sequence is:

- Repetition of the preceding level to confirm the failure
- Decrease the level step by step (0.5 g rms) to find the new threshold level
- Return at the first step of the test loop.

The mass X-axis accelerometer curve in the figure shows that the threshold phenomenon still exists, with a dispersion on the level probably due to a slight aging effect that occurred after the two first failures. So, at latch s/s level, the threshold is defined as follows:

- In the frequency range of 300 to 400 Hz, the power spectra density peak level must be less than $10 \text{ g}^2/\text{Hz}$
- It must be noted that during test at latch s/s level, the failure was simulated for a PSD peak level quite similar to the one witnessed at DBS/qualification model (R+M) level ($8 \text{ g}^2/\text{Hz}$) in the frequency range of 300 to 400 Hz.

Disfunctioning Repetition of DBS/Qualification Model and FMI Hardwares. The hardware at the origin of the latch s/s functioning problems were tested with the same test setup and test conditions. Both qualification model latch s/s failed for a simulated PSD quite identical to the one recorded at (R+M) level. It is also demonstrated that the threshold level decreased due to a lack of molybdenum disulfide (MoS_2) coating at the pawl/latch contact level.

Key Words:

Latch Mechanism, Stiffness, No Backlash

Mechanisms:

Latching Mechanism

Systems:

Eureca, Interorbital Communications Experiment, Antenna Pointing Mechanism

Author; Experts:

F. del Campo

Address:

SENER S.A., Madrid, Spain

Telephone:

Title:

Latching Mechanisms for Interorbital Communications

Source:

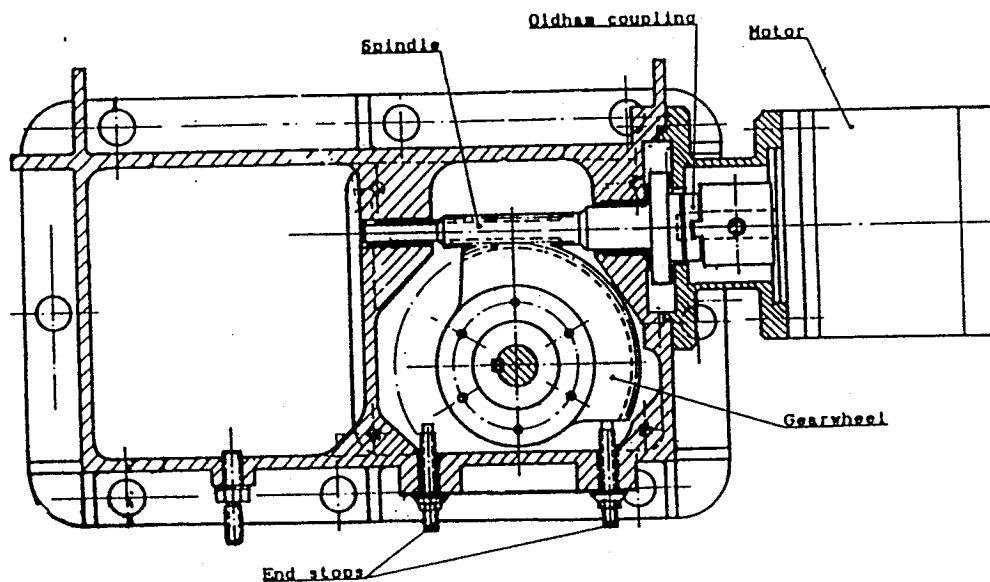
Proceedings of the 3rd European Space Mechanisms and Tribology Symposium, Madrid, Spain, 30 September-2 October 1987, ESA SP-279 (December 1987).

Abstract:

Two different latch mechanisms have been designed under European Space Agency (ESA) contract for the interorbital communications experiment in Eureca. They are both intended for helping the antenna pointing mechanism to withstand the flight loads and to increase its first natural eigenfrequency. In both cases, the main objective has been to obtain a high stiffness paying special attention to the structural discontinuities (clamp, hinges, etc.) in order to eliminate the backlash. This is obtained mainly by preloading these discontinuities and by selecting the adequate materials to avoid problems of differential coefficient of thermal expansion that could change the preload in some critical areas.

Anomalies:

A jamming problem was found when operating after a temperature change (i.e., when trying to open the mechanism at 25°C after it was closed at 65°C). The reason for this problem is that the motor is stopped by mechanical end stops through the nonbackdriveable reducer (see Figure 1). The spindle of the motor then gets jammed between its thrust bearing and the tooth of the wheel in contact at this moment (the spindle remains compressed at the end of the latching and tensioned at the end of the unlatching). The torque required then to unjam the reducer is lower than that applied to jam it, and the motor is able to provide this torque. The problem arises when the temperature changes. Then, if the spindle was compressed (tensioned), and the temperature decreases (increases), the compression (tension) on the spindle increases, due to the differential coefficient of thermal expansion between the stainless steel spindle and the aluminum alloy housing. Under those conditions, the torque required to unjam the reducer is higher than the one applied initially to jam it, and sometimes the motor is unable to provide it. The solution of the problem was to turn the motor backward a small number of steps at the end of each operation unlocking the spindle. This implies a modification of the control electronics to send the corresponding pulses automatically at the end of each operation. Then the thermal expansion of the spindle is free and the problem disappears.



95TR4/V2

Figure 1. Motor Reducer

Lessons Learned:

- The test results of the first latching system show the problems related to the materials with different coefficients of thermal expansion when using mechanical end stops through a nonbackdriveable reducer. Although it is not a very common problem, it reflects how some unexpected problems can be detected by means of some very simple tests.
- Thermal problems are prevalent with actuation and retention and relay mechanisms. Differences in coefficients of thermal expansion must be thoroughly explored to avoid jamming and excessive torque.

Description:

First Latching System. The first latching system consists of two mechanisms plus the corresponding electronics. Each of the mechanisms is an overcenter latch driven by a stepper motor through a worm gear reducer. Each of them is intended to lock one of the two degrees of freedom of the antenna pointing mechanism during launch and reentry. A breadboard model of one of the mechanisms has been built and tested, revealing a jamming problem due to the differential coefficient of thermal expansion in the worm gear reducer area.

Mechanisms Description. The two mechanisms are identical. Only the housings are different, due to interface requirements. Each of the mechanisms has two pairs of hinged bars that are aligned in the final position (overcenter mechanism, see Figure 2). The main characteristics of this mechanism are:

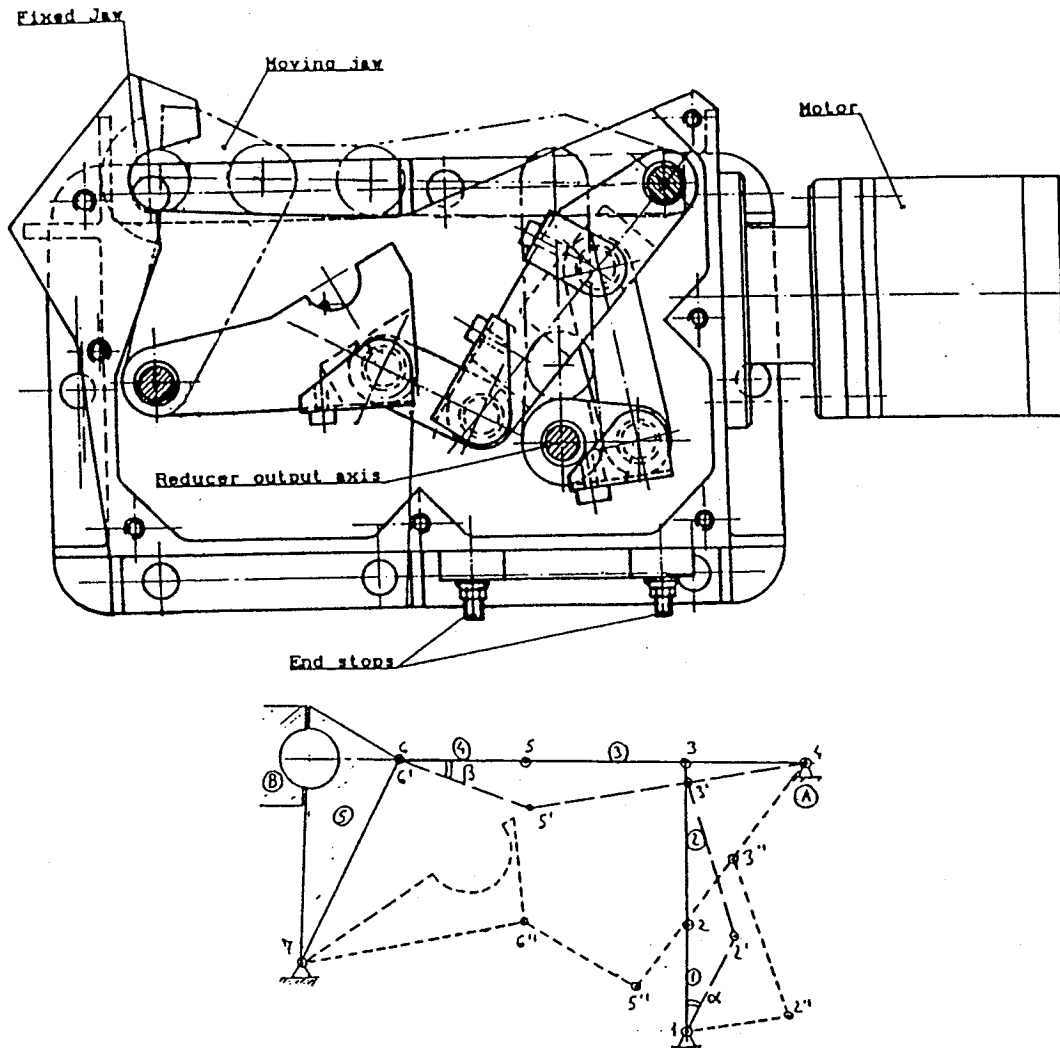
- It is possible to obtain a high clamping force with a low driving torque.
- The clamping force is independent of the driving torque. It only depends on the geometry and stiffness of the links, bearings, and housing.
- The mechanism is self locking without the help of any other mechanical elements.
- By adjusting the clamping force (preload) at a high enough value, the stiffness of the mechanism is not affected by the flexibility of the links.

The shape of the fixed claw and the finger (the element to be caught by the latch) is selected in order to obtain the maximum stiffness in the three directions. By means of a double-conical contact surface (see Figure 3), the finger is fixed between the moving and fixed claws without backlash, provided the preload is high enough.

The mechanism is driven by a stepper motor and a worm gear reducer (see Figure 1). The motor shaft and the reducer spindle are joined by a cross coupling (Oldham joint), which permits a low misalignment between them. The resulting backlash does not affect the final position of the links. The mechanical end stops for the mechanism movement are in the reducer housing. They limit the stroke of the reducer output shaft at both ends of travel by stopping the reducer wheel (see Figure 1).

All the rotating elements are mounted on Ampep bearings, which are made of PTFE reinforced with glass fiber. The worm gear reducer is lubricated with MoS₂.

A flip-flop device is mounted on the output shaft of the reducer. This device has a spring and a lever (see Figure 4). It improves the self locking of the mechanism and reduces the maximum torque required from the reducer.



95TR4/V2

Figure 2. Overcenter Mechanism

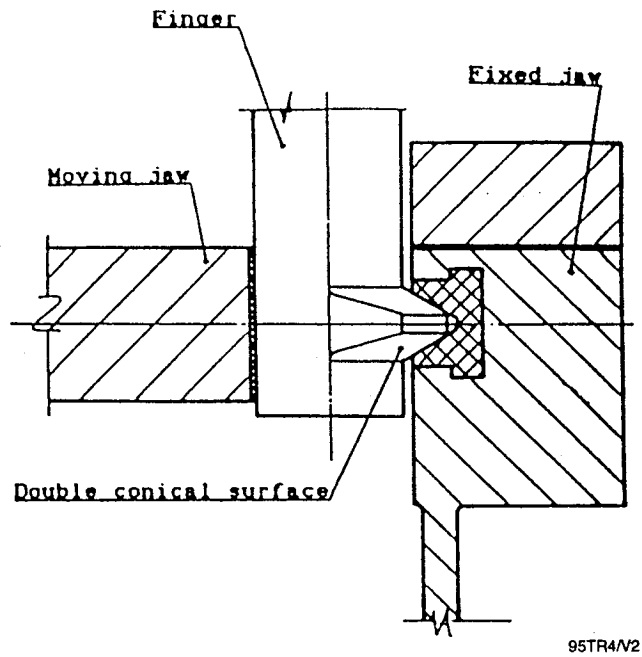


Figure 3. Latching Point

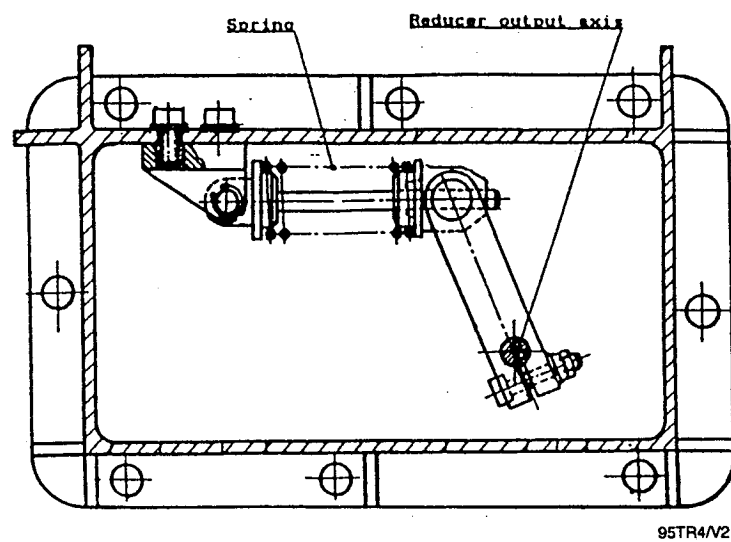


Figure 4. Flip-Flop Device

The material selected for almost all the elements (housing, links, finger, backing of the bearings, etc.) is aluminum alloy. The reason for this is to have a good mass to stiffness ratio and a constant preload when the temperature changes. The reducer contains different materials: stainless steel for the spindle and aluminum bronze for the wheel. The breadboard model can be seen in Figure 5.

Testing:

As stated above, a breadboard of the mechanism has been built and tested. Except for minor details, the model is fully representative of the flight standards. The tests performed were as follows.

Static Load Test. The mechanism was loaded in the three directions up to the yield loads (forces of 250 and 770 N within the mechanism plane, and a force of 1260 N perpendicular to it). The deflection of the mechanism was measured during the test, giving stiffness values between 5 and 30×10^6 N/m, depending on the direction.

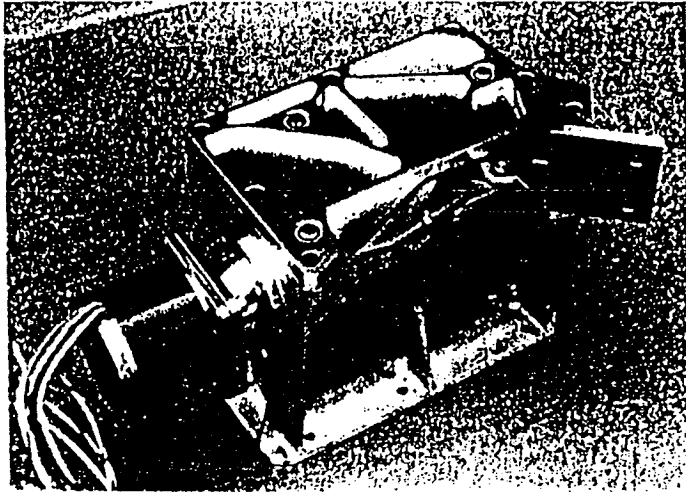
This test was repeated again with link 1 (see Figure 2) slightly shorter than previously (25.00 mm against 25.08 mm). The effect of this change is to reduce the preload, consequently reducing the required driving torque and the stiffness. The effect of this change in the stiffness is negligible. This is partly due to the high stiffness of the linkage (approximately 5×10^6 N/m) that maintains a good stiffness of the mechanism even with low preloads.

Torque Test. The torque required to operate the mechanism was measured by removing the motor and applying a torque meter to the reducer input. The measurements were done to check the influence of the different preload and the flip-flop device, which is always performed in air and at room temperature. The results were:

- Length of link 1: 25.08/25.00 mm
- Maximum torque without flip-flop device: 0.30/0.22 Nm
- Maximum torque with flip-flop device: 0.21/0.14 Nm.

It can be seen that the required torque is reduced by the change of link (without affecting the stiffness) and the implementation of the flip-flop device (improving at the same time the safety against vibrations).

Operational Test in Thermal Chamber. This test was done in a climatic chamber (in air), submitting the mechanism to thermal cycles between its maximum and minimum operational temperatures (-25 to +65°C). The latch was opened and closed at +25, -25, +25, +65, and +25°C in each cycle. Dry nitrogen was injected into the mechanism to avoid ice formation at low temperatures.



95TR4/V2

Figure 5. Breadboard Model

Key Words:

Shutter, Kapton, Exposure, Solar Ultraviolet, Thermal Control

Mechanisms:

Shutter

Systems:

Eureca I, Exobiology and Radiation Assembly

Author; Experts:

W.A. Henton-Jones

Address:

Sira Limited
Chislehurst Kent England

Telephone:

Title:

Shutter Mechanism for Controlling the Exposure of Samples to Solar Radiation

Source:

Proceedings of the Fourth European Symposium on Space Mechanisms and Tribology, Cannes, France, 20-22 September 1989, ESA SP-299 (March 1990).

Abstract:

The Eureca I microgravity mission carries a biological experiment ERA as a part of the core payload. This experiment employs a shutter for controlling the amount of exposure some of the biological specimens received from solar ultraviolet radiation. The biological samples are installed in the facility shortly before launch. Thus, the shutter must be simple to install and check out. This paper describes the modular approach to the final design together with its principal functional details.

PRECEDING PAGE BLANK NOT FILMED

PAGE 480 INTENTIONALLY BLANK

Anomalies:

- The ERA has been subjected to qualification and acceptance testing. This includes vibration and thermal vacuum testing with either full or abridged functional tests at the beginning and at various intermediate times during these tests.
- A defect in the shutter system showed up in vibration testing. The shutter material on the take-up spool tended to unwind like a coil spring, thus producing a linear movement of the blind. Although springs were incorporated in the original design to provide tension in the blind (and electrical contact with the aluminizing), these proved insufficient to prevent movement.

Lessons Learned:

- The problem was overcome by providing a leaf spring to maintain the blind in a tight coil on the take-up spool. Subsequent vibration tests verified the adequacy of this modification.
- The results from these tests verified the design and manufacture of the shutter system and it performed as predicted.

Description:

Shutter System. The system is shown schematically in Figure 1. It is divided into two distinct parts: the shutter cassette (Figure 2) and the shutter drive module (Figure 3). The shutter blind is made from metalized Kapton with predetermined apertures cut in it.

The shutter cassette integrates both thermally and mechanically directly with the fixed double tray and the system drive module. The direct thermal interface enables the cassette top plate to form ERAs principle space radiator.

The interface between the shutter cassette and the transmission module is via a slotted coupling enabling the drive torque to be transmitted to the cassette spool without slippage and simultaneously facilitating cassette integration.

System Principle. The shutter is based on the familiar film cartridge system presently used in 35-mm still cameras. The shutter screen (aluminized Kapton) slides directly beneath the cassette top plate and the surface generated by the window clamp plates on the fixed sample tray. The Kapton shutter blind is in two strips moving along the length of the tray. This facilitates operation and allows a further thermal interface to be made on the cassette top plate. Integration of the cassette on the sample tray creates a guide and slideway for the Kapton with approximately 0.3-mm gap (see Figure 4).

The shutter is drawn from a storage bin where it is loosely coiled through the guided straight section and onto a driven spool. One revolution of this driving spool corresponds to one complete exposure cycle. Hence, each successive revolution of the spool advances the exposure sequence one step. A schematic representation of this system is illustrated in Figure 5.

The system itself is unidirectional and is nonbackdrivable. The spool is rigidly constrained and has no out-of-balance mass and, when coupled to the transmission module, it cannot be turned (except by the powered motor). The Kapton blind is supported over its entire surface area on both sides. Its edges are constrained by the cassette and a slight tension is maintained by the resistance to unwinding from the cassette.

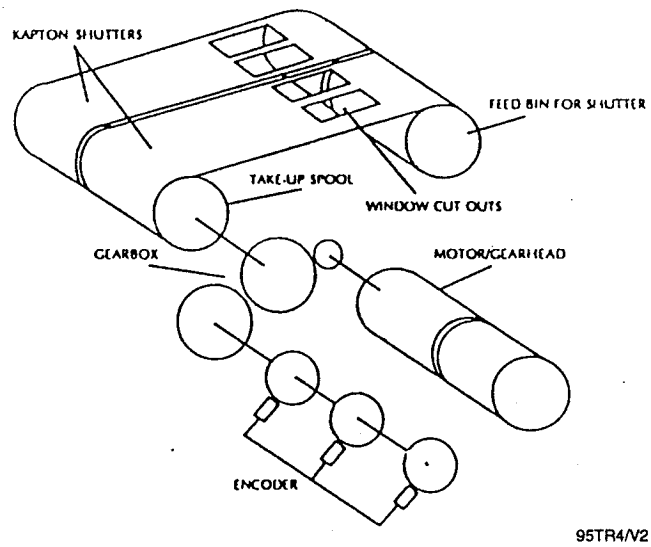


Figure 1. Shutter System Arrangement

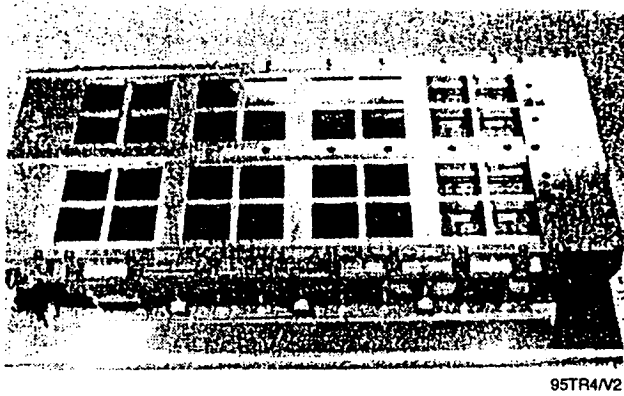


Figure 2. Shutter Cassette

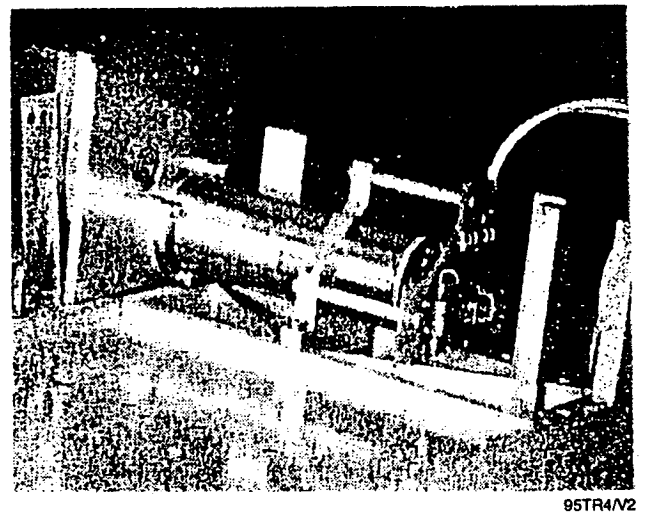
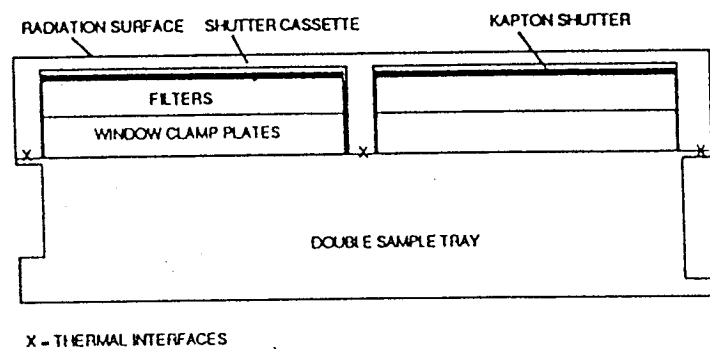
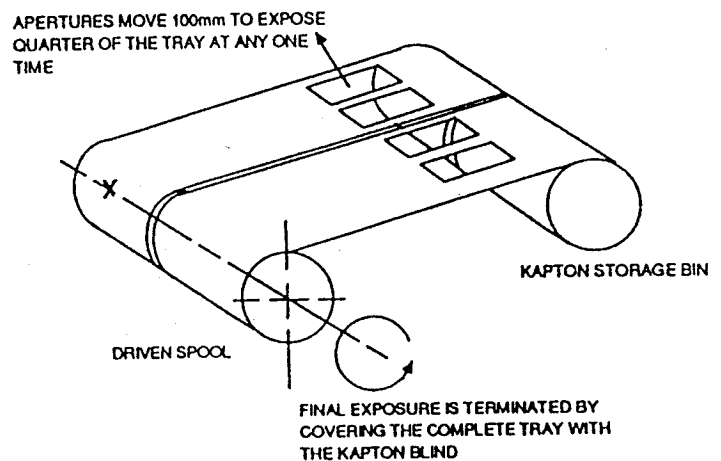


Figure 3. Shutter Drive Module



95TR4/V2

Figure 4. Cross Section of Shutter and Cassette



95TR4/V2

Figure 5. Shutter Operation

Bearings, Lubrication, and Tribology Considerations

Key Words:

Planetary Swivel Mechanism, Thrust Bearings, Slip Rings

Mechanisms:

Planetary Swivel Mechanism

Systems:

MARSNET, ROSETTA

Author; Experts:

1. R. Birner and J. Kaese
2. F. Koller and E. Muhlner
3. H.J. Luhmann

Address:

1. Deutsche Aerospace AG, Munich, Germany
2. ORS, (Osterreichische Raumfahrt- und Systemtechnik GmbH) Vienna, Austria
3. ESTEC, Noordwijk, The Netherlands

Telephone:**Title:**

Parachute Swivel Mechanism for Planetary Entry

Source:

Proceedings of 27th Aerospace Mechanisms Symposium Moffett Field, California, pp. 237-254 (1993).

Abstract:

A parachute swivel mechanism for planetary entry missions, such as a Mars probe (MARSNET) or return of cometary material samples (ROSETTA mission), has been developed. The purpose of the parachute swivel mechanism is to decouple the spin of the probe from the parachute with low friction torque during both the deployment and descent phases. Critical requirements are high-shock loads, low friction, low temperatures, and several years of storage in the deep space environment (during the cruise phase of the probe prior to operation).

The design uses a main thrust ball bearing to cope with the load requirement and a smaller thrust ball bearing for guiding of the shaft. Except for use on the Viking and Galileo swivels, it appears that this type of bearing has very rarely been employed in space mechanisms, so that little is known of its friction behavior with dry lubrication. A slip ring assembly allows the transfer of electrical power for post-reefing of the parachute. A test program has been conducted covering the environmental conditions of Mars entry and Earth reentry.

This paper describes requirement constraints, model missions of planetary entries, a bearing trade-off, analyses performed, design details, the lubrication system, and test results (friction torque versus load/spin rate). In addition, the design of the test rig is addressed.

Anomalies:

- A typical torque test record in the simulated Mars environment is shown in Figure 1. Plots of the test results are depicted in Figures 2 and 3. The mean torque is determined by the difference of torque at rate reversals. The parachute swivel mechanism survived the test program without detrimental degradation in performance.
- The influence of rate on the torque that was experienced had not been predicted. The measured torque was lower than the predicted torque at high loads and vice versa at low loads. For low-load cases, one has to consider that the predictions by the European Space Tribology Laboratory (ESTL) did not cover the friction of the cages. The slip ring friction (not directly measured) is considerably below the predicted value of 0.4 Ncm.

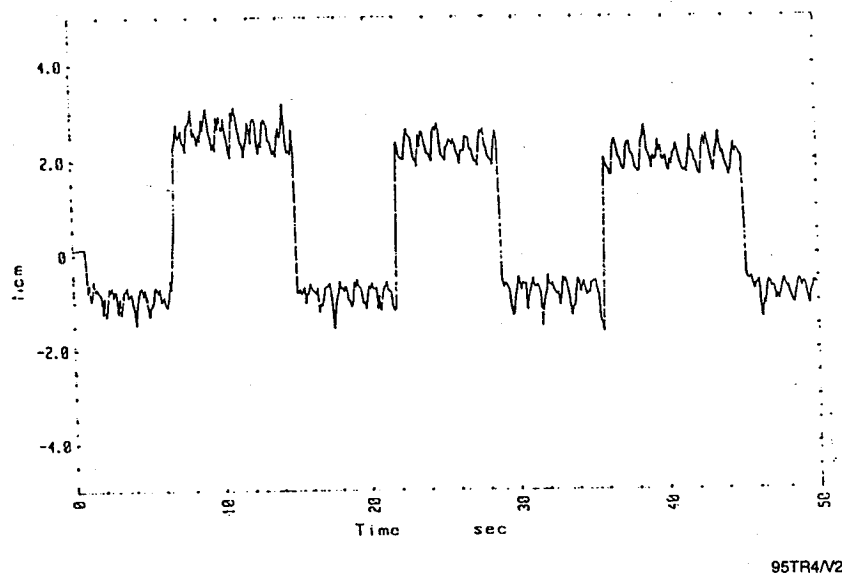


Figure 1. Torque versus Time at 500-N Load, 60 rpm, -55°C, 1-mbar CO₂

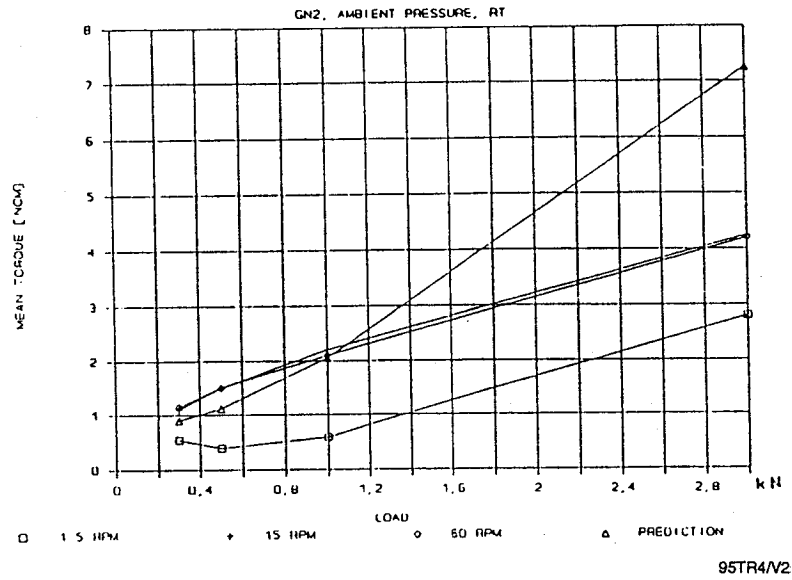


Figure 2. Torque versus Load Up to 3 kN

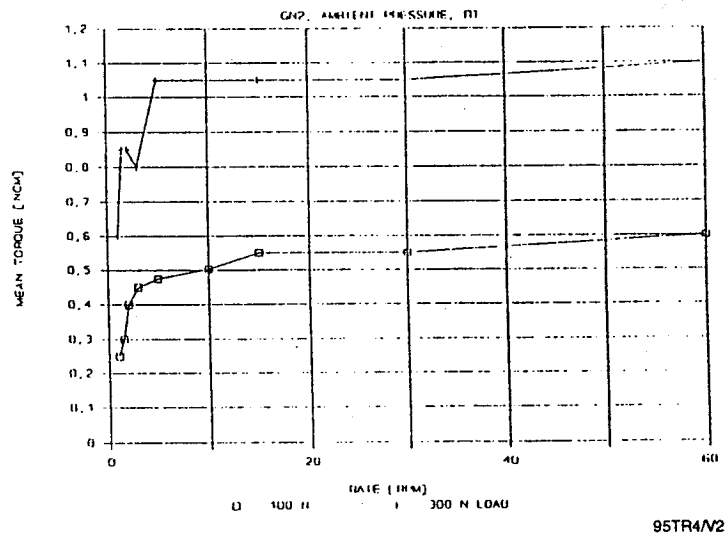


Figure 3. Torque versus Rate at 300-N Load, 1.5 rpm

Lessons Learned:

- A low-torque parachute swivel mechanism for planetary entry missions has been developed. Analysis of the loads acting on the probe parachute system during parachute inflation and parachute-borne descent showed that radial loads are negligible. A test model was built and subjected to torque measurement. Descents in the low-temperature Mars and Earth atmosphere were simulated. The tests were successful. The mean friction torque at -55°C, 1-mbar CO₂, was about the same as measured at room temperature at 1-bar GN₂. The friction torque of thrust ball bearings exhibited an unexpected increase in friction at rates above 1.5 rpm on both unlubricated and lubricated bearings. The thin, dense chromium plating survived all tests.
- Friction torque of ball bearings under thrust load and low temperature are difficult to predict. Unexpected increases in function torque have been experienced.

Description:

The parachute swivel mechanism for decoupling the parachute rotation from spinning probes during descent is a critical device that must operate after long storage time under severe environmental conditions. Very low friction torque is required and knowledge of its characteristics is essential for managing the spin of the probe, by means of vanes, for stabilization and scanning on-board instruments. The operational conditions and requirements have been identified and analyzed. A parachute swivel mechanism has been designed, manufactured, and tested. The basic parachute swivel mechanism design will be used on swivels of the Huygens probe parachutes for Titan entry.

The baseline design (see Figure 4) employs axial ball bearings for the main and guiding bearing (FAG types 51203/51100). This combination was found to be optimum with respect to the restricting demands of very low torque and mass under the applicable load conditions. The maximum static load capacity of the parachute swivel mechanism main bearing is 27 kN.

The housing is made of aluminum 7075. The housing and shaft include lugs for the interface to the parachute and to the probe. Low friction between the parachute clevis and parachute swivel mechanism is attained by use of a bonded MoS₂ film in order to minimize radial loads on the swivel bearings. The same treatment was applied on the lug of the shaft. The shaft is made from titanium, which matches the thermal expansion coefficient of the bearing races.

Power transfer through the swivel for the post-reefing system of the parachute (pyrocutter or release device) is accomplished with a Mecanex slip ring assembly. The slip ring has five lines of 2-A capacity. One of the slip rings serves as electrical bonding between shaft and housing. The four remaining lines allow power transfer to a redundant post-reefing actuator, if required. The slip rings are of an alloy composed of gold, silver, and copper, while the brushes are made from an alloy composed of gold, silver, and palladium. Each brush contact is redundant. The brushes are embedded in a block of epoxy resin. The parachute swivel mechanism size and mass is:

- Outer diameter: 46 mm
- Length: 120 mm
- Mass: 38 gm.

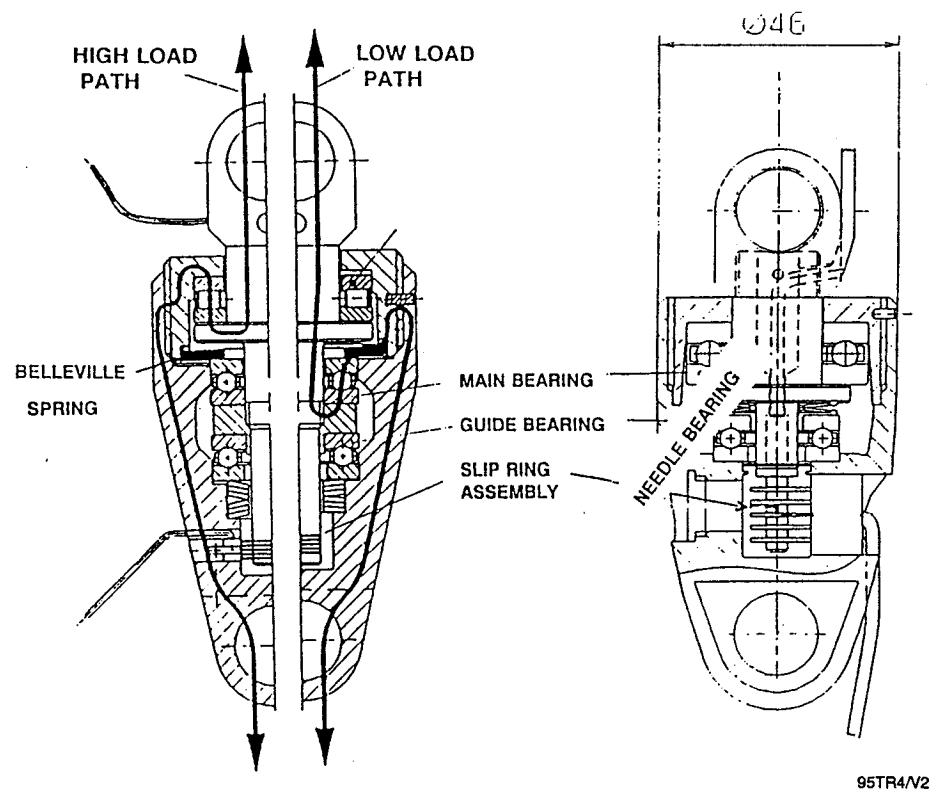


Figure 4. Parachute Swivel Mechanism Baseline Design

The applied tribological system is as follows. The balls, made from AISI 440C stainless steel, are coated with titanium carbide (TiC). The nominal thickness of the coating is 3 to 4 μm , with a fine-grained microstructure (typically 0.1 μm) and high hardness (3500 HV). High-accuracy balls (Grade 3) and a very smooth surface finish (0.006 μm Ra) are obtained. The race washers of 1.3505 steel are coated with 3 to 5 μm of thin dense chromium for corrosion protection and are lubricated with 0.4- μm MoS₂ (PVD process). The bearing cage is machined from Rulon A. The cage has been designed to achieve low friction by low surface roughness and to ensure a positive clearance for the balls under temperature extremes.

The total friction torque comprises the contributions of friction in the main bearing, the guiding bearing, and the slip rings. The main bearing is loaded with the descent load and the preload, whereas the guiding bearing is loaded with the low preload of 100 N only.

Torque predictions were performed by ESTL using a sliding friction coefficient of 0.07 for MoS₂ on steel in vacuum (worst case). A comparison of prediction and test results is shown in Figure 2.

Testing:

The test sequence comprised electrical tests of slip rings, followed by a torque characterization test at room temperature with loads from 100 N to 8800 N at rates between 1.5 and 60 rpm. A shock-load test at no rotation consisted of 10 load cycles up to 8800 N (7000-N parachute-inflation load times and an uncertainty factor of 1.25). A life test in a simulated Mars environment (CO₂) required 4-hr operation at 500-N load at -55°C and at a pressure of 1 mbar.

An Earth environment life test in humid air of 70% relative humidity required 10 min of operation at 3000 N at 15 rpm. A static load test of 20 kN completed the test program.

Key Words:

Linear Bearings, Michelson Interferometer

Mechanisms:

Linear Bearings

Systems:

Michelson Interferometer for Passive Atmosphere Sounding

Author; Experts:

1. E.W. Roberts, R.B.Watters, and S. Gill
2. R. Birner, G. Lange, and W. Posselt

Address:

1. European Space Tribology Laboratory, AEA Technology
Risley, United Kingdom
2. Deutsche Aerospace AG
Ottobrun, Germany

Telephone:

1. (UK)-0925-253015

Title:

Development of Long-Life, Low-Noise Linear Bearings for Atmospheric Interferometry

Source:

Preprint of Paper to Be Presented at the 28th Aerospace Mechanisms Symposium, Cleveland, Ohio, USA (May 1994).

Abstract:

This paper describes the development of dry-lubricated linear bearings for use on the Michelson interferometer for passive atmospheric sounding. Two candidate bearing systems were developed and tested. In the first, use was made of linear roller (needle) bearings equipped with a pulley-and-cable arrangement to prevent cage drift and to minimize roller slip. The second design was of a roller-guided bearing system in which guidance was provided by ball bearings rolling along guide rods.

The paper focuses on the development of these linear bearing systems and describes the approach taken in terms of bearing design, lubrication methods, screening programs, and thermal vacuum testing. Development difficulties are highlighted and the solutions ultimately adopted are described.

Anomalies:

A major finding of these screening tests was that those bearings that utilized rolling elements (i.e., all the bearings except the slide bearing) were adversely affected by creep of the rolling elements and cages. In all cases, this led to high force spikes at one or both ends of travel. These high forces were generated as the cages were driven into contact with the bearing end stops at which point any further movement of the nonstationary races resulted in sliding motion between races and rolling elements. In addition to causing higher friction forces, this effect also resulted in more rapid wear of the MoS₂ film.

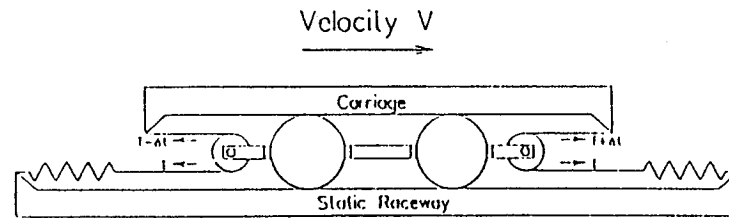
Lessons Learned:

- In order to prevent roller and cage creep, and, thus, eradicate high end forces, a pulley guide system was devised that ensured that the cages were driven at half the speed of the linear carriage. This was achieved as follows. Each end of the cage was fitted with a Vespel SP1 pulley, which ran on an MoS₂-coated steel axle. A thin-stranded steel cable looped around each pulley and was solidly clamped to the end of the carriage-mounted raceway, while being flexibly loaded via a spring to the end of the static raceway. A schematic diagram illustrating the principle of the pulley guide system is shown in Figure 1.
- Linear rolling elements and cages can creep, which leads to high torque spikes at the end of travel. These high forces were generated as the cages were driven into contact with the bearing end stops at which point any further movement of the nonstationary races resulted in sliding motion between races and rolling elements. In addition to causing higher friction forces, this effect also resulted in more rapid wear of the MoS₂ film. To prevent roller and cage creep, and, thus, eradicate high end forces for a speed control device is required to ensure cages are driven at the correct speed ratio.

Description:

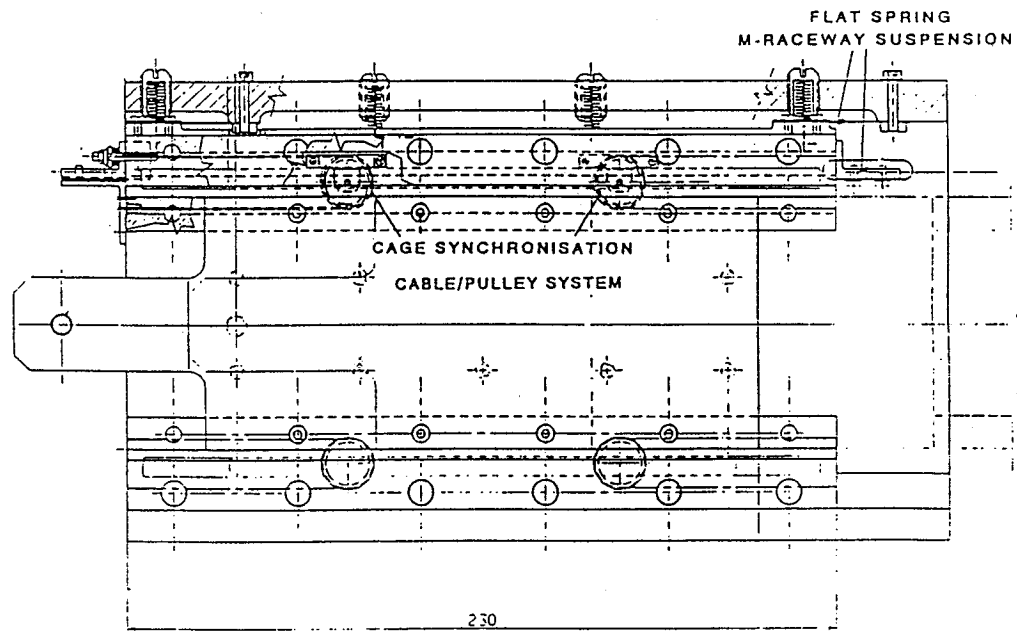
The linear roller bearing guided slide (Figure 2) consisted of 2 sets of Hydrel V- and M-shaped raceways (Figure 3). The bearings were preloaded by a compliant suspension (achieved using flat springs) of one stationary raceway. This compliant suspension provided a constant preload, insensitive to thermal changes, wear-out, and residual misalignment. Preloading was adjustable using four compression springs housed in special set screws (Figure 4).

Each bearing (Figure 3) was fitted with a PTFE-coated (ALTEF coating 40 to 50 μ m) aluminum cage of length 165 mm, the length of the races being 230 mm. Each bearing contained 12 5.4-mm long, 2-mm dia steel rollers with six rollers arranged symmetrically at each end of the cage. The roller groups at each end were separated at a distance greater than the travel of the rollers so as to prevent overlapping of the wear tracks. The bearing races and rollers were lubricated with sputtered MoS₂ (thickness 1 μ m).



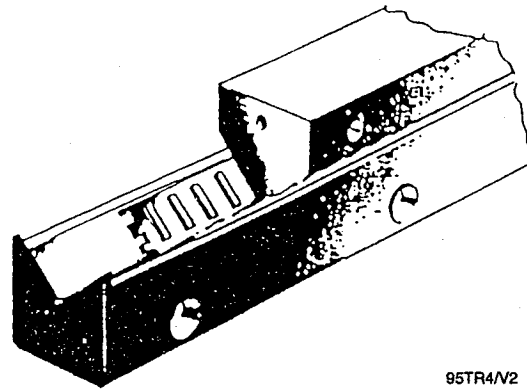
95TR4/V2

Figure 1. Principle of Pulley/Cable System for Controlling Cage Speed



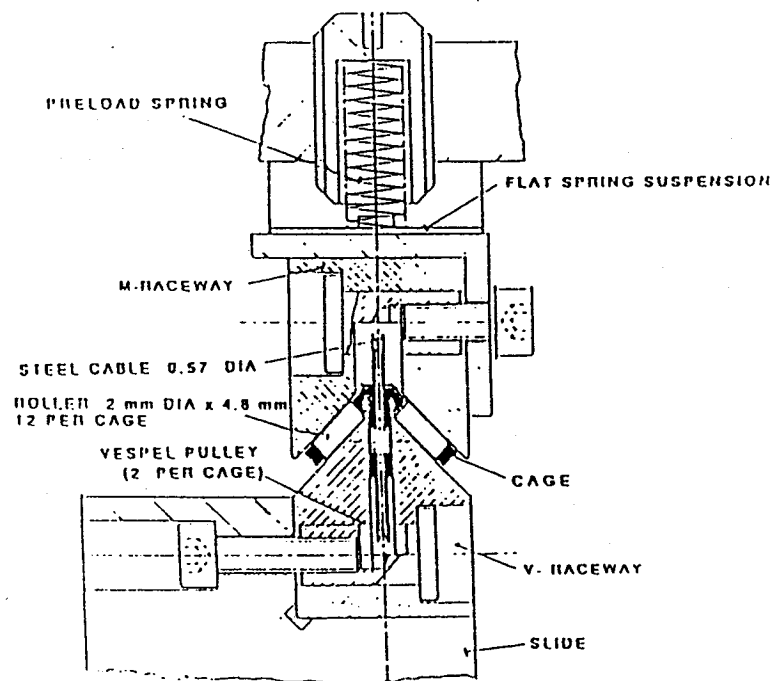
95TR4/V2

Figure 2. Linear Roller Bearing Guided Slide



95TR4/V2

Figure 3. Hydrel Roller Bearing



95TR4/V2

Figure 4. Cross Section of Hydrel Roller Bearing Showing Preloaded System

Actuators, Transport Mechanisms, and Switches

Key Words:

Deployment Mechanism, Boom Actuator, High Torque, Drive Stall

Mechanisms:

Boom Actuator

Systems:

Space Telescope

Author; Experts:

T.R. Cawsey

Address:

British Aerospace P.L.C.
Dynamics Group, Bristol Division, England

Telephone:

Title:

A Deployment Mechanism for the Double-Roll-Out Flexible Solar Array on the Space Telescope

Source:

Proceedings of 16th Aerospace Mechanisms Symposium, Kennedy Space Center, Florida, pp. 223-232 (1982).

Abstract:

British Aerospace (BAe), as prime contractor to the European Space Agency (ESA), has developed a roll-out flexible array that provides more than 4 kW of power for the NASA/ESA space telescope. The array is configured as two wings. The deployment mechanism for each wing is based on the flight-proven Hughes Aircraft Company (HAC) FRUSA design. However, modifications have been incorporated to accommodate an increase in size and the space telescope mission requirements. The assembly and operation of the deployment mechanism are described together with environmental and functional tests results.

Anomalies:

- During thermal vacuum testing of the boom actuator unit at -35°C and maximum loading conditions, a problem occurred in the redundant one-motor-drive mode. The detent torque of the backdriven motor increased from its normal 0.42 Nm to about 1.41 Nm (Figure 1). This increase in detent torque, attributed to a reduction in gearhead clearances (backlash) and possibly some increase in lubricant viscosity, was deemed to be a major factor in a drive condition occurring before retraction was complete.

Lessons Learned:

- As a result of this test failure, a decision was taken to fit heaters to the gearhead and increase the gear ratio between the gearhead output and cassette drive from 1.943 to 3.579:1 to further reduce the load on the drive motor.
- The adoption of an existing design, coupled with direct access to supporting data, has reduced design and development time. It enabled major effort to be concentrated on design modifications and additions with the knowledge that the concept was proven. An initial concern was the 5-yr life with exposure to approximately 30,000 eclipse thermal cycles. However, the results of the thermal vacuum testing, particularly with regard to the lubrication aspects, have instilled a high degree of confidence in the design and laid the foundation for the future development of this and other mechanisms that have to comply with similar requirements. The mechanism has proven its ability to stow, protect, and deploy the solar cell blankets. The final inspection of the blankets after completion of the qualification program showed that the cover glass on 28 real cells and 22 dummy cells out of a total of 24,370 cells had been cracked as a result of handling and testing.
- Low temperature can cause reduction in clearances and consequently higher torques. Heaters may have to be applied to gearheads and other devices if excessive friction results.

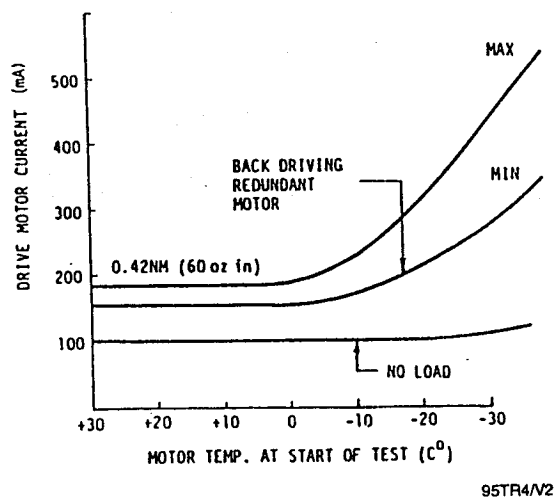


Figure 1. Relationship between Detent Torque and Temperature

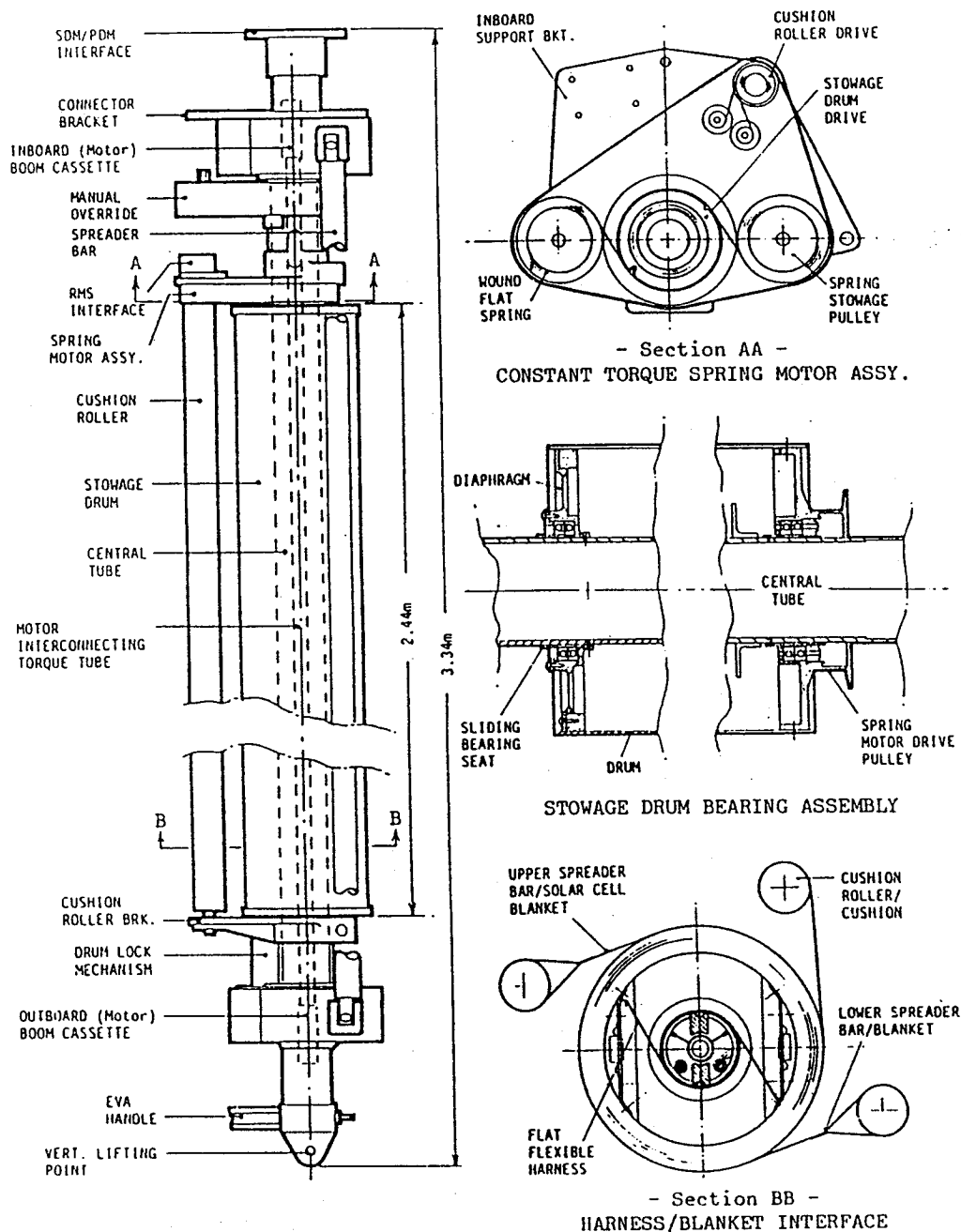
Description:

The stowage drum is a one-piece aluminum alloy tube (203.2-mm OD, 2-mm wall). It rotates about the static central tube via duplex bearing units in each titanium alloy end support (Figure 2). The inner race of the inboard bearing pair is locked to the central tube's titanium alloy seat but the outboard bearing is free to slide axially to accommodate differential expansion between drum and tube. The outboard bearing seat is hard-anodized aluminum-alloy coated with a resin-bonded MoS_2 .

The thin-section bearings, which are ABEC 7 and 440C stainless steel, have ion-plated lead on the races and a lead-bronze cage. They are mounted face to face under a spring preload of 22.25 to 40.00 N. The free rotation of the stowage drum is essential for the successful operation of the SDM. To ensure that axial bearing overload does not occur if the sliding interface seizes, the outboard bearing unit is also housed in a diaphragm mount. This diaphragm is 0.5 mm thick with an axial stiffness of 200 N/mm. It is manufactured from a titanium alloy forging with radial grain flow to reduce the possibility of circumferential cracking when deflected. The electrical interface with each blanket is through soldered connections at the drum surface and the mechanical interface is a glass fiber-reinforced Kapton strip bonded to the drum with epoxy adhesive. The drum also contains flat flexible harnesses that provide the electrical interface between the rotating drum and static control tube. These harnesses are 1524 mm long and manufactured from a base laminate of 0.068-mm (2-oz) rolled copper foil on 0.051-mm (2-mil) Kapton film with an overcoat of 0.051-mm Kapton film bonded with an acrylic adhesive. Each power harness is 311 mm wide and has 20 serrated conductors. The data harnesses are 155 mm wide, each with 30 conductors. These harnesses (Figure 2) unwind as a spiral for half the solar blanket deployed length and then rewind to the completion of deployment to attain a similarly wound configuration in the fully deployed state as in the blankets stowed condition.

Deployed blanket tension (22.25 N) is provided by redundant constant torque springs (Figure 2). The spring storage pulleys are attached to the inboard support brackets, which also incorporate an SDM lifting point and a grapple-fixture interface to enable possible use of the orbiter's remote manipulator system. The springs are stainless steel coated with bonded MoS_2 . The carbon fiber-reinforced plastic cushion roller is also driven by constant torque springs which impart a 5.5-N cushion tension. The cushion roller has stainless steel end fittings that rotate in bearing units, which comprise a spherical bearing with two small flanged ball bearings fitted into its inner diameter. This arrangement accommodates misalignment, provides redundancy, and off-loads the small low friction bearings during launch.

The boom actuator comprises two cassette assemblies. Each assembly contains two deployable and retractable BI-STEM booms (23-mm OD, 5.85 m long). The cassette assemblies are dry lubricated, gears are lubricated by a bonded solid lubricant, and the boom element guides are a polyimide/ MoS_2 composite. The power unit in each two-boom cassette assembly is a Size 13 PM dc brush motor driving through a three-stage epicyclic gearhead (113:1). The gearhead is lubricated with Braycote 3L-38-RP grease and the phenolic retainers of the output shaft bearings are vacuum impregnated with Bray 815Z oil. An external molecular seal surrounds the output shaft and a lip seal is fitted at the motor/gearhead interface to protect the dry lubricated motor. The spring-loaded radial composite brushes run on a 7-bar commutator of zirconium copper with mica insulators. Anticreep film is used within the gearhead and motor to prevent internal oil migration and leakage from the unit. The two geared motors are connected by a torque tube to provide an electrically redundant drive.



95TR4/V2

Figure 2. SDM Major Components

The outer edge of each solar cell blanket is attached to a carbon fiber-reinforced plastic spreader bar (50.8 mm, 2-mm wall), which is located between and attached to the outer tips of each pair of booms via fixed extension rails. The spreader bar houses a spring mechanism that compensates for mismatch in boom extension rates and final boom deployed length to maintain a uniform tension across the blankets. The compensator mechanism is connected to the extension rails by stainless steel tapes and includes a linear potentiometer that senses spring extension, from which the blanket tension is determined. The potentiometer movement is limited to ~25 mm; to provide a readout over full extension rail length (127 mm), the potentiometer is enclosed by a secondary spring in series with the primary spring such that the load that results in 228.6-mm extension of the primary spring causes the secondary spring to extend 25.4 mm.

The manual override gearbox has a ratio of 0.711:1 and is in constant mesh with an output gear on the torque tube. The drum lock mechanism also interfaces with the torque tube and the design is such that in the locked position the load on the release cam passes through the axis of its carrier shaft which results in a very low torque transfer to the release quadrant.

The overall mass of the SDM is 54.72 kg. However, approximately 10 kg of this is for instrumentation and astronaut extra vehicular activity interfaces. Apart from thermostatically controlled heaters on the motor units, the thermal design is passive with most of the exposed external surfaces covered with self-adhesive aluminized Kapton film and some internal surfaces black anodized.

Operation. A tension of 111.25 N is applied to the solar cell blankets to prevent slippage during launch. This tension is maintained by the drum lock mechanism. After primary deployment, the SDM is activated and during the initial revolution of the torque tube the drum lock releases. This is possible because the first revolution of the boom stowage cassettes is used to open out the elements from their tightly wound condition prior to their exit from the cassette housing. The booms are driven out and the blankets are pulled from the stowage drum via the spreader bar. The cushion rolls onto the cushion roller and the main spring motors act against drum rotation to ensure tension in each blanket. At the completion of deployment, or in any interim position, the booms remain locked by virtue of the high gearing within the actuator unit. For full deployment, the stowage drum rotates approximately 8 revolutions and the cushion roller 32 revolutions.

For normal deployment and retraction, both motors are driven together to deploy or retract one wing at a time. However, if electrical failure occurs in one motor, each motor is capable of driving both boom cassette assemblies and backdriving the failed motor. The drive electronics also has the capability to drive one motor in each SDM to simultaneously deploy or retract both wings. The drive motors are switched off at the completion of deployment or retraction by preset microswitches within each cassette assembly. Normal two-motor-drive deployment time is approximately 5 min and the manual input torque required for blanket deployment is <5 Nm.

Antennas, Booms, and Masts

Key Words:

Ulysses Spacecraft, Space Mechanisms, Radial Booms, Wire Booms, Axial Booms, Space Antennas

Mechanisms:

Wire Booms, Axial Booms

Systems:

Ulysees (Antenna)

Author; Experts:

1. F. Abarrategui, M. Fuentes, and S. Ugaldea
2. M. Aguirre

Address:

1. SENER, SA, Spain
2. European Space Agency/ESTEC, Noordwijk, The Netherlands

Telephone:

Title:

The Ulysses Mechanisms

Source:

Proceedings of the Second European Space Mechanisms and Tribology Symposium, 9-11 October 1985, Meersburg, Germany (ESA SP-231).

Abstract:

This paper describes the Ulysses mechanisms subsystem consisting of the following three types of mechanisms: a radial boom, two wire booms, and a rigid axial boom. The radial boom is used to deploy away from the spacecraft body five experiment sensors. This rigid boom is constructed with nonmagnetic materials and consists of two articulated arms. The wire boom antennas form (when deployed) a 72-m tip-to-tip dipole for the radio and plasma wave experiment. The antenna element is a tape of 5- x 0.04-mm section in CuBe₂ material. The axial boom antenna, located at the spinning axis of the spacecraft, is used as a monopole antenna by the radio and plasma wave experiment. This antenna consists of a tube of lenticular section. The section shape permits to press the tube flat and then roll it into a drum.

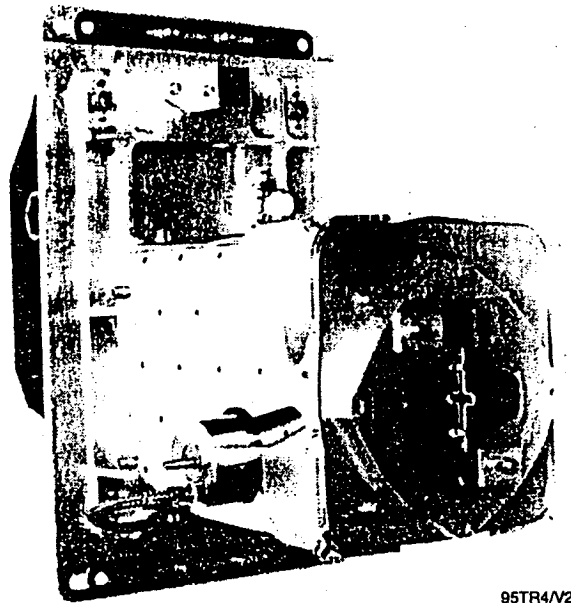
PRECEDING PAGE BLANK NOT FILMED

Anomalies:

- During the ISEE-2 flight, it was observed that after attitude maneuvers, the wire boom tapes slowly oscillated for quite a while. Therefore, in addition to modifying the drum to be able to store 35 m of tape, a tubular damper 15 cm long was installed to help in the damping of this motion. The damper is surrounded by a trumpet-like protecting cone for thermal reasons. The tip mass is guided in this cone at the beginning of the deployment.
- When the axial boom tube is stored in the drum, the stored elastic energy in the tube is not capable of overcoming the friction inside the mechanisms and therefore does not deploy by itself, but during the vibration test, some partial deployment of the tube occurs. To avoid this unwanted phenomenon, the tip of the tube was fitted with a small (1-mm diameter) cross bar. The two ends of this cross bar were held down against the unit box by two small leaf springs (see Figure 1). This avoided deployment due to vibration. When the motor is activated, the cross bar pushes both the springs and scape using only 2 of the 28 V supplied to the motor (20 mA of motor current) during the first 2 cm of deployment when the motor is cold and the output power is at its maximum.

Lessons Learned:

- Mechanisms must be evaluated for vibration problems and appropriate damping applied. Vibrations can also cause unwanted deployment which must be constrained.



95TR4/V2

Figure 1. Axial Boom (Top View) Showing the Leaf Springs and Cross Bar

Description:

Wire Boom Description. The two wire booms are located at opposite sides of the spacecraft so that when deployed they form a 72-m tip-to-tip dipole antenna for the radio and plasma wave experiment. These units are a modification of those flying in the ISEE-2 spacecraft, which are only 30 m tip to tip.

Although called wire booms, the antenna element is a tape of 5- x 0.04-mm section of CuBe2 material. This tape is stored in a drum and is deployed by centrifugal force pulling from a tip mass of 16 g. The deployment speed is controlled by a stepper motor which allows the tape to deploy at 7 to 10 mm/sec. The motor used is a variable-resistance stepper motor (SAGEM, p/n IIPP940486) driven from a common electronic unit, so both tapes will deploy symmetrically. This electronic unit also drives an identical stepper motor used in the axial boom.

The drum that the tape is stored in is made of Delrin and carries the sliding contacts of the slip ring, which transfer the antenna signal to a coax connector at the aluminum box of the unit. The drum has a worm gear engaged with a worm in the motor axis. Only when the motor rotates does the antenna tape deploy.

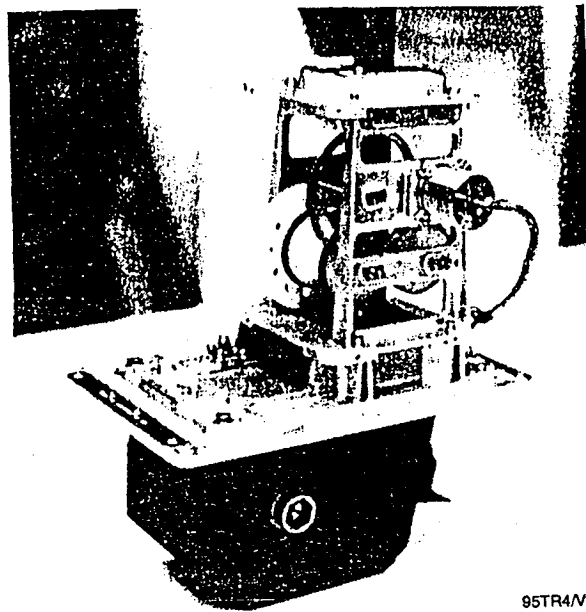
The worm/worm gear combination is irreversible, so the antenna does not deploy by centrifugal force. Nevertheless, this irreversibility is lost in the presence of vibrating loads. An adjustable friction brake (acting on the motor axis) has been added to preclude the possibility of a partial deployment of the antenna during launch when vibration plus centrifugal force (provided by lateral acceleration) are present. This friction brake holds the motor axis still during launch and uses approximately 1/3 of the motor power available during antenna deployment.

Axial Boom Description. The axial boom is located at the spinning axis of the spacecraft and is used as a monopole antenna by the radio and plasma wave experiment. This antenna consists of an 8-m biconvex tube that can be flattened and then rolled up in a 60-mm diameter drum (see Figure 2). The tube is constructed of two halves of annealed CuBe2, 40- x 0.05-mm tape, spot welded at the edges, and age hardened with an internal mandrel.

The tube is deployed by pulling from the spot-welded edges with friction rollers driven through a set of spur gears by a stepper motor identical to those used in the wire booms. Retraction (not required in orbit) is performed using a handle acting on the axis of the storage drum. The drum in which the tube is stored, is made of Delrin and carries the sliding contacts of the slip ring that transfer the antenna signal to a coax connector at the aluminum box of the unit.

In addition to the driving rollers used for deployment of the antenna tube, another set of free rollers have been incorporated to improve the alignment and the stiffness of the root attachment.

The axial boom is mounted on the spacecraft using an intermediate plate that allows the location of the antenna tube at the spacecraft spin axis, once this has been determined by test.



95TR4/V2

Figure 2. Axial Boom with Partially Deployed Tube

Testing:

Wire Boom Development Anomalies. As the wire boom units were already qualified and flown without problems in the ISEE-2 satellite, their implementation in the Ulysses spacecraft did not seem at all problematic. The increase of the storage capacity of the drum, and the inclusion of a damper, seemed to be only a geometrical change without affecting the unit performance, so no DM was built, and the changes were made directly in the spare unit remaining from the ISEE-2 program.

When the modifications were made in the first vibration test, the antenna tape broke at the attachment point with the tip mass. This was due to the cantilever-mounted tube damper movement, which bent the tape back and forth while it vibrated. The tip mass was modified so that it held the tip of the tube damper centered at the protecting core.

This solved the problem of the tape integrity, but the damper continued to move the tape during vibration, forcing use of a very high brake setting to avoid tape deployment. It was then obvious that the inclusion of the damper was not a minor modification. It would probably have been better to redesign the unit and use another device to avoid partial tape deployment at launch.

An assessment of the brake setting of 15.6 g rms compared with the system level test data for the direction perpendicular to the tape, which is the only direction that produces significant tip movement, showed that we have been extremely conservative.

When the test was repeated at 3.7 g rms (1.5-g margin over the expected level), the brake setting was reduced to 1/3 of the available motor power, which seems to be a good compromise between precluding the tip movement at launch (only 10-mm movement) and ensuring the antenna deployment after launch.

The friction force, used for pulling the tube by its edges, is communicated using neoprene rings at the drive rollers. This material is not recommended for use in space because of its outgassing and weight loss at high temperature. Therefore, a test was made to check on the suitability of this material in the environment to be used.

The qualification model unit was installed in a vacuum chamber for 28 days at the maximum expected temperature 20°C (maximum outgassing), and after that time, a deployment test of the unit was performed at -20°C (minimum friction expected in the neoprene rings) without any change in unit performance. Also spare neoprene rings were measured before and after this test with no significant changes in hardness (48 shore A before, 50 after), weight loss (1%), and elasticity.

Key Words:

European Remote Sensing Satellite (ERS-I), Synthetic Aperture Radar Antenna, Deployment Delay, Sticking

Mechanisms:

Antenna Deployment Mechanism

Systems:

ERS-I, Synthetic Aperture Radar Antenna

Author; Experts:

R. Barho

Address:

Dornier GmbH
Friedrichshafen, Germany

Telephone:

Title:

Investigations into Deployment Complications of the EER-I SAR Antenna

Source:

Proceedings of Fifth European Space Mechanisms and Tribology Symposium, ESTEC, Noordwijk, The Netherlands, 28-30 October 1992, ESA SP- 334 (April 1993).

Abstract:

The synthetic aperture radar antenna is an important part of the first European Remote Sensing Satellite (ERS-I). In deployed configurations it consists of a 10-m x 1-m planar array, divided into five single-panel arrangements. A deployable truss structure at the rear side of the antenna guarantees the alignment requirements in the deployed configuration. During launch, this framework is partly embedded into rubber supports to overcome the vibration loads without damage. In the launch configuration, the folded antenna is stowed as a compact package and clamped by six hold-down and release levers, which hold the deployable

panels closed and safe in front of the rigid midpanel. After a period of nine months clamped in the stowed configuration, a final on-ground deployment test was performed with the flight model antenna, which resulted in a delay of approximately 22 sec after the hold-down and release levers release before the deployment started. In up to 10 previous deployment tests, no delay was detected. This presentation shows the results of the investigations and tests on the antenna and component level (to find out the reason of this deployment hindrance).

Anomalies:

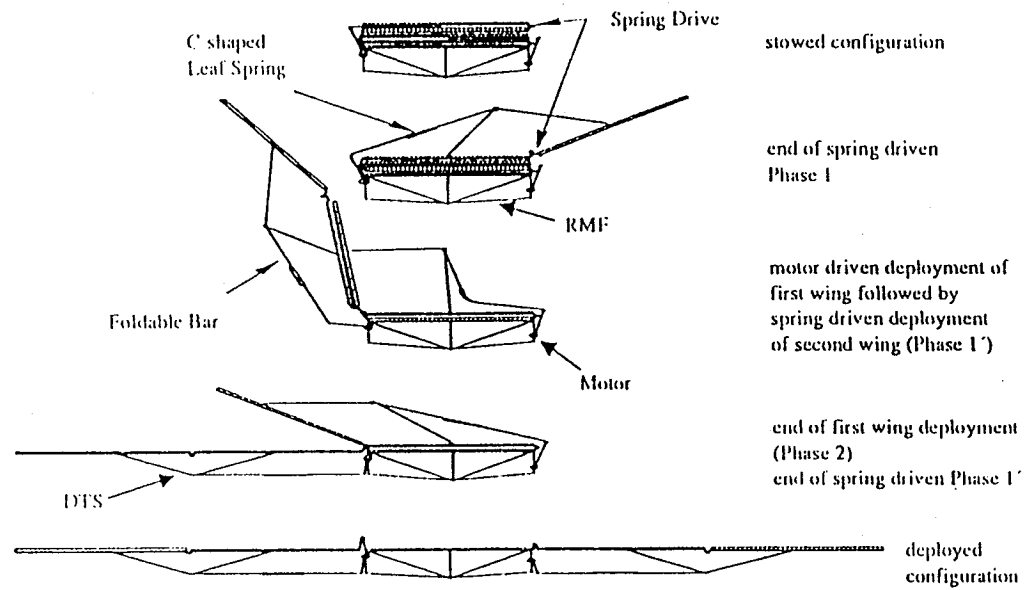
During all the previous deployment tests, five performed with the engineering model and three with the flight model. No deployment delay after opening of the clamping levers occurred. The unexpected 22-sec deployment delay of the first spring-driven phase (Phase I) during the last planned deployment test was the reason for an additional expanded test program (to find out the source of this failure and to correct it).

Lessons Learned:

- The investigations of the separation problems were satisfactory. Following the test results and corrective actions for the ERS-I flight model, there was a successful deployment in space. The MoS₂ powder treatment of the rubber surfaces and a small hardware modification for ERS-2 were acceptable.
- The project did not perform any further basic research investigations to find out the physical explanation for this sticking or sucking phenomena detected on a rubber material, which was specified as having excellent release characteristics.
- To avoid similar problems in other projects, it is recommended to close the gap of knowledge concerning this phenomenon by a test program, or at least to verify long-term stowage properties by component tests.
- Stowage time can effect deployment mechanisms, especially where soft-contact interfaces are required to separate at deployment.
- Rubber contact could cause separation problems by sucking or sticking. MoS₂ coatings could alleviate this problem.

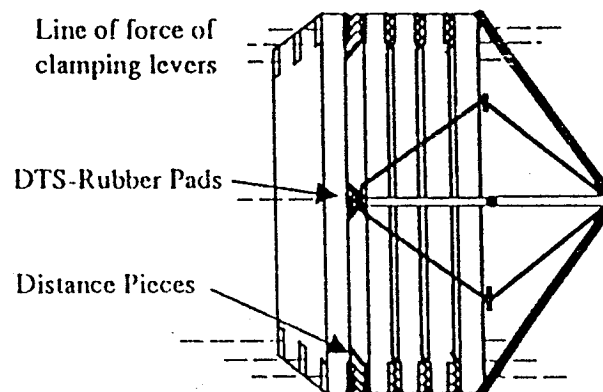
Description:

Antenna Deployment. The center panel of the five-panel arrangement is fixed to the three mounting points of the satellite by a rigid mounting frame (see Figure 1). The four panels of the right and left antenna wing are folded in front of the center panel and held by the hold-down and release levers. The clamps were positioned at the four corners of the panel package and in the center of the two longer rims of the panel package. Together with special tooth-shaped pairs of distance pieces (see Figures 2 and 3) located between each panel in the line of clamping force of the hold-down and release levers (~3100 N), the launch loads on the panel hinge assemblies and the folded framework were limited. In addition, the folded framework structure (deployable truss structure) is held by supporting rubber pads (see Figures 2 and 4).



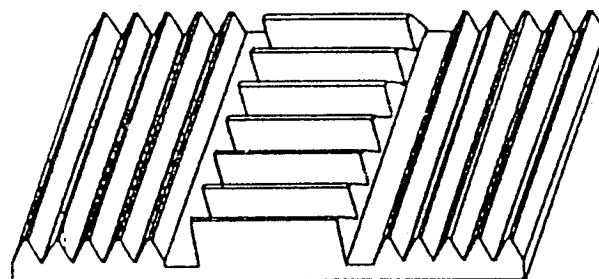
95TR4/V2

Figure 1. Synthetic Aperture Radar Antenna Deployment Sequence



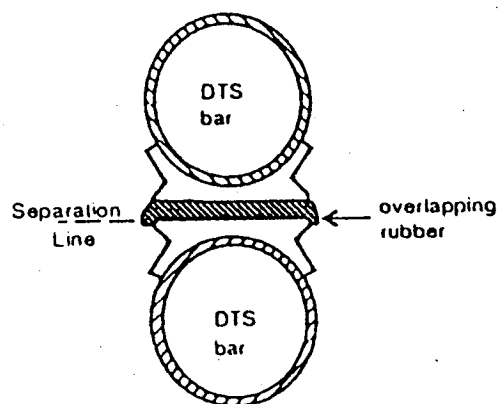
95TR4/V2

Figure 2. Arrangement of Distance Pieces and Rubber Pads



95TR4/V2

Figure 3. Tooth Profile of a Single-Distance Piece



95TR4/V2

Figure 4. Flat Rubber Pad/Aluminum Bracket I/F

The deployment of the antenna starts after release of the clamping levers, which are activated in a defined sequence by a rope tension coming from a central unit. The release consists of a first phase in which the clamp force is removed and a second phase in which the clamps are turned aside.

In the first phase of the deployment, the tip panel deploys under the drive torque leg springs. The end of this deployment phase is when the C-shaped leaf spring of the foldable bar latches is reached (Figure 1). After a waiting period, the motor-driven Phase 2 follows, in which the two-panel wing completes its deployment. This enables the deployment of the second spring-driven phase (Phase 1). After another waiting period, the final motor-driven deployment phase (Phase 2) deploys the antenna to its final configuration. To compensate for the gravity influence on ground deployment tests, a special crane with two movable axes per wing was developed. The resistive forces of the crane are kept very small and were measured before and after each deployment test to exclude them from the calculation of the actual drive torque margin of the antenna.

Testing:

In order to check whether long-term stowage was responsible for the delay, a further deployment test (FM6) was performed after an antenna stowage time of 30 days. A deployment delay of 6.5 sec was measured. It was now very clear, that the deployment delay has to be seen in direct relation with the stowage time of the antenna. The following factors, possibly responsible for the deployment delay after long-term stowage, were investigated:

- Disturbances caused by misaligned thermal hardware
- The intermediate MoS₂-sputtered distance pieces (Figure 2) located between each panel
- The interface between deployable truss structure bars and the supporting rubber pads (Figures 2 and 4).

The arrangement of the thermal hardware in the stowed configuration of the antenna and also during opening of the tip panel by hand was observed with an endoscope. The investigation showed that the arrangement of the thermal hardware between the spring-driven panels caused no deployment disturbances.

Microscopic investigations of the MoS₂-sputtered surfaces of the distance pieces showed tiny particles of elastic adhesive at several distance pieces. Thermal tape glue residues may be the source of these particles. As corrective action, the surfaces of all the teeth of all distance pieces were checked and cleaned of adhesive particles.

The surface finish of the rubber pads has a uniform arrangement of small molds. Tiny particles of adhesive were found on only two rubber pads during a microscopic examination. At the thermal isolation foil of the embedded deployable truss structure bars, residues of adhesive were found at the borders of the scaling thermal hardware strips. It was assumed that sticking of the rubber pads and the helical covered thermal hardware strips may have hindered the tip panel opening.

As a further possible deployment hindrance, a sticking effect between rubber pads and thermal hardware was taken into account. The corrective action to eliminate both possible holding effects, was to cover each deployable truss structure bar that contacts a rubber support with a thin teflon foil. The surfaces of the flat aluminium brackets were sprayed

C. Le.

with liquid Teflon. Another possible source of failure was found at the flat rubber pad/aluminum bracket interfaces positioned at every supporting interface between two opposite bars, and between the connection interfaces of the C-shaped leaf spring. At these interfaces the aluminum brackets enable the rubber pads in the stowed antenna configuration to surround the edges of the brackets and hinder the separation (Figure 4).

To eliminate this possible source of failure, the edges of the rubber pads were shaped at 20° angles. After these investigations and corrective actions, the antenna was restowed for 30 days and then was to be retested. The result will be discussed later. In the meantime, several tests at component level have been performed.

Final Deployment Tests and Corrective Actions on the Flight Model Antenna Before Launch. The deployment tests performed after a stowage time of 30 days did not proceed totally normally. A deployment delay just after release of the hold-down and release levers could not be measured, but the deployment time for the Phase I deployment was longer than specified. After evaluation of the video records in slow motion, it could be seen very clearly, that some deployable truss structure bars oscillated just after release from the embedding rubber supports. The deduction was that the holding effect between the rubber pads and deployable truss structure struts could not have been eliminated totally after covering the struts and the flat aluminum interfaces with Teflon foil or Teflon spray.

After having a normal deployment behavior in the follow-on deployment test, it was decided that additional kick springs had to be positioned between the spring-driven panels to overcome the residual sticking forces after long-term stowage.

The next deployment test after integration of the kick springs and one day of stowed configuration showed no deployment delay. However, since no more time was available, the antenna was stowed and prepared for shipment to Kourou for final integration in the ERS-I satellite.

In addition to the integration of the kick springs, it was decided that the antenna must not be stowed for more than four weeks before launch without panel release. The launch delay made it necessary to perform a double release of the spring-driven panels on the synthetic aperture antenna while mounted on the satellite. This was performed by turning the complete satellite with a multipurpose trolley until the antenna was positioned horizontally to enable the opening of the six hold-down and release lever clamps. After the panels were unlocked between the spring-driven panels, four intermediate Teflon brackets were fixed to let the rubber pads relax for 24 hr.

Investigations at the component level with one of the test specimens were performed after a stowage time of approximately six months. The test results showed a small holding force of 0.1 N in the separation test of the V-shaped interface, and a higher holding force of 0.76 N in the separation test of the flat interface.

Both tests were repeated after a further six-months stowage. One specimen was stowed without any surface treatments and gave a small holding force of 0.02 N at the V-shaped interface and a holding force of 1.5 N at the flat interface (contact area about 2 cm²). The interfaces on the second specimen were coated with MoS₂ powder in order to avoid sticking or sucking at the separation interfaces. Both these interfaces separated without any measureable holding force.

Key Words:

Hemispherical Pointing Mechanism, Microgravity

Mechanisms:

Encoders

Systems:

Eureca, Interorbital Communications Antenna Pointing Mechanism

Author; Experts:

Karl Gallagher

Address:

Marconi Space Systems Ltd.
Portsmouth, England

Telephone:

Title:

Hemispherical Pointing Mechanism

Source:

Proceedings of the Fourth European Symposium on Space Mechanisms and Tribology, Cannes, France, 20--22 September 1989, ESA SP-299 (March 1990).

Abstract:

A description of the design, development, build, and test of a hemispherical pointing mechanism. The equipment was designed for pointing the interorbital communications antenna on the European Recoverable Carrier (Eureca) spacecraft. The Eureca mission was to perform microgravity experiments; the hemispherical pointing mechanism design includes features to reduce microgravity disturbance to the host spacecraft caused by operation of the hemispherical pointing mechanism.

Anomalies:

- The wear test consisted of driving the hemispherical pointing mechanism around a rectangular solid angle of $90^\circ \times 100^\circ$ for 500 continuous cycles in ambient conditions. This duty cycle was intended to be representative of the projected nine-month operation of Eureka. At the end of the test, no sign of performance degradation was detected (with the exception of the encoders).
- Both encoders in the qualification model revealed signs of wear on at least one of their tracks, and consequent errors in their feedback. By examining the bad data from the azimuth encoder (the most severely affected), it was concluded that metallic debris was accreting on the 7th track, causing zones of uncertainty 0.7° wide every 22.5° (during which the encoder output could be seriously inaccurate).
- Although the azimuth encoder on the qualification model was the most seriously affected at the end of the wear test, all four encoders on the qualification and flight models showed some signs of the problem at some stage during testing.

Lessons Learned:

- The brush contact encoders are prone to a wear problem that renders them unsuitable for use on high-accuracy, high-reliability space mechanisms.

Description:

In June 1985 Marconi Space Systems won a contract from the European Space Agency (ESA) to design, build, test, and qualify a hemispherical pointing mechanism suitable for flying on the Eureka scientific satellite. Three models were built: breadboard model, qualification model, and flight model. Each consisted of the pointing mechanism itself, a separate box of control electronics, and the cable connecting the two (see Figure 1).

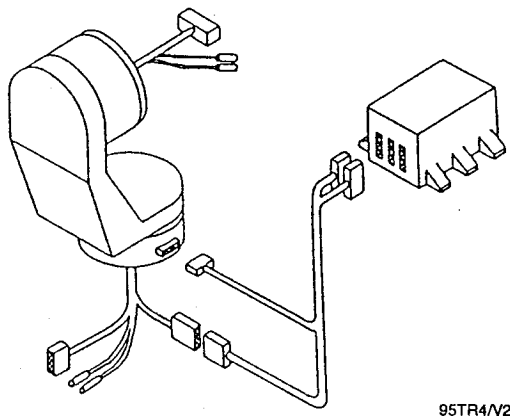


Figure 1. The Hemispherical Pointing Mechanism, Control Electronics, and Cable

The hemispherical pointing mechanism is required to support a large antenna (approximately 20 kg) and point this payload anywhere within a full hemisphere providing feedback to enable the controlling computer to know the orientation at all times. The payload is serviced by a harness consisting of 33 wires and 2 coaxial radio frequency cables, which have to pass through the hemispherical pointing mechanism.

The short period allowed for the program (initially 18 months) did not permit the development of radically new technology, so existing technology was applied in unorthodox ways. Volume and mass of the hemispherical pointing mechanism were critical, as the accommodation available on Eureka was already fixed and limited. The completed flight model hemispherical pointing mechanism and control electronics are shown in Figure 2.

The hemispherical pointing mechanism comprises two rotary actuators separated by an L-shaped bracket (see Figures 3 and 4). Each actuator utilizes a stepper motor with dual windings for reliability and a gearbox incorporating a worm drive for movement. An absolute brush contact encoder provides positional feedback. During launch, the hemispherical pointing mechanism shares the 20-kg load with additional launch locks. To carry this share of the load, each actuator utilizes a pair of needle roller bearings for strength and compactness (see Figure 5).

Encoder. Each actuator incorporates an encoder. This has been developed by Moore Reed as part of a separate contract with ESA. The unit is an absolute brush contact encoder that requires 32 full turns of its output shaft to complete one full count.

Designation: 11 DG 210

Resolution: 13 bit

Code: Gray

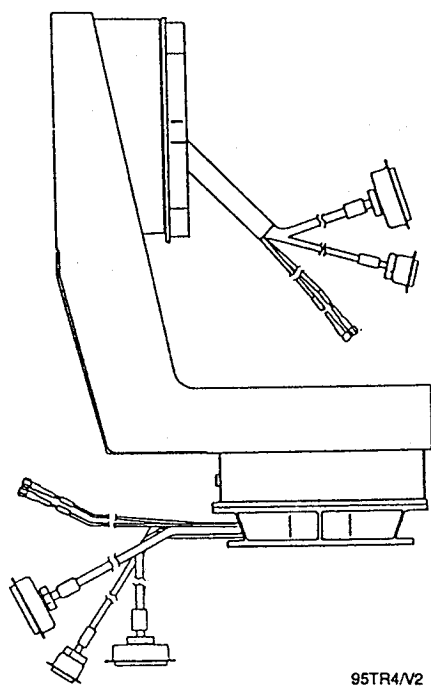
Mass: 60 g

This is mounted on the stationary flange of the actuator, and connects to the moving flange by a two-pass gearbox with a total ratio of 32. The first pass is a bevel gear with a ratio of 4:1, and the second pass is a spur pinion driven by the same ring gear that is driven by the motor gearbox, with a ratio of 8:1 (see Figure 7). The gears carry negligible load and are cut from stainless steel, unhardened, but with the same lubricants as the motor gears.



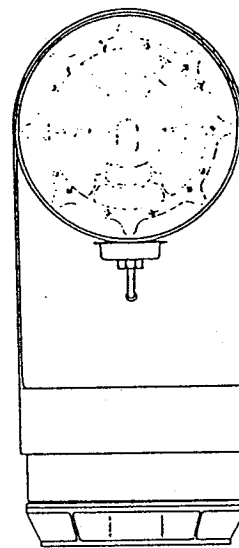
95TR4/V2

Figure 2. Flight Model Hemispherical Pointing Mechanism and Control Electronics



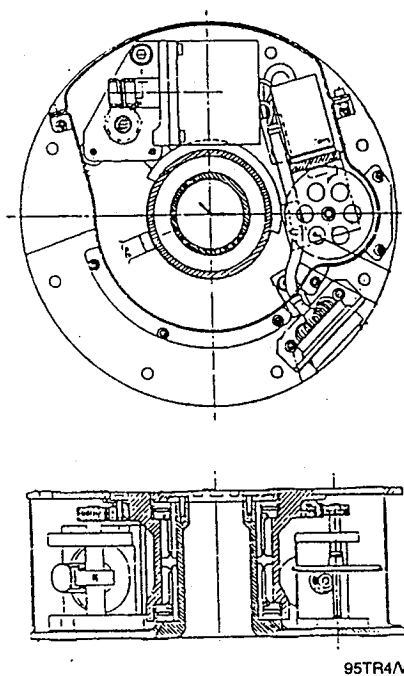
95TR4/V2

Figure 3. Side View of the Hemispherical Pointing Mecahnism



95TR4/V2

Figure 4. Front View of the Hemispherical Pointing Mechanism



95TR4/V2

Figure 5. Internal Detail of a Rotary Actuator

Key Words:

Axial Booms, Incomplete Deployment, Release Mechanism Jamming, Friction

Mechanisms:

Axial Booms

Systems:

GEOS

Author; Experts:

Gunter K. Schmidt

Address:

Dornier Systems GmbH
Friedrichshafen, Germany

Telephone:

Title:

GEOS Axial Booms

Source:

Proceedings of 12th Aerospace Mechanisms Symposium.

Abstract:

A booms and mechanisms subsystem was designed, developed, and qualified for the geostationary scientific satellite GEOS. The project was sponsored by the European Space Agency (ESA) as part of the GEOS development contract. Part of this subsystem are four axial booms consisting of one pair of 1-m booms and one pair of 2.5-m booms. Each of these booms carries one bird cage electric field sensor. Alignment accuracy requirements led to a telescopic-type solution. Deployment is performed by pressurized nitrogen. The main components of this system are:

- Telescopic section
- Release mechanism
- Pressure system
- Triax cable harness
- Experiment canister.

At deployment in orbit, two of these booms showed some anomalies and one of these two deployed only about 80%. Following this malfunction, a detailed failure investigation was performed resulting in a design modification of some critical components as release mechanism, guide sleeves of the telescopic elements, and pressure system.

Anomalies:

- After positioning GEOS in its final orbit, its eight booms and five mechanisms were deployed. However, two axial booms showed some anomalies during deployment and one of these two, a long axial boom, extended to only about 80 to 90% of its full length. Table 1 provides an interpretation of deployment data of the axial booms as observed in orbit on April 30, 1977. The observations are based on telemetry data from the accelerometer output and the boom status switches. Several of the interpretations are conclusive, while others remain inconclusive.
- The information gained from spacecraft data is not totally unambiguous. The -X PM/SAB data can be interpreted in two ways:
 - Release occurred very late and was followed by a fast deployment.
 - Release occurred for both short axial booms (+X and -X axes) at the same time. This occurs under normal conditions within a few milliseconds.
- For the +X SAB, release was followed by a nominal deployment. However, deployment of the -X SAB may have momentarily halted after an initial start, due to stiction, and then continued some 11 sec later. According to the HK signal, the release of the +Y long axial boom occurred approximately 6 to 7 sec too late. Following

Table 1. Axial Boom Deployment Data Observed During Orbit

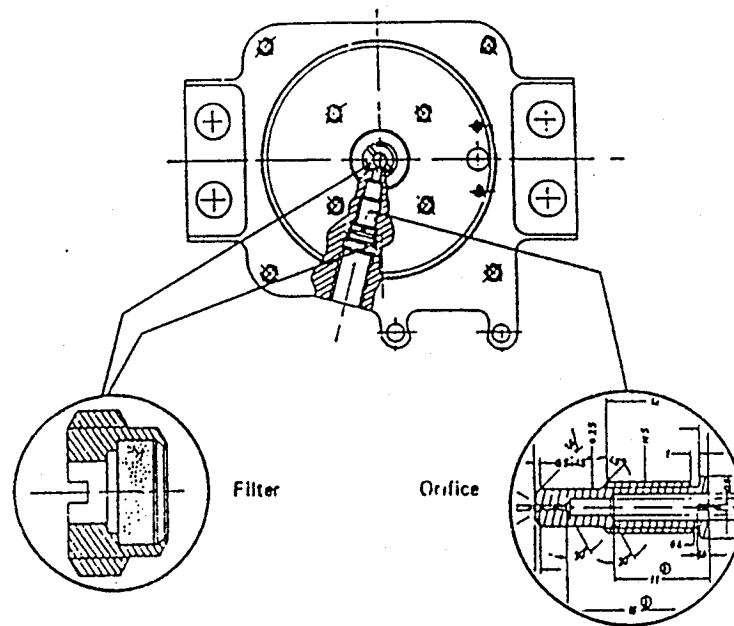
Configuration Data:	Short Axial Booms		Long Axial Booms	
	+X/FS	-X/PM	+Y/FM	-Y/FM
Deployment length	1 m		2,5 m	
overall length	1,6 m		3,1 m	
tip alignment	$\pm 0,02$ m		$\pm 0,02$ m	
release delay:	(sec)	(sec)	(sec)	(sec)
t_r nominal	$0,5 \pm 0,05$	$0,5 \pm 0,05$	$0,35 \pm 0,05$	$0,25 \pm 0,05$
t_r observed	0,5	0,5 or 10,9	6,6	$0,8 \pm 0,6$
deploy time:				
t_d nominal	$1,5 \pm 1$	$1,5 \pm 1$	$2,7 \pm 1,6$	$2,7 \pm 1,5$
t_d observed	0,9	10,8 or 0,8	0,8	$0,55 \pm 0,8$
Deployment time:				
$t_D = t_r + t_d$				
t_D nominal	2 ± 1	2 ± 1	3 ± 2	3 ± 2
t_D observed	1,4	11,3		$1,45 \pm 0,6$
HK — Signal	yes	no	yes	no
achieved deployment length	full	full or nearly full	80 to 90 %	full

95TR4/V2

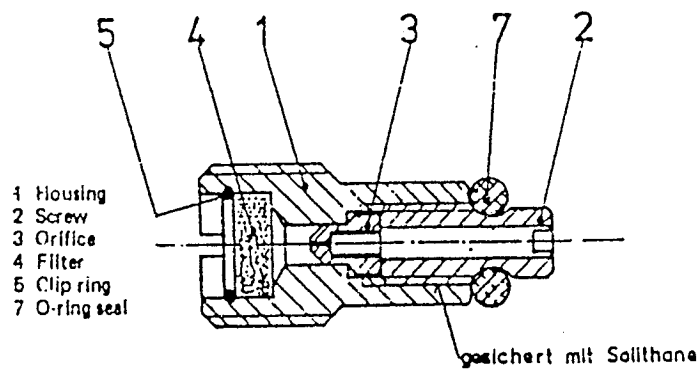
the delayed release, a deployment action of this boom was observed at the accelerometer output. However, any conclusions are subject to doubt, as the accelerometer went into saturation when the -Y LAB deployed, and the connection of HK data and accelerometer readings were considered ambiguous for the long axial boom. The actual deployed length achieved by the +Y long axial boom was determined from attitude maneuver and shadow spike data from the LAB experiment sensors.

Lessons Learned:

- To reduce the possibility of friction due to cold flow of guide rings, the tightening torque for the fixation crews has been reduced to decrease the local stress concentrations at the guide ring. In addition, the Teflon guide sleeve for RE1 was slightly modified to prevent possible jamming forces caused by cold flow resulting in configuration instability.
- In GEOS-1, the orifice and filter were screwed separately into the release block. During integration of the filter, loose particles may have been created by the screwing operation, and trapped between the filter and orifice (Figure 1a). During failure investigation, this condition was observed once. For GEOS-2, a filter orifice assembly was developed, which is assembled separately, using increased cleanliness conditions with careful control under the microscope. This new design significantly reduces the possibility of particle creation and trapping (Figure 1b).
- The release mechanism modification mainly concerned the ball release piston and ball cage area (Figure 2). The hard edge of the titanium sleeve was replaced by a soft aluminum chamfer to prevent indentation of the balls. The ball cage holes that were cylindrical in GEOS-1 are now conical to improve the ball release. This modification significantly increases the friction safety margin for ball jamming from $\mu_1 = 0.41$ to $\mu_2 = 0.77$.
- Considering the GEOS-1 housekeeping data, accelerometer data, and the failure investigation results, there is no indication that orifice contamination caused the observed anomalies. The data indicate that the reduced deployment length of the +Y LAB was caused by a malfunction of the release mechanism. The anomaly in the SAB deployment behavior was caused either by increased friction of one tube element or by malfunction of the release mechanism.
- After positioning GEOS in its final orbit, its eight booms and five mechanisms were deployed. Two axial booms showed anomalies during deployment and one of these, a long axial boom, extended to only about 80 to 90% of its full length. The anomalies were caused by malfunction of the release mechanism or by increased friction of one tube element (guide ring).
- To reduce the possibility of friction due to cold flow of guide rings, the tightening torque was reduced and the Teflon guide sleeve modified.
- The release mechanism modification mainly concerned the ball release piston and ball cage area. The hard edge of the titanium sleeve was replaced by a soft aluminum chamfer to prevent indentation of the balls. The ball cage holes which were cylindrical in GEOS-1 are now conical to improve the ball release.



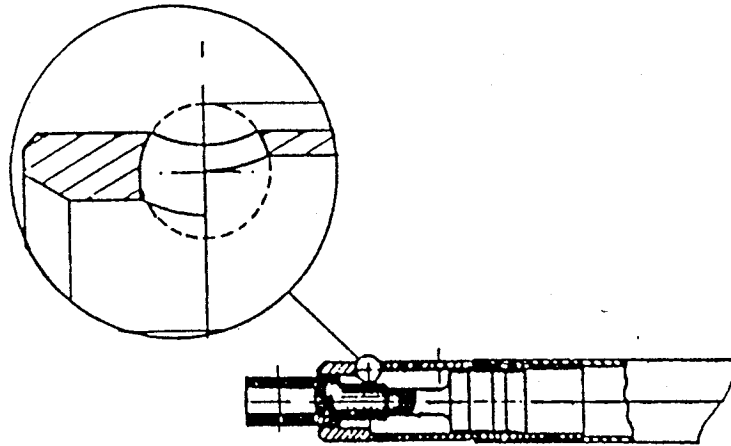
a) GEOS-1 Design



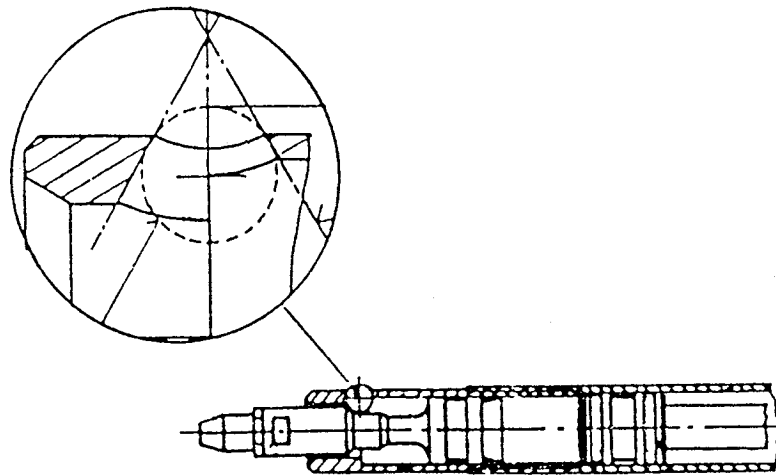
b) GEOS-2 Filter Orifice Assembly

95TR4/V2

Figure 1. Axial Booms Release Block



a) GEOS-1 Design



b) GEOS-2 Design

95TR4/V2

Figure 2. Axial Booms Release Mechanisms

Description:

Four special telescopic booms were developed for the scientific satellite GEOS as part of the booms and mechanisms subsystem. GEOS is a spin-stabilized satellite with a number of booms extending from the spacecraft body for positioning experiment probes. The experiments measure magnetic and electric fields in the low-frequency spectrum. One of the experiments requires two pairs of wire sphere sensors of 100 mm diameter to be extended 1 m and 2.5 m above the spacecraft body, at approximately 70-cm distance parallel to the spin axis. The design requirements led to the development of telescopic booms that are deployed by a nitrogen gas pressure system.

The four axial booms deploy and support GEOS's four wire-sphere electric-field sensors. During launch, the experiment spheres are stored at the base of the spacecraft in canister-like containers, which are sealed by thin aluminum foil membranes. The spheres are electrically connected by helically wound triaxial cables routed within the telescopic booms. Sufficient stiffness was achieved by using aluminum alloy tubes with a large outer diameter and thin walls to withstand the bending loads from centrifugal forces induced by the maximum deployment spin rate of 30 rpm.

Torsional orientation is provided by a keyway. The axial booms are linked by a three-ball mechanism during launch and are released and deployed by pressurized nitrogen stored in pyrotechnically activated tank valve assemblies at 110 bar. Gas flow during deployment is controlled by orifices at the base of each boom providing a deployment time of 1 to 4 sec. The gas system maintains a continuous flow for 15 to 20 sec to provide an adequate safety margin. Numerous deployment tests in vacuum were necessary to define the optimum parameters for this pressure system. Because of the extreme magnetic and chemical cleanliness required for GEOS, very careful selection of materials and processes was mandatory.

Testing:

Possible explanations for the anomalies were:

- Change in friction properties at seals, seal ring, and guide rings due to effects of hard vacuum, effects of Van Allen radiation exposure, and temperature effects creating cold flow of the teflon guide rings.
- Reduction of gas flow due to filter contamination, orifice choking, and piping leakage.
- Release mechanism jamming due to ball latch tolerances, piston over travel, and increased friction between ball and ball cage.
- An incident due to launch failure.
- A 0-g effect.

Most of the above explanations are essentially irrelevant since they would have caused different deployment data. Only the effects of stiction, orifice choking, and delayed release can be considered as valid explanations for the observed anomalies.

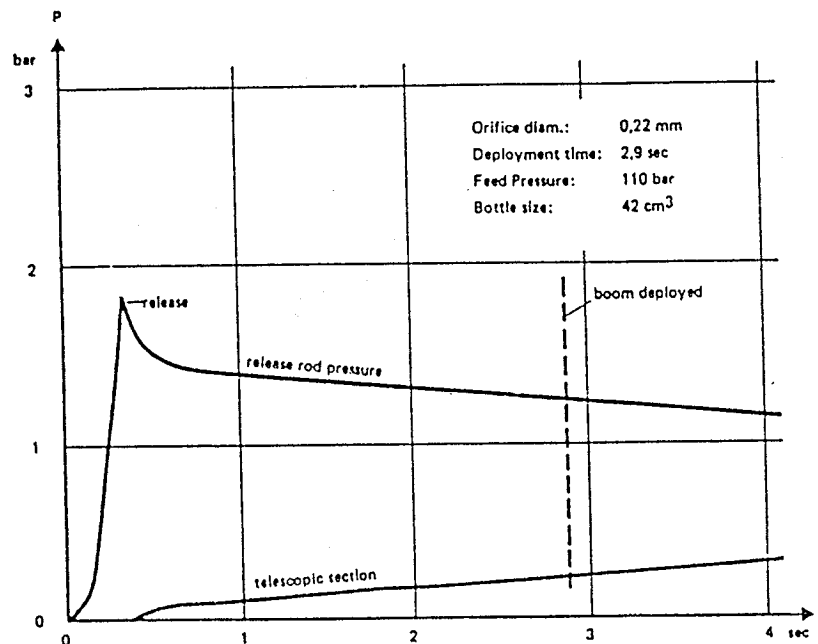
To gain additional information about the failure behavior, a test program was begun. This program consisted of three test series: single gas bottle tests, release mechanism failure simulation tests, and orifice choke simulation tests.

Approximately 100 vacuum deployments have been performed in the course of this investigative program.

Tests with a single gas bottle for each pair of the axial booms with increased charge pressure. For GEOS-2, it is proposed to keep a second gas bottle for each boom pair in reserve. For this reason, the single-bottle pressure had to be determined duplicating deployment times of the GEOS-1 two-bottle arrangement charged with 110-bar pressure. The tests demonstrated that the deployment times, using a single bottle with pressures of 150 to 160 bar, are nearly identical to the required deployment time with two bottles at 110- to 115-bar pressure.

In a second test series, jamming of the release balls in the release cage was simulated. The test setup allowed the release piston to move, but the release of the boom was delayed by a restraining wire that was melted following the required delay times.

In the third test series, an orifice choke was simulated by a thin wire inlay in the orifice channel. During these tests, the axial booms were equipped with a special-release block that allowed recording of the pressure profiles in the release rod and the telescopic section. A typical pressure profile is shown in Figure 3.



95TR4/V2

Figure 3. Long Axial Boom Pressure Profile

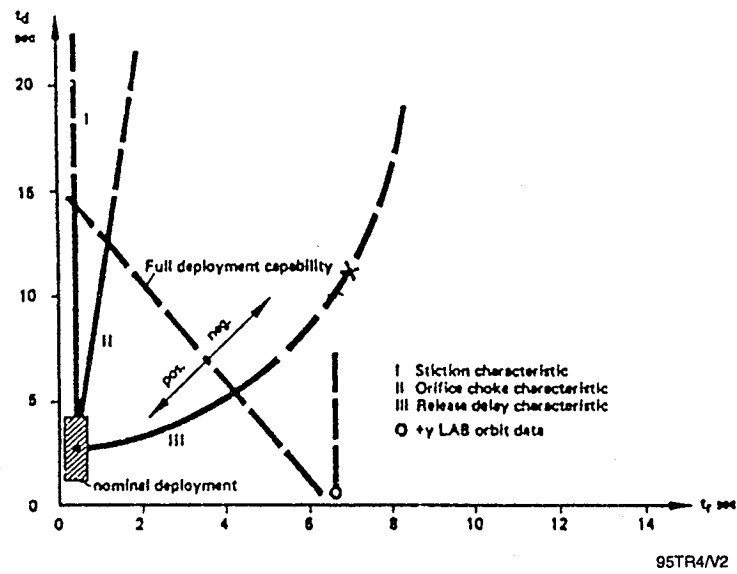
As a result of the above investigations, the release delay (t_r) and the deploy time (t_d) are determined to be the critical parameters. These parameters indicate a characteristic dependency for each of the possible failure explanations. Figure 4 illustrates these characteristics. Curve I shows the relationship attributable to increased friction. The release delay is not influenced by increased friction in the seal and guide system. Therefore, this failure develops as a vertical line (Figure 4). Curve II shows the relationship of t_r and t_d for the condition of a reduced gas flow. The reduced flow influences the deploy time significantly. Its influence on the release delay is less distinct.

Curve III shows the t_r , t_d dependency for the condition of release mechanism jamming. This failure mode causes the pressure to increase in the release rod end and the stowed telescopic sections. When release occurs, there is an increase in deployment speed. This behavior is more pronounced for the SAB than for the LAB, due to the lower deployed-to-stowed volume ratio of the SAB. The full deployment capability is limited by the amount of gas available. If we apply the orbit data to this diagram, the following can be derived:

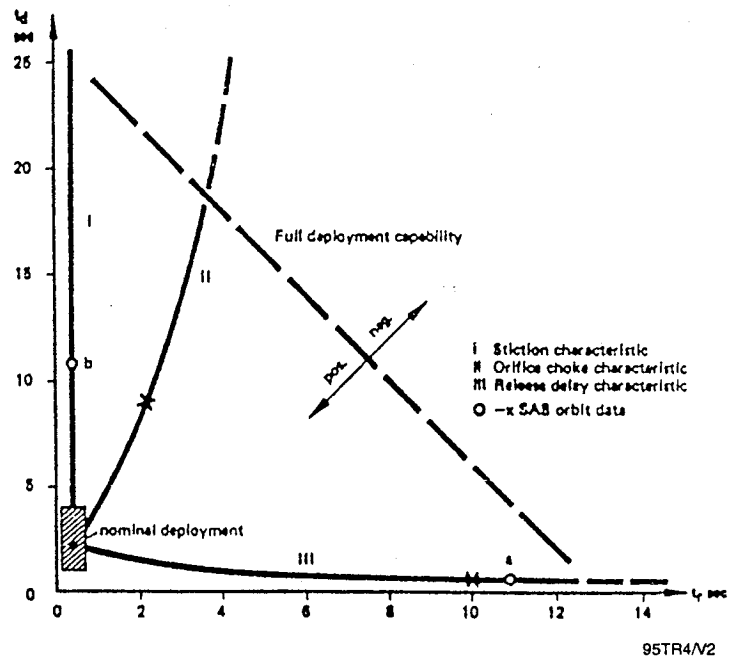
- The SAB data substantiate a position on either Curve I or Curve III (point b and a) depending on individual interpretation of the orbit data. There is no substantive evidence from the orbit data that orifice contamination has to be considered. The diagram demonstrates that any partial orifice choking would cause only a small release delay, followed by a slow deployment of the SAB. The orbit data does not support this interpretation. If the delayed release of the long axial boom has to be considered as definite, any friction has to be excluded, since the +Y LAB still deployed about 80% following the delayed release. Orifice choking can also be excluded, as it was impossible to generate release delays of greater than 4 sec during the tests. The release pressure level could not be achieved for the delayed boom at higher choke rate. This condition is valid also during orbit. Therefore, a malfunction in the release mechanism can be assumed only for the long axial boom. During the first few seconds of deployment, motion following this delayed release was relatively rapid. However, as the accelerometer was in saturation, this was not indicated in telemetry data. Following the initial rapid deployment, the deployment speed was reduced significantly for approximately 5 sec and motion finally ceased at about 80% deployment length.
- Increased deployment times due to stiction were observed occasionally during temperature tests. At higher temperatures, the Teflon guide rings show a cold-flow tendency, which can result in a friction increase. However, this friction increase was found within acceptable limits at temperatures below 60°C.

Release Mechanism Jamming. The friction conditions between ball and ball cage had been carefully calculated for GEOS-1. The calculations demonstrated a sufficient safety margin to jamming of 1.5 to 2. However, an indentation caused by the sharp edge of the titanium bushing (Figure 5a) could have resulted in increased friction, leading to a kinematic failure as indicated in Figures 5a, b, and c. Inspection of GEOS-1 spare unit release balls proved that the indentations exist. Repeated stowage and release increased the number of indentations and the likelihood of two indentation positions is highly probable (Figure 5c).

The proper functioning of the +X FS/SAB flight spare short axial boom lends support to this theory, since this boom had not been exposed to repeated testing.

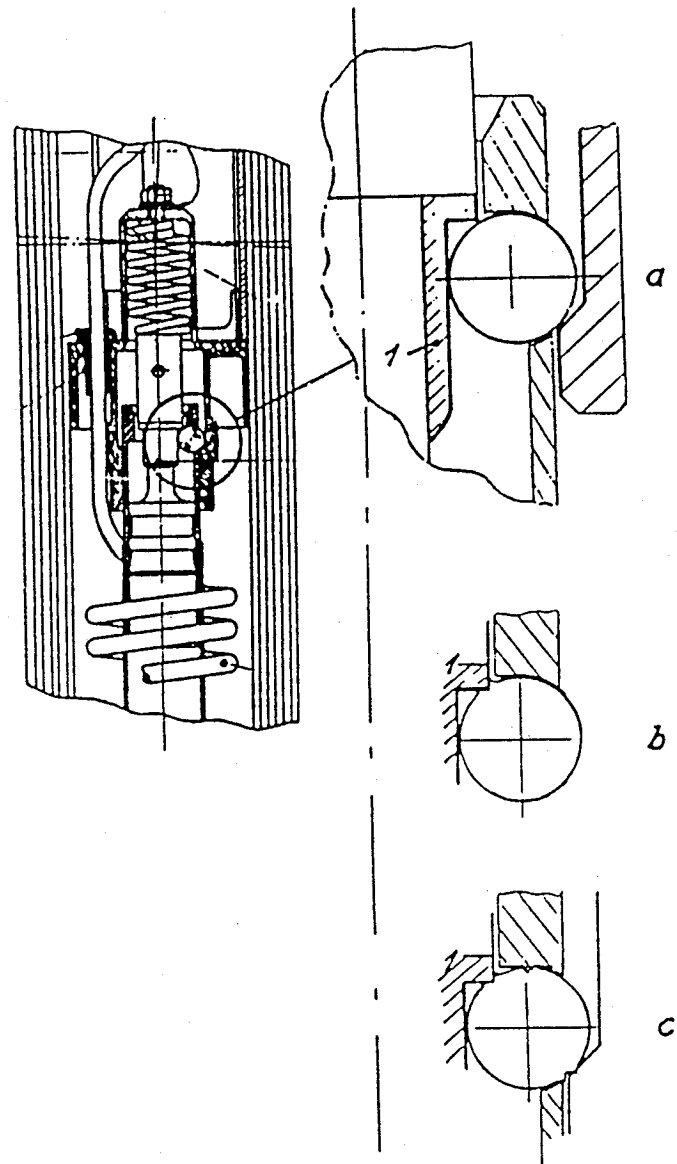


Long Axial Boom



Short Axial Boom

Figure 4. Axial Booms Deployment Characteristics



95TR4/V2

Figure 5. Release Mechanism – Possible Kinematic Failure

Following actuation of the pyrovalves for boom deployment, all four release pistons moved forward and 10 balls moved freely, except for one ball at the +Y LAB and most likely a second ball at the -X SAB may have stuck, as shown in Figure 5c. The gas expanded through the outlet hole into the telescopic sections, as shown by the pressure profile. After a few seconds, the pressure in the telescopic section nearly equalized to the release rod pressure. At this time, the release spring, which was still compressed, may have started to move the release piston in reverse direction due to the reduced pressure differential. It is very likely that this piston motion released the stuck ball in the jammed mechanism and movement continued.

Reaction Wheels

Key Words:

Wheel Start-Up Anomalies, Wheel Oscillations, Solid Friction Model, Electromagnetic Interaction, Ball Bearing, Attitude Control

Mechanisms:

Reaction Wheels

Systems:

Not Specified

Authors; Experts:

R. Stapf, T.H. Lange, and H. Holzach

Address:

DFVLR
Oberpfaffenhofen, FR Germany

Telephone:

Title:

Torque Irregularities in Reaction Wheels

Source:

Proceedings of the Second European Space Mechanisms and Tribology Symposium,
9-11 October 1985, Meersburg, Germany (ESA SP-231).

Abstract:

Experimental investigations on torque irregularities in reaction wheels revealed two classes of unexpected effects: frictional effects, which could be interpreted with Dahl's model of solid friction, and effects due to electromagnetic interactions in the dc motor. The most remarkable phenomenon was an extreme dependency of the wheel start-up current on the rotor's angular position. Equidistant current spikes, exceeding the nominal start current by up to one order of magnitude were found producing an exceptionally high start-up torque.

PRECEDING PAGE BLANK NOT FILMED

Anomalies:

Prestart Oscillations in Reaction Wheels. A very remarkable phenomenon has been observed during wheel run-up tests at certain rotor positions. Before wheel start, rotor oscillations could be found that were completely undamped, so that an external power input by electromagnetic interaction in the dc motor was assumed (Figure 1). Taking into consideration the appertaining power amplifier characteristics, an explanation of this effect could be given.

In Figure 2, the rotor is depicted schematically in some position relative to the stator. The rotor is supposed to be in the state of stiction, which means that a displacement of the rotor will cause a restoring force in the opposite direction. Together with the variable magnetic forces, the restoring force can produce rotor oscillations, which, however, are influenced by nonlinear effects, as can be seen from the shape of the torque oscillations in Figure 2.

Due to the rotor oscillations, the magnetic induction in the stator coils becomes time variable, thus, producing a corresponding generator voltage, U_g . The variation with time of the energy fed into the magnetic circuit depends crucially on the motor control. If the supply voltage, U , is kept constant, the stator current will alter according to the induced generator voltage, U_g ; the electrical power at the power input terminals is:

$$P_u = U (I_0 - (U_g / |Z_{sp}| \cos(\omega t + Y)) \quad (1)$$

where Z_{sp} is the coil impedance causing a phase angle Y .

If a constant current is fed to the motor, a variation of U_g has to be compensated by an in-phase variation of U :

$$P_i = (U_0 + U_g \cos(\omega t)) i \quad (2)$$

Corresponding equations are valid for the energy in the magnetic circuit.

From this, it is clear that for $U = \text{constant}$, the induced generator voltage causes an energy loss, which means that the oscillation will be damped. For $I = \text{constant}$, however, the time-dependent energy portion is provided by the supply voltage in phase, thus leading to a destabilization of the system.

Angular Dependency of Wheel Start Torque. The most remarkable effect found in the present tests was an extreme dependency of the starting current and of the breakaway torque from the rotor position. A uniform start-up current, with mean value of 70 mA, is superimposed by spikes at certain rotor start positions, the height of which exceeds the normal starting current by up to more than one order of magnitude. Furthermore, the spikes are equidistant with an angular separation of exactly 20° from peak to peak.

Evidently, the source of this unexpected behavior is the wheel motor, which is a brushless dc motor with 16 pole pairs (i.e., their angular distance is 20°). Some kind of deadband effect related to the motor geometry is assumed to be the reason for the anomalous start-up behavior at certain rotor positions.

Moreover, a considerable variance of the start-up currents was found from multiple measurements at identical critical positions, indicating a very sensitive dependency of the deadband effect from the rotor position. The resolution of the built-in angular encoder (1) is obviously too coarse for a detailed analysis of that phenomenon. The typical variance is about 50%, however, sometimes wheel start-up could not be obtained even with the maximum tolerable current of 2.5 A.

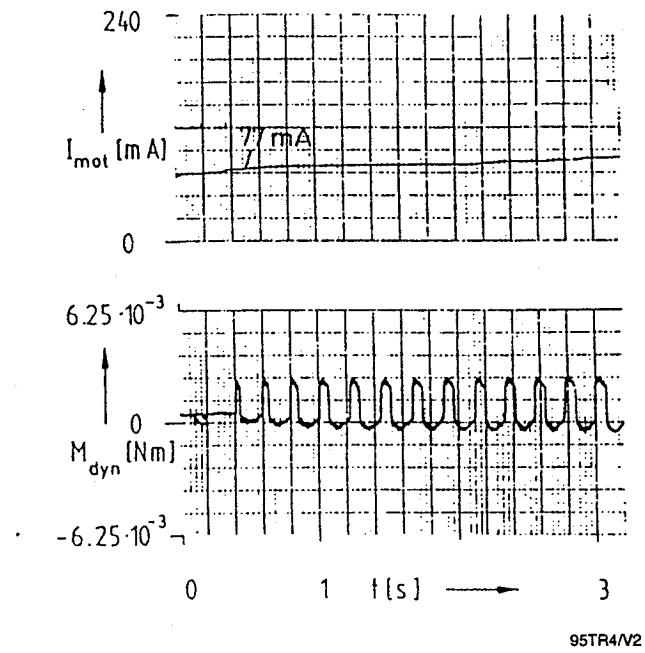


Figure 1. Prestart Oscillations in Reaction Wheels

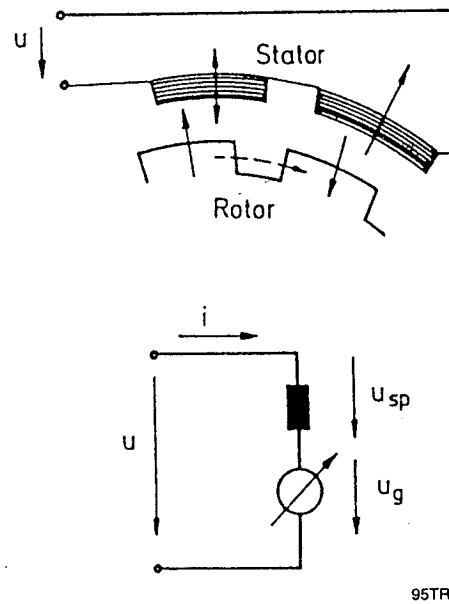


Figure 2. Electromagnetic Interactions Between Rotor and Stator at Wheel Stop

Regarding the start-up torques, the measured torques at noncritical positions correspond to those calculated from the motor scale factor (0.05 Nm/A). At the critical rotor positions, however, motor scale factors between 0.07 and 0.1 Nm/A were calculated from the torque and current measurements, confirming the very sensitive angular dependency of the effect and indicating its nonlinearity.

Probably the reason for the deadband effect is electromagnetic interactions in the wheel motor, similar to those causing prestart oscillations of the wheel. An indication for this is that such oscillations could be found sporadically at critical positions, but never at noncritical positions.

Lessons Learned:

- The present investigations show that the operation of reaction wheels at near-zero wheel speeds may be a critical mode of operation, possibly exhibiting a number of peculiar effects that can be revealed only by lengthy tests. The disturbing torques produced by these effects are considerably greater than the normal torque noise level, so that a disadvantageous influence on the performance of attitude control systems has to be expected. For sensitive missions, adequate tests are therefore indispensable in order to take them into consideration for controller design.

Key Words:

Reaction Wheels, Torque Noise, Audible Noise, Cage Instability, Olympus

Mechanisms:

Reaction Wheels, Angular-Contact Ball Bearings

Systems:

Olympus, 10-Nms Reaction Wheel

Author; Experts:

G.I. Sturtivant

Address:

British Aerospace
Space and Communications Division
Stevenage, United Kingdom

Telephone:**Title:**

Results of a 10-Nms Reaction Wheel Test Program, Including Tests on a Nylon Pore Lubrication System

Source:

Proceedings of the Second European Space Mechanisms and Tribology Symposium, 9-11 October 1985, Meersburg, Germany (ESA SP-231).

Abstract:

The Olympus 10-Nms reaction wheel test program philosophy and results are presented. The test program is designed to fully characterize the reaction wheel assembly and to verify that the unit is capable of surviving both the launch and operating environments. In addition, the lubrication system theory and test program is discussed. A history of the testing and difficulties is also included and the resulting design modifications are detailed.

Anomalies:

- The design of the Olympus reaction wheel is based around its ED20 SNFA angular-contact ball bearings. The bearings were chosen not only for their static capacity and life rating, but also because both British Aerospace (BAe) and the European Space Tribology Laboratory (ESTL) have extensive experience of SNFA angular-contact bearings. Torque losses and elastohydrodynamic film thicknesses for these bearings have previously been empirically measured for a range of space-suitable lubricants that enabled KG80 to be quickly identified as the preferred lubricant for this application; an initial quantity of oil (5 μ l) was also identified.
- The flight model reaction wheel W89 was built using these standard bearings with 5 μ l of KG80 oil per bearing as lubrication. During initial testing of the wheel, both torque noise and audible noise from the wheel at particular speeds were apparent. These were quickly identified as bearing cage instabilities.

Lessons Learned:

- Bearing cage instability is a very difficult phenomena to predict, and is essentially a rapid oscillation of the bearing cage relative to both the balls and the races. It can be thought of as a resonance and will only occur under certain conditions and, if sufficiently severe, it can cause cage break-up. It is dependent upon many factors, which include, for example, lubricant viscosity and quantity, rotational speed of the bearing, cage mass and material, ball pocket clearance, pocket spacing, and pocket design.
- ESTL and SNFA were quickly contacted and a temporary cure was arranged; cages with loose-fit pockets were fitted to a replacement pair of bearings. These were installed into the reaction wheel with 10 μ l of oil and the problem was solved. The flight bearings will, however, have a different solution, with nonequispaced pockets of the original diameter. This will give lower friction levels than the close-fit pocket cages now fitted to the engineering model.

Description:

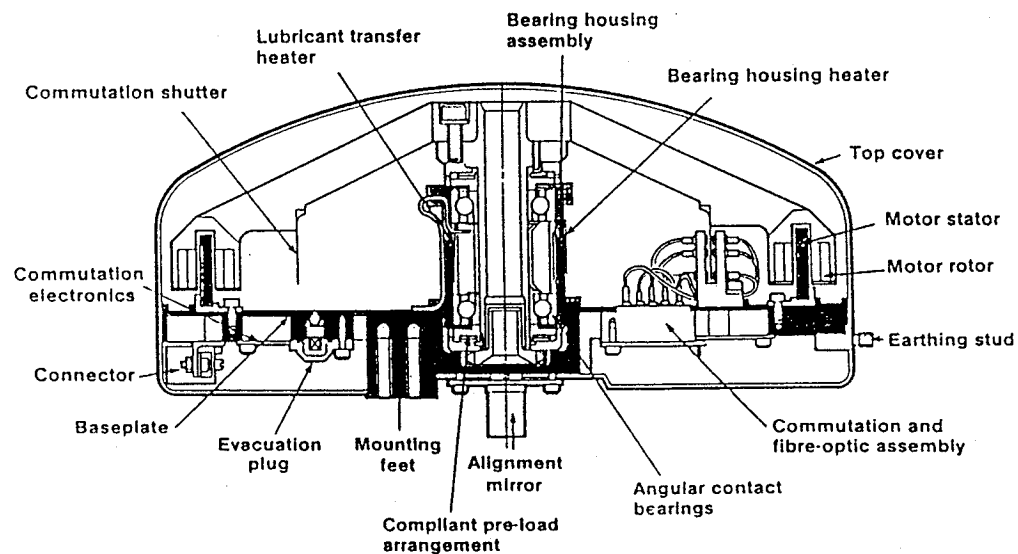
The 10-Nms reaction wheel is a derivative of previous BAe experience, in particular the 2-Nms reaction wheel. The design and development of the 2-Nms reaction wheel was successfully completed in 1977 since when it has continued to perform without fault during a real-time life test, which has now exceeded its design life of seven years and is well into its eighth year.

The success of this first unit resulted in the initial design of a much larger 10-Nms reaction wheel. This was subsequently to form the basis of the Olympus (formerly L-SAT) wheel. The basic design has previously been described in detail in a paper presented at the first European Space Mechanisms Symposium. This wheel will also be life tested after completion of the qualification testing.

The engineering model Olympus reaction wheel comprises five main subassemblies:

- Bearing assembly
- Flywheel and rotor assembly
- Stator assembly
- Motor commutation electronics assembly
- Baseplate and cover assembly.

The Olympus reaction wheel is an integrated mechanical and electronic unit (see Figure 1). It comprises the baseplate, the wheel and bearing assembly, and the motor and associated commutation electronics. The rim of the spoked flywheel contains the magnetic rotor assembly of the dc motor, and the flywheel is supported by a pair of compliantly preloaded angular-contact ball bearings. The motor stator, flywheel, and bearing assembly are mounted in the rear of the assembly and are protected by a simple cover. The incorporation of a depressurised housing reduces windage losses during testing and eliminates the risk of contamination.



95TR4/V2

Figure 1. Olympus Reaction Wheel Assembly

Key Words:

Mechanisms, Microvibration, Olympus, Infrared Sensor Vibrations

Mechanisms:

Reaction Wheels

Systems:

Olympus, PSDE Accelerometer, Infrared Sensors

Author; Experts:

D. Tunbridge

Address:

Communications Satellites Department
European Space Agency Directorate for Telecommunications, ESTEC
Noordwijk, The Netherlands

Telephone:

Title:

The Olympus PAX, Measurement of Mechanism-Induced Vibration

Source:

Proceedings of the 5th European Space Mechanisms and Tribology Symposium, ESTEC, Noordwijk, The Netherlands, 28-30 October 1992, ESA SP-334 (April 1993). A modified version of the paper appears in ESA Bulletin No. 64, but contains no additional material that is relevant.

Abstract:

The Olympus telecommunications spacecraft carries an ultrasensitive accelerometer package known as the PSDE accelerometer experiment (or PAX), designed to measure the minute disturbances caused by the operation of onboard equipment. This novel data has been used to study the operating environment that will be experienced by a highly sensitive laser-based communications package called Silex to be flown on the next generation of European Space Agency (ESA) telecommunications spacecraft, ARTEMIS and DRS.

PAGE 536 INTENTIONALLY BLANK

PRECEDING PAGE BLANK NOT FILMED

Anomalies:

A faulty infrared Earth sensor was monitored and found to have a changed vibration characteristic. A vibration instability triggered intermittently by the reaction wheels was detected.

Lessons Learned:

- At present, the major limitation on the use of PAX, or similar equipment for monitoring high-frequency events, is the need for a large bandwidth for data transmission to Earth and analyze Gbyte quantities of data. The current development is concentrated on the automation of the real-time data reduction. In the future, it may be possible to perform all the routine signal analysis and data reduction on board. The data transfer requirements would then be acceptable to a wider range of spacecraft.
- Instruments must be isolated from reaction wheel disturbances.

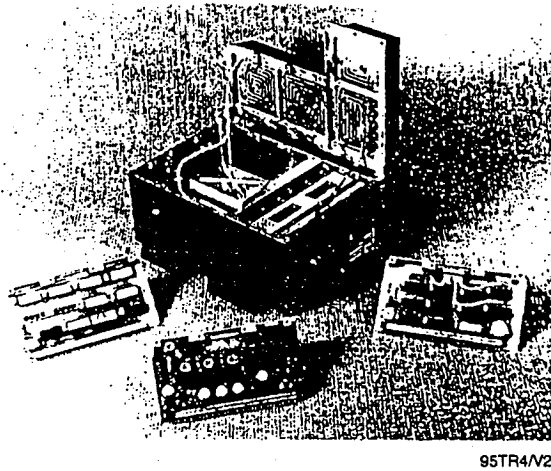
Description:

The primary purpose of PAX is to measure the in-orbit behavior of a typical telecommunications satellite structure in order to obtain design data for the Silex optical payload. A secondary purpose of PAX is to monitor the different mechanisms onboard Olympus at intervals throughout their lifetime in order to detect trends in performance. This technique has been used, for example, in the monitoring of helicopter gearboxes, but this is the first time (to the author's knowledge) that such a facility has been flown on a spacecraft in geostationary orbit.

The PAX flight hardware consists of five elements contained in a single box (Figure 1). These elements are:

- The Accube, containing three accelerometers, a calibration thermistor, and some proximity electronics.
- The analog processing electronics that convert the Accube's outputs into 12-bit digital signals.
- The digital processing electronics, which convert the digital signals into serial data words (80 bit) for telemetry purposes.
- The power converter (dc/dc), which interfaces with the 50-V power bus and provides six regulated voltages within the PAX. It also contains redundant on/off relays and generates a telemetry status signal.
- The radio frequency unit, which generates a carrier signal (12.1 GHz) modulated by the serial digital data.

The accelerometers are manufactured by Centre Suisse pour Electronique et Microtechnique (CSEM) in Neuchatel, Switzerland, using silicon chip integrated-circuit technology. A capacitive output is produced by movement of the seismic mass between electrodes. Each one is hermetically sealed at reduced pressure to provide controlled damping.



95TR4/V2

Figure 1. PAX Flight Hardware

The complete Accube assembly weighs just 150 gm and has a fundamental resonant frequency above 1.5 kHz. The total package, weighing 2.3 kg, is mounted on the lower side Earth-facing (+Z) platform of Olympus to the television broadcast payload (TVB1) (Figure 2). The PAX signal is transmitted as a sideband of the TVB1 payload transmission.

Testing:

The infrared Earth sensor had developed a mechanical interference problem that was causing the mirror to stop oscillating around local midnight, when the solar input to the unit was maximum. It was found that the fundamental frequency of the infrared Earth sensor could be heard in the PAX audio signal as a knocking sound at any time of day. On a frequency plot, all the higher harmonics were clearly visible. This can be seen in a waterfall plot (Figure 3), which shows the moment at which the infrared Earth sensor was switched off.

The noise generated by the reaction wheels was more difficult to deal with. It was intermittent and no clear correlation could be established with expected parameters such as wheel speed, time of day, and temperature. Also, it must be emphasized that there was no deterioration in the affectivity of the wheels in the attitude control system. It was therefore decided that effort should concentrate on observing the phenomenon, by now known colloquially as the screech, and attempting to determine the cause.

An automatic event logging technique was quickly developed to monitor its occurrence. The characteristics of a screech could be clearly distinguished aurally and as a dramatic change to a waterfall plot (Figure 4), but this was not so easy to reproduce in hardware. Monitoring of rms level or bandpass filtration was not effective as many other events, such as thrusters firing, could also act as triggers. It was eventually discovered that the autocorrelation function on a digital signal processor could be used to uniquely detect a screech.

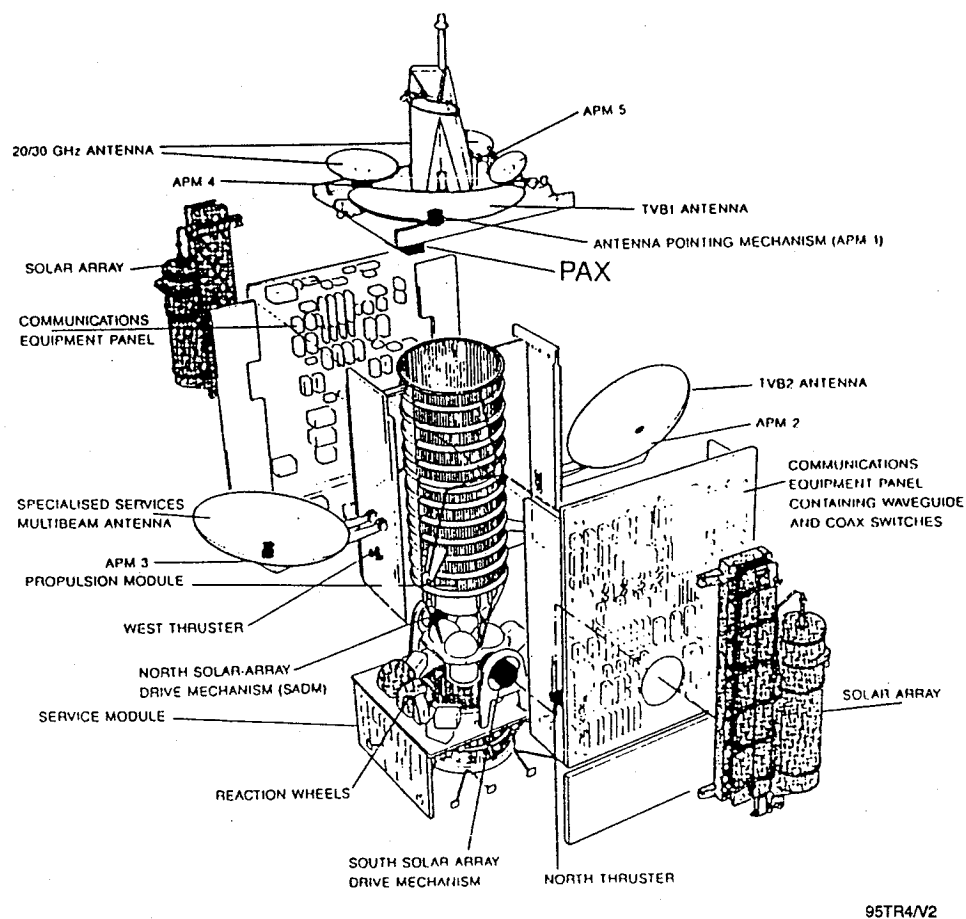
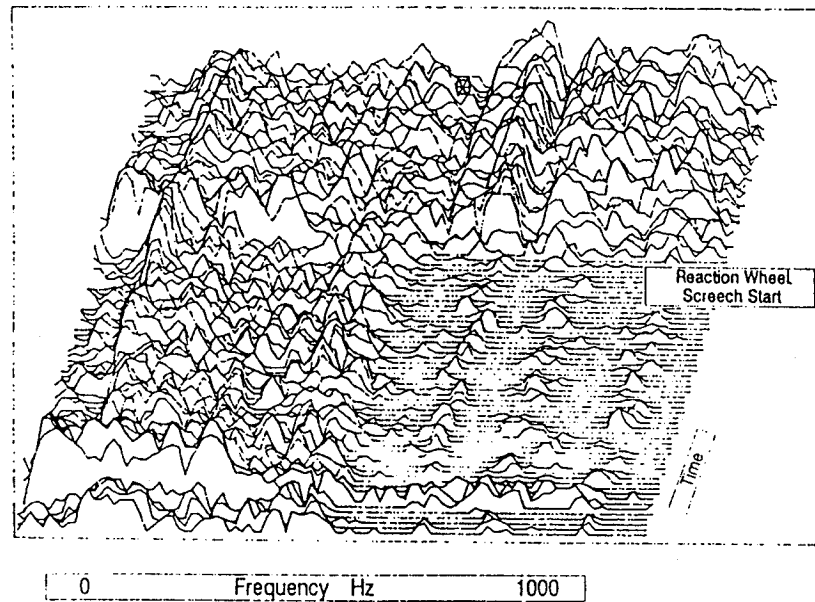
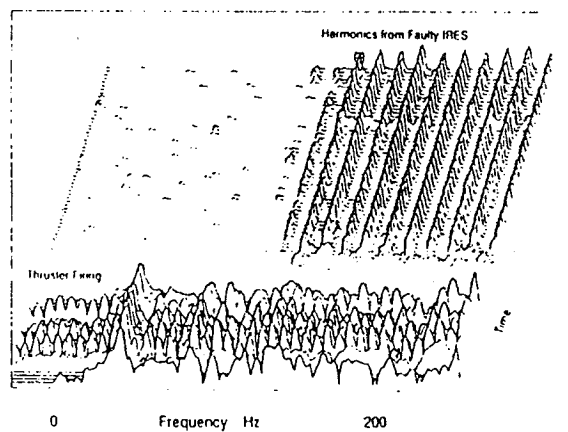


Figure 2. Exploded View of the Olympus Spacecraft Showing the Position of PAX and Many of the Vibration Sources



95TR4/V2

Figure 3. A Waterfall Plot Showing the Moment When the Earth Sensor was Switched Off



95TR4/V2

Figure 4. A Waterfall Plot Showing the Change of Spectrum as the Reaction Wheel Starts

Slip Rings and Roll Rings

Key Words:

Solar Array Drive, Speed Anomalies, Slip Rings, High Torque, Pollutants

Mechanisms:

Solar Array Drive Mechanism

Systems:

SPOT-1 Earth Observation Satellite

Author; Experts:

1. G. Atlas
2. G. Thomin

Address:

1. Societe Europeenne de Propulsion (SEP), Vernon, France
2. Centre National d'Etudes Spatiales (CNES), Toulouse, France

Telephone:

Title:

Experiences of CNES and SEP on Space Mechanisms Rotating at Low Speed

Source:

Proceedings of 21st Aerospace Mechanisms Symposium, L.B. Johnson Space Center, pp. 131-144 (1987).

Abstract:

This paper describes some aspects of the knowledge acquired in the field of space mechanisms by SEP and CNES, in international and French national space programs. The experience described centers on the development of the following major mechanism programs:

The MEGS (Mechanisme d'Entrainement du Generateur Solaire). This is a solar array drive mechanism developed and flown under a CNES-led program and is now flying on the Earth observation SPOT-1 satellite.

The MOGS (Mecanisme d'Orientation de Generateur Solaire). This is a solar array drive designed by SEP under CNES contract and currently being developed for application in the EUTELSAT II program.

PRECEDING PAGE BLANK NOT FILMED

For these mechanisms, the paper highlights key design areas and the mechanism performance obtained. Various test problems with the MEGS slip rings are discussed.

Anomalies:

- Flight measurements have been made on the SPOT-1 satellite. Results of these measurements are shown in Figure 1 and Table 1, which also shows the results of ground testing in air. H1 to H8 represent the harmonics of the speed variation (expressed in percent), which were derived for the flight case at different orbit positions. It can be seen that H1 is not measurable in the flight case, but in any event is less than on ground. The reason for this change is not yet clear, but could derive from a change in the compensation parameters.
- H2, H3, and H8 are remarkably similar to the ground test results. On the other hand, H4 is significantly greater. It is thought that this change comes from the altered slip ring friction torques in vacuum, which have the effect of modifying the equilibrium or detent position that the motor assumes during its movement. The effective torque of the motor around the detent position is shown in Figure 2.
- The motor torque acts against the rotor and is resisted by the frictional torques in the MEGS. If those torques change (e.g., due to an increase in friction of the bearings or the slip ring unit), then the equilibrium point also changes, with consequent effect on the speed stability.
- During ground testing, the change in H4 from an average of 0.9% to an average of around 2.2% in flight, can be correlated with the frictional change in the slip rings. In fact, there is an almost linear relationship between the resistive friction and the 4th harmonic, such that a 0.1-Nm change in friction equates with a 1% change in H4. The observed change in H4 is therefore thought to correspond with an expected change in friction of the MoS₂/Ag/C brushes against the silver slip ring, where the nominal frictional torque was 0.2 to 0.3 Nm in vacuum, compared with 0.4 to 0.6 Nm in air.

Lessons Learned:

- This paper has described the salient features of two solar array drives whose development has been undertaken by SEP and CNES. The designs illustrate the radically different approaches that originated from the differing design requirements. A slip ring problem occurred late in the development of the MEGS and the paper indicates how recovery action can be taken with this type of failure.
- Long storage can result in slip ring contamination. They must be examined and cleaned prior to installation. Also, investigations should be conducted to provide nonpollutant materials.

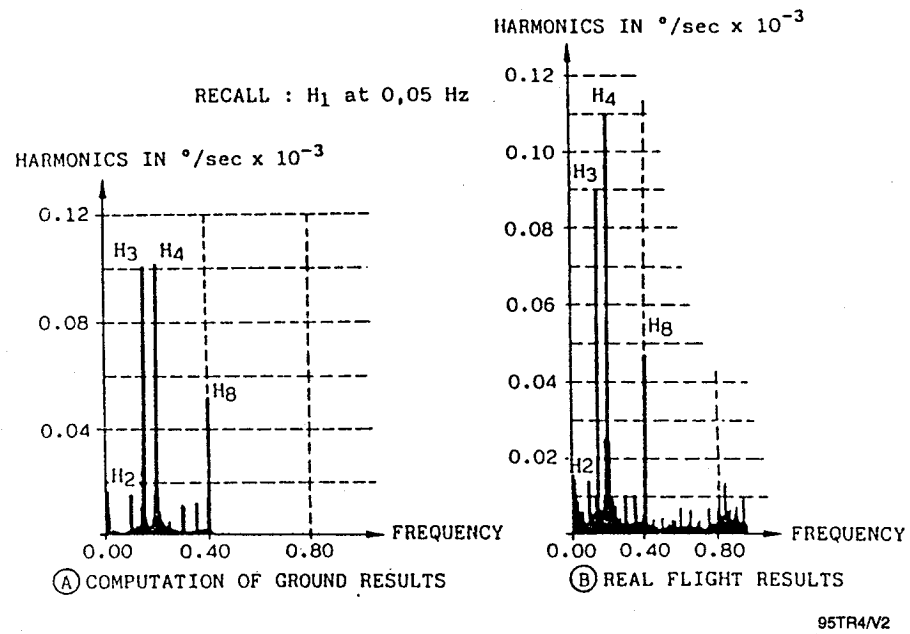
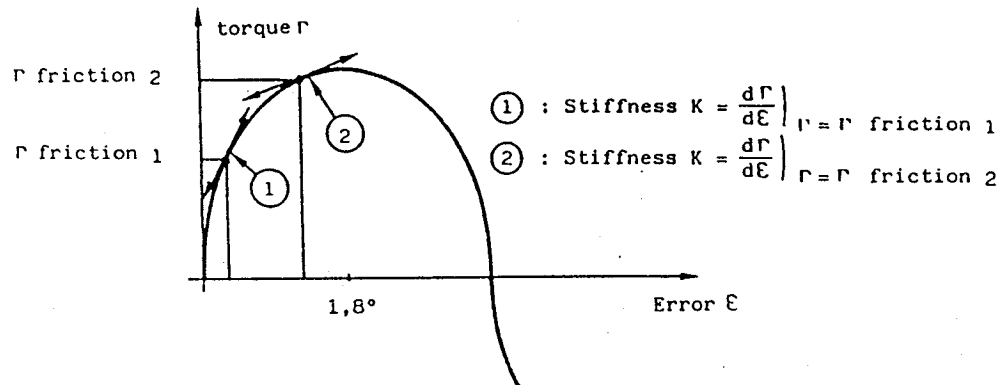


Figure 1. MEGS Orbital Performance Measurements

Table 1. Comparison of Flight and Ground Performance Data

IN FLIGHT				ON GROUND + 20°C		
IN ORBIT POSITION	107 110°	140 200°	140 95°	MEASURE 1	MEASURE 2	MEASURE 3
H1 (%)	Noise			1.75	2.24	1.53
H2 (%)	0.73	0.65	0.64	0.53	0.83	0.36
H3 (%)	0.51	0.59	0.56	0.56	0.63	0.41
H4 (%)	2.43	2.02	2.41	0.63	0.73	1.26
H5 (%)	0	0.18	0.34	-	-	-
H6 (%)	0.53	0.37	0.56	-	-	-
H7 (%)	0.69	0.62	0.64	-	-	-
H8 (%)	3.33	2.69	3.23	2.67	2.96	2.77

95TR4/V2



95TR4/V2

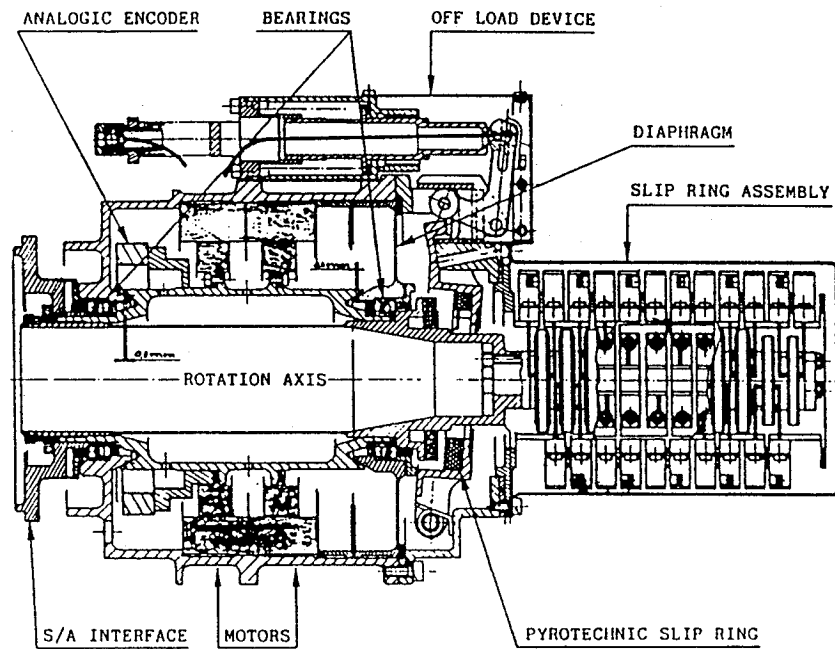
Figure 2. Detent Position Motor Torques

Description:

The MEGS. The SPOT mission was to provide precise images of the Earth, these images having a resolution of 10 m. This was a very severe requirement for the control stability of the satellite and made large corresponding demands on the stability and uniformity of motion made by the MEGS. This speed stability was required to remain within 10% of the nominal speed of 1 rev/100 min (no stepping was allowed). Particularly important was the avoidance of frequencies between 0.15 and 0.2 Hz that might have excited the solar arrays. The MEGS is shown in Figure 3.

In order to achieve these speed uniformity requirements, a direct-drive design was chosen. The motor selected was a SAGEM variable-reluctance stepper motor (nominal 1200 steps per revolution), but driven not in stepping mode, but in synchronous mode. This is achieved by applying to adjacent motor coils currents that vary sinusoidally in time, the current in adjacent coils being out of phase by π . This has the effect of moving the detent position of the motor progressively in the desired direction at (for a perfect motor) a constant speed. However, since the coils of the motor are not absolutely identical, either electrically or physically, some small variation can occur. There can also be interaction with resistive torques arising from position or time dependent friction.

A similar synchronous drive technique was applied by SEP to the despin mechanism of the ESA satellite GIOTTO. This despin mechanism is still operating successfully after the encounter with the Halley comet.



95TR4/V2

Figure 3. The MEGS

The MEGS Slip Ring Aging Problem. One year after delivery of the MEGS, during integration testing on the SPOT1 satellite at the Matra facilities at Toulouse, anomalous values of contact resistance were found in both the pyrotechnic and the power/signal slip ring assemblies. The problem was particularly severe for the pyrotechnic slip rings that had to be tested before launch where a typical value found was 1000-ohm resistance compared with the expected value of 1 ohm. Since the circuit was designed to cater for 40 mohm under a 7.5-A nominal current, action was necessary to examine the phenomenon and find a remedy.

Although such a high-contact resistance had not been identified previously either at SEP or at MECANEX, Switzerland, where the slip rings were manufactured, some anomalies had been observed during tests to determine the breakdown current on the pyrotechnic slip ring assembly. Figure 4 shows the results of such a test, where it can be observed that the voltage drop that can be maintained across the slip ring rises steeply until about 2 A has been applied, and then breaks away, rising only slightly for the remaining rise to 7.5 A, the nominal operating current. From these tests, it appeared that there was some form of diode effect, the contact behaving normally after the nominal current was applied.

It was concluded that the high friction observed during integration was caused by a local pollutant that even if it were generated during ground use or storage, would normally be rubbed off during operation by either mechanical or electrical action. The long storage prior to integration had enabled the pollutant to build up.

II-4 Slip Ring Assembly. Because of the low torques requirement on the slip ring, a large diameter disk concept for the slip rings was abandoned in favor of a modular cylindrical assembly with a small external radius. Figure 5 shows the principle of the slip ring geometry. Note that the brush pressure is applied by means of a soft-blade spring. This technique reduces the effect of temperature differentials and also allows for the 0.3-mm displacement of the rotor when the off-load mechanism is applied. The slip ring materials were chosen after a series of tests performed by CNES with material from Le Carbone Lorraine. The material chosen was Ag/Carbon/MoS₂ (12% MoS₂). As described above, the pyrotechnic slip rings were incorporated in the off-load device. In this way, they did not contribute to the in-orbit frictional torques.

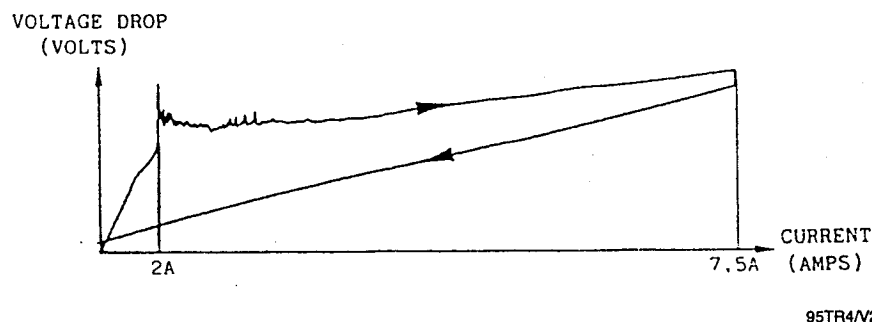


Figure 4. Evidence of the Diode Effect During Testing

Testing:

In order to check the electrical effect, a breakaway test was done on the failed unit where the current was increased up to the nominal current density of 30 A/cm². The results had uniformly the same uniform characteristics for all slip ring circuits, and exhibited the features shown in Figure 6, with some variation in the current at which the different stages in the phenomenon were observed.

Referring to Figure 6, Phase 1 ($I < 0.5$ A for the power lines) indicates a normal resistance/current relationship. The peaks, such as that indicated by "A" in the figure, correspond to the burning off of the pollutant layer. Phase 2 is diode-type behavior and indicates a semiconductor presence, possibly a layer of Ag₂O or Ag₂S. At point "B", where the nominal current density is achieved, all the pollutant layer has been burnt off; in Phase 3, the slip ring shows a nominal performance, indicating that the contact area has been cleaned.

Although these tests showed that current alone could clean the surface, and, in fact, gives a predominant effect, both current and movement are necessary to eliminate the pollutant layer. The results also showed that the attainment of a critical breakaway point was necessary to achieve the cleaning function.

Following these investigations, the SPOT-1 MEGS slip rings were cleaned just prior to launch in 1986 and subsequently operated well within their specifications in orbit. Investigations are now being performed to investigate the source of the pollutant layer and to identify materials that could be used to avoid the problem.

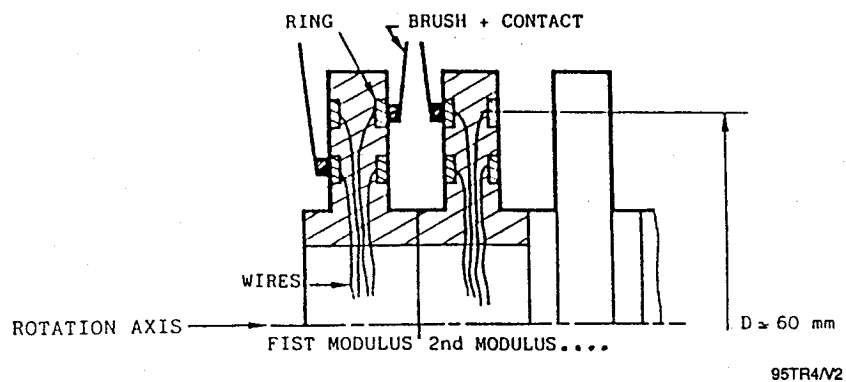


Figure 5. MEGS Slip Ring Geometry

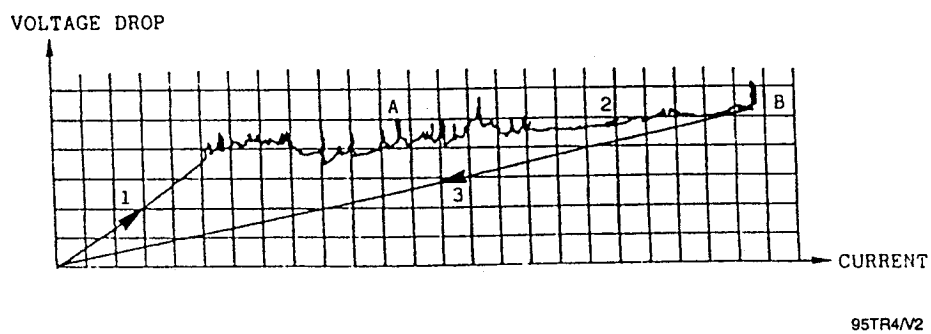


Figure 6. Breakaway Tests on MEGS Slip Rings

Rotating Systems

Miscellaneous

Key Words:

Vapor Compressor, Tribological Problems, Spacelab

Mechanisms:

Vapor Compressor

Systems:

Spacelab, Heat Pump for Refrigeration Unit

Author; Experts:

1. F. Berner, H. Oesch, and K. Goetz
2. C.J. Savage

Address:

1. Swiss Federal Aircraft Factory
6032 Emmen, Switzerland
2. ESTEC, European Space Agency
2200 AG Noordwijk, The Netherlands

Telephone:**Title:**

The Mechanical Design of a Vapor Compressor for a Heat Pump to Be Used in Space

Source:

Proceedings of 16th Aerospace Mechanisms Symposium, Kennedy Space Center, Florida, pp.329-339 (1982).

Abstract:

The most important elements of the mechanical design of a reciprocating compressor have been discussed. Since this compressor is a component of a reversed Carnot-cycle heat pump that will be used on space missions, its design is strongly influenced by two requirements: the capability of operating in the absence of gravity, and the necessity of achieving as high an efficiency as possible in order to minimize the heat pump's power consumption.

Because of the 0-g environment, we have replaced oil with grease as a lubricant, which made it necessary to strictly separate the heat pump's working fluid from the lubricants. This requirement led to the incorporation of metal bellows with extremely long operating lifetimes.

The concept of a semiautomatic discharge valve was introduced in order to optimize the compressor efficiency. This valve opens automatically when the pressure in the cylinder starts exceeding the pressure in the discharge manifold, but it is closed by means of a mechanism such that complete closing is reached at a particular crank angle or piston position. The main features of this mechanism have been described.

Anomalies:

Because of the small size of the compressor, we had initially designed the tappet as a simple, single element. Friction and wear between tappet and cam were reduced through oil lubrication. Unfortunately, we could not maintain a stable oil film between the gliding elements at high camshaft speeds, and excessive wear resulted under these conditions. Since an effective oil lubrication would be even more difficult to maintain under null gravity condition, owing to the absence of a defined level of the oil pool, we have abandoned the gliding contact with oil lubrication, in favor of a practically pure rolling contact between the cam and a roller held in the tappet head with miniature ball bearings. Whereas the ball bearings are grease lubricated for life, there is no lubrication at all between roller and cam.

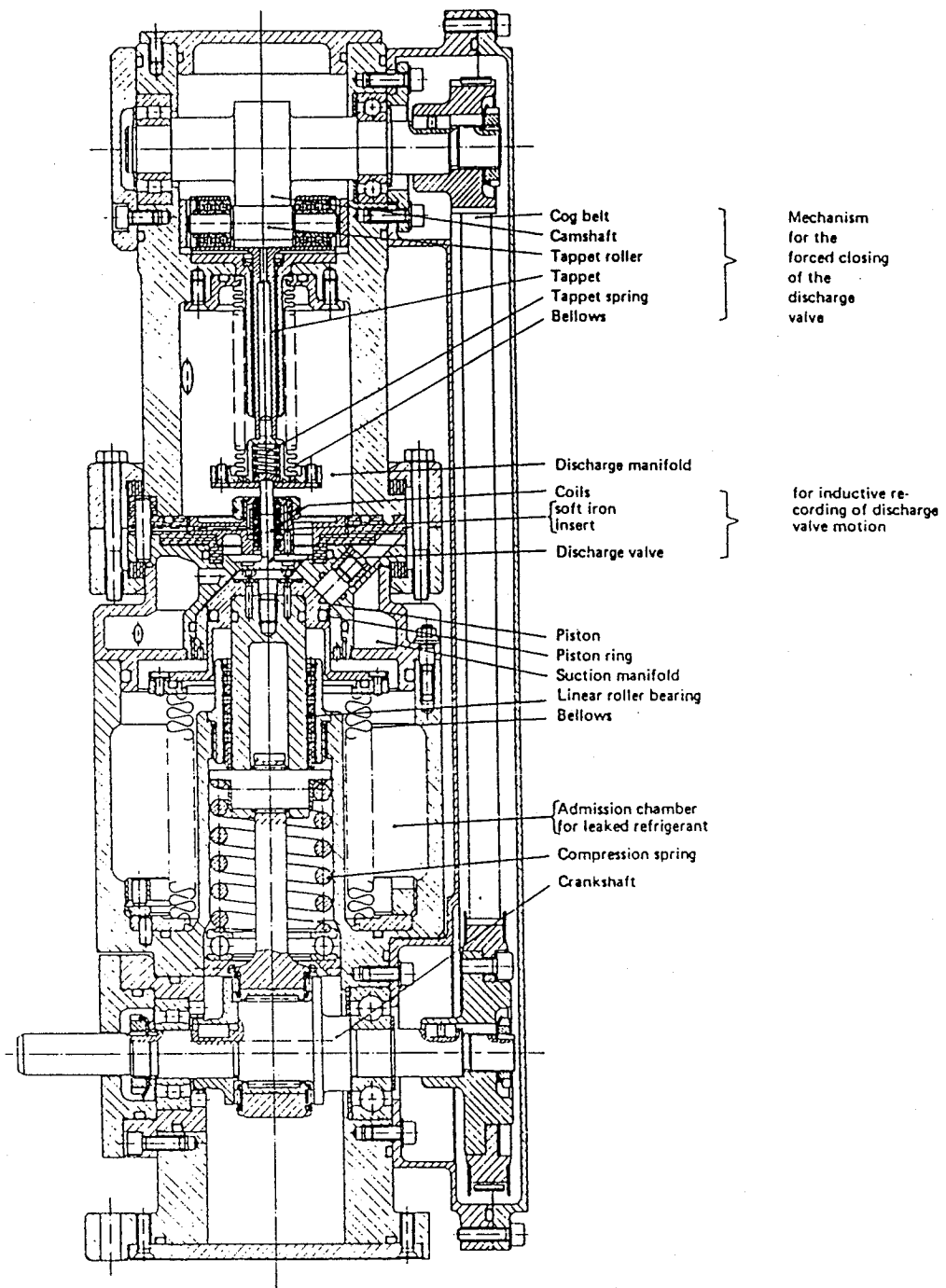
Lessons Learned:

- Oil lubrication is not feasible for reciprocating machines in space because of zero gravity. Grease-packed rolling elements are generally used.
- Cam interfaces are critical life-limiting elements because of the large radii of curvature of the cam's surface compared with the roller radius. Cams made of nitrided steel or coated with tungsten carbide or titanium carbide deteriorated rapidly. Excellent results were obtained with through-hardened steels for cam and roller and also with boronized cam surfaces.

Description:

Special Elements of the Mechanical Design. A section through the vapor compressor is presented in Figure 1, in which some of the special elements of the mechanical design are annotated.

The Semiautomatic Discharge Valve. Reciprocating compressors are usually of the automatic type (i.e., they feature suction and discharge valves that open and close automatically in response to a positive or negative pressure difference across their ports). Most designs feature a series of reed-type suction valves and one or two disk-type, spring-loaded discharge valves per cylinder. Whereas reed valves have been found to perform satisfactorily in our application, the characteristics of automatic discharge valves lead to an unacceptably low volumetric efficiency, particularly at high compression ratios and when the compressor is not operated at the speed for which the disk valve was



95TR4/V2

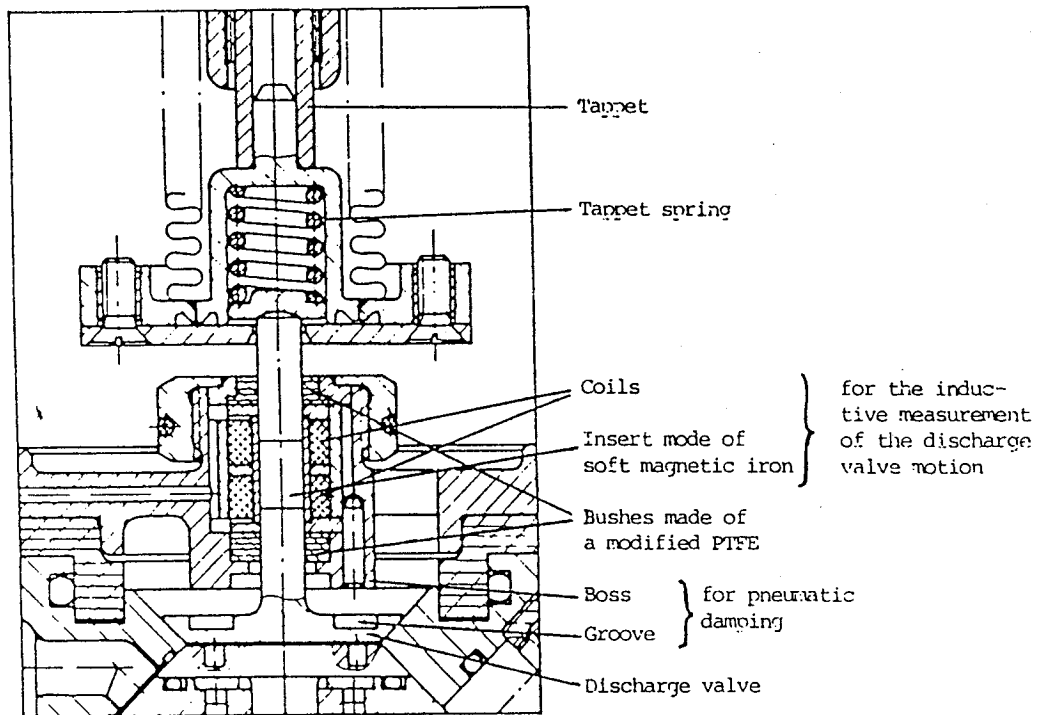
Figure 1. Section through Vapor Compressor

optimized. Hence, we decided to retain the concept of automatic valves for the suction valves only, which in our compressor are a series of reed valves arranged around a centrally positioned disk-type discharge valve. The discharge valve should ideally open when, during a compression phase, the pressure in the cylinder reaches the level of the discharge pressure. This event is delayed if the compression ratio is increased (i.e., the crank angle at which equality of pressures is reached on the two sides of the valve disk increases with the compression ratio). Therefore, we allow the discharge valve to open automatically, but we have developed a concept for its forced closing, such that it hits its seat at a selected crank angle (e.g., when the piston just reaches its upper dead center). This new concept of a semiautomatic discharge valve and the mechanism with which it is realized are described in this section.

Concept of a Semiautomatic Discharge Valve. Closing of the discharge valve is achieved by pushing on its stem with a tappet, whose motion is controlled by a camshaft that is driven off the crankshaft by means of a cog belt. While the tappet is in permanent contact with the camshaft, it touches the valve stem only during (and a very short time after) valve closing. At other times, the valve is either in its seat and the tappet above its lower dead position or, during valve opening, the valve moves toward its open position while the tappet is at its upper dead position.

Only this higher camshaft speed allows achieving sufficiently fast valve closing for the maximum compression ratio of 10 specified by the client. The additional stroke carried out by the tappet between two closing strokes does not have any influence on the discharge valve, because the latter is firmly retained in its seat during this phase due to the positive difference between discharge and cylinder pressures. Notice that the tappet's stroke is slightly larger (in our case 0.5 mm) than the valve's stroke. This difference was introduced for reasons of dimensional inaccuracy. One cannot rigidly push with the tappet against the valve while the latter rests in its seat, i.e., one has to incorporate a spring between actual tappet and valve stem as shown in Figure 2. This spring makes it unnecessary to incorporate special damping means to prevent too large a jumping back of the discharge valve from its seat. On the other hand, we have incorporated means for the pneumatic damping of the valve when, at the end of the opening phase, it hits its stop. As can be seen in Figure 2, these consist of a circular groove on the upper side of the valve disk, and a matching counterpart in the structure that provides the guidance for the valve stem.

Mechanism for the Forced Closing of the Discharge Valve. The camshaft/tappet mechanism makes the duration of the valve closing phase dependent on the compressor speed so that it is always the same fraction of the time of one revolution. Additional measures are necessary to minimize the valve closing in terms of the crank angle interval. Another consideration for the design of the cam contour is the possibly uncontrolled movement of the discharge valve near the end of the closing phase. Ideally, the control mechanism should achieve closing at a very specific crankshaft position, which is not really possible. The tappet, together with the discharge valve, is accelerated during most of the closing phase. However, the tappet reaches a position from which it must be decelerated, since it must then come to a full stop. The valve does not follow this movement (i.e., it remains in contact with the tappet only during the acceleration portion and then proceeds at a constant speed when the tappet is decelerated; meaning that it precedes the tappet from this moment onward). Obviously then, a further aim is to postpone the start of tappet deceleration to the last possible moment (i.e., to keep as short as possible the crank angle interval during which the tappet decelerates). There is a limit to the delay of the beginning of the deceleration because the rate of deceleration increases if the deceleration phase is reduced. Noting that, during deceleration the tappet roller would jump off the cam if not

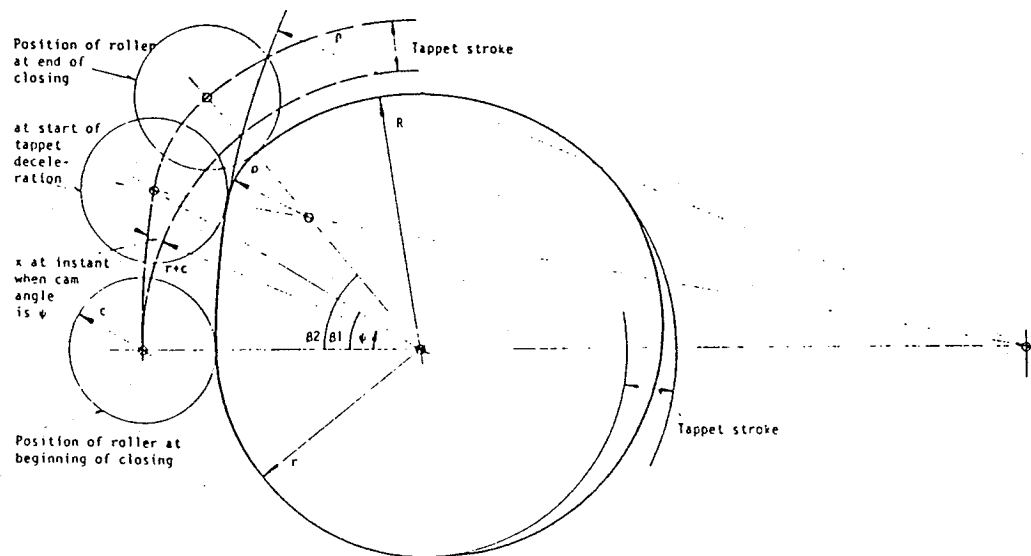


95TR4/V2

Figure 2. Details of Lower Portion of Tappet, Discharge Valve, and Means of Recording the Valve Motion

pushed against it, and it is evident that the larger the deceleration rate, the larger the force must be with which the tappet is pushed against the cam. This force then causes a larger Hertzian surface pressure at all other times and, hence, increased wear. Thus, a compromise must be found between the duration of the deceleration phase and the mean force with which the tappet is pushed against the cam. To meet the different requirements mentioned above, we had to design a cam of a size that is rather large when compared with the crankshaft. The cam shape is depicted in Figure 3, which is not to scale but illustrates all relevant features.

As noted previously, the discharge manifold is hermetically sealed from the tappet/camshaft assembly by means of a metal bellows. This element has an additional function: the pressure in the discharge manifold being typically between 5 and 10 bar higher than in the camshaft housing. The bellows furnishes a pressure force with which the tappet is pushed against the camshaft, thereby assuring a permanent contact between the two elements. With a maximum crankshaft speed of 1000 rpm, the bellows is subjected to load cycles at a frequency of 33 Hz. This value is about an order of magnitude above the maximum frequency recommended by the bellows manufacturers. Moreover, the client having specified a minimum operating lifetime of 500 hr at maximum compressor speed, the bellows must survive at least 60 million load cycles, which again is one or two orders of magnitude above manufacturer's specifications. We believe that such a requirement can be met only if, unlike what seems to be general practice, the bellows is deflected only in the strictly elastic range of its material's stress deflection curve. This means that the ratio of the bellows' stroke to its free length has to be limited to a few percent. The stroke and free length are 3.3 mm and 60 mm, respectively, in our design.



95TR4/V2

Figure 3. Cam Geometry and Motion of the Tappet Roller Over the Cam Surface During the Closing Phase

Testing:

Rather extensive testing with camshafts and rollers of different materials, different surface treatments, and/or coatings were required to identify that material combination that resulted in the least wear of the cam and roller surfaces. Generally speaking, the camshaft has been found to be the critical element, apparently because of the large radii of curvature of the cam's surface compared with the roller's radius. Specifically, the surfaces of cams made of nitrided steel or coated with tungsten carbide or titanium carbide were found to deteriorate rather rapidly. All roller materials tested performed satisfactorily. These were nitrided steel 34CrAlMo5 and through-hardened steel X102CrMo17 or X165CrMoV12. Excellent results have been obtained with a camshaft made of X102CrMo17 steel, through-hardened, and paired with a roller made of the nitrided steel mentioned above. Also very good results were obtained with boronized cam surfaces (material: steel 42CrMo4 boronized to a depth of 100 μm and steel X165CrMoV12 boronized 20- μm deep), paired with rollers made of either one of the three materials mentioned above. With the Hertzian pressure varying between 450 N/mm^2 and 550 N/mm^2 during one revolution of the camshaft, we observed some minor wear of these cams during the first 50 hr of testing at a camshaft speed of 2000 rpm and practically no wear thereafter during several thousand hours of testing.

Guidance of the tappet is provided by a dry bearing material consisting of a layer of sintered bronze that is impregnated with PTFE. The tappet is made of titanium which, according to the dry bearing material's manufacturer, is not hard enough for minimum wear of its material. Therefore we have coated the tappet surfaces with tungsten carbide that is applied with a flame-plating process.

Guidance of the discharge valve stem is less critical than tappet guidance because, in contrast to the tappet, the valve is not subjected to significant moments or forces normal to the stem axis. Hence, the guiding bushes for the valve stem are made of a modified PTFE only, and the titanium valve is not coated. However, as can be seen in Figure 2, a piece of soft iron is interposed between upper and lower stem portion. Since titanium is a reasonably good dielectric, this intermediate stem piece, together with the two coils shown in Figure 2 inside of a tube made of soft magnetic iron, allows the inductive measurement and recording of the discharge valve motion.

Additional Information

Additional Information

In addition to the items in the Literature Review (Section 2.0), the European Space Tribology Laboratory (ESTL) is aware of a number of other problems and anomalies that have occurred in satellites or during ground testing. We include a list of such events for your information, but we are not aware of any detailed investigations of these faults or anomalies that have been published in the open literature.

HIPPARCOS Astronomy Satellite

Failure of two onboard gyroscopes providing spin-axis attitude information. Operating mode/software adjusted to compensate for this. Reported in ESA Bulletin No. 67 (August 1991), No. 68 (November 1991), No. 72 (November 1992), and No. 73 (February 1993).

In tests of protoflight model, differential focussing problem due to creep of mirror glue, arising from thermal cycling and high humidities. Mirror replaced by spare in which the glue was more stable, not having experienced high temperatures or humidities. Reported in ESA Bulletin No. 52 (November 1987).

ERS-1

Blocking of wind-scatterometer antenna movement. Problem corrected from ground by use of backup systems. Failure attitude control system to converge to fine-pointing mode; attributed to software error, corrected from ground. Reported in ESA Bulletin No. 68 (November 1991), No. 70 (May 1992), and No. 73 (February 1993).

Ulysses

Developed a wobble (nutation) problem, thought to be due to solar heating of axial boom. Problem disappeared when boom in the shadow of the spacecraft. Onboard control strategies developed to control any recurrences. Reported in ESA Bulletin No. 65 (February 1991).

IUE

Gyroscope failure reported. Problem had been anticipated, and alternative control software was implemented for use with the two remaining gyroscopes. Software to permit control with only one gyroscope was being developed. Reported in ESA Bulletin No. 45 (February 1986).

EUREKA

Two antenna booms failed to latch closed after launch by shuttle. Boom held in closed position by astronaut while ESOC sent latch commands, and positive latching was achieved. Reported in ESA Bulletin No. 75 (August 1993).

Spacelab-1

High data rate recorder drive belt broke during flight. Attributed to belt being wider than those used previously. Corrective action was to return to previous size of drive belts. Reported in ESA Bulletin No. 38 (May 1984).

Spacelab-2

One of three fixed-head star trackers failed, affecting operation of instrument pointing system optical sensor. Faulty unit returned to Dornier for examination. Reported in ESA Bulletin No. 45 (February 1986).

Spacelab-3

Scientific airlock failed after preliminary use; was to be examined after recovery. Reported in ESA Bulletin No. 43 (August 1985).

Addresses and Telephone Numbers

BERTIN & Cie
B.P. 3
F-78373
Plasor Cedex, France
Telephone: 1-34-81-85-00/Fax: 1-30-54-04-14

BRITISH AEROSPACE SYSTEMS LIMITED
Communications Satellites Division
Gunnels Wood Road
Stevenage, Hertfordshire, United Kingdom
Telephone: 438-313456/Fax: 438-736637

BRITISH AEROSPACE SYSTEMS LIMITED
Earth Observation and Science Division
P.O. Box 5
Filton, Bristol, United Kingdom
Telephone: 272-693831/Fax: 272-363812

CNES
Center National d'Etudes Spatiale
Avenue Edouard Belin
F-31055 Toulouse Cedex, France
Telephone: 61-27-31-31/Fax: 61-27-31-79

DEUTSCHE AEROSPACE AG
P.O. Box 80 1109
D-8000 Munchen (Munich) 80, Germany
Telephone: 89-607-0/Fax: 89607-26481

DORNIER GmbH
P.O. Box 1420
D-7990 Friedrichshafen, Germany
Telephone: 7545-80/Fax: 7545-84411

EUROPEAN SPACE AGENCY (ESTEC)
P.O. Box 299
NL-2200
AG Noordwijk ZH, The Netherlands
Telephone: 1719-86555/Fax: 1719-17400

MATRA MARCONI SPACE UK
Anchorage Road
Portsmouth PO3 5PU, United Kingdom
Telephone: 705-664966

ORS
The Austrian Aerospace Company
Osterreichische Raumfahrt und Systemtechnik Gesellschaft MbH
Operngasse 20b
A-1040 Wien (Vienna), Austria
Telephone: 1-588-140/Fax: 1-588-14-221

SENER Ingenieria y Sistemas SA
Calle Severo Ochoa, Parque Tecnologica de Madrid
E-28760 TRES CANTOS (Madrid), Spain
Telephone: 1-807-7000/Fax: 1-807-7201

S.E.P.
Societe Europeene de Propulsion
Division Propulsion a Liquids et Espace
Foret de Vernon
B.P. 27207 Vernon, France
Telephone: 32-21-72-00/Fax: 32-21-27-01

SWISS FEDERAL AIRCRAFT FACTORY
CH-6032
Emmen, Switzerland
Telephone: 41-59-41-11/Fax: 41-55-25-88

REPORT DOCUMENTATION PAGEForm Approved
OMB No. 0704-0188

Public reporting burden for this collection of information is estimated to average 1 hour per response, including the time for reviewing instructions, searching existing data sources, gathering and maintaining the data needed, and completing and reviewing the collection of information. Send comments regarding this burden estimate or any other aspect of this collection of information, including suggestions for reducing this burden, to Washington Headquarters Services, Directorate for Information Operations and Reports, 1215 Jefferson Davis Highway, Suite 1204, Arlington, VA 22202-4302, and to the Office of Management and Budget, Paperwork Reduction Project (0704-0188), Washington, DC 20503.

1. AGENCY USE ONLY (Leave blank)		2. REPORT DATE September 1995	3. REPORT TYPE AND DATES COVERED Technical Memorandum	
4. TITLE AND SUBTITLE Space Mechanisms Lessons Learned Study Volume II—Literature Review			5. FUNDING NUMBERS WU-297-10-00	
6. AUTHOR(S) Wilbur Shapiro, Frank Murray, Roy Howarth, and Robert Fusaro				
7. PERFORMING ORGANIZATION NAME(S) AND ADDRESS(ES) National Aeronautics and Space Administration Lewis Research Center Cleveland, Ohio 44135-3191			8. PERFORMING ORGANIZATION REPORT NUMBER E-9892	
9. SPONSORING/MONITORING AGENCY NAME(S) AND ADDRESS(ES) National Aeronautics and Space Administration Washington, D.C. 20546-0001			10. SPONSORING/MONITORING AGENCY REPORT NUMBER NASA TM-107047	
11. SUPPLEMENTARY NOTES Wilbur Shapiro, Frank Murray, and Roy Howarth, Mechanical Technology Incorporated, Latham, New York 12110 (work funded under NASA Contract NAS3-27086); Robert Fusaro, NASA Lewis Research Center. Responsible person, Robert Fusaro, organization code 5230, (216) 433-6080.				
12a. DISTRIBUTION/AVAILABILITY STATEMENT Unclassified - Unlimited Subject Categories 18, 37, and 27 This publication is available from the NASA Center for Aerospace Information, (301) 621-0390.			12b. DISTRIBUTION CODE	
13. ABSTRACT (Maximum 200 words) Hundreds of satellites have been launched to date. Some have operated extremely well and others have not. In order to learn from past operating experiences, a study was conducted to determine the conditions under which space mechanisms (mechanically moving components) have previously worked or failed. The study consisted of (1) an extensive literature review that included both government contractor reports and technical journals, (2) communication and visits (when necessary) to the various NASA and DOD centers and their designated contractors (this included contact with project managers of current and prior NASA satellite programs as well as their industry counterparts), (3) requests for unpublished information to NASA and industry and (4) a mail survey designed to acquire specific mechanism experience. The information obtained has been organized into two volumes. Volume I provides a summary of the lessons learned, the results of a needs analysis, responses to the mail survey, a listing of experts, a description of some available facilities and a compilation of references. Volume II contains a compilation of the literature review synopsis.				
14. SUBJECT TERMS Mechanisms; Systems; Problems; Space; Mechanical components; Tribology; Lubrication; Deployables; Lessons learned			15. NUMBER OF PAGES 536	
			16. PRICE CODE A23	
17. SECURITY CLASSIFICATION OF REPORT Unclassified	18. SECURITY CLASSIFICATION OF THIS PAGE Unclassified	19. SECURITY CLASSIFICATION OF ABSTRACT Unclassified	20. LIMITATION OF ABSTRACT	